

INFORMATION TO USERS

This manuscript has been reproduced from the microfilm master. UMI films the text directly from the original or copy submitted. Thus, some thesis and dissertation copies are in typewriter face, while others may be from any type of computer printer.

The quality of this reproduction is dependent upon the quality of the copy submitted. Broken or indistinct print, colored or poor quality illustrations and photographs, print bleedthrough, substandard margins, and improper alignment can adversely affect reproduction.

In the unlikely event that the author did not send UMI a complete manuscript and there are missing pages, these will be noted. Also, if unauthorized copyright material had to be removed, a note will indicate the deletion.

Oversize materials (e.g., maps, drawings, charts) are reproduced by sectioning the original, beginning at the upper left-hand corner and continuing from left to right in equal sections with small overlaps.

Photographs included in the original manuscript have been reproduced xerographically in this copy. Higher quality 6" x 9" black and white photographic prints are available for any photographs or illustrations appearing in this copy for an additional charge. Contact UMI directly to order.

ProQuest Information and Learning
300 North Zeeb Road, Ann Arbor, MI 48106-1346 USA
800-521-0600

UMI[®]

University of Alberta

SCOUR OF CLAY BY JETS

By

Kerry Anne Mazurek



A thesis submitted to the Faculty of Graduate Studies and Research in partial fulfillment of
the requirements for the degree of Doctor of Philosophy

in

Water Resources Engineering

Department of Civil & Environmental Engineering

Edmonton, Alberta

Spring 2001



National Library
of Canada

Acquisitions and
Bibliographic Services

395 Wellington Street
Ottawa ON K1A 0N4
Canada

Bibliothèque nationale
du Canada

Acquisitions et
services bibliographiques

395, rue Wellington
Ottawa ON K1A 0N4
Canada

Your file Votre référence

Our file Notre référence

The author has granted a non-exclusive licence allowing the National Library of Canada to reproduce, loan, distribute or sell copies of this thesis in microform, paper or electronic formats.

The author retains ownership of the copyright in this thesis. Neither the thesis nor substantial extracts from it may be printed or otherwise reproduced without the author's permission.

L'auteur a accordé une licence non exclusive permettant à la Bibliothèque nationale du Canada de reproduire, prêter, distribuer ou vendre des copies de cette thèse sous la forme de microfiche/film, de reproduction sur papier ou sur format électronique.

L'auteur conserve la propriété du droit d'auteur qui protège cette thèse. Ni la thèse ni des extraits substantiels de celle-ci ne doivent être imprimés ou autrement reproduits sans son autorisation.

0-612-60324-5

Canada

University of Alberta

Library Release Form

Name of Author: Kerry Anne Mazurek

Title of Thesis: Scour of Clay by Jets

Degree: Doctor of Philosophy

Year this Degree Granted: 2001

Permission is hereby granted to the University of Alberta Library to reproduce single copies of this thesis and to lend or sell such copies for private, scholarly or scientific research purposes only.

The author reserves all other publication and other rights in association with the copyright in the thesis, and except as herein before provided, neither the thesis nor any substantial portion thereof may be printed or otherwise reproduced in any material form whatever without the author's prior written permission.

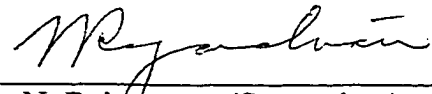

102 John's Drive
Lac La Biche, Alberta
Canada T0A 2C0

Date: January 29, 2001

University of Alberta

Faculty of Graduate Studies and Research

The undersigned certify that they have read, and recommend to the Faculty of Graduate Studies and Research for acceptance, a thesis entitled "**Scour of Clay by Jets**" submitted by **Kerry Anne Mazurek** in partial fulfillment of the requirements for the degree of **Doctor of Philosophy in Water Resources Engineering**.



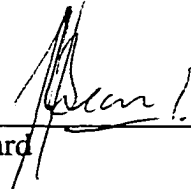
Dr. N. Rajaratnam (Supervisor)



Dr. D. C. Segó (Cosupervisor)

Z. Zhu

Dr. D. Zhu



Dr. J. Leonard



Dr. J.D. Scott

Z. Zhu (for)

Dr. P.Y. Julien (Eternal Examiner)

Date: 26 Jan 2001

**TO THOSE BEFORE ME WHOSE WORK HELPED ME
UNDERSTAND.**

TO THOSE WHO SUPPORTED ME.

TO THOSE WHO ENCOURAGED ME.

ABSTRACT

The work described herein is a laboratory study of the scour of clays by two types of jets: a submerged vertical circular impinging jet and a submerged plane turbulent wall jet. The scour tests were undertaken using one type of soil composed of 40 % clay, 53 % silt, and 7 % fine sand. The first objective was to examine the characteristics of scour in clay by these jets, including the form of erosion of the clay and the dimensions of the scour hole produced by the jets. The second objective was to develop a method of predicting the scour hole dimensions in a clay from the hydraulic properties of the jet and the properties of the soil.

For the scour by the circular impinging jet, an analysis based on the mechanics of impinging jets shows the dimensions of the scour hole at an equilibrium state of scour are a function of the momentum flux from the jet, the impingement height (for "large" impingement heights), the viscosity and density of the eroding fluid, and the critical shear stress of the soil. Equations were developed to predict the scour hole dimensions for the asymptotic or equilibrium state of scour (for a scour hole eroded by mass erosion). A dimensionless scour hole profile was also developed. Measurements showed that the scour hole dimensions appear to grow linearly with the logarithm of time, except at times very near the beginning of scour and as the scour hole nears equilibrium state, as has previously observed in scour by jets in sand. In a similar method as for impinging jet scour, equations were developed to predict the maximum depth of scour, the distance to the maximum depth, the length of the scour hole, and scour hole profile, for scour in a cohesive soil by a plane turbulent wall jet. This work shows that repeatable experiments in the scour by jets of cohesive materials can be performed.

ACKNOWLEDGEMENTS

I would like to sincerely thank Dr. N. Rajaratnam and Dr. D.C. Sego for their support and guidance through the course of this study. Both have provided excellent supervision for this work. Gratitude is extended to P. Fedun for building and then helping with the experimental arrangement.

There have been many students through my years in the T. Blench Hydraulics laboratory that have encouraged me in my work. Here I thank F. Ade, M. Chamani, C. Albers, A. Mainali, A. Moawad, S. Ead, G. Sikora, and G. Arnold, for their advise and encouragement at different times during the course of my graduate studies.

Great appreciation is expressed to my parents for their continued support.

Funding for both myself and the project was provided by the Natural Science and Engineering Research Council in the form of an NSERC Postgraduate scholarship and a research grant to Dr. Rajaratnam and is gratefully acknowledged.

Table of Contents

CHAPTER 1: INTRODUCTION	1
1.1 Introduction	1
1.2 Objectives	2
1.3 Organization of the Thesis	2
CHAPTER 2: THE BEHAVIOR AND EROSION OF CLAYS	4
2.1 Background	4
2.2 Clay Particles and their Behavior	7
2.3 Characteristics of Erosion in Clay Soils	10
2.3.1 <i>Introduction</i>	10
2.3.2 <i>Erosion of Muds or High Void Ratio Soils</i>	10
2.3.3 <i>Erosion of Low Void Ratio Soils</i>	12
2.4 Factors Affecting the Erodibility of Cohesive Soils	17
2.4.1 <i>Background</i>	17
2.4.2 <i>Clay Content and Soil Gradation</i>	18
2.4.3 <i>Mineralogy of the Clay Particles</i>	19
2.4.4 <i>Fabric of the Clay</i>	19
2.4.4.1 <u><i>Saturated Soils</i></u>	19
2.4.4.2 <u><i>Unsaturated Soils</i></u>	20
2.4.5 <i>Interparticle Bonds</i>	21
2.4.5.1 <u><i>Effect of the Pore and Eroding Water Chemistry</i></u>	21
2.4.5.2 <u><i>Effect of the Soil Density</i></u>	23

2.4.5.3 <i><u>Effect of Test Temperature</u></i>	26
2.4.6 <i>Macroscopic Strength of the Bed</i>	27
2.4.7 <i>Summary</i>	30
CHAPTER 3: JETS AND EROSION BY JETS	32
3.1 Introduction	32
3.2 Jet Characteristics	32
3.2.1 <i>Submerged Circular Turbulent Impinging Jets</i>	33
3.2.2 <i>Submerged Plane Turbulent Wall Jets</i>	34
3.3 Jet Scour in Cohesionless Soils	36
3.3.1 <i>Scour in Cohesionless Soils by Submerged Circular Turbulent Impinging Jets</i>	36
3.3.2 <i>Scour in Cohesionless Soils by Submerged Plane Turbulent Wall Jets</i>	37
3.4 Previous works in Erosion of Cohesive Soils by Jets	39
3.4.1 <i>Introduction</i>	39
3.4.2 <i>Jets Used in the Evaluation of Soil Resistance to Scour</i>	40
3.4.2.1 <i><u>Dunn (1959)</u></i>	40
3.4.2.2 <i><u>Dash (1968)</u></i>	41
3.4.2.3 <i><u>Bhasin, Lovell, and Toebe (1969)</u></i>	42
3.4.2.4 <i><u>Hollick (1976)</u></i>	43
3.4.2.5 <i><u>Kuti and Yen (1976)</u></i>	44
3.4.2.6 <i><u>Krishnamurthy (1983)</u></i>	45
3.4.3 <i>Scour by Jets in Cohesive Soils</i>	46
3.4.3.1 <i><u>Moore and Masch (1962)</u></i>	46
3.4.3.2 <i><u>Mirtskhulava et al (1967)</u></i>	48

3.4.3.3	<i><u>Abt (1980)</u></i>	50
3.4.3.4	<i><u>Hedges (1990)</u></i>	52
3.4.3.5	<i><u>Hanson (1990a)</u></i>	54
3.4.3.6	<i><u>Hanson (1991)</u></i>	55
3.4.3.7	<i><u>Stein (1990)</u></i>	56
3.5	Discussion	58
CHAPTER 4: EXPERIMENTAL SETUPS & EXPERIMENTS		63
4.1	Introduction	63
4.2	Experimental Setup I - Impinging Jet Tests	63
4.2.1	<i>Experimental Setup and Experiments</i>	63
4.2.2	<i>Measurements</i>	64
4.3	Experimental Setup II - Wall Jet Tests	66
4.3.1	<i>Experimental Setup and Experiments</i>	66
4.3.2	<i>Measurements</i>	67
4.4	Clay Samples	69
4.4.1	<i>Description of Samples</i>	69
4.4.2	<i>Manufacture of the Clay</i>	69
4.4.3	<i>Preparation of the Samples for Testing</i>	70
4.4.3.1	<i><u>Impinging Jet Tests</u></i>	70
4.4.3.2	<i><u>Wall Jet Tests</u></i>	71
4.5	Water Chemistry of the Eroding Fluid	71

CHAPTER 5: EROSION CHARACTERISTICS	81
5.1 Introduction	81
5.2 Flake Erosion	81
<i>5.2.1 Impinging Jet Tests</i>	81
<i>5.2.2 Wall Jet Tests</i>	82
5.3 Mass erosion	83
<i>5.3.1 Impinging Jet Tests</i>	83
<i>5.3.2 Wall Jet Tests</i>	83
5.4 Rapid Surface Erosion	84
<i>5.4.1 Impinging Jet Tests</i>	84
<i>5.4.2 Wall Jet Tests</i>	85
CHAPTER 6: RESULTS AND ANALYSIS OF IMPINGING JETS TESTS	92
6.1 Introduction	92
6.2 Results	94
6.3 Developing Dimensionless Parameters for Impinging Jet Scour of Clay	95
<i>6.3.1 Dimensional Analysis for Scour Hole Dimensions at Equilibrium</i>	95
<i>6.3.2 Development of a Dimensionless Time Scale</i>	98
6.4 Analysis of Equilibrium State Results	100
<i>6.4.1 Scour Hole Dimensions at Equilibrium</i>	100
<i>6.4.2 Scour Hole Profiles at Equilibrium State</i>	102

6.5 Growth of the Scour Hole	105
6.6 Analysis of Errors	107
6.7 Discussion	108
CHAPTER 7: RESULTS AND ANALYSIS OF WALL JETS TESTS	151
7.1 Introduction	151
7.2 Results	152
7.3 Dimensional Analysis for Plane Wall Jet Scour of Clays	153
<i>7.3.1 Dimensional Analysis for Scour Hole Dimensions at Equilibrium State</i>	153
<i>7.3.2 Dimensionless Parameters for the Growth of the Scour Hole</i>	155
7.4 Analysis of Equilibrium State Results	156
<i>7.4.1 Dimensions of the Scour Hole at Equilibrium State</i>	156
<i>7.4.2 Scour Hole Profiles at Equilibrium State</i>	157
<i>7.4.3 Geometry of the Scour Holes</i>	159
<i>7.4.4 Variability in the Scour Holes</i>	160
7.5 Growth of the Scour Holes	161
7.6 Analysis of Errors	161
7.7 Discussion	162
CHAPTER 8: CONCLUSION	201
8.1 Summary of Observations	201
8.2 Conclusions	205

8.3 Recommendations for Future Research	205
REFERENCES	207
Appendix A: Scour hole growth data for impinging jet tests.	219
Appendix B: Growth of the scour hole volume, maximum scour depth, and centreline scour depth for the impinging jet tests (plots).	239
Appendix C: Scour hole profile data for impinging jet tests.	251
Appendix D: Scour hole profiles for impinging jet tests.	266
Appendix E: Scour hole profile data for wall jet tests.	277
Appendix F: Scour hole profiles for wall jet tests.	294
Appendix G: Data for wall jet evolution tests.	309

List of Tables

<u>Table</u>	<u>Page</u>
2-1 Typical values for critical shear stress.	30
4-1 Details of experiments for impinging jet tests.	71
4-2 Details of experiments for wall jet tests.	72
4-3 Eroding water chemistry data for impinging jet tests.	73
4-4 Eroding water chemistry data for wall jet tests.	74
6-1 Location of first eroded particle.	110
6-2 Scour hole volume, maximum scour depth, and centreline scour depth at equilibrium state.	111
6-3 Scour hole radius and half-widths based on the maximum depth of scour at equilibrium state.	112
6-4 Half-widths based on the centreline depth of scour at equilibrium state.	113
6-5 Time scales for impinging jet scour tests.	114
6-6 Maximum errors in measurements and derived quantities.	115
7-1 Maximum scour depth, location of the maximum scour depth, and length of the scour holes at equilibrium state for the wall jets tests.	163
7-2 Variability in the dimensions of a scour hole.	164
7-3 Maximum errors in measured and derived quantities for wall jet tests.	165

List of Figures

<u>Figure</u>		<u>Page</u>
2-1	Examples of different types of clay fabrics.	31
3-1	The submerged circular impinging jet (a) definition sketch (b) pressure distribution on boundary for typical test conditions (c) shear stress distribution on boundary.	59
3-2	The plane turbulent wall jet.	60
3-3	Typical scour holes (a) a weakly deflected jet type scour hole (b) a strongly deflected jet scour hole.	61
3-4	Scour by a plane wall jet in sand.	62
4-1	Experimental setup I - impinging jet apparatus.	75
4-2	Experimental setup II - wall jet apparatus.	76
5-1	Flake Erosion (a) erosion of a particle (b) in plan.	85
6-1	Typical scour hole profiles for impinging jet tests.	116
6-2	Definition sketch for impinging jet tests.	117
6-3	Growth of the scour hole volume (a) arithmetic scale (b) semi-log plot (all tests at $X=1214$ Pa).	118
6-4	Growth of the maximum scour depth (a) arithmetic scale (b) semi-log plot (all tests at $X=1214$ Pa).	119
6-5	Growth of the centreline scour depth (a) arithmetic scale (b) semi-log plot (all tests at $X=1214$ Pa).	120
6-6(a)	Dimensionless scour hole volume at equilibrium state.	121
(b)	Data Point No. 1 (8/14.5/9.0/4) $U_o=8.95$ m/s $d=8$ mm $H=116$ mm ($X-X_c$)/ $X_c=0.27$ $t_d=67.6$ h	122
(c)	Data Point No. 2 (4/29.0/25.9/2) $U_o=25.86$ m/s $d=4$ mm $H=116$ mm ($X-X_c$)/ $X_c=1.65$ $t_d=114.4$ h	122
(d)	Data Point No. 3 (8/8.1/7.4/1) $U_o=7.44$ m/s $d=8$ mm $H=65$ mm ($X-X_c$)/ $X_c=1.80$ $t_d=117.4$ h	122
(e)	Data Point No. 4 (4/16.3/19.9/1) $U_o=13.93$ m/s $d=4$ mm $H=65$ mm ($X-X_c$)/ $X_c=4.00$ $t_d=103.9$ h	122
(f)	Data Point No. 5 (4/10.0/13.9/1) $U_o=13.93$ m/s $d=4$ mm $H=40$ mm ($X-X_c$)/ $X_c=5.46$ $t_d=90.9$ h	122
(g)	Data Point No. 6 (4/10.0/15.9/2) $U_o=15.92$ m/s $d=4$ mm $H=40$ mm	122

	$(X-X_c)/X_c=7.44$ (after 49 h 54 min)	
(h)	Data Point No. 6 (4/10.0/15.9/2) $U_o=15.92$ m/s $d=4$ mm $H=40$ mm $(X-X_c)/X_c=7.44$ $t_d=116.1$ h	123
(i)	Data Point No. 7 (4/10.0/15.9/1) $U_o=15.92$ m/s $d=4$ mm $H=40$ mm $(X-X_c)/X_c=7.44$ $t_d=93.12$ h	123
(j)	Data Point No. 8 (4/10.0/17.9/1) $U_o=17.90$ m/s $d=4$ mm $H=40$ mm $(X-X_c)/X_c=9.69$ $t_d=123.9$ h	123
(k)	Data Point No. 9 (4/10.0/19.9/1) $U_o=19.89$ m/s $d=4$ mm $H=40$ mm $(X-X_c)/X_c=12.19$ $t_d=96.3$ h	123
6-7	Scour hole profile (a) for a strongly deflected jet and (b) for a weakly deflected jet.	124
6-8	Dimensionless scour hole volume at equilibrium state with dimensionless excess stress.	125
6-9	Dimensionless maximum scour hole depth at equilibrium state with dimensionless excess stress.	126
6-10	Dimensionless centreline scour hole depth at equilibrium state with dimensionless excess stress.	127
6-11	Ratio of the maximum scour depth to the centreline scour depth at equilibrium state with the dimensionless excess stress.	128
6-12	Dimensionless scour hole radius at equilibrium state.	129
6-13	Ratio of the scour hole volume to the centreline scour depth at equilibrium state with dimensionless excess stress.	130
6-14	Ratio of the radius of the scour hole to the centreline scour depth at equilibrium state with dimensionless excess stress.	131
6-15	Effect of temperature on the scour hole volume at equilibrium.	132
6-16	Dimensionless scour hole profile at equilibrium nondimensionalized with the maximum scour depth and scour hole radius.	133
6-17	Dimensionless scour hole profile at equilibrium nondimensionalized with the centreline scour depth and scour hole radius.	134
6-18	Curve fits for the dimensionless scour hole profile that uses the maximum scour depth and scour hole radius as scales.	135
6-19	Curve fits for the dimensionless scour hole profile that uses the centreline scour depth and scour hole radius as scales.	136
6-20	Dimensionless scour hole profile at equilibrium nondimensionalized with the maximum depth of scour and half-widths.	137

6-21	Dimensionless scour hole profile at equilibrium nondimensionalized with the centreline depth of scour and half-widths.	138
6-22	Curve fit for the dimensionless scour hole profile that uses the maximum depth of scour and half-widths as scales.	139
6-23	Curve fit for the dimensionless scour hole profile that uses the centreline depth of scour and half-width as scales.	140
6-24	Variation of the ratio of the scour hole radius and the half-width based on the maximum scour depth at equilibrium with the dimensionless excess stress.	141
6-25	Variation of the ratio of the scour hole radius to the half-width based on the centreline scour depth at equilibrium with dimensionless excess stress.	142
6-26	Half-width based on the maximum scour depth at equilibrium with dimensionless excess stress.	143
6-27	Half-width based on the centreline scour depth at equilibrium with dimensionless excess stress.	144
6-28	Ratio of the half-width based on the maximum scour depth to the nozzle diameter at equilibrium with the dimensionless excess stress.	145
6-29	Growth of the dimensionless scour hole volume.	146
6-30	Variation of the dimensionless time scale with dimensionless excess stress.	147
7-1	Scour hole profiles at equilibrium along jet centreline.	166
7-2	Definition sketch for wall jet tests.	167
7-3	Growth of the scour holes (a) Test No. 2.33/10.5/1/E (b) Test No. 2.33/8.9/1/E	168
7-4	Growth of the maximum scour depth with time (a) arithmetic scale (b) semi-log plot.	169
7-5	The location of the maximum scour depth with time (a) arithmetic scale (b) semi-log plot.	170
7-6	Growth of the scour hole length with time (a) arithmetic scale (b) semi-log plot.	171
7-7 (a)	Dimensionless average maximum scour hole depth at equilibrium.	172
(b)	Point 1 (5.10/6.5/1) $U_o=6.54$ m/s $a=5.10$ mm $(\lambda-\lambda_c)/\lambda_c=1.14$ $t_d=149.2$ h	173
(c)	Point 2 (2.33/8.0/2) $U_o=8.00$ m/s $a=2.33$ mm $(\lambda-\lambda_c)/\lambda_c=2.20$ $t_d=101.0$ h	173

(d)	Point 2 plan view	173
(e)	Point 3 (5.10/7.0/3) $U_o=7.03$ m/s $a=5.10$ mm $(\lambda-\lambda_c)/\lambda_c=1.47$ $t_d=120.0$ h	173
(f)	Point 4 (2.33/10.2/1) $U_o=10.23$ m/s $a=2.33$ mm $(\lambda-\lambda_c)/\lambda_c=4.23$ $t_d=126.0$ h	173
(g)	Point 4 plan view	173
(h)	Point 5 (2.33/9.5/1) $U_o=9.50$ m/s $a=2.33$ mm $(\lambda-\lambda_c)/\lambda_c=3.52$ $t_d=140.6$ h	174
(i)	Point 6 (2.33/8.5/2) $U_o=8.46$ m/s $a=2.33$ mm $(\lambda-\lambda_c)/\lambda_c=2.58$ $t_d=120.7$ h (side view)	174
(j)	Point 6 plan view	174
(k)	Point 7 (2.33/12.0/1) $U_o=12.03$ m/s $a=2.33$ mm $(\lambda-\lambda_c)/\lambda_c=6.23$ $t_d=93.2$ h	174
(l)	Point 7 plan view	174
(m)	Point 8 (2.33/12.7/1) $U_o=12.72$ m/s $a=2.33$ mm $(\lambda-\lambda_c)/\lambda_c=7.08$ $t_d=118.2$ h	174
(n)	Point 8 plan view	174
7-8	Dimensionless average maximum scour hole depth at equilibrium state with the dimensionless parameter λ .	175
7-9	Average location of the maximum depth of scour at equilibrium state with the dimensionless parameter λ .	176
7-10	Average length of the scour hole at equilibrium state with the dimensionless parameter λ .	177
7-11	Typical scour hole profiles (a) Type 1 profiles (b) a Type 2 profile (S2) and a Type 3 profile (S1) and (c) Type 4 profiles.	178
7-12	Dimensionless scour hole profile for the Type 1 scour hole.	179
7-13	Dimensionless scour hole profile for the Type 2 scour hole.	180
7-14	Dimensionless scour hole profile for the Type 3 scour hole.	181
7-15	Dimensionless scour hole profile for the Type 4 scour hole.	182
7-16	Dimensionless average length scale b_w at equilibrium state with	183

dimensionless λ .

7-17	Dimensionless maximum scour depth at equilibrium sorted by scour hole type (no averaging).	184
7-18	Dimensionless location of the maximum scour depth sorted by scour hole type.	185
7-19	Dimensionless scour hole length sorted by scour hole type.	186
7-20	Dimensionless length scale of scour sorted by scour hole type.	187
7-21	Variation of the ratio of the location of maximum scour to the maximum scour depth at equilibrium as sorted by the scour hole profile type.	188
7-22	Variation of the ratio of the scour hole length to the maximum depth at equilibrium as sorted by the scour hole profile type.	189
7-23	Variation of the ratio of the scour length scale to the maximum scour depth at equilibrium as sorted by scour hole type.	190
7-24	Variation of the ratio of the length of the scour hole to the location of the maximum depth as sorted by scour hole type.	191
7-25	Variation of the ratio of the average location of maximum scour to the average maximum scour depth at equilibrium.	192
7-26	Variation of the ratio of the average scour hole length to the average maximum depth of equilibrium.	193
7-27	Variation of the ratio of the average length scale of scour to the average maximum scour depth at equilibrium.	194
7-28	Variation of the ratio of the average scour hole length to the average location of maximum scour at equilibrium.	195
7-29	Dimensionless scour hole profile with time for Test No. 2.33/10.5/1/E.	196
7-30	Dimensionless scour hole profile with time for Test No. 2.33/8.9/1/E.	197
7-31	Growth of the dimensionless scour hole length with time.	198

List of Plates

<u>Plate</u>	<u>Page</u>
4-1 Experimental setup I - impinging jet.	77
4-2 Experimental setup II - plane wall jet (a) flume, storage tank, and pump (b) front view of nozzle and sample.	78
4-3 Electron micrograph of the soil (a) at 1500X magnification (b) at 7500X magnification.	79
4-4 Section of clay manufacturing equipment where the soil and water are mixed.	80
4-5 Section of clay manufacturing equipment from which the clay is extruded.	80
5-1 Beginning of flake erosion for an impinging jet (a) early on in the test (b) later in the test.	86
5-2 Pattern of scour on the surface of the clay for flake erosion for two tests.	87
5-3 Flake erosion pattern in a wall jet test.	88
5-4 Mass eroded hole in impinging jet tests with eroded clay chunks.	88
5-5 (a) Some eroded chunks form the scour hole shown in (b) for wall jet tests.	89
5-6 Rapid surface erosion in an impinging jet test (a) after 2 h (b) after 4 h.	90
5-7 Rapid surface erosion in two wall jet tests (a) after 1 h (b) after 1 h 20 min.	91
6-1 Typical scour holes (a) Test no. 8/14.5/10.9.1 $U_o=10.94$ m/s $d=8$ mm $H=65$ mm $(X-X_c)/X_c=0.90$ (after 71h 17 min) (b) Test no. 8/8.0/9.0/4 $U_o=8.95$ m/s $d=8$ mm $H=65$ mm $(X-X_c)/X_c=3.05$ (after 116h 49min).	148
6-2 Scour hole growth for Test no. 8/8.1/9.0/1 $U_o=8.95$ m/s $d=8$ mm $H=65$ mm $(X-X_c)/X_c=3.05$ after (a) 15min (b) 30min (c) 1h 8min (d) 2h 30min (e) 5h (f) 9h 44min (g) 23h 21min (h) 30h 21min (i) 46h 6min (j) 55h 42min (k) 96h 36 min (l) 124h 15min.	150
7-1 Scour hole growth for Test no. 2.33/8.9/1/E $U_o=8.89$ m/s $a=2.33$ mm $(\lambda-\lambda_c)/\lambda_c=3.05$ after (a) 30 min (b) 2 h (c) 4.5 h (d) 25 h (e) 25 h (in plan) (f) 50 h (g) 50 h (in plan) (h) 72 h (i) 72 h (in plan)	199

List of Symbols

The following symbols are used:

a	=	thickness of the jet at the nozzle for wall jet tests
b_{∞}	=	half-width of scour hole at equilibrium for impinging jet tests
$b_{cl\infty}$	=	radial distance from the jet centreline where the scour depth is half the centreline scour depth at equilibrium for the impinging jet tests
$\bar{b}_{cl\infty}$	=	average for a section of the radial distance from the jet centreline where the scour depth is half the centreline scour depth at equilibrium
$\bar{\bar{b}}_{cl\infty}$	=	average for scour hole of the radial distance from the jet centreline where the scour depth is half the centreline scour depth at equilibrium
$b_{m\infty}$	=	radial distance from the jet centreline where the scour depth is half the maximum scour depth at equilibrium for the impinging jet tests
$\bar{b}_{m\infty}$	=	average for a section of radial distance from the jet centreline where the scour depth is half the maximum scour depth at equilibrium
$\bar{\bar{b}}_{m\infty}$	=	average for scour hole of radial distance from the jet centreline where the scour depth is half the maximum scour depth at equilibrium
b_w	=	length scale for wall jet tests
$b_{w\infty}$	=	length scale at equilibrium (wall jet tests)
$\bar{b}_{w\infty}$	=	average of the sectional measurements for a test of the length scale at equilibrium (wall jet tests)
B	=	width of flow
B_o'	=	thickness of jet as it enters the tailwater
B_o	=	thickness of jet
B_w	=	maximum width of scour hole
c	=	parameter describing physiochemical properties of soil (Chapter 3)
c_f	=	skin friction coefficient
c'	=	fatigue strength to rupture of soil
C_d	=	diffusion coefficient

d	=	jet diameter at nozzle
d_c	=	diameter of culvert
d_t	=	tailwater depth
D	=	particle grain size
\dot{E}	=	erosion rate
F_o	=	densiometric Froude number
g	=	gravitational acceleration
h	=	an exponent
H	=	height of jet above sample surface (impingement height)
H'	=	distance from the nozzle to the clay surface along the jet centreline (for oblique jets)
J_i	=	jet index
K	=	soil erodibility coefficient
n	=	a coefficient
m	=	an empirical constant
m'	=	a coefficient
M_o	=	momentum flux from the nozzle
p_w	=	pressure at the clay surface
P_d	=	pressure exerted by the jet on the aggregates (Chapter 3)
P_h	=	factor to take into account hydrostatic pressure effects
PI	=	plasticity index
Q	=	flow rate
Q_c	=	scouring rate
r	=	distance from jet centreline
r_i	=	distance from centreline of first eroded particle
r_o	=	radius of scour hole
r_{∞}	=	radius of scour hole at equilibrium

\bar{r}_{∞}	=	average radius of scour hole at equilibrium for a section
$\bar{\bar{r}}_{\infty}$	=	average for scour hole of the radius of scour hole at equilibrium
r'	=	distance from the jet centreline to top of ridge
R	=	Reynolds number
R_h	=	hydraulic radius
\bar{R}^2	=	correlation coefficient
s	=	settling velocity of the soil particles
S_g	=	specific gravity of the particles
S_{gt}	=	specific gravity of the soil (bulk)
S_v	=	vane shear strength of soil
t	=	time
t_d	=	total test duration
t_{80}	=	time to reach 80% of the specified scour hole dimension
t_{90}	=	time to reach 90% of the specified scour hole dimension
t_+	=	dimensionless time scale
t_1	=	time scale (Chapter 3)
U_{es}	=	velocity as jet enters the tailwater
U_m	=	maximum velocity of the jet
U_n	=	noneroding velocity
U_o	=	velocity of the jet at the nozzle (jet origin)
U_1	=	velocity at approach section
V	=	average velocity
w	=	water content
w_c	=	water content of sample just after cutting
w_p	=	water content of sample just prior to test
w_f	=	water content of sample after test

x	=	distance from nozzle along the direction of flow
x_m	=	distance from nozzle of location of the maximum depth
$x_{m\infty}$	=	distance from nozzle of location of the maximum depth at equilibrium
$\bar{x}_{m\infty}$	=	average of sectional measurements for a test for distance from nozzle of location of the maximum depth at equilibrium
x_p	=	length of jet potential core
x_o	=	length of scour hole
$x_{o\infty}$	=	length of scour hole at equilibrium state
$\bar{x}_{o\infty}$	=	average of sectional measurements for a test for the length of scour hole at equilibrium state
x'	=	distance from nozzle to top of mound (in sand scour)
\bar{x}	=	distance along the jet axis from the water surface
x_1	=	distance along the jet axis from the water surface to original bed level
x_2	=	distance along the jet axis from the water surface to the bottom of the scour hole
X	=	parameter describing hydraulic properties of jet for impinging jet tests
X_c	=	value of X at which mass erosion first occurs
y	=	distance across width of sample measured from edge of sample
y_1	=	depth of flow at approach section
z	=	vertical distance measured from the surface of the sample (wall jet tests)
Z	=	soil factor
α	=	a constant
β	=	angle of inclination of the jet with the clay surface
δ	=	a constant; in chapter 3, the height above the bed where the velocity is maximum
$\delta_{1/2}$	=	height above the bed where the velocity is half the maximum velocity
Δh_m	=	mercury manometer reading (head of mercury)

ϵ	=	scour depth (measured from original clay surface)
$\bar{\epsilon}$	=	average depth of erosion (Chapter 3)
ϵ_{∞}	=	scour depth at equilibrium state
ϵ_{cl}	=	centreline scour depth
$\epsilon_{cl\infty}$	=	centreline scour depth at equilibrium
ϵ_m	=	maximum scour depth
$\epsilon_{m\infty}$	=	maximum scour depth at equilibrium
$\bar{\epsilon}_{m\infty}$	=	average maximum scour depth at equilibrium of sectional measurements for a test
κ	=	soil homogeneity coefficient
λ	=	parameter describing jet characteristics for wall jet tests ($\lambda = \rho U_0^2$)
λ_c	=	critical value of λ below which no significant erosion occurs
μ	=	dynamic viscosity of the eroding fluid
ν	=	kinematic viscosity of the eroding fluid
θ	=	an angle; an empirical constant
ρ	=	density of the eroding fluid
ρ_d	=	dry density of soil
ρ_o	=	density of water taking into account aeration
ρ_s	=	density of the particle
ρ_t	=	bulk density of the soil
σ	=	normal stress on soil due to jet
σ_s	=	sediment resistance parameter
σ_{tc}	=	tensile strength of the soil
τ	=	shear stress on the surface of the soil

τ_c	=	critical shear stress of the soil
τ_{om}	=	maximum shear stress on clay surface
τ_s	=	shear strength of the soil
ξ	=	volume of scour
ξ_∞	=	volume of scour at equilibrium
ψ	=	finest content of the soil (silt and clay)

CHAPTER 1: INTRODUCTION

1.1 Introduction

Research into the erosion of cohesive soils has made little progress that can be applied directly to field situations. In Northern Alberta, much of the soil is glacial or lacustrine clay, and engineers have had difficulty effectively accounting for erosion when designing hydraulic works for that area (Andres, 1985). Study of the problem is complicated by the many factors that affect the erodibility of clay, such as the clay mineralogy and pore fluid chemistry, the natural inhomogeneity of soil, and the fact that the soil is most often eroded by a turbulent fluid flow which in itself is not well understood. Irrespective of the present state of knowledge, there are still bridge piers to be designed for scour, river banks to be protected from erosion, canals to be designed against degradation, and soil losses from fields to be estimated. As well, there is the local scour downstream of hydraulic structures, created by flow in the form of turbulent water jets, that may undermine the stability of these structures. Examples are the scour downstream of vertical gates, flip bucket spillways, weirs, drops, and culverts.

The jet is a concentrated flow, where the higher velocity fluid of the jet discharges into an ambient fluid that is either at rest or in motion. The jet can be either unsubmerged, such as the case of a water jet discharging into air, or it can be submerged, where the jet is discharging into the same fluid. The jet can also be of several different forms, with the focus herein on the circular turbulent impinging jet and the plane turbulent wall jet. The circular impinging jet is a jet produced by a flow through a circular nozzle to impinge against a wall or boundary. The plane wall jet is a two dimensional jet produced from a rectangular nozzle with a large aspect ratio to flow tangentially along a boundary. The jet produced by flow under a sluice gate or that of a hydraulic jump in a rectangular channel behaves similarly to a plane wall jet. A flip bucket produces an impinging jet that acts to scour the downstream bed.

Much work has been done on the study of scour by jets of cohesionless materials such as sand. Relatively little work has been carried out on the scour of cohesive soils. The work presented herein focuses on the scour of clay by jets. The first case studied is the scour of clay by a submerged circular turbulent jet impinging at 90° to the sample surface. The second case is the scour created by a submerged plane turbulent wall jet.

1.2 Objectives

The objectives of this study are:

- 1) To examine the characteristics of scour in clay by submerged circular turbulent impinging jets and submerged plane turbulent wall jets. This includes study of the form of erosion of the clay and the dimensions of the scour hole produced by the jets. This is done by varying the hydraulic properties of the system (the velocity and diameter of the jet at its origin and the height of the jet above the clay surface) rather than through a change in the properties of the soil.
- 2) To develop a method of predicting the scour hole dimensions in a clay from the hydraulic properties of the jet and the properties of the soil.

1.3 Organization of the Thesis

This thesis is organized into eight chapters. Chapters 2 and 3 are a review of the literature. Chapter 2 provides a general overview of the characteristics and behavior of clay particles and how these particles are affected by environmental conditions. It also includes discussion of the many factors that affect the erosion of clays or cohesive soils and how these are related to clay particle behavior. As well, this chapter provides a discussion of the different erosion characteristics of cohesive soils previously observed by other researchers. Chapter 3 provides a discussion of the mechanics of jets, the previous work done on erosion by jets in cohesive soils, and the relevant results from the work done on jet scour of sand. Chapter 4 provides information on the experimental setup and program. Chapter

5 is a discussion of the different types of erosion observed during testing. Chapter 6 and Chapter 7 present the results and analysis of the scour tests with the impinging jets and wall jets respectively. Finally, Chapter 8 consists of a summary of observations, the conclusions of this work, and suggestions for future research.

CHAPTER 2: THE BEHAVIOR AND EROSION OF CLAYS

2.1 Background

Cohesive soil erosion has been studied for about 150 years, with reviews provided by the ASCE Task Committee on Sedimentation (1966,1968), Andres (1985), Croad (1981), Partheniades and Paaswell (1968), Paaswell and Partheniades (1968), Paaswell (1973), Grissinger (1982), Zeman (1983), and Mirstkhoulava (1989). Typical of the first attempts to quantify the susceptibility of clay to erosion was the work done by Fortier and Scobey (1925). Clay soils were categorized as, for example “stiff clay” or “clay loam” and a range for the maximum permissible velocity was given for each type of soil. This maximum permissible velocity was the average velocity of flow in a canal for which the canal would neither fill with sediments (or “silt”) nor scour.

With time, erosion studies included more detailed descriptions of the physical properties of the clay soil as well as the hydraulic conditions. Middleton (1930) suggested the use of the “dispersion ratio”, the ratio of the percent of silt and clay found by settling a small sample of soil in distilled water without chemical or mechanical dispersion to the amount of silt and clay found with dispersion, to help determine whether a soil would be erosive or nonerosive. Bouyoucos (1935) suggested erosiveness should be related to the “clay ratio”, the ratio of the percentage of mass of sand and silt in the soil to the percentage of clay. Laflen and Beasley (1960) determined the critical shear stress for several soils and related it to the different soil physical properties such as void ratio, plasticity, vane shear strength, and percent clay. Dunn (1959) correlated the critical shear stress of several clays to the vane shear strength, percentage of fines ($< 60 \mu\text{m}$), and plasticity of the soil using a submerged vertical circular impinging jet to create erosion.

The critical shear stress of a soil can loosely be defined as the stress created on the soil surface by the flow below which no erosion occurs. Flaxman (1963) collected observations of several channels in the field and then related estimates of the “tractive power” (stream power) of the stream for the maximum observed flow to the unconfined compressive strength of the soil. He then drew a dividing line on this plot to differentiate channels that had been qualitatively described as either erodible or nonerodible. The United States Bureau of Reclamation also performed several studies (Thomas and Enger, 1961; Carlson and Enger, 1962; Enger, 1963; Lane, 1952).

The work on clay erosion became increasingly more complicated as it became more evident that the pore and eroding water chemistry and mineralogy of the clay are important to its resistance to erosion. Arulanandan and his colleagues at the University of California at Davis undertook a series of studies to investigate the effect of these properties (Alizadeh, 1974; Ariathurai and Arulanandan (1978); Arulanandan et al, 1973; Arulanandan, 1975; Arulanandan et al, 1975; Sargunam, 1973; Sargunam et al, 1973). Largely due to this work, it is now recognized that physicochemical factors can play a strong role in the erosion of clays.

In this chapter, clay particles and their behavior are discussed. Next, the characteristics of erosion of clays are described. It is found that there is more than one form of erosion of a clay. Finally, there is a discussion of what factors influence the erodibility of a clay with both the macroscopic and electrochemical properties of the clay influencing its erosion resistance.

2.2 Clay Particles and their Behavior

In order to understand what factors affect a clay and therefore the erosion resistance of a clay soil, the characteristics of the material must be understood. In this section, the characteristics of clay particles and how they behave are briefly described. This discussion is based on the work of Mitchell (1993), Van Olphen (1963), and Grimm (1953, 1962).

Clay particles are those particles in a soil less than 2 μm in size. These particles are composed of layered, sheet minerals. The atomic structure of clay mineral sheets is commonly made up of two structural units, the silicon tetrahedron and the aluminum or magnesium octahedron. The different clay mineral groups are characterized by the stacking arrangement of the octahedral and silica sheets and the manner in which two or three layers of these sheets are held together. Differences in clays within a clay mineral group are usually due to differences in substituted cations in their structure called isomorphous substitution. The isomorphous substitution of cations into the clay mineral structure causes the clay particles to have a net negative electrical charge.

The negative charge on the clay particles is usually balanced by the adsorption of cations from solution (the pore fluid). These cations are either held between the clay structural layers or on the surfaces and edges of the particles. Many of the cations held within the clay are “exchangeable cations”. These are cations that can be replaced by cations of another type. There is a relative order of replaceability known as the lyotropic series. This order is given as $\text{Li}^+ < \text{Na}^+ < \text{K}^+ < \text{NH}_4^+ < \text{Mg}^{2+} < \text{Ca}^{2+} < \text{Al}^{3+} < \text{Fe}^{3+}$, so that for example Na^+ ions will be replaced by Ca^{2+} if there is Ca^{2+} available. The quantity of exchangeable cations is referred to as the Cation Exchange Capacity (CEC). Overall, the

CEC indicates the sensitivity of a clay to changes in its environment, as the exchangeable cations can have a considerable influence on the interparticle forces between clay particles (Arulanandan, 1975).

This attraction of cations by the clay particles results in the formation of what is called the diffuse double layer (a cloud of cations surrounding the negatively charged particle). The tendency for the cations to diffuse is balanced by their attraction to the negatively charged particle, with the result that the concentration of cations is high near the particle surface and decreases exponentially with distance from the particle. The energy of repulsion or repulsive potential, which is the work it takes for another negatively charged particle to move from an infinite distance to a given distance between the particles, then also decreases exponentially from the particle surface. These repulsive forces are counteracted by the attractive van der Waals forces of the particle that act at small distances from the particle surface. The van der Waals forces are not affected by the chemical environment.

Overlap of the double layers of two particles is a source of interparticle repulsion. The balance or "net interaction" between the repulsive forces and the van der Waals forces determine whether two clay particles in a quiescent environment will aggregate or flocculate (when attractive forces predominate) or stay dispersed (when repulsive forces predominate). Since the van der Waals forces are essentially fixed, whether a clay will flocculate or disperse is controlled by size and extent of the repulsive forces which can be affected by the environment. If the repulsion is reduced by reducing the extent of the double layer the particles can be brought closer together and the tendency of the particles to flocculate is increased. Factors that affect the extent of the double layer include the

concentration and type of ions in the pore fluid, and the pH, temperature, and dielectric constant¹ of the pore fluid.

The fabric of clay is one factor that affects the erosion resistance of a clay soil. The “fabric” of a soil is the arrangement of the particles, particle groups, and pore spaces in soil as opposed to the “structure”, which is the combined effect of the fabric, composition, and interparticle forces (Mitchell, 1993). Van Olphen (1977) defined several types of association of clay particles that form the fabric of a soil (Figure 2-1):

1. *Dispersed* - no face-to-face particle associations.
2. *Aggregated* - face-to-face associations of clay particles.
3. *Deflocculated* - no association between aggregates.
4. *Flocculated* - edge-to-face or edge-to-edge association of aggregates.

The net interparticle forces are different in each case because of the different particle orientations and therefore interactions.

Clays are distinguished from other soil particles by their net negative electrical charge, the plasticity of the material when mixed with water, and the particles high resistance to weathering (Mitchell, 1993). Clay minerals are often platy in shape (kaolinite), but can also be needlelike or tubular (halloysite). The mineralogy of the clay controls its particle size and shape and chemical and physical properties. Three common minerals are kaolinite, smectite, and illite. Kaolinite has a CEC in the range of 3 to 15 meq/100 g. The particles are relatively thick and the clay is not prone to swelling. Smectites (montmorillonite is in this clay mineral group) have a high CEC of about 80 to

¹ The dielectric constant of a medium, for example water, is the ratio of the electrostatic capacity of condenser plates, separated by the given material, to that of the same condenser with a vacuum between the plates (Mitchell, 1993).

150 meq/100 g. Montmorillonite has very thin flakes and is very much prone to swelling. Illite, like the smectites, also has extensive isomorphous substitution, but because the negative charge on the particles is partly balanced by a layer of K^+ ions between the clay layers, the CEC is in the range of about 10 to 40 meq/100 g. Illites are small flaky particles that are most often mixed with other types of clays.

2.3 Characteristics of Erosion in Clay Soils

2.3.1 Introduction

Clay soils do not erode in one manner, but show a number of different types of erosion depending on the properties of the soil, particularly the density and the degree of inhomogeneity, and the shear stress on the bed. Very high void ratio materials behave much like a fluid, with the interaction between the eroding fluid and the sediment layer behaving much like a stratified flow. Muds, or high void ratio clay soils, are typically eroded particle by particle or in flocs, named “surface erosion”, or by the removal of clumps of soil named “mass” or “bulk” erosion. More heavily consolidated clay soils can be eroded particle by particle as surface erosion, by the removal of flakes from the surface, named “flake erosion”, or by the removal of small to large chunks of the soil, again named mass erosion. The following is a review of the different types of erosion previously reported in clay erosion studies.

2.3.2 Erosion of Muds or High Void Ratio Soils

Mehta et al (1989) and Mehta (1991) provide a good description of the erosion of mud beds. The mode of erosion varies both with the magnitude of the bed shear stress and the nature of the deposit. Surface erosion is the erosion of particles, flocs, or

aggregates at the surface of the bed where “the flocs or aggregates, initially attached to their neighbors by interparticle bonds, break up and are entrained as a result of hydrodynamic lift and drag” (Mehta, 1991). Erosion rates depend strongly on the interparticle forces and the fabric of the bed (Krone, 1983; Paaswell, 1973). Gularte et al (1979a) suggested that when the clay fabric is more dispersed erosion takes place by the removal of individual particles. As the clay fabric becomes more flocculated (with increasing pore water salinity) erosion occurs along weak planes in the soil structure, resulting in the removal of flocs and aggregates rather than the removal of individual particles.

Mass or bulk erosion occurs when the bed fails at a plane underneath the surface of the soil, and all the material above that plane is removed by the flow in clumps (Mehta, 1991). This occurs at higher shear stresses, when the flow shear stresses exceed the bulk shear strength of the bed (Mehta, 1991; Krone, 1983). The erosion rate by mass erosion is much greater than that of surface erosion. It is first seen as pits on the clay surface and then progresses to a rapid deterioration of the bed with increasing shear stress (Krone, 1999).

Einsele et al (1974) observed erosion of angular shaped crumbs, shreds, and flat cakes of clay in testing several mud beds. These different erosion characteristics were attributed to the fabric of the bed, the shear strength of the soil, and the shear stress on the bed. Crumbs eroded when the soil showed vertical microjointing, whereas the erosion of flat cakes occurred when the weak planes in the clay were horizontal. They also found that mass erosion first occurred at one or several locations on the sample surface.

The work of Huang (1993) suggests that there is a link between the type of erosion observed and the bulk density of the bed. He described the erosion characteristics for sediments collected from Lianyung Harbour in China tested in terms of the bulk density of the sediments. For a bulk density in the range of 1030 to 1180 kg/m³, he reported that the deposits behaved as “a Bingham plastic fluid with large fluidity” and scouring occurred as “the wavy interface between the muddy flow and clear water breaks”. For bulk densities of the bed of 1180 to 1500 kg/m³, the deposit scoured as “wisps of thread-like clouds that appeared on the surface of fluidified mud”. For bulk densities of the soil greater than 1500 kg/m³, the material scoured “by a peeling off of the deposit surface, discontinuously as small lumps”. This would indicate that mass erosion occurred at the higher bulk densities.

Perigaud (1984b) defined a high mud concentration or low void ratio soil in regards to erosion as that having a porosity less than 0.5, where the porosity is the ratio of the volume of voids in a soil sample to the total volume of the sample. This corresponds to a void ratio of less than 1, where void ratio is the ratio of the volume of voids in a soil sample to the volume of solids (particles). Partheniades and Paaswell (1968) also divided the erosion of muds from the erosion of more consolidated clays, although they did not suggest a criteria.

2.3.3 Erosion of Low Void Ratio Soils

The most common type of erosion for low void ratio or high mud concentration, consolidated soils is mass erosion (Karasev, 1964). Mass erosion is the erosion of soil chunks or large aggregates and has been observed by Abdel-Rahman (1963), Epsley (1963), Christensen and Das (1973), Hall (1981), Kamphuis (1983, 1988, 1990),

Kamphuis and Hall (1983), Lefebvre et al (1986), McNeil et al (1996), Masch et al (1963), Moore and Masch (1962), Perigaud (1984b), Rohan et al (1980, 1986), Terwindt et al (1968), and Zeman (1982). However, mass erosion can be divided into two classes: (1) erosion due to disturbances in the clay (such as those created by sampling) or along preexisting planes of weakness (such as fissures or silt layers) and (2) erosion that is not associated with disturbances in the clay structure but occurs at high bed shear stresses due to failure of the clay.

Mass erosion due to disturbances of the clay sample was reported by Kamphuis (1983), who noted that damage to the sample resulted in erosion at lower shear stresses than the critical shear stress of the soil. Kamphuis (1990) noted:

“The water will normally remove the cohesive materials by pitting and flaking, removing the material in very small pieces. When fractures or sandy seams are present, the material will be removed in larger pieces (spalling), as separation occurs along the fractures and sandy planes... On portions of the samples where fracturing was absent, the samples were hardly eroded by clear water. Thus the same soils yielded widely varying values for initiation of erosion and for erosion volumes, depending on the extent of fracturing.”

Kamphuis (1988) also describes how in flume testing of natural clays, in one of the clays erosion took place by the removal of chunks that were bounded by fractures, with an erosion rate that was high initially and gradually tapered off to nearly zero. For another clay, the fractures were more widely spaced so that:

“The standard pattern of erosion at almost all of the velocities tested was to have large particles either spall or peel away leaving a local inhomogeneity in the sample surface. Smaller particles then flaked and peeled away from the margins of these hollows until some state of equilibrium was reached and no further erosion occurred until further larger particles were eroded away. If no large particles eroded from the sample surface, this surface appeared to remain untouched, with the exception of very small particles flaking away.”

Mirskhoulava (1989) suggested that the flow would be concentrated near any defects, cracks, or mechanical damage in the clay which would result in the widening of the cracks and the detachment of particles.

Rohan et al (1980) tested two sensitive, structured natural clays in flume tests on samples collected from Eastern Canada. Erosion in their samples occurred in three ways. The first was a selective erosion of silty nodules, where the silt was picked out of the clay surface by the flow, leaving the surrounding clay uneroded. The second was an erosion of chunks which was attributed to disturbances of the clay in preparation for testing. This usually occurred only in the first few minutes of testing. The final type of erosion was removal of particles along preexisting planes of weakness and fissures. Lefebvre et al (1986) felt that “for natural intact structured clays, erosion at the particle level does not appear to be significant ... links between structure clay particles are such that to be eroded, structure clays need to have some planes or weakness or defects such as microfissures, planes of bedding, or lenses of sand or silt.” They also give that:

“For natural intact structured clays erosion takes place rather by the pulling out of coarse grains or chunks and do not involve failure. Erosion is then associated with defects in the clay matrix, which act as zones or planes or weakness. As a consequence, the chemistry of the soil/water complex plays a very minor role, if any in the erodibility of intact structured clays. The physical or the physicochemical processes that are responsible for weathering and fissuring or surficial clays can however, drastically change the erodibility of a clay, as a result of the creation of defects”.

Preliminary work done by the author on clay scour by jets showed that creating a disturbance in a clay soil could cause mass erosion to develop. In testing a clay for erosion with a plane submerged wall jet (the apparatus described in Chapter 4), only erosion of small thin flakes from the clay surface was observed until a very small mark

was made on the sample surface. After a few hours, a scour hole that was an order of magnitude larger than the size of the original mark on the sample surface had formed. Further testing showed that mass erosion could be induced to occur if marks were made on the surface of the clay.

Mass erosion will also develop for undisturbed clay tested at high stresses. Perigaud (1984b) described flume testing for erosion for a soil with a “high mud concentration”:

“One can see small blocks pulled out of the bed and carried individually by the flow; the size of these blocks (a few millimetres in these experiments) are much bigger than the size of the individual particles (a few microns)”.

Epsey (1963) also describes the results of his erosion tests on a consolidated clay in rotating cylinder tests:

“At some critical point, a large amount of material is suddenly ripped loose from the sample, resulting in a high rate of scour for the particular shear stress. ... The preparation of the soil sample was a very important part of the test. If any small cracks formed in the samples during molding, failure of the samples was premature. The samples would fail along the planes formed by the cracks.”

Photographs included in Epsey (1963) show samples that are degraded by the removal of very large chunks (several centimetres in size), resulting in a very uneven sample surface. The mass erosion rate appeared to increase with increasing shear stresses on the clay.

Others who have observed mass erosion include Terwindt et al (1968), who performed field tests in a flume on a natural soil that was called a “well-consolidated clay.” They found the soil eroded by the detachment of clay fragments or “pebbles”, but did not discuss the size of the particles eroded. Moore and Masch (1962) observed sudden jumps in the relation between the scour depth and time and attributed these to the erosion of large chunks in testing for scour of clays by a circular impinging jet.

Some researchers have observed a pitting of the surface of the clays. Kamphuis and Hall (1983) found in most tests that their samples eroded by the formation of small pit marks in the sample surface. These pits expanded in size (diameter and depth) with time. Partheniades (1984) in a discussion of this work, thought that the pit marks were an indication of mass erosion. Mehta (1991) noted that "when the soil is hard, pitting of the bed due to dislodgment of large pieces of soil is often observed".

Surface erosion has been observed also in consolidated clays. The erosion rates are usually extremely small as compared to mass erosion. Those who have observed surface erosion include Dunn (1959), who described the initiation of erosion in the jet testing of several field soil samples as when the water in the jet tank became cloudy. He did not report removal of chunks of clay. In flume testing, Kamphuis and Hall (1983) found in a few tests that the bed eroded "in a general fashion at a very slow rate". Hedges (1990) observed particle by particle erosion at lower stresses tested for his impinging jet and the removal of "flat aggregates with a maximum thickness 1/4 in" at the higher stresses tested.

McNeil et al (1996) also observed surface erosion at low shear stresses and mass erosion at higher shear stresses. They asserted that if the flow was hydraulically smooth, erosion would occur primarily in the form of surface erosion. Observations showed that surface erosion occurred at the lower shear stresses tested in flume tests when the flow was estimated to be hydraulically smooth. As the shear stress increased and the flow became hydraulically rough, pits on the order of 1 mm in size were observed, indicating mass erosion occurred.

Of the studies where the erosion of flakes or “flake erosion” was observed are Epsy (1963), Masch et al (1963), and Zeman (1982). In rotating cylinder tests, Epsy (1963) saw flakes were eroded from the surface of his samples at the lower shear stresses tested, which he described as a washing of the surface of the sample. He felt that this erosion might be due to sample surface conditions. Flake erosion results in the erosion of only a very thin layer of soil at the clay surface and gives very low erosion rates.

Based on the above, it may be concluded that at lower stresses, surface erosion, flake erosion, or pitting of the sample surface might be observed. For higher stresses, it is likely the bed will be eroded by the erosion of chunks of clay or mass erosion. However, if there are disturbances in the clay such as fractures, silt layers, or other inhomogenities erosion of large clay chunks will occur along these discontinuities at stresses much lower than would occur for the intact clay.

2.4 Factors Affecting the Erodibility of Cohesive Soils

2.4.1 Background

The erodibility of a clay soil can be described by both the erosion rates for a given shear stress and the critical shear stress. The number of factors known to affect the erodibility of a cohesive soils are many including the type and amount of clay; shear strength; plasticity index; the pore and eroding fluid chemistry, the density of the soil, and the temperature. Herein, these factors are separated into independent properties of the soil that control the erosion of clay. They are the clay content and gradation of the soil, the mineralogy of the clay particles, and the structure of the soil. Other factors such as the pore and eroding water chemistry, strength of the soil (based on the vane shear or unconfined compression strength test), density, and temperature, either influence or are

influenced by these factors. This discussion of the factors that affect erosion does not extend to those changes in the flow that may affect erosion rates such as turbulence levels.

2.4.2 *Clay Content and Soil Gradation*

Many studies indicate that increasing the clay content in a soil increases its erosion resistance as the critical shear stress increases and the erosion rates decrease (Bouyoucous, 1935; Dunn, 1959; Smerdon and Beasley, 1961; Grissinger, 1966; Dash, 1968; Bhasin et al, 1969; Kuti and Yen, 1976; Thorn and Parsons, 1980; Kamphuis and Hall, 1983; Hanson, 1990; Torfs et al, 1994; Hosny, 1995; Huygens and Verhoeven, 1996). These studies have included mud, more consolidated soils, and unsaturated soils. Increasing the clay content increases the interparticle forces within the soil, thus increasing erosion resistance (Partheniades and Paaswell, 1968).

Several studies also report increasing erosion resistance with the plasticity index of soil (Dunn, 1959; Smerdon and Beasley, 1961; Lyle and Smerdon, 1965; Kamphuis and Hall, 1983). Plasticity index (PI) is a function of both the clay content and the type of clay minerals present in the soil (and therefore not an independent property of the soil).

For soils with similar activity, where the activity $A = \frac{PI}{\%clay}$, an increasing plasticity

index indicates an increasing clay content. Partheniades and Paaswell (1968) analyzed the work of Dunn (1959) and found that his clays had similar activities. It was thus concluded that the increase in critical shear stress that Dunn (1959) observed with increasing plasticity index was due to an increasing clay content in the soils.

The gradation of the soil also has an affect on its erodibility. As the sand constituent in a soil becomes more well-graded, erosion rates decrease (Bhasin et al, 1999). It has also been observed that deposits with a high percentage of sand and silt particles or with sand or silt nodules of lenses are more erodible than a homogeneous clay (Lefebvre et al, 1985).

2.4.3 Mineralogy of the Clay Particles

The mineralogy of the particles can affect the erosion resistance of a clay soil. Mitchener and Torfs (1996) found that the increase in the critical shear stress with the clay content depended on the type of clay mineral added. Partheniades and Paaswell (1970) suggested that adding some very active clays, such as bentonite, to a soil has been shown to increase erosion resistance. In general, it has been found that clays with higher plasticities are more erosion resistant for the same clay content (Sargunam, 1973), so that montmorillonite is less erodible than illite, and illite is less erodible than kaolinite. A more dispersed montmorillonite may even show a higher erosion resistance than a flocculated kaolinite (see discussion below) (Sargunam, 1973).

2.4.4 Fabric of the Clay

2.4.4.1 Saturated Soils

A flocculated soil has a critical shear stress that is much higher than one with a dispersed structure (Arulanandan et al, 1975). As such, the pH of the pore fluid may have an effect on the fabric of the clay in some circumstances. Dennett et al (1995) found for a kaolinite clay with a 60 % water content that was settled in a flume, that at low pH the clay was flocculated and had increased cohesion and increased erosion

resistance. At high pH, the clay was dispersed with a reduced resistance to erosion. This is likely because kaolinite particles are charged positively on their edges in a low pH environment (Mitchell, 1993). However, Raudviki and Tan (1984) found that, in general for clays, as the pH increases erosion rates increase. For bentonite, Raudviki and Tan (1984) noted an initial rapid increase in erosion rates with increasing pH, with a leveling of the erosion rates with further increases in pH.

The type of fabric also affects the form of erosion. Gularte et al (1979b) found a marked increase in the critical shear stress for an illitic clay with increasing pore water salinity (a range from 2.5 to 10 % NaCl). They noted that at low salinities clays have a more dispersed fabric in which erosion should take place by the removal of individual particles. With increasing salinity, the clay particles will flocculate and erosion should occur through flocs or aggregates rather than individual particles. Raudkivi and Tan (1984) found that the eroded surface of some clays looked distinctly pitted, whereas clays with face to face stacking of the particles appear to flake. Similarly, Minks (1983) found mass erosion as flat plate like particles for an unsaturated soil with parallel particle orientation and erosion in more spherical chunks for soils with a random particle orientation.

2.4.4.2 Unsaturated Soils

There have been a number of papers that investigate the influence of fabric on the erosion of compacted unsaturated soils. These studies use the observations of Lambe (1955a,b) who found that if a cohesive soil is compacted wet of optimum the soil will have a more dispersed fabric as the particles become aligned perpendicular to the direction of loading. If the soil is compacted on the dry side of optimum, the soil will

have a more flocculated fabric. Unlike that found for saturated soils by Arulanandan (1975), the work on unsaturated soils found that the more flocculated fabric had erosion rates much higher than the dispersed fabric (Shaikh, 1986; Shaikh et al, 1988a,b; Grissinger, 1966). Shresta and Arulanandan (1988) suggested, however, that since the soils are unsaturated it is likely that the soils are undergoing slaking so that erosion rates are much higher than if the soil was only eroding. Slaking is the disintegration of an unsaturated soil after immersion in water into a pile of pieces or small particles (Mitchell, 1993). The flocculated soils have a higher permeability than the dispersed soils, allowing water to penetrate the unsaturated soil much more quickly resulting in much higher slaking rates than the dispersed soil. It can be concluded, whether the clay is either slaking eroding, that the erosivity for compacted soils depends strongly on the water content of the soil (Kandiah and Arulanandan, 1976).

2.4.5 *Interparticle Bonds*

2.4.5.1 Effect of the Pore and Eroding Water Chemistry

There is a strong affect on erosion of the pore and eroding water chemistry and, in particular, of the difference between the pore and eroding water chemistry. One method of describing the water chemistry is through the use of the sodium adsorption ratio (SAR). It is defined as:

$$\text{SAR} = \frac{(\text{Na}^+)}{\sqrt{0.5[(\text{Ca}^{2+}) + (\text{Mg}^{2+})]}} \quad (2.1)$$

where Na^+ , Ca^{2+} , and Mg^{2+} are the concentrations of the sodium, calcium, and magnesium ions respectively. If the pore and eroding water are the same, an increase in salt concentration in the pore fluid with any composition (any SAR) will give an increase in

the erosion resistance of a soil (Arulanandan et al, 1973). This is because there is a reduction in the double layer thickness and therefore the repulsive forces in the clay and the clay tends to flocculate. However, there is a limit to the increase in erosion resistance with an increase in salinity, after which the increasing salinity will not have a strong effect (Parchure and Mehta, 1985; Raudkivi and Tan, 1984). As well, if the SAR increases, the critical shear stress decreases. With increasing SAR the interparticle bonds weaken and the surface soil particles detach more easily (Arulanandan et al, 1973). There can be a substantial increase in the critical shear stress and decrease an erosion rates when exchangeable sodium is replaced with high exchangeable cations with higher valencies (Arulanandan, 1975).

Arulanandan (1975) observed that the critical shear stress (for surface erosion) increased with increasing CEC at low SAR and decreased with increasing CEC at high SAR. This is likely because at low SAR, there are more higher valence ions which produces a shrinking double layer and higher bonding between the particles. Increasing CEC would indicate a higher capacity to “use” these ions in solution and a result there would be a higher strength. For high SAR, the increased sodium in the pore fluid would result in a tendency of the clay particles to disperse and therefore there would be less erosion resistance with increasing SAR. Arulanandan (1975) suggested at high SAR, the clay is in a dispersed state and therefore there is more swelling reducing the erosion resistance. The low SAR clays were thought to have reduced swelling, and “as swelling is reduced, larger critical shear stresses are required to detach particles.”

If the eroding water is less saline than the pore fluid, an osmotic pressure is set up so that water moves into the clay surface, creating swelling and weakening the

interparticle bonds (Karasev, 1964; Arulanandan, 1975; Arulanandan and Heinzen, 1977). If the eroding water is more saline than the pore fluid or contains ions that are of higher valence than that of the pore fluid, the clay will absorb those ions. This results in an increase in the strength of the clay (at the clay surface). Partheniades (1962,1965) found that absorption of iron from the eroding water into the clay surface made his clay more erosion resistant. He also found that this only affected the surface of the clay bed.

Dispersive clays are ones with essentially no critical shear stress. They will erode, significantly, under any flow. It is thought that a clay will behave as dispersive when the repulsive forces in the clay are strong and the clay is “deflocculated” (Sherard et al, 1972). When the clay comes in contact with water, individual clay particles detach from the clay surface and are carried away by the flow. This dispersive behavior of a clay may occur when the clay has a high amount of exchangeable sodium in the pore fluid and the eroding water has a low salt content.

2.4.5.2 Effect of the Soil Density

Both the fabric and interparticle forces are affected by a change in density of the clay soil. There is a strong dependence of the critical shear stress of a soil on the bulk density of the soil (Jakobsen and Diegaard, 1996; Mitchener and Torfs, 1996; Berlamont et al, 1993; Huang, 1993; Hanson, 1992, 1996; Hanson and Robinson, 1993; Kamphuis and Hall, 1983; Thorn and Parsons, 1980; Thomas and Enger, 1961). It was found that the critical shear stress increases for increasing soil density for muds, more consolidated soils, and unsaturated soils. Some typical values for the critical shear stress at different densities for saturated soils are given in Table 2-1. This increase in erosion resistance has been attributed to the increase in contact between the particles because of the reduced

interparticle spacing and therefore increased interparticle bond strength (Gularte et al, 1979a; Partheniades and Paaswell, 1968).

Krone (1999) describes the effect of increasing density on erosion rates for self-weight consolidated mud:

“The resistance to shear is clearly determined by the mass of solids overburden and can be described as progressive collapse of the aggregate structure that creates increasing numbers of interparticle bonds. At the depth where the overburden causes collapse to a nearly homogeneous structure, such as that of first-or-zero order aggregates, the resistance to erosion increases linearly with increasing overburden but at a much slower rate. Small increases in shear stress above the threshold for this structure causes rapid erosion. The final change in structure is that from collapsing pores of aggregates to one where simple particle arrangement will be the response to increasing overburden.”

This change in structure with increasing overburden (or consolidation) pressures will depend on the fabric of the clay. Raudkivi and Tan (1984) suggested that if the clay had a “card house” structure the effect of consolidation would be small until the card house structure collapsed. However, if the clay particles were stacked face to face, the consolidation pressure would affect the interparticle distance and thus the interaction of the particles (the van der Waals forces would become more predominant).

The bulk density can be related to the water content, dry density, and void ratio of the soil by:

$$\rho_t = \rho_d(1 + w) = \frac{\rho_s + \rho_s e}{1 + e} \quad (2.2)$$

where:

$$\rho_t = \frac{M_t}{V_t} \quad (2.3)$$

$$\rho_d = \frac{M_s}{V_t} \quad (2.4)$$

$$e = \frac{V_v}{V_s} \quad (2.5)$$

$$w = \frac{M_w}{M_s} \quad (2.6)$$

with:

- e = void ratio
- M_s = mass of solids in soil
- M_t = total mass of soil
- M_w = mass of water
- S = saturation ($S = V_w/V_v$)
- V_s = volume of solids
- V_t = total volume of soil
- V_v = volume of voids
- V_w = volume of water $S = V_w/V_v$
- w = water content
- ρ_t = bulk density of the soil
- ρ_d = dry density of the soil
- ρ_s = density of the solids
- ρ = density of water (or fluid in the voids)

Thus studies that show an increasing critical shear stress and decreasing erosion rates with decreasing water content (Gularte et al, 1979a and 1980; Dash, 1968; Bhasin et al, 1969; Hosny, 1995) also indicate that the critical shear stress increases and erosion rates decrease with increasing density. Similarly an increasing critical shear stress with decreasing void ratio as found by Laflen and Beasley (1960), Lyle and Smerdon (1965), Ghebriyessus et al (1994) indicates an increasing critical shear stress with increasing density.

Variation of the critical shear stress with soil density may vary with the soil structure. Gularte et al (1979a) tested saturated soil samples of 50 % illite and 50 % silt

at water contents of 50 to 80 % at the different salinities of 2.5, 5.0, 7.5, and 10.0 % NaCl in the pore and eroding fluid. The drop in critical shear stress (for surface erosion) with increasing water content was much more pronounced for the soils with the higher salinities. This may indicate a more flocculated structure is more sensitive to changes in density for erosion resistance.

Lefebvre et al (1986) (see also Lefebvre and Rohan (1986)) studied the effect of consolidation on erosion of natural clays. They found that if the clay is originally structured, consolidation pressures above the preconsolidation pressure can damage bonding that has developed between the particles and thus weaken the links between the particles. They saw a drop in the critical shear stress by an order of magnitude for a clay consolidated to 1.5 to 3.5 times the preconsolidation pressure. Thus, increasing the soil density to decrease erosion rates will not be helpful in all cases.

2.4.5.3 Effect of Test Temperature

The temperature affects the double layer thickness and thus the interparticle bond strength in many ways. Increasing temperature, directly, has the effect of increasing the double layer thickness. However, increasing temperature also causes a decrease in the surface potential for a constant charge and the dielectric constant of the pore fluid, which decreases the double layer thickness. Thus, these effects of increasing temperature work against each other and the growth of the double layer with temperature is not clear (Mitchell, 1993). Thus, the dependence of erosion on temperature is also not clear.

Many researchers have observed an increase in erodibility with increasing temperature (Christensen and Das, 1973; Kelly et al, 1979; Zreik et al, 1998). For erosion resistance, Kelly et al (1979) found an increasing surface erosion rate with

temperature in a remolded illitic clay at 40 % water content. Grissinger (1966) saw increasing erosion rate with increasing eroding water temperature for compacted unsaturated samples in flume tests. Liou (1970) also found decreasing critical shear stress with temperature in testing of a high water content ($w=510\%$) bed. Zreik et al (1998) found that a younger bed (just settled) at higher temperature eroded more quickly than a young bed at low temperature. They believed it was a result of a decrease in bond strength with an increasing temperature. Zreik et al (1998) also suggested that the effect of temperature on the erosion behavior of the high void ratio, self-weight consolidated sediments tested only was important for about the top 0.5 cm of the bed, below which the bed structure and age were the dominant factors.

Croad (1981), however, found that the relation between surface erosion rates with temperature was more parabolic in shape (instead of only increasing with temperature) that and could have either positive or negative curvature. This behavior was also shown by Raudkivi and Hutchison (1974) who found that the effect of temperature on surface erosion rates was reduced for increasing pore water salinity and decreasing particle size. Raudviki and Hutchison (1974) also suggested that “temperature is not going to be a variable of primary importance in natural conditions.”

2.4.6 Macroscopic Strength of the Bed

The macroscopic strength of the bed such as the tensile strength, the vane shear strength, and the unconfined compressive strength are a function of the properties described above. Several researchers have correlated the erosion resistance of clay soils to these measurements. However, there is some argument as to what the appropriate measurement is for determining the erodibility of a soil. Many researchers believe that it

is the tensile strength of the soil that should be used (Martin, 1962; Dash, 1968; Mirstkhoulava, 1975; Nearing, 1991). Others have used the vane shear strength or the unconfined compressive strength measurements in determining erodibility of the soil (Lyle and Smerdon, 1965; Kamphuis and Hall, 1983).

Some of the confusion on what strength measurement should be used to determine the erosion resistance of a soil, comes from the fact that the cohesion measured in current geotechnical testing methods comes from not only the interparticle bond strength, but other sources (Reddi and Bonala, 1997; Mitchell, 1993). Mitchell (1993) classified the sources of strength in a soil as true and apparent cohesion. True cohesion involves short-range and cementation bonds and electrostatic and electromagnetic attractions and can be related to the interparticle bond strength. Apparent cohesion involves capillary stresses due to the surface tension of the fluid in the void space and mechanical forces due to interlocking rough surfaces on the failure plane (friction). However, true and apparent cohesion cannot be measured separately at this time. Erosion is considered as a plucking of the particles from the bed (Nearing, 1991) so that frictional strength should not be a large component of the erosion resistance of a soil. Others believe that erosion occurs when the moving water flows through the open pores of the soil skeleton and detaches the flocs through a lifting and drag action (Zreik et al, 1998), again not requiring frictional strength. The critical shear stress has been found to increase with increasing vane shear strength and unconfined compressive strength (Dunn, 1959; Flaxman, 1963; Hall, 1983; Kamphuis and Hall, 1983).

However, in an early study of erosion of mud beds, Partheniades (1965) concluded from three experiments with two muds of high water content that there was no

dependence of erosion rate for surface erosion on vane shear strength. "The minimum scouring shear stresses and the erosion rates are independent of the strength of the bed material, provided that the flow does not induce stresses of an order higher than the order of the macroscopic strength of the bed" (to induce mass erosion). His supporting idea for this conclusion was that the strength of the bonds between the flocs (the interparticle bonds) did not change significantly with a change in void ratio, until the material was highly consolidated. The conclusion that the erosion is independent of the shear strength of the bed has spread in the literature. However, the vane shear strength for the bed at high water content is difficult to measure and it is likely that his measurements of the shear strength of the bed were in error (Zreik et al, 1998) indicating that his original conclusions may be questionable as well.

The typical magnitude of the critical shear stress is usually several orders of magnitude less than the macroscopic shear strength of the bed (Partheniades, 1971). Dunn (1959) found critical shear strength values (likely for surface erosion) that were about 1/2000 of the values for the vane shear strength for low void ratio soils. Zreik et al (1998) found that the critical shear stress (for surface erosion of aggregates and flocs) was one order of magnitude smaller than both the undrained and drained shear strength of the soil in tests of a high void ratio soil. They attributed the difference between the shear strength and the critical shear stress to the frictional components of strength in their measurements and that "the resistance to the erosive action of the water is provided by the individual bonds between the flocs, with the weakest bond governing, while the resistance to the shearing action of the cone penetration and the slope failure is provided by the ensemble of bonds between the flocs available in the shear soil mass". They also

thought the difference between the shear strength of the soil and the critical shear stress was that turbulent fluctuations greatly increase the actual shear stress on the bed over the average measured value. Mehta (1991) suggested that the erosion resistance of a soil for surface erosion was in the same order as the interparticle forces of the aggregates of the particles.

2.4.7 Summary

As a summary of the above, in general erosion resistance will increase for a homogeneous saturated clay soil that is not fissured, stratified, cemented, or disturbed by sampling:

- for increasing clay content.
- for increasing density of the soil.
- for increasing salinity of the pore and eroding fluid.
- for decreasing SAR of the pore fluid.
- if the fabric of the soil is flocculated rather than dispersed.
- for increasing shear strength of the soil.

The studies reviewed in this chapter indicate that one must be careful to observe the temperature and the eroding water chemistry in carrying out experiments in the erosion of cohesive soils (if they are not strictly controlled). The studies also show that the density, gradation, clay mineralogy, and structure of cohesive soil influence the erosion characteristics and these properties of the soil should be determined.

Table 2-1: Typical values for critical shear stress.

Author	Description of Soil	Type of Erosion	Given	ρ_s (kg/m ³)	ρ (kg/m ³)	τ_c (Pa)
Jakobsen and Deigaard (1996)	- mud - 25 % clay - self-weight consolidation for 0.86 days.	- flume test	$\rho_s = 300$ kg/m ³	300		0.75
			$\rho_s = 200$ kg/m ³	200		0.41
			$\rho_s = 100$ kg/m ³	100		0.07
Kusuda et al (1985)	- 30 % clay - $\rho_s = 2610$ kg/m ³	- rotating annular cylinder	w = 325 %	275	1170	0.18
			w = 1000 %	96	1060	0.03
Skafel and Bishop (1994)	- soil: 2% sand and gravel, 33 % silt, 46% clay - LL=27%, PL=17% - $S_u = 86$ kPa - consolidated clay	- surface erosion - flume test				7
Huang (1993)	- natural mud	- flume test	$\rho_s = 200$ kg/m ³ $\rho_s = 600$ kg/m ³	200 600		0.18 1.8
Otsubo and Muraoka (1988)	- mud - $\rho_s = 2510$ kg/m ³	- flume test (lots of scatter)	w = 450 %	200	1120	0.4
Terwindt et al (1988)	- $S_v = 15$ kPa (consolidated clay) - PI=40 - 22% clay, 45 % silt	- erosion by detachment of clay fragments of pebbles				1.1
Thom and Parsons (1988)	Soil 1: CEC=20 meq/100g - 51 % clay: 17 % kaolin; 17 % illite, 17 % chlorite; 39 % non-clay minerals; 10 % organics salinity: 26 g/L Soil 2: CEC=35 meq/100g - 50 % clay: 30 % montmorillonite, 15 % kaolin; 50 % non-clay minerals salinity: 26 g/L Soil 3: CEC=25 meq/100g - 75 to 80 % clay: 15 to 20 % montmorillonite, 30 % kaolin; 30 % illite; 20 % non-clay minerals salinity: 33 g/L	- pore and eroding water at same salinity - flume test	$\rho_s = 200$ kg/m ³	200		0.48
			$\rho_s = 100$ kg/m ³	100		0.12
			$\rho_s = 38$ kg/m ³	38		0.055
			$\rho_s = 200$ kg/m ³	200		0.8
			$\rho_s = 65$ kg/m ³	65		0.14
Kamphuis and Hall (1983)	Soil A: 60 % clay; 35 % silt; 5 % sand - PI=23.5 % w=34.5 % $S_v = 9.6$ kPa Soil B: 60 % clay; 38 % silt; 2 % sand - PI=35.6 % w=35.6 % $S_v = 17.1$ kPa	- flume test	w=34.5 %	1380	1860	10.5
			w=35.6 %	1360	1850	12.8
Chapius (1986)	Soil 1: 36.7 % clay; 48.7 % silt; 12.0 % sand; 2.6 % gravel - PL=15.4 LL=26.6 % w=25.4 % - CEC=10.9 meq/100g Soil 1: 65.6 % clay; 27.6 % silt; 6.8 % sand - PL=22.2 % LL=44.4% w=53.0 % - CEC=15.3 meq/100g	- rotating cylinder	w=25.4 %	1584	1990	4.2
			w=53.0 %	1100	1690	8.7
Masch et al (1963)	- 100 % Taylor Marl	- rotating cylinder (for mass erosion)	w=28 %	1520	1950	83.3
			w=31 %	1454	1905	93.8
			w=31 %	1454	1905	69.9
			w=31%	1454	1905	83.3
			w=28%	1520	1950	87.1
Epsey (1963)	- 30 % clay, LL=47 %, PL=21 % w=46 % - $\rho_s = 2751$ kg/m ³	- rotating cylinder (for mass erosion)	w=30%	1476	1920	83.3
			w=46 %	1214	1773	85.2
Chow (1959)	- reports on data collected in U.S.S.R - for a "heavy clay soil"		e=1.2	1350	1750	3.8
			e=0.7	1160	1970	9.1
			e=0.3	1330	2270	22
Zeman (1982)	- w=14.3 %	- rotating cylinder	e=0.45	1265	2150	20
Partheniades (1983)	- 60 % clay, 40 % silt, small amount of fine sand LL=99% PL=44% - $\rho_s = 584$ kg/m ³ Salinity: 33 grams/L	- flume test (surface erosion)	w=110 %	584	1226	0.48
Einsele et al (1984)	- kaolinite	- mass erosion	w=350 %	260	1160	0.98
			w=70 %	930	1580	1.28
Rohan et al (1986)	- 63 % clay; 32 % silt; 5 % sand - LL=36 %, PL=23 % w=36 %	- drill hole test - mass erosion	w=36 %	1356	1844	170

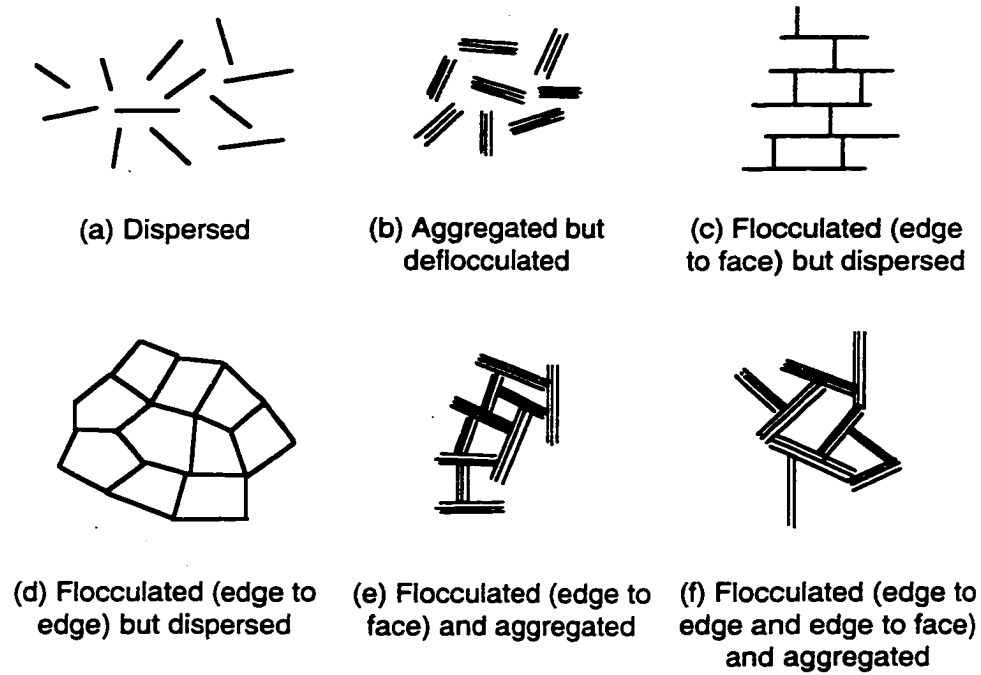


Fig. 2-1: Examples of different types of clay fabrics (adapted from Van Olphen (1977) and Mitchell (1993)).

CHAPTER 3: JETS AND EROSION BY JETS

3.1 Introduction

In this chapter, the mechanics of the two different types of jets used in the present experiments are discussed. These are the submerged circular turbulent impinging jet and the submerged plane turbulent wall jet. As well, as much work has been done on the scour of cohesionless materials such as sand by these jets, the main characteristics of scour found in these studies are presented. Finally, a review and discussion of the literature on the scour of clay or cohesive soils by jets is given.

3.2 Jet Characteristics

3.2.1 Submerged Circular Turbulent Impinging Jet

A circular impinging jet is a jet produced from a circular nozzle that is issuing into a stationary fluid and is directed to impinge against a boundary or wall. Only the case of the submerged jet is considered here. The jet of diameter d and velocity U_o at the nozzle is set at a height H above the surface on which it impinges. A sketch is given in Figure 3-1. It is generally accepted that the flow of this type of jet can be divided into three regions: (1) the "free jet region", where the jet essentially behaves as if there were no boundary (such as described in Albertson et al, 1950) (2) the "impingement region", where the flow begins to stagnate and is redirected to flow along the wall and (3) the "wall jet region", where the flow behaves as a radial wall jet. The behavior of the jet strongly depends on the relative impingement height H/d .

When the jet is at a "large" impingement height, defined by Beltaos and Rajaratnam (1977) as $H > 8.3d$, the jet is fully developed before it impinges on the wall. As a result, the jet properties can be combined into the momentum flux $M_o = \frac{\pi}{4} \rho U_o^2 d^2$ so that the characteristics of the flow at the boundary are a function of M_o , ρ , μ , and H . Here ρ and μ are the density and dynamic viscosity of the fluid. The free region has been found to

extend to about $x=0.86H$ from the nozzle, where x is the distance from the nozzle measured along the jet centreline, based on a comparison of the velocity of the jet to that of a free jet. Based on considerations of the pressure at the wall, the impinging region extends to about $r=0.22H$, where r is the radial distance from the jet centreline (Beltaos and Rajaratnam, 1977).

The impingement region is where there is the most severe hydrodynamic action on the bed. The shear stress and pressure distribution in this region for typical experimental conditions for the present study are shown in Figure 3-1. The maximum shear stress on the bed created by a jet at a large impingement height for the case of impingement on a smooth wall can be estimated from (Beltaos and Rajaratnam, 1974):

$$\tau_{om} = 0.16\rho U_o^2 \left(\frac{d}{H}\right)^2 \quad (3.1)$$

The wall shear stresses in the impingement region showed no dependence on the Reynolds number at the nozzle ($R = \frac{U_o d}{\nu}$). For the wall jet region, for a range of Reynolds numbers from 64000 to 288000, Poreh et al (1967) found that the wall shear stresses showed only a mild dependence on the Reynolds number, varying with $R^{-0.3}$.

When the jet is at a “small” impingement height, defined as $H < 5.5d$ (Beltaos and Rajaratnam, 1977), the jet does not fully develop and the potential core of the jet impinges on the boundary (Beltaos and Rajaratnam, 1977; Pamadi and Belov, 1980). This significantly changes the flow as compared to the large impingement height case. The flow characteristics at the wall have been shown to be a function of U_o , d , ρ , and μ . The shear stress distribution will show “two peaks” as compared to the wall shear stress for the large impingement height case, due to a transition from a laminar to turbulent boundary layer on the wall (Pamadi and Belov, 1980). For the transition between the small and large impingement heights, the flow in the impingement region will be a function of U_o , ρ , μ , d , and H (Beltaos and Rajaratnam, 1977).

Only jets at large impingement heights were used for the present study. At present there is little information on the behavior of an impinging jet on a scoured bed.

3.2.2 *Submerged Plane Turbulent Wall Jets*

The plane turbulent wall jet is a two dimensional flow that flows tangentially along a boundary. Only the case of the submerged jet that is issuing into a stationary fluid, at no offset distance (the distance between the wall and the jet), and with no pressure gradient is considered here. Some of the many studies of this type of jet include Glauert (1956), Myers et al (1961, 1963), Schwarz and Cosart (1961), Rajaratnam (1967), Launder and Rodi (1981, 1983), and Gerodimos and So (1997). Once fully developed, the wall jet flow is considered to consist of two regions: an inner layer near the wall that extends up to the location of the maximum velocity in the velocity profile and an outer layer that extends from the location of the maximum velocity to the edge of the jet (sketched in Figure 3-2). The inner layer is treated as a boundary layer while the outer layer is treated as a plane free jet. As with a free jet, there exists a region that extends from the nozzle called the potential core where the velocity is equal to the velocity at the nozzle U_o . The boundary layer and free jet shear layer grow to extend through the entire wall jet flow after a distance of about $6a$ (Rajaratnam, 1976), where "a" is the thickness of the jet at the nozzle. This distance is the length of the potential core.

The boundary layer is thin near the nozzle and grows with distance from the nozzle. As such, the wall jet flow can be hydraulically rough near the nozzle and hydraulically smooth at distances far from the nozzle (Rajaratnam, 1967). The shear stresses created by the jet on the wall for the hydraulically rough flow do not depend on the Reynolds number at the nozzle ($R = \frac{U_o a}{\nu}$). The wall shear stresses for the hydraulically smooth flow have been found to depend only weakly on the Reynolds number at the nozzle, with τ varying with $R^{-1/12}$ (Myers et al, 1963; Hogg et al, 1997). Others have suggested that τ varies with $R^{-1/4}$ (Schwarz and Cosart, 1961). The wall shear stresses can be expressed as a function

of the flow properties at the nozzle $\tau = c_f \frac{\rho U_o^2}{2}$ (Myers et al, 1963), where c_f is the skin friction coefficient. The shear stresses on the wall decrease with distance from the nozzle so that the maximum shear stress will occur very near the nozzle. The wall shear stresses increase and the velocity of the jet decays more quickly with increasing wall roughness (Rajaratnam, 1967). Both the decay of the velocity of the jet and the growth of the jet with distance from the nozzle have been found not to depend on Reynolds number (Schwarz and Cosart, 1961).

Little is known about the properties of a wall jet flow once a scour hole created by it has formed. Chatterjee and Ghosh (1980) found a steep drop in bed shear stress just after scouring starts for beds of sand and gravel. The velocity distribution of the flow was also found to substantially change from that of a wall jet once the bed was scoured. It should also be noted the jet flow may be substantially changed by changing tailwater conditions.

3.3 Jet Scour in Cohesionless Soils

3.3.1 Scour in Cohesionless Soils by Submerged Circular Turbulent Impinging Jets

As cohesionless particles such as sand behave as individual particles, the erosion of sand will be different from that of a clay. The resistance to erosion of sand results from its buoyant weight so that the size and density of the particle and gravity must be considered in determining this resistance. In a clay, the electrochemical forces that bind the particles together control the clay resistance to erosion. Nevertheless, studies of the scour by jets in sand give an indication of what may be expected in the scouring by jets in clays.

There have been many studies of the scour of cohesionless soils by submerged circular impinging jets including Doddiah et al (1953), Johnson (1967), Westrich and Kobus (1973), Rajaratnam and Beltaos (1977), Kobus et al (1979), Rajaratnam (1982), Mih and Kabir (1983), and Aderibigbe and Rajaratnam (1996). One of the important observations was that there are two main forms of scour hole: one that is wide and shallow or “weakly deflected” and the other that is narrow and deep where the jet is almost

completely turned back on itself or “strongly deflected” (Rouse, 1939; Westrich and Kobus, 1973; Kobus et al, 1979; Aderibigbe and Rajaratnam, 1996). In general, the shallow scour holes form at lower flows and/or large impingement heights and the deep scour holes forms at higher flows and/or small impingement heights. The typical shapes of scour holes are shown in Figure 3-3. The scour hole has a ridge built up around its outer edges made up of the particles removed from the scour hole.

Growth of the scour hole has been found to be linearly related to the logarithm of time (Doddiah et al, 1953; Rajaratnam and Beltaos, 1977). Scouring continues with a decreasing scour rate until the scour hole reaches an “asymptotic”, “equilibrium”, or “ultimate state”, when there is no noticeable change in the scour hole dimensions (Westrich and Kobus, 1973). There is a difference between the static scour found where the jet flow is stopped and the dynamic scour created by the flowing jet (Doddiah et al, 1953; Rajaratnam and Beltaos, 1977; Aderibigbe and Rajaratnam, 1996). The dynamic scour is generally greater (particularly for the narrow deep) scour holes with any sand settling back into the scour hole upon cessation of flow (creating the static scour depth).

Jets at small and large impingement heights show different behavior (Mih and Kabir, 1983). The scour hole dimensions for jets at small impingement heights have been found to scale with the diameter of the jet at the nozzle, d , while scour holes formed by jets at large impingement heights scale with the impingement height H (Westrich and Kobus, 1973; Rajaratnam and Beltaos, 1977; Mih and Kabir, 1983). The scour hole profiles at equilibrium were made dimensionless using the maximum depth of scour as the scale for the scour depths and the radius of the scour hole for the radial distance from the jet centreline (Aderibigbe and Rajaratnam, 1996). The half-width of scour, b , of the distance from the jet centreline where the depth of scour is half the maximum depth, also worked well as a scale for the distance from the jet centreline (Rajaratnam and Beltaos, 1977; Rajaratnam, 1982; Aderibigbe and Rajaratnam, 1996). The scour hole profiles have also

been found to be similar through the scouring process, using the scales described above (Rajaratnam and Beltaos, 1977).

3.3.2 Scour in Cohesionless Soils by Submerged Plane Turbulent Wall Jets

There have also been many studies of the erosion or scour of cohesionless soils by submerged plane turbulent wall jets including Laursen (1952), Tarapore (1956), Chatterjee and Ghosh (1980), Rajaratnam (1981), Ali and Lim (1986), Ali and Salehi Neyshaboury (1991), and Chatterjee et al (1994), and Aderibigbe and Rajaratnam (1998). The typical scour hole profile for scour in sand is sketched in Figure 3-4. At the end of the scour hole a mound forms made up of the particles from the scour hole. In addition, as for the scour by impinging jets there is the dynamic scour as the jet flow continues and a shallower static scour hole that forms when the jet flow is stopped (Aderibigbe and Rajaratnam, 1998).

The growth of the scour hole dimensions have been observed to follow a linear relation with the logarithm of time (Laursen, 1952; Tarapore, 1956). Again at long times, the scour rate becomes very small and the scour hole profile reaches an “asymptotic”, “equilibrium”, or “ultimate” state (Laursen, 1952; Rajaratnam, 1981; Chatterjee et al, 1994). As the scour hole dimensions near asymptotic state, the linear relation between the scour depth and the logarithm of time is no longer applicable.

The scour hole profiles have been found to be similar through the scouring process (Laursen, 1952; Tarapore, 1956; Ali and Salehi Neyshaboury, 1991). Some of the scales that have been used to nondimensionalize the scour hole profiles include the maximum scour depth ϵ_m and the distance to the top of the mound x' for the scour depths and the length of the scour hole, x_o , x' , and the distance to the maximum scour depth x_m for the distance from the origin of the jet (the nozzle).

As for the impinging jets, the resistance to scour for cohesionless materials is typically defined by the size and density of the particles that make up the soil bed. For example, Rajaratnam (1981) suggested that for the scour of cohesionless materials by a

plane turbulent wall jet flowing tangentially to the bed, the maximum scour depth at equilibrium was a function of:

$$\varepsilon_{\text{max}} = f\{U_o, a, \rho, g(\rho_s - \rho), v, D\} \quad (3.2)$$

where: g = gravitational acceleration
 ρ_s = density of the sand particles
 D = the sand grain size (the size for 50 % passing for a uniform sand gradation)

Using dimensional analysis he found:

$$\frac{\varepsilon_{\text{max}}}{a} = f \left\{ F_o = \frac{U_o}{\sqrt{\frac{g(\rho_s - \rho)}{\rho} D}}, \frac{U_o a}{v}, \frac{a}{D} \right\} \quad (3.3)$$

Experiments showed that the scour hole dimensions were strongly related to F_o , where F_o can be considered as a ratio of the shear forces acting on a particles to the resistance to erosion (the buoyant weight of the particle) and that the Reynolds number could be neglected from the analysis.

3.4 Previous works in Erosion of Cohesive Soils by Jets

3.4.1 Introduction

Only a few researchers have performed experiments in the erosion of cohesive soils using turbulent jets. In most studies, a jet was used to create erosion as a means to evaluate the erosivity of different soils in terms of the soil properties (Dunn, 1959; Dash, 1968; Bhasin, Lovell, and Toebes, 1969; Hollick, 1976; Kuti and Yen, 1976; Krishnamurthy, 1983). In these tests, the flow was typically constant and the soil properties were varied. Fewer works have focused on the effect of the flow properties on the scour by jets (Moore and Masch, 1962; Mirtskhulava et al, 1967; Abt, 1980; Hedges, 1990; Hanson, 1990a, 1991; Stein, 1990), with these studies being of much more concern to the present work.

3.4.2 Jets Used in the Evaluation of Soil Resistance to Scour

3.4.2.1 Dunn (1959)

Dunn (1959) was one of the first to test the erosiveness of cohesive soils using turbulent jets. The objectives of his study were to determine the influence of soil properties on the erosiveness of a variety of soils in terms of the critical shear stress and to develop a method of estimating this critical shear stress from the vane shear strength of the soil. He first collected soil samples from several locations. Jet testing of the soils used a submerged vertical circular impinging jet to create erosion. For each test, the jet velocity was slowly increased until the water in the jet tank became and stayed cloudy. The associated shear stress was deemed the critical shear stress. This was determined by measuring the shear stress on the bed at the location where erosion first occurred by placing a shear plate on the bottom of the tank. This was a small distance away from the centreline of the jet, although Dunn does not specify this location. He also found that this distance did not depend on the impingement height. The independence of the location of the maximum shear stress from the impingement height indicates that the jet was likely at a “small” impingement height ($H < 5.5d$) (Beltaos and Rajaratnam, 1977). It was found that the critical shear stresses were about 1/2000 of the vane shear strength values, with the shear strengths in a range of 2.4 to 23.9 kPa.

Dunn goes on to develop a relation for the critical shear stress and the properties of the soil using his experimental data:

$$\tau_c = 0.02 + \frac{S_v \tan \theta}{1000} + 0.18 \tan \theta \quad (3.4)$$

The constant 0.02 is a factor he attributed to the normal pressure on the soil created by the impinging jet. He then correlated the angle θ from his critical shear stress equation to different soil properties. For the plasticity index, PI (%), he found:

$$\theta^\circ = 30 + 1.73(\text{PI}) \quad (3.5)$$

for a range of plasticity index of 5 to 16. He also correlated θ with the amount of fines in the soil, ψ , defined as the percentage by weight of soil particles less than 60 μm . This gave:

$$\theta = 0.6\psi \quad (3.6)$$

The formula using the plasticity index gave a better fit to the data.

Dunn likely was testing for surface erosion, as he noted a general cloudiness in the jet tank and did not report any removal of the soil in chunks. The general conclusions from this work include that the critical shear stress increases with increasing vane shear strength, increasing fines content (clay content), and plasticity. The most important observation in regards to scour is that the erosion first occurred at a location away from the centreline of the jet.

3.4.2.2 *Dash (1968)*

Dash (1968) performed experiments with a circular submerged impinging jet to examine the effect on erosion rates of several soil parameters such as the clay and water content. In this work, he developed a jet erosion index based on dimensional analysis and an evaluation of an energy balance between the energy flux from the jet and the work done by the fluid on the soil. For erosion by an impinging circular submerged turbulent jet, Dash (1968) assumed :

$$\xi S_{gt} = f\{U_o, \rho, d, \mu, \sigma_{te}, t\} \quad (3.7)$$

where:

- ξ = the volume of scour
- S_{gt} = specific gravity of the soil
- ρ = density of eroding fluid
- μ = dynamic viscosity of the eroding fluid
- σ_{te} = tensile strength of the soil
- t = time

Dimensional analysis gave that:

$$\frac{\xi S_{gt}}{d^3} = f \left\{ \frac{tU_o}{d}, \frac{U_o d \rho}{\mu}, \frac{\sigma_{te}}{\rho U_o^2} \right\} \quad (3.8)$$

The jet used had a diameter at the nozzle of 3.2 mm and was set at 25.4 mm above the sample. This gives an $H/d=7.9$, which is close to what would be considered a large impingement height. The given dimensional analysis appears to be more appropriate for a jet at a small impingement height. The jet used for testing the samples was confined to a 76.2 mm diameter, 305 mm tube. The samples were held at the bottom of the tube. Only the weight loss of the sample with time was reported. There is no discussion of the characteristics of the scour holes created by the jet or the characteristics of erosion of the material.

3.4.2.3 *Bhasin, Lovell, and Toebes (1969)*

The work of Bhasin, Lovell, and Toebes (1969) follows that of Dash (1968). Bhasin et al used a submerged, vertical, circular jet (Dash's apparatus) to test the influence of sand/clay ratio, water content, and mixing and curing times of the soil, as well as the sand content in the flow on erosion. They also investigated the effect on erosion rates of the jet velocities, nozzle diameter, and impingement height. The jet was confined to a 76.2 mm diameter erosion tube as in Dash (1968), with a 50.8 mm deep sample at the end of the tube. The nozzle sizes used were either 4.7 or 9.5 mm, with the jet velocity as high as 15.5 m/s. Erosion was determined by stopping the tests and weighing the sample at 2.5 or 5 min intervals. The tests were run for 20 min.

The erosion rate was found to increase with increasing jet velocity, decreasing jet height above the sample surface (as might be expected for a jet at a large impingement height), and increasing diameter of the jet. Erosion rate was also found to increase with an increasing soil water content, increasing sand/clay ratio, and decreasing time of curing of the soil. Sand in the jet flow increased the erosion rates of the samples.

3.4.2.4 *Hollick (1976)*

Hollick (1976) used a vertical, submerged circular jet in trying to develop charts that could be used for predicting the critical shear stress of a soil based on the amount of scour seen during jet testing. He tested a number of soil samples using the same nozzle diameter, impingement height, and test temperature and duration for all tests. He then plotted a dimensionless average scour depth, $\frac{\bar{\epsilon}}{d} = \frac{\sqrt[3]{\xi}}{d}$, where ξ is the volume of scour, against a dimensionless soil resistance parameter, $\frac{\tau_c d^2}{\rho v^2}$, for a number of Reynolds numbers to develop his design curves. These parameters were based on the dimensional analysis of Moore and Masch (1962) (discussed in section 3.4.3.1). However, Hollick (1976) used the nozzle diameter, d , to nondimensionalize the scour depth instead of the impingement height used by Moore and Masch (1962). He also used the critical shear stress as the soil resistance parameter. The critical shear stress for each soil was determined in flume tests, with a visual criterion for the beginning of erosion that was not specified.

For the jet testing, the nozzle diameter used was 4 mm and the impingement height was set at 80 mm. Based on the ratio $H/d=20$, the jet was at a large impingement height. For the given test temperature of 20°C and a range of Reynolds numbers of 6000 to 18000, the range of jet velocities at the nozzle can be calculated as 1.5 to 4.5 m/s with the maximum bed shear stress ranging from 0.9 to 8.2 Pa. However, these velocities are somewhat lower than would be predicted by the given range of head of the gravity driven flow of 330 to 1250 mm (2.5 to 5.0 m/s). The durations of the tests were either 100 min or 10 min (for the weaker soils).

After developing his curves using kaolinite /sand mixtures, Hollick jet tested compacted natural clays to try and predict the critical shear stress of these soils. He compared the predicted critical shear stress from the jet tests to that determined from flume tests and did not get a good correlation. This may be because he did not test until the scour

holes reached equilibrium and thus was actually testing erosion rates of the soil which do not necessarily depend on the critical shear stress (a soil can have a high erosion rate even though it has a high critical shear stress (Moore and Masch, 1962)).

Important observations included that there were two main scour hole types: (1) a narrow, deep scour hole and (2) a wider, more shallow bowl shaped scour hole. There were also intermediates scour hole shapes between these two types. Moore and Masch (1962) saw a similar phenomenon and attributed the different scour hole shapes to the relative impingement height H/d . Moore and Masch (1962) suggested that at the lower values of H/d , the narrow, deep scour holes formed, and at the high values of H/d , the wide and shallow scour hole formed. However, since Hollick did not change the impingement height or nozzle diameter for any of his tests, the scour hole shape cannot strictly be a function of H/d . Mirtskhoulava (1989) reports similar work to Hollick (1976) was done in Russia, although no details are given.

3.4.2.5 Kuti and Yen (1976)

Kuti and Yen (1976) experimentally studied the scour of a cohesive material by a hydraulic jump created at the end of an apron at the bottom of a model spillway, which can be considered a case of scour by a plane wall jet (Rajaratnam, 1965). They examined the effect of varying the void ratio and clay content of the soil on the volume of scour with time. For this work, they suggest a relation between the volume of scour and the soil and flow properties as:

$$\frac{\Delta\xi}{\Delta t} = f\{y_1, \nu, \rho, \rho_s, U_1, s, D, B, t, c\} \quad (3.9)$$

where:

- ξ = volume of scour
- U_1 = average velocity of approach flow (supercritical velocity for jump)
- y_1 = depth of approach flow at the apron (supercritical depth for jump)
- B = width of channel
- ν = kinematic viscosity of the eroding fluid

- ρ_t = bulk density of the soil
- s = terminal velocity of soil particles
- D = mean grain size of soil particles
- c = parameter describing the physiochemical forces of the soil

With dimensional analysis, they found:

$$\frac{\Delta\xi}{U_1 y_1 B \Delta t} = f \left\{ \frac{y_1}{D}, \frac{U_1 y_1}{v}, \frac{U_1 t}{y_1}, \frac{U_1}{s}, \frac{\rho_t}{\rho}, \frac{B}{y_1}, c \right\} \quad (3.10)$$

Since the ratio $\frac{\rho_t}{\rho}$ depends on the void ratio, e , and the settling velocity of the soil particles and cohesion depend the clay content (but was really the fines content, ψ), the void ratio and fines content were used to replace these parameters in the analysis. With the flow depth and velocity held constant and for a particular type of clay mineral, they reduce eqn. 3.10 to:

$$\frac{\Delta\xi}{U_1 y_1 B \Delta t} = f \left\{ \frac{U_1 t}{y_1}, e, \psi \right\} \quad (3.11)$$

Observations included that there was a rapid erosion rate initially that gradually tapered off, with an asymptotic approach to the final volume of scour. They concluded that the volume of scour was reduced with increasing clay content. However, they included soil particles of up to 0.060 mm in their clay content and their reported clay contents of 20 to 80 % are actually in the range of about 3 to 12.5% from the given grain size distribution curves. The lower clay content materials had no plasticity and thus cannot be considered cohesive soils.

3.4.2.6 *Krishnamurthy (1983)*

Krishnamurthy (1983) used both a vertical circular jet and flume testing to examine the variation of the critical shear stress with the soil strength found by both the direct shear and unconfined compressive strength tests for two clays. However, he does not report the criteria used for determining the critical shear stress or the erosion characteristics of the

materials. There is also scant reporting of the test procedures. The critical shear stresses for the jet tests ranged from about 1.5 to 25 Pa, whereas for the flume tests these range from 0.2 to 1.1 Pa. Details of how the shear stress on the bed was calculated for the jet tests are not presented.

3.4.3 Scour by Jets in Cohesive Soils

3.4.3.1 Moore and Masch (1962)

The work of Moore and Masch (1962) is closest in scope to the present study. They used a submerged vertical circular impinging jet to examine the evolution of scour in three clays. These were a natural stratified sediment (with a bulk density of 2490 kg/m³), a natural jointed sediment, and a laboratory remolded sediment (bulk density of 2484 kg/m³). Unfortunately, no other soil properties are given. For each test, clay samples were inserted into a 127 mm diameter, 102 mm deep cylinder. The cylinder was then placed in a recess in the floor of a 0.91 by 0.91 by 0.46 m tank and submerged for testing. A circular turbulent jet that impinged at 90° to the samples was produced by flow through nozzles of either 15.9, 9.5, or 4.8 mm diameter. With the jet Reynolds numbers reported to be in the range of about 10000 to 40000, this gives velocities of the jet at the nozzle in a range of 0.63 to 8.4 m/s for a test temperature of 20°C. The impingement heights ranged from H/d of 6 to 10 (corresponding to impingement heights of 57 to 95 mm). From this data, the maximum shear stress on the bed can be calculated as ranging from about 0.6 to 310 Pa.

The duration of the tests at a given velocity were 60 minutes. At ten minute intervals, the test was stopped and the sample weighed to determine the weight of the soil scoured. Using this weight, the volume of scour was calculated. The average depth of scour was determined by taking the cube root of this scour volume. After each test the jet velocity was then increased and the same procedure was repeated. However, it is uncertain whether the authors used the same scoured out sample for all testing and just increased the velocity after 60 min or used a new sample of the material.

The data collected was evaluated through the use of dimensional analysis. They suggested the average depth of scour, $\bar{\epsilon} = \sqrt[3]{\xi}$, was a function of:

$$\bar{\epsilon} = f\{U_o, d, H, \rho, \mu, \sigma_s, t\} \quad (3.12)$$

where σ_s is a scour resistance property of the sediment (with dimensions of a stress) that was not defined. Using dimensional analysis, they found:

$$\frac{\bar{\epsilon}}{H} = f\left\{\frac{t\mu}{\rho d^2}, \frac{\rho U_o d}{\mu}, \frac{H}{d}, \frac{\sigma_s \rho d^2}{\mu^2}\right\} \quad (3.13)$$

Results showed that the average scour hole depth grew in a linear relation with the logarithm of time. Large discontinuities in these curves were observed to correspond to episodes of “large pieces breaking out of the sample and being carried away by the jet”. As well, average scour depths were observed to be in a range of about 5 to 60 mm. It thus can be concluded that Moore and Masch (1962) observed mass erosion. On plots that relate scour depth and time, the dimensionless time $\frac{t\mu}{\rho d^2}$ is shown to range from 0.03 to 0.4. However, this corresponds to times of about 3 to 36 s (a 36 s long test). Since this contradicts their reported test times of 60 min, it appears there is an error in the reporting of this data.

Observations include that the clay did not scour in symmetrical patterns which they attributed to the nonuniformity of the samples. However, this may be partly due to the scour hole not reaching equilibrium state. They also found that each sample required a given jet velocity before scour began. Unfortunately, they do not report the impingement height used for the test so that the critical shear stress cannot be calculated. As well, for the range of $6 \leq H/d \leq 10$ and for a constant jet Reynolds number the maximum amount of scour occurred at an H/d of around 8.0. This is interesting as an H/d of 8 is in the range of H/d where there is a transition between the small and large impingement height behavior of the jet (Beltaos and Rajaratnam, 1974). Significant scatter in the data seen at an H/d of 7.0 was thought to be due to a change in the type of scour hole that “may be associated with the

geometry of the jet.” They recognized that for the lower impingement heights, the potential core of the jet may reach the bed, and that this was different than the jet behavior at larger impingement heights. They also found:

“For values of H/d less than 7.0, the scour hole was deep and localized. At the higher H/d values the scour hole was wider and shallower covering a larger portion of the sediment sample. At the lower H/d values the jet was almost completely reversed, and very little scour took place once the scour hole developed. In the latter case the scour rate was lower, as the energy of the jet was dissipated in a relatively deep narrow hole. For the high H/d values, the potential core of the jet did not strike the sample and the jet was of broader extent, causing a relatively shallow scour hole.”

The two regimes of scour are similar to the weakly-deflected and strongly-deflected jet regimes found by Aderibigbe and Rajaratnam (1996), in their work with impinging vertical circular turbulent jets on cohesionless soils. It is thought that for the deep, narrow scour hole the observed decrease in scour is due to a decrease in the momentum of the jet caused by the entrainment of the fluid that is turned in the direction opposite to the jet in the deep scour hole (i.e. the momentum of the jet is diminished by the entrainment of its own return flow).

3.4.3.2 *Mirtskhulava et al (1967)*

Mirtskhulava et al (1967) appear to have developed a method to quantify the local scour due to jets in cohesive soils. It is not explicitly stated in this work that the authors are considering scour by two dimensional plane impinging jets. However, descriptions of the flow and scour holes suggest that this is the case. This work is similar in concept to that of Stein et al (1993). Mirtskhulava et al proposed that the condition of equilibrium scour is reached when “the maximum average velocity on the bottom is equal or less than the bottom non-eroding velocity” (the permissible velocity). The change of “axial velocity of the falling stream” with distance along the jet axis was given by:

$$U_m = \frac{U_{es}}{0.9 + 0.09(x_1/B_o) + 0.12(x_1 / B_o)} \quad (3.14)$$

- where:
- U_{es} = velocity at the “entrance section” (this is can be interpreted as the velocity of the jet at the water surface)
 - U_m = maximum velocity of the jet at a distance x from the entrance section
 - B_o' = width of the “stream” (the thickness of the jet) at the entrance section
 - B_o = “the stream width” at the distance \bar{x} from the entrance section (thickness of the jet at a distance \bar{x} from the water surface), where $B_o = B_o' + 0.43\bar{x}$
 - x_1 = distance “along the stream” (along the jet axis) from the stream entrance to the “downstream base” (the original bed level)
 - x_2 = distance along the axis from the “base” to the scour hole bottom (the scour hole depth)

Equilibrium occurs when U_m is equal to the non-eroding velocity, U_n , given as:

$$U_n = 1.25 \sqrt{\frac{2gm'}{0.3\rho_o n} \{\rho_s - \rho_o\} D + 1.25\{C'\kappa + P_d + P_h\}} \quad (3.15)$$

- where:
- g = acceleration due to gravity (assumed by the writer)
 - n = coefficient that takes into the pulsating nature of the velocities in the jet (given as $n=4.0$ for natural conditions and $n=2.25$ for laboratory testing)
 - m' = a factor adjusting the eroding capacity for the flow for added sediment (given as $m=1.0$ for clear water scour and $m=1.6$ with sediment)
 - ρ_o = density of water taking into account aeration
 - ρ_s = density of the particles
 - D = diameter/size of the aggregates (the eroded particles)
 - C' = “fatigue strength to rupture depending on the cohesion in the state of saturation”
 - κ = homogeneity coefficient for the soil ($\kappa \approx 0.5$)
 - P_d = pressure exerted by the jet on the aggregates washed away, depending on the stream velocity at the bottom of the hole
 - P_h = “a ‘hydrostatic pressure’ effect on the contact between the aggregates” ($P_h = \alpha\rho_o\varepsilon_m$ where $\alpha=0.010$)

An equation for the maximum depth of scour and the time necessary to reach specified scour depths is also given.

Other comments of interest include that there is an asymptotic approach to the state of equilibrium scour:

“when actual velocities of flow exceed the permissible value for the given soil sufficiently the detachment of aggregates takes places comparatively in a short period of time and vice-versa - at the end of erosion process the necessary number of loading cycles approximates infinity.”

They also note that, in general, larger aggregates were removed at the beginning of scour. The size of the aggregates were reported to be “conditioned by the soil’s texture and structure indices and also by the degree of “active” forces exceeding the passive ones, which determine the soil resistance to erosion.”

3.4.3.3 *Abt (1980)*

Abt (1980) studied the erosion at a culvert outlet of a cohesive soil at prototype scale. This is a case of scour by a circular horizontal wall jet. His objectives were to determine the form and dimensions of the scour hole created by the culvert flow and to predict this scour hole geometry based on parameters developed through the use of dimensional analysis. Testing was conducted in an outdoor flume that was 30.5 m long, 6.1 m wide, and 2.4 m deep, with the culvert invert at the same level as the soil bed. Three culverts of 273, 356, and 457 mm diameters were used with flow rates ranging from 0.05 to 0.824 m³/s. The test duration was 1000 min. The scour hole profile was measured using a point gauge after 31.6, 100, 316, and 1000 minutes of testing. The tailwater was maintained at 0.45 ± 0.05 times the diameter of the culvert.

Only one type of soil was tested and the same bed was used for all tests. The scour hole was dewatered and refilled after each test. The soil was a sandy clay made up of 58 % sand, 28 % clay, 14 % silt, and 1 % organic material. It had a liquid limit of 34 %, a plastic limit of 19 %, and a plasticity index of 15. The soil was placed in the flume using a loader and was compacted in lifts to 90 ± 2 % of optimum density.

Using dimensional analysis, Abt suggested that the parameters significant to the scour at the outlet of the culvert are:

$$\frac{\varepsilon}{d_c}, \frac{B_w}{d_c}, \frac{x_o}{d_c}, \text{ or } \frac{\xi}{d_c^3} = f \left\{ \frac{R_h}{d_c}, \frac{d_t}{d_c}, \frac{Q}{g^{1/2} d_c^{5/2}}, \frac{\tau_c}{\rho V^2}, \frac{t}{t_d} \right\} \quad (3.16)$$

where:

- d_c = culvert diameter
- R_h = hydraulic radius (of the culvert flow)
- B_w = maximum width of the scour hole
- x_o = maximum length of scour hole (distance from nozzle where $\varepsilon \rightarrow 0$)
- V = average velocity of culvert flow at the outlet
- d_t = tailwater depth
- t = time of measurement from start of test
- t_d = duration of test

The main parameters used in his analysis were the “discharge intensity” $\frac{Q}{g^{1/2} d_c^{5/2}}$, and the “modified shear number” $\frac{\tau_c}{\rho V^2}$. The discharge intensity varied from about 0.35 to 3.5. For the second parameter, the modified shear number, the critical shear stress was not measured, but calculated based on an equation modified from Dunn (1959).

General observations of cavity growth and formation showed that the cavities were circular in shape when $\frac{Q}{g^{1/2} d_c^{5/2}} < 1$ and elongated to an oval shape for $\frac{Q}{g^{1/2} d_c^{5/2}} > 1$. The maximum scour depth consistently occurred at about $0.35 x_o$. Sand and clods deposited at the downstream end of the scour hole in a mound. This mound was never larger than $0.25d_c$ in height. The small silt and clay sized material in the soil was either carried away by the flow or could be found in the void space of the mound. It should be noted that the final dimensions of the scour hole likely do not correspond to an equilibrium state of scour, as the tests were stopped after 1000 minutes.

Abt related the maximum scour hole length, width, and volume of scour to maximum scour hole depth (the geometry after 1000 minutes) in a series of plots. All scour hole dimensions were nondimensionalized using the culvert diameter. He also related scour hole dimensions to the discharge intensity and the modified shear number.

For the scour hole profiles, Abt nondimensionalized the scour hole depth with the maximum scour hole depth and the distance from the end of the culvert with the length of the scour hole and found that there was significant scatter. The scatter may have been reduced if the tests had been run to equilibrium state and if the half-width (the location past the maximum depth of scour where the scour is half the maximum depth) was used to nondimensionalize the distance from the culvert outlet, as suggested by Aderibigbe (1996) in his work with scour in sand.

This work suggests that dimensional analysis is suitable to determine the scour hole geometry in a cohesive soil eroded by jets. Abt also provides the data from his experiments, so that it may be used in future analyses of the scour of cohesive soils by circular horizontal wall jets. Abt (1980) is summarized in Abt and Ruff (1982).

3.4.3.4 *Hedges (1990)*

Hedges (1990) studied scour in clays with an inclined submerged turbulent circular impinging jet. He compared jet scour to the problem of scour produced on the banks of narrow channels due to ship thruster usage. The concern was the potential effect of this localized scour on bank stability. The objective of the study was to determine the relationship between scour and the time of impingement, the clay shear strength, the height of the jet above the sample, and the impingement angle. He also examined the velocity and pressure distribution of the jet acting on a smooth, flat surface.

Dimensional analysis was used to evaluate the data. The dimensionless parameters thought to control scour of clays were:

$$\frac{\xi}{d^3} = f \left\{ \frac{H'}{d}, \frac{\tau_s d}{U_o \mu}, \frac{\tau_{tr} d}{U_o \mu}, \frac{\rho U_o d}{\mu}, \beta, PI, \frac{U_o t}{d} \right\} \quad (3.17)$$

where: H' = distance from the nozzle to the clay surface along the jet centreline
 τ_s = shear strength of the soil
 τ_{tr} = tractive shear force on the soil caused by the jet
 PI = plasticity index of the soil

$\beta =$ angle of inclination of the jet

Since Hedges believed the tractive shear stress, τ_{tr} , acting on the soil is difficult to define, the maximum pressure force created by a jet acting on the clay surface was substituted in that parameter. This stress was measured in alternate experiments using pressure transducers embedded into a plexiglass box and placed under the jet. The water content, w , of the soil was added to the scour volume parameter, $\frac{\xi}{wd^3}$, in hopes of reducing variability in the scour data. A parameter for scour rate, Q_c , was also developed and given as $\frac{Q_c}{d^2U_o}$.

A soil test sample consisted of one large block of clay, 267 mm wide by 406 mm long by 102 mm deep, made up of four smaller blocks that had been pressed together. Only one type of clay was tested. Tests were conducted in a 457 mm wide by 889 mm long by 533 mm deep jet tank. Variables included the angle of inclination of the jet, which was alternately set at 90° (vertical), 75°, 60°, or 45°. The jet height above the sample varied from 63.5 to 101.6 mm, while the jet velocity at the nozzle was held constant at 11.4 m/s. Total test duration was 15 min. Scour volume was measured at 5 min intervals by draining the tank and measuring the volume of water left in the scoured out areas on the surface of the soil.

Results showed that there were two mechanisms of scour. At higher stresses on the sample (smaller jet height and/or larger angles of inclination), clay was removed as flat pieces with a maximum 6.4 mm thickness. At the lower stresses, the clay eroded particle by particle, as evidenced by a cloudiness in the jet tank. Scour volume was found to be linearly related to time. However, this included only three data points and the tests were conducted for only 15 min. He also found that scour decreases with increasing jet height from the sample and with a decreasing angle of inclination. Scour rate also decreased with increasing shear strength of the clay, although there was a large amount of scatter. All four

angles of inclination showed approximately the same scour rate for a given tractive pressure on the clay surface. He concluded that this indicates that the tractive shear force is the controlling factor for erosion rather than the angle of inclination of the jet.

Problems encountered during testing included that the scour was confined to the centre block of clay, as erosion did not continue across the interface of two combined blocks. This indicates that one large, continuous clay sample must be used. For the dimensional analysis, many variables seem redundant, as both the tractive shear stress on the soil and the jet characteristics ρ , U_o , d , H' , and β are included. Use of the plasticity index may also not be useful as it has been concluded by many (Paaswell, 1973) that plasticity index is not an adequate parameter to use to describe soil erosion resistance. Hedges (1990) does not report dimensions of the scour holes for his tests.

3.4.3.5 *Hanson (1990a)*

Hanson (1990a) developed an in-situ jet testing device to evaluate the erodibility of cohesive soils that uses a submerged circular turbulent impinging jet to create erosion. He based his analysis on the work of Moore and Masch (1962), but used the coefficient of erodibility, K , for the soil resistance parameter σ_s . This coefficient is from the equation described by Foster et al (1977) $\dot{E} = K(\tau - \tau_c)^m$ that relates the erosion rate \dot{E} to the excess shear stress applied to the soil. In previous testing of soils in an open channel, Hanson (1990b) found that for cohesive soils $m \cong 1$. The units used for K were cm/h/Pa. The dimensionless parameters that describe scour were thus:

$$\frac{\sqrt[3]{\dot{E}}}{H} = f \left\{ \frac{t\mu}{\rho d^2}, \frac{\rho U_o d}{\mu}, \frac{H}{d}, \frac{\mu K}{d} \right\} \quad (3.18)$$

Jet tests were performed on four soils that had been previously tested for erosion rates in an open channel (Hanson, 1989, 1990b). The jet tests were carried out using a portable device that was set on top of the soil to be tested. The jet diameter and impingement height were held constant for all tests at 13 and 220 mm respectively

($H/d=16.9$). The scour hole profile was measured at 10, 30, 60, and 100 min intervals for a total test time of 200 min. For more resistant soils, a 1000 min interval was added.

Hanson then compared the effect of the different dimensionless parameters on the dimensionless scour hole volume using the data from three of the four soils tested. On performing a statistical analysis of the data, he determined (for a constant impingement height and nozzle diameter):

$$\frac{\sqrt[3]{\xi}}{H} = 0.0436 \left(\frac{\rho U_o d}{\mu} \right)^{0.67} \left(\frac{t\mu}{\rho d^2} \right)^{0.065} \left(\frac{\mu K}{d} \right)^{0.138} \quad (3.19)$$

The equation for scour volume was then rearranged to yield K and used to predict the erodibility factor for the fourth soil.

Hanson's method shows interesting results. However, more tests on other cohesive soils must be performed for verification of his analysis. Of interest is the use of the erodibility coefficient K in the analysis. This seems to be a much better parameter for estimating scour dimensions that are dependent on the scour rates than the critical shear stress. However, Hanson's method is based on a linear relation between erosion rate and excess shear stress which has not been found by all researchers (Foster et al, 1977; Owoputi and Stolte, 1995).

3.4.3.6 Hanson (1991)

Using the results found in the in-situ jet testing present in Hanson (1990a), Hanson developed a dimensionless jet index used to describe the erodibility of a soil. He assumed:

$$\dot{E} = \frac{\xi_m}{t} = \omega t^{-\delta} \quad (3.20)$$

where ω and δ are constants. From a regression with the data from jet testing from one soil he found $\delta=0.931$. He then suggested that for a given soil in a given condition $\omega = Zf(U_o)$, where Z is a soil factor and $f(U_o)$ is a function that characterizes the properties of the jet flow. He assumed that the function $f(U_o)$ is dependent only on the

velocity of the jet at the nozzle, U_o , as, for his jet tests, the nozzle diameter, impingement height, and fluid density and viscosity were held constant. This gives:

$$\frac{\epsilon_m}{t} = ZU^\alpha t^{-0.931} \quad (3.21)$$

Using data from the jet tests on another soil, he then found that $\alpha \approx 1$. To avoid the soil factor Z having dimensions of time, Hanson suggested the use of the “Jet Index”, J_i , where $Z = J_i t_1^h$, where t_1 is “1 s or the time unit of 1 s if Z is in the units of 1 s (i.e. if Z is in minutes then $t_1=1/60$ min)”. He thus wrote an equation for the erosion of a soil caused by a circular impinging jet:

$$\frac{\epsilon_m}{t} = J_i U_o \left(\frac{t}{t_1} \right)^{-0.931} \quad (3.22)$$

Hanson found fairly good fit to his data from Hanson (1990a) for this erosion rate equation on a log-log scale. It should be noted it is likely that scour did not reach equilibrium for that data for which he is developing his equations.

3.4.3.7 *Stein (1990)*

Stein (1990) studied the erosion created by an inclined plane impinging jet. The focus of the work was to develop an understanding of the mechanics of headcut migration. The work of Beltaos (1974) in the characterization of impinging jets is used in combination with the sediment detachment equation $\dot{E} = K(\tau - \tau_c)^m$ to predict both the equilibrium scour depth and the rate of scour hole development. Stein (1990) is also described in Stein and Julien (1991), Stein et al (1993), and Stein and Julien (1994).

For the decay of maximum velocity along the centreline of a plane turbulent jet, an equation from Rajaratnam (1976) is used:

$$\frac{U_m}{U_o} = C_d \sqrt{\frac{B_o'}{\bar{x}}} \quad \text{for } \bar{x} > x_p \quad (3.23)$$

where: U_m = jet centreline velocity.

U_o = jet entrance velocity (velocity at the jet origin).

x_p = length of the jet potential core.

\bar{x} = distance along the jet centreline from the jet origin.

C_d = diffusion coefficient of the jet.

B_o' = jet thickness at entrance to the tailwater surface.

with a value for $C_d=2.6$. The origin of the jet is the location where it first enters the tailwater surface. He then related the shear stresses created by the jet, τ , to the maximum velocity using $\tau = c_f \rho U_m^2$, where c_f is the coefficient of friction. Next, an expression was used to relate the depth of scour in terms of the distance along the jet centreline and the impingement angle. The equilibrium scour depth, ϵ_{∞} , measured from the original bed level is:

$$\epsilon_{\infty} = x_2 \sin \beta - d_t \quad (3.24)$$

where: x_2 = the distance along the jet centreline from tailwater entry to the bed impingement at equilibrium

d_t = the tailwater depth above the original bed

β = jet impingement angle (measured from the horizontal)

Then, assuming that equilibrium is reached (i.e. there is no more significant erosion) when the shear stress decreases to the critical shear stress τ_c , the equation for shear stress and depth of scour was combined to give an expression for the equilibrium scour depth:

$$\epsilon_{\infty} = \frac{C_d^2 c_f \rho U_o^2 B_o'}{\tau_c} \sin \beta \quad (3.25)$$

It was assumed here that the tailwater depth is insignificant compared to the depth of scour. This equation is independent of the type of soil although it may not be applicable to dispersive clays where $\tau_c \approx 0$.

Stein (1990) went on to develop an equation for the rate of scour hole development using the equation $\dot{E} = K(\tau - \tau_c)^m$ and the above ideas. His analysis showed that there are three main stages to the evolution of scour for a jet flow with a negligible tailwater: an

initial period when the soil is within the jet potential core and the relation between scour depth and time is linear; a second stage, where the relation of the scour hole depth grows in a linear relation with the logarithm of time; and a final period where the scour is approaching equilibrium depth.

To test his theory, experiments were performed using an plane impinging jet created by an overall fixed within a 10.4 cm wide, 200 cm long, 33 wide flume. Three soils were tested: a cohesive agricultural soil with a d_{50} of 0.045 mm; a fine sand with a d_{50} of 0.15 mm; and a coarse sand with a d_{50} of 1.5 mm. Observations showed that the scour hole profile was fairly symmetrical about the maximum depth of scour, but was slightly lengthened in the direction of flow. The maximum depth was shifted slightly upstream of the centreline of the jet.

This work is interesting in the attempt to predict theoretically the equilibrium scour depths and erosion rates of both sand and clays created by impinging jets. The method of estimating the shear stress that is causing erosion is a weakness, however, as it is known that the boundary strongly affects the behavior of the jet. This is a result of the lack of study of the shear stress produced on the boundaries formed by impinging jets.

3.5 Discussion

From the above described studies, there are several characteristics of scour by circular impinging jets in clays that suggest what will be observed in the present experiments. First, from the observations of Dunn (1959), erosion should first occur at a location away from the centreline of the jet. This can also be expected based on the shear stress distribution created by an impinging jet on the clay surface, as the maximum shear stress on the bed occurs not at the jet centreline, but a distance of about $r=0.14H$ from the centreline (Beltaos and Rajaratnam, 1974). Second, the erosion of more consolidated clays most often occurs as the intermittent removal of chunks of varying size or “mass” erosion (Moore and Masch, 1962; Mirstkhulava et al., 1967; Hanson, 1990). Third, Moore and

Masch (1962) showed that the average scour depth (the cube root of the scour hole volume) grows approximately in a linear relation with the logarithm of time, and it may be expected that the other dimensions of the scour hole may grow in this type of relation as well (although this must be confirmed). These growth of the scour hole would then be consistent with what has been observed for jet erosion in cohesionless soils. Moore and Masch (1962) also observed two forms of scour hole: one that is narrow and deep and one that is wide and shallow. The shape of the scour hole appears to depend on the relative impingement height H/d , but not solely on that parameter as Hollick (1976) also found two forms of scour hole but did not change either the diameter of the jet or the impingement height (and therefore H/d) in his experiments. These two different regimes of scour must be further investigated. Unfortunately, the data from the experiments that used circular impinging jets described in this chapter are not useful for the present work as either the soil properties were not defined (for Moore and Masch, 1962), and tests variables are not described in detail (for Moore and Masch, 1962; and Hollick, 1976), or the experiments were run in such a way as to alter the jet flow (for Dash, 1968; Bhasin et al, 1969).

For the scour in cohesive soils for a plane wall jet, the only previous study to use of flow similar to this type of jet was Kuti and Yen (1976). Observations of Kuti and Yen included that there was a rapid erosion rate initially that gradually tapered off, with an asymptotic approach to the final volume of scour. However, they were studying the erosion by a hydraulic jump downstream of a model dam and did not locate the jump on the apron of the model so that the shear stresses acting on their test samples cannot be estimated. Thus, there are no previous data on cohesive soil erosion by plane turbulent wall jets that will be useful to the present study.

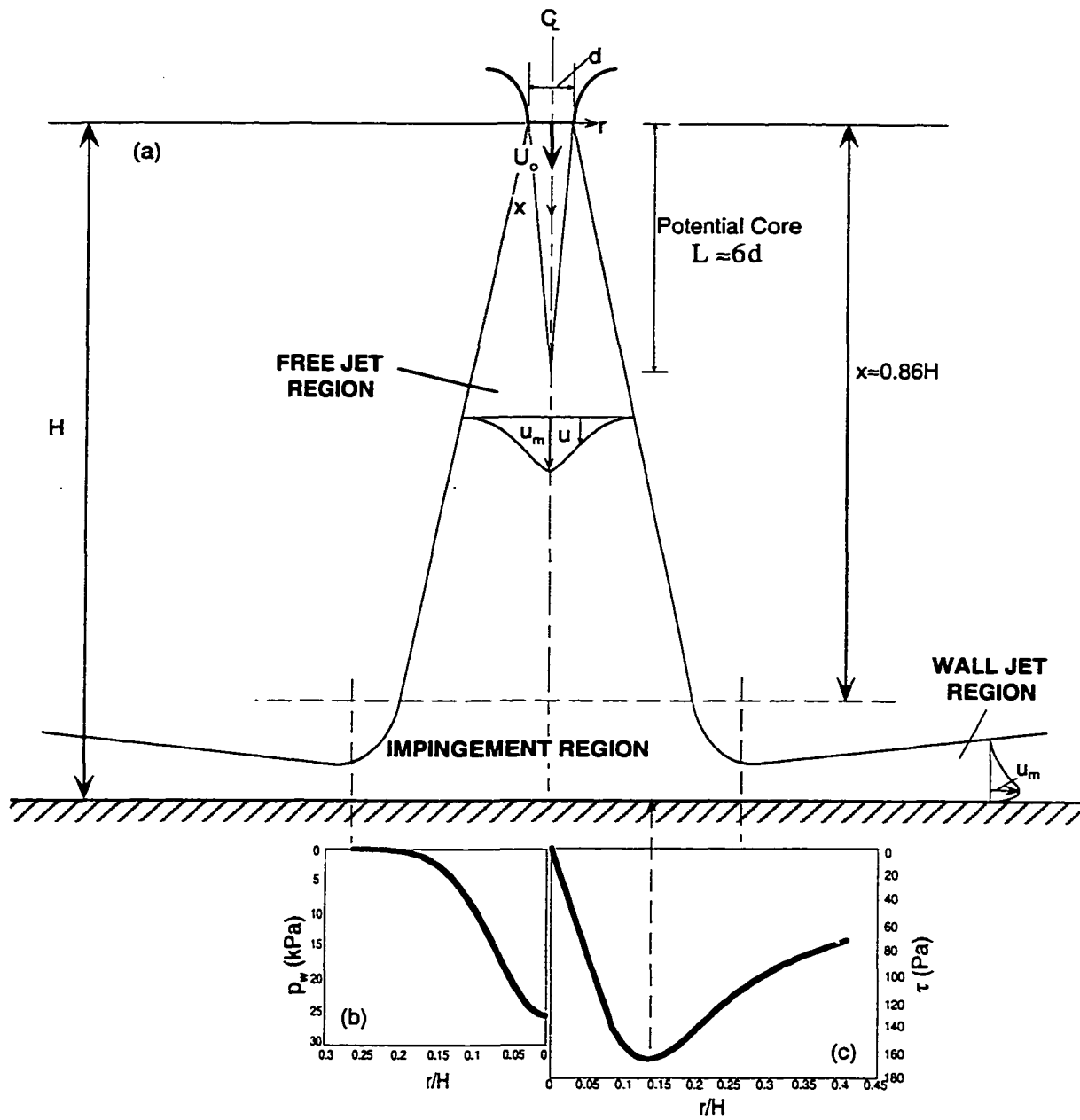


Figure 3-1: The submerged circular turbulent impinging jet (a) definition sketch (b) pressure distribution on boundary for typical test conditions (c) shear stress distribution on boundary (adapted from Beltaos and Rajaratnam, 1974).

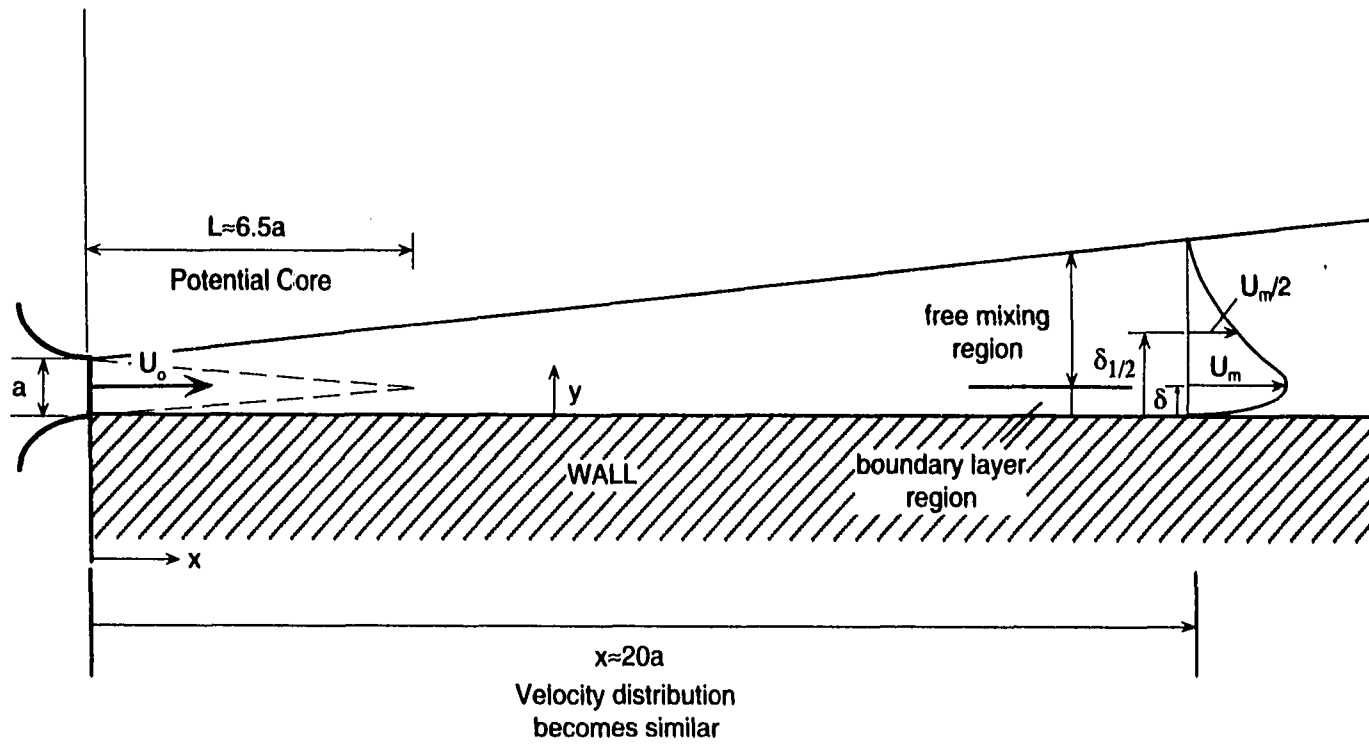


Fig. 3-2: The plane turbulent wall jet.

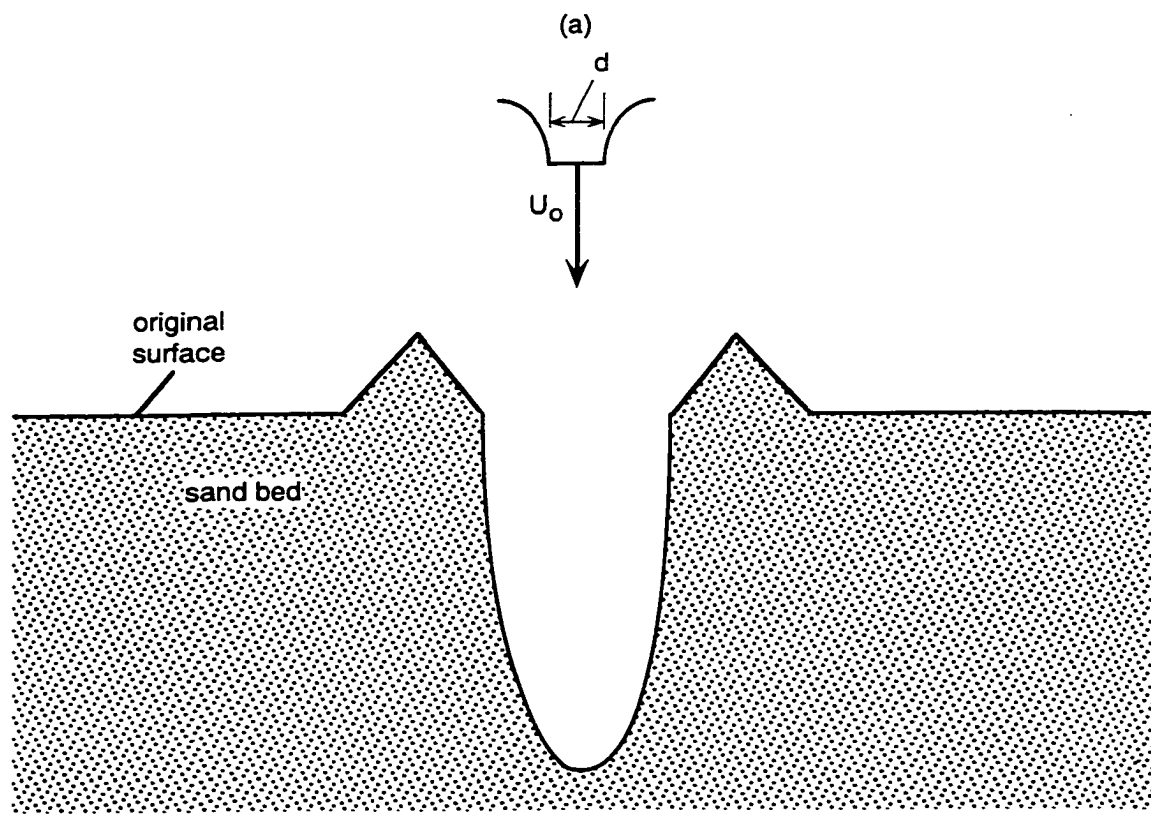
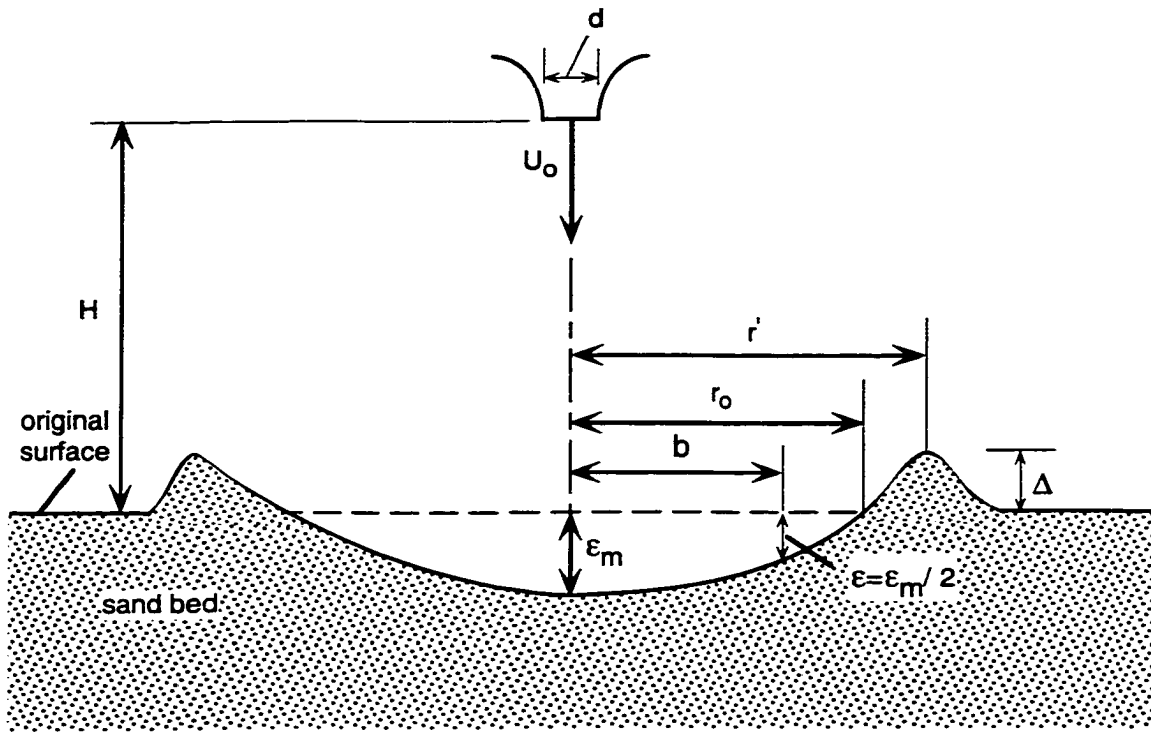


Fig. 3-3: Typical scour holes (a) a weakly deflected jet type scour hole (b) a strongly deflected jet scour hole (adapted from Aderibigbe and Rajaratnam (1996)).

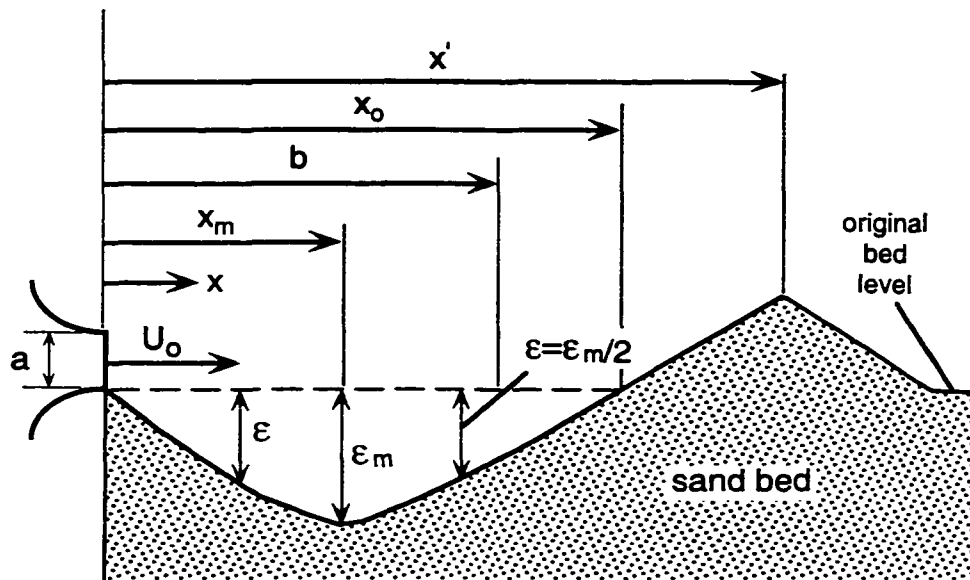


Fig. 3-4: Scour by a plane wall jet in sand.

CHAPTER 4: EXPERIMENTAL SETUPS & EXPERIMENTS

4.1 Introduction

Two experimental setups were employed in carrying out the present study of the scour of clay by jets. The first set of experiments used a submerged circular turbulent impinging jet to create scour. The second set of experiments used a submerged turbulent plane wall jet. Only one type of clay was tested. The experimental setups, testing program, and the properties of the tested clay are described in this chapter.

4.2 Experimental Setup I - Impinging Jet Tests

4.2.1 Experimental Setup and Experiments

The first experimental setup employed a submerged vertical circular turbulent impinging jet to scour several samples of clay of similar properties (Figure 4-1 and Plate 4-1). The jet was created by pumping tap water from a large 880 L fiberglass tank through an 830 mm long, 120 mm diameter cylindrical plenum and then a well designed nozzle to impinge at 90° to the clay surface. The nozzle diameter used was either 4 or 8 mm and velocities at the nozzle ranged from 4.97 to 25.9 m/s for the scour tests. This gave jet Reynolds numbers in the range of 26000 to 98500. Flow rates ranging from 0.1 to 0.71 L/s could be produced in the apparatus for the 8 mm nozzle, with a maximum of 0.35 L/s for the 4 mm diameter nozzle. These flow rates were measured through the use of a magnetic flow meter, however periodic checks of the flow meter readings were carried out by taking volumetric flow measurements in the jet tank. Water was not recirculated in the apparatus to avoid a buildup of ions in the water and a steadily increasing water temperature during each test. The test temperatures varied from 3.5 to 23.6 °C and depended on the temperature of the tap water fed to the laboratory. During each test, at least one reading of the eroding water conductivity, pH, and temperature was taken.

The 244 mm long, 175 mm wide, 85 mm high clay samples were set on a platform inside an octagonal tank of 572 mm width and 610 mm height that was filled with tap water

before the start of testing so that both the sample and the jet were submerged. The jet nozzle was submerged by at least 100 mm and the jet impingement height ranged from 40 to 116 mm, with a range for H/d of 8.1 to 29.0 (large impingement heights only). Details of the experiments are given in Table 4-1.

4.2.2 Measurements

For impinging jet tests, the maximum scour depth, centreline scour depth, and scour hole volume were measured from the start of each test at times of approximately 2 min, 5 min, 15 min, 30 min, 1 h, 2 h, 4 h, 8 h, 24 h, 48 h, 72 h, and 96 h, depending on the change in scour in the sample, and then at 24 h intervals until equilibrium conditions were reached. The test was shut down and the jet tank drained for each measurement. As the scour hole remained full of water, the maximum and centreline scour hole depths were determined by using a thin wooden rod to lightly touch the clay surface in the appropriate location. The length of the water mark on the rod then gave the scour depth. Care was taken not to disturb the sample, as this could cause erosion to occur in the disturbed area. The scour hole volume was measured by first using a vacuum pump to remove the water from the scour hole, then refilling the cavity with water measured in a small graduated cylinder (0.2 mL graduations) until the water just overflowed from the scour hole onto the undisturbed sample surface. The dimensions of the scour hole across the width and along the length of the block were also noted to aid in determining whether the scour had reached equilibrium state. A photographic record of the scour hole was also kept, with a picture taken of the scour hole at the time of each measurement. After the measurements were taken, the tank was again filled with water by using the jet which was directed to impinge against the wall of the jet tank and away from the sample. To centre the jet again above the scour hole, the flow rate was reduced to a very low, noneroding velocity so that the jet could be brought across the sample surface. The jet plenum was then centred within wooden guides and tied down. The flow was then increased to the desired rate.

Once equilibrium had been reached, the jet tank was drained and the jet centreline marked on the clay surface. The sample was then brought out of the jet tank and was set in an apparatus designed for convenient measurement of the scour hole. Two perpendicular cross-sections of the scour hole were taken, one across the width of the sample and the other along the length of the sample. The equilibrium dimensions of the scour hole were measured using a point gauge that could be read to 0.1 mm. After measuring the scour hole profiles, two measurements were made of the vane shear strength of the sample. Samples were then removed from the area around where the vane shear strength measurements were taken for soil water content determination.

Equilibrium state was assumed to have been reached when the scour hole volume and depths did not change over 24 h. The scour hole volume was used as the primary means of determining when equilibrium state was reached, however, as the measurements were considered to be more reliable. Not all samples reached equilibrium. Sometimes the clay block would split in half, a very large chunk would be removed by slaking (a chunk considered much too large to be eroded hydraulically), or the edges of the block would spall so that the scour hole would be affected. At the larger impingement heights tested, the latter occurred frequently.

4.3 Experimental Setup II - Wall Jet Tests

4.3.1 Experimental Setup and Experiments

The second experimental setup used a submerged turbulent plane wall jet to create scour in the clay samples. This apparatus is shown in Figure 4-2 and Plate 4-2. Tap water was pumped through a 670 mm long, 144 mm wide, 100 mm high rectangular plenum through a 144 mm wide nozzle to create a jet that issued into a 4.1 m long, 150 mm wide flume with a depth of submergence of 350 mm. Two nozzles were used with heights of 2.33 or 5.10 mm. The clay was carefully set in the flume so that the clay surface was the same height of the bottom of the nozzle. In these tests, a 150 mm wide, 90 mm high, and

242 mm long clay sample was used. These samples were contained within a 2 mm thick metal band used to ensure that all samples were of the same dimensions. A false flume bed was constructed which was placed downstream of the clay block to try to ensure an even surface for the flow and so that the sample would not be moved out of place by the flow. This false bed could be removed as needed when placing or removing the clay sample from the flume.

Flow rates through the nozzle varied from 1.63 to 5.40 L/s and had a range for the velocity at the nozzle of 4.86 to 13.56 m/s. For most of the tests, the velocity was measured through the use of a pressure tap on surface of the plenum, placed a few centimetres before the flow began to constrict within the nozzle along with a mercury manometer. For the first few tests, a very small 1.59 mm outside diameter Prandtl tube (United Sensor Corporation No. PAA-12-KL) was used to measure the jet velocity at the nozzle. Table 4-2 gives the details of the experiments for the wall jet tests.

Due to the large flow rates as compared to the impinging jet tests, in the wall jet tests some of the water was recirculated through the apparatus. The flow was redirected at the end of the flume through a return line to the large storage tank from which the tap water was pumped. However, a constant inflow of water from the city supply line was also required due to leakage in the flume. The recirculating flow system was not used whenever there was a large suspended sediment concentration in the flow such as at the start of each test. These tests ran continuously until the end of a test and were not stopped for scour hole measurements.

4.3.2 Measurements

Visual estimates of the length of scour, the maximum depth of scour, the distance of the maximum scour depth from the nozzle, and the uniformity of the scour hole were taken at various intervals during the tests until equilibrium was considered to be reached. The condition of the sample was also monitored through a photographic record of the tests.

The scour hole was assumed to be at equilibrium when the length of scour did not change for a period of at least 24 h, with a typical time to reach equilibrium of 100 h. The length of the scour hole was used as the scour hole was too variable to get a good estimate of the maximum scour depth. It was less obvious than for the impinging jet tests that a scour hole had reached equilibrium as the effects of the side walls of the flume became increasingly predominant at longer test times. There tended to be increased scour on the sides of the block which progressively moved inward with time. After about 140 h, side wall effects on the scour hole were very strong.

Once equilibrium had been reached, the sample was removed from the flume and three longitudinal scour hole profiles (profiles parallel to the direction of flow) were measured using a point gauge of a 0.1 mm resolution. These sections were at about 50, 75 (centreline), and 100 mm across the width of the block measured from the side of the sample nearest the front plexiglass of the flume. The exact location of the sections were varied so that the measurements would give the most representative profiles for a test. After the scour hole profile measurements were complete, vane shear strength tests were carried out on the sample. Samples were then taken from the sample from the area around where the vane shear tests were carried out for water content determination.

Two tests were also undertaken to examine the growth of the scour hole with time. For the selected time intervals of 30 min, 1 h, 2 h, 4 h, 24 h, and at each 24 h interval thereafter, the test was shut down and the sample removed from the flume so that profile measurements along the jet centreline could be taken. After each set of measurements, the sample was replaced in the flume. The flume was then filled with water using a hose and then jet flow was slowly reinitiated. Unfortunately, in both tests the samples did not reach equilibrium because of a sudden, unexplained increase in velocity during the first test and the due to very large eroded pieces that completely eroded the sample in the second.

4.4 Clay Samples

4.4.1 Description of Samples

Only one type of clay was used for testing. This clay was a manufactured clay obtained from Plainsman Clays Ltd. of Medicine Hat, Alberta, Canada (M390 is the company designation of the clay used). The clay blocks were periodically tested for homogeneity and generally had uniform vane shear strength, water content, grain size distribution, Atterberg Limits, and activity. The samples contained about 40 % clay, 53 % silt, and 7 % fine sand, and consistently had a vane shear strength of 20 kPa, a liquid limit of 36 %, a plastic limit of 18 %, a dry density of about 1540 kg/m³, and an activity of 0.4. Details of this testing are included with the data given in Appendix A. The water content of the blocks prior to testing averaged 26.0 % with a 97 % saturation. After testing the water content increases to a depth averaged value over the top 30 mm of the sample of about 27.7 %. No fissuring was visually evident in these blocks prior to, or after submergence, or after drying. Electron micrographs produced by a scanning electron microscope of the structure of the clay, given in Plate 4-3, showed that the clay had an aggregated structure with random particle orientations. An X-Ray diffraction test of the soil showed that the clay component of the soil consisted of kaolinite and illite.

4.4.2 Manufacture of the Clay

A tour of Plainsman Clays Ltd. provided an opportunity to observe how the clay blocks were made. The Plainsman clay material comes from a mine in Saskatchewan. The clay occurs in layers in their pit. They have divided this mine into different clay types according to how similar a particular seam is in its properties in comparison to other seams and sort the material into different piles as they mine it. Then enough material from each pile is transported to Medicine Hat and left at the Plainsman site in the same piles as at the mine to supply the plant for up to five years.

The different Plainsman pottery clay types are made up of the clays in the different piles at the mine. The pottery clays are mixed up using the Plainsman “recipes” that have

been determined mostly by experience. These recipes are based on so many loader buckets of one clay pile and so many of another. To mix up the clays, the loader brings the materials from the piles to a "corral" where the different recipes are mixed up using the loader. After the clay is mixed in this method, the material for the desired clay type is dried in an oven to remove any excess moisture, although the clay mix is not completely dry. The dried mixture is brought into the plant and loaded onto a conveyance system.

Within the plant, the material passes along the conveyance system through a series of three hoppers where the materials are better mixed. From the final hopper the material moves into a mixing section which is a long cylindrical tube with a rod in the middle. The mixing section looks very much like an auger. It is here that technicians add water (Medicine Hat tap water) to the dry soil mixture (Plate 6-4). The addition of water is based only on the visual assessment and experience of the technicians. The wetted clay was then moved into a rectangular vacuum chamber by a continuous feed to be consolidated into a long rectangular block (Plate 6-5). The vacuum chamber was effective in removing any air voids in the sample, as noted from experience in testing the clay blocks. The block is automatically cut with a wire to a preset size as it was extruded from the vacuum chamber. The dimensions of the block are thus fixed by the dimensions of the extruder. The blocks are then sealed in plastic bags.

For the particular batch used for testing, 1392 boxes of clay were produced. Of these, 60 boxes of this batch was used for the testing described herein. Almost 90 % of testing was performed with clay from this particular batch for the impinging jet tests and all of the tests for the wall jet test used clay from this batch.

4.4.3 Preparation of the Samples for Testing

4.4.3.1 Impinging Jet Tests

The samples were prepared for the impinging jet tests by first pushing a 0.5 mm thin rectangular metal band with the same dimensions of the test block into the sample. The

confining band were used to help prevent the block from splitting apart during testing by providing a slight confining pressure on the sides of the sample. The surface of the clay was then cut with a very thin metal wire using a guide to ensure all the samples were the same height. The water content of the sample was taken using the material trimmed off the original clay block. The block was then placed in the jet tank and the tank was then filled with water. In most cases, the test was started immediately after the block was cut. For a few tests, the sample was left submerged for some time before testing (this information is included with the data in Appendix A). In these cases, a water content sample of material from the sides of the sample was taken just prior to starting the test.

4.4.3.2 *Wall Jet Tests*

The clay block was prepared in much the same way for the plane wall jet tests as for the vertical jet tests. A 2 mm thick rectangular confining band was pushed into the sample using a press for even pressure around the edges of the sample. The clay was then cut using a thin metal wire to the dimensions of the band using the top of the band as a guide. The block was always tested immediately after preparing the sample for testing. Water content samples of the material trimmed from the original sample were taken for every test.

4.5 Water Chemistry of the Eroding Fluid

The water temperature, pH, and conductivity were recorded for each test. A water sample was taken from the large storage tank and tested using a Fisher 101 pH/conductivity meter. Conductivity and pH values were consistent with water chemistry data given by Epcor, the company that supplies water for the City of Edmonton. A summary of the water chemistry data provided by Epcor through the duration of testing is given in Tables 4-3 and 4-4. This table also includes the water pH, conductivity, and temperature measurements. The water chemistry of the eroding fluid appears to have been fairly consistent through the course of testing.

Table 4-1: Details of experiments for the impinging jet tests.

Test No.	Q (L/s)	H (mm)	d (mm)	H/d	U _o (m/s)	R	$\rho U_o^2(d/H)^2$ (Pa)	t _e (h)	w _c (%)	w _p (%)	w _r (%)	S _v (kPa)	Notes
8/8.1/5.0/1	0.250	65	8	8.1	4.97	31715	374.7	69.8	25.38	25.38			*
8/8.1/6.1/1	0.310	65	8	8.1	6.17	43241	576.2	76.3	26.50	26.50	28.09	20.5	**
8/8.1/6.1/2	0.310	65	8	8.1	6.17	43343	576.2						
8/8.1/7.0/1	0.350	65	8	8.1	6.96	53605	734.4	98.7	26.18	29.99	27.41	20.8	**
8/8.1/7.4/1	0.374	65	8	8.1	7.44	56123	838.6	117.4	26.20	28.23	27.55	18.9	**
8/8.1/8.1/1	0.405	65	8	8.1	8.06	43647	983.4	68.5			29.20	17.7	*
8/8.1/8.4/1	0.420	65	8	8.1	8.36	58585	1057.6	72.5	26.43	30.43		19.6	**
8/8.1/9.0/1	0.450	65	8	8.1	8.95	64279	1214.1	124.3			28.04	20.4	*
8/8.1/9.0/2	0.450	65	8	8.1	8.95	76829	1214.1	44.7	26.21		27.90	20.5	*
8/8.1/9.0/3	0.450	65	8	8.1	8.95	69458	1214.1	92.0	25.52	29.63	27.41	20.2	*
8/8.1/9.0/4	0.450	65	8	8.1	8.95	62769	1214.1	93.0	26.50		27.26	16.1	**
8/8.1/9.0/5	0.450	65	8	8.1	8.95	46813	1214.1	95.4	25.50	30.14	27.54	21.7	*
8/8.1/9.0/6	0.450	65	8	8.1	8.95	46813	1214.1	166.0	25.81	25.81	27.56	22.6	*
8/8.1/9.0/7	0.450	65	8	8.1	8.95	62769	1214.1				28.53		
8/8.1/9.0/8	0.450	65	8	8.1	8.95	69278	1214.1				28.04		
8/8.1/9.9/1	0.499	65	8	8.1	9.93	73035	1492.8	94.4	26.85	29.15	28.59	18.4	*
8/8.1/9.9/2	0.499	65	8	8.1	9.93	71278	1492.8		26.95	29.19	28.07	20.5	
8/8.1/9.9/3	0.500	65	8	8.1	9.95	62433	1498.8		25.19	29.63			
8/8.1/9.9/4	0.500	65	8	8.1	9.95	62433	1498.8		26.15	29.50			
8/8.1/9.9/5	0.500	65	8	8.1	9.95	60839	1498.8	91.9	27.12	29.73	27.60	19.9	**
8/8.1/9.9/6	0.500	65	8	8.1	9.95	56979	1498.8		26.24	26.24			
8/8.1/9.9/7	0.500	65	8	8.1	9.95	56979	1498.8				30.08		
8/14.5/9.0/1	0.400	116	8	14.5	7.96	41463	301.2	45.6	26.72	30.49			*
8/14.5/9.0/2	0.450	116	8	14.5	8.95	70188	381.2	97.4	26.06	30.05	27.83	17.5	*
8/14.5/9.0/3	0.450	116	8	14.5	8.95	70188	381.2	70.7	26.51	29.01	27.80	14.8	*
8/14.5/9.0/4	0.450	116	8	14.5	8.95	74371	381.2	105.5	26.16	29.42	27.36	18.1	*
8/14.5/9.0/5	0.450	116	8	14.5	8.95	74713	381.2	67.6		29.52	27.17	19.6	*
8/14.5/9.0/6	0.450	116	8	14.5	8.95	46154	381.2	96.2	26.72		27.95	20.9	*
8/14.5/9.0/7	0.450	116	8	14.5	8.95	71907	381.2		26.04	30.22			
8/14.5/9.0/8	0.450	116	8	14.5	8.95	76829	381.2		26.69	29.53			
8/14.5/9.9/1	0.500	116	8	14.5	9.95	49708	470.6	70.9		29.93	27.27	23.2	*
8/14.5/9.9/2	0.500	116	8	14.5	9.95	50049	470.6		25.87				
8/14.5/10.9/1	0.550	116	8	14.5	10.94	59105	569.4	71.3	26.43	28.59	27.56	21.7	*
8/14.5/11.9/1	0.600	116	8	14.5	11.94	60666	677.7		26.39	29.95			
4/10.0/9.9/1	0.125	40	4	10.0	9.95	26007	989.5	141.8	25.51	25.51			*
4/10.0/11.9/1	0.150	40	4	10.0	11.94	30661	1424.8	145.0	25.52	25.52	27.28	23.3	*
4/10.0/11.9/2	0.150	40	4	10.0	11.94	31098	1424.8	144.1	25.47	25.47			*
4/10.0/13.9/1	0.175	40	4	10.0	13.93	48678	1939.4	90.9	25.49	25.49	26.94	28.4	**
4/10.0/15.9/1	0.200	40	4	10.0	15.92	42381	2533.0	93.1	25.05	25.05	27.35	25.6	*
4/10.0/15.9/2	0.200	40	4	10.0	15.92	58258	2533.0	166.1	25.46	25.46	27.54	24.7	**
4/10.0/17.9/1	0.225	40	4	10.0	17.90	63819	3205.9	123.9	25.93	25.93	27.53	23.3	**
4/10.0/19.9/1	0.250	40	4	10.0	19.89	52200	3957.9	96.3	25.26	25.26			*
4/16.3/15.9/1	0.200	65	4	16.3	15.92	49947	959.3	188.7	25.79	25.79	28.08	24.1	*
4/16.3/19.9/1	0.250	65	4	16.3	19.89	71250	1498.8	103.9	25.57	25.57	27.53	22.9	*
4/29.0/19.9/1	0.250	116	4	29.0	19.89	71250	470.6		25.56	25.56			
4/29.0/21.9/1	0.275	116	4	29.0	21.88	76494	569.4	90.7	26.01	26.01	27.39	25.2	**
4/29.0/25.9/1	0.325	116	4	29.0	25.86	98536	795.3	141.4	25.39	25.39	27.29	22.9	*
4/29.0/25.9/2	0.325	116	4	29.0	25.86	91527	795.3	114.4	25.37	25.37			*

* signifies completed runs with equilibrium depth and volume measurements only

** signifies completed runs with scour hole profile measurements

Code for Test No.: diameter (mm)/(H/d)/U_o(m/s)/No. of test for given conditions

Table 4-2: Details of experiments for wall jet tests.

Experiment	a (mm)	U_o (m/s)	Q (L/s)	R (in 10^3)	ρU_o^2 (Pa)	t_d (h)	Temp (°C)	w_p (%)	w_f (%)	S_v (kPa)	Notes
2.33/5.2/1	2.33	5.16	1.73	9.97	26566	96.88	13.1	25.43	27.15	25.3	*
2.33/6.2/1	2.33	6.16	2.07	12.84	37866	128.95	15.9	26.19	26.94	26.8	*
2.33/7.0/1	2.33	6.98	2.34	10.59	48736	101.23	4.7	26.28		22.9	*
2.33/7.2/1	2.33	7.17	2.41	10.73	51444	96.23	4.3	25.73	26.67	28.5	*
2.33/7.2/2	2.33	7.16	2.40	14.48	51154	121.98	14.7	25.63	27.32	22.9	*
2.33/7.4/1	2.33	7.36	2.47	11.36	54214	94.38	5.2	26.04			†
2.33/8.0/1	2.33	7.97	2.67	12.22	63506	163.53	5.0	25.85	27.81	21.1	*
2.33/8.0/2	2.33	8.00	2.69	17.89	63898	101.00	18.7	26.19	27.48	19.6	*
2.33/8.1/1	2.33	8.13	2.73	12.51	66173	167.57	5.1	25.90	27.71	22.9	†
2.33/8.1/2	2.33	8.05	2.70	12.26	64845	122.05	4.8	24.72			†
2.33/8.2/1	2.33	8.18	2.75	12.91	66948	117.33	6.0	25.99	27.17	22.3	*
2.33/8.5/1	2.33	8.52	2.86	12.79	72551	169.78	4.4	25.97	27.12	22.9	†
2.33/8.5/2	2.33	8.46	2.84	12.94	71629	120.67	4.9	26.21	27.87	18.7	*
2.33/8.7/1	2.33	8.67	2.91	13.02	75208	141.42	4.4	25.72			†
2.33/8.8/1	2.33	8.84	2.97	13.32	78132	96.63	4.5	26.51	28.01	23.1	†
2.33/9.0/1	2.33	9.03	3.03	16.37	81443	96.25	10.7	25.93	27.23	21.7	*
2.33/9.3/1	2.33	9.31	3.12	14.08	86636	120.10	4.6	25.90	26.83	26.7	†
2.33/9.7/1	2.33	9.74	3.27	14.13	94872	142.85	3.4	25.88	27.76	24.7	†
2.33/9.5/1	2.33	9.50	3.19	15.00	90330	140.58	6.0		27.53	19.9	*
2.33/9.8/1	2.33	9.85	3.31	18.64	96926	146.08	12.3	26.02	27.38	21.1	*
2.33/10.2/1	2.33	10.23	3.43	21.29	104503	126.00	15.8	25.81	27.99	22.9	*
2.33/11.3/1	2.33	11.31	3.80	20.79	127940	93.00	11.2	26.12	27.20	22.9	*
2.33/11.7/1	2.33	11.66	3.91	21.03	135824	97.00	10.5	26.35	27.58		*
2.33/12.0/1	2.33	12.03	4.04	24.92	144588	93.15	15.6	25.88	27.05	23.8	*
2.33/12.3/1	2.33	12.25	4.11	25.50	149993	100.60	15.8	26.15			*
2.33/12.7/1	2.33	12.72	4.27	27.18	161518	118.18	16.9	25.96			*
2.33/8.9/1/E	2.33	8.89	2.98	13.98	79009	72.00	5.9	25.54			*
2.33/10.5/1/E	2.33	10.54	3.54	15.88	111011	4.00	4.5	26.10	28.06	19.6	*
5.10/4.9/1	5.10	4.86	3.73	17.28	23628	120.42	7.0	25.35	27.24	21.7	*
5.10/6.0/1	5.10	6.04	4.63	20.38	36430	148.95	5.2	25.28	27.63	20.8	*
5.10/6.5/1	5.10	6.54	5.02	22.10	42830	149.23	5.2	25.97	27.32	22.6	*
5.10/7.0/3	5.10	7.03	5.40	23.95	49475	120.00	5.5	25.30	26.95	22.3	*

Code for Test No.: a (mm) / U_o (m/s) / No. of tests for given conditions E=evolution test

† velocity measured using Prandtl Tube

* velocity measured using nozzle pressure

Table 4-3: Eroding water chemistry data for impinging jet tests.

Eroding Water Chemistry Data (City of Edmonton Tap Water)								Measurements				
Month	Major ions - average concentration (mg/L)							Impinging Jet Tests				
	Ca ²⁺ as CaCO ₃	Total Hardness as CaCO ₃	Na ⁺	K ⁺	HCO ₃ ⁻ as CaCO ₃	Cl ⁻	SO ₄ ²⁻	Test Date	Test No.	pH	Conductivity (µs/cm)	Temp (°C)
Apr 1998	86	133	4.7	1.5	72	2.74	59.8	12-Apr-98	8/8.1/8.1/1			6.0
May 1998	84	128	5	1.0	67	2.28	61.3	1-May-98	8/8.1/9.0/7			15.0
								5-May-98	8/8.1/9.0/1			16.0
								28-May-98	8/8.1/9.0/8			19.0
Jun 1998	87	133	4.0	0.8	76	2.08	61.3	3-Jun-98	8/8.1/9.9/2	7.81	273	15.8
								7-Jun-98	8/8.1/9.9/1	7.87	283	16.9
Jul 1998	91	133	9.5	1.4	50	2.29	69.2	8-Jul-98	8/14.5/9.0/6			20.5
								10-Jul-98	8/14.5/9.0/1	7.87	299	20.1
								17-Jul-98	8/14.5/9.0/2	7.95	288	20.1
								25-Jul-98	8/14.5/9.0/3	7.88	286	22.2
Aug 1998	88	131	3.8	0.8	66	2.04	48.9	3-Aug-98	8/14.5/9.0/4	7.86	279	22.2
								7-Aug-98	8/14.5/9.0/7	7.88	273	23.6
								16-Aug-98	8/8.1/9.0/2	7.87	274	22.3
								25-Aug-98	8/8.1/9.0/3	7.97	274	19.9
Sep 1998	88	133	2.8	0.6	82	2.01	51.4	4-Sep-98	8/8.1/7.0/1	8.09	240	18.9
								11-Sep-98	8/8.1/7.4/1	7.92	277	18.3
								20-Sep-98	8/8.1/8.4/1	8.05	260	15.6
								29-Sep-98	8/8.1/6.1/2	7.97	286	15.1
Oct 1998	88	135	3.9	0.6	70	2.39	54.5	1-Oct-98	8/8.1/6.1/1	8.09	278	14.9
								13-Oct-98	8/8.1/5.0/1	8.28	253	11.8
								22-Oct-98	8/8.1/9.0/3	8.36	248	10.7
								28-Oct-98	8/8.1/9.9/4	8.34	276	11.8
								31-Oct-98	8/8.1/9.9/5	8.22	285	9.7
Nov 1998	79	127	4.2	0.7	72	2.77	53.5	4-Nov-98	8/8.1/9.9/6	7.67	282	7.9
								7-Nov-98	8/8.1/9.9/7	7.67	282	7.9
								11-Nov-98	8/14.5/8.0/1	8.29	292	4.7
								13-Nov-98	8/14.5/9.0/5	8.24	278	4.4
								18-Nov-98	8/14.5/9.9/2	8.27	274	3.7
								21-Nov-98	8/14.5/9.9/1	8.33	277	3.5
Dec 1998	75	125	3.8	0.7	73.0	2.42	55.7	3-Dec-98	8/14.5/10.9/1	8.29	270	6.4
								8-Dec-98	8/14.5/11.9/1	8.24	270	4.1
Jan 1999	73	125	4.4	0.8	71.0	2.52	59.0	15-Jan-99	4/10.0/11.9/1	8.45	206	4.3
								22-Jan-99	4/10.0/15.9/1	8.31	268	5.4
								28-Jan-99	4/10.0/19.9/1	8.32	252	4.9
Feb 1999	76	126	4.0	0.7	74.0	2.83	59.6	8-Feb-99	4/10.0/9.9/1	8.41	270	4.8
								19-Feb-99	4/10.0/11.9/2	8.45	274	4.7
Mar 1999	70	117	4.3	0.6	58.0	4.56	59.5	9-Mar-99	8/8.1/9.0/5			4.8
								16-Mar-99	8/8.1/9.0/6	8.26	285	4.8
May 1999	72	114	7	1.9	45.0	3.38	81.1	12-May-99	4/16.3/15.9/1	8.16	260	11.0
								25-May-99	4/16.3/19.9/1	8.25	274	15.9
Jun 1999	65	115	6	1	65.0	2.52	66.3	8-Jun-99	4/29.0/19.9/1	8.37	272	15.9
								14-Jun-99	4/29.0/25.9/1	8.22	261	18.4
								25-Jun-99	4/29.0/25.9/2	8.35	265	15.4
								30-Jun-99	4/29.0/21.9/1			14.9
Jul 1999	85	126	4.9	1.4	23.0	2.68	84.7	5-Jul-99	4/10.0/13.9/1	8.08	299	14.9
								9-Jul-99	4/10.0/15.9/2	8.05	297	16.8
								14-Jul-99	4/10.0/17.9/1	8.04	280	15.7

*Taken from: Aqualta (1998a-i), Aqualta (1999a-f)

Table 4-4: Eroding water chemistry data for wall jet tests.

Eroding Water Chemistry Data (City of Edmonton Tap Water)								Measurements				
Month	Major ions - average concentration (mg/L)							Wall Jet Tests				
	Ca ²⁺ as CaCO ₃	Total Hardness as CaCO ₃	Na ⁺	K ⁺	HCO ₃ ⁻ as CaCO ₃	Cl ⁻	SO ₄ ²⁻	Test Date	Test No.	pH	Conductivity (µs/cm)	Temp (°C)
Nov 1998	79	127	4.2	0.7	72	2.77	53.5	12-Nov-98	2.33/9.3/1	8.24	276	4.6
								18-Nov-98	2.33/9.7/1	8.27	270	3.4
Dec 1998	75	125	3.8	0.7	73.0	2.42	55.7	7-Dec-98	2.33/8.8/1	8.14	275	4.5
								14-Dec-98	2.33/8.1/1	8.16	268	5.1
Jan 1999	73	125	4.4	0.8	71.0	2.52	59.0	4-Jan-99	2.33/8.5/1			4.4
								12-Jan-99	2.33/8.7/1	8.41	220	4.4
								22-Jan-99	2.33/7.4/1	8.30	271	5.2
								28-Jan-99	2.33/8.1/2	8.34	260	4.8
Feb 1999	76	126	4.0	0.7	74.0	2.83	59.6	11-Feb-99	2.33/7.0/1	8.38	267	4.7
								17-Feb-99	2.33/7.2/1	8.46	273	4.3
Mar 1999	70	117	4.3	0.6	58.0	4.56	59.5	15-Mar-99	2.33/8.0/1	8.23	280	5.0
								30-Mar-99	2.33/8.5/2	8.19	278	4.9
Apr 1999	76	116	8.0	2.9	47.0	5.42	97.0	6-Apr-99	2.33/8.2/1	7.93	311	6.0
								13-Apr-99	2.33/9.5/1	7.83	265	6.0
May 1999	72	114	7	1.9	45.0	3.38	81.1	3-May-99	2.33/9.8/1	8	289	12.3
								13-May-99	2.33/11.3/1	8	260	11.2
								19-May-99	2.33/9.0/1	8.44	272	10.7
								25-May-99	2.33/10.2/1	8.25	277	15.8
Jun 1999	65	115	6	1	65.0	2.52	66.3	8-Jun-99	2.33/6.2/1	8.36	273	15.9
								15-Jun-99	2.33/8.0/2	8.21	258	18.7
								25-Jun-99	2.33/12.0/1	8.34	264	15.6
								30-Jun-99	2.33/13.6/1			15.6
Jul 1999	85	126	4.9	1.4	23.0	2.68	84.7	5-Jul-99	2.33/13.5/1	8.18	300	15.1
								9-Jul-99	2.33/12.7/1	8.04	298	16.9
								15-Jul-99	2.33/12.3/1	8.03	278	15.8
Sep 1999	81	128	3.7	0.8	80.0	2.36	55.4	9-Sep-99	2.33/7.2/2	8.06	268	14.7
								20-Sep-99	2.33/4.9/1			16.4
								24-Sep-99	2.33/5.2/1	8.12	282	13.1
								30-Sep-99	2.33/11.7/1	8.11	282	10.5
Nov 1999	82	133	3.7	0.6	76.0	2.61	56.3	2-Nov-99	2.33/10.5/1/E	8.05	276	4.5
								22-Nov-99	2.33/8.9/1/E	8.25	259	5.9
Jan 2000	89	145	4.2	0.7	76.0	2.41	58.2	10-Jan-00	5.10/6.5/1	8.33	275	5.2
								20-Jan-00	5.10/7.0/3	8.09	305	5.5
								26-Jan-00	5.10/6.0/1	8.11	331	5.2
Feb 2000	113	170	5.1	0.8	108.0	3.22	60.0	8-Feb-00	5.10/4.9/1	7.97	332	7.0

*Taken from: Aqualta (1998h-i), Aqualta (1999a-h), Epcor (1999), Epcor (2000a-b)

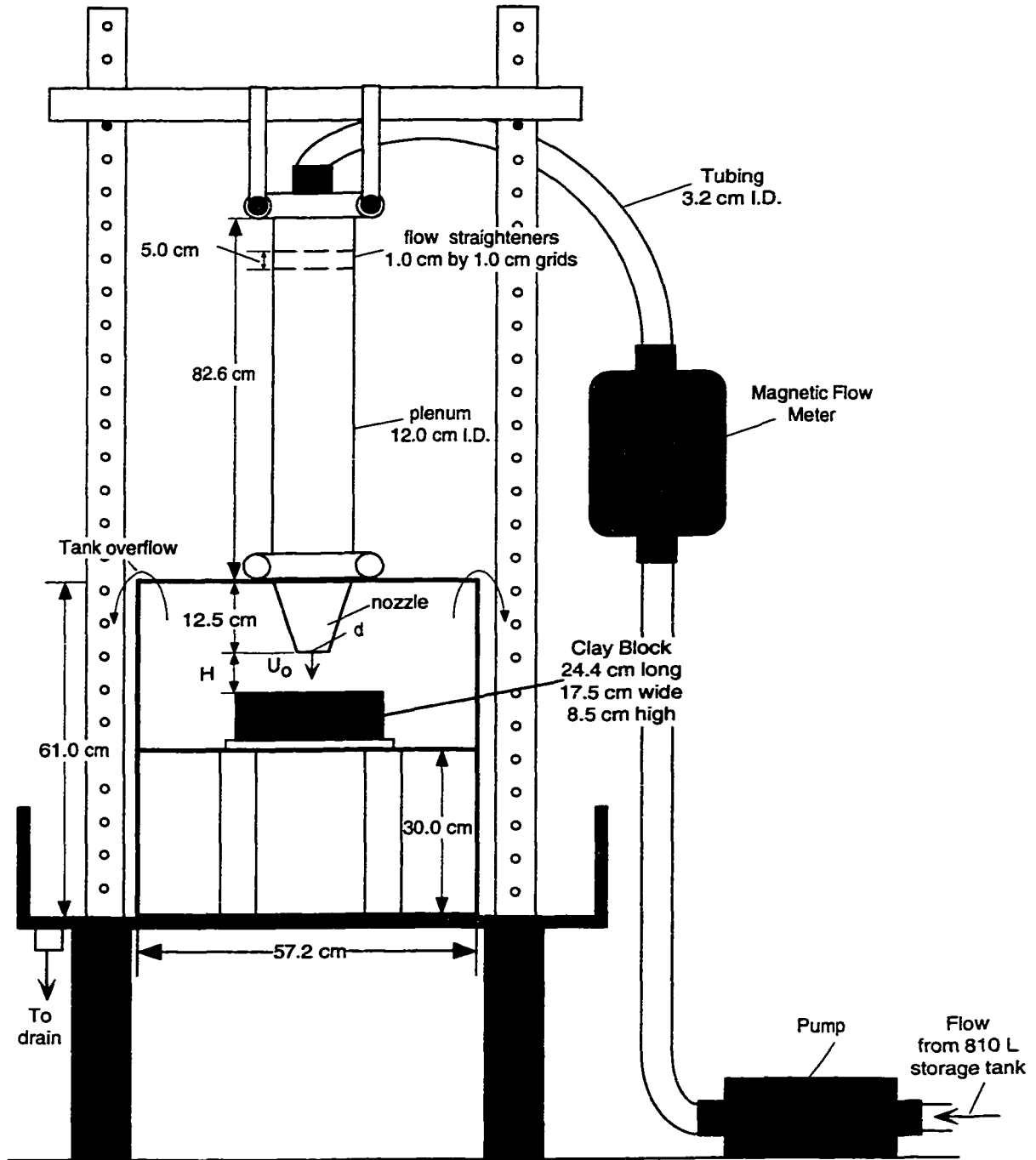


Fig. 4-1: Experimental setup I - impinging jet apparatus.

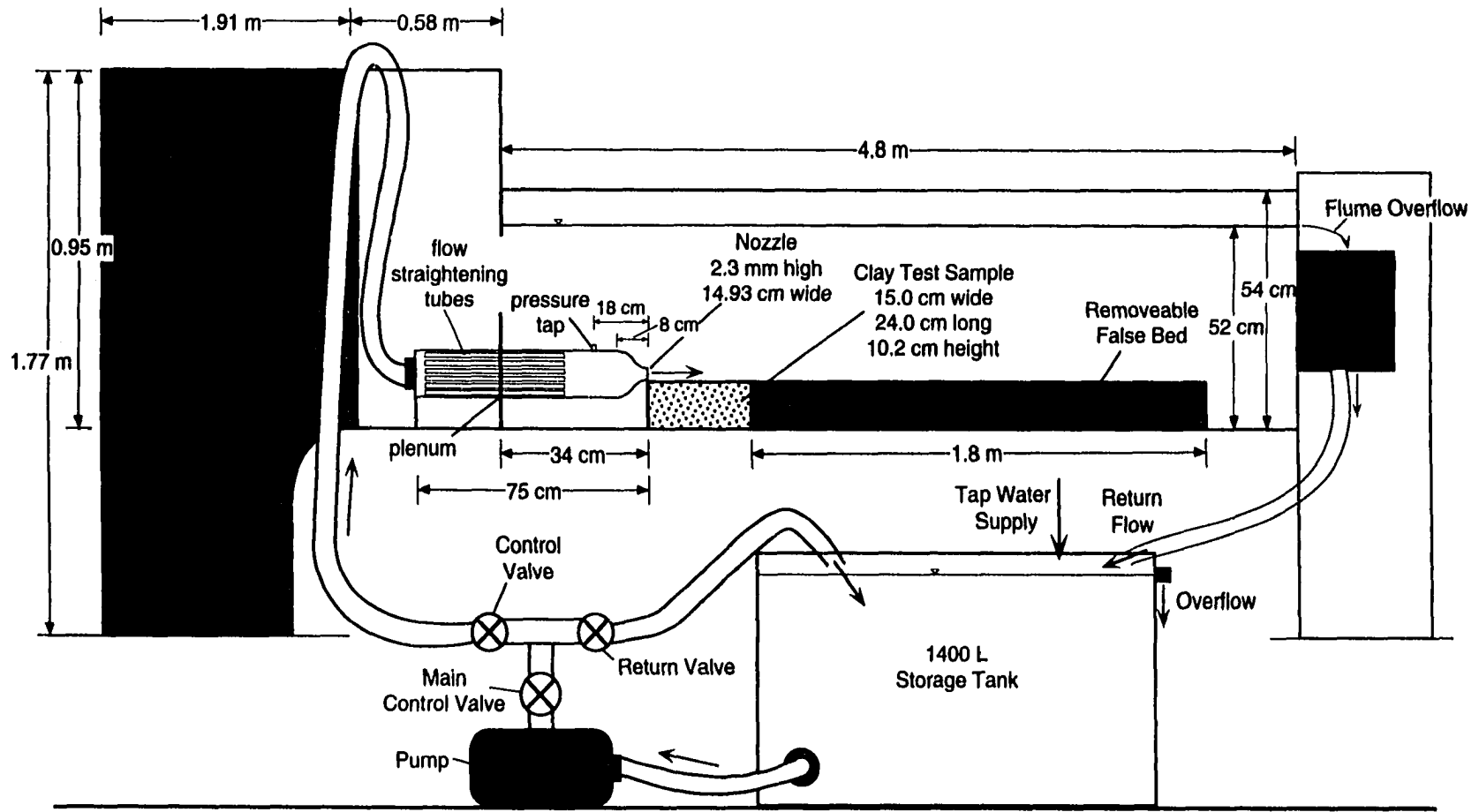


Fig. 4-2: Experimental setup II - wall jet apparatus.

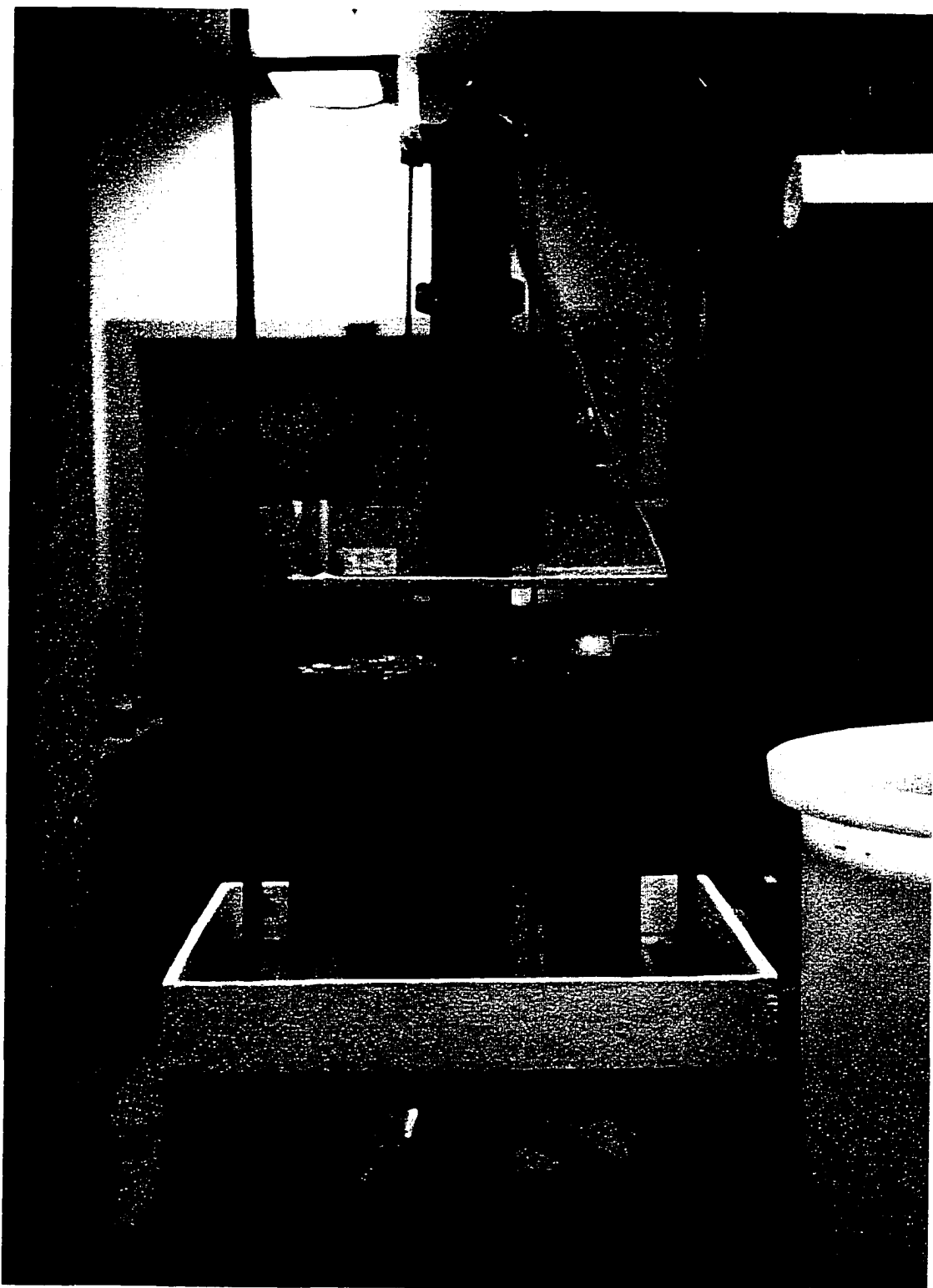
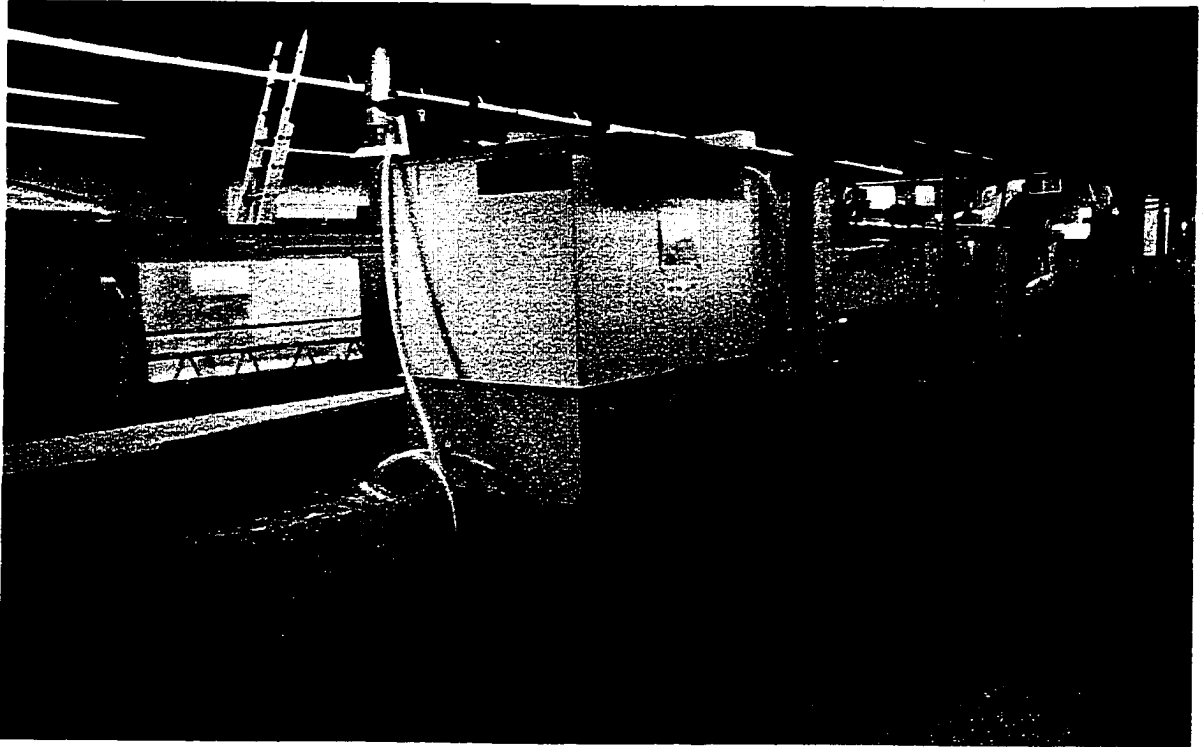
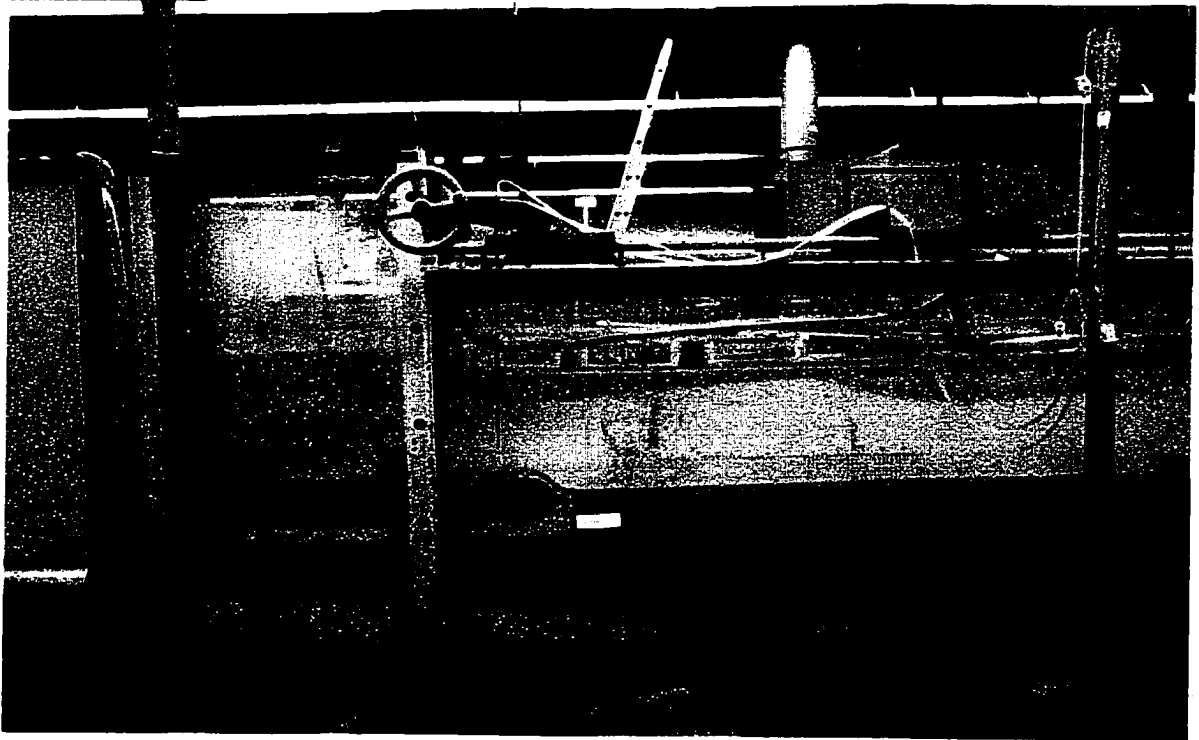


Fig. 4-1: Experimental setup I – impinging jet.

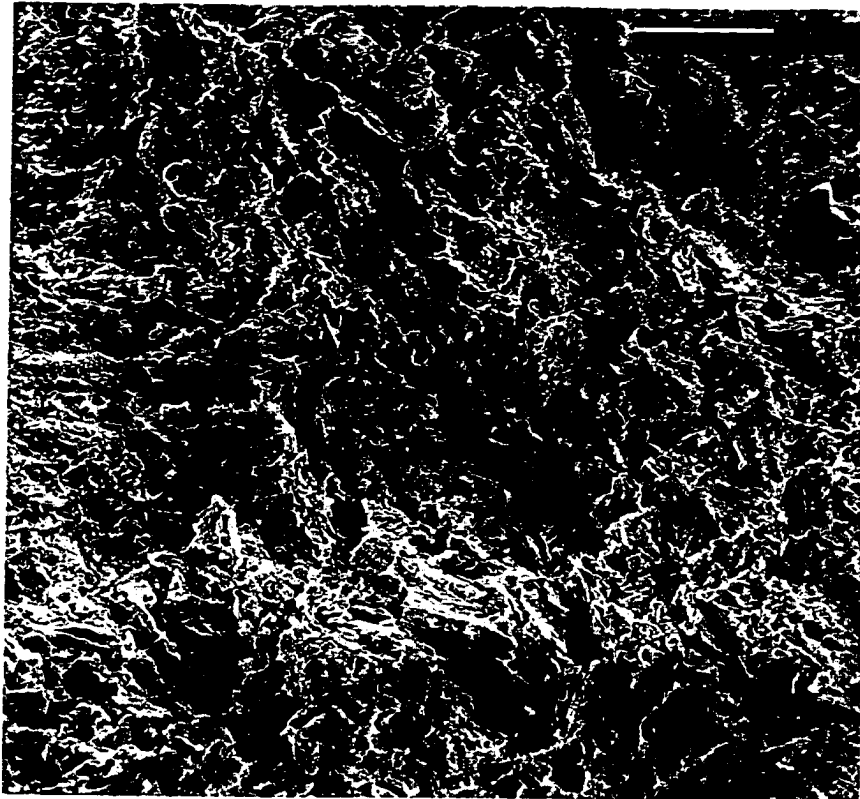


(a)



(b)

Plate 4-2: Experimental setup II – plane wall jet (a) flume, storage tank, and pump (b) front view of nozzle and sample.



(a)



(b)

Plate 4-3: Electron micrograph of the soil (a) at 1500X magnification (b) at 7500X magnification.



Plate 4-4: Section of clay manufacturing equipment where the soil and water are mixed.



Plate 4-5: Section of clay manufacturing equipment from which the clay is extruded.

CHAPTER 5: EROSION CHARACTERISTICS

5.1 Introduction

During both the impinging and wall jet scour experiments, three types of erosion were observed: flake erosion; mass erosion; and rapid surface erosion. In this chapter, the characteristics of these types of erosion and under what conditions they occurred are discussed.

5.2 Flake Erosion

5.2.1 *Impinging Jet Tests*

For the impinging jet tests, the only type of erosion that occurred at the lower shear stresses was flake erosion. In flake erosion, only thin flakes are removed from the clay surface. The flake sizes were typically 1 to 3 mm in diameter (the shape is somewhat circular) and were much less than a millimetre thick. The erosion was confined only to a very thin layer and the erosion rate was very small compared to the other types of erosion. Flake erosion first is seen as a few small pits on the clay surface (shown in Plate 5-1). The scour hole grows when a flake flips out of the edge of one of the pits and is carried away. The edge of the flake closest to the jet is bent and lifted up and the particle is rotated about the edge of the flake that is furthest from the jet before being lifted away (Figure 5-1 (a)). Often another flake just behind the first eroded flake becomes the new eroded particle, so that there is a line scoured out that radiates from the jet centreline due to the continuously eroding flakes (Figure 5-1(b)).

The result of flake erosion was a pattern on the clay surface that was circular or elliptical in shape on the clay surface with a depth of at most a millimetre. Outside this eroded area the clay surface was not affected by the flow. The scour pattern grew in diameter for about 9 h after which it did not change. The typical pattern of scour in its equilibrium state is shown in Plate 5-2. The edge of the scour pattern is jagged

corresponding to the size of the flakes. The size of the scour hole is dependent on the bed shear stress, but was typically 60 to 80 mm in diameter.

There appears to be a critical shear stresses below which this type of erosion does not occur for the tested clay. This was about 15 Pa. At shear stresses just above critical, often a small uneroded patch was left in the centre of the scour hole (like that shown in Plate 5-2(a)). This might be explained by the distribution of shear stress on the clay surface as the shear stress is small near the jet centreline and increases to maximum at distance from the nozzle of about $r=0.14H$ (Beltaos and Rajaratnam, 1974). The size of the flakes did not appear to change with increasing shear stress. This type of erosion likely can be attributed in part to the alignment of the particles during cutting of the surface of the sample (Mitchell, 1993). Flake erosion occurs in combination with mass erosion once the critical shear stress for mass erosion is reached.

5.2.2 Wall Jet Tests

The wall jet tests were never run at a velocity low enough to have only flake erosion occur. Flake erosion was observed on the surface of the mass eroded scour holes past the end of the scour holes as marks on the surfaces of the sample. No significant erosion of the samples occurred due to flake erosion as again the depth of scour due to flake erosion was less than a millimetre. The scour pattern looked like a jagged line between the eroded and uneroded clay surface as shown in Plate 5-3.

5.3 Mass erosion

5.3.1 Impinging Jet Tests

As discussed in Chapter 2, mass erosion is the erosion of small to large chunks of clay from the clay body. A small chunk was about 3 mm long, 2 mm thick, and a few millimetres wide. A large chunk was about 100 mm long, 40 mm thick, and about 30 mm wide and was angular in shape. A mass eroded scour hole with several moderately sized chunks are shown in Plate 5-4. In mass erosion, the chunks of clay appear to be ripped or

torn from the clay surface intermittently. The chunks were removed in much the same way as in flake erosion. First, part of the clay surface was seen to be lifted up from the rest of the surface. As the flow gets underneath this small piece of clay and begins to move it away, the part of the surface still connected to the initially eroded piece is torn off with it to form a larger, angular chunk. The initial part of the chunk lifted up by the flow is always closest to the jet centreline. The part of the chunk that was furthest from the jet is usually the thickest. Often when chunks are removed, there will be a cloud of individual particles that appear almost as a burst during the mass erosion event.

There is a definite critical shear stress below which no mass erosion occurs. Smaller chunks tended to be eroded for lower shear stresses or at longer times. As well, the mass erosion process was intermittent with the frequency of a mass erosion event observed to be lowest at longer times (>24 h). Most mass erosion occurred during the first few hours of a test. Mass erosion was the predominant type of erosion for the impinging jet tests.

5.3.2 Wall Jet Tests

Mass erosion occurred in the wall jet tests in much the same manner as the impinging jet tests. Plate 5-5 shows some eroded chunks from one of the wall jet tests. The chunk size tended to be smaller for the wall jet tests than the impinging jet tests, likely because the tests could not be run at as high of stresses (the clay sample could be completely destroyed by mass erosion within a few minutes at the high stresses). The chunks also tended to be more flat than angular. As in the impinging jet tests, mass erosion was the predominant form of erosion for the wall jet tests.

5.4 Rapid Surface Erosion

5.4.1 Impinging Jet Tests

A form of erosion named "rapid surface erosion" sometimes occurred at very high shear stresses in the impinging jet tests. When this type of erosion occurred, at the start of

the test the jet tank suddenly became very cloudy. After only a short time (about 20 minutes), an obvious symmetrical depression formed in the clay. The surface of the clay was very smooth. It was a particle by particle erosion, as noted by the cloudiness in the jet tank and the lack of any clay chunks in the jet tank. This scour hole was never observed in its equilibrium state as mass erosion always occurred to disturb the scour hole. The maximum time a test was run with only rapid surface erosion occurring was 4 hours. Plate 5-6 shows some typical scour holes eroded by rapid surface erosion.

Two tests in which this type of erosion occurred for the 8 mm nozzle had a maximum shear stress on the bed of about 260 and 400 Pa. During testing for erosion at these higher stresses, the volume of scour was much less than that would be created by mass erosion. When mass erosion does occur at these high stresses, it is thought that it is in conjunction with rapid surface erosion as the scour hole tended to be very smooth, while it appeared to be more rough at the lower shear stresses.

Mass erosion appears to occur in a lower stress range (bed shear stresses) than rapid surface erosion. The lower critical shear stress for mass erosion may be an indicate of strength of groups of aggregates or the chunks of soils. The higher critical shear stress for rapid surface erosion, may indicate that the stresses require to break up the aggregates into particles or remove the aggregates for the larger chunks are higher than those required to break up groups of aggregates or chunks of clay.

5.4.2 Wall Jet Tests

At the beginning of the wall jet tests, the scour holes were always very smooth and there was no noticeable removal of soil chunks. As such, it is thought rapid surface erosion was the mechanisms of erosion for the first few hours of the wall jet tests. Typical scour hole profiles for early in two tests are shown in Plate 5-7.

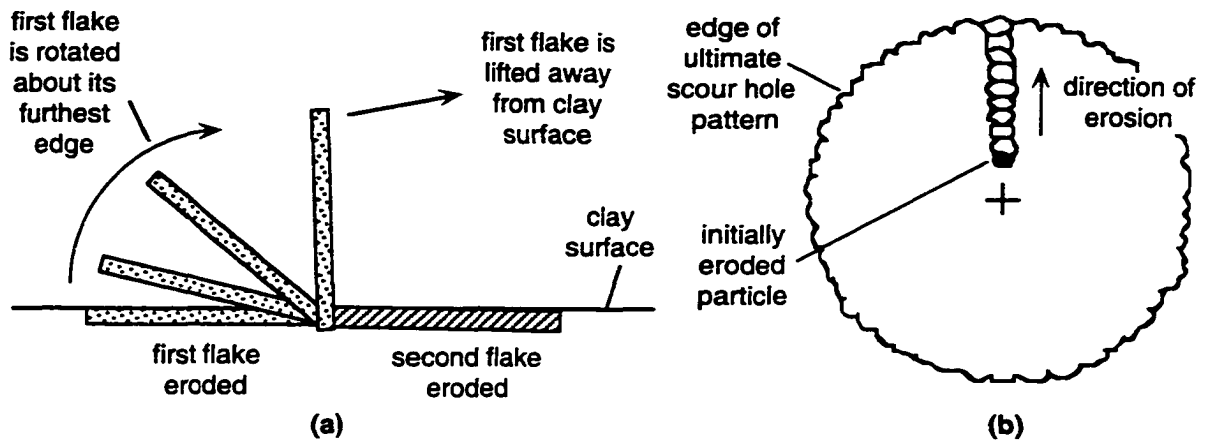
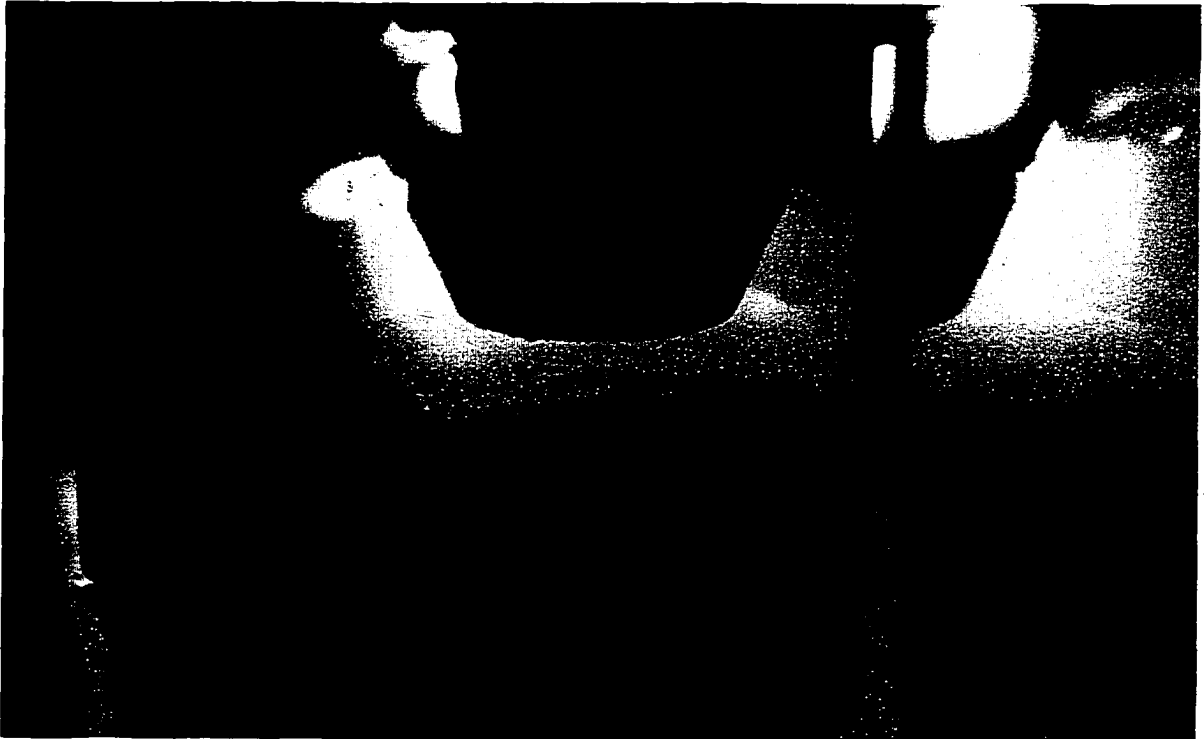


Fig. 5-1: Flake Erosion (a) erosion of a particle (b) in plan.



(a)



(b)

Plate 5-1: Beginning of flake erosion for an impinging jet test (a) early on in the test (b) later in the test.



(a)



(b)

Plate 5-2: Pattern of scour on the surface of the clay for flake erosion for two tests.

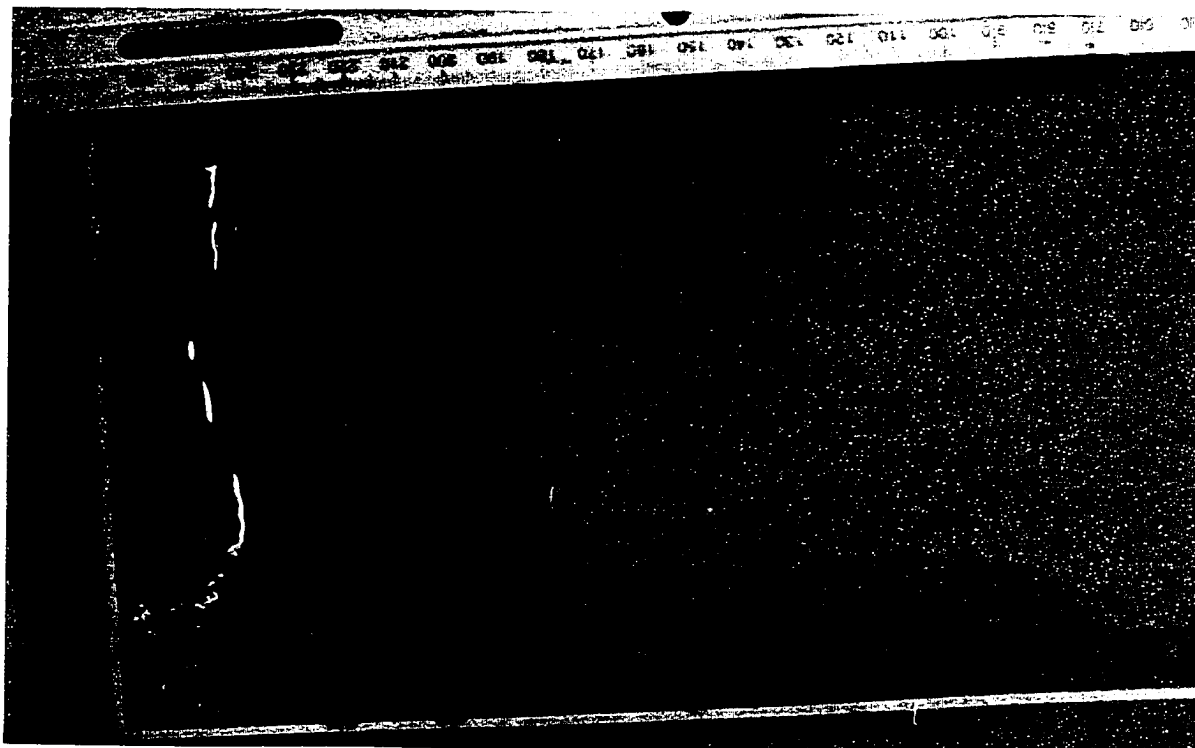


Plate 5-3: Flake erosion pattern in a wall jet test.

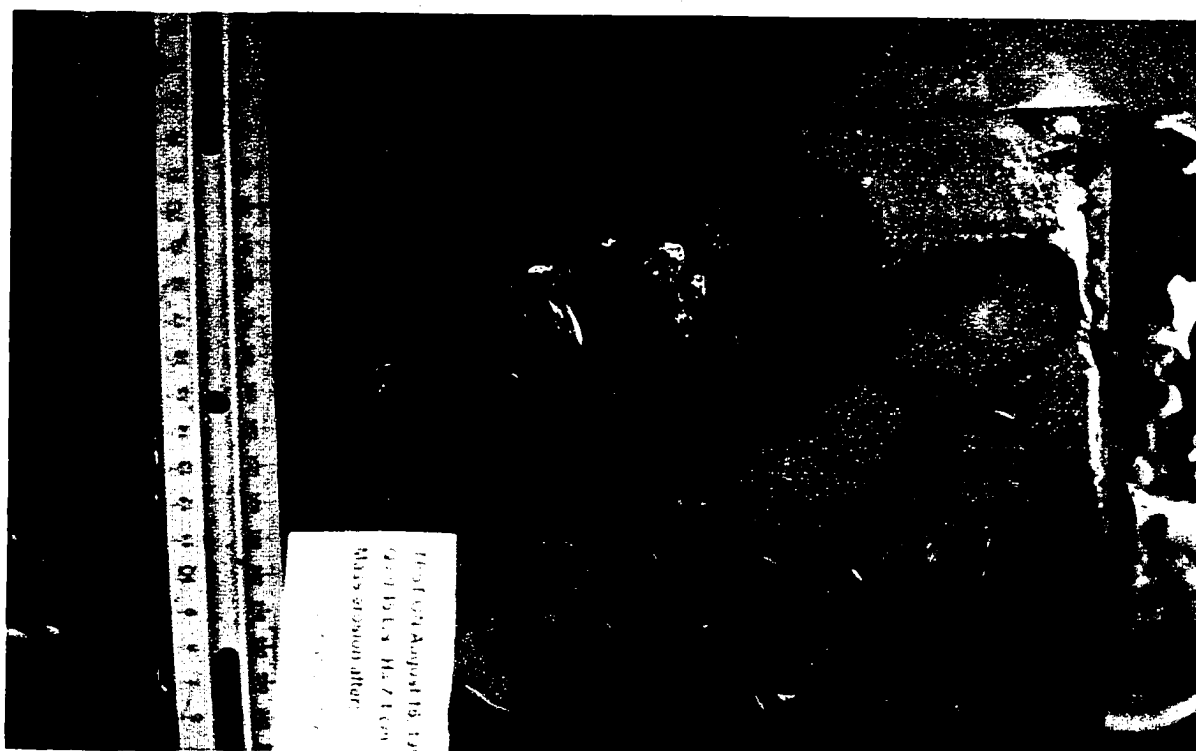
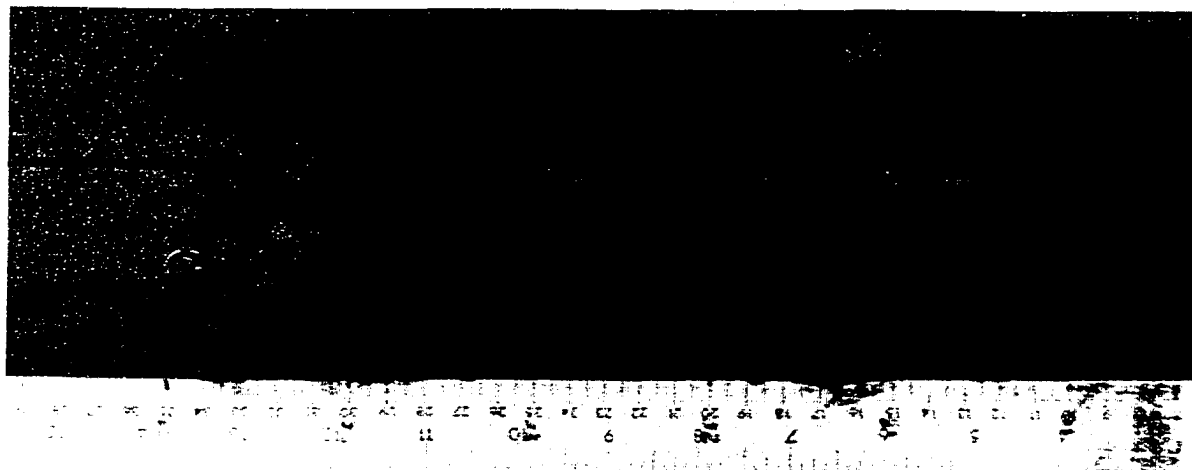
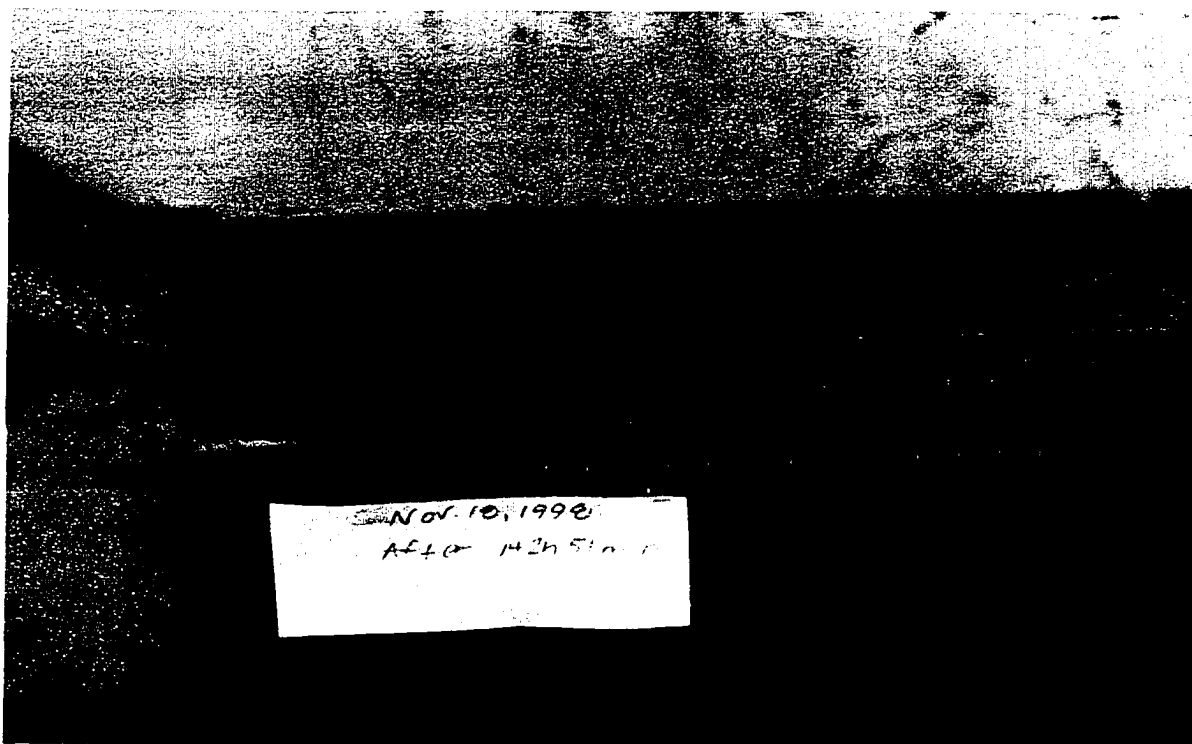


Plate 5-4: Mass eroded hole in impinging jet tests with eroded clay chunks.



(a)



(b)

Plate 5-5: (a) Some eroded chunks from scour hole shown in (b) for wall jet tests.

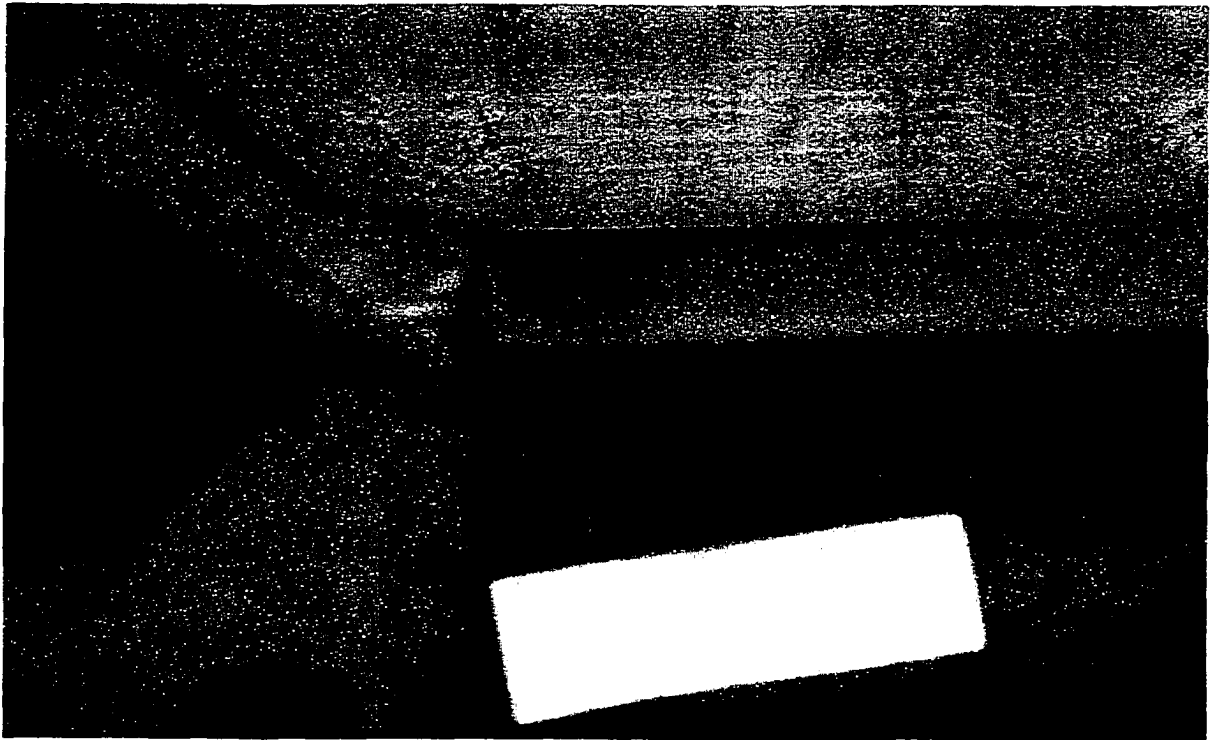


(a)

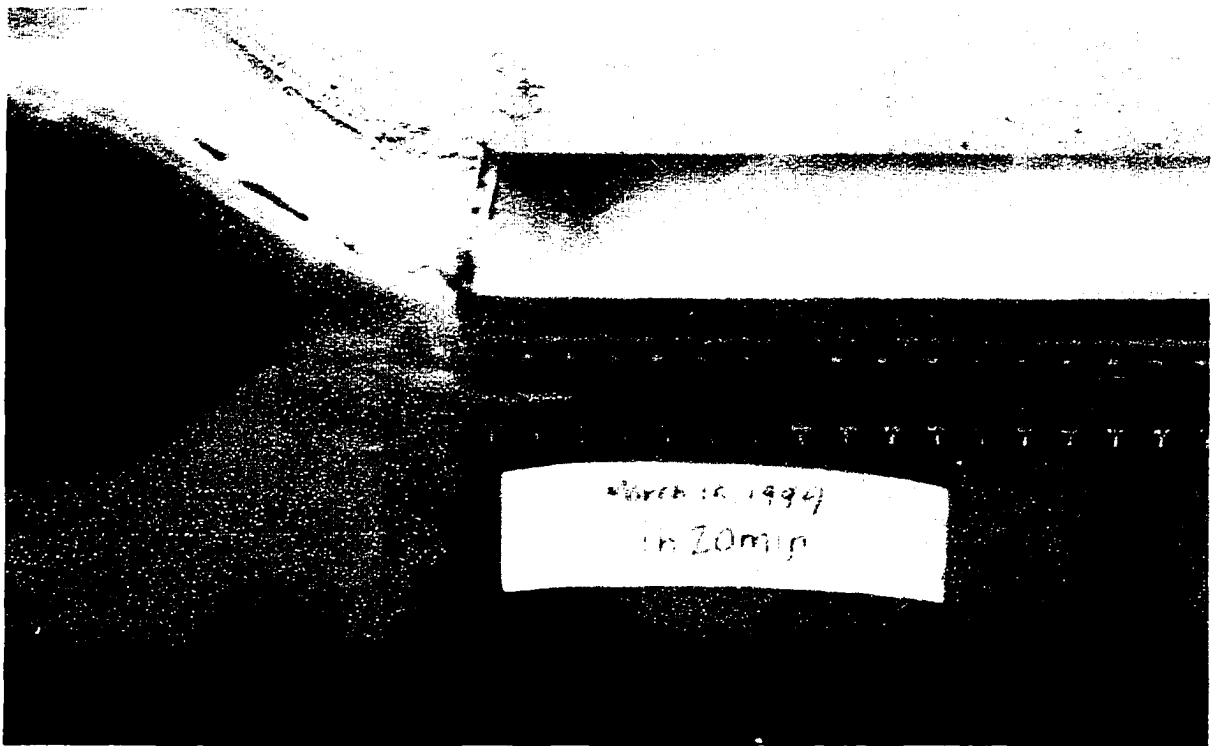


(b)

Plate 5-6: Rapid surface erosion in an impinging jet test (a) after 2 h (b) after 4 h.



(a)



(b)

Plate 5-7: Rapid surface erosion in two wall jet tests (a) after 1 h (b) after 1 h 20 min.

CHAPTER 6: RESULTS AND ANALYSIS OF IMPINGING JETS TESTS¹

6.1 Introduction

As found in the review of the literature on jet erosion of clays, vertical circular turbulent impinging jets are often used as a means to create erosion in erodibility testing of soils. In many of the studies, the hydraulic properties of the jet were held constant while soils with varying properties were tested. The amount of scour for a given soil was then compared to that found for other soils to give an indication of its erodibility and the soil properties that affect erosion rates. Others have begun to develop methods of evaluating erodibility based on the amount of scour created in a soil using varying properties of the jet such as the velocity, nozzle diameter, and impingement height. However, there has been limited success in developing equations to predict the scour created by these jets.

An attempt is made herein to use dimensional analysis to aid in developing parameters and empirical equations that are appropriate to predict the scour in clay due to a submerged circular turbulent impinging jet. Only the case where the jet is impinging at 90° to the clay surface is considered. Results found in the impinging jet tests of a clay, described in Chapter 4, are presented and analyzed using these parameters. The dimensions of the scour hole considered to be of most concern were the maximum scour depth, the scour depth along the jet centreline, the scour hole radius, and the volume of scour. The centreline scour depth was measured in addition to the maximum scour depth as it was thought that in field erodibility testing of soils with impinging jet devices, it may be easier to measure the scour along the jet centreline rather than trying to find the maximum scour depth (this is not necessarily along the jet centreline) and may give more consistent results. In addition to the above scour hole dimensions, the scour hole profiles are also analyzed.

¹ The main content of this chapter has been accepted for publication in the ASCE Journal of Hydraulic Engineering.

The study focuses on scour holes that have reached an equilibrium state, where the dimensions of the scour hole do not change over significant periods of time (the scour has become asymptotic to an ultimate state of scour). This was done because it is intuitive that critical shear stress is the appropriate soil “property” to describe the soil erosion resistance for scour at equilibrium state as it is by definition the critical shear stress that controls when scour can no longer occur, whereas a review of the literature showed that there has been some difficulty in finding an appropriate soil property to describe soil erodibility in terms of erosion rates. Allowing the scour holes to reach equilibrium was thought also to better serve the elucidation of this problem, as scour holes in the same state are being compared. Finally, the equilibrium state gives the largest scour that can be expected for given hydraulic conditions giving an appreciation for the maximum possible size of the scour hole. Also presented are observations made of the growth of the scour holes with time.

Since mass erosion was the type of erosion that contributed most to the scour of the clay, the impinging jet tests were run for a range of velocities where mass erosion of the samples occurred. Rapid surface erosion was also observed in the formation of the scour holes, although it did not appear to be the dominant erosion mechanism. Thus the dimensions given in the following are for those scour holes formed primarily by mass erosion. Little concern was placed on the scour created by flake erosion due to the minute amounts of scour it caused.

6.2 Results

Typical scour hole profiles found in the impinging jet tests are shown in Figure 6-1 with a definition sketch given in Figure 6-2. Typical profiles are also shown in Plate 6-1. It is seen that the radius of the scour hole is quite distinct. It was also often found that the maximum depth of scour did not occur at the jet centreline.

Erosion first occurred at a small distance away from the jet centreline as shown in Plate 6-2(a) and as might be expected from the observations of Dunn (1959). Whenever conditions permitted, the distance of the nearest edge of the first eroded particle from the jet

centreline, r_j , was measured. This distance varied from 5 to 13 mm, with an r_j/H of 0.8 to 0.2 and an average $r_j/H=0.15$ (Table 6-1). This data is limited because erosion of several clay chunks usually occurred very quickly so that the location of the first eroded particle could not be determined. Some of the variability in this data may be partly attributed to the difficulty in determining the location of the jet centreline on the clay surface during a test. The average value of $r_j/H=0.15$ compares well with the location of the maximum bed shear stress, which occurs at a distance of about $r/H=0.14$ for a smooth bed (Beltaos and Rajaratnam, 1974). This indicates that initiation of erosion occurs in the location of maximum bed shear stress.

Measurements of the evolution of the scour hole showed that the scour hole typically reached an equilibrium state within 80 to 100 h of testing. The typical growth of the scour hole volume, ξ_{∞} , is given in Figure 6-3, with the corresponding growth of the maximum and centreline depths given in Figures 6-4 and 6-5. Photographs of the growth of the scour hole for one of these tests are shown in Plate 6-2. The growth of the scour hole volume, maximum depth, and centreline depth appear to follow a linear relation with the logarithm of time except at times very near the beginning of scour and as the scour hole nears equilibrium. The tests shown in these figures are all at the same hydraulic conditions, but do not fall on the same curve. This may be due to the different sized chunks of clay removed by mass erosion very near the start of each test that may have significantly changed the behavior of flow over each sample. It also may be due to variations in the sample such as the water content and saturation that affected erosion rates of the clay. The scour hole growth data is given in Appendix A, with plots of the growth of the scour hole given in Appendix B. Typically there was more scatter in the relation between maximum depth and time than for either the scour hole volume or centreline scour. This was due to the removal of large chunks of clay that would cause the maximum scour depth to remain constant for long periods during a test. The maximum scour depth was also often not in a consistent location in the scour hole through a test due to this erosion of

chunks. As well, in the earlier times of a test the scour hole profiles tended to be much more irregular in shape than at later times.

6.3 Developing Dimensionless Parameters for Impinging Jet Scour of Clay

6.3.1 Dimensional Analysis for Scour Hole Dimensions at Equilibrium

Results from earlier studies on the scour of clays by submerged vertical circular impinging jets, for example, Moore and Masch (1962) and Hanson (1990), suggest that dimensional analysis can be used to develop parameters to describe the scour hole. As well, in studies of the mechanics of this type of turbulent jet for the case of the jet impinging at 90° to a smooth wall, it has been found that the jet characteristics in the impingement region for large impingement heights ($H > 8.3d$) depend on the momentum flux from the nozzle, the density of the fluid, the height of the jet above the surface, and the viscosity of the fluid (Beltaos and Rajaratnam, 1974). Extending these ideas from jet mechanics to the scour created by these jets and using the critical shear stress to describe the soil erosion resistance, the maximum depth of scour at equilibrium state, ϵ_{∞} , can be considered to be a function of:

$$\epsilon_{\infty} = f_1 \{ M_o, \rho, H, \mu, \tau_c \} \quad (6.1)$$

where:

- M_o = momentum flux from the nozzle ($M_o = \frac{\pi}{4} \rho U_o^2 d^2$)
- d = nozzle diameter
- H = impingement height of the jet
- U_o = velocity of the jet at the nozzle
- ρ = density of the eroding fluid
- μ = dynamic viscosity of the eroding fluid
- τ_c = critical shear stress for mass erosion of the clay

These properties have the dimensions of length (L), mass (M), and time (T) of:

$$\begin{aligned} \epsilon_{\infty} &\rightarrow L \\ M_o &\rightarrow (M/L^3)(L/T)^2 L^2 \rightarrow ML/T^2 \\ \rho &\rightarrow M/L^3 \end{aligned}$$

$$\begin{aligned}
H &\rightarrow L \\
\tau_c &\rightarrow M/(LT^2) \\
\mu &\rightarrow M/(LT)
\end{aligned}$$

Then using the Buckingham π -theorem with the repeating variables M_o , ρ , and H :

$$\pi_1 = M_o^a \rho^b H^c \epsilon_{mso}$$

$$\pi_1 = (ML/T^2)^a (M/L^3)^b L^c L$$

$$\begin{array}{l}
\text{T:} \quad -2a=0 \quad a=0 \\
\text{M:} \quad a+b=0 \quad b=0 \\
\text{L:} \quad a-3b+c+1=0 \quad c=-1
\end{array}$$

$$\therefore \pi_1 = \frac{\epsilon_{mso}}{H}$$

$$\pi_2 = M_o^a \rho^b H^c \tau_c$$

$$\pi_2 = (ML/T^2)^a (M/L^3)^b L^c M/(LT^2)$$

$$\begin{array}{l}
\text{T:} \quad -2a-2=0 \quad a=-1 \\
\text{M:} \quad a+b+1=0 \quad b=0 \\
\text{L:} \quad a-3b+c-1=0 \quad c=2
\end{array}$$

$$\therefore \pi_2 = \tau_c H^2 / M_o$$

$$\text{or } \pi_2 = M_o / (\tau_c H^2)$$

This reduces to:

$$\pi_2 = \frac{\rho U_o^2}{\tau_c} \left(\frac{d}{H} \right)^2$$

$$\pi_3 = M_o^a \rho^b H^c \mu$$

$$\pi_3 = (ML/T^2)^a (M/L^3)^b L^c M/(LT)$$

$$\begin{array}{l}
\text{T:} \quad -2a-1=0 \quad a=-1/2 \\
\text{M:} \quad a+b+1=0 \quad b=-1/2 \\
\text{L:} \quad a-3b+c-1=0 \quad c=0
\end{array}$$

$$\therefore \pi_3 = \mu / (\rho M_o)^{1/2} = \mu / (\rho U_o d)$$

$$\text{or } \pi_3 = \frac{\rho U_o d}{\mu} = \frac{U_o d}{\nu}$$

Therefore:

$$\frac{\varepsilon_{\text{max}}}{H} = f_1 \left\{ \frac{\rho U_o^2}{\tau_c} \left(\frac{d}{H} \right)^2, \frac{U_o d}{\nu} \right\} \quad (6.2)$$

The parameter $\frac{\rho U_o^2 (d/H)^2}{\tau_c}$ can be considered as the ratio of the maximum shear

stress on the bed to the critical shear stress of the soil. Letting $X = \rho U_o^2 \left(\frac{d}{H} \right)^2$, it is

assumed that there is a value of X , X_c , below which there is no mass erosion of the soil which can be related to the critical shear stress of the soil, τ_c . To develop a dimensionless

parameter that is of more general applicability, $\frac{\rho U_o^2 (d/H)^2}{\tau_c}$ can be rewritten as an excess

shear stress term $\frac{X - X_c}{X_c}$. Use of this parameter as $\frac{X - X_c}{X_c}$ assumes that the soil has a

critical shear stress which is not true of dispersive soils. Then to relate τ_c and X_c , τ_c is

related to the maximum bed shear stress created by the jet, τ_{om} , which can be estimated

from (Beltaos and Rajaratnam, 1974):

$$\tau_{\text{om}} = 0.16 \rho U_o^2 \left(\frac{d}{H} \right)^2 = 0.16 X \quad (6.3)$$

This assumes that the jet is impinging on a smooth, flat bed (which may be a reasonable assumption for the initial surface of the soil) and that the jet is at a large impingement height. This gives that $\tau_c = 0.16 X_c$.

The parameter $\frac{\rho U_o d}{\mu}$ can be recognized as the jet Reynolds number at the nozzle.

As discussed in Chapter 3, the bed shear stresses created by a circular impinging jet do not depend strongly on Reynolds number. Thus the Reynolds number can be neglected in the analysis so that:

$$\frac{\epsilon_{\text{max}}}{H} = f_1 \left\{ \frac{X - X_c}{X_c} \right\} \quad (6.4)$$

Following similar dimensional reasoning, expressions can be written for the scour hole volume, ξ_{∞} , centreline scour depth, $\epsilon_{\text{cl}\infty}$, and scour hole radius, r_{∞} , at equilibrium:

$$\frac{\epsilon_{\text{cl}\infty}}{H} = f_2 \left\{ \frac{X - X_c}{X_c} \right\} \quad (6.5)$$

$$\frac{\sqrt[3]{\xi_{\infty}}}{H} = f_3 \left\{ \frac{X - X_c}{X_c} \right\} \quad (6.6)$$

$$\frac{r_{\infty}}{H} = f_4 \left\{ \frac{X - X_c}{X_c} \right\} \quad (6.7)$$

6.3.2 Development of a Dimensionless Time Scale

To nondimensionalize the data of the growth of the scour hole dimensions, a time scale is needed. Previous work by Rajaratnam and Beltaos (1977) showed that the time to reach a scour depth that is some percentage of the equilibrium scour depth can be used to nondimensionalize the test duration for scour of sand by submerged circular impinging jets. Assuming that the time to 80 % of the equilibrium state of a given dimension of the scour hole, t_{80} , can be used to properly nondimensionalize the data of the growth of the scour holes, this time scale must then be predicted based on the hydraulic properties of the jet and the parameters describing the soil erosion resistance. Following the previous analysis it is assumed:

$$t_{80} = f_5 \{ M_o, \rho, H, \mu, \tau_c \} \quad (6.8)$$

This analysis would also apply to time scales that use some other percentage of the equilibrium scour depth.

Again using the Buckingham π -theorem with the repeating variables M_o , ρ , and H :

$$\pi_1 = M_o^a \rho^b H^c t_{80}$$

$$\pi_1 = (ML/T^2)^a (M/L^3)^b L^c T$$

$$\begin{array}{l} \text{T:} \quad -2a+1=0 \quad a=1/2 \\ \text{M:} \quad a+b=0 \quad b=-1/2 \\ \text{L:} \quad a-3b+c=0 \quad c=-2 \end{array}$$

$$\therefore \pi_1 = \frac{t_{80}}{H^2} \sqrt{\frac{M_o}{\rho}} = \frac{t_{80} U_o}{H} \left\{ \frac{d}{H} \right\}$$

with $\pi_2 = \frac{\rho U_o^2}{\tau_c} \left(\frac{d}{H} \right)^2$ and $\pi_3 = \frac{\rho U_o d}{\mu}$ as before. Thus, from these dimensional considerations it can be concluded:

$$t_+ = \frac{t_{80} U_o}{H} \left(\frac{d}{H} \right) = f_1 \left\{ \frac{\rho U_o^2}{\tau_c} \left(\frac{d}{H} \right)^2, \frac{U_o d}{\nu} \right\} \quad (6.9)$$

Rewriting the relation and assuming that the effect of the Reynolds number can be neglected as before:

$$t_+ = f_6 \left\{ \frac{X - X_c}{X_c} \right\} \quad (6.10)$$

6.4 Analysis of Equilibrium State Results

6.4.1 Scour Hole Dimensions at Equilibrium

To test the dimensionless relationships developed above, the scour hole volume at equilibrium was plotted against the parameter X (Figure 6-6(a)). From this the critical value of X below which there is no scour can be estimated as $X_c=300$ Pa. This corresponds to a maximum shear stress on the bed and thus a critical shear stress of the clay about 48 Pa. Figure 6-6(b-g) show the different shapes of scour holes corresponding to the points indicated in Figure 6-6(a). The low values of scour hole volume for points 7, 8, and 9 are due to the different scour hole shapes for these tests, which were narrow and deep. In this type of scour hole, the jet was almost completely reversed or "strongly deflected" (SD) (Figure 6-7(a)). The other scour holes were wide and shallow with a "weakly deflected" jet (WD) (Figure 6-7(b)). The reduction in scour hole volume for the

strongly deflected scour holes is likely due to a decrease in the momentum of the jet caused by the entrainment of the fluid that is turned in the direction opposite the jet in the deep scour hole (i.e. the momentum of the jet is reduced by the entrainment of its own return flow). For one test (data point number 6 in Fig 6-6(a)), the strongly deflected jet regime occurred initially (Figure 6-6(f)) but, with time, the edges of the scour hole were eroded away to form a wider scour hole (Figure 6-6(g)).

Using the value for $X_c=300$ Pa found from Figure 6-6, the equilibrium scour data were replotted as functions of the excess stress $\frac{X - X_c}{X_c}$. This was done for the scour hole volume and maximum and centreline scour depth data (Figures 6-8 to 6-10) given in Table 6-2. The results show the scour hole dimensions are well correlated with $\frac{X - X_c}{X_c}$ and can be given by the equations:

$$\frac{\sqrt[3]{\epsilon_{\infty}}}{H} = 0.37 \left\{ \frac{X - X_c}{X_c} \right\}^{0.51} \quad (6.11)$$

$$\frac{\epsilon_{\text{max}}}{H} = 0.19 \left\{ \frac{X - X_c}{X_c} \right\}^{0.74} \quad (6.12)$$

$$\frac{\epsilon_{\text{cl}}}{H} = 0.17 \left\{ \frac{X - X_c}{X_c} \right\}^{0.79} \quad (6.13)$$

with respective correlation coefficients \bar{R}^2 of 0.87, 0.87, and 0.86. The data for the strongly deflected regime scour holes were not included in the curve fits for the scour hole volume as this introduced significant scatter, but were included with the data for the maximum and centreline scour depths. There was not enough data to develop a predictive equation for the scour hole volume for the strongly deflected jet regime.

The different relations given for the maximum and centreline scour depths reflect the observation that the maximum depth of scour did not always occur at the jet centreline. The ratio of $\epsilon_{\text{max}}/\epsilon_{\text{cl}}$ varied from 1.0 to 1.75, with the extreme value 1.75 occurring for a

very shallow scour hole. The percent difference between the maximum and centreline depths ranged 0 to 42.9 %. The ratio of the maximum depth to the centreline depth at equilibrium state did not depend on $\frac{X - X_c}{X_c}$, as shown in Figure 6-11. At the higher values of $\frac{X - X_c}{X_c}$, $\epsilon_{\text{max}}/\epsilon_{\text{cl}} \cong 1$ which indicates that the maximum depth occurs at the jet centreline for the strongly deflected jet regime. For the weakly deflected jet regime, the location of the maximum depth was much more variable.

Four measurements of the radius was taken for each test as two cross-sections were taken for each scour hole in the scour hole profile measurements. The scour hole radius can be estimated from (Figure 6-12):

$$\frac{\bar{r}_{\text{cl}}}{H} = 0.44 \left\{ \frac{X - X_c}{X_c} \right\}^{0.37} \quad (6.14)$$

with an $\bar{R}^2=0.81$. The strongly deflected jet regime data were not included for this correlation. The data on the scour hole used in this relationship are the average of the four radius measurements taken for each test. The radius measurements for a cross-section differed by 0 to 77.3%, while the average radius measurements between the two cross-sections taken for each tests differed by 0 to 29.2%.

The ratio $\frac{\sqrt[3]{\epsilon_{\text{cl}}}}{\epsilon_{\text{cl}}}$ shows a change in the geometry of the scour hole with increasing

$\frac{X - X_c}{X_c}$ (Figure 6-13). The ratio of the cube root of the scour hole can be taken as the average scour depth. At low values of $\frac{X - X_c}{X_c}$, the average scour depth is about 2 to 3.5 times the centreline scour depth indicating that the scour hole is relatively wide and shallow. At values of $\frac{X - X_c}{X_c} \geq 5$, this ratio appears to become constant and equal to

about $\frac{\sqrt[3]{\xi_{\infty}}}{\epsilon_{cl\infty}} \approx 1$, indicating that the scour hole is more narrow and deep. The change in geometry is also suggested by the change in the ratio $\frac{\bar{\Gamma}_{0\infty}}{\epsilon_{cl\infty}}$ (Figure 6-14), which also decreases to a value of $\frac{\bar{\Gamma}_{0\infty}}{\epsilon_{cl\infty}} \approx 1$ for $\frac{X - X_c}{X_c} \geq 5$. Thus, the transition from a wide and shallow scour hole to a more narrow and deep scour hole occurs at about $\frac{X - X_c}{X_c} \cong 5$.

From the earlier discussion of the factors affecting the erosion of cohesive soils in Chapter 2, it was found that the temperature was one of these variables. To examine whether the temperature had a significant effect on the equilibrium dimensions of the scour hole, the scour hole volume data were divided into groups based on the test temperature (Figure 6-15). As there are no obvious trends in the data, the equilibrium dimensions of the scour hole do not appear to depend on temperature for this clay.

6.4.2 Scour Hole Profiles at Equilibrium State

As discussed above, two profile measurements were taken for each scour hole once equilibrium had been reached. One was taken along the length of the block (“lengthwise section”) and the other was taken along the width of the block (“widthwise section”) perpendicular to the first section. Appendix C gives the complete data for the scour hole profile measurements with the scour hole profiles given in Appendix D.

The scour hole profiles nondimensionalized well with both the maximum and centreline scour depth as the scale for the scour measurements and the radius of the scour hole as the scale for the radial distance from the jet centreline (Figures 6-16 and 6-17). No scour data were excluded from the profile data, as the strongly deflected jet regime profiles fell on the same dimensionless scour hole profile as the weakly deflected jet profiles. The dimensionless scour hole profiles fit well with both quadratic and sine functions (Figures 6-18 and 6-19) given by:

$$\frac{\epsilon_{\infty}}{\epsilon_{m\infty}} = 1.08(r/r_{\infty})^2 + 0.03(r/r_{\infty}) - 1.00 \quad (6.15)$$

$$\frac{\epsilon_{\infty}}{\epsilon_{m\infty}} = \sin\left\{\frac{2\pi(r/r_{\infty})}{-3.90} - 1.60\right\} \quad (6.16)$$

$$\frac{\epsilon_{\infty}}{\epsilon_{cl\infty}} = 1.07(r/r_{\infty})^2 + 0.03(r/r_{\infty}) - 1.00 \quad (6.17)$$

$$\frac{\epsilon_{\infty}}{\epsilon_{cl\infty}} = \sin\left\{\frac{2\pi(r/r_{\infty})}{3.93} - 1.54\right\} \quad (6.18)$$

with respective correlation coefficients of $\tilde{R}^2=0.93$, 0.94, 0.93, and 0.94. These equations were developed using the program Kaleidograph which uses an iterative least squares procedure.

Alternatively, the half-width of scour also worked well to nondimensionalize the radial distance from the jet centreline for the scour hole profiles. The half-width, $b_{m\infty}$ is the radial distance from the jet centreline where the scour depth is half the maximum scour depth (i.e. where $\epsilon_{\infty} = \epsilon_{m\infty}/2$). Similarly, $b_{cl\infty}$ is the distance from the centreline where the scour depth is half the centreline depth. The dimensionless profiles using the half-widths are given in Figures 6-20 and 6-21. These profiles were found to be best approximated by a sine function of the form (Figures 6-22 and 6-23):

$$\frac{\epsilon_{\infty}}{\epsilon_{m\infty}} = \sin\left\{\frac{2\pi(r/b_{m\infty})}{-6.30} - 1.54\right\} \quad (6.19)$$

$$\frac{\epsilon_{\infty}}{\epsilon_{cl\infty}} = \sin\left\{\frac{2\pi(r/b_{cl\infty})}{-6.26} - 1.54\right\} \quad (6.20)$$

both with $\tilde{R}^2=0.92$. A Gaussian equation given by (Figure 6-22):

$$\frac{\epsilon_{\infty}}{\epsilon_{m\infty}} = \exp\left\{-0.693\left(\frac{r}{b_{m\infty}}\right)^2\right\} \quad (6.21)$$

also fit the data well for $\frac{r}{b_{m\infty}} \leq 1.0$ but departed strongly from the data at large values of r .

This is because the equation indicates infinite values for the scour hole radius. The data for

the radius of the scour hole and the maximum and centreline half-widths are given in Tables 6-3 and 6-4. The ratio of the radius of the scour hole to the half-width was found to be $\bar{r}_{\text{osc}}/\bar{b}_{\text{moo}} = 1.55$ and $\bar{r}_{\text{osc}}/\bar{b}_{\text{cloo}} = 1.54$ (Figures 6-24 and 6-25).

To predict the half-widths, it was assumed that the half-width followed the same functional relation as the other dimensions of the scour hole:

$$\frac{b_{\infty}}{H} = f_6 \left\{ \frac{X - X_c}{X_c} \right\} \quad (6.22)$$

As for the prediction of the scour hole radius, the average of the data for each scour hole was used for correlation. The maximum and centreline depth half-widths were found to be given by (Figures 6-26 and 6-27):

$$\frac{\bar{b}_{\text{moo}}}{H} = 0.270 \left\{ \frac{X - X_c}{X_c} \right\}^{0.345} \quad (6.23)$$

$$\frac{\bar{b}_{\text{cloo}}}{H} = 0.274 \left\{ \frac{X - X_c}{X_c} \right\}^{0.341} \quad (6.24)$$

with \bar{R}^2 of 0.82 and 0.79 respectively. These data did not include the half-widths for the strongly deflected jet regime. The half-widths for each cross-section differed in a range from 0 to 122.6 % for the half-widths based on the maximum scour depth and 2.0 to 111.8 % for the half-widths based on the centreline scour depth. The variation was reduced for the difference between the section-averaged half-widths for each scour hole, varying from 0.7 to 31.4 % for the maximum depth half-width and 0.7 to 32.4 % for the centreline half-width. The centreline half-width was at most 13.0 % larger than the half-width based on the maximum depth for each section, 7.5 % larger for the averaged values for a section, and 4.1 % larger for the average values for each scour hole.

An often used scale for nondimensionalizing the scour hole dimensions in previous analyses of impinging jet scour by other researchers has been the diameter of the jet d (see Chapter 3). The variation of \bar{b}_{moo}/d with $\frac{X - X_c}{X_c}$ (Figure 6-28) indicates that d is a poor

scale to nondimensionalize the length scale for these data. It also confirms that the impingement height is a much better scale for impinging jet tests with large impingement heights as in the present experiments.

6.5 Growth of the Scour Hole

The data on the growth of the scour hole volume can be nondimensionalized using the time to 80 % of the scour hole volume, t_{80} , for the time scale (Figure 6-29). For the growth of the cube root of the scour hole volume, the maximum scour depth, and the centreline scour depth, the time to 90 % of the respective dimension worked well as the time scale to collapse the data onto one dimensionless curve. These time scales, given in Table 6-5, were estimated from the scour hole data by three methods. If the curve fit for the data for a particular test was good and provided reasonable estimates for the time scale, this time scale was used. If the estimate from the curve fit to the data was not reasonable, a linear interpolation between the data points for the appropriate time interval was used. If the depth corresponding to the required percentage of the given dimension was actually measured, the time of the measurement was used as the time scale.

From dimensional analysis it was found that:

$$t_+ = \frac{t_{80} U_o}{H} \left(\frac{d}{H} \right) = f_4 \left\{ \frac{X - X_c}{X_c} \right\} \quad (6.25)$$

However, a very poor correlation of this dimensionless time scale to $\frac{X - X_c}{X_c}$ was found (Figure 6-30). This weak correlation may result from the same factors that do not allow the growth of the scour hole under the same hydraulic conditions to fall on one curve (shown in Figure 6-3). These include that different sized chunks were removed very near the start of each test and that the initial water contents of the blocks were slightly different resulting in different erosion rates. The time to ultimate scour may also be partly controlled by the time of the submergence of the clay (i.e. the time it takes for the clay to absorb water into

its structure and come to an equilibrium water content is a separate time scale operating for this system).

It is also likely that the critical shear stress is not the only soil parameter needed to describe erosion rates. Studies have shown that a soil with a low critical shear stress may not give high erosion rates and vice versa (Moore and Masch, 1962). This indicates that the erodibility of a soil in terms of its erosion rates may be decoupled from the critical shear stress. Often the erosion rate model $\dot{E} = K(\tau - \tau_c)^m$ is used to predict the erosion rates of a soil (Stein et al. 1993; Hanson 1990), where \dot{E} is the erosion rate, K is the coefficient of erodibility, τ is the shear stress on the surface of the soil, and m is an empirical constant with $m \approx 1$ for clays (Hanson, 1990; Stein et al., 1993). It is likely that a parameter such as K should be included in an analysis in erosion rate problems such as the growth of the scour hole with time.

6.6 Analysis of Errors

The following provides estimates of the errors in the different measured and derived quantities in the impinging jet tests. The errors given are the maximum errors and therefore are the worst case. The calculations used in estimating these errors are based on Topping (1957).

The flow was measured using a Foxboro 2802 Magnetic Flow Meter, with a manufacturer specified accuracy of 1.0 % of the flow rate. The nozzle diameter had an estimated error in measurement of 0.1 mm, which was the precision of the calipers used for the nozzle measurements. This gives an error of 2.5 % for the 4 mm nozzle and 1.25 % for the 8 mm nozzle. The maximum error in the velocity of the jet at the nozzle is thus about 6.0 % for the 4 mm nozzle and 3.5 % for the 8 mm nozzle. The error in measurement in the impingement height was estimated at 1 mm, with a largest percent error then of 2.5 %. Using these errors, the error in the derived parameter $X = \rho U_o^2 \left(\frac{d}{H} \right)^2$ can

thus be estimated as 11.0 % for the 4 mm nozzle and 6.3 % for the 8 mm nozzle. Assuming the percent error in X_c is the same as the error in X , the error in the parameter $\frac{X - X_c}{X_c}$ can be estimated as 22 % and 12.58 % for 4 and 8 mm nozzles respectively.

For the measurements of the scour hole taken with time, the error in measurement of the maximum and centreline depths is about 0.5 mm. For the scour hole volume, the graduated cylinder could be read to 0.1 mL, but the error in measurement in the volume is likely a little larger at 0.2 mL. The smallest non-zero volume measurement (for scour holes at equilibrium) was 0.3 mL. However, since a measurement for this small of a volume was repeated several times the error in measurement could be taken as 0.1 mL giving a 33 % error in the measurement. For the next smallest volume at equilibrium, the 0.2 mL error estimate in the measurement gives a 4.0 % error in the volume. The error in the dimensionless ratio $\frac{\sqrt[3]{\epsilon_{\infty}}}{H}$ is then 3.8 %.

For the scour hole profile measurements taken after the tests (equilibrium state measurements), the point gauge used to measure the maximum and centreline scour depths could be read to 0.1 mm. However, an error in measurement of 0.2 mm will be used. This gives a maximum percent error in the maximum scour depth at ultimate state of 3.0 % and a 3.2 % error in the centreline scour depth at ultimate state. For the dimensionless ratios $\frac{\epsilon_{m\infty}}{H}$ and $\frac{\epsilon_{cl\infty}}{H}$ the errors are then 5.5 % and 5.7 % respectively. For the scour hole radius at ultimate state, an 1 mm error in measurement is estimated. This gives an error for the smallest radius of 5.3 %. For the ratio r/H , the maximum error would then be 7.76 %. For the half-width, b , the half-width is about $0.67r$ so that the error in b should be proportional to r and equal to about 0.7 mm. This gives a maximum error in the half-widths of about 5.4 %. For the dimensionless ratio b/H , the error can then be estimated at about 7.9 %. The errors are summarized in Table 6-6.

6.7 Discussion

These experiments confirm that dimensional analysis is a useful tool in describing the scour of clay by a vertical circular turbulent submerged impinging jet. The scour hole dimensions at equilibrium appear to be a function of $X = \rho U_0^2 \left(\frac{d}{H} \right)^2$, which can be written in the form $\frac{X - X_c}{X_c}$. For the clay tested in this study, X_c was found to be approximately 300 Pa, which corresponds to a critical shear stress of the clay tested in this study of about 48 Pa. The scale of the scour hole dimensions for these tests at a large impingement height ($H/d > 8.3d$) was the impingement height H . The nozzle diameter d was a poor scale for the data. Equations were developed to predict the scour hole dimensions at equilibrium. However these equations are for scour holes predominately formed by mass erosion, and are unlikely to apply to mass erosion in a clay sample that is fissured, disturbed by sampling, slaking, layered, or inhomogeneous. They would also apply only to jets with Reynolds numbers greater than about 10000, when the growth of the jet becomes independent of the Reynolds number (Rajaratnam and Flint-Peterson, 1989).

Two types of scour holes were found, similar to that seen by Moore and Masch (1962) and Hollick (1976), one that is wide and shallow, named the weakly deflected jet regime, and one that is narrow and deep, named the strongly deflected jet regime. Herein, it is suggested that the transition from the weakly to strongly deflected jet regime occurs at about $\frac{X - X_c}{X_c} \cong 5$. The scour hole profiles at equilibrium for both weakly and strongly deflected jet scour hole types are fall on the same dimensionless profile if nondimensionalized by using either ϵ_{∞} or $\epsilon_{cl\infty}$ as a scale for the scour depths and either r_{∞} or b_{∞} as a scale for the radial distance from the jet centreline.

The scour hole dimensions, the cube root of the scour hole volume, the maximum scour depth, and the centreline scour depth, appear to grow in a linear relation with the

logarithm of time except for near the start of a test and as the scour hole dimensions approach equilibrium. These observations are similar to that found in jet scour in cohesionless soils. Tests at the same hydraulic conditions did not fall on the same curve for the growth of the scour hole dimensions. This is thought to be due to different sized chunks of clay being removed near the start of each test that significantly changed the flow characteristics and an influence of slightly different water contents and saturations at the start of the tests on erosion rates.

Table 6-1: Location of first eroded particle.

Test No.	Test Date	U_o (m/s)	d (mm)	H (mm)	$(X-X_c)/X_c$	r_i (mm)	r_i/H
8/8.1/5.0/1	13-Oct-98	4.97	8	65	0.25	12	0.18
8/8.1/6.1/2	29-Sep-98	6.17	8	65	0.92	8	0.12
8/8.1/7.0/1	4-Sep-98	6.96	8	65	1.45	5	0.077
8/8.1/9.0/3	25-Aug-98	8.95	8	65	3.05	9	0.14
8/8.1/9.9/4	28-Oct-98	9.95	8	65	4.00	13	0.20
4/8.1/9.9/6	4-Nov-98	9.95	8	65	4.00	11	0.17

Table 6-2: Scour hole volumes, maximum depths, and centreline depths at equilibrium state.

Test No.	Test Date	Q (L/s)	H (mm)	d (mm)	U _o (m/s)	R	τ_{om} (Pa)	X (Pa)	H/d	Temp (°C)	t _d (h)	$\frac{X-X_c}{X_c}$	ξ_{om} (cm ²)	$\sqrt{\xi_{om}}$ (cm)	ϵ_{om} (cm)	ϵ_{clm} (cm)	ϵ_{om}/H	ϵ_{clm}/H	ξ_{om}/H^3	$\sqrt{\xi_{om}}/H$	Type	
8/8.1/5.0/1	13-Oct-98	0.250	65	8	4.97	31715	60.0	374.7	8.1	11.8	69.78	0.25	0.3	0.67	0.35	0.20	0.054	0.031	0.001	0.103	WD	
8/8.1/6.1/1	1-Oct-98	0.310	65	8	6.17	43241	92.2	576.2	8.1	14.9	76.28	0.92	16.5	2.55	1.30	1.26	0.200	0.194	0.060	0.392	WD	
8/8.1/7.0/1	4-Sep-98	0.350	65	8	6.96	53605	117.5	734.4	8.1	18.9	98.73	1.45	14.5	2.44	1.27	1.27	0.195	0.195	0.053	0.375	WD	
8/8.1/7.4/1	11-Sep-98	0.374	65	8	7.44	56123	134.2	838.6	8.1	18.3	117.43	1.80	30.0	3.11	2.08	2.08	0.320	0.320	0.109	0.478	WD	
8/8.1/8.1/1	12-Apr-98	0.405	65	8	8.06	43647	157.3	983.4	8.1	6.0	68.50	2.28	51.5	3.72	2.10	-	0.323	-	0.188	0.572	WD	
8/8.1/8.4/1	20-Sep-98	0.420	65	8	8.36	58585	169.2	1057.6	8.1	15.6	72.45	2.53	104.0	4.70	4.22	4.22	0.649	0.649	0.379	0.723	WD	
8/8.1/9.0/1	5-May-98	0.450	65	8	8.95	64279	194.2	1214.1	8.1	16.0	124.25	3.05	78.0	4.27	2.80	-	0.431	-	0.284	0.657	WD	
8/8.1/9.0/2	16-Aug-98	0.450	65	8	8.95	76829	194.2	1214.1	8.1	22.3	44.67	3.05	85.0	4.40	3.70	3.50	0.569	0.538	0.310	0.676	WD	
8/8.1/9.0/3	25-Aug-98	0.450	65	8	8.95	69458	194.2	1214.1	8.1	19.9	92.00	3.05	90.0	4.48	3.25	3.25	0.500	0.500	0.328	0.689	WD	
8/8.1/9.0/4	16-Oct-98	0.450	65	8	8.95	62769	194.2	1214.1	8.1	11.8	92.95	3.05	108.0	4.76	4.35	4.35	0.669	0.669	0.393	0.733	WD	
8/8.1/9.0/5	9-Mar-99	0.450	65	8	8.95	46813	194.2	1214.1	8.1	4.8	95.35	3.05	132.0	5.09	4.01	4.00	0.617	0.615	0.481	0.783	WD	
8/8.1/9.0/6	16-Mar-99	0.450	65	8	8.95	46813	194.2	1214.1	8.1	4.8	166.02	3.05	70.0	4.12	3.51	3.45	0.540	0.531	0.255	0.634	WD	
8/8.1/9.9/1	7-Jun-98	0.499	65	8	9.93	73035	238.9	1492.8	8.1	16.9	94.42	3.98	149.0	5.30	3.70	3.70	0.569	0.569	0.543	0.816	WD	
8/8.1/9.9/5	31-Oct-98	0.500	65	8	9.95	60839	239.8	1498.8	8.1	9.7	91.88	4.00	-	-	3.95	3.93	0.608	0.605	-	-	WD	
8/14.5/8.0/1	11-Nov-98	0.400	116	8	7.96	41463	48.2	301.2	14.5	4.7	45.63	0.00	0.0	0.00	0.00	0.000	0.000	0.000	0.000	0.000	0.000	WD
8/14.5/9.0/1	10-Jul-98	0.450	116	8	8.95	70188	61.0	381.2	14.5	20.1	97.42	0.27	24.5	2.90	0.90	0.80	0.078	0.069	0.016	0.250	WD	
8/14.5/9.0/2	17-Jul-98	0.450	116	8	8.95	70188	61.0	381.2	14.5	20.1	70.65	0.27	43.0	3.50	1.40	1.20	0.121	0.103	0.028	0.302	WD	
8/14.5/9.0/4	3-Aug-98	0.450	116	8	8.95	74713	61.0	381.2	14.5	22.2	67.57	0.27	18.0	2.62	0.80	0.75	0.069	0.065	0.012	0.226	WD	
8/14.5/9.0/5	13-Nov-98	0.450	116	8	8.95	46154	61.0	381.2	14.5	4.4	96.15	0.27	13.5	2.38	0.66	0.62	0.057	0.053	0.009	0.205	WD	
8/14.5/9.9/1	21-Nov-98	0.500	116	8	9.95	49708	75.3	470.6	14.5	3.5	70.92	0.57	33.0	3.21	1.56	1.54	0.134	0.133	0.021	0.277	WD	
8/14.5/10.9/1	3-Dec-98	0.550	116	8	10.94	59105	91.1	569.4	14.5	6.4	71.28	0.90	99.0	4.63	2.47	2.24	0.213	0.193	0.063	0.399	WD	
4/10.0/9.9/1	8-Feb-99	0.125	40	4	9.95	26007	158.3	989.5	10.0	4.8	141.83	2.30	8.0	2.00	1.09	1.04	0.273	0.260	0.125	0.500	WD	
4/10.0/11.9/1	15-Jan-99	0.150	40	4	11.94	30661	228.0	1424.8	10.0	4.3	144.95	3.75	22.5	2.82	1.45	1.30	0.363	0.325	0.352	0.708	WD	
4/10.0/13.9/1	5-Jul-99	0.175	40	4	13.93	31099	310.3	1939.4	10.0	14.9	90.92	5.46	65.0	4.02	3.78	3.36	0.945	0.840	1.016	1.005	WD	
4/10.0/15.9/2	9-Jul-99	0.200	40	4	15.92	42382	405.3	2533.0	10.0	16.8	166.07	7.44	85.0	4.40	3.14	2.95	0.785	0.738	1.328	1.099	WD	
4/16.3/15.9/1	12-May-99	0.200	65	4	15.92	49947	153.5	959.3	16.3	11.0	188.72	2.20	34.0	3.24	1.59	1.55	0.245	0.238	0.124	0.498	WD	
4/16.3/19.9/1	25-May-99	0.250	65	4	19.89	71250	239.8	1498.8	16.3	15.9	103.88	4.00	90.0	4.48	3.59	3.52	0.552	0.542	0.328	0.689	WD	
4/29.0/21.9/1	30-Jun-99	0.275	116	4	21.88	76494	91.1	569.4	29.0	14.9	90.65	0.90	20.0	2.71	0.87	0.82	0.075	0.071	0.013	0.234	WD	
4/29.0/25.9/1	14-Jun-99	0.325	116	4	25.86	98538	127.3	795.3	29.0	18.4	141.37	1.65	112.0	4.82	2.88	2.68	0.248	0.231	0.072	0.416	WD	
4/29.0/25.9/2	25-Jun-99	0.325	116	4	25.86	91527	127.3	795.3	29.0	15.4	114.38	1.65	88.0	4.45	2.34	2.34	0.202	0.202	0.056	0.383	WD	
4/10.0/11.9/2	19-Feb-99	0.150	40	4	11.94	31098	228.0	1424.8	10.0	4.7	144.08	3.75	5.0	1.71	0.95	0.90	0.238	0.225	0.078	0.427	SD	
4/10.0/15.9/1	22-Jan-99	0.200	40	4	15.92	42381	405.3	2533.0	10.0	5.4	93.12	7.44	19.5	2.69	2.68	2.68	0.670	0.670	0.305	0.673	SD	
4/10.0/17.9/1	14-Jul-99	0.225	40	4	17.90	63819	512.9	3205.9	10.0	15.7	123.88	9.69	20.0	2.71	3.44	3.44	0.860	0.860	0.313	0.679	SD	
4/10.0/19.9/1	28-Jan-99	0.250	40	4	19.89	52200	633.3	3957.9	10.0	4.9	96.30	12.19	57.0	3.85	4.35	4.35	1.088	1.088	0.891	0.962	SD	

Table 6-3: Scour hole radius data and half-widths based on maximum depth of scour at equilibrium state.

Test No.	Test Date	Q (L/s)	H (cm)	d (mm)	τ_{om} (Pa)	X (Pa)	$(X-X_c)/X_c$	Lengthwise section (all in cm)							Widthwise section (all in cm)							For Test (cm)					
								b_{m+}	b_{m-}	\bar{b}_m	r_{m+}	r_{m-}	\bar{r}_m	ϵ_{m+}	ϵ_{m-}	b_{m+}	b_{m-}	\bar{b}_m	r_{m+}	r_{m-}	\bar{r}_m	ϵ_{m+}	ϵ_{m-}	\bar{b}_m	\bar{r}_m	ϵ_{m+}	ϵ_{m-}
8/8.1/7.0/1	4-Sep-98	0.350	6.5	8	117.5	734.4	1.45	1.625	2.038	1.831	3.00	3.50	3.25	1.27	1.13	2.020	2.130	2.075	4.00	3.00	3.50	1.27	1.27	1.953	3.38	1.27	1.27
8/8.1/7.1/1	11-Sep-98	0.374	6.5	8	134.2	838.6	1.80	2.011	2.138	2.075	3.50	4.00	3.75	2.08	2.08	1.740	2.180	1.960	3.50	4.00	3.75	2.02	2.02	2.017	3.75	2.08	2.08
8/8.1/8.1/1	20-Sep-98	0.420	6.5	8	169.2	1057.6	2.53	2.766	2.305	2.536	4.60	3.30	3.95	4.22	4.22	3.629	2.188	2.908	6.10	3.00	4.55	4.22	4.22	2.722	4.25	4.22	4.22
8/8.1/6.1/1	1-Oct-98	0.310	6.5	8	92.2	576.2	0.92	1.875	1.875	1.875	3.10	3.00	3.05	1.30	1.28		2.759	2.759		4.00	4.00	1.36	1.25	2.170	3.37	1.36	1.28
8/8.1/9.0/4	16-Oct-98	0.450	6.5	8	194.2	1214.1	3.05	2.463	2.669	2.566	3.50	4.40	3.95	4.35	4.35	2.616	2.482	2.549	4.70	3.65	4.18	4.26	4.26	2.558	4.08	4.35	4.35
8/8.1/9.6/5	31-Oct-98	0.500	6.5	8	239.8	1498.8	4.00	2.399	2.797	2.598	4.20	4.00	4.10	3.93	3.91	2.257		2.257	3.90		3.90	3.95	3.93	2.484	4.03	3.95	3.93
8/14.5/9.9/5	13-Nov-98	0.450	11.6	8	61.0	381.2	0.27	2.129	1.671	1.900	3.25	2.70	2.98	0.57	0.57	1.688		1.688	2.75		2.75	0.86	0.82	1.829	2.90	0.86	0.82
8/14.5/9.9/1	21-Nov-98	0.500	11.6	8	75.3	470.6	0.57	1.820		1.820	3.50		3.50	1.51	1.51		3.305	3.305		4.80	4.80	1.56	1.54	2.563	4.15	1.56	1.54
8/14.5/10.9/1	3-Dec-98	0.550	11.6	8	91.1	569.4	0.90	2.735	3.673	3.204	5.00	5.40	5.20	2.28	2.23	3.549	4.130	3.840	5.40	5.80	5.60	2.47	2.24	3.522	5.40	2.47	2.24
4/10.0/11.9/1	15-Jan-99	0.150	4.0	4	228.0	1424.8	3.75	1.232		1.232	2.10		2.10	1.45	1.45	1.248		1.248	2.00		2.00	1.54	1.54	1.239	2.05	1.54	1.54
4/10.0/13.9/1	22-Jan-99	0.200	4.0	4	405.3	2533.0	7.44	1.553	1.650	1.602	2.10	1.90	2.00	2.83	2.83	1.565	1.232	1.399	2.10	1.70	1.90	2.88	2.88	1.500	1.95	2.88	2.88
4/10.0/9.9/1	8-Feb-99	0.125	4.0	4	158.3	989.5	2.30	1.337	1.405	1.371	2.20	2.30	2.25	1.04	1.03	1.663	1.428	1.548	2.75	2.30	2.53	1.09	1.00	1.458	2.39	1.09	1.03
8/8.1/9.0/5	9-Mar-99	0.450	6.5	8	194.2	1214.1	3.05	3.080	3.438	3.259	5.20	5.30	5.25	4.01	4.00	3.019	3.442	3.231	4.80	5.30	5.05	3.98	3.98	3.245	5.15	4.01	4.00
8/8.1/9.0/8	16-Mar-99	0.450	6.5	8	194.2	1214.1	3.05	1.695	2.598	2.148	3.20	3.60	3.40	3.49	3.45	2.758	2.257	2.508	4.20	3.80	4.00	3.51	3.45	2.327	3.70	3.51	3.45
4/16.3/15.9/1	12-May-99	0.200	6.5	4	153.5	959.3	2.20	2.240	2.491	2.368	4.60	3.80	4.20	1.59	1.55	1.918	2.398	2.158	3.70	3.75	3.73	1.59	1.52	2.262	3.96	1.59	1.55
4/16.3/19.9/1	25-May-99	0.250	6.5	4	239.8	1498.8	4.00	3.210	2.577	2.894	4.40	3.80	4.10	3.59	3.52	2.765	2.868	2.817	4.80	3.75	4.28	3.49	3.48	2.855	4.19	3.59	3.52
4/29.0/25.9/1	14-Jun-99	0.325	11.6	4	127.3	795.3	1.65	4.289	3.623	3.956	5.90	6.20	6.05	2.79	2.68	2.848	2.941	2.895	5.70	5.10	5.40	2.68	2.64	3.425	5.73	2.68	2.68
4/29.0/25.9/2	25-Jun-99	0.325	11.6	4	127.3	795.3	1.65	3.077	3.480	3.279	5.50	5.50	5.50	2.34	2.34	3.525	4.022	3.774	5.10	5.90	5.50	2.26	2.25	3.526	6.50	2.34	2.34
4/29.0/21.9/1	30-Jun-99	0.275	11.6	4	91.1	569.4	0.90	2.395	2.762	2.579	3.80	4.40	4.10	0.82	0.82	2.813	3.157	2.985	5.10	5.90	5.50	0.87	0.80	2.782	4.80	0.87	0.82
4/10.0/13.9/1	5-Jul-99	0.175	4.0	4	310.3	1939.4	5.46	1.413	3.112	2.263	2.80	4.60	3.70	3.78	3.34	2.205	1.281	1.743	3.80	2.80	3.30	3.69	3.36	2.003	3.50	3.78	3.36
4/10.0/15.9/2	9-Jul-99	0.200	4.0	4	405.3	2533.0	7.44	2.247	1.970	2.109	6.30	4.70	5.50	3.00	2.95	1.265	4.523	2.894	2.70	8.10	4.40	3.14	2.91	2.501	4.95	3.14	2.95
4/10.0/17.9/1	14-Jul-99	0.225	4.0	4	512.9	3205.9	9.69	1.608	1.638	1.622	2.20	1.90	2.05	3.44	3.44	1.197	1.291	1.244	1.90	1.90	1.90	3.44	3.44	1.433	1.98	3.44	3.44

Table 6-4: Half-widths based on the centreline depth of scour at equilibrium state.

Test No.	Test Date	Q (L/s)	H (cm)	d (mm)	τ_{cm} (Pa)	X (Pa)	$(X-X_c)/X_c$	Lengthwise section (cm)							Widthwise section (all in cm)							For Test (cm)					
								b_{c+}	b_{c-}	\bar{b}_{c+}	\bar{b}_{c-}	\bar{r}_{c+}	\bar{r}_{c-}	\bar{r}_{cm}	ϵ_{c+}	ϵ_{c-}	ϵ_{cm}	\bar{b}_{c+}	\bar{b}_{c-}	\bar{r}_{c+}	\bar{r}_{c-}	\bar{r}_{cm}	ϵ_{c+}	ϵ_{c-}	\bar{b}_{c+}	\bar{b}_{c-}	\bar{r}_{c+}
8/8.1/7.0/1	4-Sep-98	0.350	6.5	8	117.5	734.4	1.45	1.728	2.136	1.932	3.00	3.50	3.25	1.27	1.13	2.020	2.130	2.075	4.00	3.00	3.50	1.27	1.27	2.004	3.38	1.27	1.27
8/8.1/7.1/1	11-Sep-98	0.374	6.5	8	134.2	838.6	1.80	2.011	2.138	2.075	3.50	4.00	3.75	2.08	2.08	1.740	2.180	1.960	3.50	4.00	3.75	2.02	2.02	2.017	3.75	2.08	2.08
8/8.1/8.1/1	20-Sep-98	0.420	6.5	8	169.2	1057.6	2.53	2.766	2.305	2.536	4.80	3.30	3.95	4.22	4.22	3.629	2.186	2.908	6.10	3.00	4.55	4.22	4.22	2.722	4.25	4.22	4.22
8/8.1/6.1/1	1-Oct-98	0.310	6.5	8	92.2	576.2	0.92	1.911	2.145	2.028	3.10	3.00	3.05	1.30	1.26	2.850	2.850		4.00	4.00	1.38	1.25	2.302	3.37	1.38	1.26	
8/8.1/9.0/4	16-Oct-98	0.450	6.5	8	194.2	1214.1	3.05	2.463	2.669	2.566	3.50	4.40	3.95	4.35	4.35	2.616	2.482	2.549	4.70	3.65	4.18	4.26	4.26	2.558	4.06	4.35	4.35
8/8.1/9.6/5	31-Oct-98	0.500	6.5	8	239.8	1498.8	4.00	2.407	2.800	2.604	4.20	4.00	4.10	3.93	3.91	2.262		2.262	3.90		3.90	3.95	3.93	2.490	4.03	3.95	3.93
8/14.5/9.9/5	13-Nov-98	0.450	11.6	8	61.0	381.2	0.27	2.141	1.684	1.913	3.25	2.70	2.98	0.57	0.57	1.750		1.750	2.75		2.75	0.68	0.62	1.858	2.90	0.68	0.62
8/14.5/9.9/1	21-Nov-98	0.500	11.6	8	75.3	470.6	0.57	1.820		1.820	3.50		3.50	1.51	1.51		3.317	3.317		4.80	4.80	1.56	1.54	2.569	4.15	1.56	1.54
8/14.5/10.9/1	3-Dec-98	0.550	11.6	8	91.1	569.4	0.90	2.809	3.699	3.254	5.00	5.40	5.20	2.28	2.23	3.708	4.360	4.034	5.40	5.80	5.60	2.47	2.24	3.644	5.40	2.47	2.24
4/10.0/11.9/1	15-Jan-99	0.150	4.0	4	228.0	1424.8	3.75	1.232		1.232	2.10		2.10	1.45	1.45	1.248		1.248	2.00		2.00	1.54	1.54	1.239	2.05	1.54	1.54
4/10.0/13.9/1	22-Jan-99	0.200	4.0	4	405.3	2533.0	7.44	1.553	1.650	1.602	2.10	1.90	2.00	2.63	2.63	1.565	1.232	1.399	2.10	1.70	1.90	2.68	2.68	1.500	1.95	2.68	2.68
4/10.0/9.9/1	8-Feb-99	0.125	4.0	4	158.3	989.5	2.30	1.343	1.412	1.378	2.20	2.30	2.25	1.04	1.03	1.781	1.487	1.624	2.75	2.30	2.53	1.09	1.00	1.501	2.39	1.09	1.03
8/8.1/9.0/5	9-Mar-99	0.450	6.5	8	194.2	1214.1	3.05	3.083	3.442	3.263	5.20	5.30	5.25	4.01	4.00	3.019	3.442	3.231	4.80	5.30	5.05	3.98	3.98	3.247	5.15	4.01	4.00
8/8.1/9.0/6	16-Mar-99	0.450	6.5	8	194.2	1214.1	3.05	1.703	2.622	2.163	3.20	3.60	3.40	3.49	3.45	2.782	2.271	2.527	4.20	3.80	4.00	3.51	3.45	2.345	3.70	3.51	3.45
4/16.3/15.9/1	12-May-99	0.200	6.5	4	153.5	959.3	2.20	2.277	2.522	2.400	4.60	3.80	4.20	1.59	1.55	1.971	2.436	2.204	3.70	3.75	3.73	1.59	1.52	2.302	3.98	1.59	1.55
4/16.3/19.9/1	25-May-99	0.250	6.5	4	239.8	1498.8	4.00	3.229	2.600	2.915	4.40	3.80	4.10	3.59	3.52	2.775	2.871	2.823	4.80	3.75	4.28	3.49	3.48	2.869	4.19	3.59	3.52
4/29.0/25.9/1	14-Jun-99	0.325	11.6	4	127.3	795.3	1.65	4.352	3.750	4.051	5.90	6.20	6.05	2.79	2.68	2.878	2.968	2.923	5.70	5.10	5.40	2.68	2.64	3.487	5.73	2.68	2.68
4/29.0/25.9/2	25-Jun-99	0.325	11.6	4	127.3	795.3	1.65	3.077	3.480	3.279	5.50	5.50	5.50	2.34	2.34	3.533	4.032	3.783	5.10	5.90	5.50	2.28	2.25	3.531	5.50	2.34	2.34
4/29.0/21.9/1	30-Jun-99	0.275	11.6	4	91.1	569.4	0.90	2.395	2.762	2.579	3.80	4.40	4.10	0.82	0.82	2.875	3.222	3.049	5.10	5.90	5.50	0.87	0.80	2.814	4.80	0.87	0.82
4/10.0/13.9/1	5-Jul-99	0.175	4.0	4	310.3	1939.4	5.46	1.499	3.246	2.373	2.80	4.60	3.70	3.78	3.34	2.283	1.327	1.805	3.80	2.80	3.30	3.69	3.36	2.089	3.50	3.78	3.36
4/10.0/15.9/2	9-Jul-99	0.200	4.0	4	405.3	2533.0	7.44	2.283	1.989	2.138	3.30	4.70	5.50	3.00	2.95	1.297	4.585	2.941	2.70	6.10	4.40	3.14	2.91	2.539	4.95	3.14	2.95
4/10.0/17.9/1	14-Jul-99	0.225	4.0	4	512.9	3205.9	9.69	1.606	1.638	1.622	2.20	1.90	2.05	3.44	3.44	1.197	1.291	1.244	1.90	1.90	1.90	3.44	3.44	1.433	1.98	3.44	3.44

Table 6-5: Time scales for impinging jet scour tests.

Test No.	Test Date	Q (L/s)	H (cm)	d (mm)	U _o (m/s)	τ _{om} (Pa)	X (Pa)	(X-X _c)/X _c	$\sqrt[3]{\xi}$	ε _m	ε _{cl}	ξ
									t ₉₀ (h)	t ₉₀ (h)	t ₉₀ (h)	t ₉₀ (h)
8/8.1/6.1/1	1-Oct-98	0.310	6.5	8	6.17	92.2	576.2	0.92	51.99	66.03	81.57	52.43
8/8.1/7.0/1	4-Sep-98	0.350	6.5	8	6.96	117.5	734.4	1.45	30.02	36.78	84.10	43.54
8/8.1/7.4/1	11-Sep-98	0.374	6.5	8	7.44	134.2	838.6	1.80	24.81	60.09	82.42	37.87
8/8.1/8.1/1	12-Apr-98	0.405	6.5	8	8.06	157.3	983.4	2.28	12.19	51.86		18.51
8/8.1/8.4/1	20-Sep-98	0.420	6.5	8	8.36	169.2	1057.6	2.53	2.69	25.6	28.46	7.80
8/8.1/9.0/1	5-May-98	0.450	6.5	8	8.95	194.2	1214.1	3.05	44.1			49.10
8/8.1/9.0/3	25-Aug-98	0.450	6.5	8	8.95	194.2	1214.1	3.05	25.0	67.7	72.2	48.00
8/8.1/9.0/4	16-Oct-98	0.450	6.5	8	8.95	194.2	1214.1	3.05	17.0	46.4	55.4	33.97
8/8.1/9.0/5	9-Mar-99	0.450	6.5	8	8.95	194.2	1214.1	3.05	31.6	60.45	59.9	42.26
8/8.1/9.0/6	16-Mar-99	0.450	6.5	8	8.95	194.2	1214.1	3.05	48.7	85.0	132.3	74.90
8/8.1/9.9/1	7-Jun-98	0.499	6.5	8	9.93	238.9	1492.8	3.98	1.239		33.1	0.99
8/14.5/9.0/1	10-Jul-98	0.450	11.6	8	8.95	61.0	381.2	0.27	30.8	13.4	27.8	28.43
8/14.5/9.0/4	3-Aug-98	0.450	11.6	8	8.95	61.0	381.2	0.27	17.3	6.27	19.4	20.89
8/14.5/10.9/1	3-Dec-98	0.550	11.6	8	10.94	91.1	569.4	0.90	74.5	63.52	63.8	58.21
4/10.0/9.9/1	8-Feb-99	0.125	4.0	4	9.95	158.3	989.5	2.30	92.9	119.05	122.9	105.90
4/10.0/15.9/1	22-Jan-99	0.200	4.0	4	15.92	405.3	2533.0	7.44	24.9	43.25	43.3	34.43
4/29.0/25.9/1	14-Jun-99	0.325	11.6	4	25.86	127.3	795.3	1.65	83.9	83.38		89.99
4/29.0/25.9/2	25-Jun-99	0.325	11.6	4	25.86	127.3	795.3	1.65	59.1	88.83	100.9	65.79

* italics indicate that the time scale was estimated through linear interpolation.

Table 6-6: Maximum errors in measured and derived quantities.

Quantity	Maximum Error	Notes
Q	up to 1 % of flow rate	from performance specifications of Foxboro 2802 Magnetic Flow Meter
d	2.5 % for the 4 mm nozzle 1.25 % for the 8 mm nozzle	
H	2.5%	
U _o	6.0 % for the 4 mm nozzle 3.5 % for the 8 mm nozzle	
X	11.0 % for the 4 mm nozzle 6.3 % for the 8 mm nozzle	
$\frac{X - X_c}{X_c}$	22.0 % for the 4 mm nozzle 12.6 % for the 8 mm nozzle	
ξ_{∞}	4.0%	very smallest volume measurement had an error of about 33 %
$\epsilon_{m\infty}$	3.0%	
$\epsilon_{c\infty}$	3.2%	
r_{∞}	5.3%	error in the smallest measured value (unaveraged)
b_{∞}	5.4%	error in the smallest measured value (unaveraged)
$\frac{\epsilon_{m\infty}}{H}$	5.5%	
$\frac{\epsilon_{c\infty}}{H}$	5.7%	
$\frac{\sqrt[3]{\xi_{\infty}}}{H}$	3.8%	
$\frac{r_{\infty}}{H}$	7.8%	error in the smallest measured value (unaveraged)
$\frac{b_{\infty}}{H}$	3.2%	error in the smallest measured value (unaveraged)

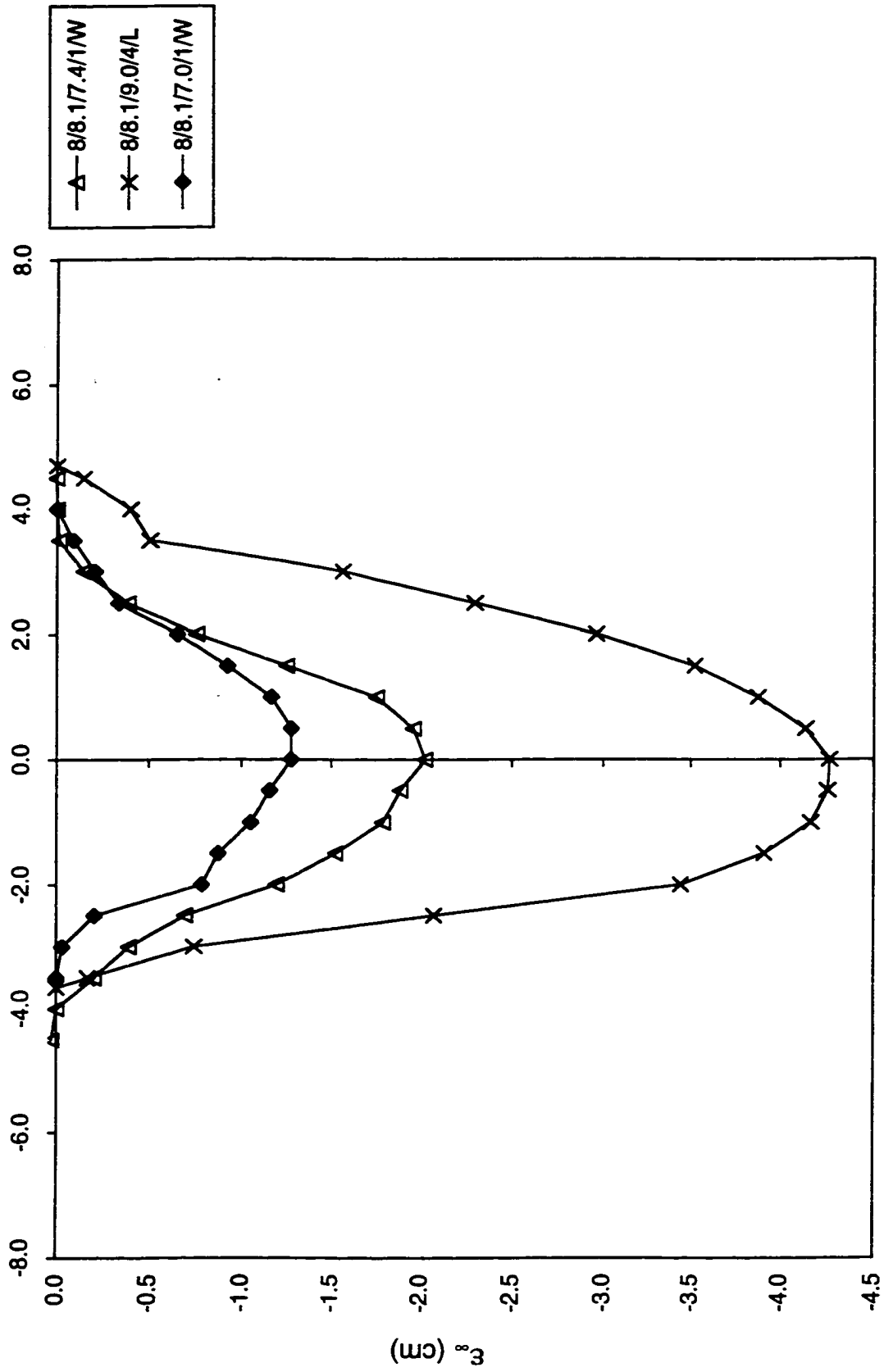


Fig. 6-1: Typical scour hole profiles for the impinging jet tests.

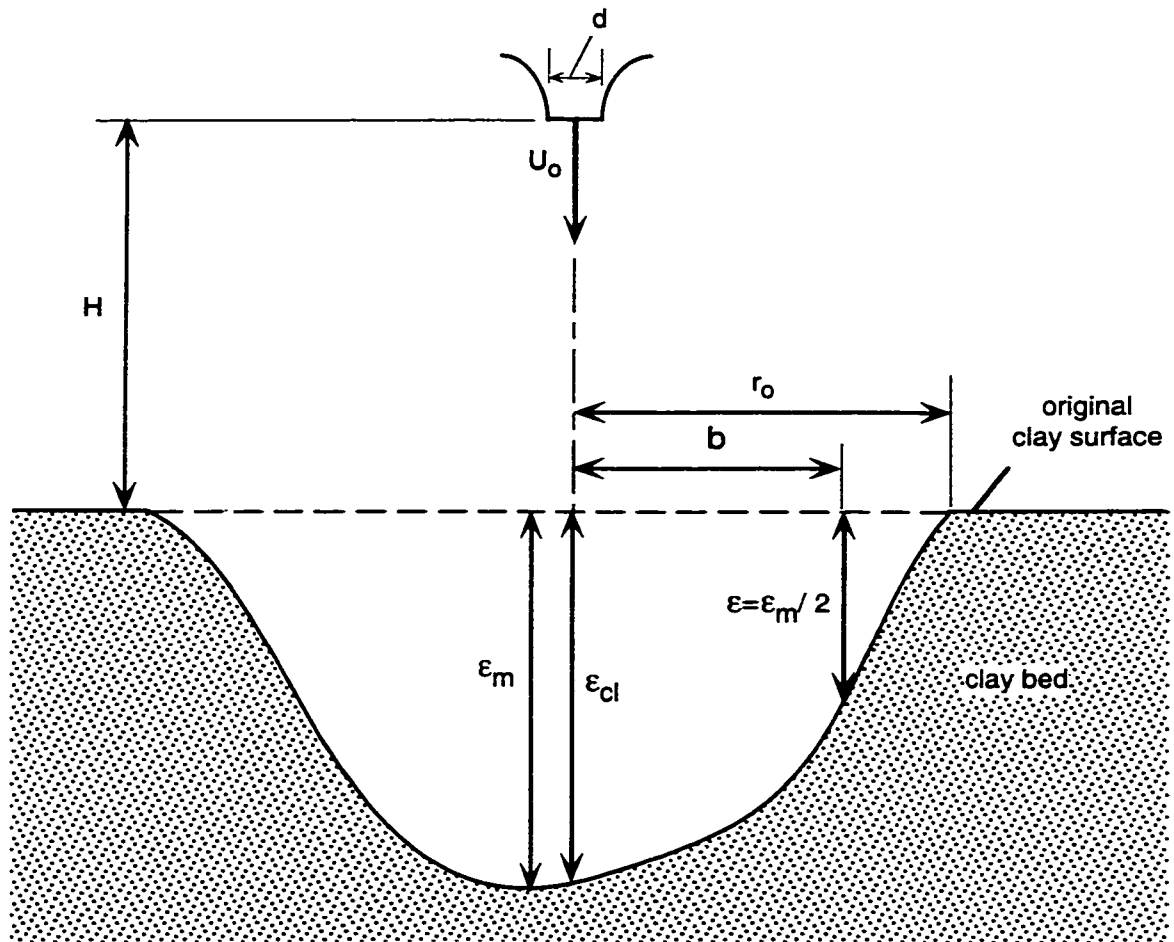
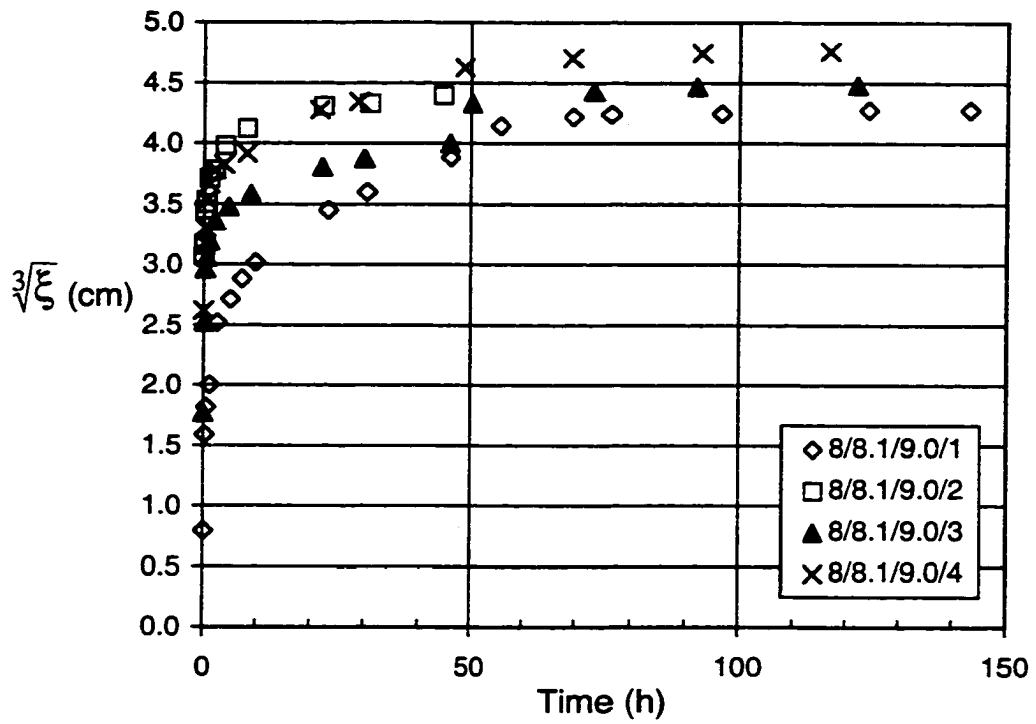
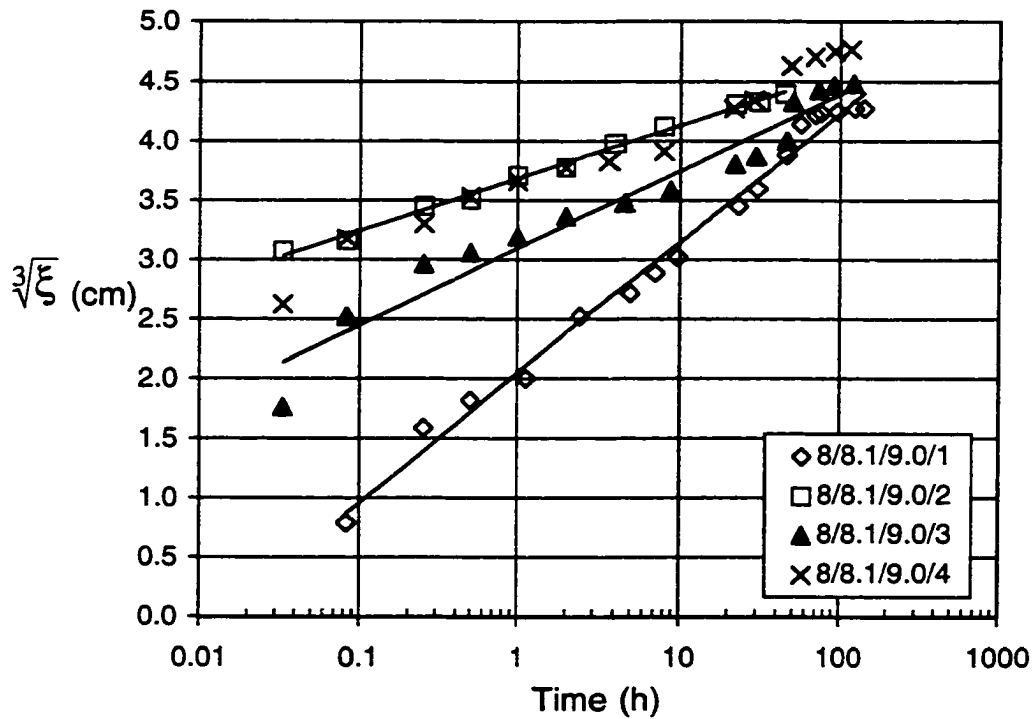


Fig. 6-2: Definition sketch for impinging jet tests.

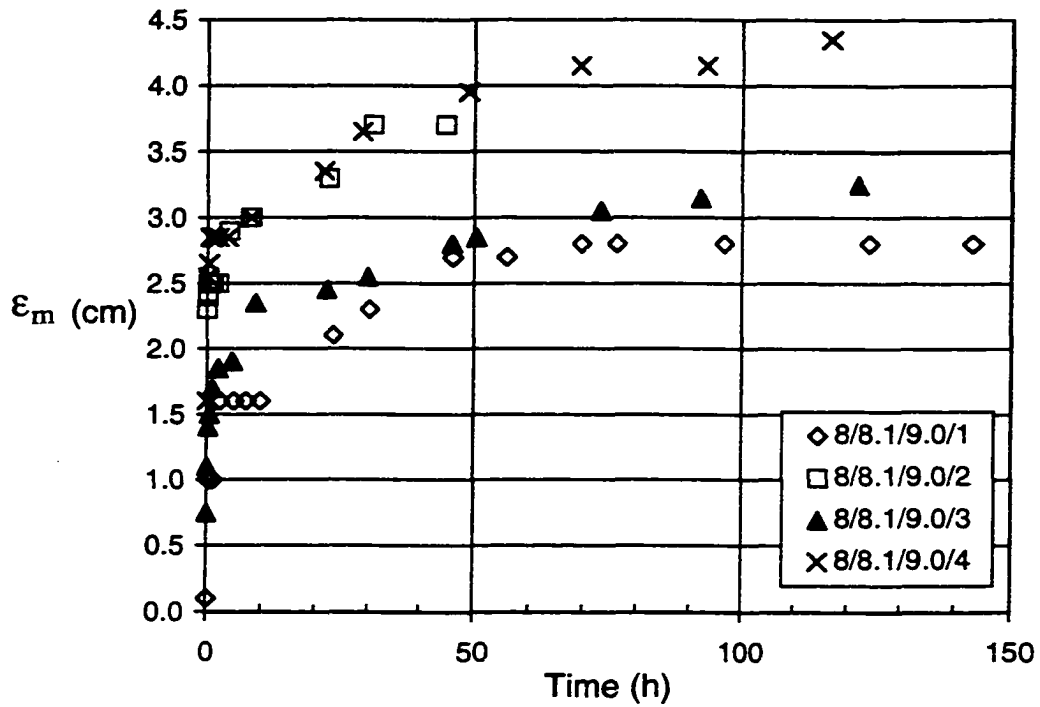


(a)

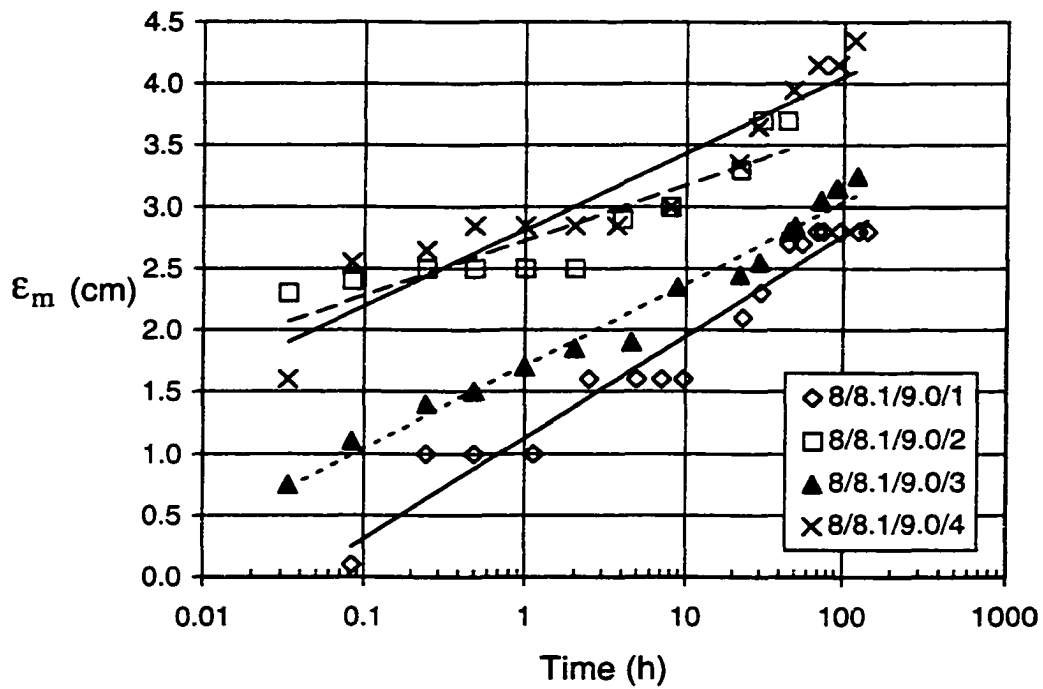


(b)

Fig. 6-3: Growth of the scour hole volume (a) arithmetic scale (b) semi-log plot (all tests at $X=1214$ Pa)

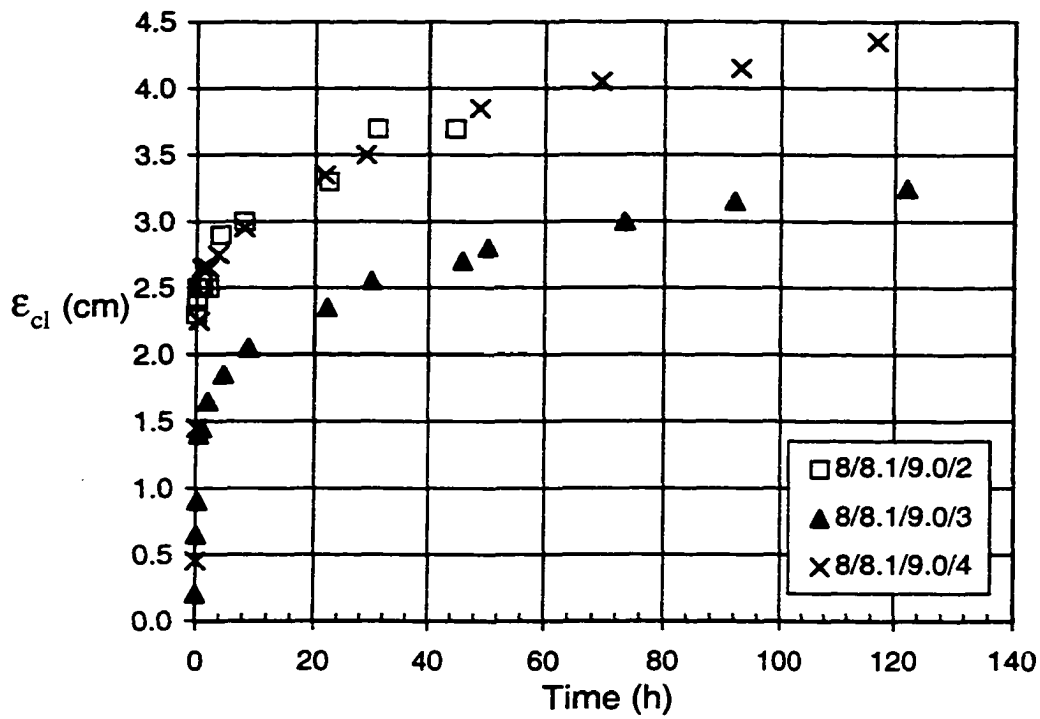


(a)

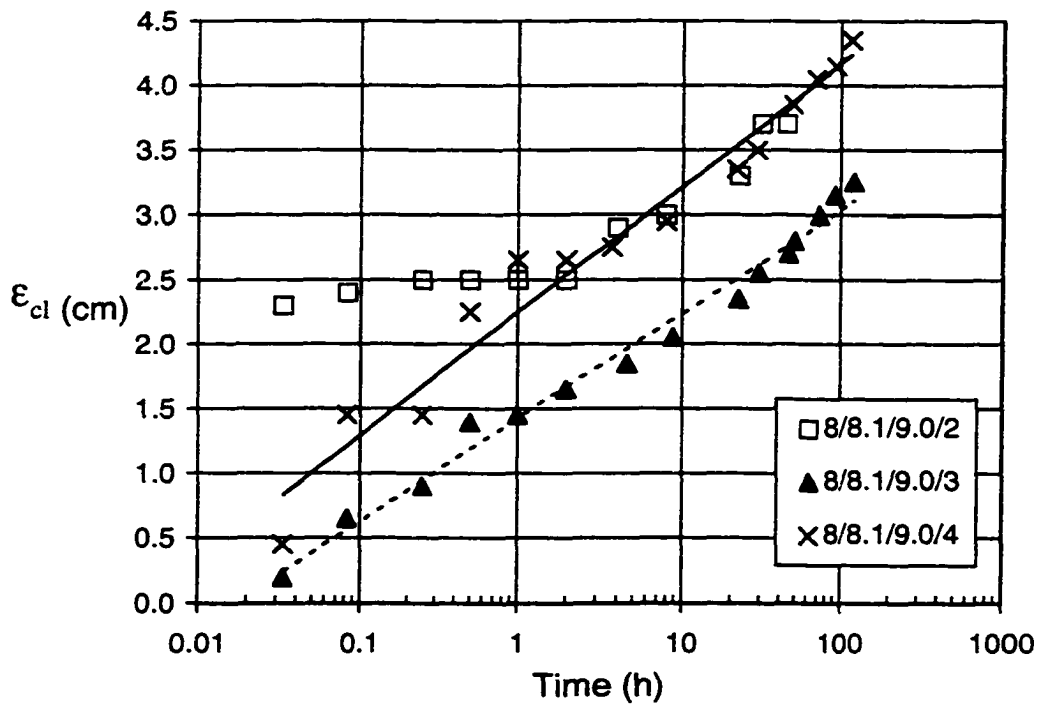


(b)

Fig. 6-4: Growth of the maximum scour depth (a) arithmetic scale (b) semi-log plot (all tests at $X=1214$ Pa)



(a)



(b)

Fig. 6-5: Growth of the centreline scour depth (a) arithmetic scale
(b) semi-log plot (all tests at $X=1214$ Pa)

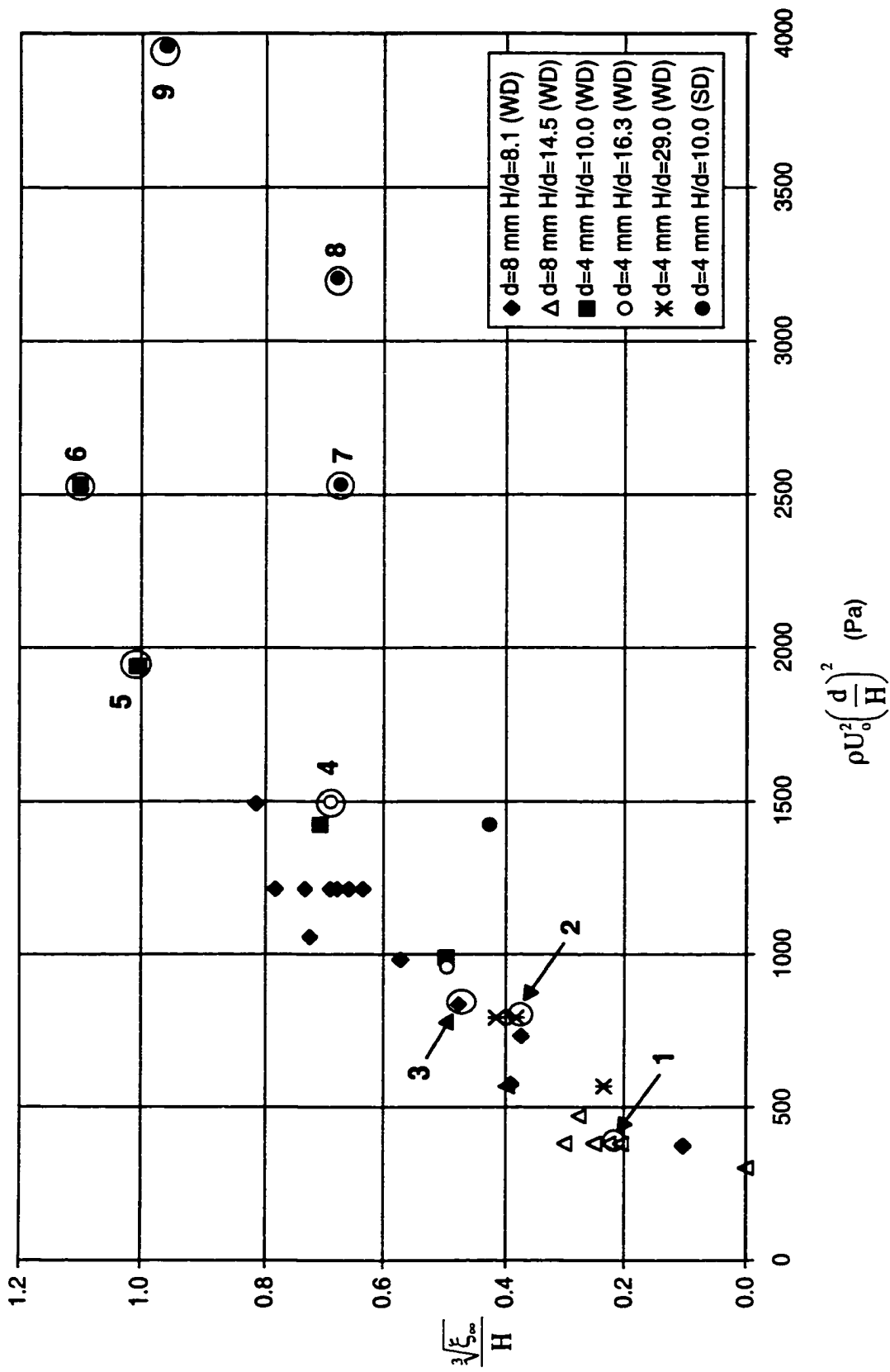


Fig. 6-6(a): Dimensionless scour hole volume at equilibrium state.

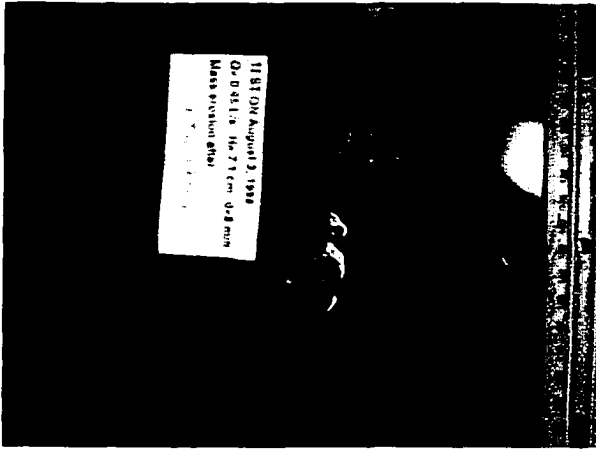
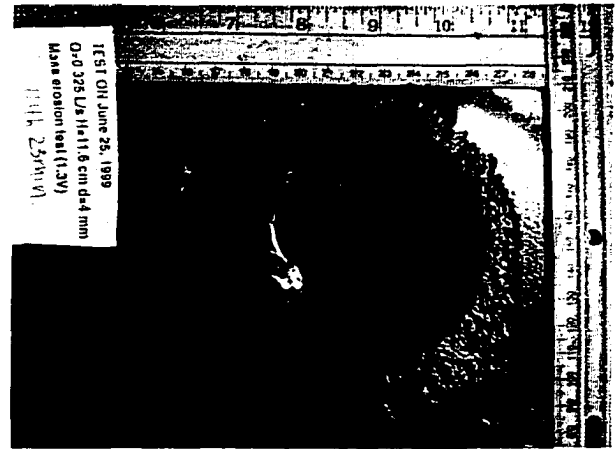
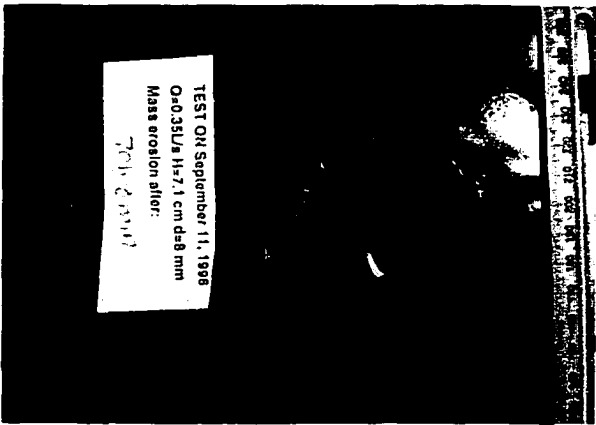


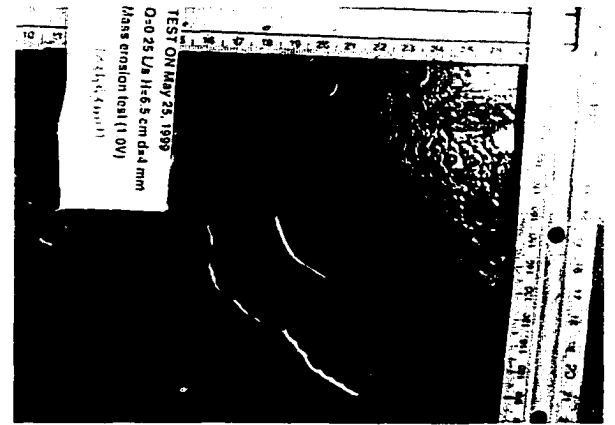
Fig. 6-6(b) Data Point No. 1 (8/14.5/9.0/4)
 $U_o=8.95$ m/s $d=8$ mm $H=116$ mm
 $(X-X_c)/X_c=0.27$ $t_d=67.6$ h



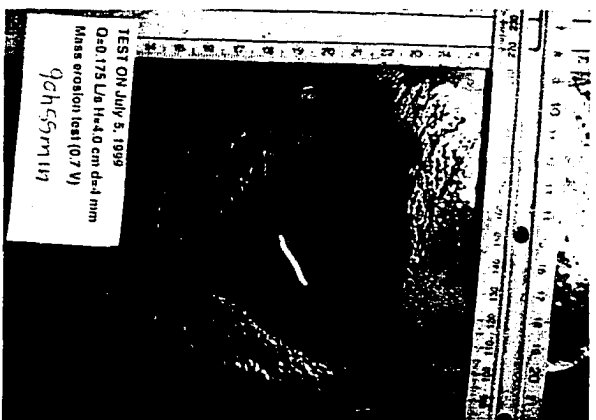
(c) Data Point No. 2 (4/29.0/25.9/2)
 $U_o=25.86$ m/s $d=4$ mm $H=116$ mm
 $(X-X_c)/X_c=1.65$ $t_d=114.4$ h



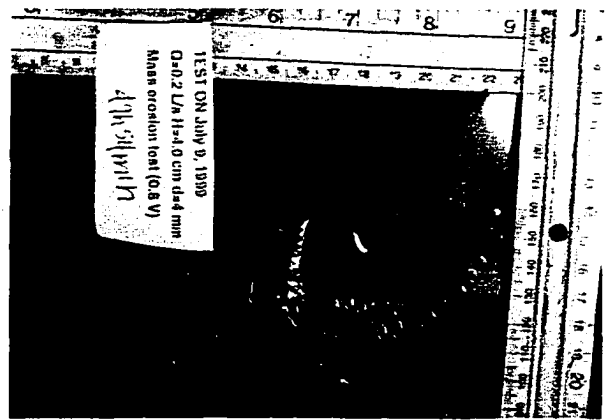
(d) Data Point No. 3 (8/8.1/7.4/1)
 $U_o=7.44$ m/s $d=8$ mm $H=65$ mm
 $(X-X_c)/X_c=1.80$ $t_d=117.4$ h



(e) Data Point No. 4 (4/16.3/19.9/1)
 $U_o=13.93$ m/s $d=4$ mm $H=65$ mm
 $(X-X_c)/X_c=4.00$ $t_d=103.9$ h



(f) Data Point No. 5 (4/10.0/13.9/1)
 $U_o=13.93$ m/s $d=4$ mm $H=40$ mm
 $(X-X_c)/X_c=5.46$ $t_d=90.9$ h



(g) Data Point No. 6 (4/10.0/15.9/2)
 $U_o=15.92$ m/s $d=4$ mm $H=40$ mm
 $(X-X_c)/X_c=7.44$ (after 49h 54min)

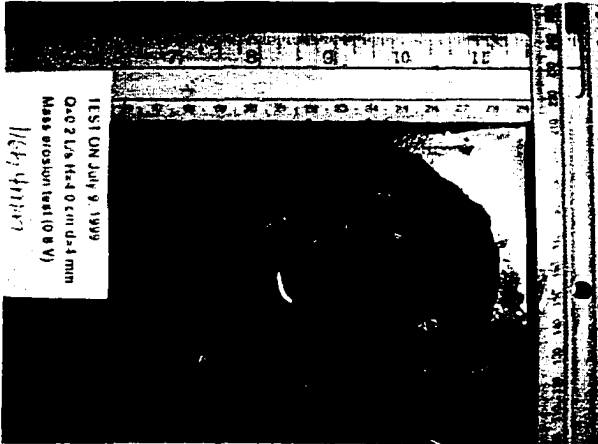
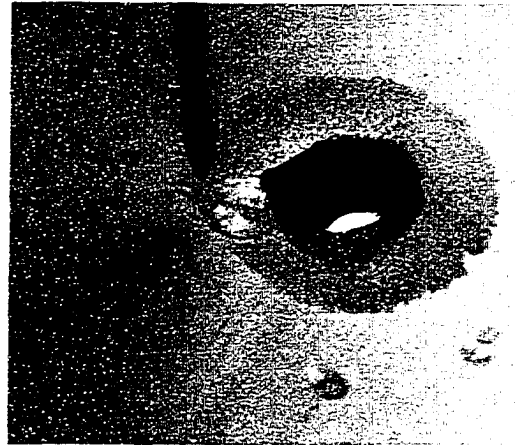
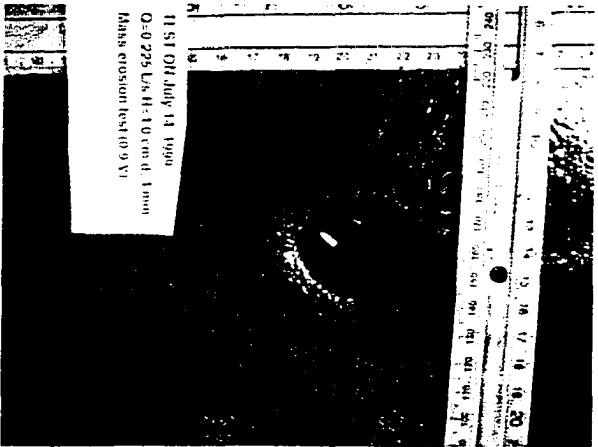


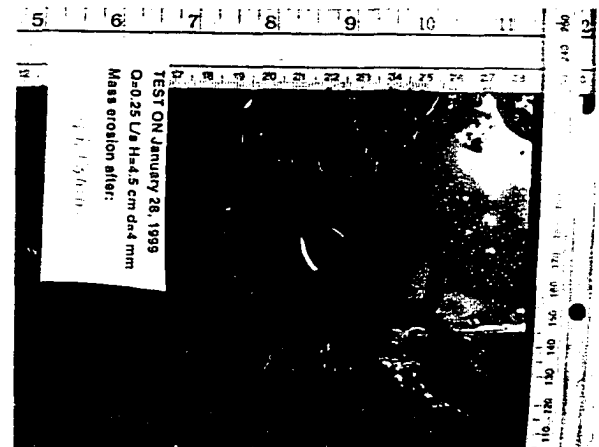
Fig. 6-6(h) Data Point No. 6 (4/10.0/15.9/2)
 $U_o=15.92$ m/s $d=4$ mm $H=40$ mm
 $(X-X_c)/X_c=7.44$ $t_d=116.1$ h



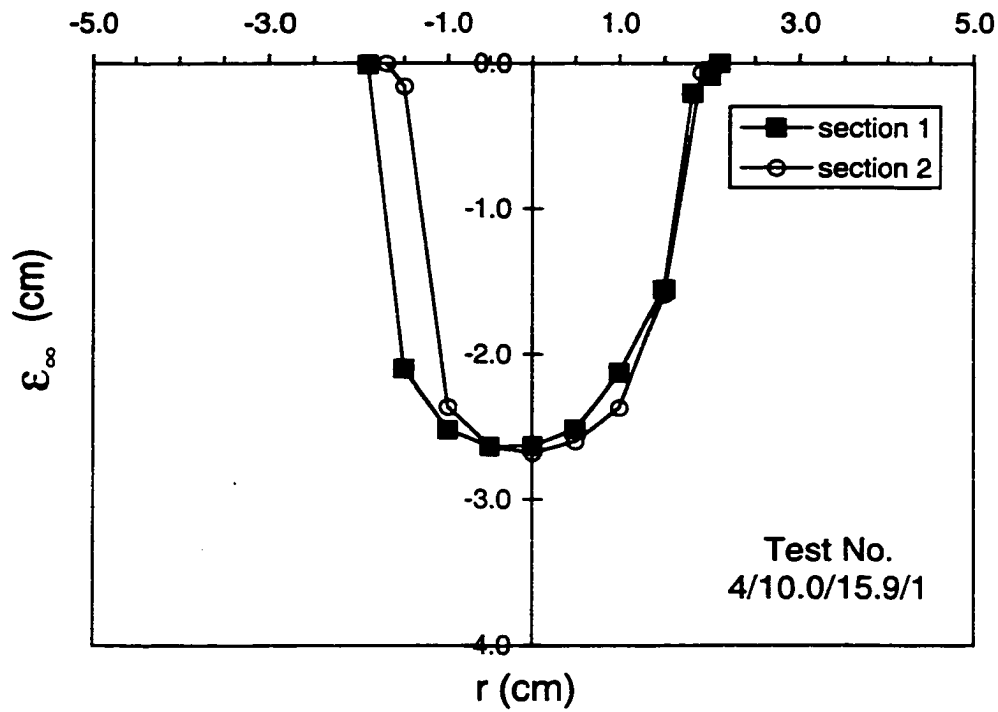
(i) Data Point No. 7 (4/10.0/15.9/1)
 $U_o=15.92$ m/s $d=4$ mm $H=40$ mm
 $(X-X_c)/X_c=7.44$ $t_d=93.12$ h



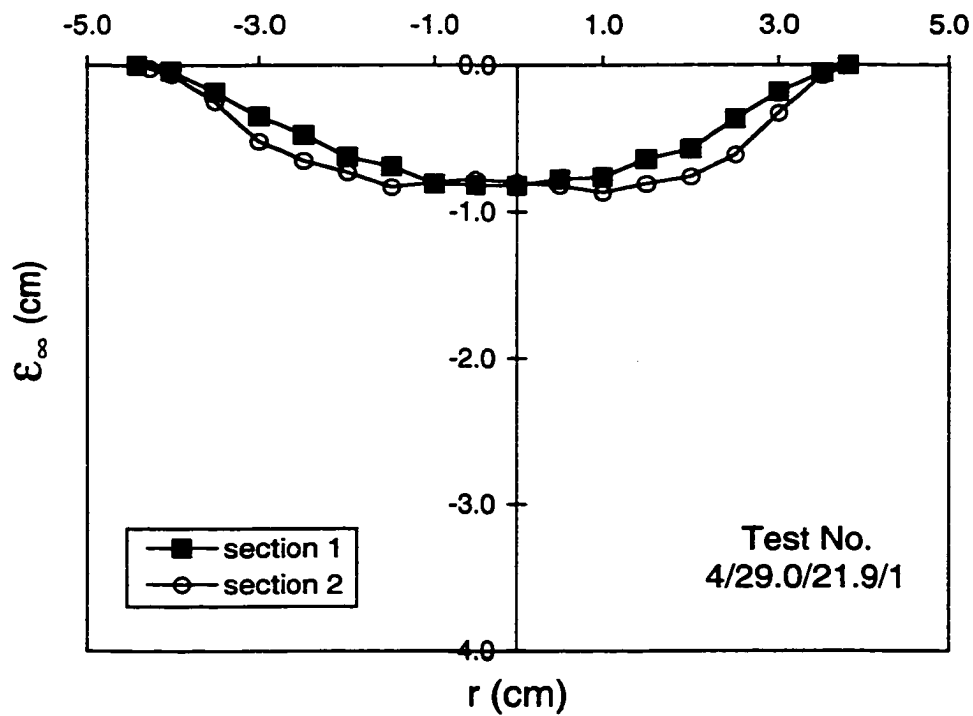
(j) Data Point No. 8 (4/10.0/17.9/1)
 $U_o=17.90$ m/s $d=4$ mm $H=40$ mm
 $(X-X_c)/X_c=9.69$ $t_d=123.9$ h



(k) Data Point No. 9 (4/10.0/19.9/1)
 $U_o=19.89$ m/s $d=4$ mm $H=40$ mm
 $(X-X_c)/X_c=12.19$ $t_d=96.3$ h



(a)



(b)

Fig. 6-7: Scour hole profile (a) for a strongly deflected jet and (b) for a weakly deflected jet.

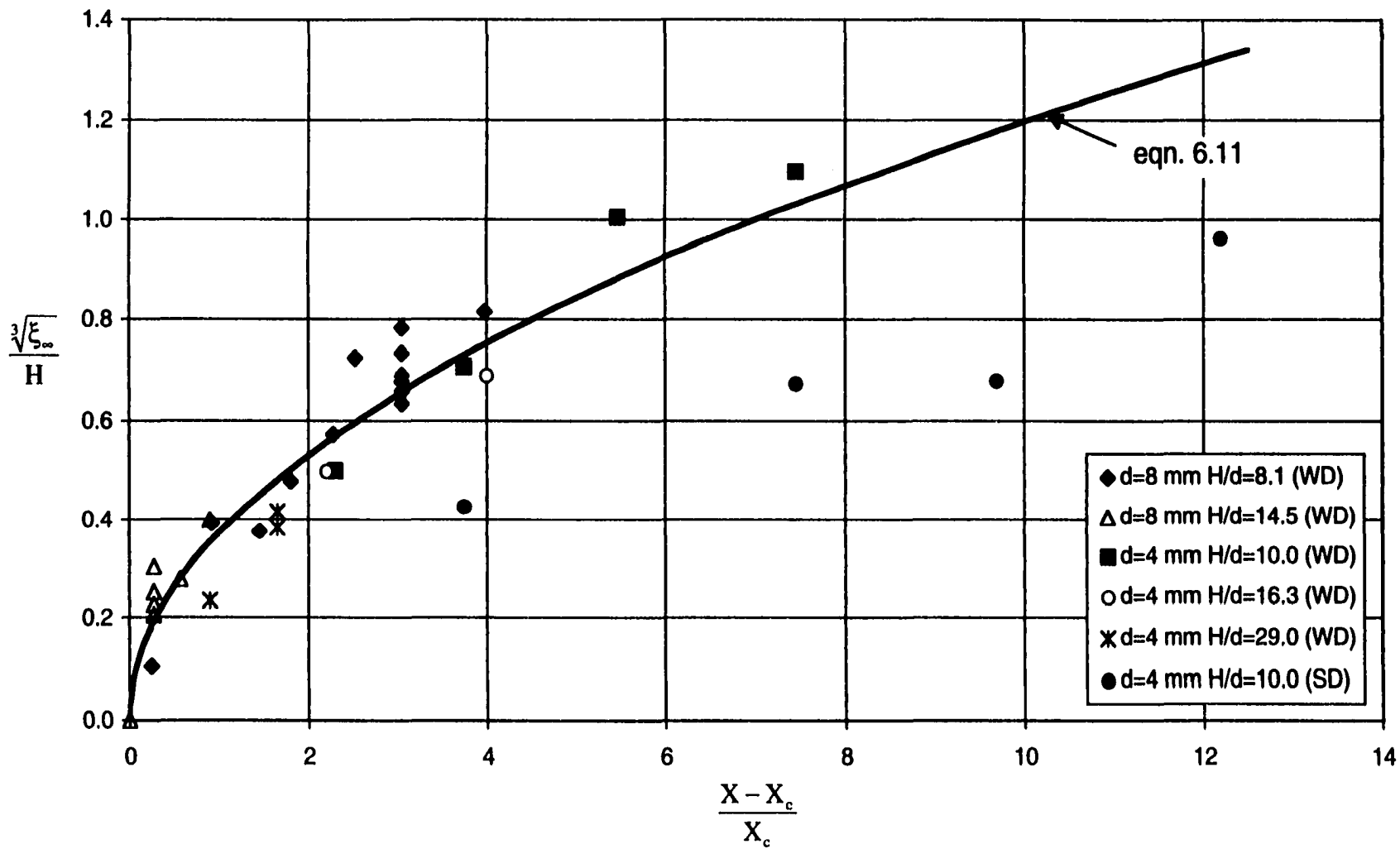


Fig. 6-8: Dimensionless scour hole volume at equilibrium state with dimensionless excess stress.

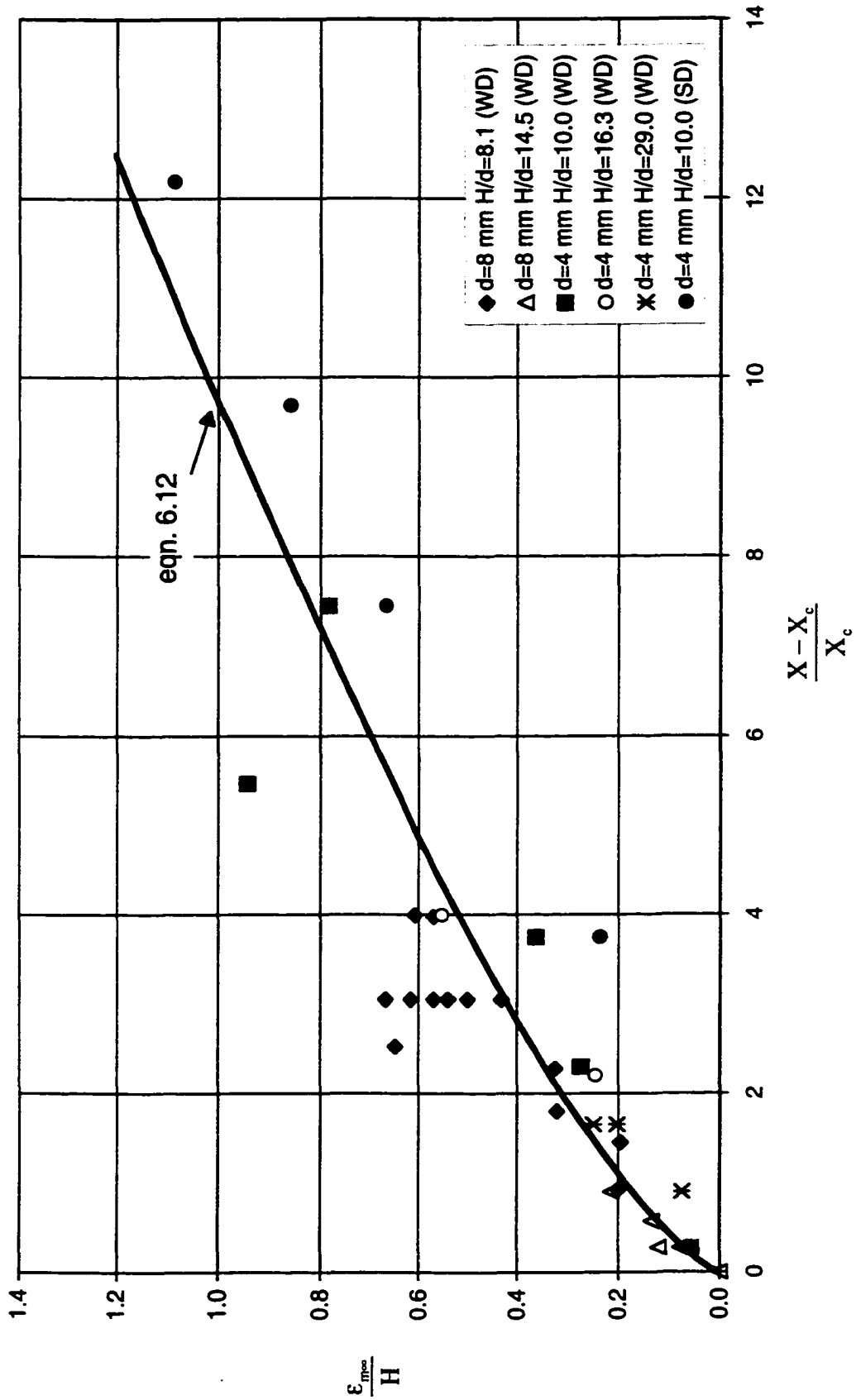


Fig. 6-9: Dimensionless maximum scour hole depth at equilibrium state with dimensionless excess stress.

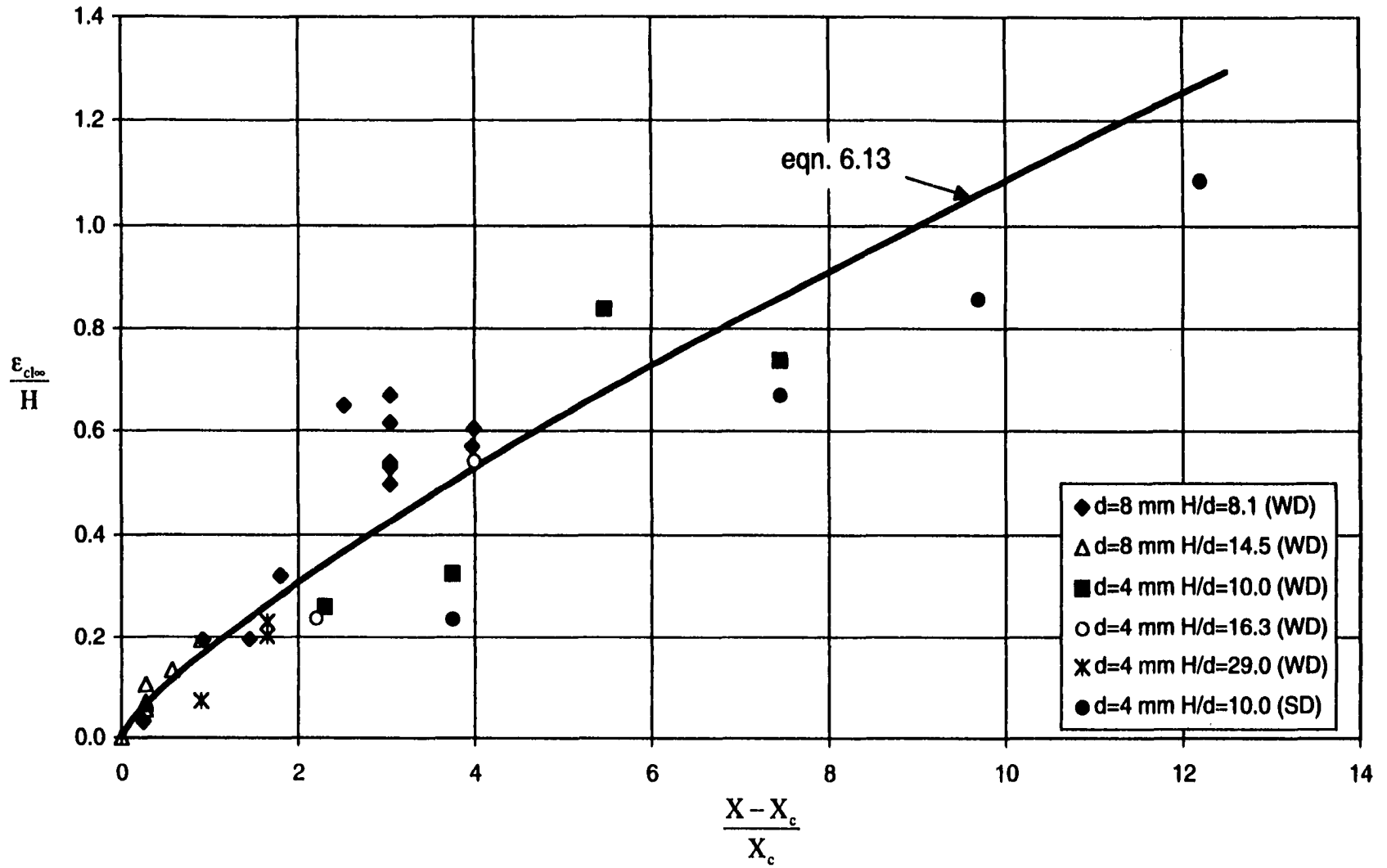


Fig. 6-10: Dimensionless centreline scour hole depth at equilibrium state with dimensionless excess stress.

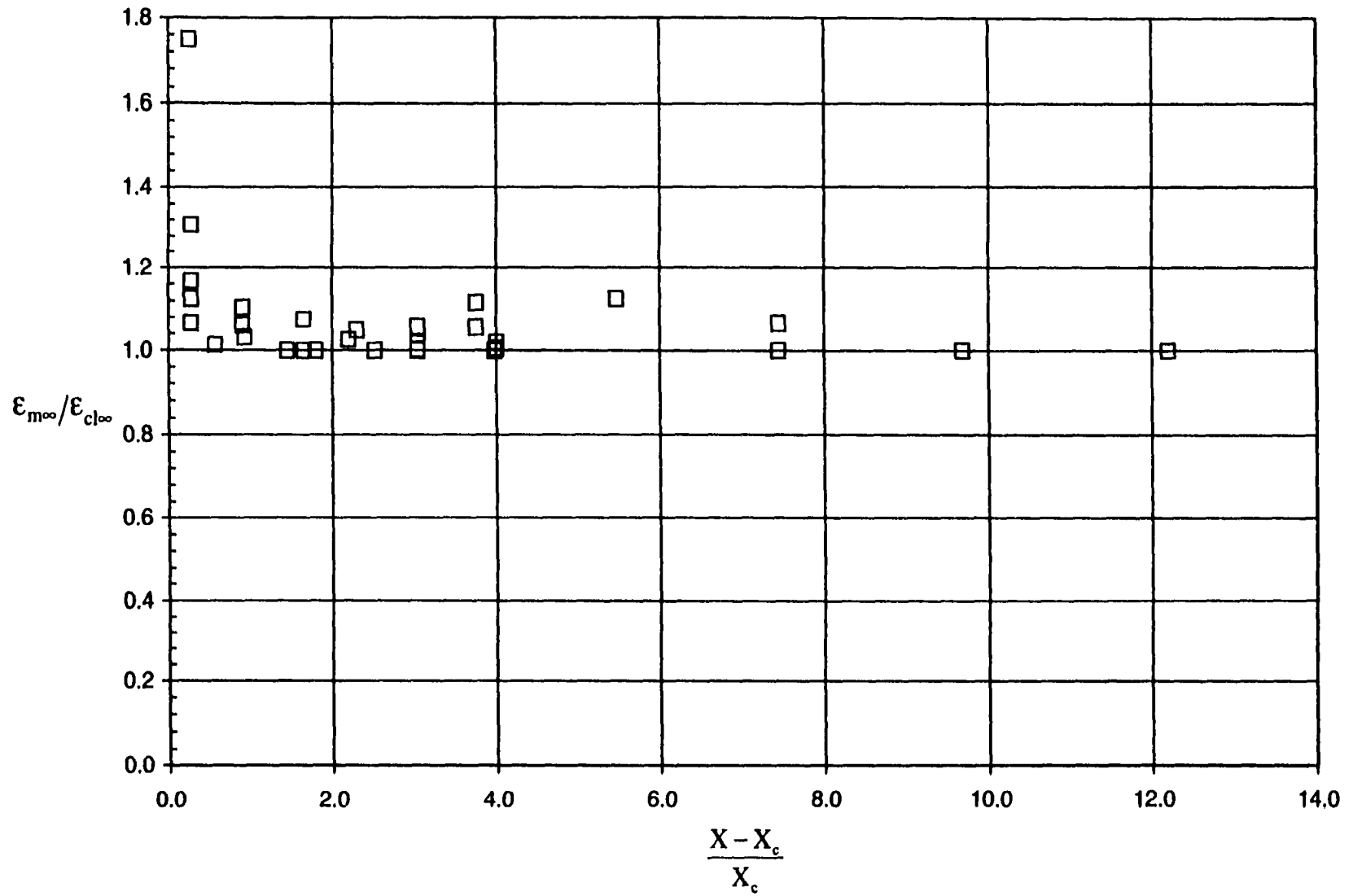


Fig. 6-11: Ratio of the maximum scour depth to the centreline scour depth at equilibrium state with the dimensionless excess stress.

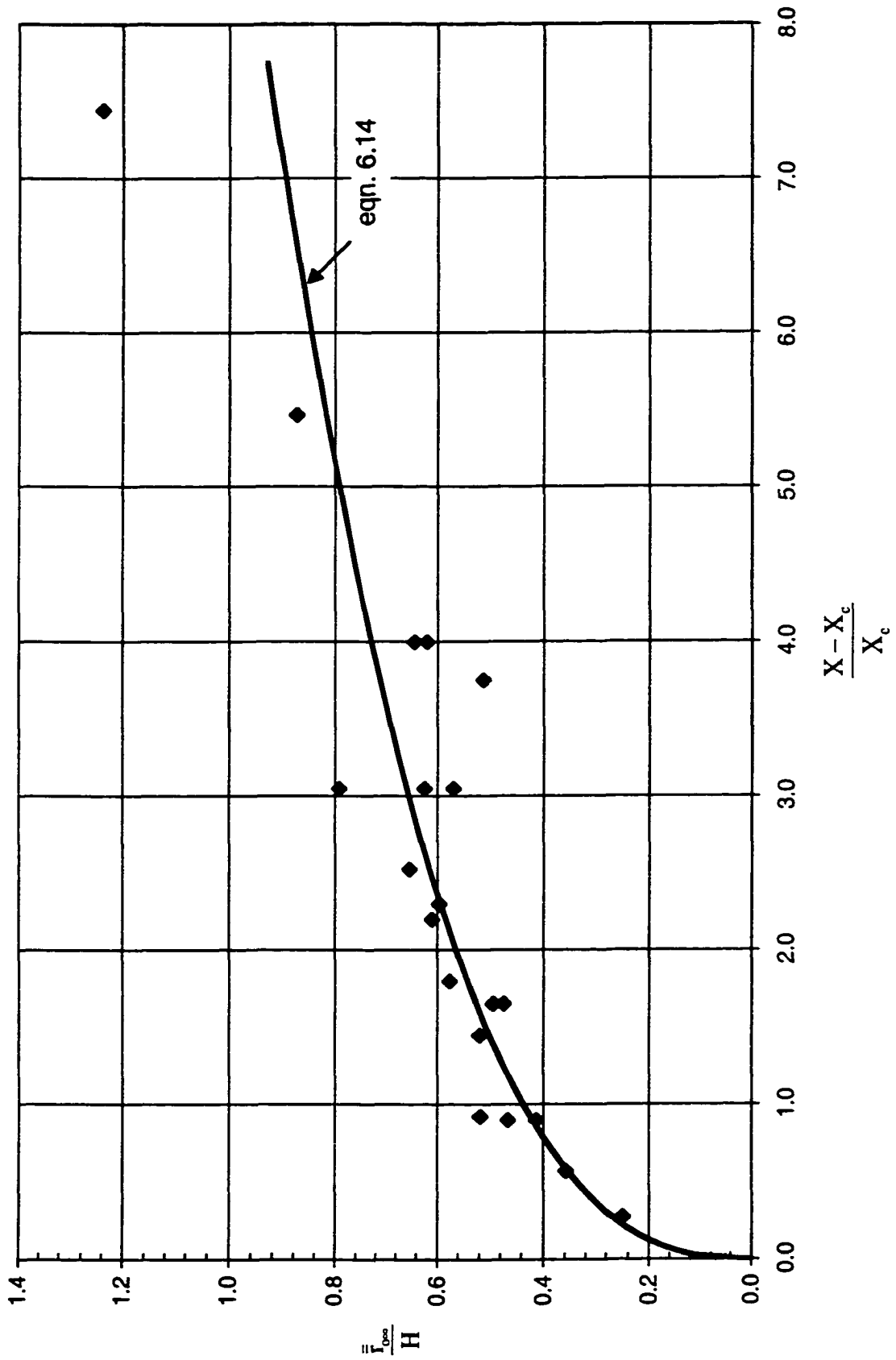


Fig. 6-12: Dimensionless scour hole radius at equilibrium state.

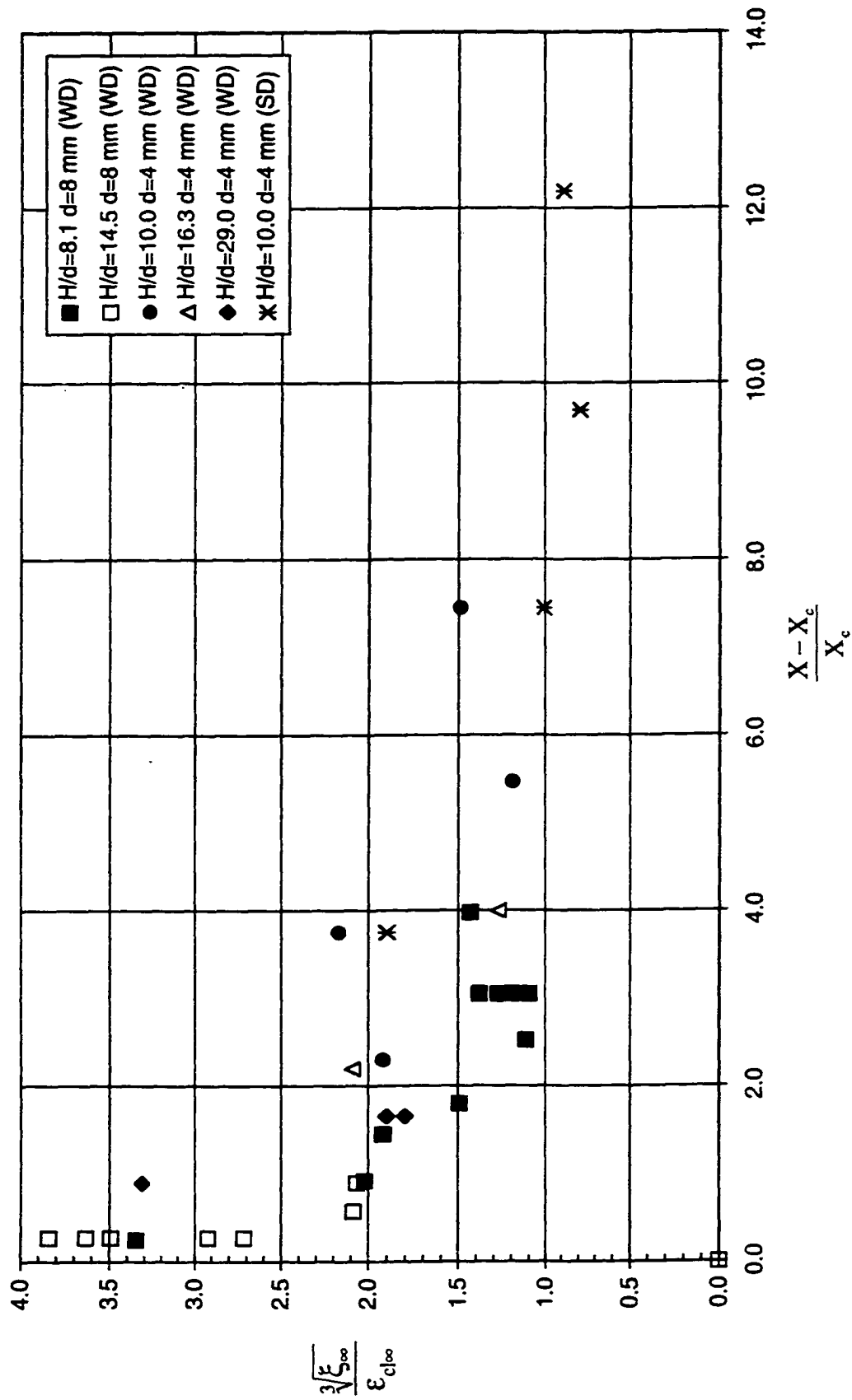


Fig. 6-13: Ratio of the scour hole volume to the centreline scour depth at equilibrium state with dimensionless excess stress.

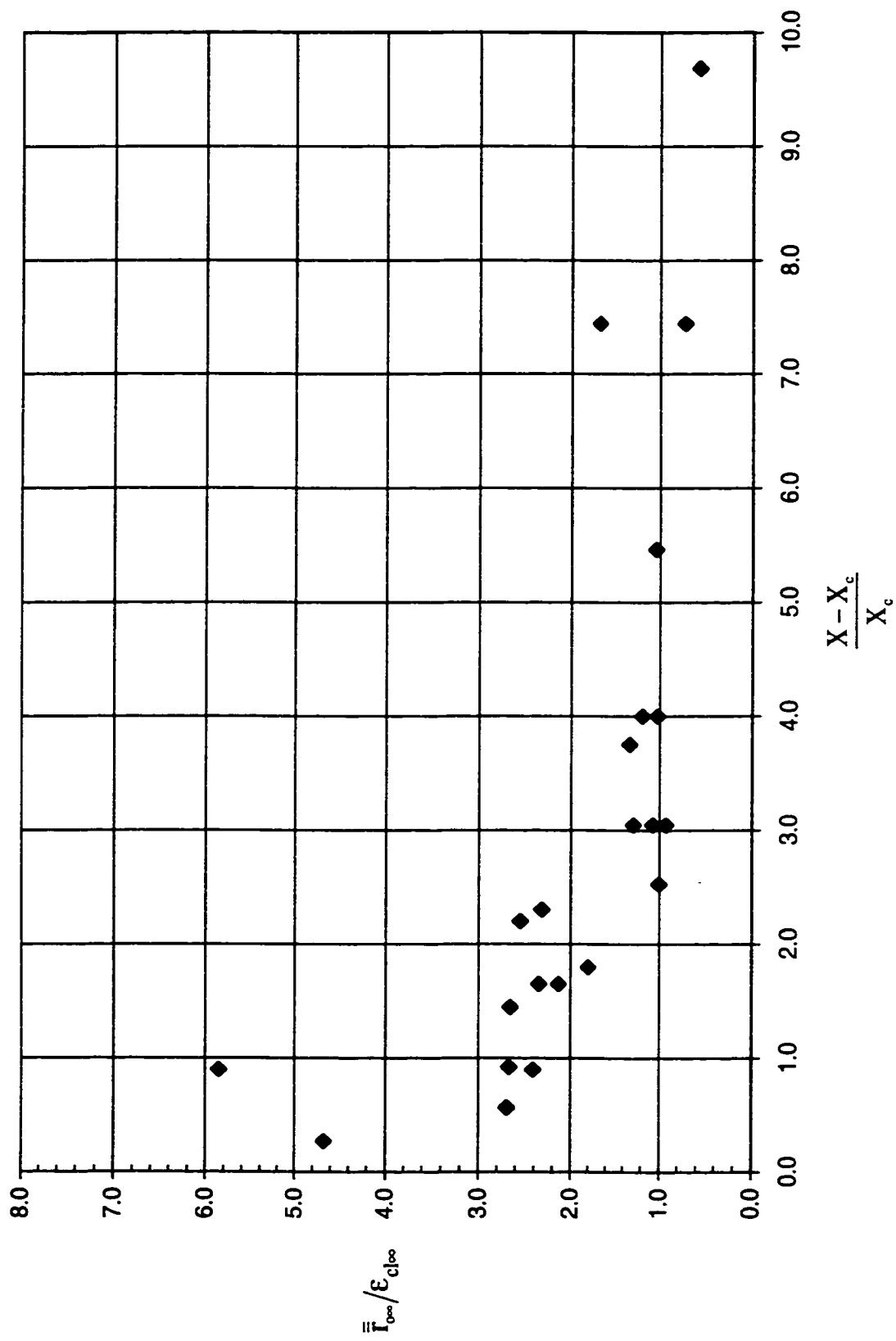


Fig. 6-14: Ratio of the radius of the scour hole to the centreline scour depth at equilibrium state with dimensionless excess stress.

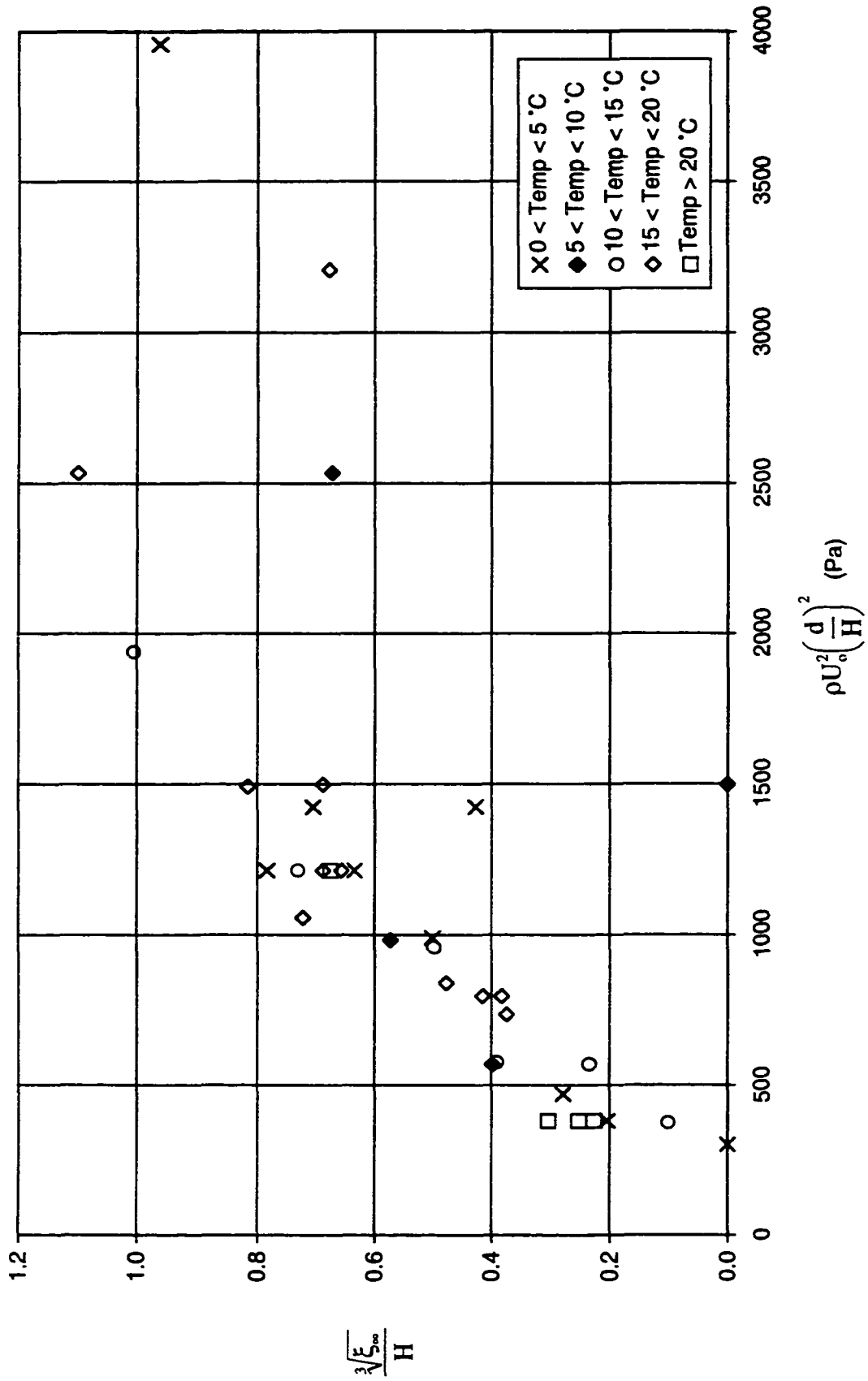


Fig. 6-15: Effect of temperature on the scour hole volume at equilibrium.

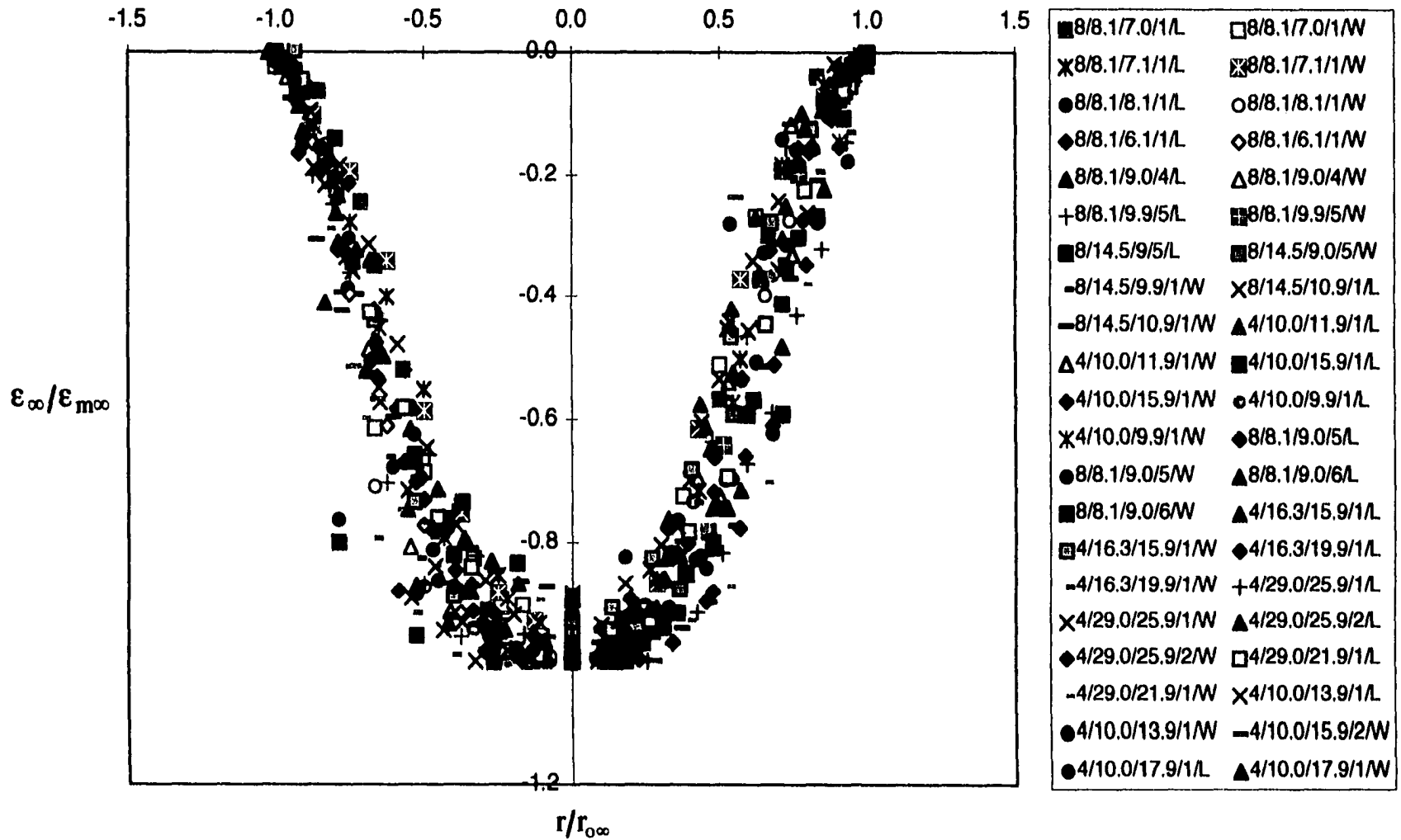


Fig. 6-16: Dimensionless scour hole profile at equilibrium nondimensionalized with the maximum scour depth and scour hole radius.

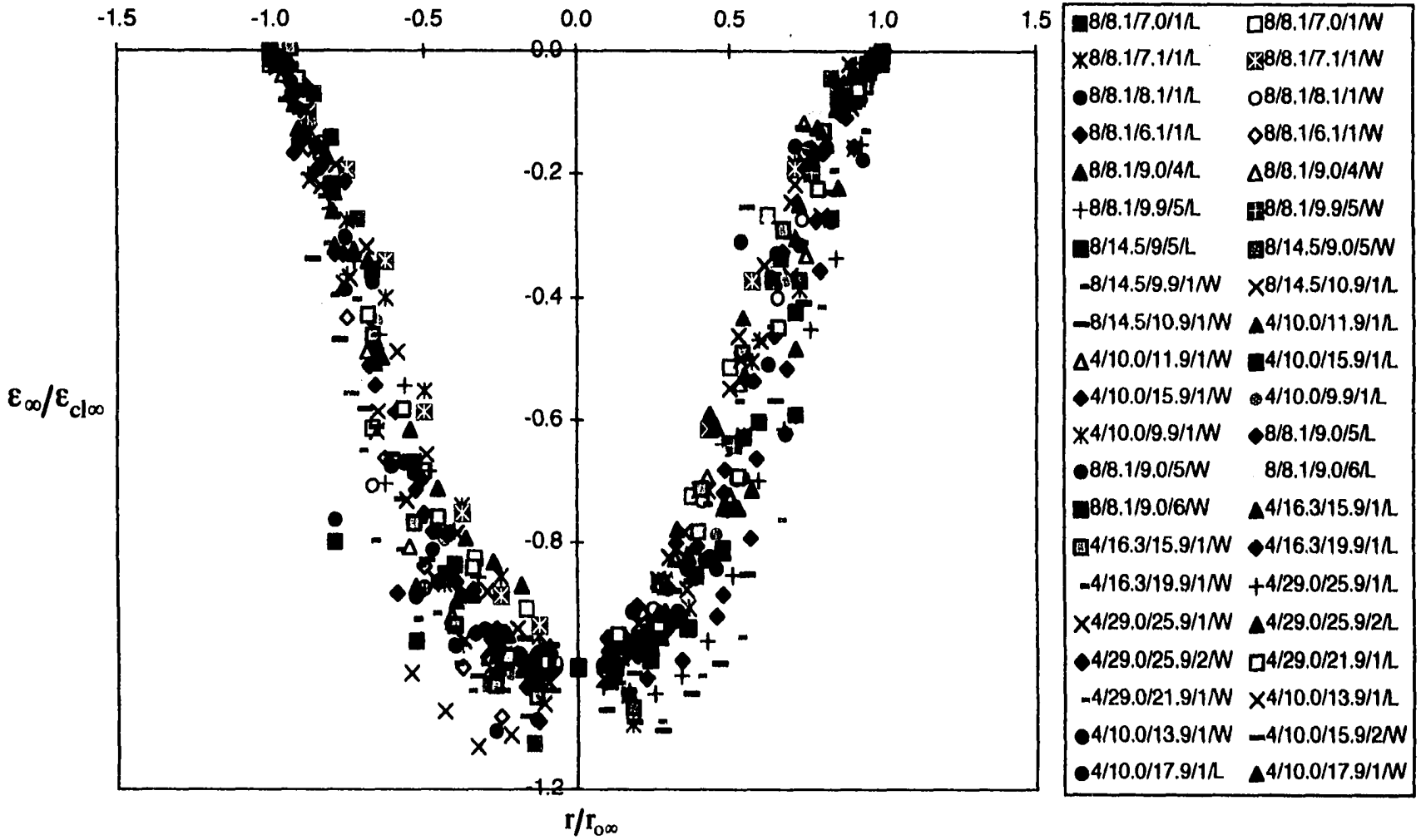


Fig. 6-17: Dimensionless scour hole profile at equilibrium nondimensionalized with the centreline scour depth and scour hole radius.

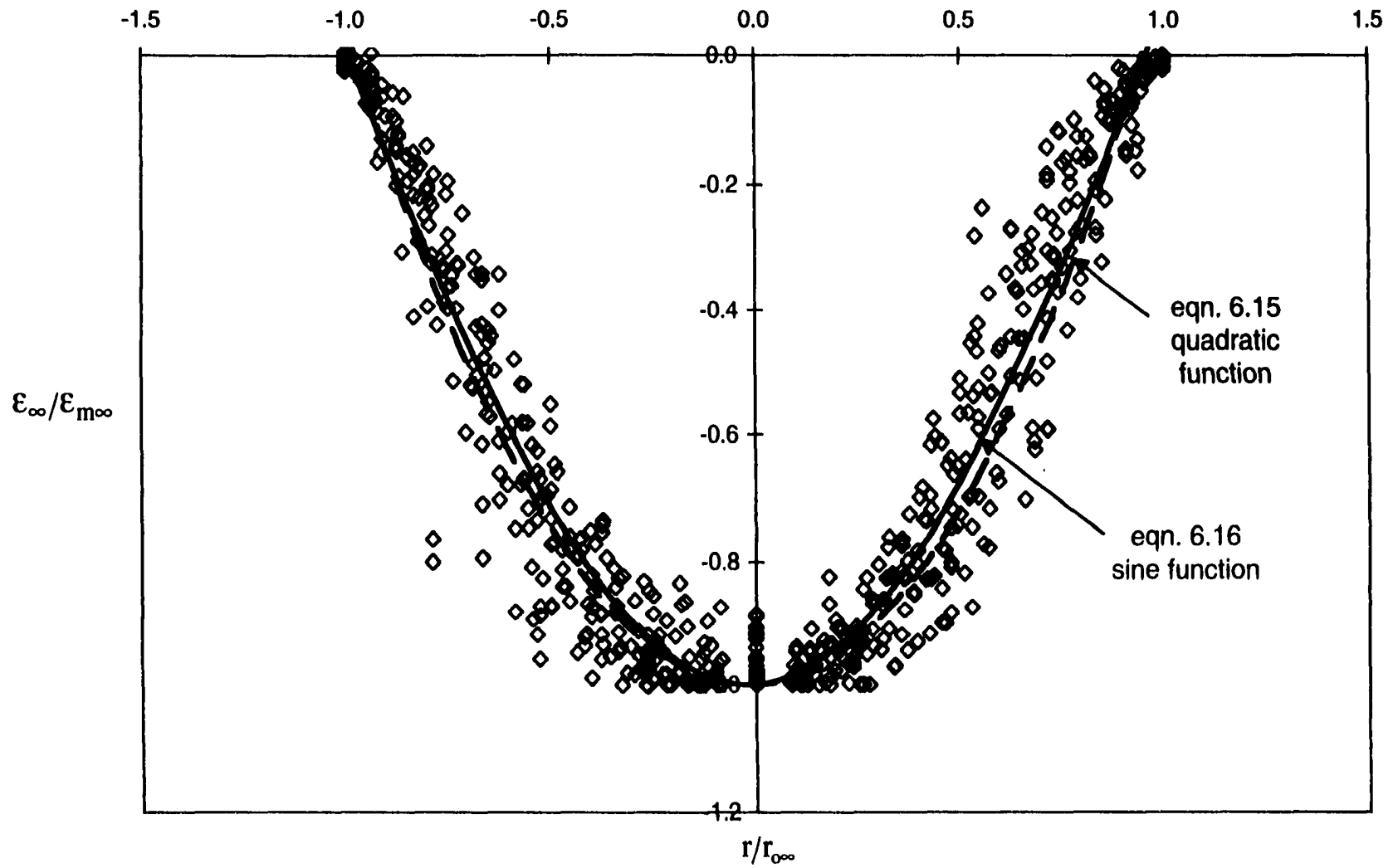


Fig. 6-18: Curve fits for the dimensionless scour hole profile that uses the maximum scour depth and the scour hole radius as scales.

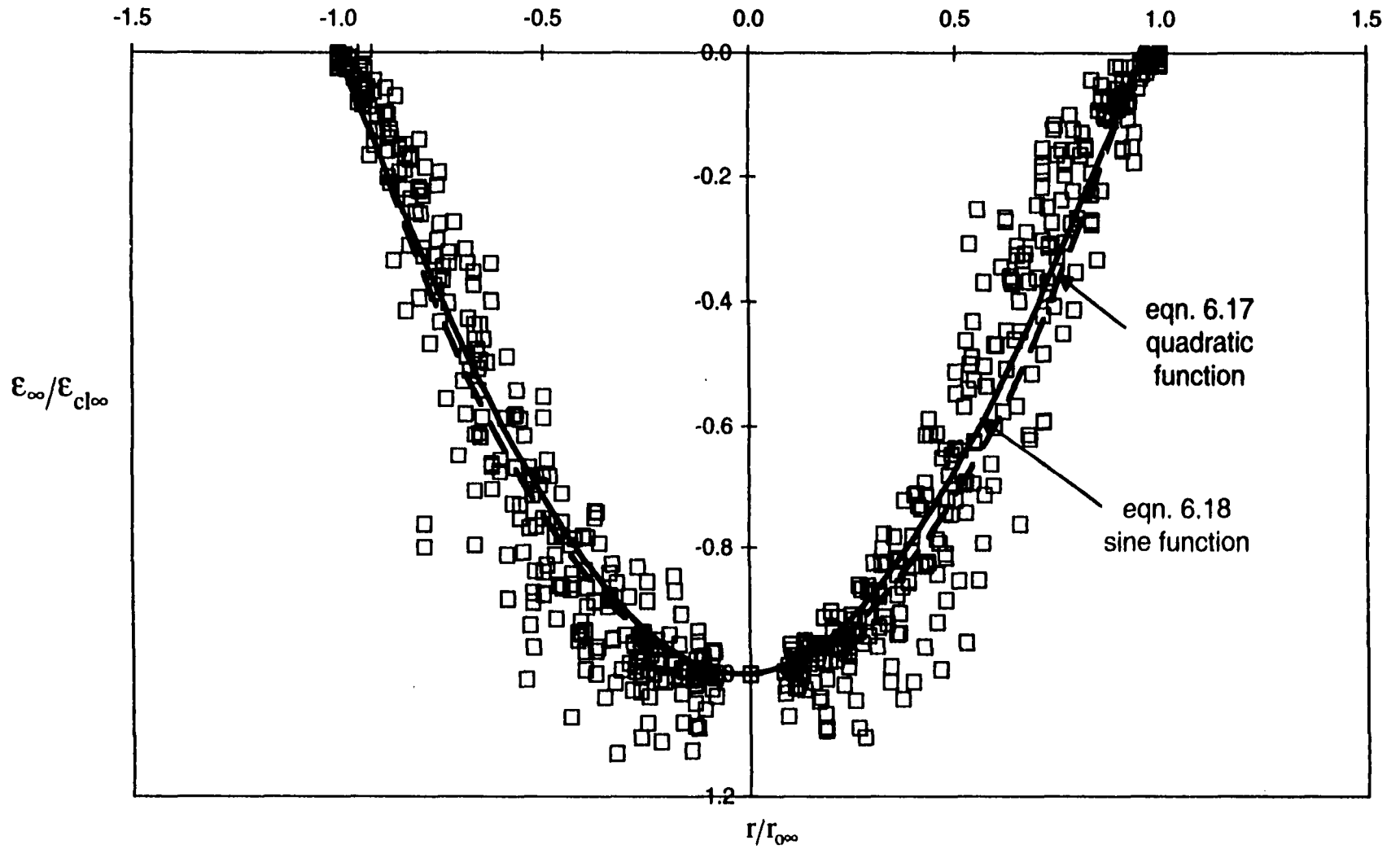


Fig. 6-19: Curve fits for the dimensionless scour hole profile that uses the centreline scour depth and scour hole radius as scales.

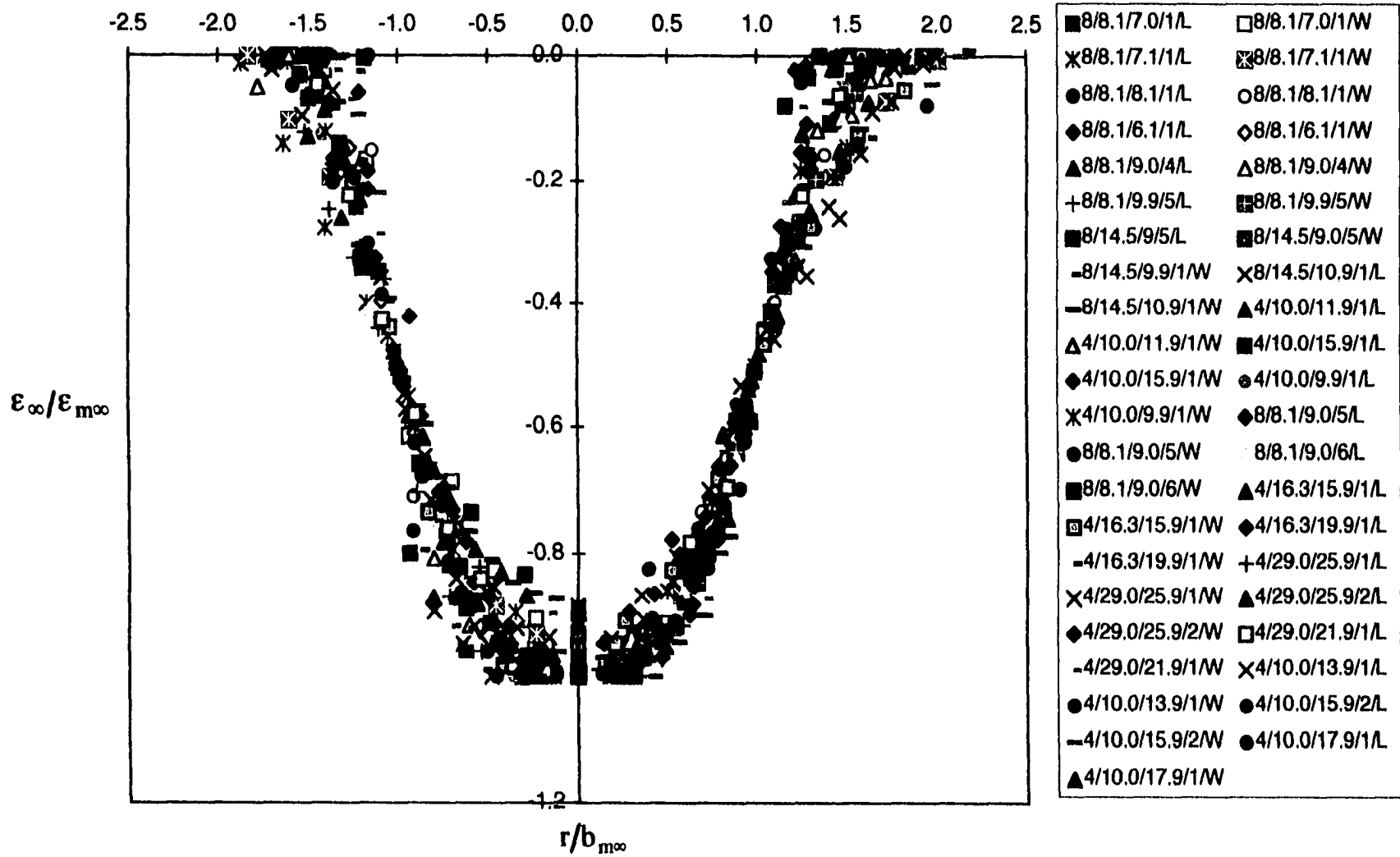


Fig. 6-20: Dimensionless scour hole profile at equilibrium nondimensionalized with the maximum depth of scour and half-widths.

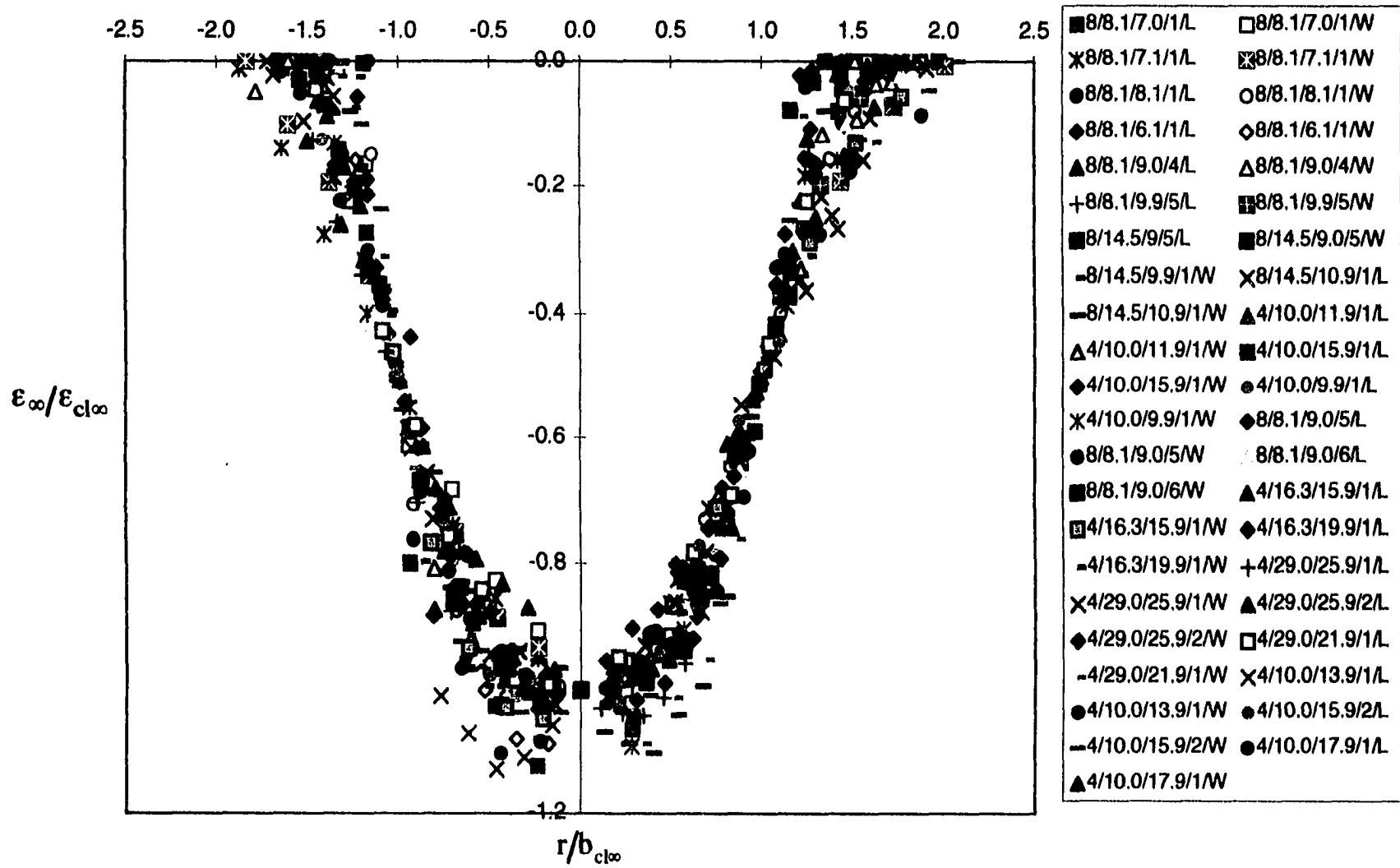


Fig. 6-21: Dimensionless scour hole profile at equilibrium nondimensionalized with the centreline depth of scour and half-widths.

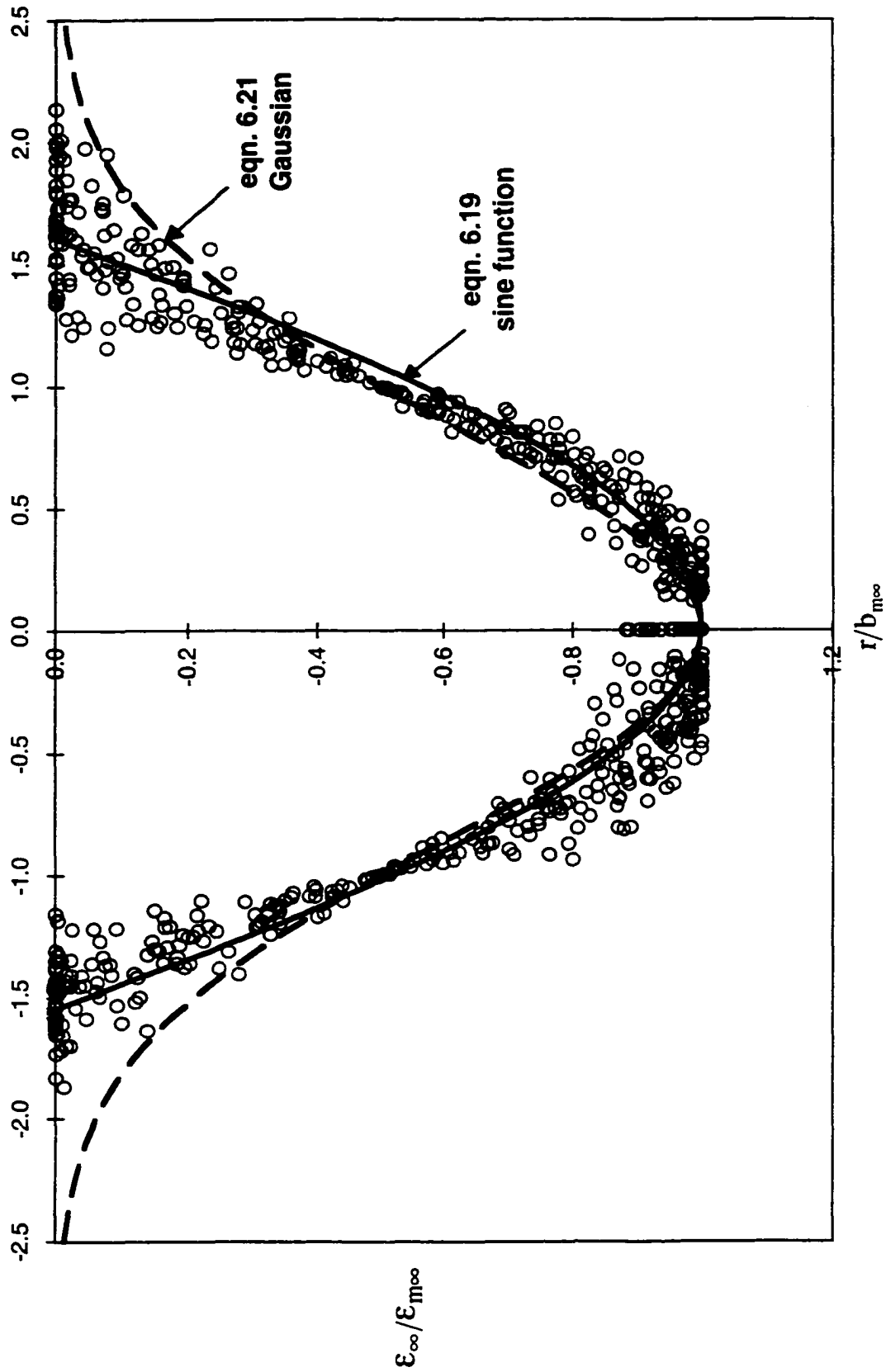


Fig. 6-22: Curve fits for the dimensionless scour hole profile that uses the maximum depth of scour and half-widths as scales.

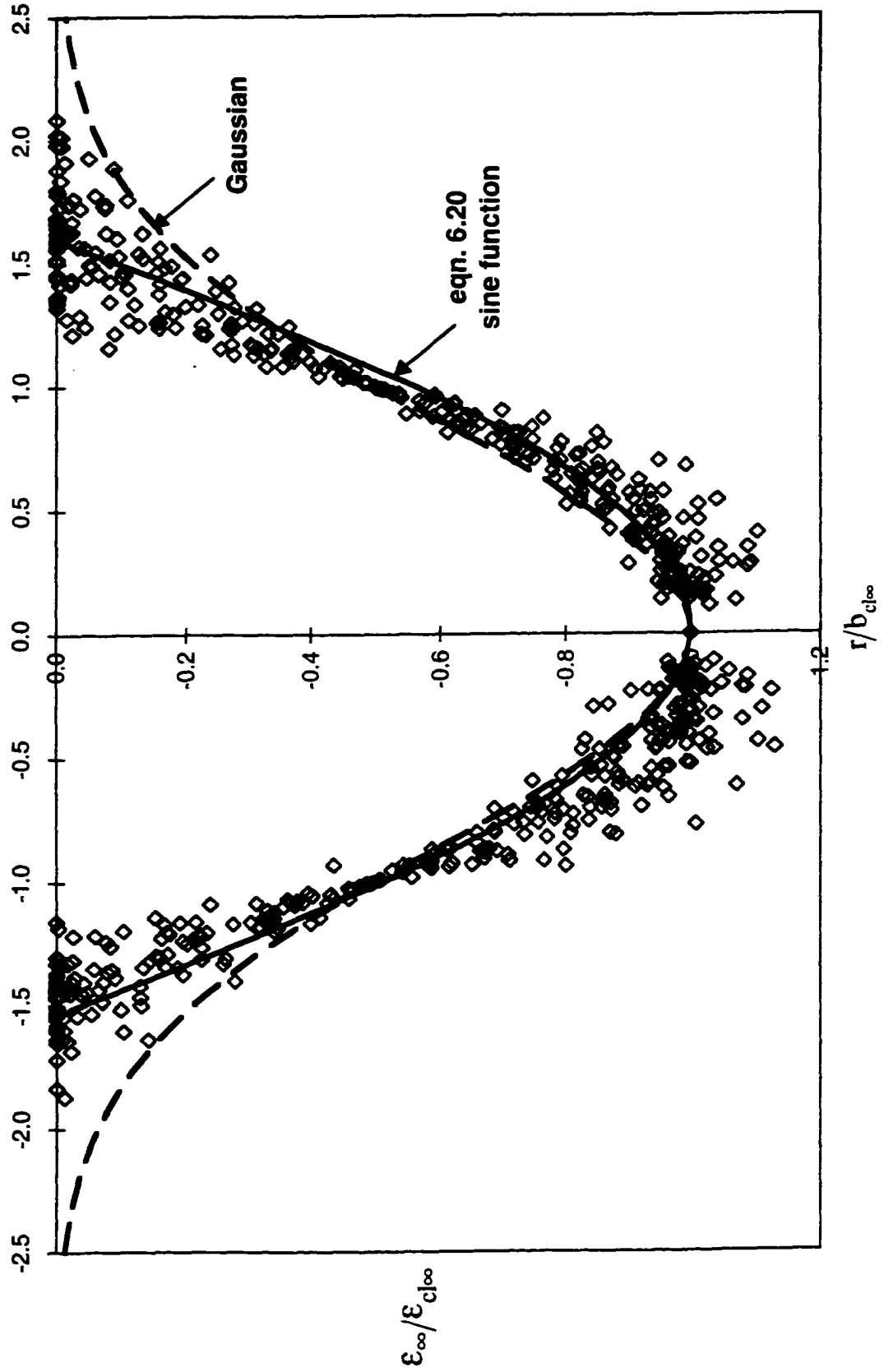


Fig. 6-23: Curve fits for the dimensionless scour hole profile that uses the centreline depth of scour and half-widths as scales.

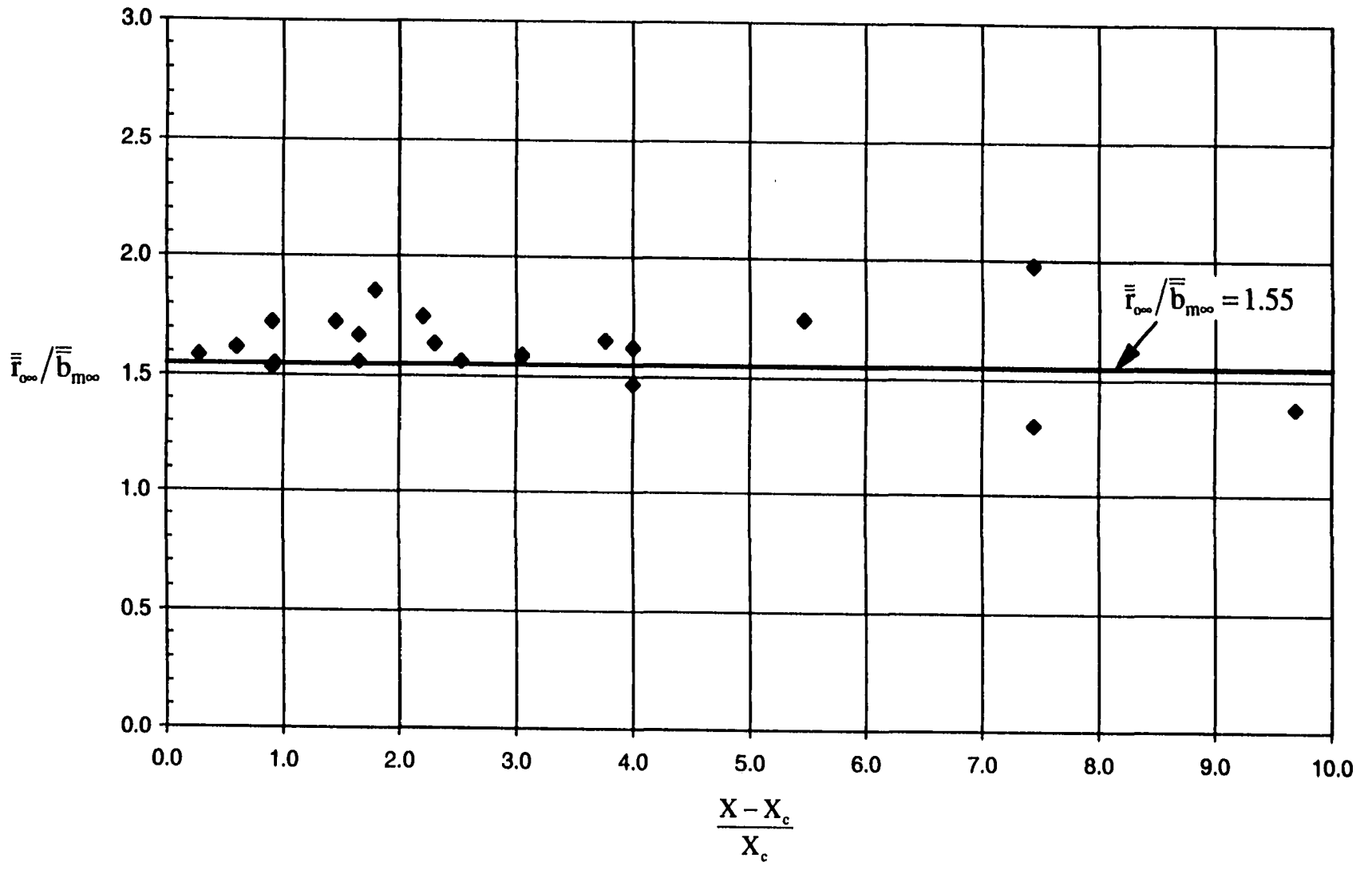


Fig. 6-24: Variation of the ratio of the scour hole radius and the half-width based on the maximum scour depth at equilibrium with dimensionless excess stress.

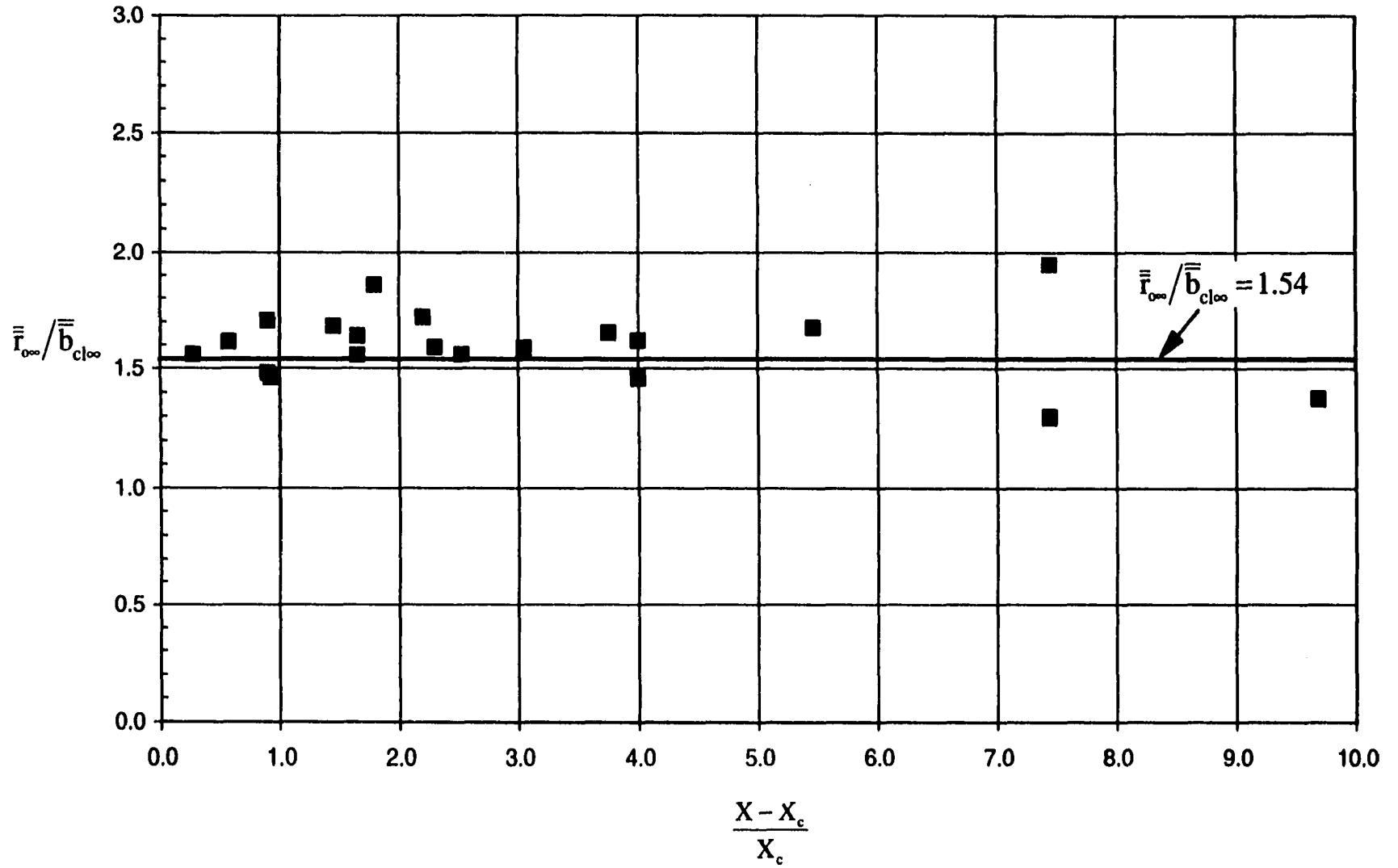


Fig. 6-25: Variation of the ratio of the scour hole radius and the half-width based on the centreline scour depth at equilibrium with dimensionless excess stress.

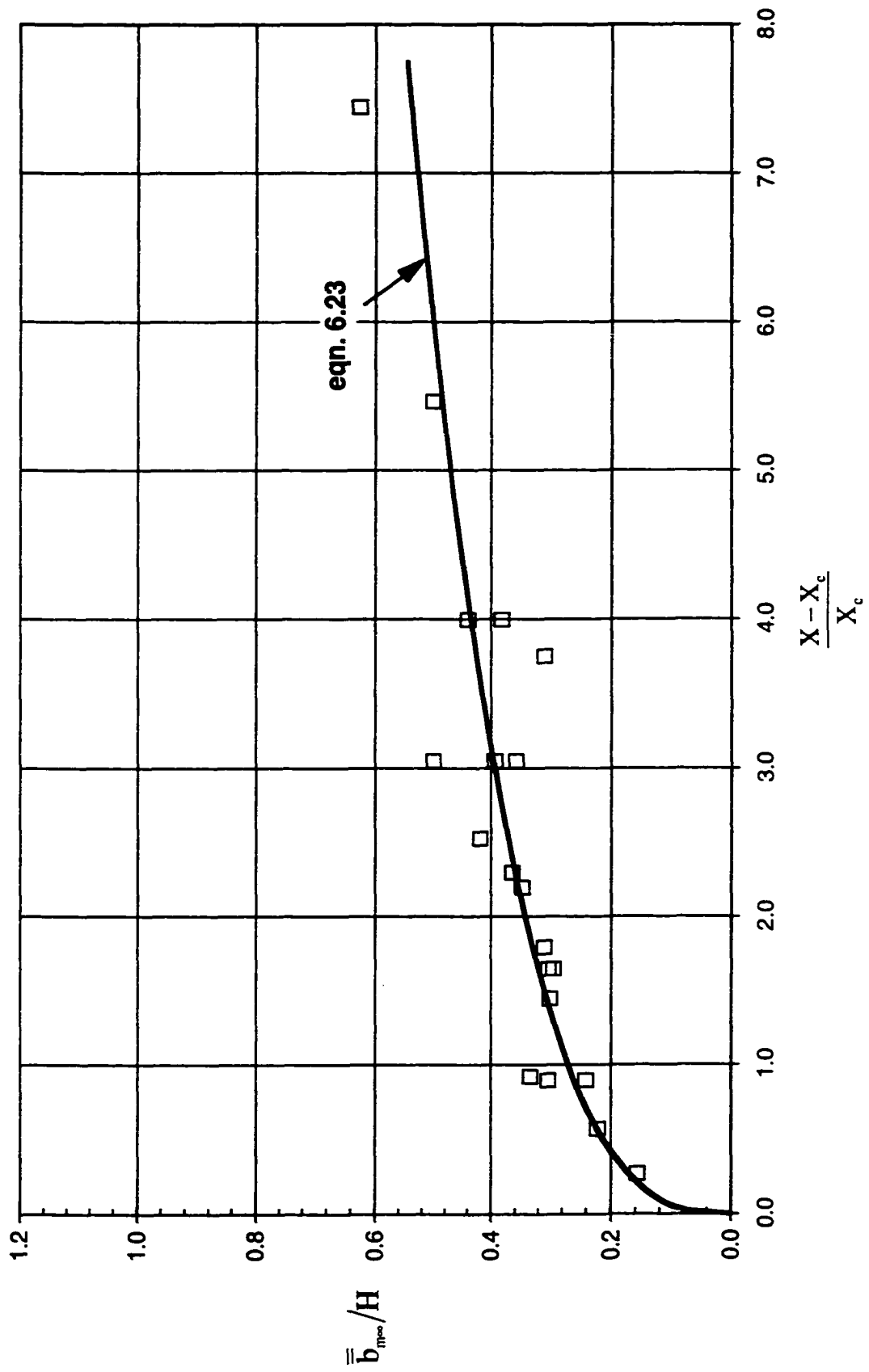


Fig. 6-26: Half-width based on the maximum scour depth with dimensionless excess stress.

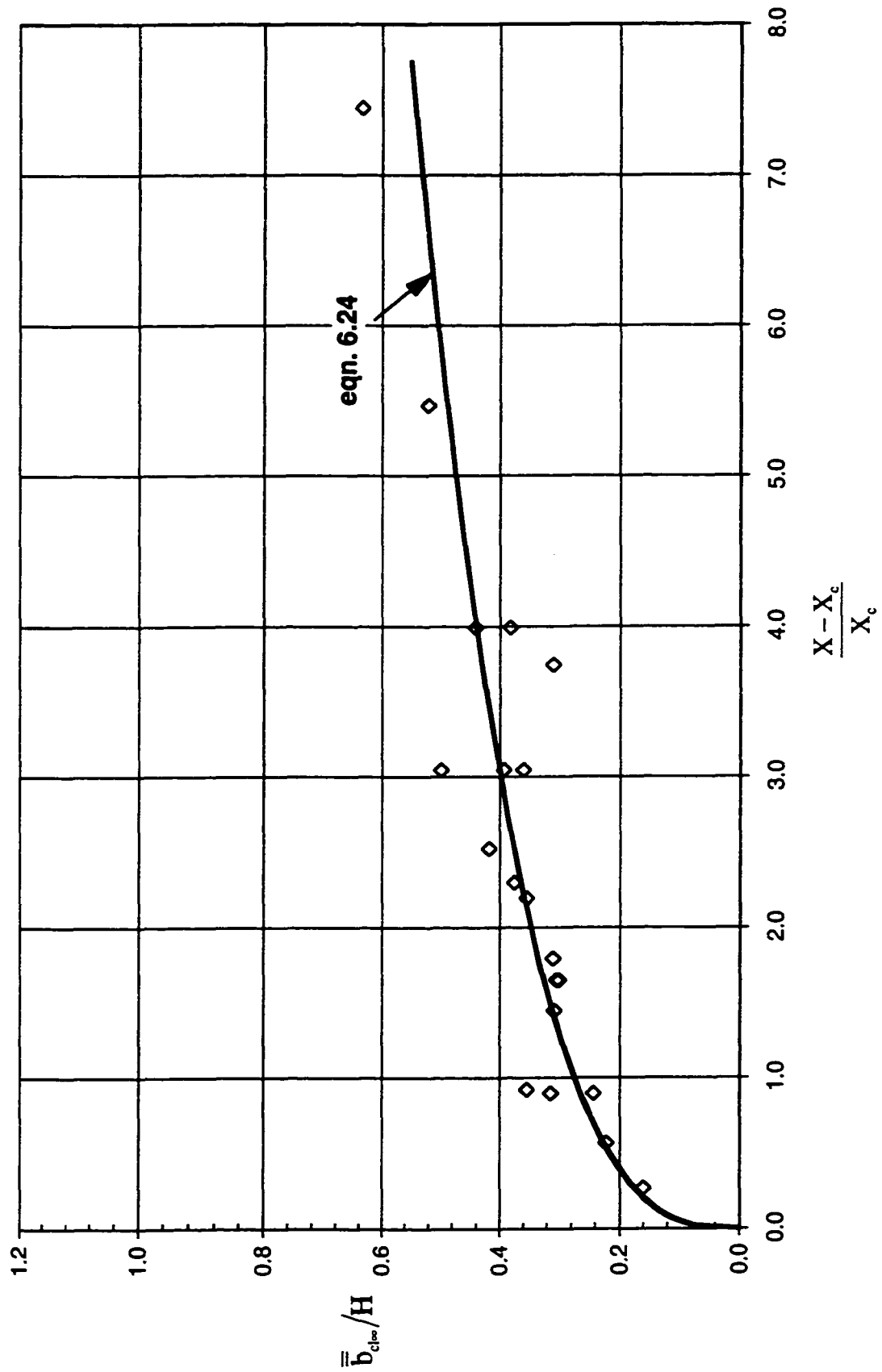


Fig. 6-27: Half-width based on the centreline scour depth with dimensionless excess stress.

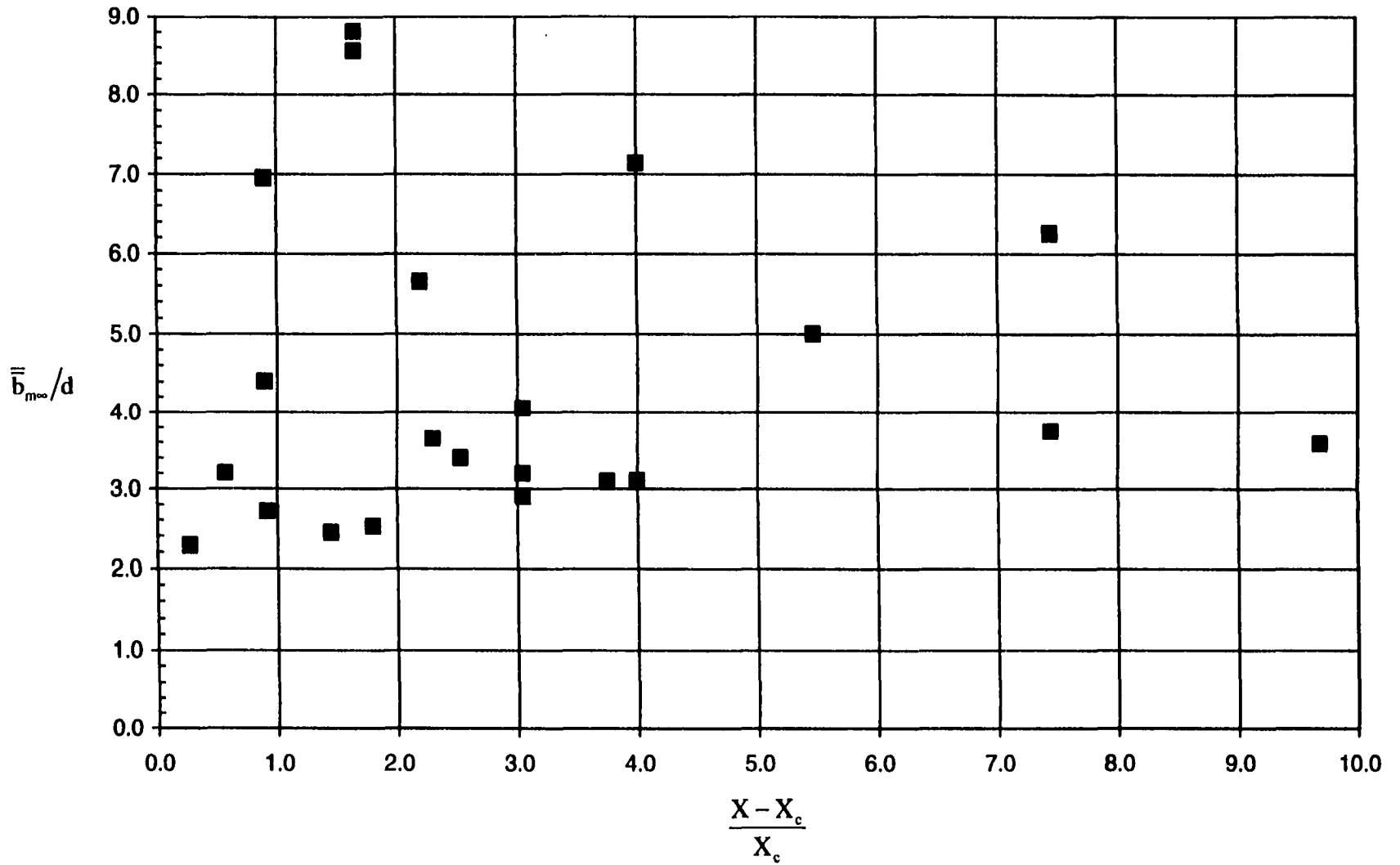


Fig. 6-28: Ratio of the half-width based on the maximum scour depth to the nozzle diameter at equilibrium with dimensionless excess stress.

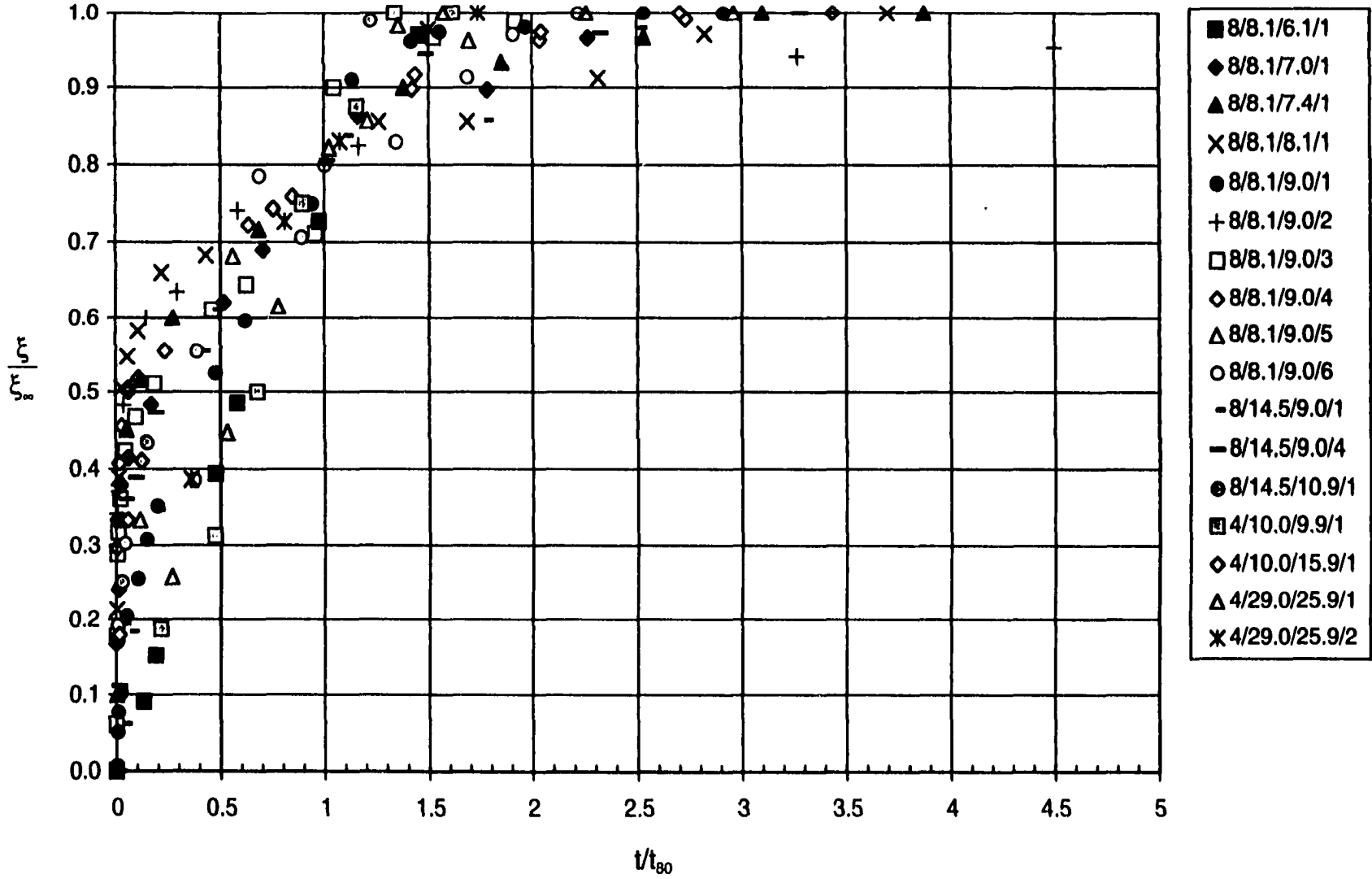


Fig. 6-29: Growth of the dimensionless scour hole volume.

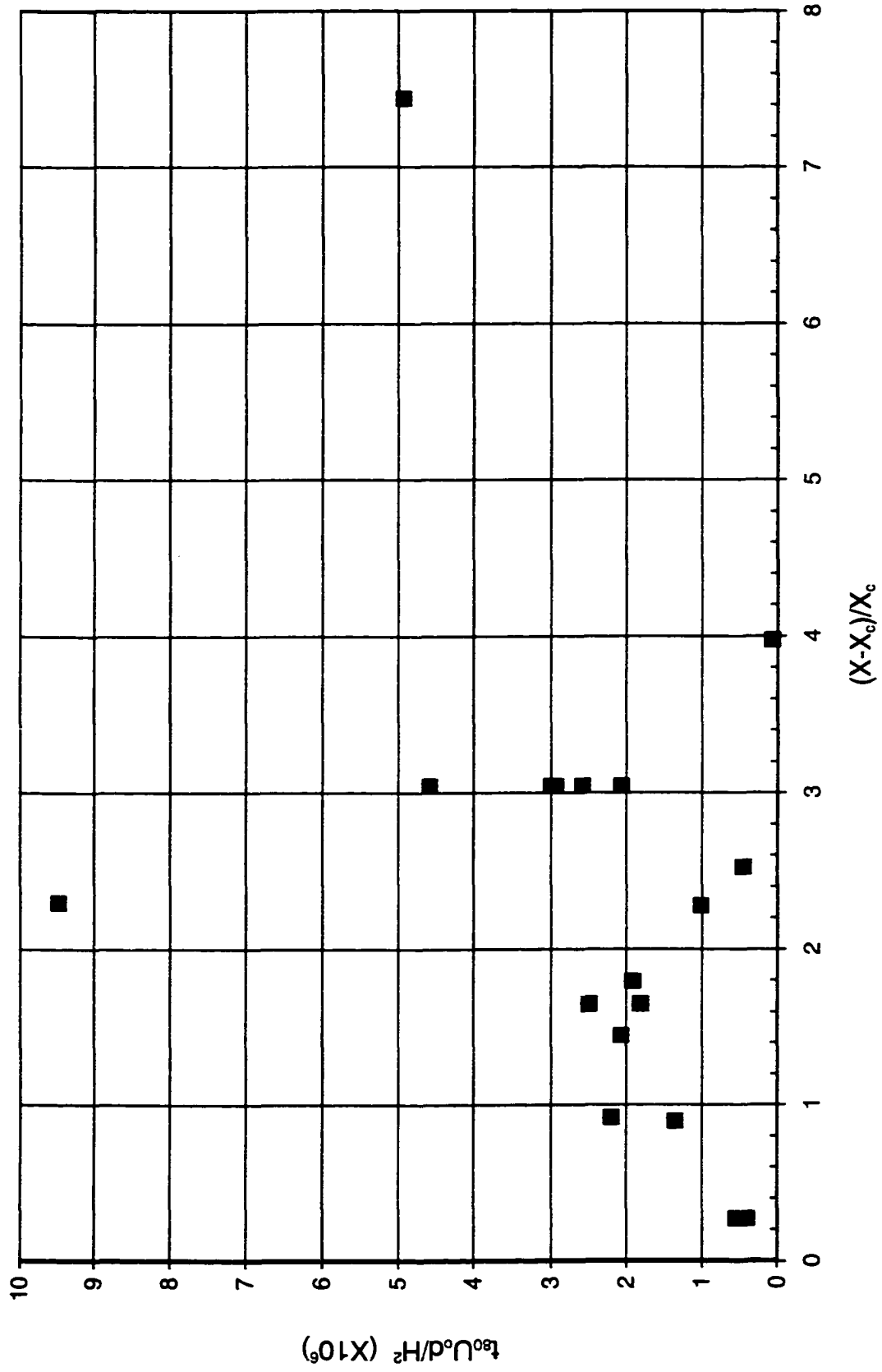


Fig. 6-30: Dimensionless time scale for scour hole volume with dimensionless excess stress.

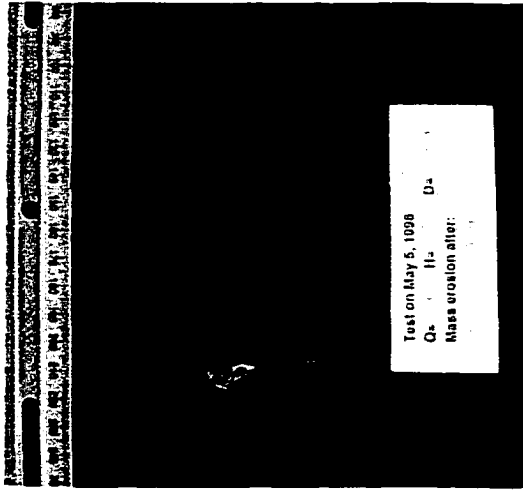


(a)

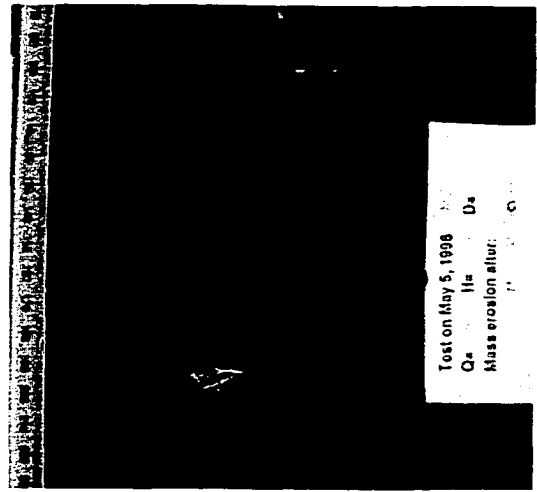


(b)

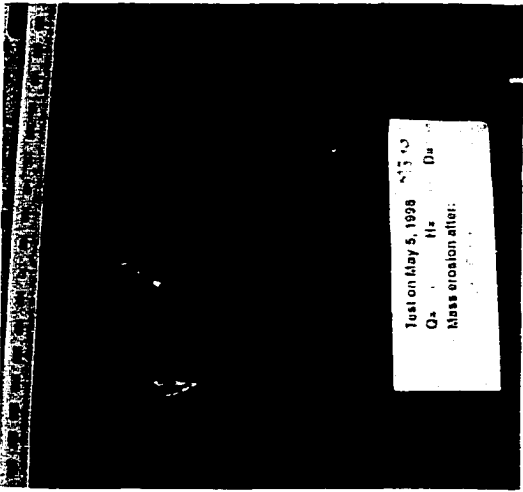
Plate 6-1: Typical scour holes (the point gauge marks the jet centerline) (a) Test no. 8/14.5/10.9/1 $U_o=10.94$ m/s $d=8$ mm $H=65$ mm $(X-X_c)/X_c=0.90$ (after 71h 17min) (b) Test no. 8/8.1/9.0/4 $U_o=8.95$ m/s $d=8$ mm $H=65$ mm $(X-X_c)/X_c=3.05$ (after 116h 49min).



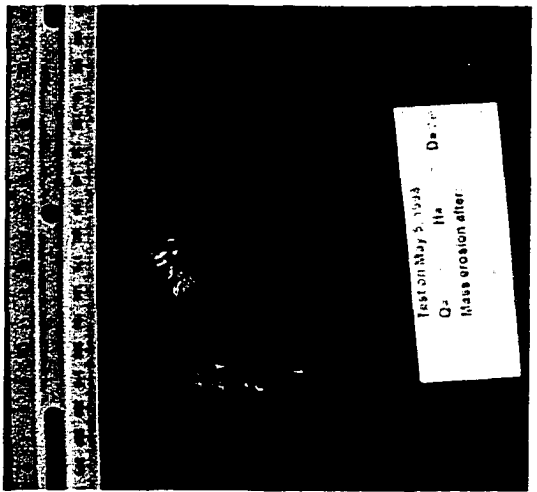
(a)



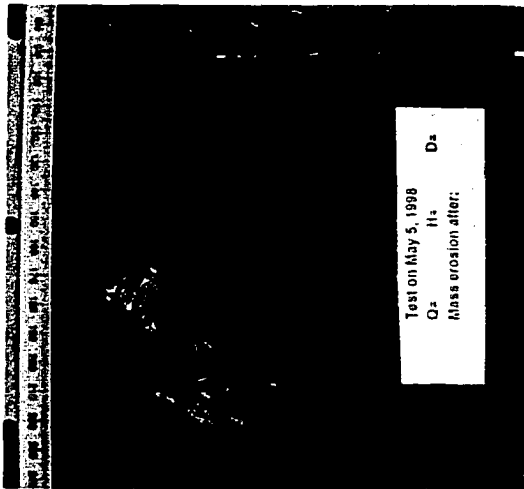
(b)



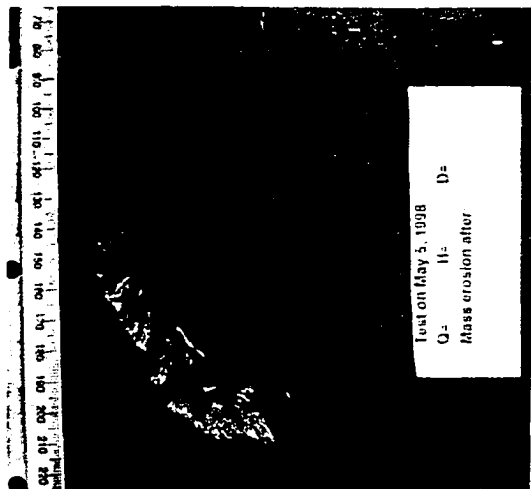
(c)



(d)

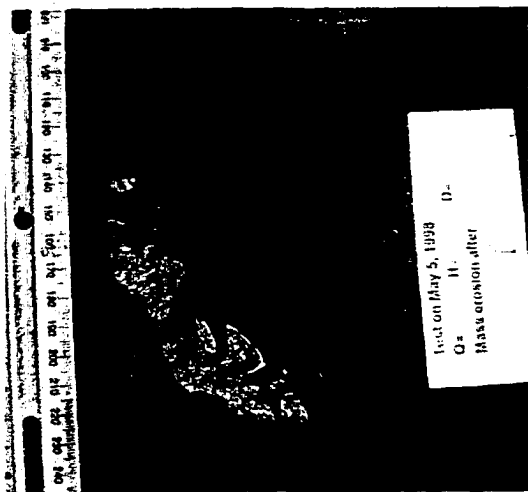


(e)

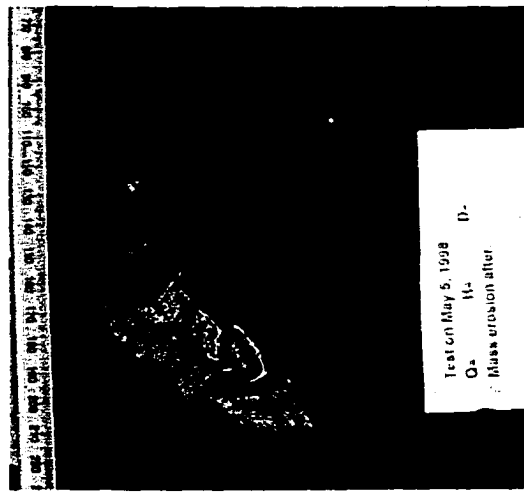


(f)

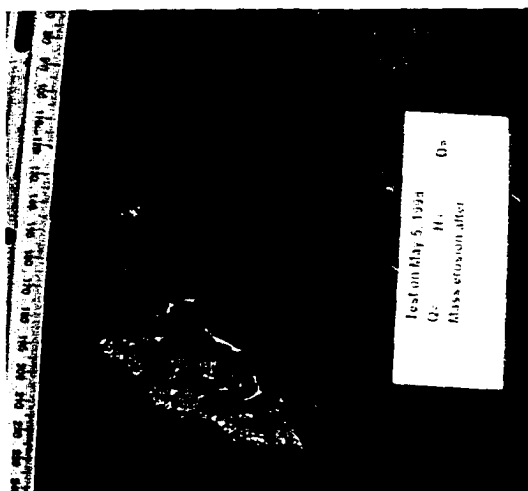
Plate 6-2: Scour hole growth for Test no. 8/8.1/9.0/1 $U_o=8.95$ m/s $d=8$ mm $H=65$ mm $(X-X_c)/X_c=3.05$ after (a) 15min (b) 30min (c) 1h 8min (d) 2h 30min (e) 5h (f) 9h 44min (g) 23h 21min (h) 30h 21min (i) 46h 6min (j) 55h 42min (k) 96h 36min (l) 124h 15min.



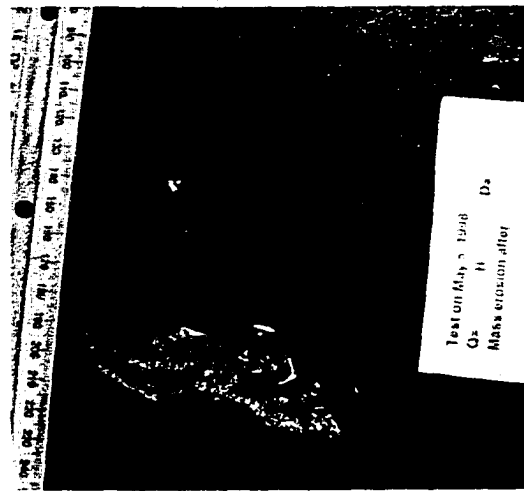
(g)



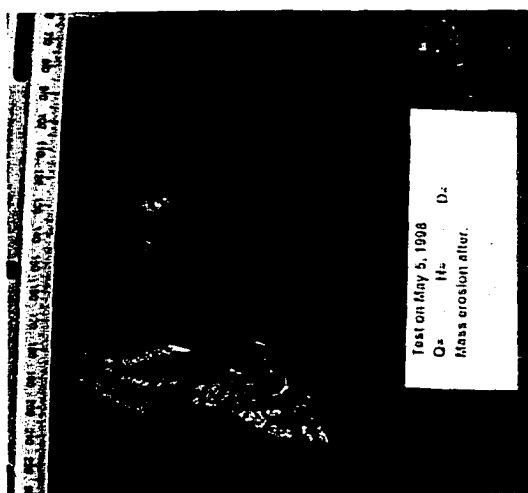
(h)



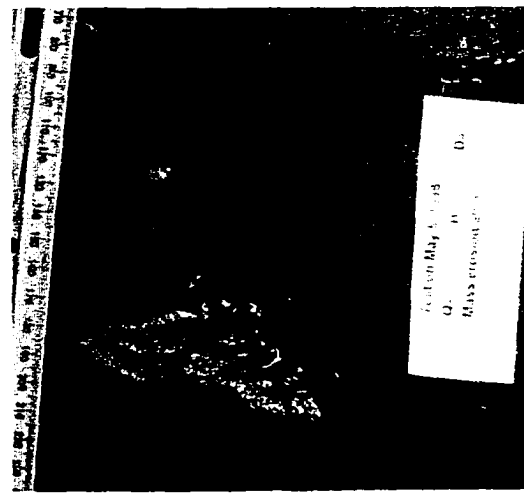
(i)



(j)



(k)



(l)

Plate 6-2: cont'd.

CHAPTER 7: RESULTS AND ANALYSIS OF WALL JETS TESTS

7.1 Introduction

Erosion by plane turbulent wall jets occurs in a number of practical situations. Examples are the scour created downstream of gates and in hydraulic jump type stilling basins. For each case, the potential amount of erosion created by the flow must be assessed, as excessive scour can cause these hydraulic structures to become unstable. There have been very few investigations that have studied the erosion of clays by wall jets. Abt (1980) studied the scour created by a horizontal circular wall jet in his study of the scour created at a culvert outlet. He measured the scour created in one cohesive soil for different flows and culvert diameters. The growth of the scour hole was observed up to a maximum test duration of 1000 min. Kuti and Yen (1976) studied the scour created by a hydraulic jump at the end of an apron at the base of a model dam. They reported the volume of scour for varying clay contents and void ratio of the soil. They did not vary the flow in these tests.

For the exploratory study described herein, a submerged plane turbulent wall jet was used to create scour in a clay. The maximum scour depth, distance to the maximum depth from the nozzle, the length of the scour hole, and scour hole profile, at equilibrium or ultimate state are related to the characteristics of the jet through the use of dimensional analysis. Equilibrium or ultimate state is defined as the asymptotic state of scour reached after a significantly long time as found by Laursen (1952), Rajaratnam (1981), and Chatterjee et al (1994), among others, in studies of the erosion by plane wall jets in cohesionless materials and Kuti and Yen (1976) for cohesive soils. Observations on the growth of the scour hole are also presented.

The study focuses on scour holes at equilibrium state because, from preliminary tests, it was found that disturbances on the clay surface, such as could occur when taking scour depth measurements, could cause erosion to occur when it would not otherwise. Secondly, the equilibrium state gives the largest scour that can be expected for given

hydraulic conditions, giving the maximum possible size of the scour hole. Finally, allowing the scour holes to reach equilibrium was thought to better serve the elucidation of this problem, as scour holes in the same state of scour are compared.

7.2 Results

As discussed in Chapter 4, measurements of the scour hole were taken along three longitudinal sections. Typically these sections were taken at about 50 mm, 75 mm, and 100 mm across the width of the sample measured from its edge, with 75 mm falling along the jet centreline. The locations of the sections were varied somewhat for each test so that the data reflected the most representative profiles for that particular test. This was done because of the sometimes great variability in the condition of the samples across the sample width. As discussed in Chapter 5, the scour holes were formed primarily by mass erosion by the removal of mostly small sized chunks (a few millimetres for the dimensions of the chunks). Rapid surface erosion was also observed during these tests, particularly for the very early times. Thus the parameters and predictive equations developed below are for those scour holes primarily formed by mass erosion.

Typical equilibrium scour profiles are shown in Figure 7-1, where ϵ_{∞} is the depth of erosion at any location in the equilibrium state with a sketch of the scour profiles shown in Figure 7-2. These typical profiles were measured along the centreline of the block. Although the flow is, at least initially, two dimensional, the scour across the width of the block was quite variable. Most often, both the scour hole dimensions and the profile shape varied across the sample. It was the unusual case where the scour hole at equilibrium remained uniform. It is seen that there is no deposition of material at the end of the scour hole for this clay (Figure 7-1), as observed for the scour of sand by wall jets (Laursen, 1952, Rajaratnam, 1981) and by Abt (1980) in his tests with a cohesive soil (a mixture of 58% sand, 14% silt, and 28% clay, and 1 % organic material).

Two tests were undertaken to examine the growth of the scour holes with time. For these tests, the samples were taken out of the experimental setup at selected times and the scour hole profile along the jet centreline were measured. The growth of the scour holes in the two evolution tests are shown in Figure 7-3, with photographic observations of the growth of one of the scour holes shown in Plate 7-1. The scour hole dimensions ϵ_m , x_m , and x_o , appear to grow in a linear relation with the logarithm of time (Figure 7-4 to 7-6). These observations are similar to that seen for the scour of cohesionless materials (Laursen, 1952). Unfortunately, in neither test did the scour hole reach an equilibrium state before the test ended.

7.3 Dimensional Analysis for Plane Wall Jet Scour of Clays

7.3.1 Dimensional Analysis for Scour Hole Dimensions at Equilibrium State

Dimensional analysis is used to develop parameters appropriate to describe the scour of clay by a plane turbulent wall jet. It is considered that the maximum depth of scour at equilibrium state, ϵ_{∞} , by a submerged plane turbulent wall jet in a clay is a function of:

$$\epsilon_{\infty} = f\{U_o, a, \rho, \mu, \tau_c\} \quad (7.1)$$

where:

- ϵ_{∞} = maximum depth of scour at ultimate state
- U_o = velocity of the jet at the nozzle
- a = jet thickness at the nozzle (nozzle height)
- ρ = density of the eroding fluid
- μ = dynamic viscosity of the eroding fluid
- τ_c = critical shear stress for mass erosion of the clay

Using the Buckingham π -theorem with the repeating variables U_o , a , and ρ it is found:

$$\frac{\epsilon_{\infty}}{a} = f\left\{\frac{\rho U_o^2}{\tau_c}, \frac{U_o a}{\nu}\right\} \quad (7.2)$$

As the shear stress on the bed (or clay surface) can be written as $\tau_o = c_f \frac{\rho U_o^2}{2}$ (Myers et al, 1963), the parameter $\frac{\rho U_o^2}{\tau_c}$ can be interpreted as the relation of the shear stress on the bed to the critical shear stress of the soil. To simplify the relation, the parameter λ is defined as $\lambda = \rho U_o^2$. Then assuming that there is a critical value of λ , λ_c , below which no significant erosion occurs, $\frac{\rho U_o^2}{\tau_c}$ can be written as an excess stress term:

$$\frac{\epsilon_{\text{max}}}{a} = f_1 \left\{ \frac{\lambda - \lambda_c}{\lambda_c}, \frac{U_o a}{v} \right\} \quad (7.3)$$

The parameter $\frac{U_o a}{v}$ can be recognized as the jet Reynolds number R. Since the shear stress on the bed has been found to have only a weak dependence on R (Myers et al, 1963; Schwarz and Cosart, 1961; Hogg et al, 1997), for R in the range of at least 7100 to 56500, it is assumed that the effect of the Reynolds number is small so that:

$$\frac{\epsilon_{\text{max}}}{a} = f_2 \left\{ \frac{\lambda - \lambda_c}{\lambda_c} \right\} \quad (7.4)$$

Expressions for the location of the maximum depth of scour, x_{max} , the length of the scour hole, x_{oo} , and the distance from the nozzle to where the scour is half the maximum scour depth, b_{wo} , can then be similarly written for equilibrium state:

$$\frac{x_{\text{max}}}{a} = f_3 \left\{ \frac{\lambda - \lambda_c}{\lambda_c} \right\} \quad (7.5)$$

$$\frac{x_{\text{oo}}}{a} = f_4 \left\{ \frac{\lambda - \lambda_c}{\lambda_c} \right\} \quad (7.6)$$

$$\frac{b_{\text{wo}}}{a} = f_5 \left\{ \frac{\lambda - \lambda_c}{\lambda_c} \right\} \quad (7.7)$$

It should be noted that for the purposes herein, the distances from the nozzle x_m , x_o , and b_w , are more precisely defined as the distance from the start of the sample. This was 2 mm away from the nozzle which was the thickness of the metal band that contained the samples.

7.3.2 Dimensionless Parameters for the Growth of the Scour Hole

To allow for analysis of the growth of the scour holes, an additional dimensionless parameter must be developed. Assuming that the maximum depth of the scour hole at any time, t , depends on time and the same parameters as the maximum scour depth at equilibrium state:

$$\epsilon_m = f\{U_o, a, \rho, \mu, \tau_c, t\} \quad (7.8)$$

Dimensional analysis then gives:

$$\frac{\epsilon_m}{a} = f_6 \left\{ \frac{\rho U_o^2}{\tau_c}, \frac{U_o a}{\nu}, \frac{U_o t}{a} \right\} \quad (7.9)$$

Rewriting this equation and assuming the effect of the jet Reynolds number is small, as above, suggests:

$$\frac{\epsilon_m}{a} = f_7 \left\{ \frac{\lambda - \lambda_c}{\lambda_c}, \frac{U_o t}{a} \right\} \quad (7.10)$$

7.4 Analysis of Equilibrium State Results

7.4.1 Dimensions of the Scour Hole at Equilibrium State

As discussed above, it is expected that the dimensions of the scour hole at equilibrium are related to the parameter $\lambda = \rho U_o^2$. To find such relations, the average dimensions of the scour hole were used. These averages are for the dimensions found from the three scour hole profiles taken for each tests. Figure 7-7(a) shows the relation with average maximum scour depth, $\bar{\epsilon}_{m\infty}$ (the average of the maximum scour depths found for each longitudinal section taken for each test), with λ . Given in Figure 7-7(b-n) is a

series of photographs showing several scour holes at equilibrium state which correspond to the data in Figure 7-7 (a). Table 7-1 gives the scour hole dimension data.

From Figure 7-7(a), and from the relations between the x_o and x_m with λ , the value of λ where no (significant) erosion occurs, λ_c , is about 20000 Pa. With an estimate for $c_f=0.005$ (Rajaratnam, 1965; Myers et al, 1963) for the shear stress on the bed in a location very near the nozzle for the range of Reynolds numbers used for the present experiments, this is equal to a maximum bed shear stress and thus a critical shear stress of about 50 Pa. This is very close to the critical shear stress value of 48 Pa found from the impinging jet tests.

Using the critical value of $\lambda_c=20000$ Pa, the scour hole dimensions were plotted with $\frac{(\lambda-\lambda_c)}{\lambda_c}$ (Figures 7-8 to 7-10). The results show that the scour hole dimensions at equilibrium correlate well with $\frac{(\lambda-\lambda_c)}{\lambda_c}$, with the data being best described by the equations:

$$\frac{\bar{e}_{m\infty}}{a} = 3.78 \frac{(\lambda - \lambda_c)}{\lambda_c} \quad (7.11)$$

$$\frac{\bar{x}_{m\infty}}{a} = 3.84 \frac{(\lambda - \lambda_c)}{\lambda_c} \quad (7.12)$$

$$\frac{\bar{x}_{o\infty}}{a} = 27.0 \left(\frac{\lambda - \lambda_c}{\lambda_c} \right)^{0.58} \quad (7.13)$$

These equations have respective correlation coefficients \tilde{R}^2 of 0.78, 0.64, and 0.82. The data for tests 2.33/8.0/1 and 2.33/8.5/1 (point 6 in Figure 7-7(a) and the point nearest to it) were not included for correlation for $\bar{e}_{m\infty}$ and $\bar{x}_{m\infty}$, as the large values for $\bar{e}_{m\infty}$ and $\bar{x}_{m\infty}$ were the result of a strongly V-shaped scour hole as compared to the other tests. It should also be noted that the two highest values of x_o in Figure 7-10 were estimated from the scour

hole profiles for these tests, as the length of the scour hole reached just beyond the end of the sample.

7.4.2 Scour Hole Profiles at Equilibrium State

There appeared to be several different shapes for the scour hole profiles that for the purposes herein have been classified into four types. For one test, a different profile may occur for each longitudinal section taken across the block as the scour holes were most often not two dimensional and had a shape that varied across the block width. Typical profiles are given in Figure 7-11 for each scour hole type. Figure 7-11 (a) shows the smooth and rounded Type 1 profile. Figure 7-11 (b) shows both the shallow and long Type 2 profile and the Type 3 profile that similar to the Type 1 profile but has a “kink” in the latter half of the profile. The Type 4 profile (Figure 7(c)) is V-shaped. It is similar to the Type 1 profile, but x_m is shifted away from the nozzle. Table 7-1 includes the classification of the profiles for each test. Some of the profiles could not be classified into one of the four scour hole types and was labeled “unknown”. Appendix E gives the data for the scour hole profiles at equilibrium with the scour hole profiles given in Appendix F.

Several different scales were tried to nondimensionalize the scour hole profile data. To nondimensionalize the distance from the nozzle, x_m and x_o (as used by Abt (1980) in his circular horizontal wall jet tests) were tried as the scales but did not work well to collapse the data. However, the distance from the nozzle, $b_{w\infty}$, where $\epsilon_{\infty} = \epsilon_{m\infty} / 2$ on the part of the profile where $x > x_m$ was found to be a suitable scale. The maximum scour depth was used as the scale for the scour depths. The dimensionless profiles for the four different scour hole types are given in Figures 7-12 to 7-15. A fifth power polynomial was used to fit to the Type 1 scour profile (Figure 7-12):

$$\frac{\epsilon_{\infty}}{\epsilon_{m\infty}} = 1.62 \left(\frac{x}{b_{w\infty}} \right)^5 - 7.45 \left(\frac{x}{b_{w\infty}} \right)^4 + 11.08 \left(\frac{x}{b_{w\infty}} \right)^3 - 4.92 \left(\frac{x}{b_{w\infty}} \right)^2 - 0.219 \left(\frac{x}{b_{w\infty}} \right) - 0.630 \quad (7.14)$$

with an $\tilde{R}^2=0.91$. This equation significantly departs from the data at about $x/b_{w\infty} \geq 1.4$. The Type 1 profile was included with the other profile types to allow for a comparison of the profile shapes. Figure 7-14 shows that the Type 3 profile is very similar to the Type 1 profile, but appears to depart from the Type 1 profile for $x/b_{w\infty} \geq 1$. The Type 4 profile also closely resembles the Type 1 profile (Figure 7-15).

To be able to use the above developed scour hole profiles, the length scale $b_{w\infty}$ must be determined. Figure 7-16 shows the relation between $\bar{b}_{w\infty}$ and $\left(\frac{\lambda - \lambda_c}{\lambda_c}\right)$. The length scale can then be found using the equation:

$$\frac{\bar{b}_{w\infty}}{a} = 15.14 \left(\frac{\lambda - \lambda_c}{\lambda_c} \right)^{0.56} \quad (7.15)$$

This equation fit the data with an $\tilde{R}^2=0.78$. Although the length scale can be predicted, the scour hole shape that will occur for a given set of conditions as yet cannot be determined. The variability of scour across the width of the sample possibly can be attributed to both the effects of the removal of clay chunks by mass erosion on the overall erosion process and the hydraulics of this type of flow. Near the beginning of a test, there was often one or two mid-sized chunks (10 mm dimensions) removed by mass erosion from the clay. It is thought that these perturbations in the sample surface changes the original two-dimensional flow over the sample into a more three-dimensional flow, thus creating the three-dimensional scour pattern. It has also been observed (Rajaratnam, 1968) that at a section near the channel wall, the average velocity in a plane turbulent jet increases over that at the jet centreline (and comes to zero at the wall). This may partly explain why there was often deeper scour near the walls of the flume when intuitively one would expect less scour in this region. However, this latter observation might also be explained by weaknesses created in the sample by inserting the metal band that contains the sample for the tests into the clay.

As the scour hole profiles showed that there were different shapes of scour holes, an analysis was carried out as to whether there was an obvious difference in the scour hole dimensions between the scour hole types. Figures 7-17 to 7-20 shows $\epsilon_{m\infty}$, $x_{m\infty}$, $x_{o\infty}$, $b_{w\infty}$ as a function of λ and scour hole type. The Type 2 profiles tend to be shallower than the other scour hole types, although they are not significantly different in depth. The Type 2 profiles also tend to have a smaller x_m (Figure 7-18). No conclusions can be drawn about the length of the scour hole (Figure 7-19) or the length scale (Figure 7-20). Since there were no strong tendencies for the scour hole dimensions to depend on the scour hole profile type, it was concluded that using average values for each test was acceptable.

7.4.3 Geometry of the Scour Holes

To elucidate the differences in the scour hole profile types, the parameters $\frac{x_{m\infty}}{\epsilon_{m\infty}}$, $\frac{x_{o\infty}}{\epsilon_{m\infty}}$, $\frac{b_{w\infty}}{\epsilon_{m\infty}}$, and $\frac{x_{o\infty}}{x_{m\infty}}$ were plotted as functions of $\frac{\lambda - \lambda_c}{\lambda_c}$ (Figures 7-21 to 7-24). The ratio $\frac{x_{m\infty}}{\epsilon_{m\infty}}$ appears to be independent of $\frac{\lambda - \lambda_c}{\lambda_c}$ (Figure 7-21) with $\frac{x_{m\infty}}{\epsilon_{m\infty}} \approx 1$. There is no indication the different scour hole types show significant differences in this parameter. For the ratio of the length of the scour hole to its maximum depth (Figure 7-22), the Type 2 scour holes have an average $\frac{x_{o\infty}}{\epsilon_{m\infty}} \approx 6$ which confirms these scour holes are long and shallow. This value is compared to $\frac{x_{o\infty}}{\epsilon_{m\infty}} \approx 3$ for the Type 4 profiles and $\frac{x_{o\infty}}{\epsilon_{m\infty}} \approx 4$ for the Type 1 profiles. The Type 3 profiles have large variability in $\frac{x_{o\infty}}{\epsilon_{m\infty}}$, as shown in the scatter in the latter half of the Type 3 scour hole profile (Figure 7-14). As may then be expected, the ratio of the length scale of scour to the maximum depth, indicates the Type 2 scour hole

profiles have a larger $\frac{b_{w\infty}}{\epsilon_{m\infty}}$ at about $\frac{b_{w\infty}}{\epsilon_{m\infty}} = 3.5$, while the Type 4 profiles have a smaller ratio at $\frac{b_{w\infty}}{\epsilon_{m\infty}} = 1.75$. All ratios indicate less scatter at high values of $\frac{\lambda - \lambda_c}{\lambda_c}$. If the differences in the scour hole profiles types are ignored and although there is a large amount of variability in the data at low values of $\frac{\lambda - \lambda_c}{\lambda_c}$, for the average scour hole $\frac{\bar{x}_{m\infty}}{\bar{\epsilon}_{m\infty}} \approx 1$, $\frac{\bar{x}_{0\infty}}{\bar{\epsilon}_{m\infty}} \approx 4$, $\frac{\bar{b}_{w\infty}}{\bar{\epsilon}_{m\infty}} \approx 2$, and $\frac{\bar{x}_{0\infty}}{\bar{x}_{m\infty}} \approx 4$ (Figure 7-25 to 7-28).

7.4.4 Variability in the Scour Holes

The scour produced in the samples was most often quite variable across the sample. Table 7-2 gives a range for the difference of the maximum sectional measurement of the scour hole (one of the longitudinal sections measured for each tests) and the average of the measurements for the scour hole. It also gives a range for difference between the maximum and minimum sectional measurements for the scour holes. The values in Table 7-2 do not include the extreme values produced from Test No. 2.33/5.2/1, where the value of λ was close to λ_c and the amount of scour was small.

7.5 Growth of the Scour Holes

The scour hole profiles measured at each time interval for each test were made dimensionless using ϵ_m and b_w as scales. It was found that the scour hole profiles are similar through the duration of a test (Figures 7-29 and 7-30). As well, the dimensionless profiles from the two tests fit well with one another and also are very close to the Type 4 profile developed from the scour hole profiles at equilibrium. As shown in Figures 7-4 to 7-6, the dimensions of the scour hole grow in a linear relation with the logarithm of time. The parameters developed in section 7.3 were used to nondimensionalize this data (Figure 7-31). However, there was not enough data to determine whether these dimensionless

parameters are adequate to describe this problem. The data from the evolution tests are given in Appendix G.

7.6 Analysis of Errors

The error analysis for the wall jet tests was carried out based on the work of Topping (1957). The velocity of the jet at the nozzle was measured through the use of a pressure tap on the nozzle and mercury manometers that could be read to 1 mm, however due to the variability in the readings the error is estimated as about 4 mm. This gives an maximum error in U_o of 2.1 %. The error in velocity thus results in an error in λ of 4.2% and in $\frac{\lambda - \lambda_c}{\lambda_c}$ of 8.3 %. Errors in the other measured quantities include a 2.0% error in the maximum scour depth at equilibrium, based on a 0.2 mm error in the point gauge measurements, and 14.2, 3.5, and 4.9 % errors in $x_{m\infty}$, $x_{0\infty}$, and $b_{w\infty}$ respectively, resulting from a 1 mm error in the measurement of these quantities. A summary of errors is given in Table 7-3.

7.7 Discussion and Conclusions

The scour of clay created by a plane turbulent wall jet was not two-dimensional for these tests, but varied across the width of the sample. This irregularity in the scour hole may be due to the walls of the flume and disturbances at the edges of the sample, but may also be due to the process of scour. For a clay eroded by mass erosion, a large eroded chunk of clay may significantly change the dynamics of the approximately two-dimensional jet flow over the sample into a much more three-dimensional flow, thus creating the uneven scour. Nevertheless, the longitudinal scour hole profiles at equilibrium were successfully made dimensionless using the maximum scour depth for the scour depths and the distance to half the maximum depth as the scale for the distance from the nozzle. These profiles did not fall on one curve, but could be divided into four types based on the shape of the

dimensionless profile. However, the type of scour hole profile that will form under given flow conditions cannot as yet be predicted.

The dimensions of the scour hole at equilibrium can successfully be correlated with the parameter $\lambda = \rho U_o^2$. There appears to be a critical value of λ below which significant erosion (i.e. more than flake erosion) does not occur and this was estimated at about 20000Pa. This gives a critical shear stress for the clay of $\tau_c = 50$ Pa which compares well to the value for the critical shear stress found in the impinging jet tests of 48 Pa. As for the impinging jet tests, the equations developed herein to predict the scour hole dimensions are for scour holes predominately formed by mass erosion. It is unlikely these equations would work well to predict scour in clays that are fissured, highly disturbed by sampling, slaking, layered, or otherwise inhomogeneous.

Observations of the evolution of two scour holes showed that the longitudinal profiles for each time through a test, made dimensionless using the maximum depth of scour and the distance to half the maximum depth of scour (for $x > x_m$) as scales, were similar. The growth of the scour hole dimensions showed a linear relation with the logarithm of time up to near the equilibrium state.

Table 7-1: Maximum scour depth, location of the maximum scour depth, and length of the scour holes, at equilibrium state for the wall jet tests.

Details of Tests							Section 1					Section 2					Section 3					Average for Scour Hole					
Test No.	Test Date	a (mm)	U_o (m/s)	R	ρU_o^2 (Pa)	$(\lambda - \lambda_c)/\lambda_c$	Type of Scour Hole	y (mm)	ϵ_{max} (mm)	x_{max} (mm)	x_{end} (mm)	b_{max} (mm)	y (mm)	ϵ_{max} (mm)	x_{max} (mm)	x_{end} (mm)	b_{max} (mm)	y (mm)	ϵ_{max} (mm)	x_{max} (mm)	x_{end} (mm)	b_{max} (mm)	$\bar{\epsilon}_{max}$ (mm)	\bar{x}_{max} (mm)	\bar{x}_{end} (mm)	\bar{b}_{max} (mm)	
2.33/9.3/1	12-Nov-98	2.33	9.31	14075	86636	3.33	2	38.5	20.6	20.0	140.0	80.3	78.5	18.2	27.0	130.0	77.5							18.4	23.5	135.0	78.9
2.33/9.7/1	18-Nov-98	2.33	9.74	14128	94872	3.74	S1-1/S2-3	38.5	31.3	38.0	190.0	112.0	76.5	36.8	43.0	193.0	88.3							34.1	40.5	191.5	100.1
2.33/8.8/1	7-Dec-98	2.33	8.84	13319	78132	2.91	S1-1/S2-2	38.5	16.0	30.0	97.5	61.1	76.5	18.7	30.0	104.0	59.2							17.4	30.0	100.8	60.1
2.33/8.1/1	14-Dec-98	2.33	8.13	12513	66173	2.31	S2-2						76.5	14.1	7.5	108.0	56.5							14.1	7.5	108.0	56.5
2.33/8.5/1	4-Jan-99	2.33	8.52	12790	72551	2.63	S1-7/S2-2	38.5	15.4	29.0	122.0	89.7	76.5	22.9	22.5	122.0	70.6							19.2	25.6	122.0	80.1
2.33/8.7/1	12-Jan-99	2.33	8.67	13022	75208	2.76	S2-2						76.5	22.0	23.0	120.0	59.2							22.0	23.0	120.0	59.2
2.33/7.4/1	22-Jan-99	2.33	7.36	11357	54214	1.71	S1-2/S2-3	38.5	12.5	10.0	86.0	55.8	76.5	16.2	15.0	84.0	30.9							14.4	12.5	85.0	43.4
2.33/8.1/2	28-Jan-99	2.33	8.05	12264	64845	2.24	S1-2/S2-2/S3-7	38.5	21.1	25.0	106.0	52.3	76.5	18.6	23.0	100.0	52.5	115.0	15.5	4.0	98.0	24.3	19.9	24.0	101.3	52.4	
2.33/7.0/1	11-Feb-99	2.33	6.98	10594	48738	1.44	7	45.0	14.4	32.5	68.0	47.74	72.0	18.0	36.0	70.0	49.4							15.2	34.3	69.0	48.8
2.33/7.2/1	17-Feb-99	2.33	7.17	10732	51444	1.57	1	59.0	12.3	26.0	70.0	39.7	83.0	12.7	25.0	72.0	44.8							12.5	25.5	71.0	42.3
2.33/8.0/1	15-Mar-99	2.33	7.97	12224	63508	2.18	4	61.0	55.4	45.0	118.0	73.44	76.5	57.0	48.0	132.5	74.7							56.2	48.5	124.3	74.1
2.33/8.5/2	30-Mar-99	2.33	8.46	12936	71629	2.58	S1-4/S2-1	68.5	61.5	55.0	141.0	77.08	85.0	61.9	55.0	136.0	74.6							61.7	55.0	138.5	75.8
2.33/8.2/1	6-Apr-99	2.33	8.18	12910	68948	2.35	S1-4/S2-3	59.0	23.3	32.0	89.0	51.48	81.0	26.7	25.0	88.0	49.3							25.0	28.5	88.5	50.4
2.33/9.5/1	13-Apr-99	2.33	9.50	14996	90330	3.52	1	62.0	48.0	25.0	147.0	67.35	83.0	52.2	30.0	120.0	68.5							50.1	27.5	120.0	67.9
2.33/8.8/1	3-May-99	2.33	9.85	18637	96928	3.85	S1-1/S2-4	81.5	31.3	40.0	107.0	62.98	107.0	35.4	42.0	116.0	64.1							33.4	41.0	111.5	63.5
2.33/11.3/1	13-May-99	2.33	11.31	20790	127940	5.40	4	56.5	59.4	60.0	155.0	92.8	78.0	60.4	60.0	180.0	94.9							59.9	60.0	167.5	93.8
2.33/8.0/1	19-May-99	2.33	9.03	16372	81443	3.07	2	50.0	19.7	32.0	122.5	79.5	85.0	23.7	32.0	132.0	68.2							21.7	32.0	127.3	73.9
2.33/10.2/1	25-May-99	2.33	10.23	21286	104503	4.23	S1-3/S2-1	53.0	40.5	41.0	175.0	87.2	94.5	40.7	37.5	152.0	89.3							40.6	39.3	163.5	88.3
2.33/8.2/1	8-Jun-99	2.33	8.16	12844	37866	0.89	S1-3	71.5	14.6	7.0	67.0	21.9												14.6	7.0	67.0	21.9
2.33/8.0/2	15-Jun-99	2.33	8.00	17891	63898	2.19	S1-4/S2-3	59.5	17.4	24.0	67.0	38.7	70.0	17.1	21.0	70.0	38.1							17.3	22.5	68.5	38.4
2.33/12.0/1	25-Jun-99	2.33	12.03	24918	144588	6.23	1	52.0	40.7	42.5	138.0	80.5	76.5	42.9	32.0	144.0	86.7							41.8	42.5	141.0	83.8
2.33/12.7/1	9-Jul-99	2.33	12.72	27182	161900	7.10	1	51.0	80.8	81.0	258	166.8	96.0	68.7	63.0	269	147.4							74.8	72.0	263.5	157.0
2.33/12.3/1	15-Jul-99	2.33	12.25	25502	149993	6.50	S1-3/S2-2	54.0	60.0	45.0	234	81.78	96.0	44.3	35.0	250	129.4							52.2	40.0	242.0	105.6
2.33/7.2/2	8-Sep-99	2.33	7.18	14484	51154	1.56	S1-3/S2-3/S3-4	50.0	9.8	14.0	60.0	24.1	75.5	12.2	14.5	63.0	23.9	110.0	17.9	21.0	61.0	32.5	13.3	16.5	61.3	26.8	
2.33/5.2/1	24-Sep-99	2.33	5.16	9974	26568	0.33	S2-7/S3-4	50.0	0.0	0.0	0.0	0	75.5	1.8	12.5	29.0	20.3	99.0	2.1	12.5	33.0	23.3	1.3	6.3	20.7	14.5	
2.33/11.7/1	30-Sep-99	2.33	11.66	21033	135824	5.79	4	50.0	38.8	44.0	141.0	75.8	75.5	43.7	42.5	120.0	72.1	100.0	45.1	39.0	143.0	72.4	42.5	41.8	134.7	73.4	
5.10/8.5/1	10-Jan-00	5.10	6.54	22096	42830	1.14	S1-3/S2-3/S3-7	50.0	20.7	42.5	153.0	86.04	75.5	16.1	30.0	149.0	74.8	100	10.2	35	130	95.48	15.7	35.8	144.0	85.4	
5.10/7.0/3	20-Jan-00	5.10	7.03	23949	49475	1.47	3	35.0	66.8	45.0	182.0	82.1	76.0	54.2	55.0	220.0	95.4	100	51.8	50	216	94.71	51.6	50.0	187.0	94.7	
5.10/6.0/1	28-Jan-00	5.10	6.04	20378	36430	0.82	7	52.0	45.9	32.5	197.5	145.0	75.5	44.23	36.0	200.0	143.8	107	44.3	39	199	138	44.8	35.8			
5.10/4.9/1	8-Feb-00	5.10	4.86	17281	23628	0.18	S1-3/S2-1/S3-1	55.0	31.3	25.0	96.0	53.08	75.5	30.83	32.0	92.0	54.0	105	21.4	30	83	50.21	27.8	29.0	83.0	52.4	

* For the 9 Jul 99 and 15 Jul 99, x_c was estimated from the scour hole profile data by extending the profile to zero scour as scour went past the end of the clay sample.
 * Italics denote that the scour hole was likely affected by slaking and this data was not included in the analysis.

Table 7-2: Variability in the dimensions of a scour hole.

Difference between section value and average value (%)							
$\epsilon_{m_{sc}}$		$x_{m_{sc}}$		$x_{o_{sc}}$		$b_{w_{sc}}$	
min	max	min	max	min	max	min	max
0.3	34.7	0	20	0	22.5	0.2	28.6

Difference between maximum and minimum section values (%)							
$\epsilon_{m_{sc}}$		$x_{m_{sc}}$		$x_{o_{sc}}$		$b_{w_{sc}}$	
min	max	min	max	min	max	min	max
0.5	66.9	0	42.4	0	22.5	0.5	57.3

Table 7-3: Maximum errors in measured and derived quantities for wall jet tests.

Quantity	Maximum Error	Notes
U_o	2.1%	
a	4.7% for the 2.33 nozzle 3.1% for the 5.10 mm nozzle	
$\epsilon_{m\infty}$	2.0%	*have an extreme value of 11.1% for a very shallow scour hole
$x_{m\infty}$	14.2%	
$x_{o\infty}$	3.5%	
$b_{w\infty}$	4.9%	
λ	4.2%	
$\frac{\lambda - \lambda_c}{\lambda_c}$	8.3%	
$\frac{\epsilon_{m\infty}}{a}$	6.8% for the 2.33 nozzle 5.2% for the 5.10 mm nozzle	*have an extreme value of 15.8 % *have an extreme value of 14.2 %
$\frac{x_{m\infty}}{a}$	19.0% for the 2.33 nozzle 17.3% for the 5.10 mm nozzle	
$\frac{x_{o\infty}}{a}$	8.2% for the 2.33 nozzle 6.6% for the 5.10 mm nozzle	
$\frac{b_{w\infty}}{a}$	9.7% for the 2.33 nozzle 8.1% for the 5.10 mm nozzle	

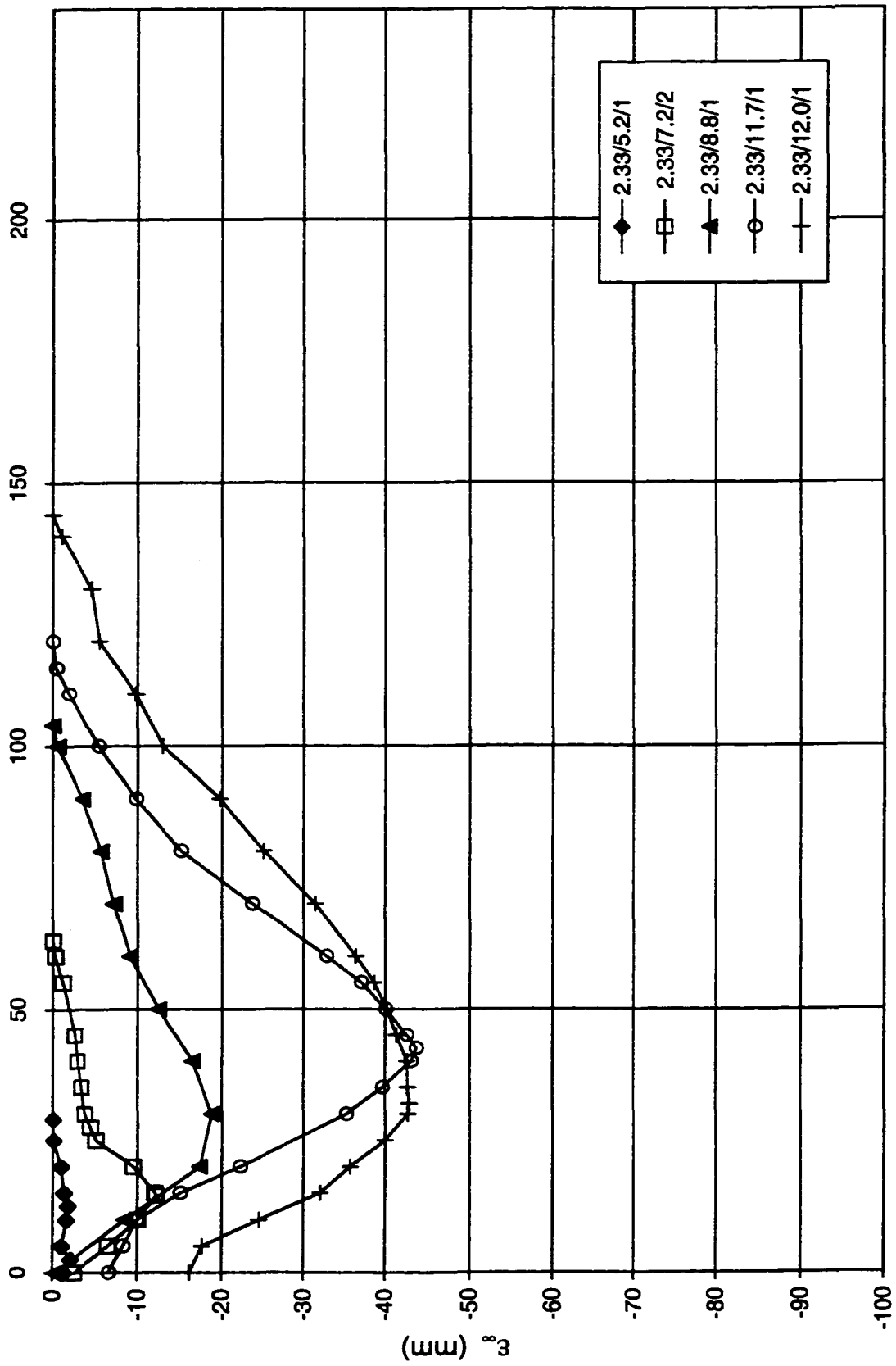


Fig. 7-1: Scour hole profiles at equilibrium along jet centreline.

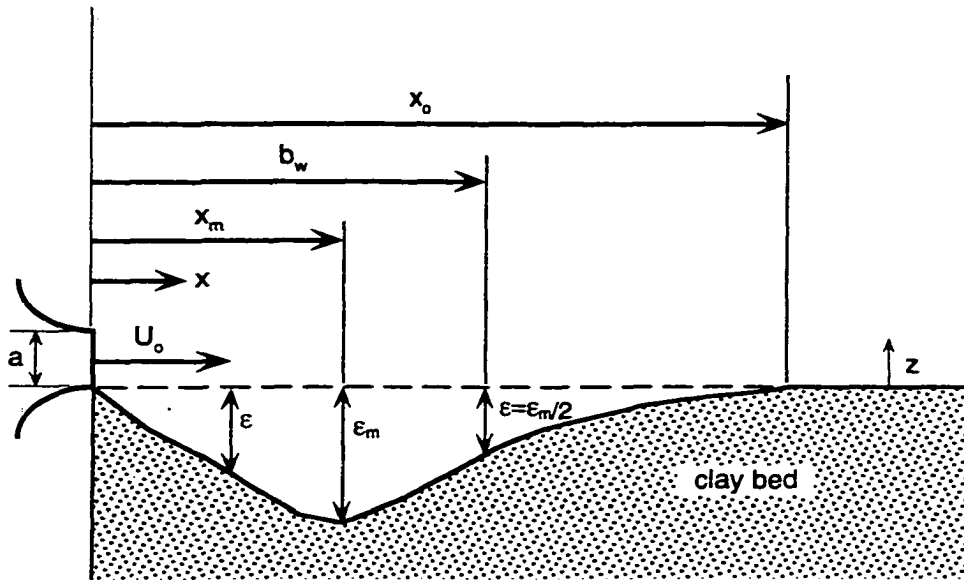
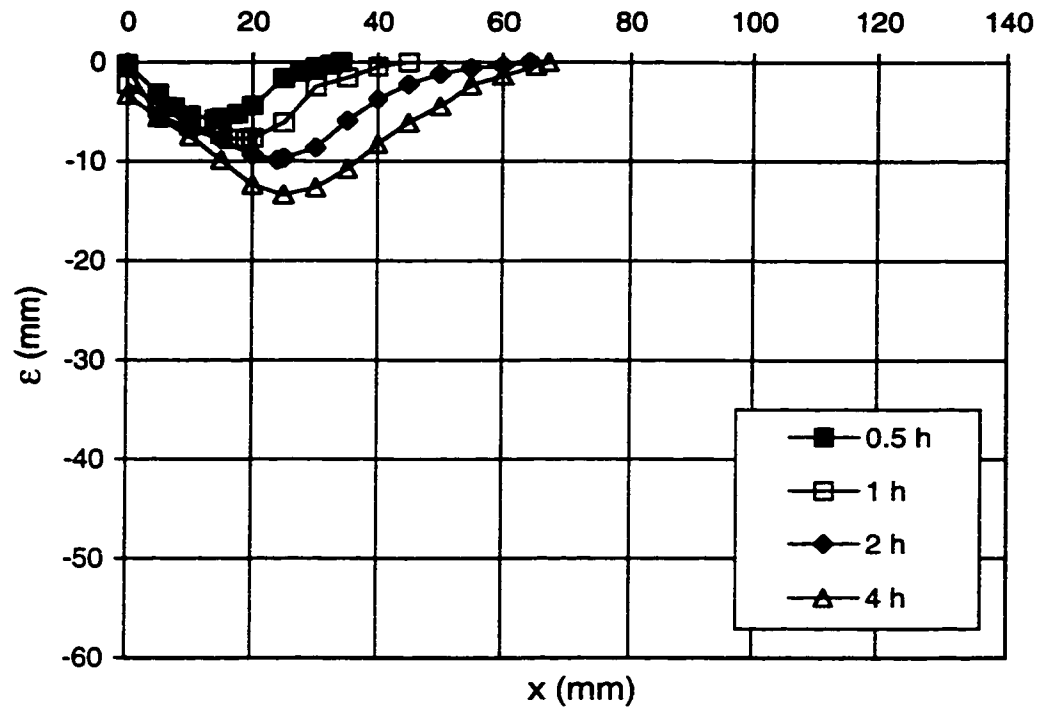
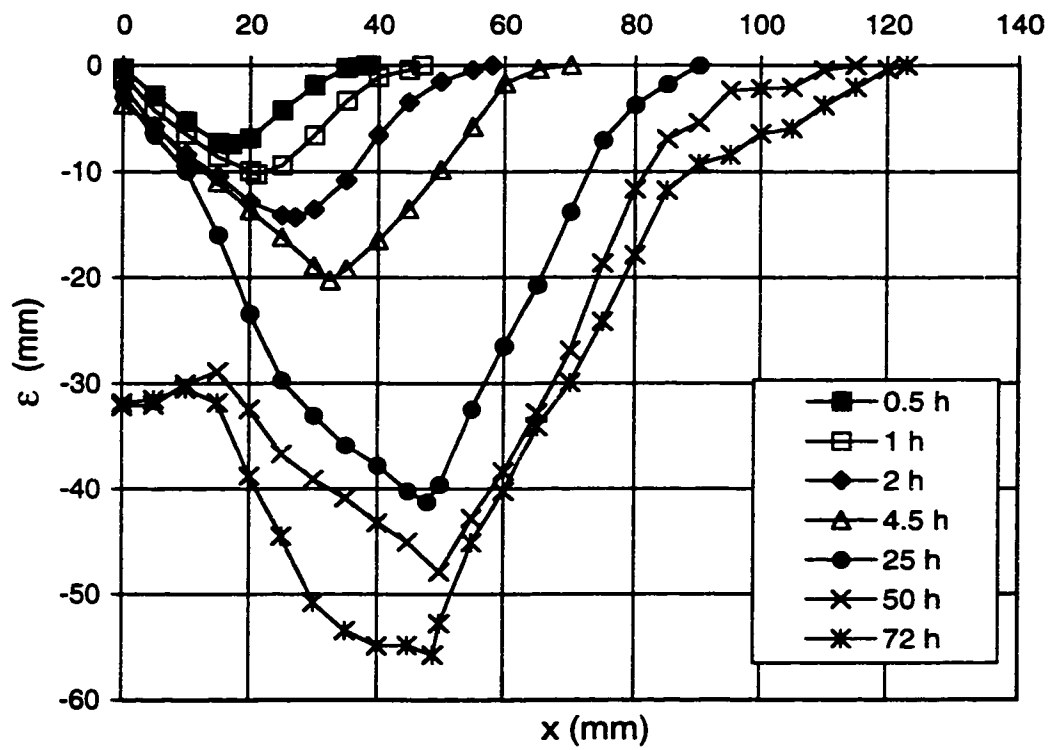


Fig. 7-2: Definition sketch of scour for wall jet tests.

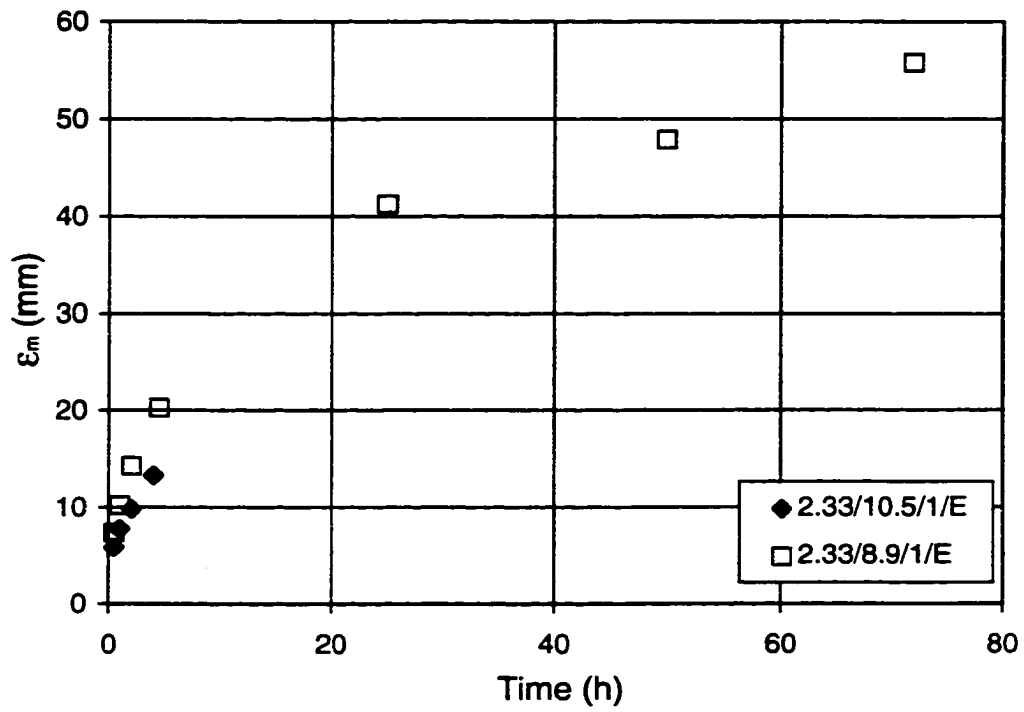


(a)

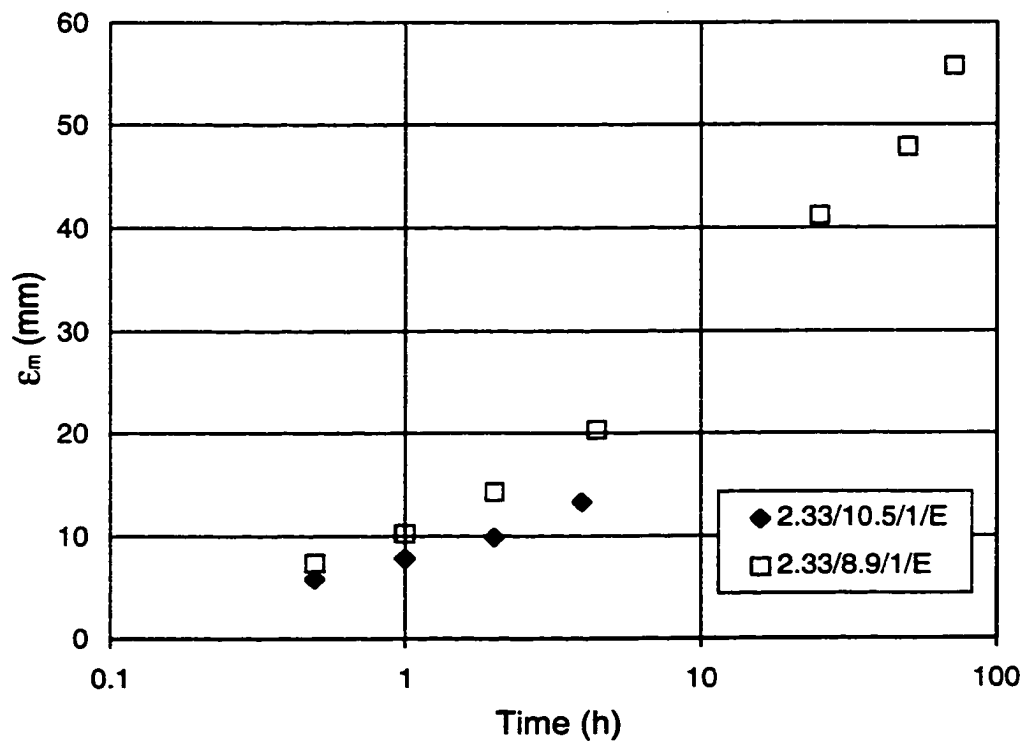


(b)

Fig. 7-3: Growth of the scour holes (a) Test No. 2.33/10.5/1/E
(b) Test No. 2.33/8.9/1/E

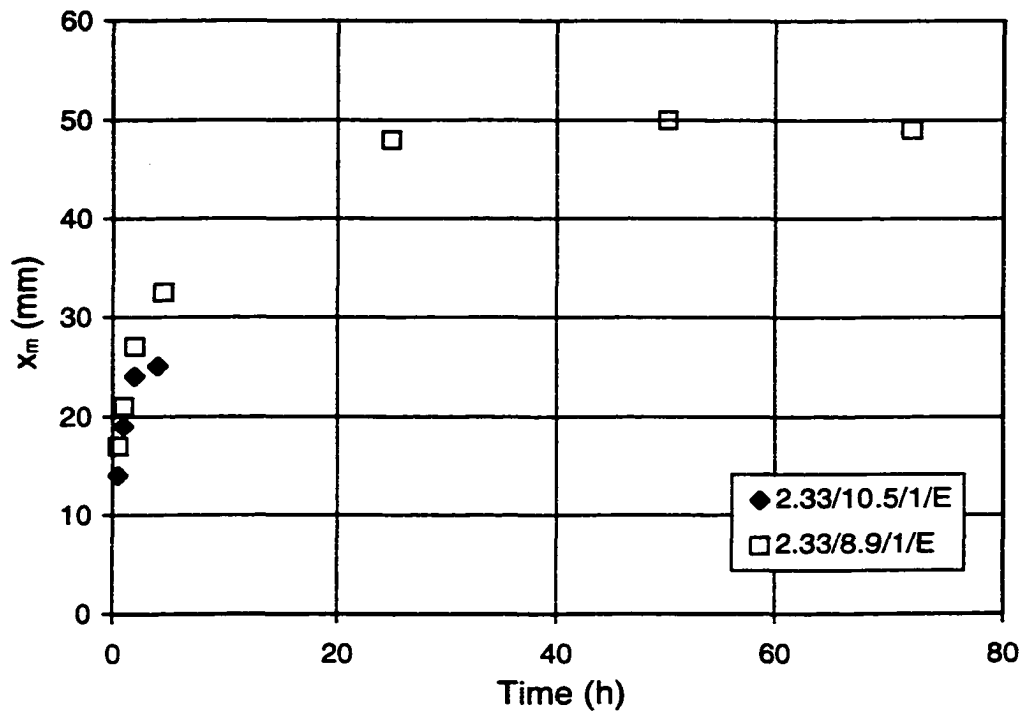


(a)

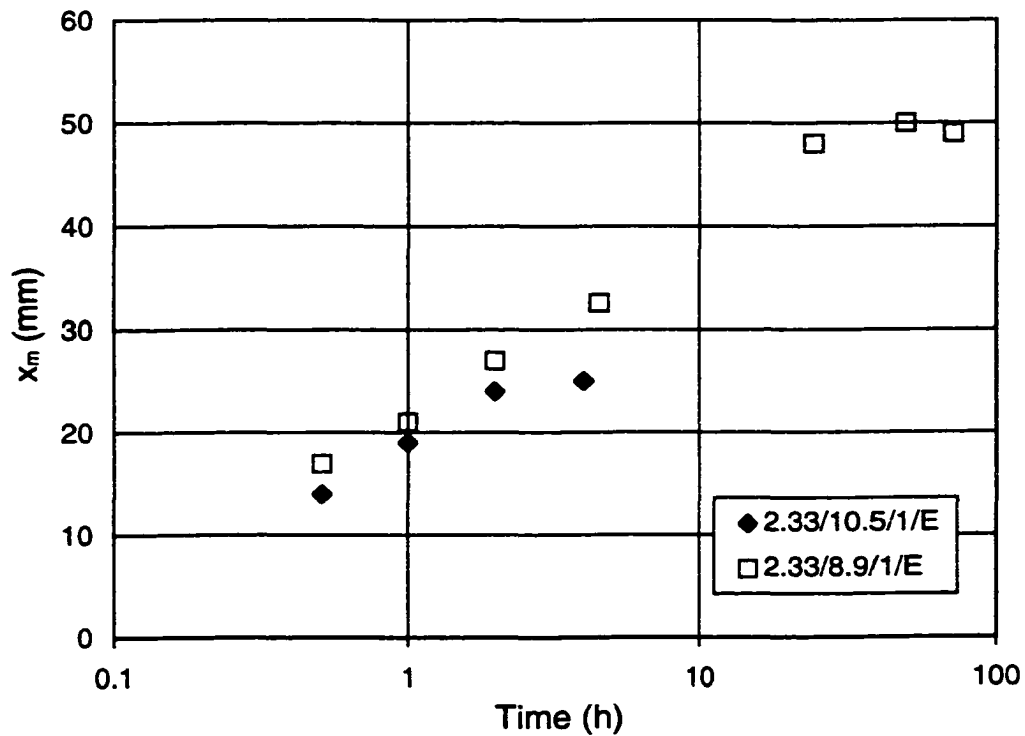


(b)

Fig. 7-4: Growth of the maximum scour depth with time
(a) arithmetic scale (b) semi-log plot.

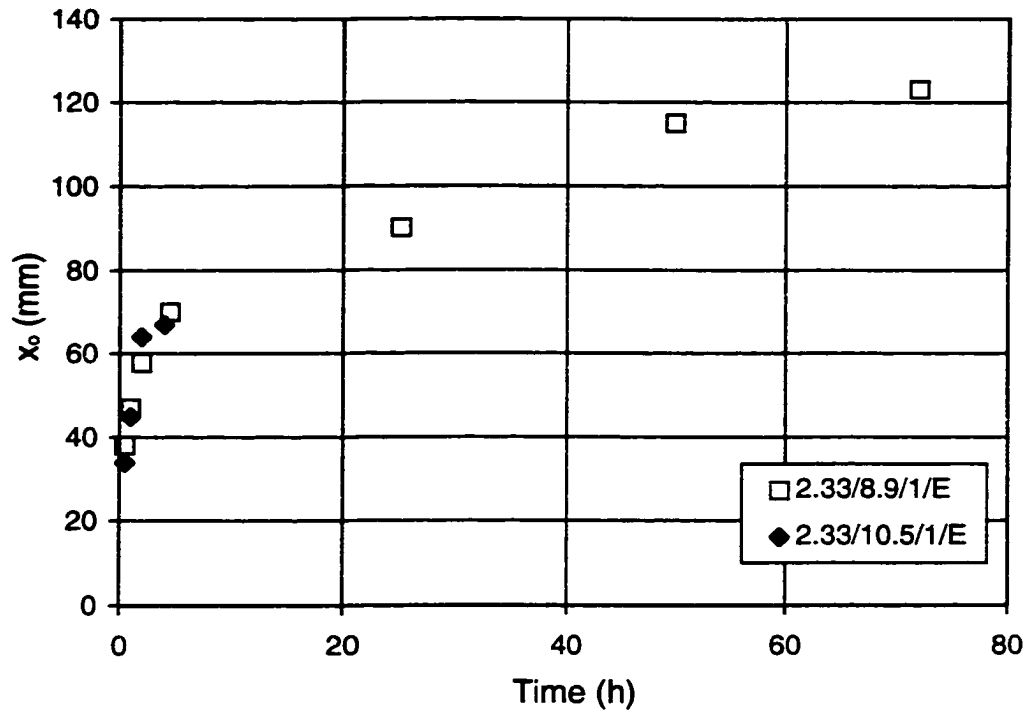


(a)

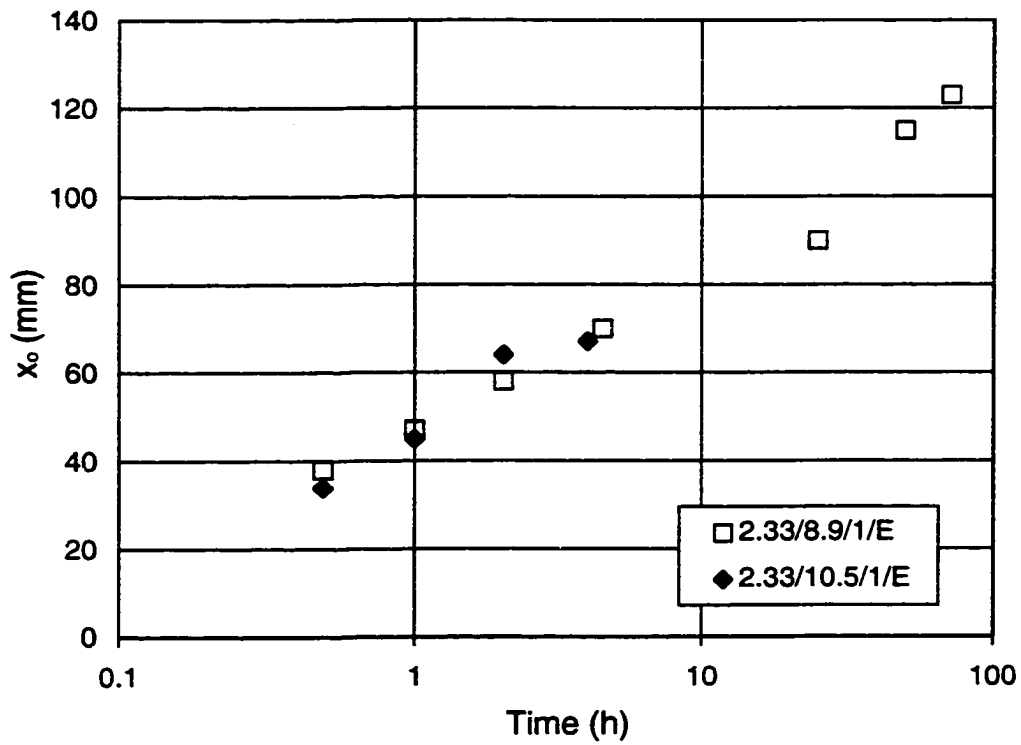


(b)

Fig. 7-5: The location of the maximum scour depth with time
(a) arithmetic scale (b) semi-log plot.



(a)



(b)

Fig. 7-6: Growth of the scour hole length with time (a) arithmetic scale
(b) semi-log plot.

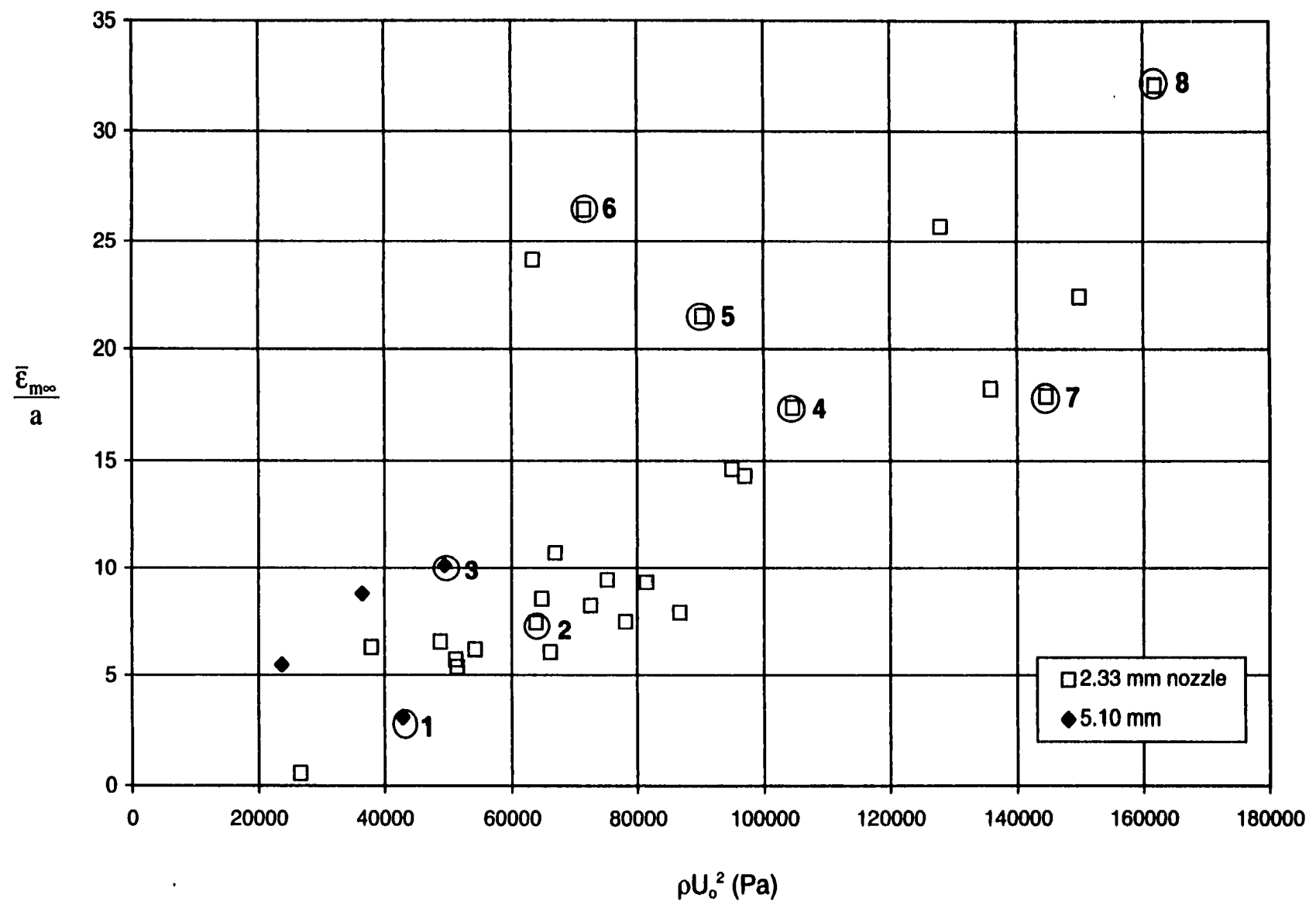


Fig. 7-7(a): Dimensionless average maximum scour hole depth at equilibrium.

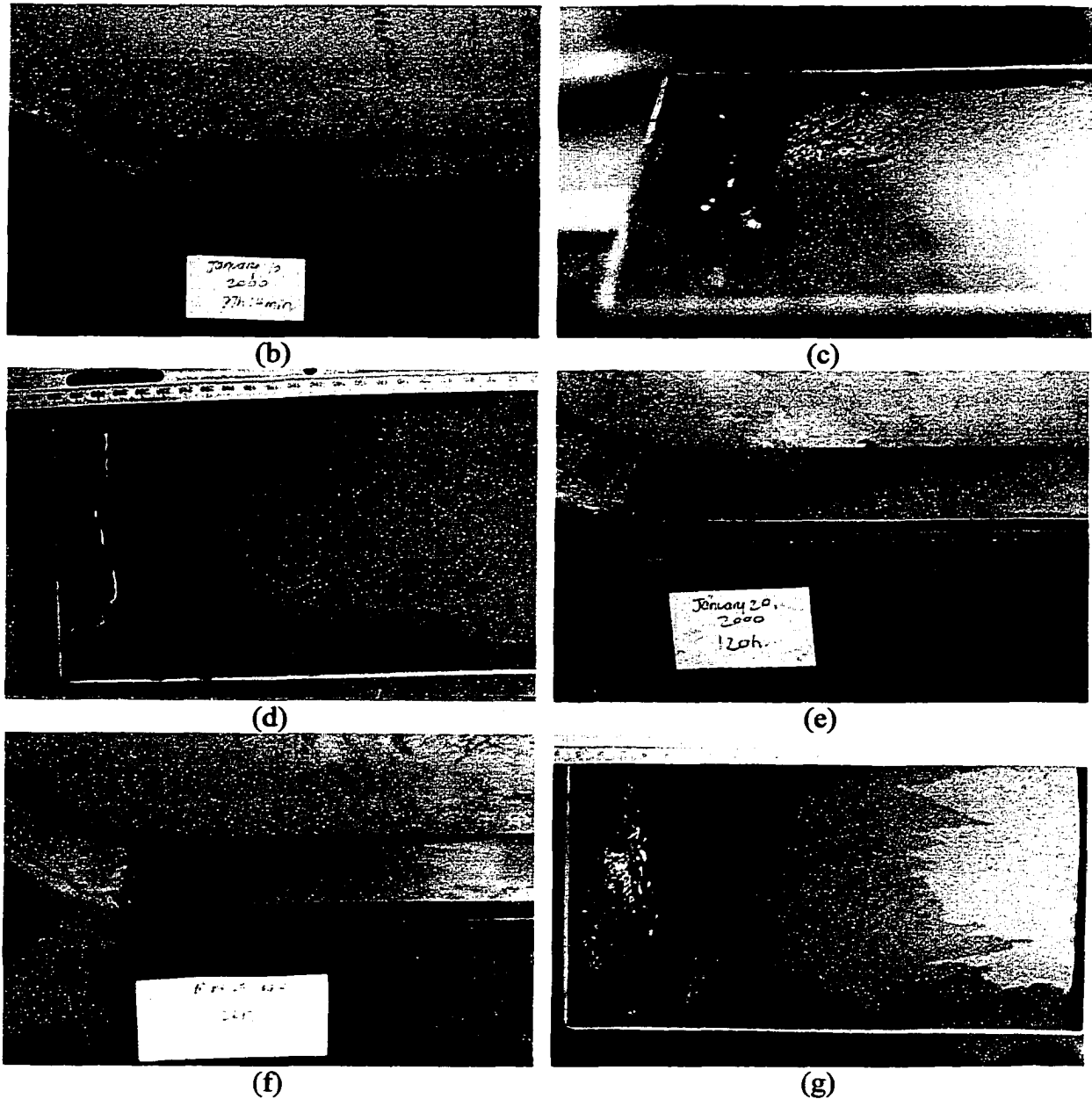
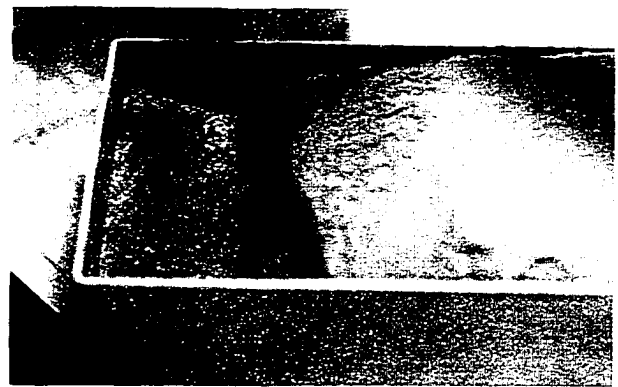


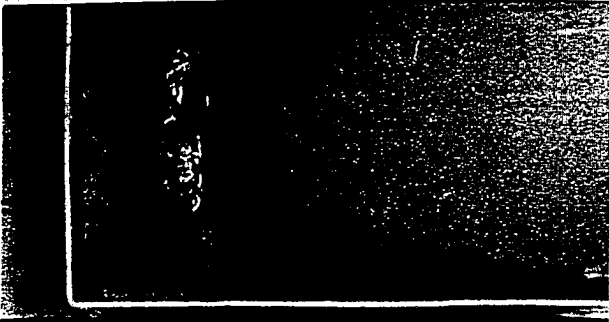
Fig. 7-7: (b) Point No.1 (5.10/6.5/1) $U_o=6.54$ m/s $a=5.10$ mm $(\lambda-\lambda_c)/\lambda_c=1.14$ $t_d=149.2$ h
 (c) Point 2 (2.33/8.0/2) $U_o=8.00$ m/s $a=2.33$ mm $(\lambda-\lambda_c)/\lambda_c=2.20$ $t_d=101.0$ h (side view) (d)
 Point 2 plan view (e) Point 3 (5.10/7.0/3) $U_o=7.03$ m/s $a=5.10$ mm $(\lambda-\lambda_c)/\lambda_c=1.47$
 $t_d=120.0$ h (f) Point 4 (2.33/10.2/1) $U_o=10.23$ m/s $a=2.33$ mm $(\lambda-\lambda_c)/\lambda_c=4.23$ $t_d=126.0$ h
 (g) Point 4 plan view (h) Point 5 (2.33/9.5/1) $U_o=9.50$ m/s $a=2.33$ mm $(\lambda-\lambda_c)/\lambda_c=3.52$
 $t_d=140.6$ h (i) Point 6 (2.33/8.5/2) $U_o=8.46$ m/s $a=2.33$ mm $(\lambda-\lambda_c)/\lambda_c=2.58$ $t_d=120.7$ h
 (side view) (j) Point 6 plan view (k) Point 7 (2.33/12.0/1) $U_o=12.03$ m/s $a=2.33$ mm
 $(\lambda-\lambda_c)/\lambda_c=6.23$ $t_d=93.2$ h (side view) (l) Point 7 plan view (m) Point 8 (2.33/12.7/1)
 $U_o=12.72$ m/s $a=2.33$ mm $(\lambda-\lambda_c)/\lambda_c=7.08$ $t_d=118.2$ h (side view) (n) Point 8 plan view



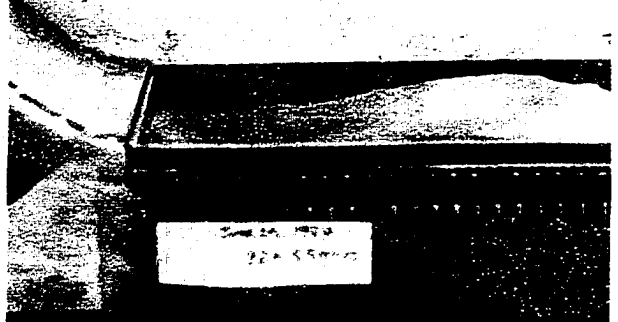
(h)



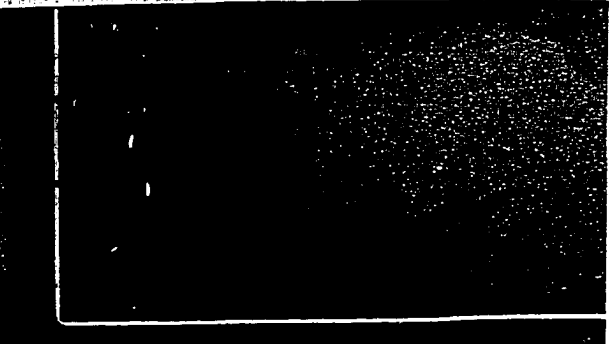
(i)



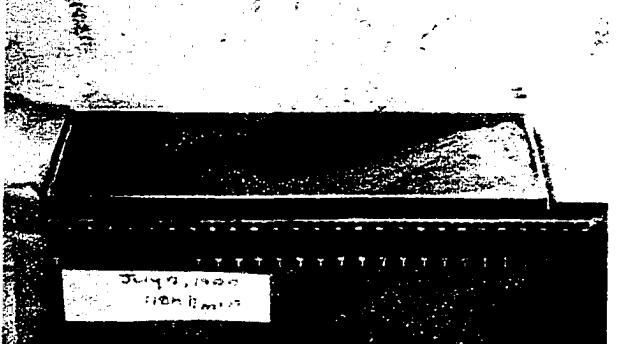
(j)



(k)



(l)



(m)



(n)

Fig. 7-7: cont'd.

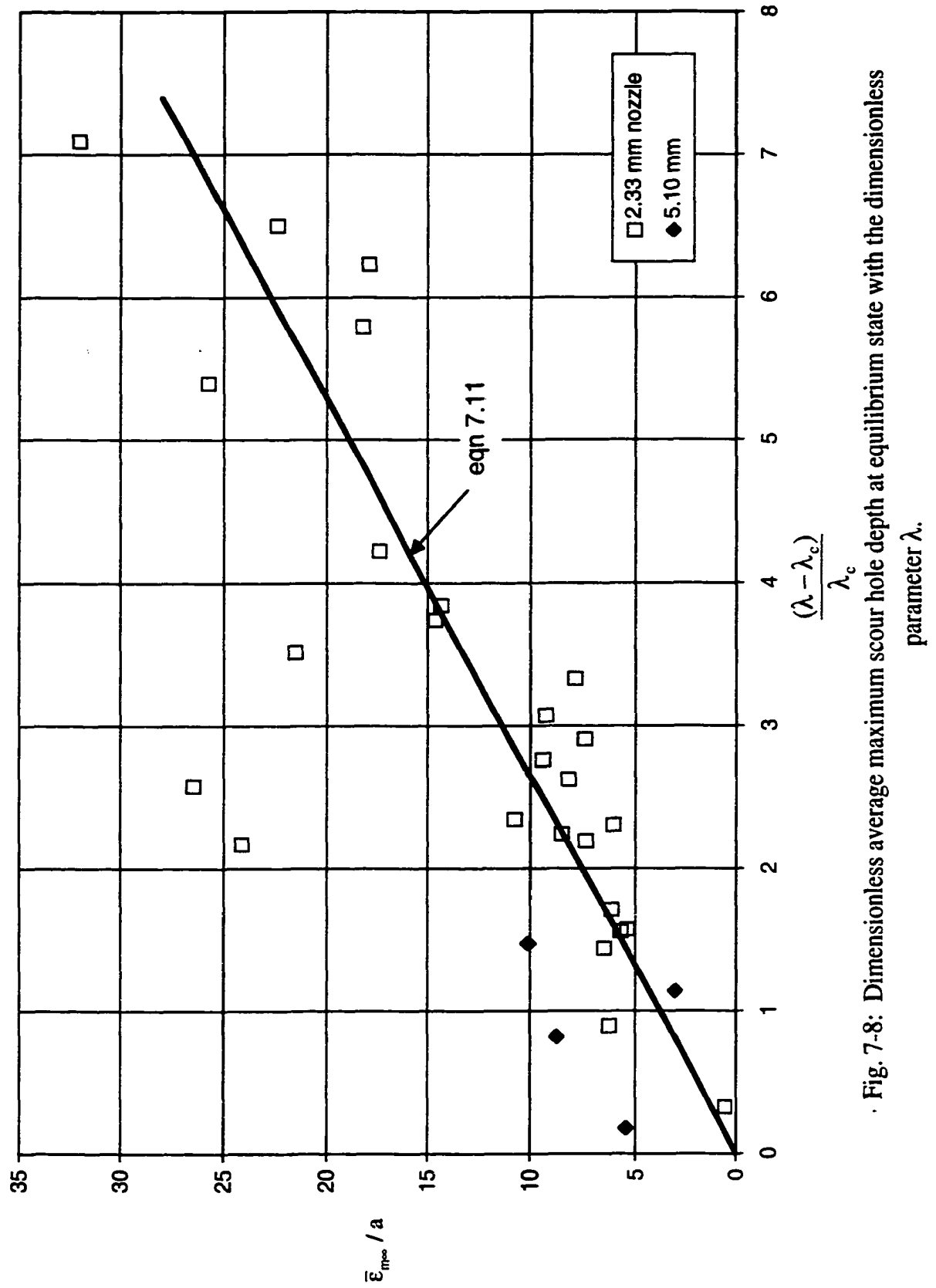


Fig. 7-8: Dimensionless average maximum scour hole depth at equilibrium state with the dimensionless

parameter λ .

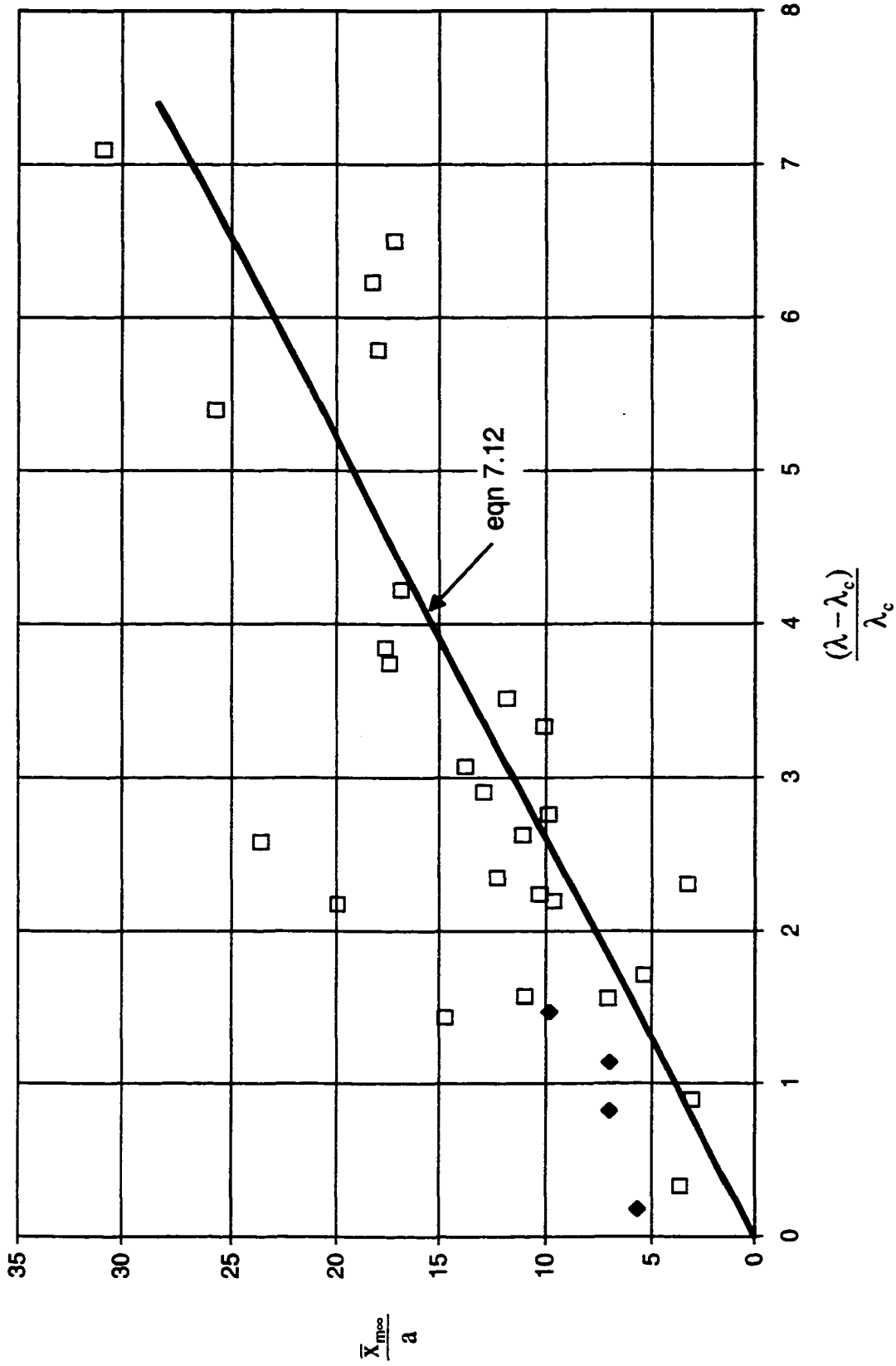


Fig. 7-9: Average location of the maximum depth of scour at equilibrium state with the dimensionless parameter λ .

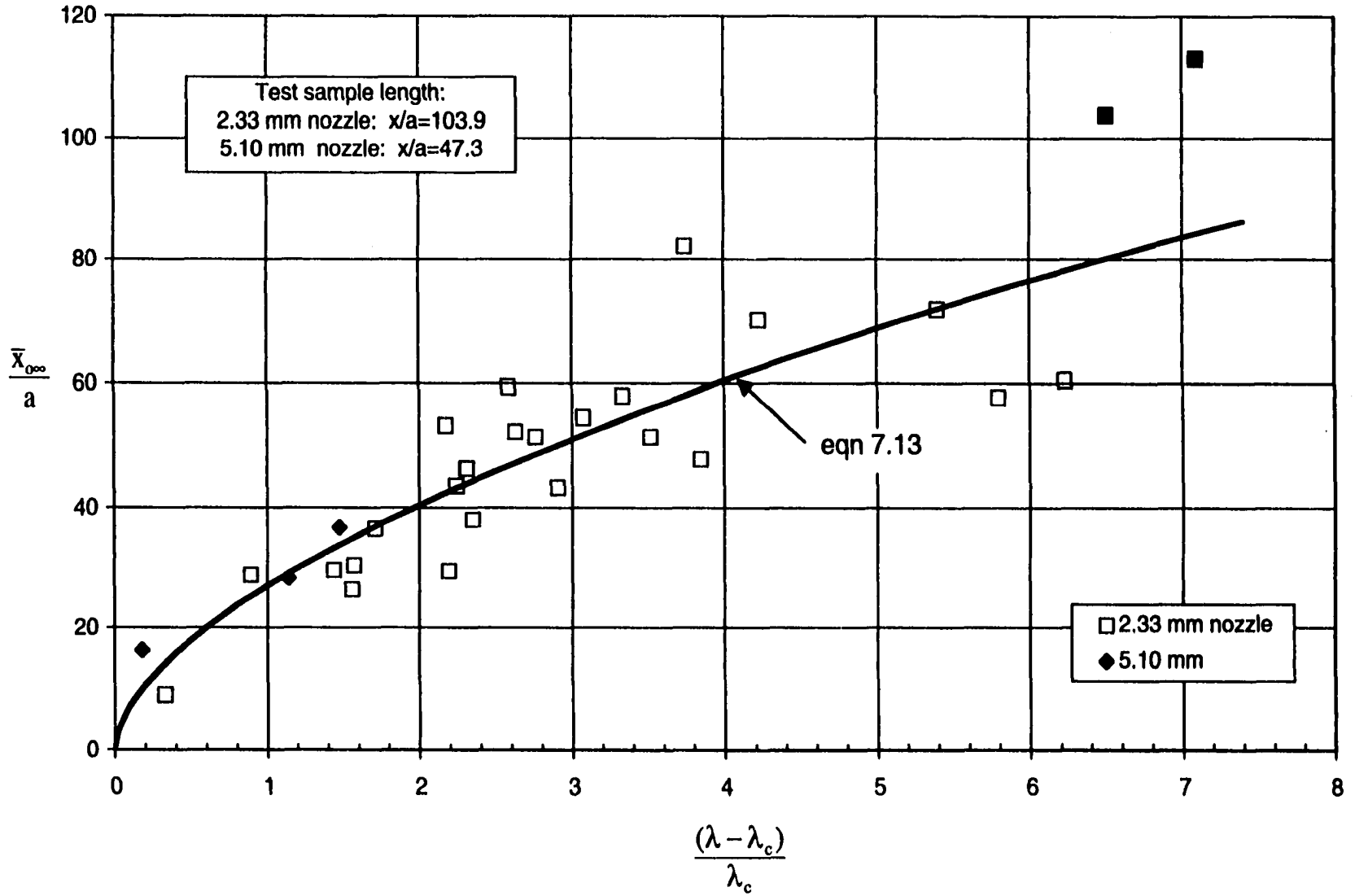
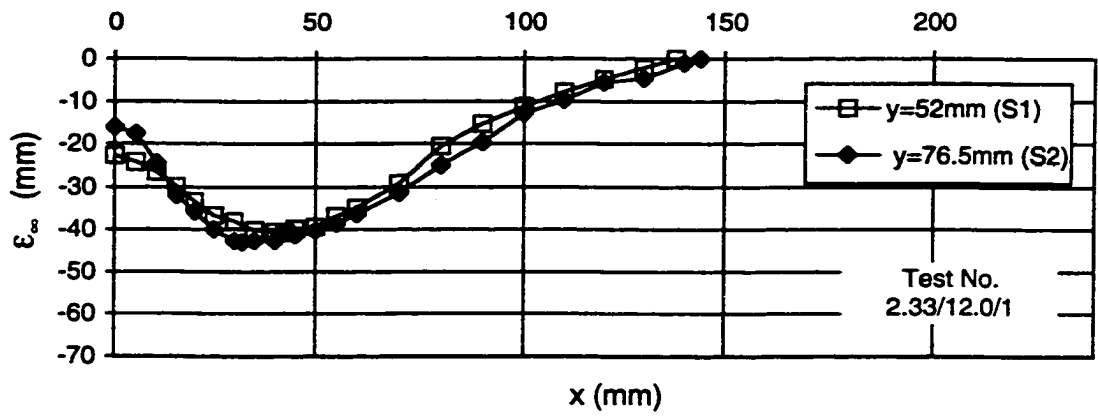
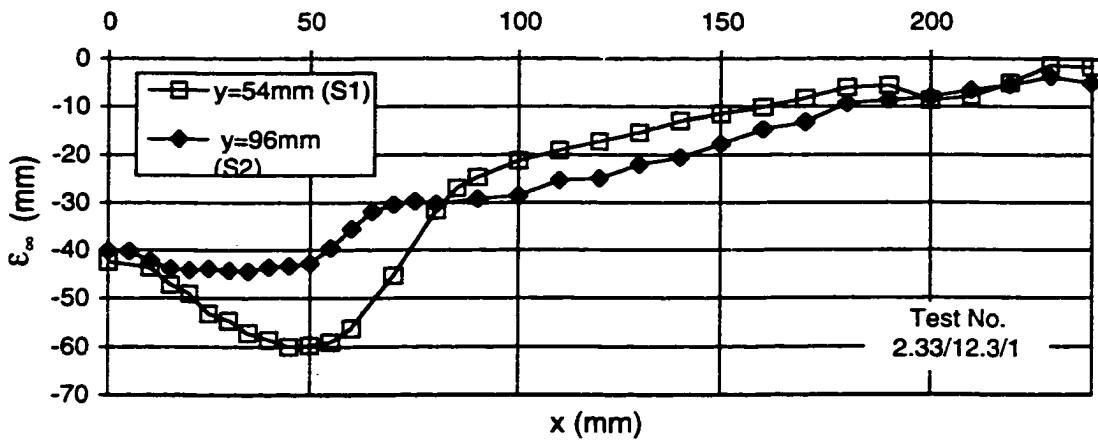


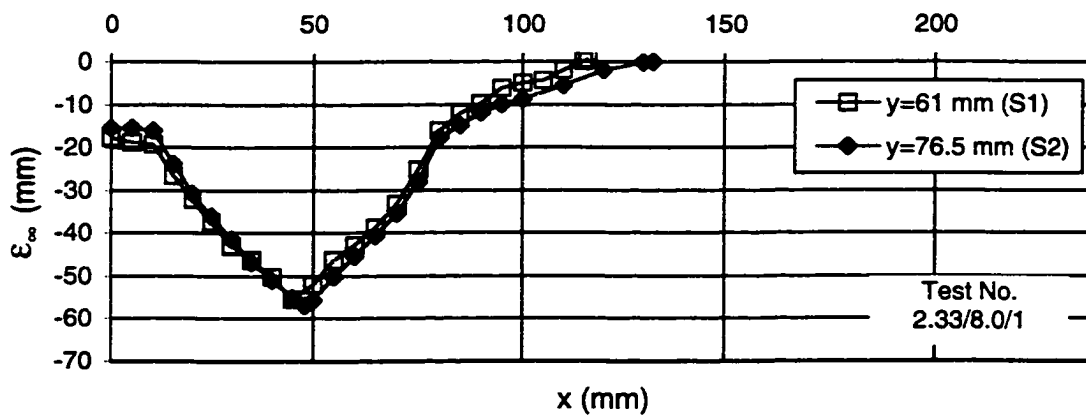
Fig. 7-10: Average length of the scour hole at equilibrium state with the dimensionless parameter λ .



(a)



(b)



(c)

Fig. 7-11: Typical scour hole profiles (a) Type 1 profiles (b) a Type 2 profile (S2) and a Type 3 profile (S1) and (c) Type 4 profiles

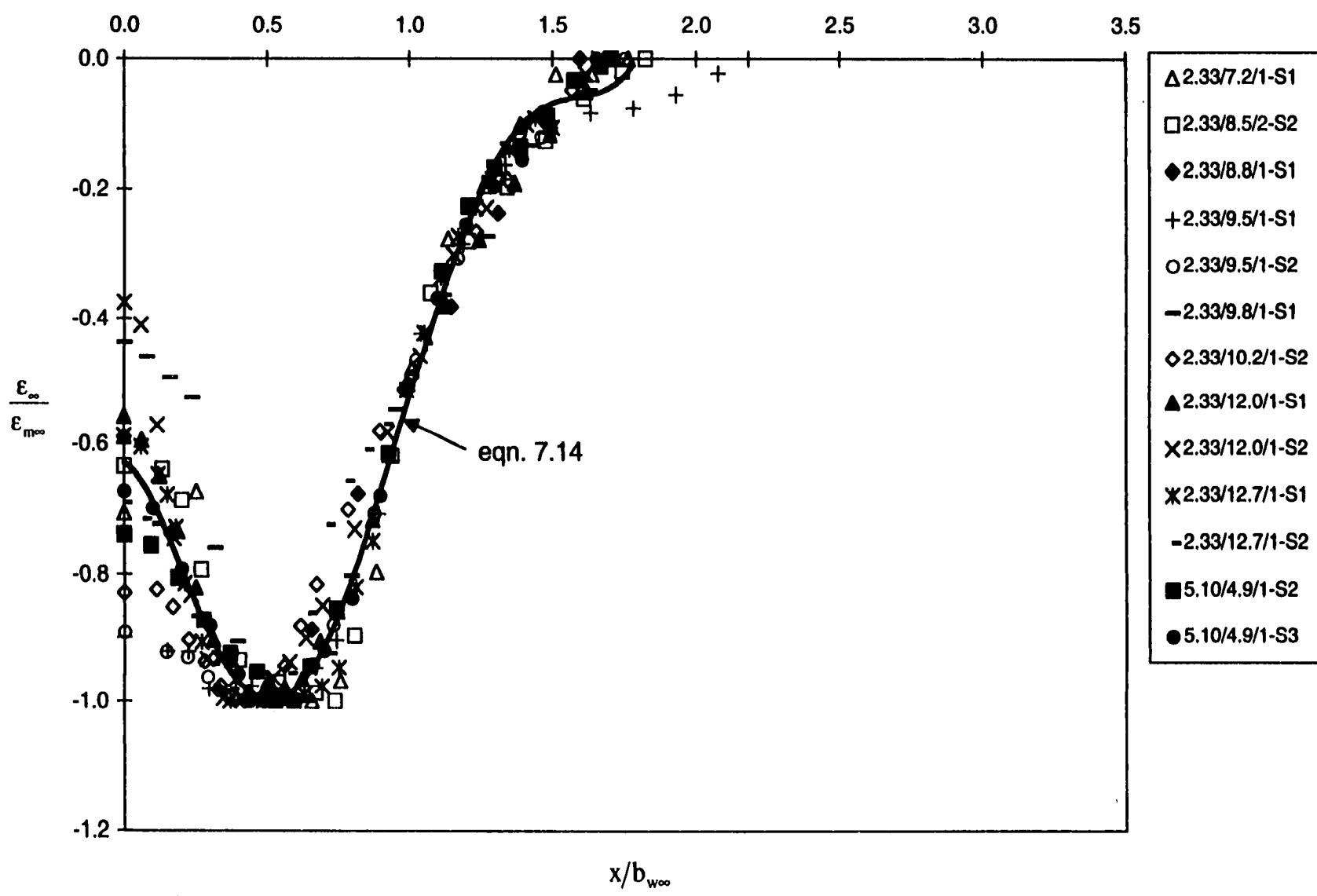


Fig. 7-12: Dimensionless scour hole profile for the Type 1 scour hole.

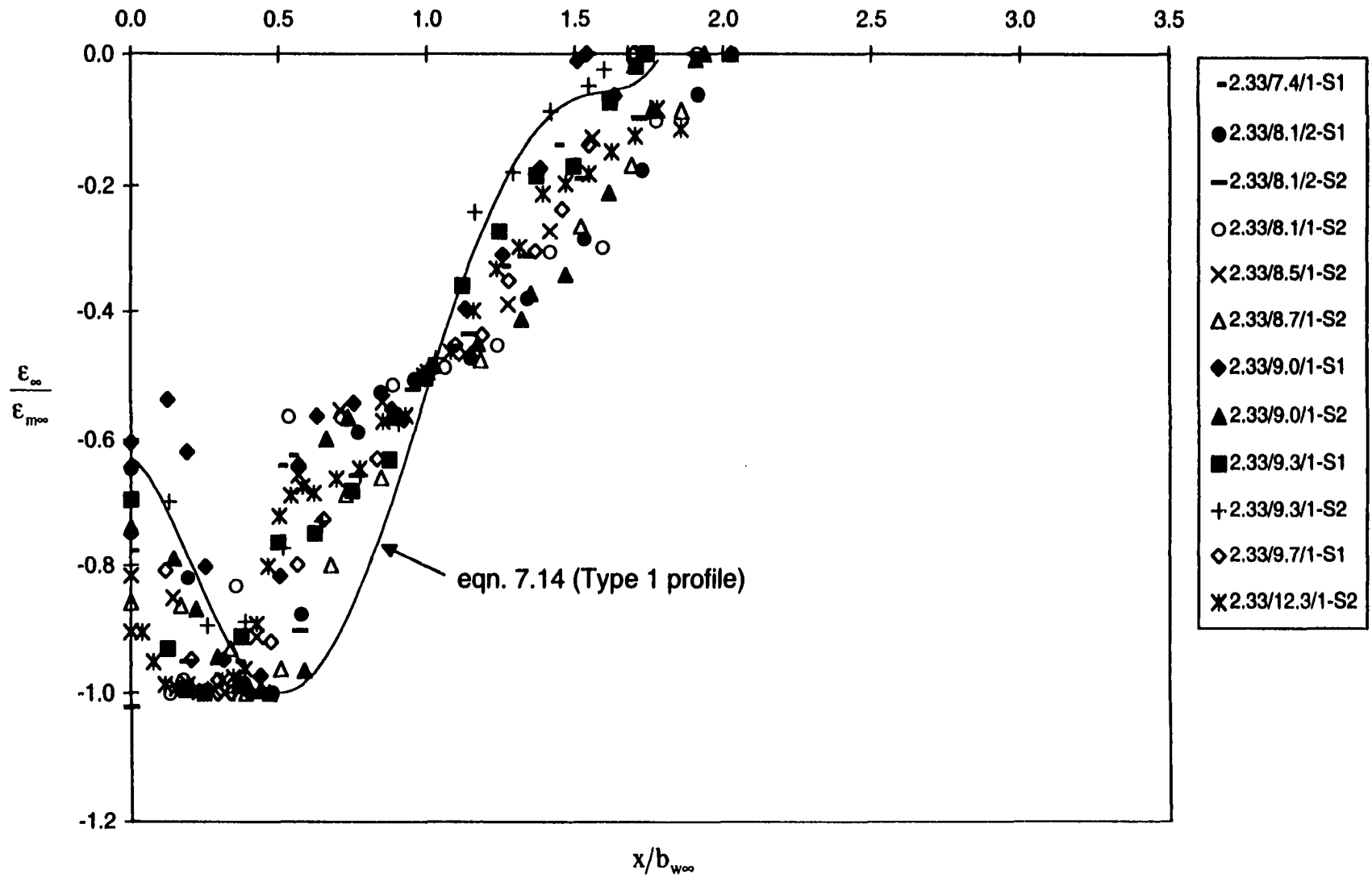


Fig. 7-13: Dimensionless scour hole profile for the Type 2 scour hole.

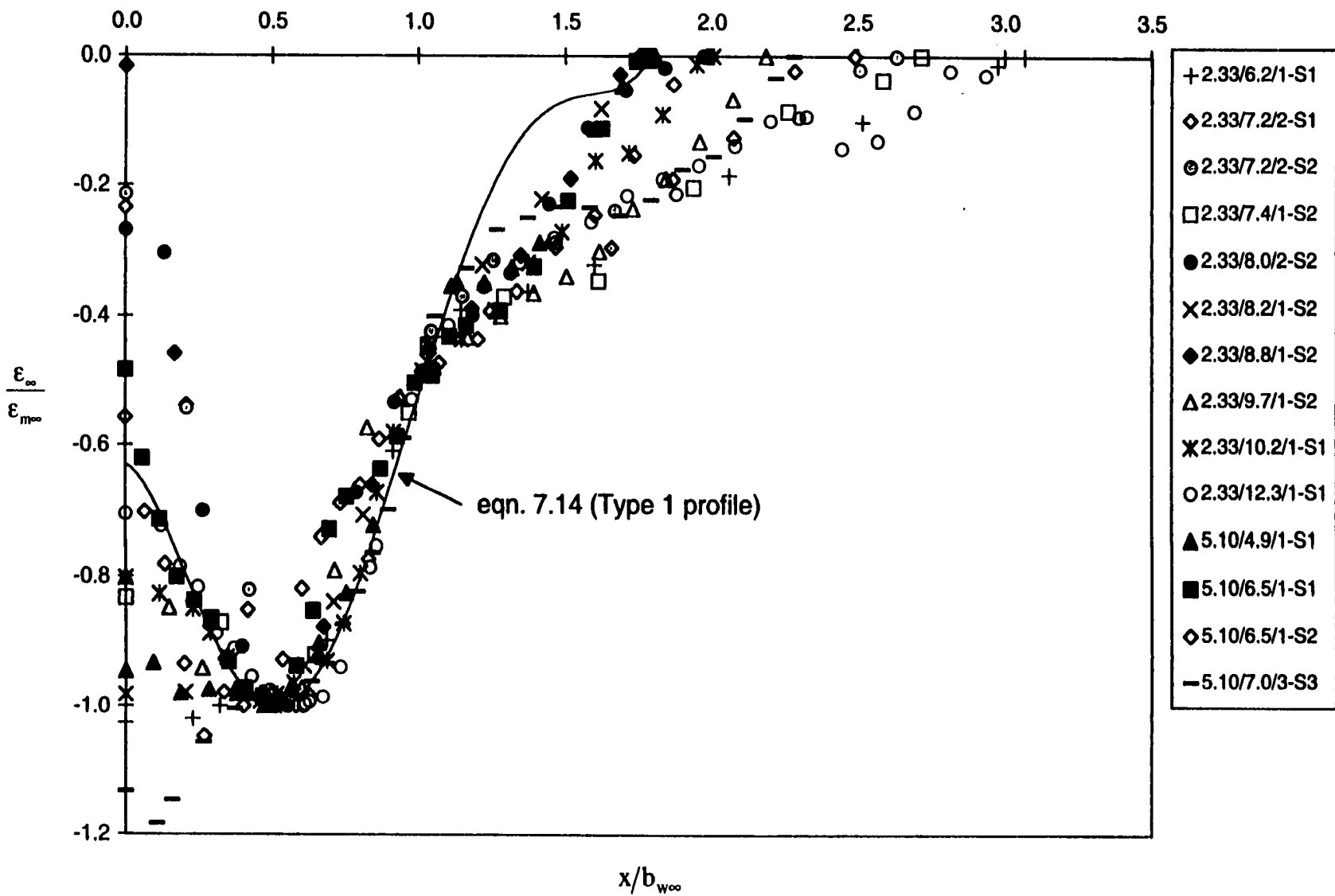


Fig. 7-14: Dimensionless scour hole profile for the Type 3 scour hole.

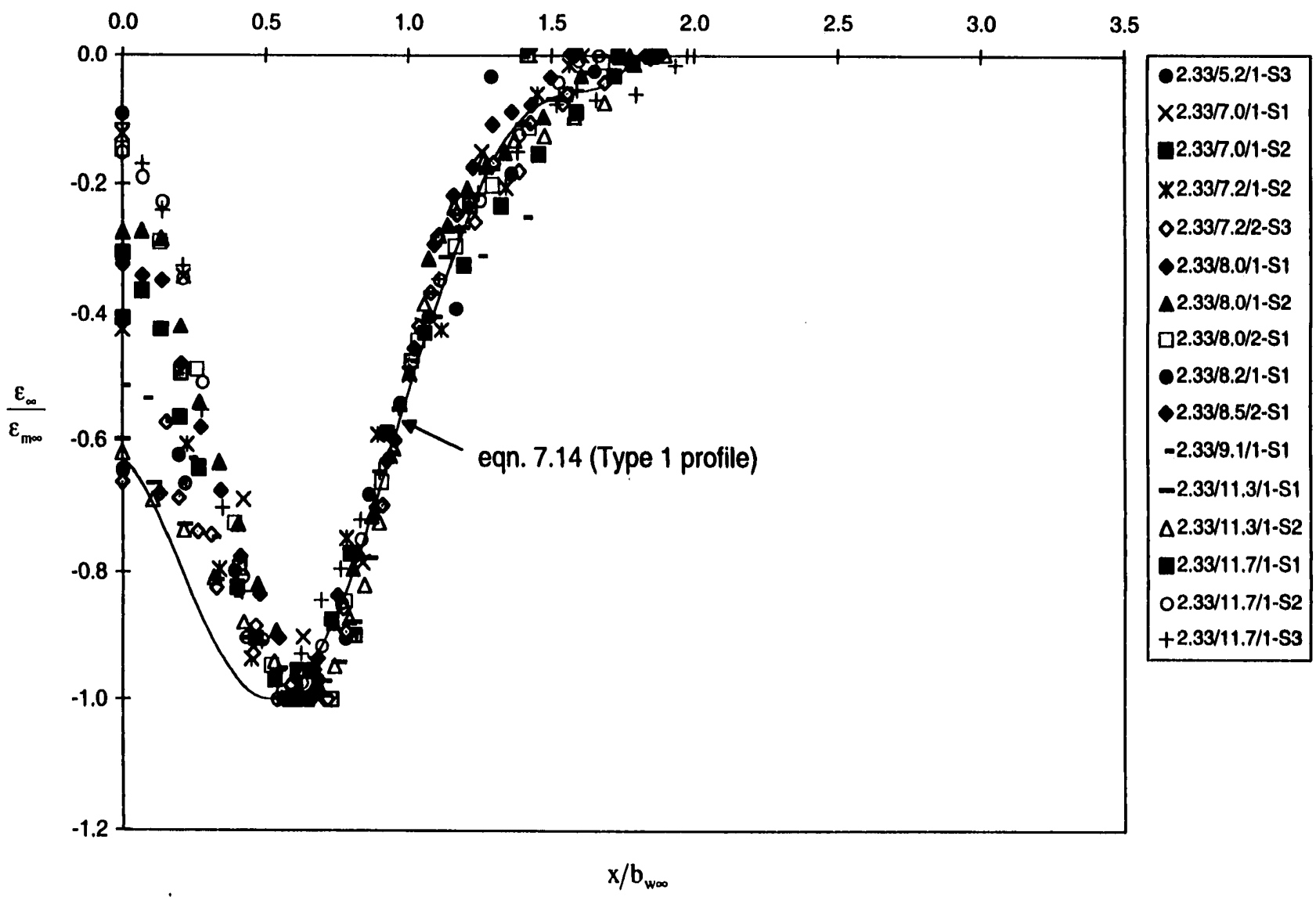


Fig. 7-15: Dimensionless scour hole profile for Type 4 scour hole.

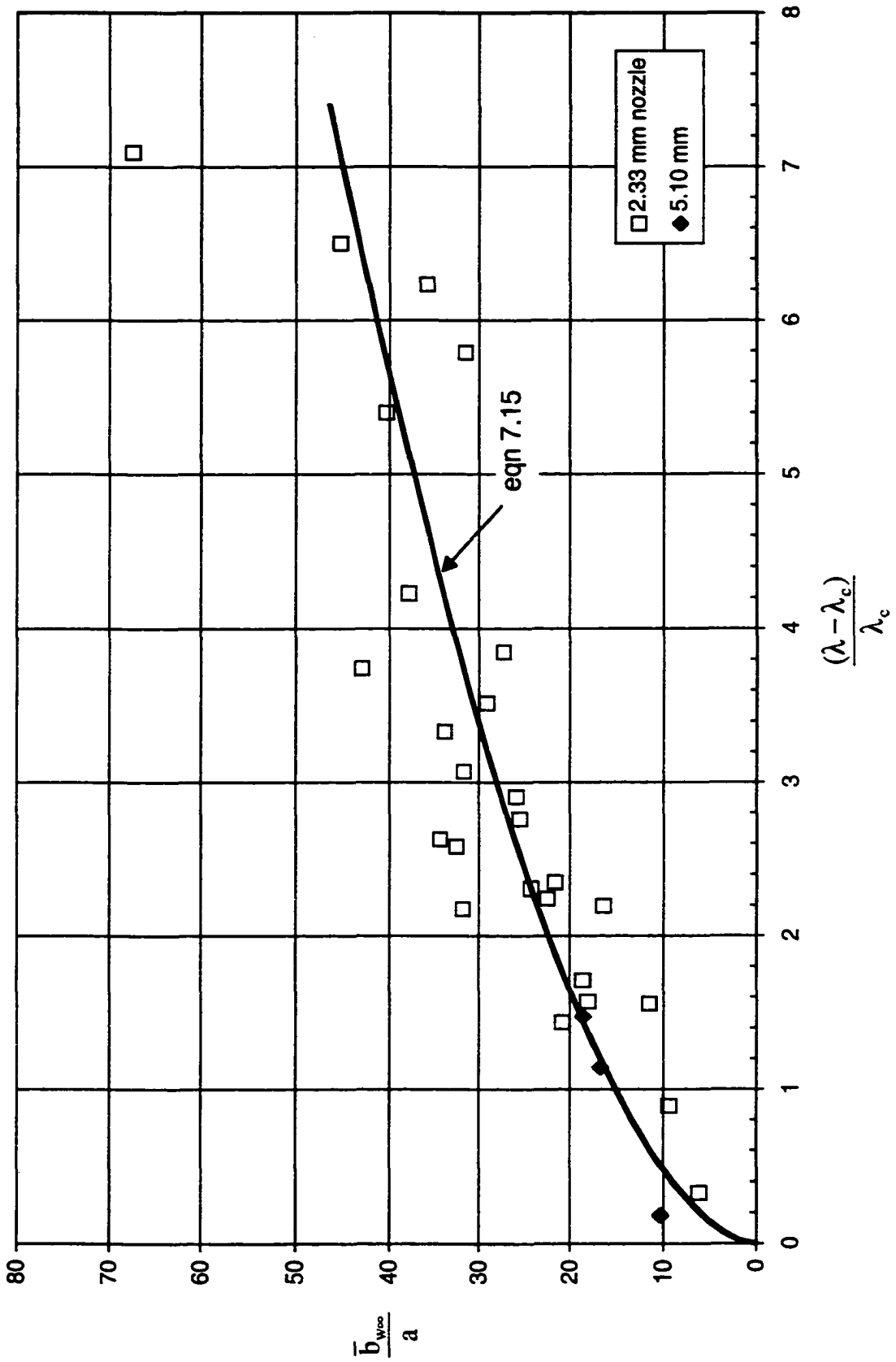


Fig. 7-16: Dimensionless average length scale b_w at equilibrium state with dimensionless λ .

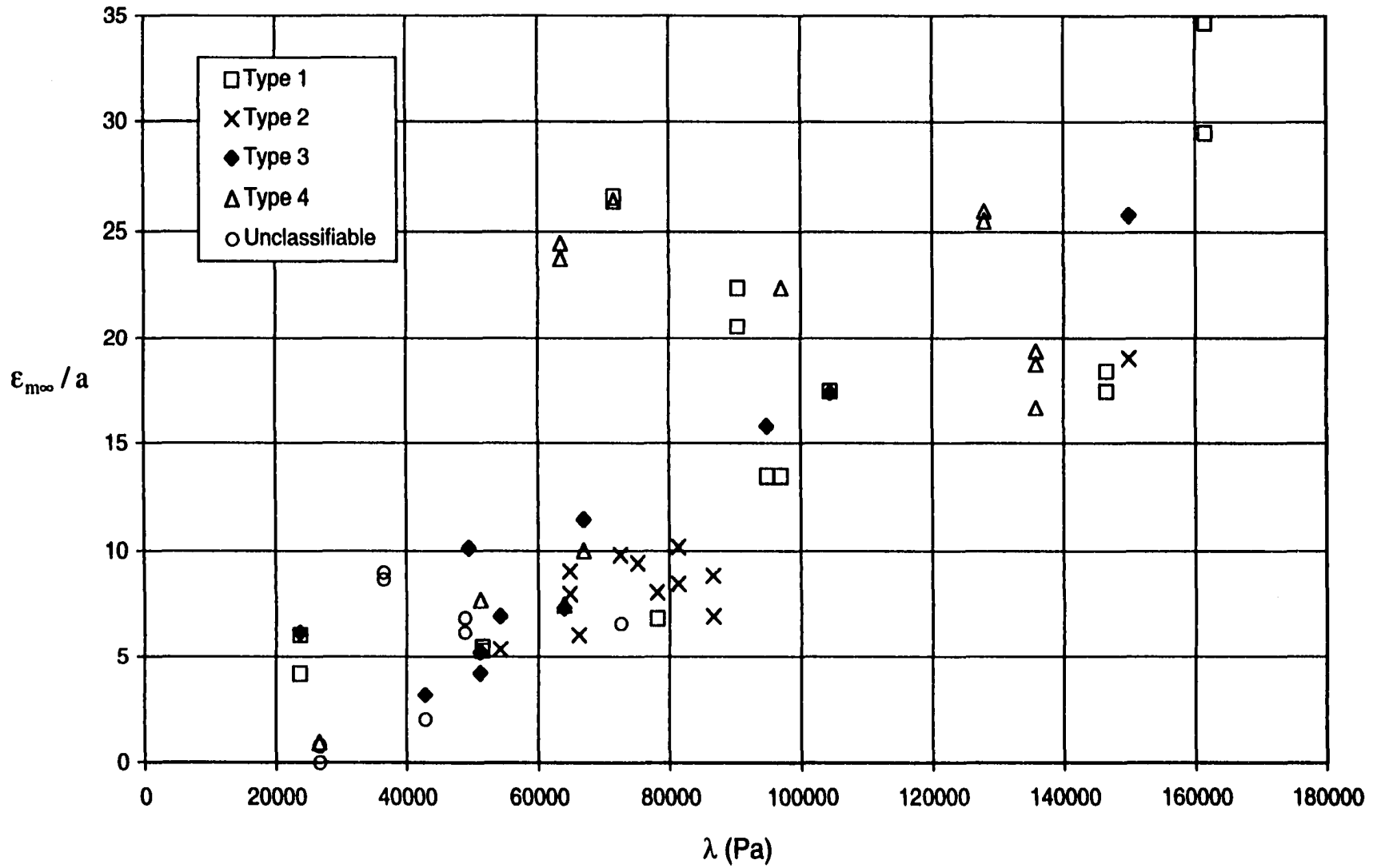


Fig. 7-17: Dimensionless maximum scour depth at equilibrium sorted by scour hole type (no averaging).

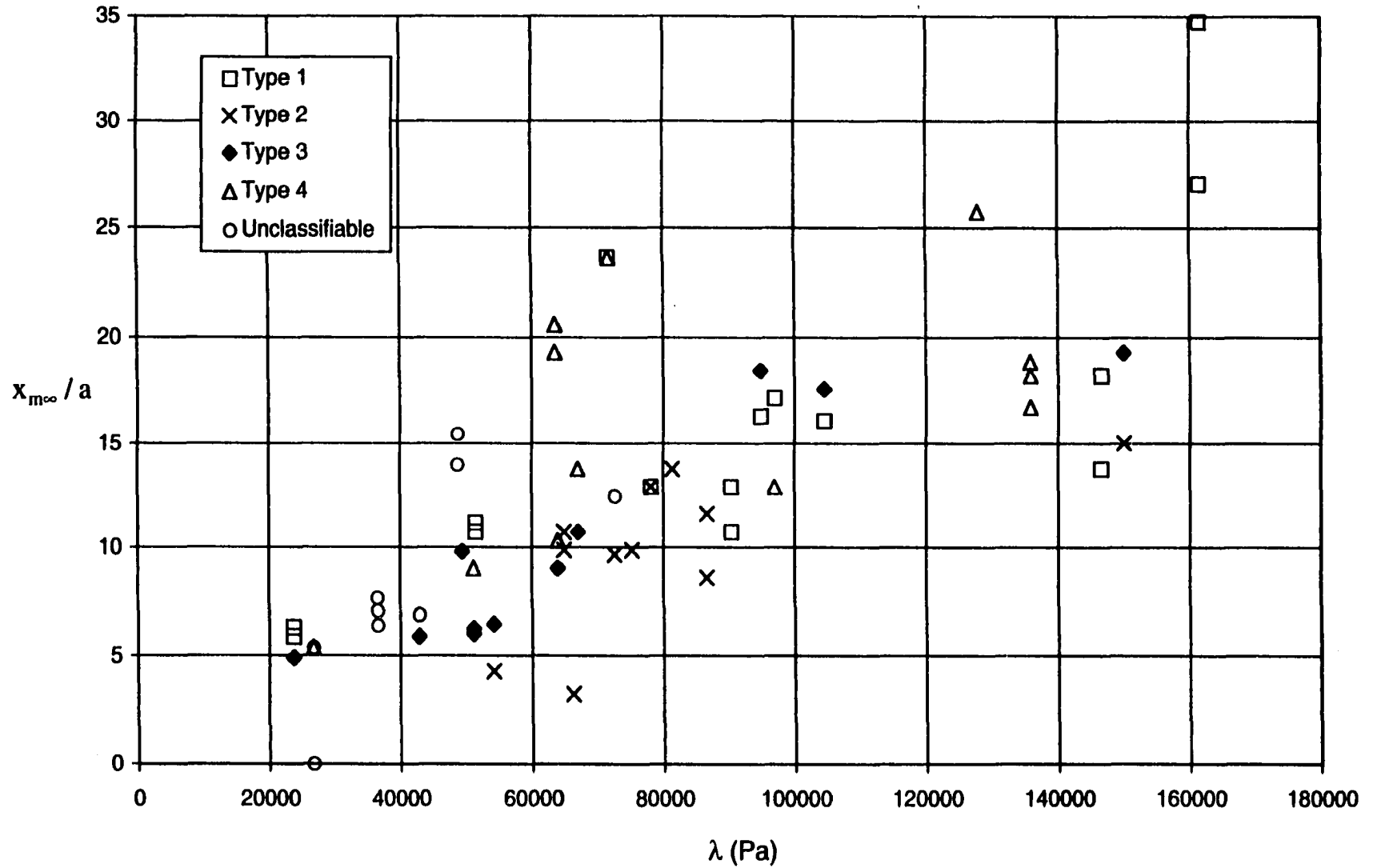


Fig. 7-18: Dimensionless location of the maximum scour depth sorted by scour hole type.

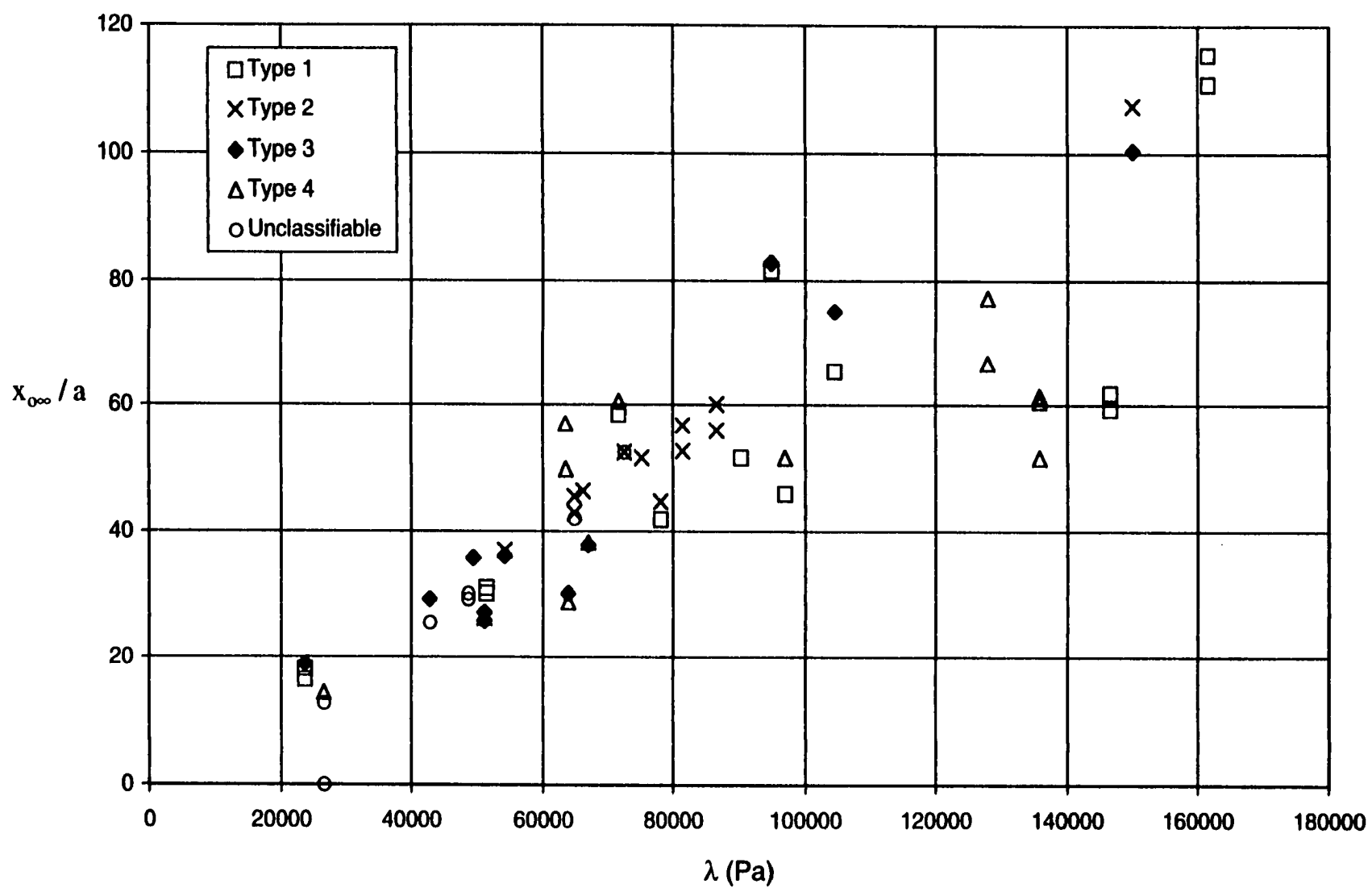


Fig. 7-19: Dimensionless scour hole length sorted by scour hole type.

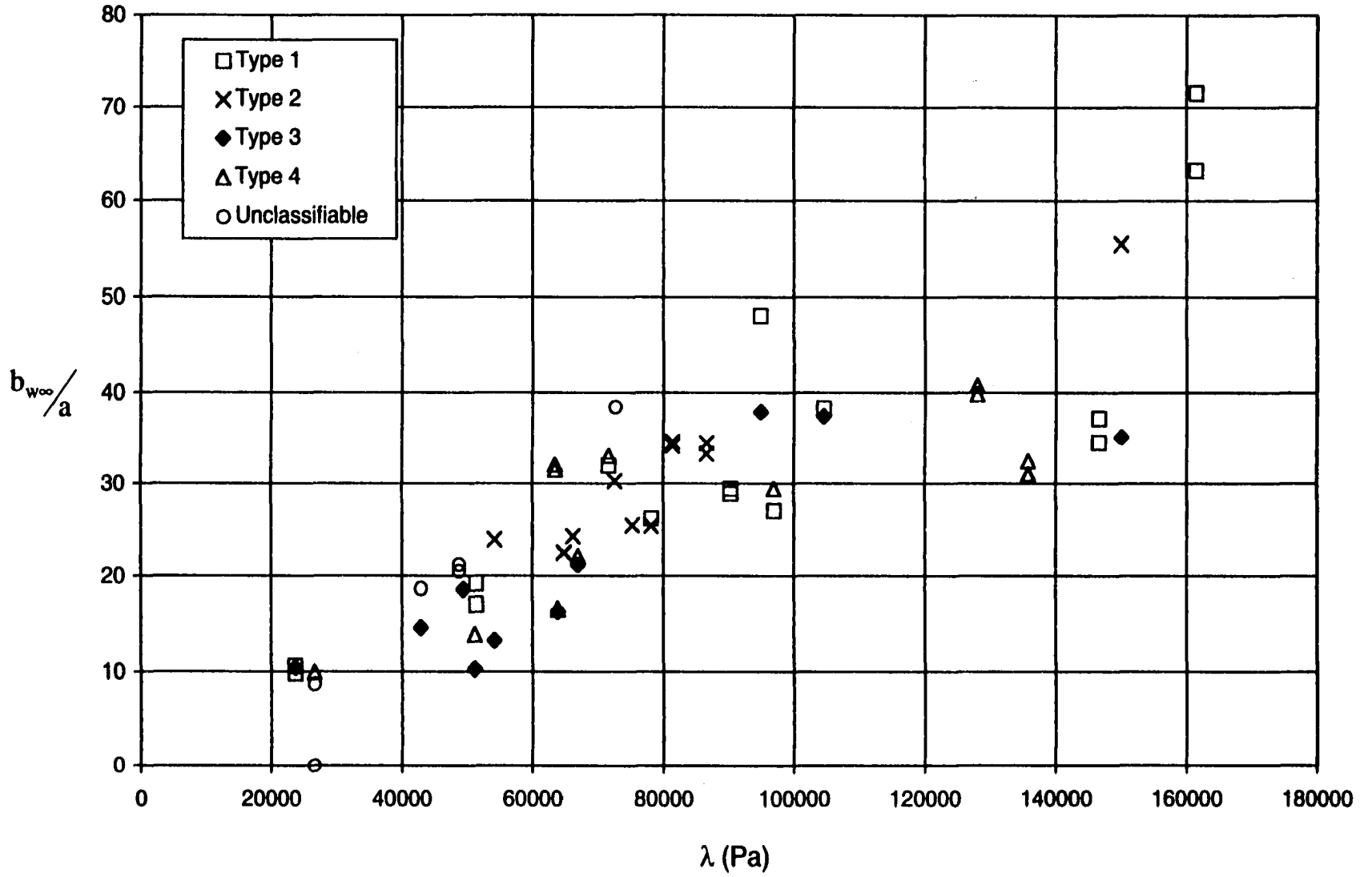


Fig. 7-20: Dimensionless length scale of scour sorted by scour hole type.

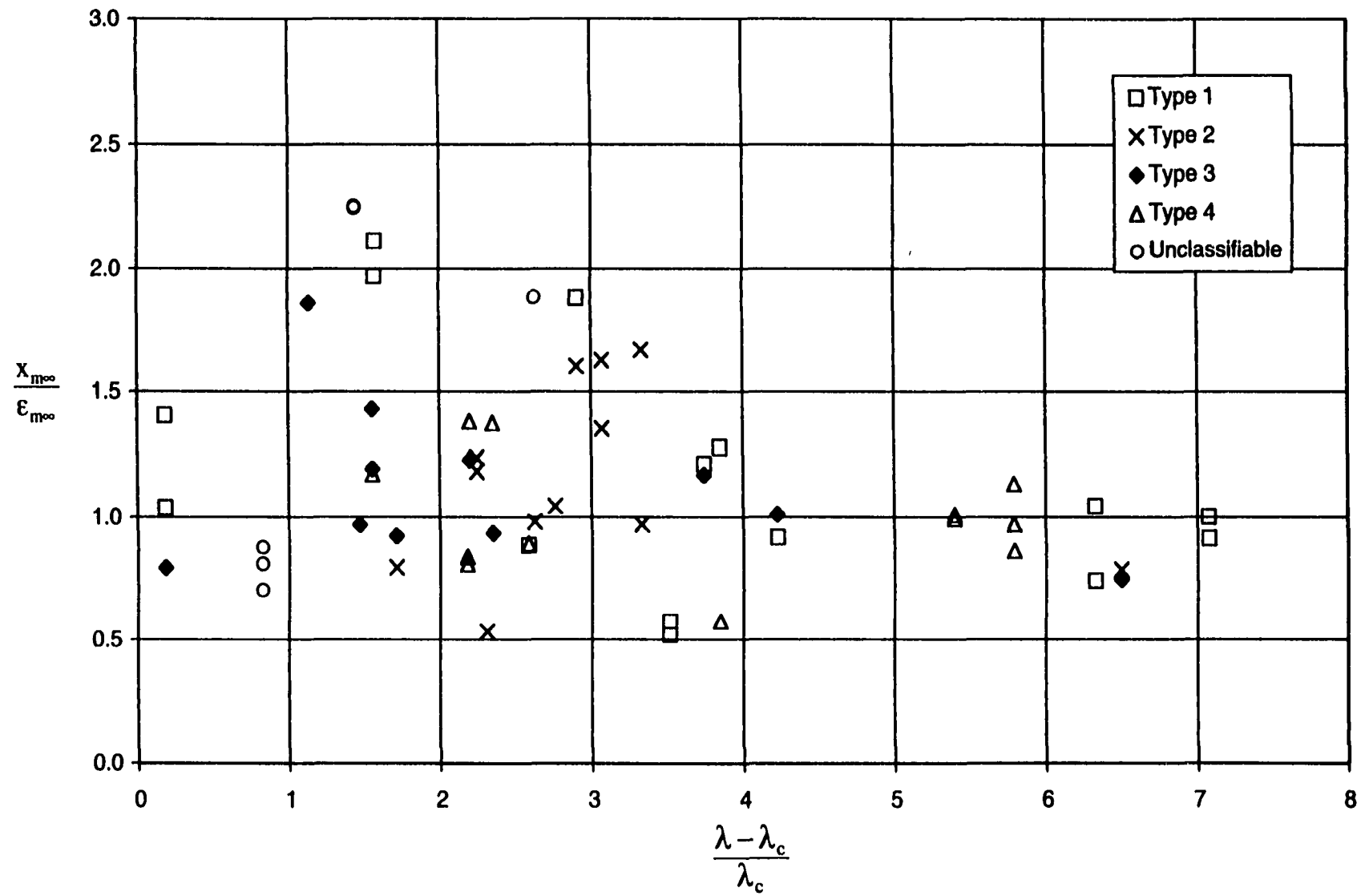


Fig. 7-21: Variation of the ratio of the location of maximum scour to the maximum scour depth at equilibrium as sorted by the scour hole profile type.

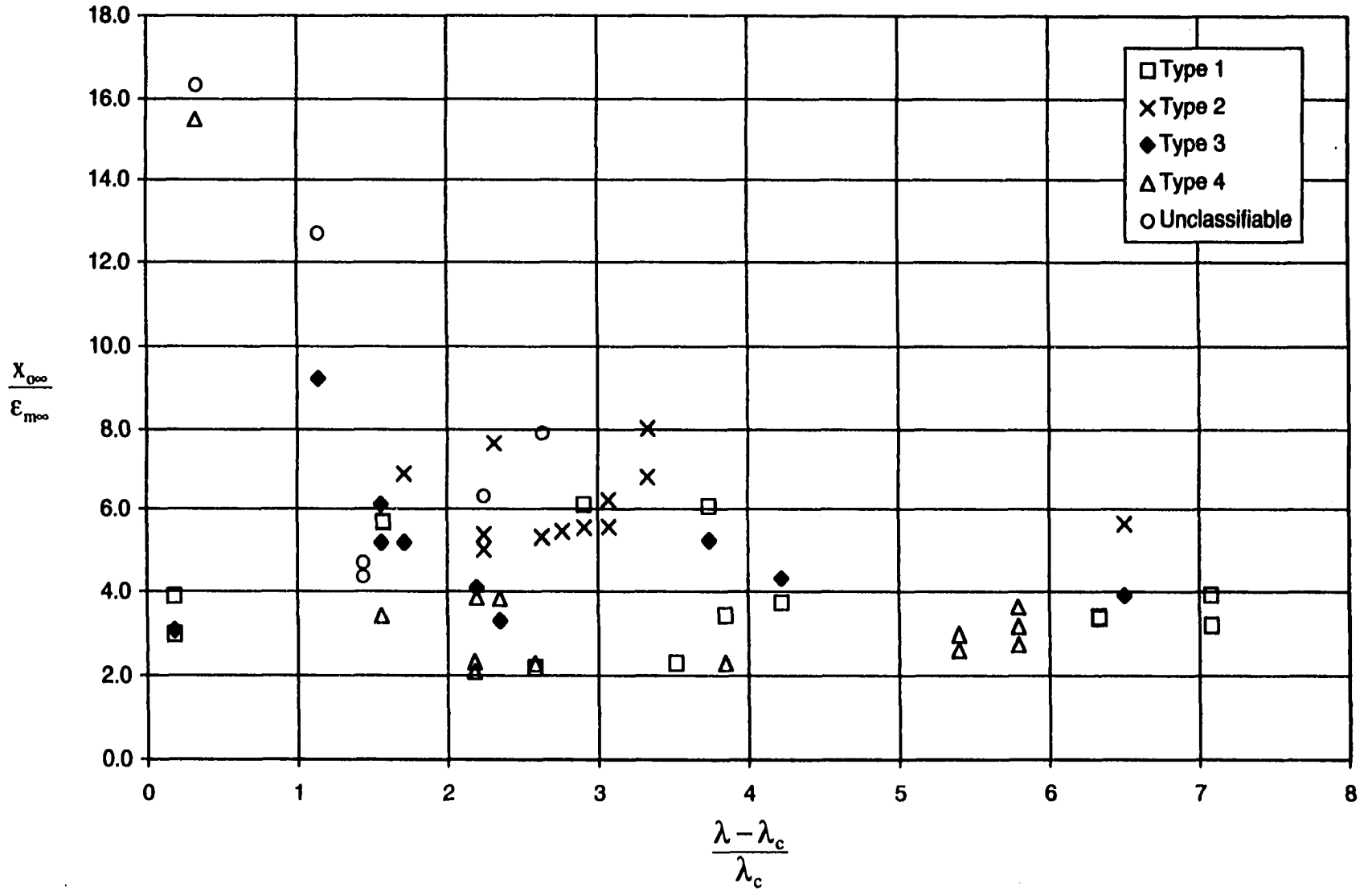


Fig. 7-22: Variation of the ratio of the scour hole length to the maximum depth at equilibrium as sorted by the scour hole profile type.

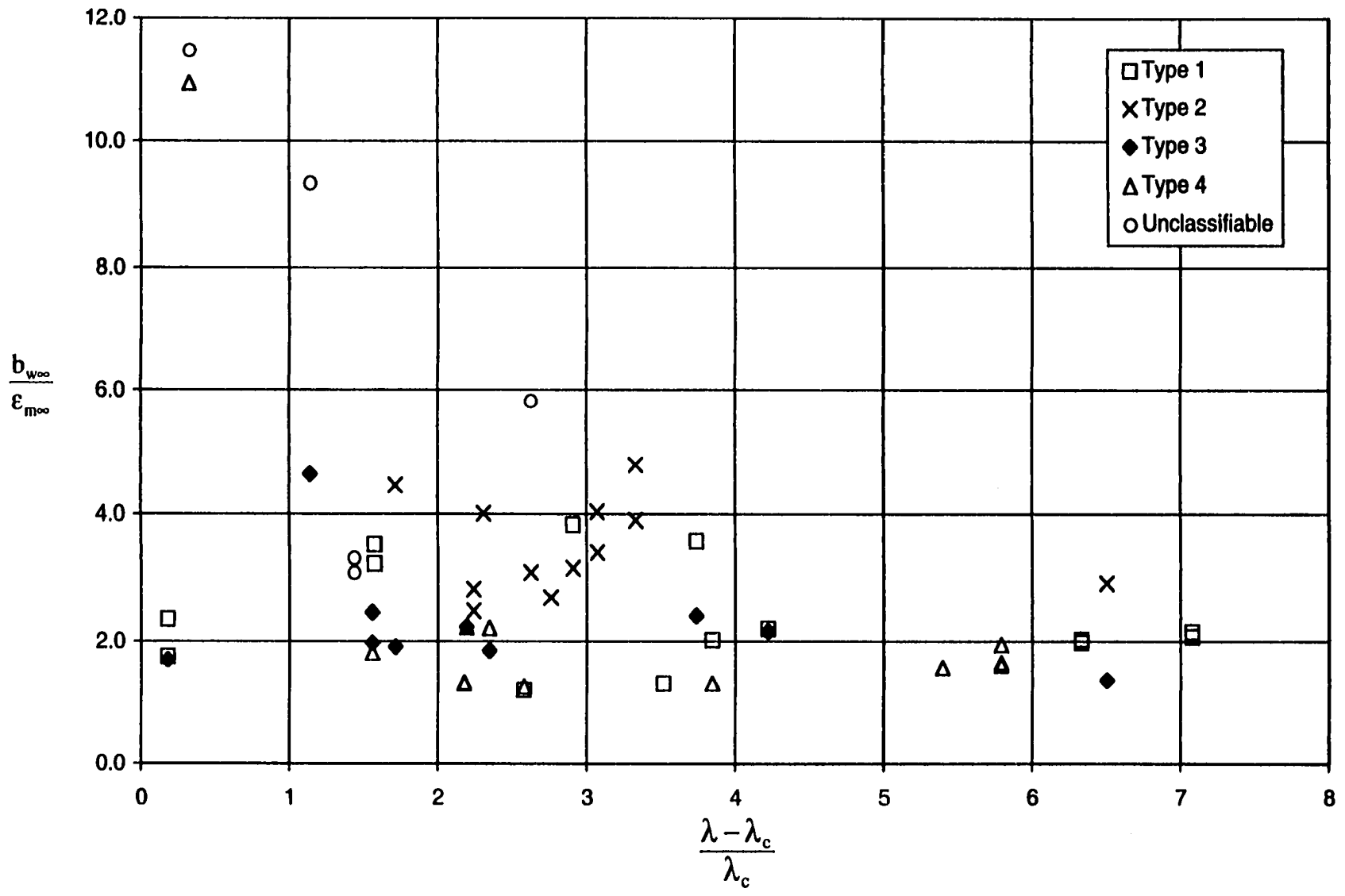


Fig. 7-23: Variation of the ratio of the scour length scale to the maximum scour depth at equilibrium as sorted by scour hole type.

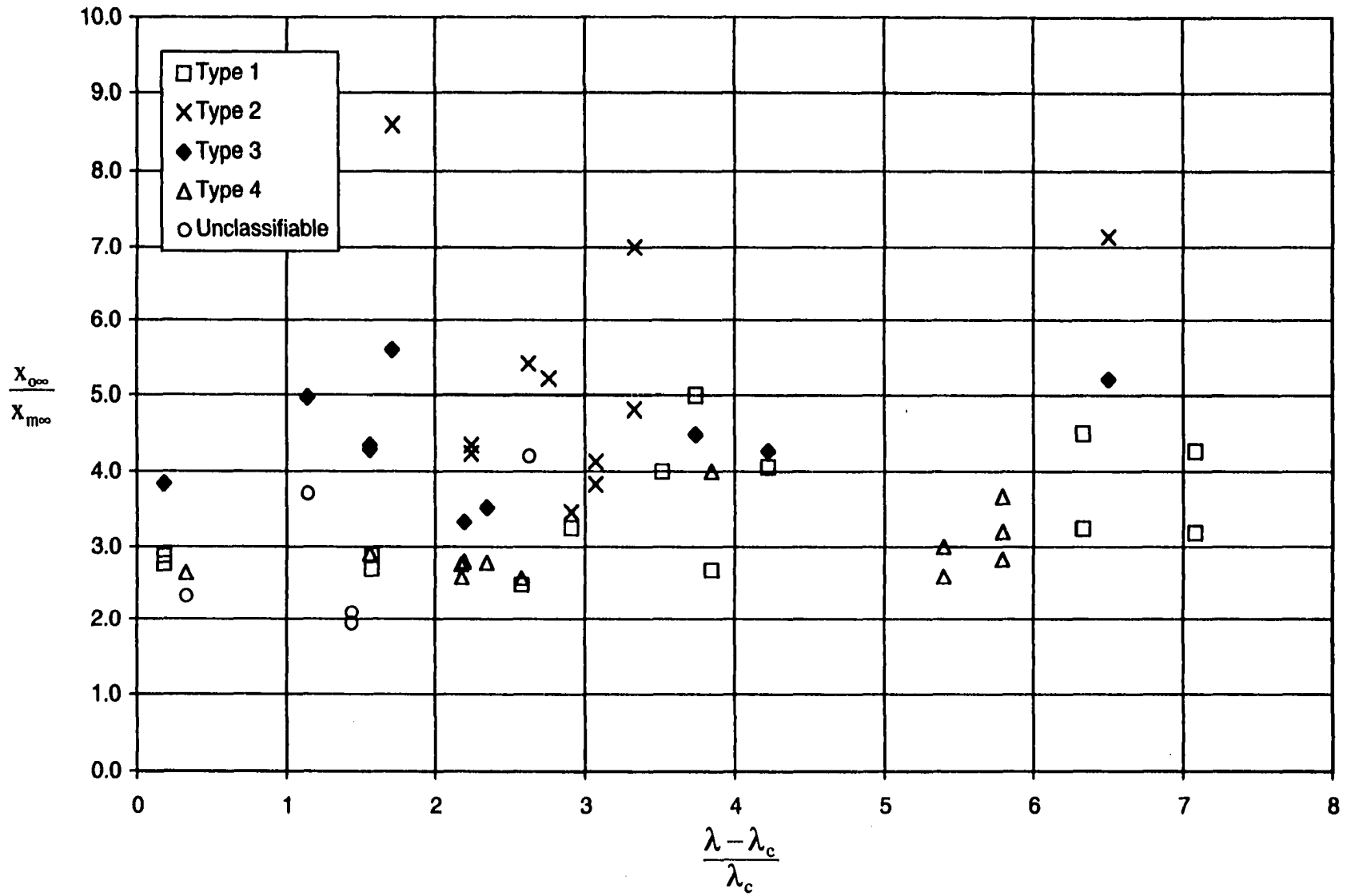


Fig. 7-24: Variation of the ratio of the length of the scour hole to the location of the maximum depth as sorted by scour hole type.

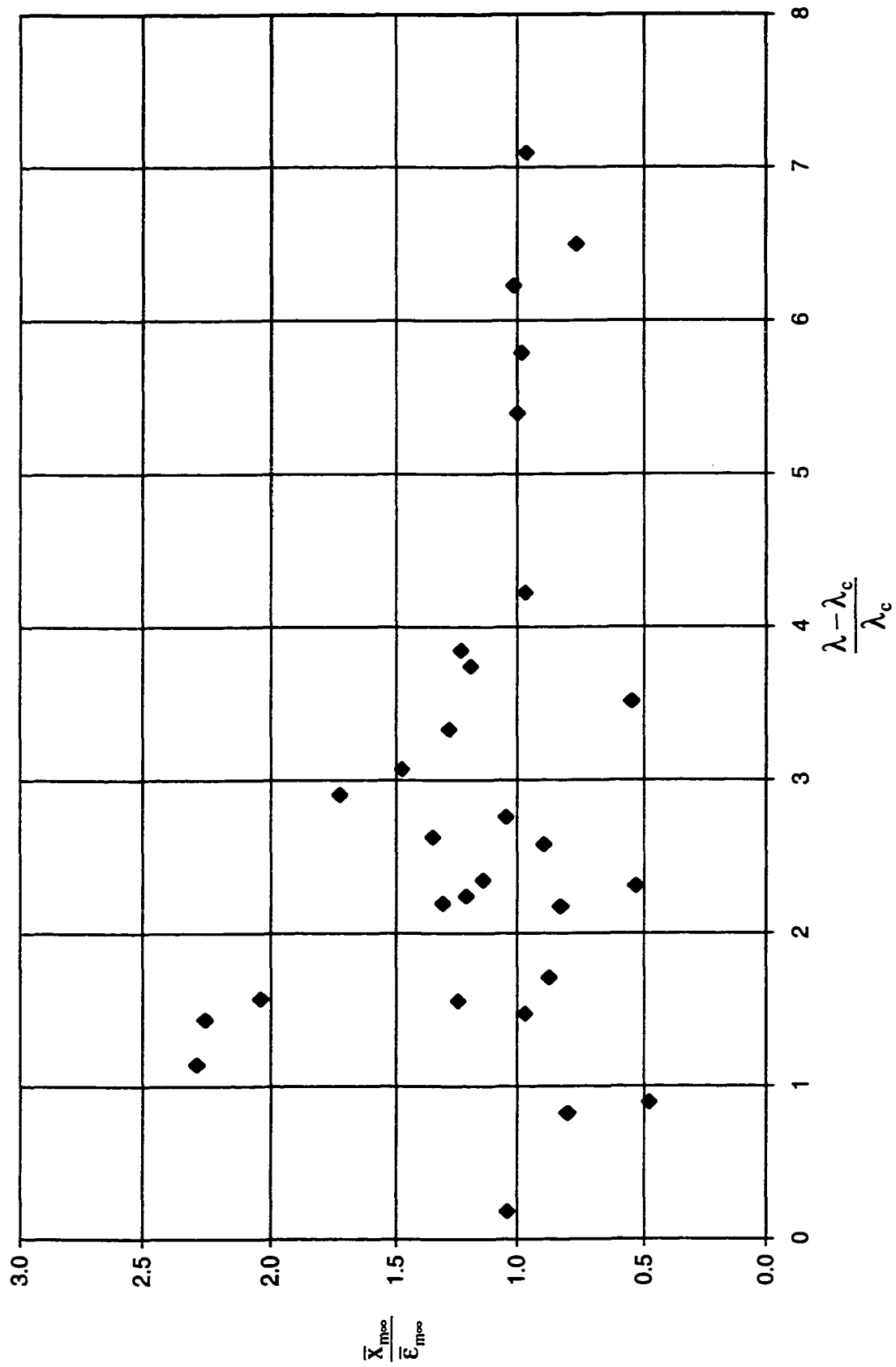


Fig. 7-25: Variation of the ratio of the average location of maximum scour to the average maximum scour depth at equilibrium.

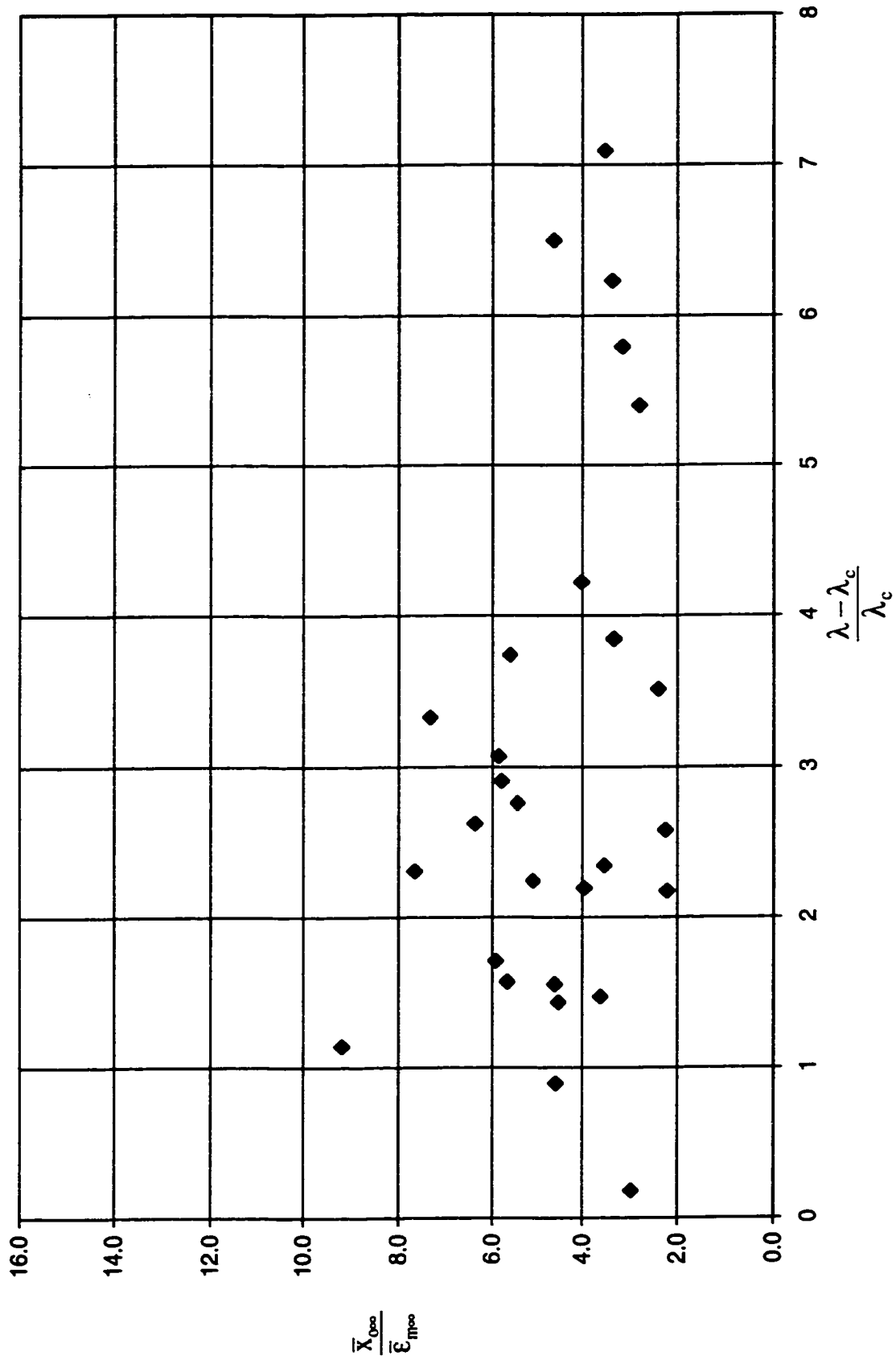


Fig. 7-26: Variation of the ratio of the average scour hole length to the average maximum depth at equilibrium.

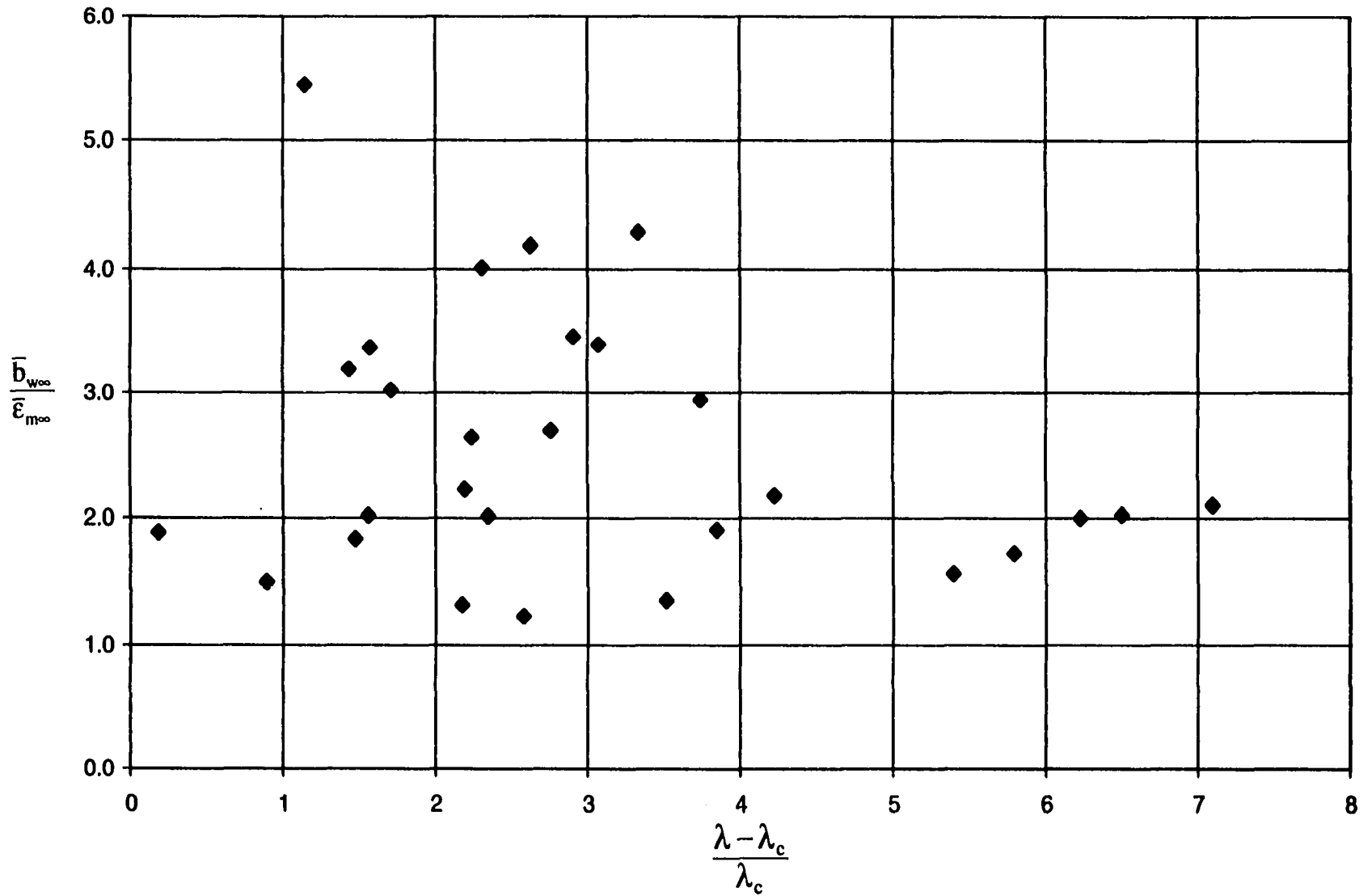


Fig. 7-27: Variation of the ratio of the average length scale of scour to the average maximum scour depth at equilibrium.

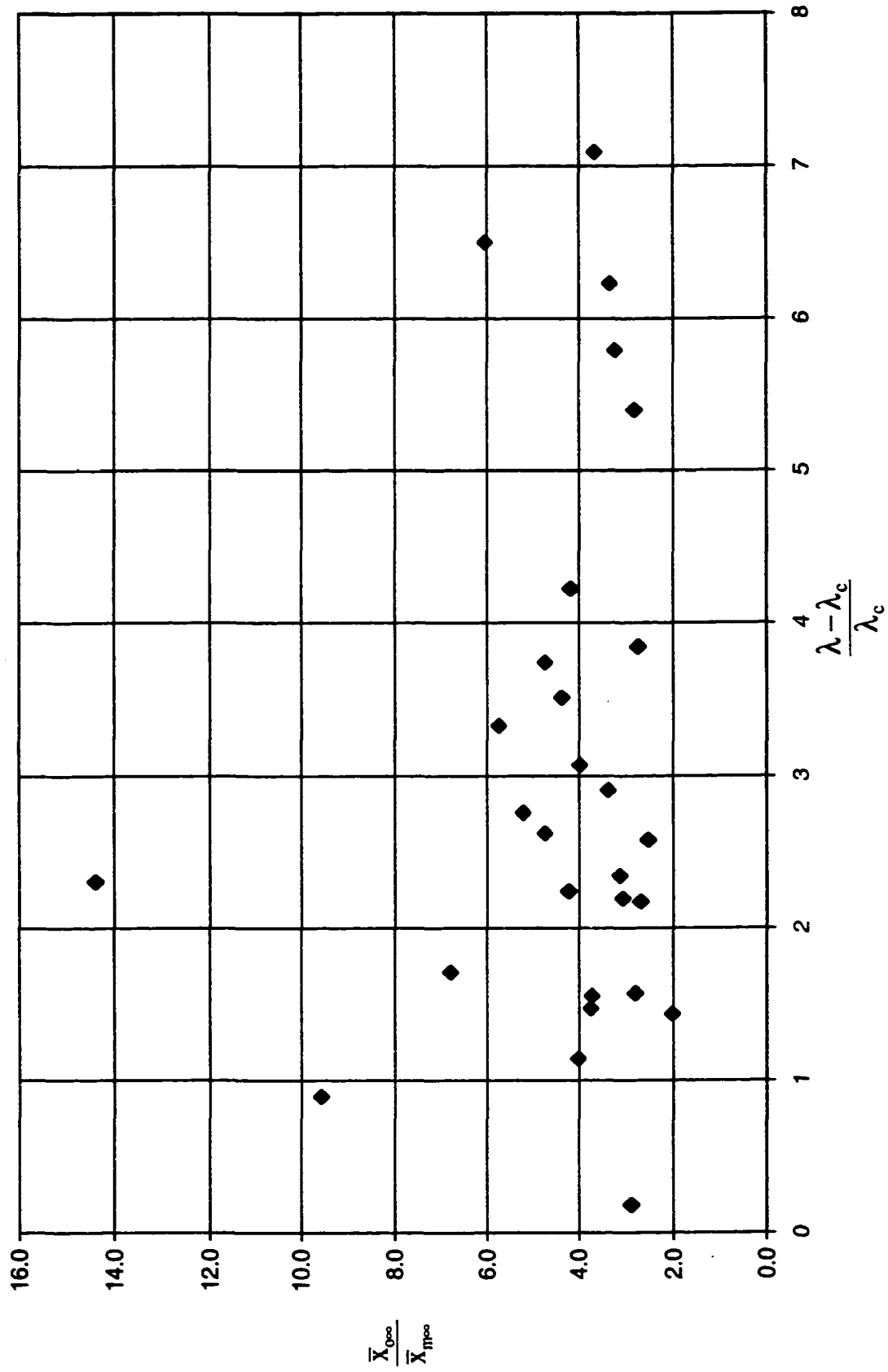


Fig. 7-28: Variation of the ratio of the average scour hole length to the average location of maximum scour at equilibrium.

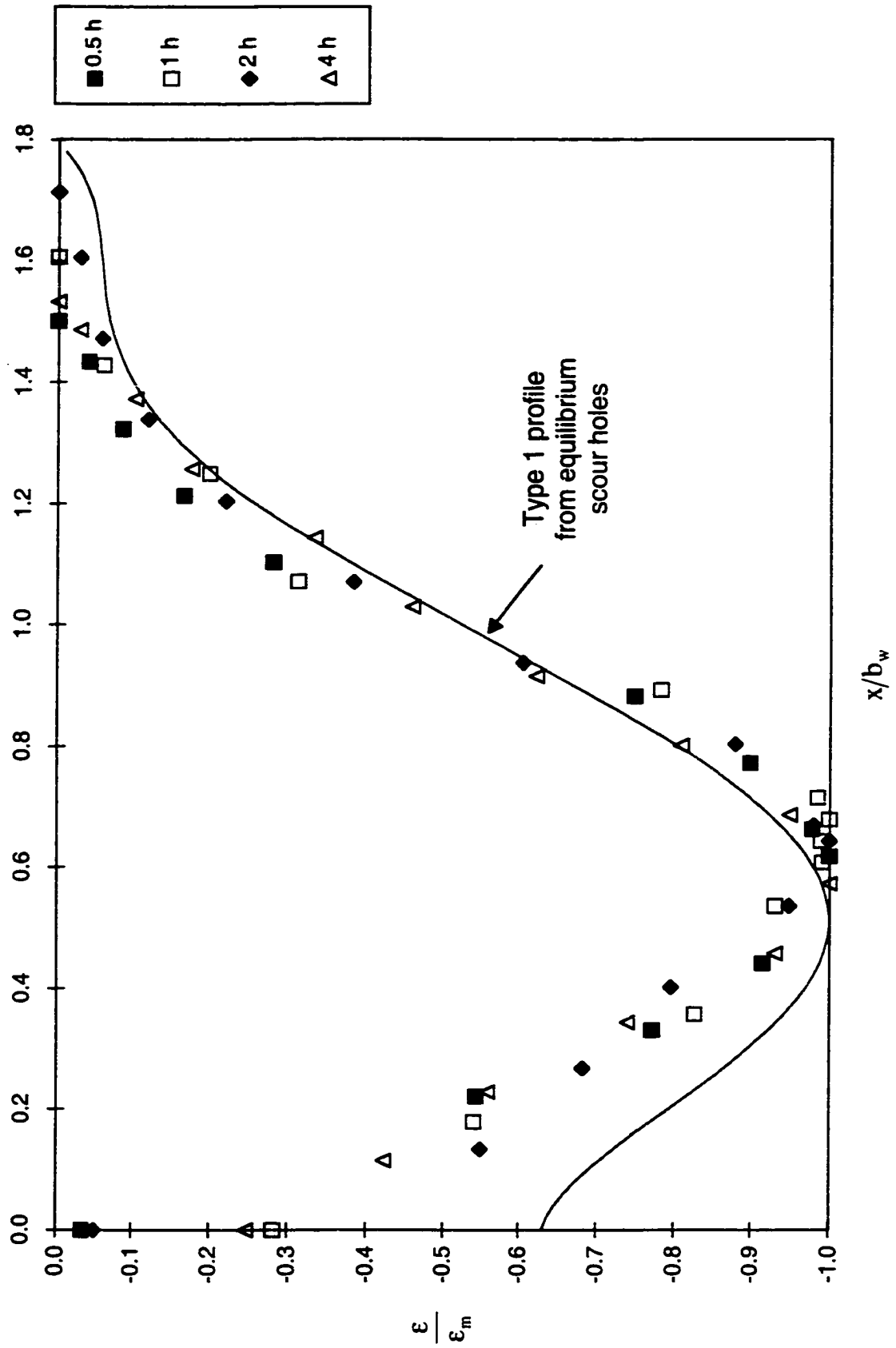


Fig. 7-29: Dimensionless scour hole profile with time for Test No. 2.33/10.5/1/E.

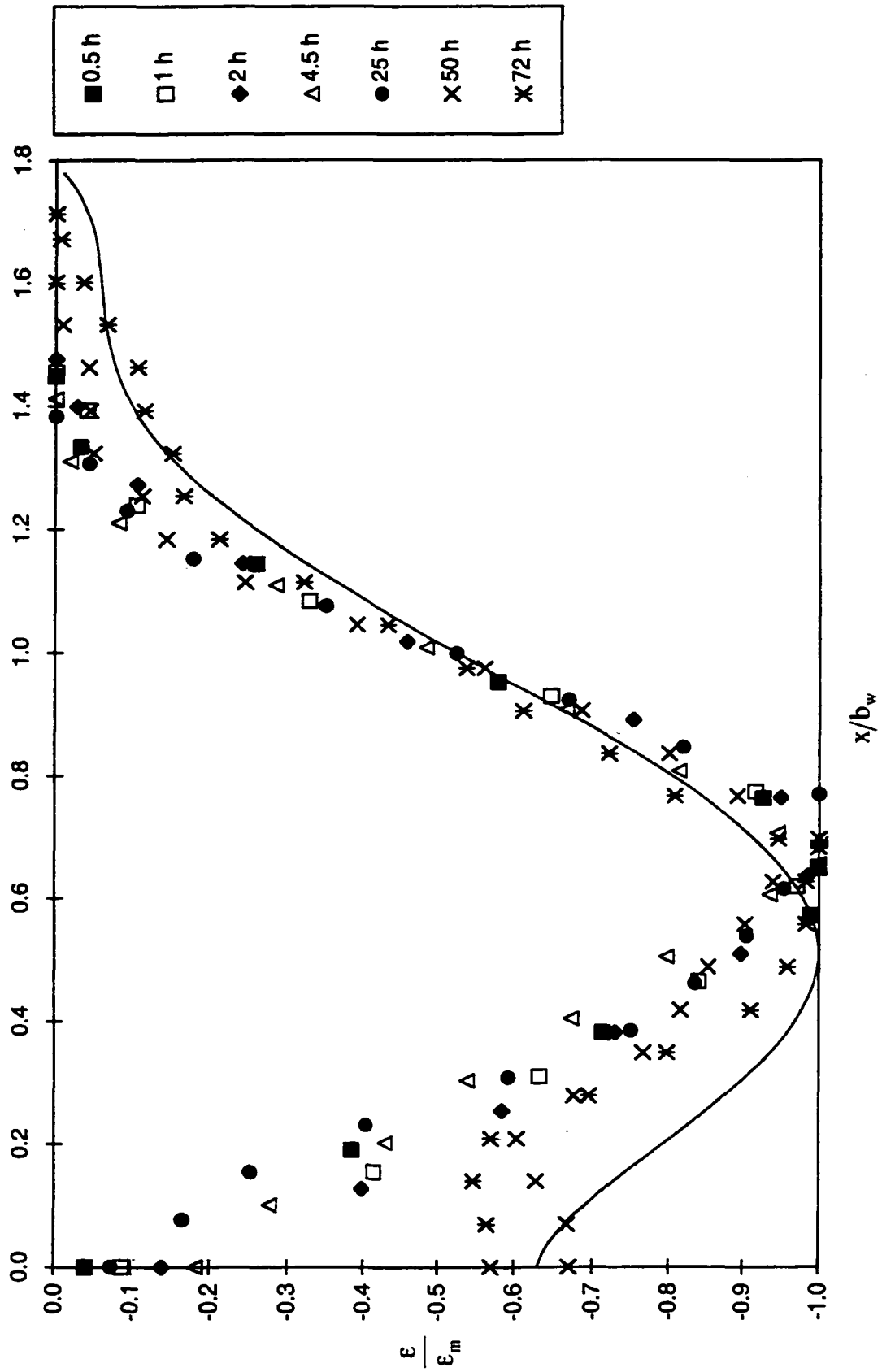


Fig. 7-30: Dimensionless scour hole profile with time for Test No. 2.33/8.9/1/E.

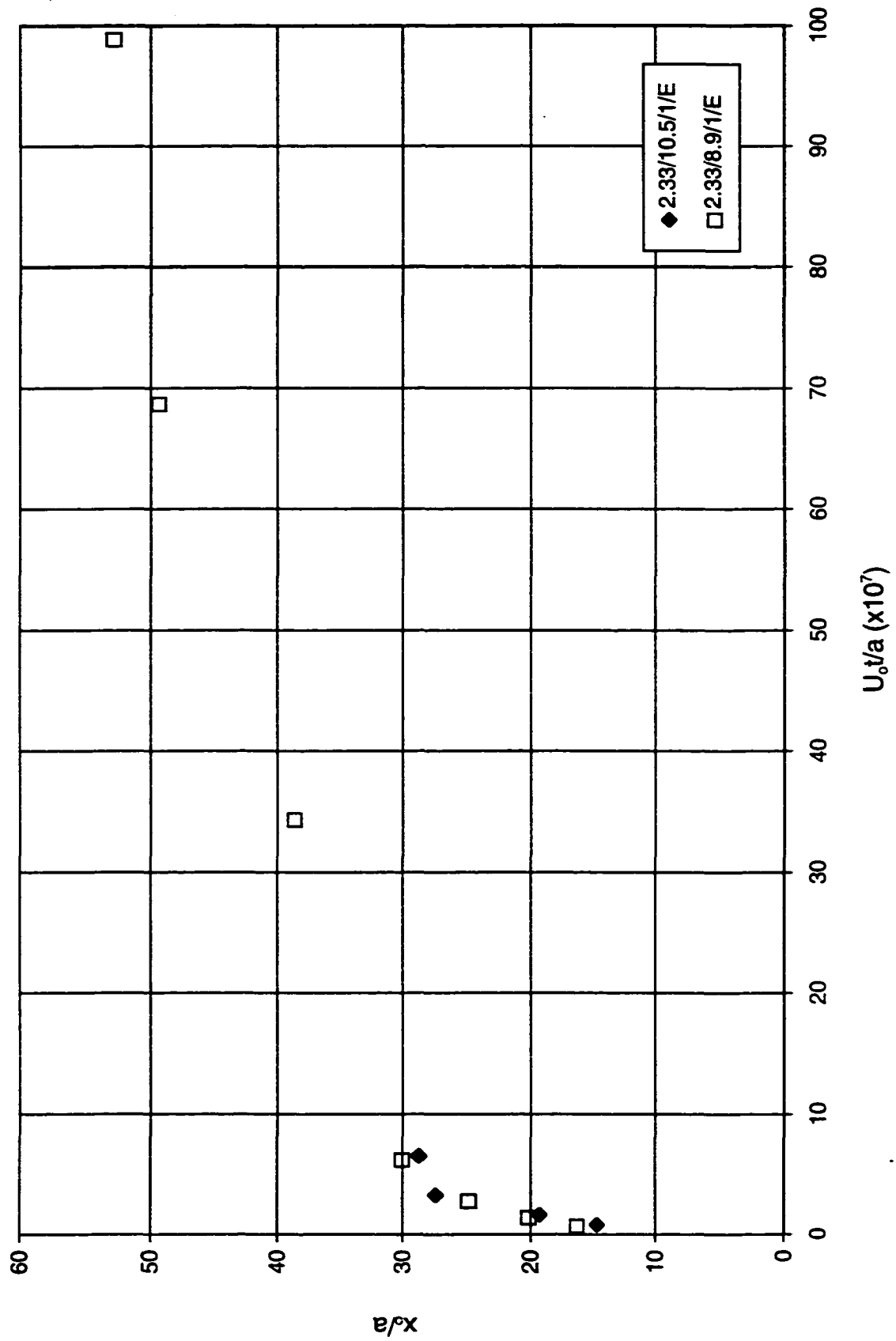


Fig. 7-31: Growth of the dimensionless scour hole length with time.

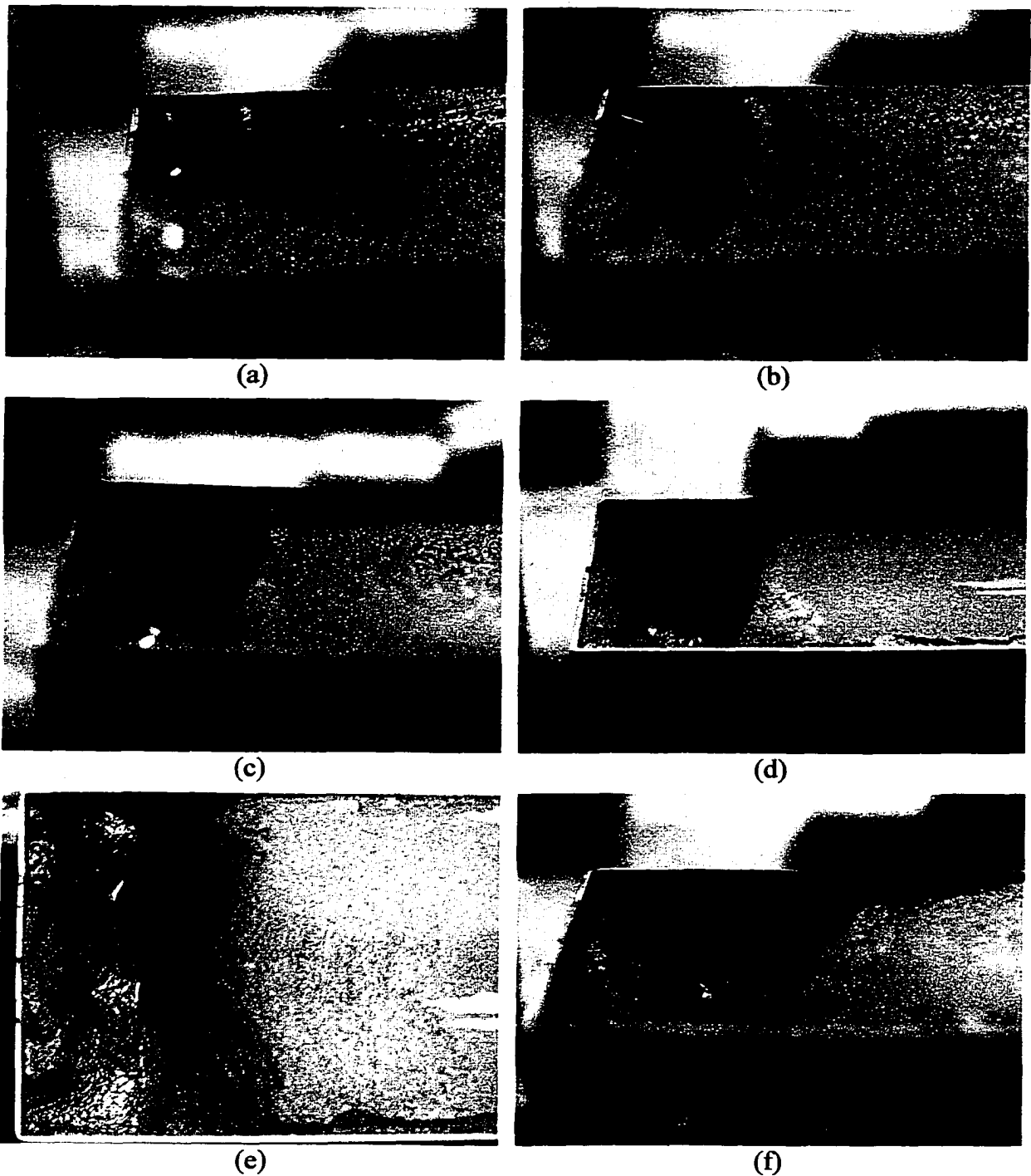
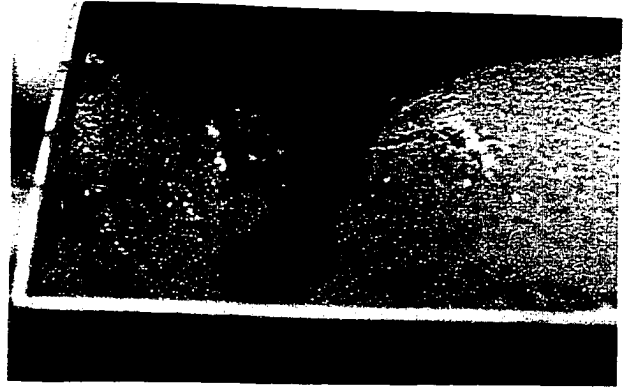


Plate 7-1: Scour hole growth for Test no. 2.33/8.9/1/E $U_o=8.89$ m/s $a=2.33$
 $(\lambda-\lambda_c)/\lambda_c=3.05$ after (a) 30 min (b) 2 h (c) 4.5 h (d) 25 h (e) 25 h (in plan) (f) 50 h (g) 50 h
(in plan) (h) 72 h (i) 72 h (in plan)



(g)



(h)



(i)

Plate 7-1: cont'd.

CHAPTER 8: CONCLUSION

8.1 Summary of Observations

In the preceding chapters, the scour of clay by two different types of submerged water jets was studied. In this last chapter, a brief discussion on the main observations from this work is presented. The first study contribution was an investigation of the scour created in a clay by a submerged circular turbulent jet impinging at 90° to the sample. This type of jet is frequently used for determining the erodibility of soils and in general studies of the characteristics of scour in soils. Some of the important observations include:

1. There appears to be a linear relation between the growth of the scour hole dimensions (the maximum scour depth, centreline scour depth, and the cube root of the scour hole volume) with time for the majority of the growth of the scour hole. At longer times, the scour hole dimensions did not appear to change (over a 24 h period) and were determined to be at an asymptotic or equilibrium state of scour. This was after about 80 to 100 hours. At times very near the beginning of scour and as the scour approached the equilibrium scour depth the growth of scour hole did not follow the linear relation with the logarithm of time. This is similar to that observed for sand erosion.
2. Tests at the same hydraulic conditions did not fall on the same curve (they did not have the same growth rate) although the scour hole at equilibrium may be of the same size. It is thought that this was due to the different sized chunks of clay being removed near the start of each test that significantly changed the flow characteristics. The influence of slightly different water content and saturation of the samples may have also affected erosion rates.
3. The scour hole radius is distinct for scour by jets in clays as compared to that in sand. There was no “ridge” that formed outside the scour hole built of material from the scour hole for the tested soil (which had a very fine gradation). As well, the maximum scour depth typically did not fall along the jet centreline.

4. The most dominant form of erosion for the impinging jet, and what should be for most consolidated clays, was mass erosion. This is the removal of the soil in the form of chunks that varied in size from a few millimetres in to hundreds of millimetres. Although the chunks of clay appear to be removed randomly from the clay, especially at very early times for the tests, the scour hole eventually does come to what appears to be an asymptotic state of scour. The dimensions of the scour hole at equilibrium then can be predicted based on the properties of the jet. These jet properties can be combined in the parameter $X = \rho U_o^2 \left(\frac{d}{H} \right)^2$ for jets at large impingement heights ($H > 8.3d$). The equations to predict the scour hole dimensions apply only to jets with Reynolds numbers greater than about 10000.
5. There is a critical value of X , X_c , below which no mass erosion occurs. For the clay used in the experiments described herein, this was about $X_c = 300$ Pa which is equivalent to a maximum shear stress on the clay surface of 48 Pa. The critical shear stress of the clay can then be assumed to be 48 Pa.
6. For the current study, which used only jets at large impingement heights, it was found that the impingement height a better scale to make the maximum scour depth, the centreline scour depth, and cube root of scour hole dimensionless rather than the diameter of the jet as used in some previous studies in scour of clay by jets.
7. The scour hole profiles can successfully be made dimensionless using the maximum scour depth as scale for the scour depths and either the radius of the scour hole or the half-width of scour, which is the radial distance from the jet centreline where the scour depth is half the maximum scour depth, for the distance from the jet centreline. The centreline scour depth also worked well as the scale instead of the maximum scour depth.
8. There were two forms of scour hole that formed: (1) a wide and shallow scour hole with a “weakly deflected” jet and (2) a narrow and deep scour hole with a “strongly

deflected" jet. The wide and shallow scour hole occurs for $\frac{X - X_c}{X_c} \leq 5$ and the narrow and deep scour hole tends to form when $\frac{X - X_c}{X_c} \geq 5$. The scour hole volume is smaller for the strongly deflected jet scour holes than the weakly deflected jet scour holes. It is thought this is due to the reduction in momentum of the jet due to the entrainment of its own return flow.

The wall jets experiments are one of the first investigations of the scour of clay by a submerged plane turbulent wall jet. There were several important observations:

1. The scour hole created by the two dimensional plane wall jet flow was not two dimensional but varied across the width of the sample. This irregularity in the scour hole was often pronounced at longer times whereas the scour holes were usually fairly uniform during the first few hours during the tests. The variable scour hole shape may have been due to the wall effects of the flume and disturbances at the edge of the sample, but may also have been due to mass erosion of the samples. When a chunk of soil is eroded in one location of the clay surface, the approximately two-dimensional jet flow over the sample becomes much more three-dimensional, potentially creating the uneven scour.
2. The scour was created for the wall jet tests by rapid surface erosion during the early times of the tests, and after a few hours, erosion of small to large soil chunks by mass erosion.
3. The scour hole profiles, although the scour hole was not uniform across the sample, could be successfully made dimensionless using the nozzle thickness as the scale for the scour depths and the distance from the nozzle where the scour depth was half the maximum depth for the distance from the nozzle. These profiles did not fall on one curve, but could be divided into four types based on the shape of the dimensionless

profile. More than one of the different types of scour hole profile could occur across the sample for a test. Under what conditions these profiles form is as yet undetermined.

4. The dimensions of the scour hole that were thought to be of most concern were the maximum depth of scour, the location of maximum scour, and the length of the scour hole. These scour hole relations at equilibrium can be related to the parameter $\lambda = \rho U_0^2$ and equations were developed to predict the scour hole dimensions.
5. There were a critical value of λ below which no significant erosion occurred. This was $\lambda = 20000$ Pa for this clay. This is equivalent to a critical shear stress of about 50 Pa, a value that is very close to that found from the impinging jet tests of 48 Pa.
6. The scour hole dimensions were found to grow in a linear relation with the logarithm of time (although in each of the tests, the scour holes failed to reach equilibrium).
7. In two tests examining the evolution of the scour holes, the scour hole profiles through the scouring process were found to be similar. The scour holes profiles were made dimensionless in the same manner as the scour hole profiles at equilibrium.

Other significant observations are the three types of erosion observed through two set of experiments and that the characteristics of erosion were similar in the two types of tests. Flake erosion is the erosion of thin, flat flakes from the clay surface. This produced minimal scour and its occurrence is thought to be related to the preparation of the sample. Mass erosion is the erosion of small to large chunks of clay from the sample. Mass erosion produced significant amounts of erosion in very short times and was the predominant type of erosion in these tests. Finally, rapid surface erosion is a particle by particle erosion that occurred at high bed stresses.

8.2 Conclusions

The main contributions of this work are as follows:

1. This work shows that repeatable experiments in the scour by jets of clay can be performed.
2. It provides several important observations of the characteristics of scour by jets of clays.
3. It includes the first study of the scour by submerged plane turbulent wall jet scour in cohesive material.
4. It introduces a method to predict the scour hole dimensions at equilibrium produced by both submerged circular turbulent impinging jets and submerged plane turbulent wall jet.

8.3 Recommendations for Future Research

As only one clay was tested for this study, there is a need to examine whether the equations for predicting scour developed herein are applicable to the scour by jets of other soils. It should also be remembered that these equations likely do not apply to soils that are fissured, disturbed by sampling, layered, or otherwise inhomogenous and, as such, research should be carried out on the erosion behavior in these types of soils as well. These equations also may not apply to unsaturated soils that can slake.

The current tests with the impinging jet examine only the scour produced by jets at large impingement heights. Study of the scour of clays by developing jets (small impingement heights) should also be undertaken. As well, there is a need to examine more closely the development of the scour holes with time so that the scour hole dimensions at any time during the scouring process can be predicted. This work also can easily be extended to the scour in cohesive material by jets of different geometries.

There is also a need to define the limits of cohesive soil behavior in regards to soil erodibility and the characteristics of soil erosion. The erosion of sand and cohesive soils is different and it is necessary to know how a soil will erode for different clay contents and clay minerals. There as yet has only been a small amount of work done on this subject. This might be done with testing using an impinging jet apparatus.

The impinging jet could easily be developed further as an erodibility device. However, there must be a comparison between the erosion created by the jet and that in an open channel flow for it to be used for determining erosion in open channel flows. The wall jet testing however is quite finicky to the placement of the block with respect to the jet flow and should not be considered as a robust test for this type of testing.

REFERENCES

- Abdel-Rahman, N.M. (1963) The Effect of Flowing Water on Cohesive Beds. Ph.D. Thesis. Swiss Federal Institute of Technology. Zurich, Switzerland.
- Abt, S.R. (1980) Scour at Culvert Outlets in Cohesive Bed Material. Ph.D. Thesis. Colorado State University, Fort Collins, Colorado.
- Abt, S.R., and J.R. Ruff (1982) "Estimating Culvert Scour in Cohesive Material." Journal of the Hydraulics Division. ASCE. **108** (HY1): 25-34.
- Aderibigbe, O. (1996) Contributions to Erosion by Jets. Ph.D. Thesis. University of Alberta, Edmonton, Alberta, Canada.
- Aderibigbe, O.O., and N. Rajaratnam (1996) "Erosion of Loose Beds by Submerged Circular Impinging Vertical Turbulent Jets." Journal of Hydraulic Research. **34** (1): 19-33.
- Aderibigbe, O., and N. Rajaratnam (1998) "Effect of Sediment Gradation on the Erosion by Plane Turbulent Wall Jets." Journal of Hydraulic Engineering. **124** (10): 1034-1042.
- Albertson, M.L., B. Dai, R.A. Jensen, and H. Rouse (1950) "Diffusion of Submerged Jets." ASCE Transactions. **115**: 639-664.
- Ali, K.H.M., and L. Lim (1986) "Local Scour Caused by Submerged Wall Jets." Proceedings, Institution of Civil Engineers. **81** (2): 607-645.
- Ali, K.H.M., and A.A. Salehi Neyshaboury (1991) "Localized Scour Downstream of a Deeply Submerged Horizontal Jet." Proceedings, Institution of Civil Engineers. **91** (2): 1-18.
- Alizadeh, A. (1974) Amount and Type of Clay and Pore Fluid Influences on the Critical Shear Stress and Swelling of Cohesive Soils. Ph.D. Thesis, University of California at Davis, Davis, California.
- Andres, D. (1985) "Hydraulic Erodability of Cohesive Materials." Alberta Research Council, Report No. SWE 83/04, Edmonton, Alberta.
- Ariathurai, R., and K. Arulanandan (1978) "Erosion Rates of Cohesive Soils." Journal of the Hydraulics Division. **104** (HY2): 279-283.
- Arulanandan, K. (1975) "Fundamental Aspects of Erosion of Cohesive Soils." Journal of the Hydraulics Division. **101** (HY5): 635-639.
- Arulanandan, K., and R.T. Heinzen (1977) "Factors Influencing Erosion in Dispersive Clays and Methods of Identification. Proceedings of the IAHR Symposium on Erosion and Solid Matter Transport, Paris, July, 1977, pgs. 404-416.
- Arulanandan, K., P. Loganathan, and R. Krone (1975) "Pore and Eroding Fluid Influences on Surface Erosion of Soil." Journal of the Geotechnical Engineering Division. **101** (GT1): 51-66.

- Arulanandan, K., S. Sargunam, P. Loganathan, and R.B. Krone (1973) "Application of Chemical and Electrical Parameters to the Prediction of Erodibility." Soil Erosion: Causes and Mechanisms, Prevention and Control. Special Report No. 135, Highway Research Board, Washington, D.C., pgs. 42 to 51.
- ASCE Task Committee on Sedimentation (1966) "Abstracted Bibliography on Erosion of Cohesive Materials." Journal of the Hydraulics Division. 92 (HY2): 243-289.
- ASCE Task Committee on Sedimentation (1968) "Erosion of Cohesive Sediments." Journal of the Hydraulics Division. 94 (HY4): 1017-1049.
- Aqualta (1998a) "Water Treatment Plants Monthly Report". City of Edmonton, April, 1998.
- Aqualta (1998b) "Water Treatment Plants Monthly Report". City of Edmonton, May, 1998.
- Aqualta (1998c) "Water Treatment Plants Monthly Report". City of Edmonton, June, 1998.
- Aqualta (1998d) "Water Treatment Plants Monthly Report". City of Edmonton, July, 1998.
- Aqualta (1998e) "Water Treatment Plants Monthly Report". City of Edmonton, August, 1998.
- Aqualta (1998f) "Water Treatment Plants Monthly Report". City of Edmonton, September, 1998.
- Aqualta (1998g) "Water Treatment Plants Monthly Report". City of Edmonton, October, 1998.
- Aqualta (1998h) "Water Treatment Plants Monthly Report". City of Edmonton, November, 1998.
- Aqualta (1998i) "Water Treatment Plants Monthly Report". City of Edmonton, December, 1998.
- Aqualta (1999a) "Water Treatment Plants Monthly Report". City of Edmonton, January, 1999.
- Aqualta (1999b) "Water Treatment Plants Monthly Report". City of Edmonton, February, 1999.
- Aqualta (1999c) "Water Treatment Plants Monthly Report". City of Edmonton, March, 1999.
- Aqualta (1999d) "Water Treatment Plants Monthly Report". City of Edmonton, April, 1999.
- Aqualta (1999e) "Water Treatment Plants Monthly Report". City of Edmonton, May, 1999.
- Aqualta (1999f) "Water Treatment Plants Monthly Report". City of Edmonton, June,

1999.

- Aqualta (1999g) "Water Treatment Plants Monthly Report". City of Edmonton, July, 1999.
- Aqualta (1999h) "Water Treatment Plants Monthly Report". City of Edmonton, September, 1999.
- Beltaos, S. (1974) Turbulent Impinging Jets. Ph.D. Thesis. University of Alberta, Edmonton, Alberta, Canada.
- Beltaos, S., and N. Rajaratnam (1974) "Impinging Circular Turbulent Jets." Journal of the Hydraulics Division. **100** (HY10): 1313-1328.
- Beltaos, S., and N. Rajaratnam (1977) "Impingement of Axisymmetric Developing Jets." Journal of Hydraulic Research. **15** (4): 311-326."
- Berlamont, J., M. Ockenden, E. Tooman, and J. Winterwerp (1993) "The Characterisation of Cohesive Sediment Properties." Coastal Engineering. **21**: 105-128.
- Bhasin, R.N., C.W. Lovell, and G.R. Toebes (1969) "Erodability of Sand-Clay Mixtures as Evaluated by a Water Jet." Technical Report No. 8. Purdue University Water Resources Research Center. Purdue University, West Lafayette, Indiana, June, 1969.
- Bouyoucos, G.J. (1935) "The Clay Ratio as A Criterion of Susceptibility of Soils to Erosion." Journal of the American Society of Agronomy. **27**: 738-741.
- Braiu, J.L., F.C.K. Ting, H.C. Chen, R. Gudavalli, S. Pergugu, and G. Wei (1999) "SRICOS: Prediction of Scour Rate in Cohesive Soils at Bridge Piers." Journal of Geotechnical and Geoenvironmental Engineering. **125** (4): 237-246.
- Carlson, E.J., and P.F. Enger (1962) "Studies of Tractive Forces of Cohesive Soils in Earth Canals." Hydraulic Branch Report No. Hyd-504, United States Department of the Interior Bureau of Reclamation, Denver, Colorado, October, 1962.
- Chatterjee, S.S., and S.N. Ghosh (1980) "Submerged Horizontal Jet Over Erodible Bed." Journal of the Hydraulics Division. **106** (HY11): 1765-1782.
- Chatterjee, S.S., and S.N. Ghosh, and M. Chatterjee (1994) "Local Scour Due to Submerged Horizontal Jet." Journal of Hydraulic Engineering. **120** (8): 973-992.
- Christensen, R.W., and B.M. Das (1973) "Hydraulic Erosion of Remolded Cohesive Soils." Soil Erosion: Causes and Mechanisms, Prevention and Control. Special Report No. 135, Highway Research Board, Washington, D.C., pgs. 8 to 19:
- Croad, R.N. (1981) Physics of Erosion of Cohesive Soils. Ph.D. Thesis. University of Auckland. Auckland, New Zealand.
- Dash, U. (1968) Erosive Behavior of Cohesive Soils. Ph.D. Thesis. Purdue University, West Lafayette, Indiana.

- Dennett, K.E., T.W. Sturm, A. Amirtharajah, and T. Mahmood (1995) "Flume Studies on the Erosion of Cohesive Sediments." Proceedings of the 1st International Conference on Water Resources, August 14-18, 1995, San Antonio, Texas, Vol. 1, pgs. 199-203.
- Doddiah, D., M.L. Albertson, and R. Thomas (1953) "Scour from Jets." Proceedings of the Minnesota International Hydraulics Convention, Minneapolis, 1953, pgs. 161-169.
- Dunn, I.S. (1959) "Tractive Resistance of Cohesive Channels." Journal of the Soil Mechanics and Foundations Division. **85** (SM3): 1-24.
- Einsele, G., R. Overbeck, H.U. Schwarz, and G. Unsold (1974) "Mass Physical Properties, Sliding and Erodibility of Experimentally Deposited and Differently Consolidated Clayey Muds." Sedimentology. **21**: 339-372.
- Enger, P.F. (1963) "Canal Erosion and Tractive Force Study - Analysis of Data from a Boundary Shear Flume." Report No. Hyd-532, United States Department of the Interior Bureau of Reclamation, Denver, Colorado, December, 1963.
- Epcor (1999) "Water Treatment Plants Monthly Report". City of Edmonton, September, 1999.
- Epcor (2000a) "Water Treatment Plants Monthly Report". City of Edmonton, January, 2000.
- Epcor (2000b) "Water Treatment Plants Monthly Report". City of Edmonton, February, 2000.
- Epsy, W.H., Jr. (1963) "A New Test to Measure the Scour of Cohesive Sediment." Technical Report No. HYD 01-6301, Hydraulic Engineering Laboratory, Department of Civil Engineering, University of Texas at Austin, April 1963.
- Flaxman, E.M. (1963) "Channel Stability in Undisturbed Cohesive Soils." Journal of the Hydraulics Division. **89** (HY2): 87-96.
- Fortier, S. and F.C. Scobey (1925) "Permissible Canal Velocities." ASCE Proceedings. **51**: 1397-1413.
- Foster, G.R., L.D. Meyer, and C.A. Onstad (1977) "An Erosion Equation Derived from Basic Erosion Principles." Transactions of the ASAE. **20** (4): 678-682.
- Gerodimos, G., and R.M.C. So (1997) "Near -Wall Modelling of Plane Turbulent Wall Jets." Journal of Fluids Engineering. **119**: 304-313.
- Ghebreiyessus, Y.T., C.J. Gantzer, E.E. Alberts, and R.W. Lentz (1994) "Soil Erosion by Concentrated Flow: Shear Stress and Bulk Density." Transactions of the ASAE. **37** (6): 1791-1797.
- Glauert, M.B. (1956) "The Wall Jet." Journal of Fluid Mechanics. **1** (Dec): 625-643.
- Grimm, R.E. (1953) Clay Mineralogy. McGraw-Hill Book Company, Inc.: New York, 384 pgs.

- Grimm, R.E. (1962) Applied Clay Mineralogy. McGraw-Hill Book Company, Inc.: New York, 422 pgs.
- Grissinger, E.H. (1966) "Resistance of Selected Clay Systems to Erosion by Water." Water Resources Research. 2 (1): 131-138.
- Grissinger, E.H. (1982) "Bank Erosion of Cohesive Materials." Gravel-Bed Rivers. R.D. Hey, J.C. Bathurst, and C.R. Thorne, eds., pgs. 273-287.
- Gularte, R.C., W.E. Kelly, and V.A. Nacci (1979a) "Scouring of Cohesive Material as a Rate Process." Civil Engineering in the Ocean IV. Proceedings of the ASCE Specialty Conference. Sept. 10 to 12th, 1979, San Francisco, California, Vol. 2, pgs. 848-862.
- Gularte, R.C., W.E. Kelly, and V.S. Nacci (1979b) "Rheological Methods for Predicting Erosion." Maritime Technology '79: Ocean Energy, 15th Annual Conference of the Marine Technological Society, New Orleans, Louisiana, pgs. 251-258.
- Hall, K.R. (1981) Initiation of Erosion of Consolidated Clays by Unidirectional Flow. M.Sc. Thesis. Department of Civil Engineering. Queen's University, Kingston, Ontario.
- Hall, K.R. (1983) "Model Investigation of Erosion of Consolidated Cohesive Soils." Proceedings of the 6th Canadian Hydrotechnical Conference, CSCE, Ottawa, Ontario, June 2 and 3, 1983, pgs. 357-377.
- Hanson, G.J. (1989) "Channel Erosion Study of Two Compacted Soils." Transactions of the ASAE. 32 (2): 485-490.
- Hanson, G.J. (1990a) "Surface Erodibility of Earthen Channels at High Stresses: Part II - Developing an In Situ Testing Device." Transactions of the ASAE. 33 (1): 132-137.
- Hanson, G.J. (1990b) "Surface Erodibility of Earthen Channels at High Stresses: Part I - Open Channel Testing." Transactions of the ASAE. 33 (1): 127-131.
- Hanson, G.J. (1991) "Development of a Jet Index to Characterize Erosion Resistance of Soils in Earthen Spillways." Transactions of the ASAE. 34 (5): 2015-2020.
- Hanson G.J. (1992) "Erosion Resistance of Compacted Soils." Transportation Research Record. No. 1369, pgs. 26-30.
- Hanson, G.J. (1996) "Investigating Soil Strength and Stress-Strain Indices to Characterize Erodibility." Transactions of the ASAE. 39 (3): 883-890.
- Hanson, G.J., and K.M. Robinson (1993) "The Influence of Soil Moisture and Compaction on Spillway Erosion." Transactions of the ASAE. 36 (5): 1349-1352.
- Hedges, J.D. (1990) The Scour of Cohesive Soils by an Inclined Submerged Water Jet. M.Sc. Thesis. Texas A & M University. College Station, Texas.
- Hogg, A.J., H.E. Buppert, and W. B. Dade (1997) "Erosion by Planar Turbulent Jets." Journal of Fluid Mechanics. 338: 317-340.

- Hollick, M. (1976) "Towards a Routine Assessment of the Critical Tractive Forces of Cohesive Soils." Transactions of the ASAE. **19**: 1076-1081.
- Hosny, M.M. (1995) Experimental Study of Local Scour around Circular Bridge Piers in Cohesive Soils. Ph.D. Thesis, Colorado State University, Fort Collins, Colorado.
- Huang, J. (1993) "Experimental Study of the Scouring of Cohesive Deposits in Salt Water." International Journal of Sediment Research. **8** (2): 67-83.
- Huygens, M., and R. Verhoeven (1996) "Some Fundamental Particularities on Partly Cohesive Sediment Transport in a Circular Test Flume." Advances in Fluid Mechanics. Proceedings of the 1st Conference on Advances in Fluid Mechanics, New Orleans. Vol. 9, pgs. 11-20.
- Jackobsen, F., and R. Deigaard (1996) "Material Parameters and Numerical Simulations of Flume Experiments on Cohesive Sediments." Prog. Report 76, July, 1996, Dept. of Hydrodynamics and Water Resources. Technical University of Denmark. pgs. 11-25.
- Johnston, G. (1967) "The Effect of Entrained Air on the Scouring Capacity of Water Jets." Proceedings of the 12th IAHR Congress, Fort Collins, Colorado, pgs. 218-226.
- Kamphuis, J.W. (1983) "On the Erosion of Consolidated Clay Material by a Fluid Containing Sand." Canadian Journal of Civil Engineering. **10**: 223-231.
- Kamphuis, J.W. (1988) Competent Scour Velocity of Cohesive Soils. Report for the Ontario Ministry of Transportation, December, 1988.
- Kamphuis, J.W. (1990) "Influence of Sand or Gravel on the Erosion of Cohesive Sediment." Journal of Hydraulic Research. **28** (1): 43-53.
- Kamphuis, J.W., and K.R. Hall (1983) "Cohesive Material Erosion by Unidirectional Current." Journal of the Hydraulics Division. **109** (1): 49-61.
- Kandiah, A., and K. Arulanandan (1974) "Hydraulic Erosion of Cohesive Soils." Transportation Research Record 497. pgs. 60-68.
- Karasev, I.F. (1964) "The Regimes of Eroding Channels in Cohesive Material." Soviet Hydrology. **6**: 551-579.
- Kelly, W.E., R.C. Gularte, and V.A. Nacci (1979) "Erosion of Cohesive Sediments as Rate Process." Journal of the Geotechnical Engineering Division. **105** (GT5): 673-676.
- Kobus, H., P. Leister, and B. Westrich (1979) "Flow Field and Scouring Effects of Steady and Pulsating Jets Impinging on a Movable Bed." Journal of Hydraulic Research. **17** (3): 175-192.
- Krishnamurthy, M. (1983) "Incipient Motion of Cohesive Soils." Frontiers of Hydraulic Engineering. Proceedings of the ASCE conference on frontiers of hydraulic engineering, Aug. 9-12, 1983, Cambridge, Massachusetts, pgs. 97 to 101.

- Krone, R.B. (1983) "Cohesive Sediment Properties and Transport Properties." Frontiers in Hydraulic Engineering. Cambridge, Massachusetts, August 9-12, 1983, pgs. 66-78.
- Krone, R.B. (1999) "Effects of Bed Structure on Erosion of Cohesive Sediments." Journal of Hydraulic Engineering. **125** (12): 1297-1301.
- Kuti, E.G., and C. Yen (1976) "Scouring of Cohesive Soils." Journal of Hydraulic Research. **14** (3): 195-206.
- Lambe, T.W. (1958a) "Compacted Clay: Structure." Journal of the Soil Mechanics and Foundations Division. **84** (SM2): Paper No. 1654, 1-34.
- Lambe, T.W. (1958b) "Compacted Clay: Engineering Behavior." Journal of the Soil Mechanics and Foundations Division. **84** (SM2): Paper No. 1655, 1-35.
- Laflen, J.M., and R.P. Beasley (1960) Effects of Compaction on Critical Tractive Forces in Cohesive Soils. University of Missouri, Agricultural Experiment Station, Research Bulletin 749, September 1960.
- Lane, E.W. (1952) "Progress Report on Results of Studies on Design of Stable Channels." Hydraulic Laboratory Report No. Hyd-352. United States Department of the Interior Bureau of Reclamation. Denver, Colorado, June, 1952.
- Lauder, B.E., W.Rodi (1981) "The Turbulent Wall Jet." Progress in Aerospace Science. **19**: 81-128.
- Lauder, B.E., and Rodi, W. (1983) "The Turbulent Wall Jet - Measurements and Modeling." Annual Review of Fluid Mechanics. **15**: 429-459.
- Laursen, E.M. (1952) "Observations of the Nature of Scour." Proceedings of the 5th Hydraulic Conference, Bulletin 34, University of Iowa, Iowa City, Iowa, 1952, pgs. 179-197.
- Lefebvre, G., K. Rohan, and S. Douville (1985) "Erosivity of Natural Intact Structured Clay: Evaluation." Canadian Geotechnical Journal. **22** (4): 508-517.
- Lefevre, G., and K. Rohan (1986) "On the Principal Factors Controlling Erosivity of Undisturbed Clay." Proceedings of the Symposium on Cohesive Shores, National Research Council of Canada, pgs. 170 to 195.
- Lefebvre, G., K. Rohan, J.P. Milette (1986) "Erosivity of Intact Clay: Influence of the Natural Structure." Canadian Geotechnical Journal. **23** (4): 427-434.
- Liou, Y. (1970) Hydraulic Erodibility of Two Pure Clay Systems. Ph.D. Thesis. Colorado State University, Fort Collins, Colorado.
- Lyle, W.M., and E.T. Smerdon (1965) "Relation of Compaction and Other Soil Properties to Erosion Resistance of Soils." Transactions of the ASAE. **8**: 419-422.
- Martin, R.T. (1962) "Discussion of Experiments of the Scour Resistance of Cohesive Sediments." by W.L. Moore and F.D. Masch, Jr. Journal of Geophysical Research. **67** (4): 1447-1449.

- Masch, F.D., W.H. Epsey, and W.L. Moore (1963) "Measurements of the Shear Resistance of Cohesive Sediments." Proceedings of the Federal Inter-Agency Sedimentation Conference, Jackson, Mississippi, pgs. 151-155.
- McNeil, J., C. Taylor, and W. Lick (1996) "Measurements of Erosion of Undisturbed Bottom Sediments with Depth." Journal of Hydraullic Engineering. **122** (6): 316-324.
- Mehta, A.J. (1991) "Review Notes on Cohesive Sediment Erosion." Coastal Sediments '91. Vol. 1, pgs. 40-53.
- Mehta, A.J., E.J. Hayter, W.R. Parker, R.B. Krone, and A.M. Teeter (1989) "Cohesive Sediment Transport. I: Process Description." Journal of Hydraulic Engineering. **115** (8): 1076-1093.
- Mih, W.C., and J. Kabir (1983) "Impingement of Water Jets on Nonuniform Streambed." Journal of Hydraulic Engineering. **109** (4): 536-548
- Middleton, H.E. (1930) "Properties of Soils which Influence Soil Erosion." USDA Technical Bulletin No. 178. pgs. 1-16.
- Minks, A.G. (1983) Investigation of the Effect of Soil Particle Orientation on the Erodibility of Kaolinite. M.Sc. Thesis. University of Missouri-Rolla. Rolla, Missouri.
- Mitchener, H., and H. Torfs (1996) "Erosion of Mud/Sand Mixtures." Coastal Engineering. **29**: 1-25.
- Mirtskhoulava, Ts. E. (1989) "Cohesive Soil Scour Processes, Mechanism, Forecast Achievements and Problems." Proceedings of the XXIII Congress of the IAHR. Ottawa, Canada, August 21-25, 1989, pgs. B-113 to B-120.
- Mirtskhulava, Ts.E. (1975) "Prediction of Erosion of Cohesive Soils." Proceedings of the 16th Congress of the IAHR, San Paulo, Brazil, pgs. 470 to 477.
- Mirtskhulava, Ts.E., I.V. Dolidze, and A.V. Magomedova (1967) "Mechanisms and Computation of Local and General Scour in Non-Cohesive, Cohesive Soils, and Rock Beds." Proceedings of 12th Congress of the IAHR, Fort Collins, Colorado, September, 1967, Vol. 3, pgs. 169-176.
- Mitchell, J.K. (1993) Fundamentals of Soil Behavior. 2nd ed. John Wiley & Sons Inc.: New York, 437 pgs.
- Moore, W.L., and F.D. Masch, Jr. (1962) "Experiments on the Scour Resistance of Cohesive Sediments." Journal of Geophysical Research. **67** (4): 1437-1449.
- Myers, G.E., J.J. Schauer, and R.H. Eustis (1961) "The Plane Turbulent Wall Jet Part 1. Jet Development and Friction Factor." Technical Report No. 1, Department of Mechanical Engineering, Stanford University, Stanford, California, June 1, 1961.
- Myers, G.E., J.J. Schauer, and R.H. Eustis (1963) "The Plane Turbulent Wall Jet Flow Development and Friction Factor." Journal of Basic Engineering. **85** (Mar), 47-53.

- Nearing, M.A. (1991) "A Probabilistic Model of Soil detachment by Shallow Turbulent Flow." Transactions of the ASAE. **34** (1): 81-85.
- Owoputi, L.O., and W.J. Slope (1995) "Soil Detachment in the Physically Based Soil Erosion Process: A Review." Transactions of the ASAE. **38** (4): 1099-1110.
- Paaswell, R.E. (1973) "Causes and Mechanisms of Cohesive Soil Erosion: State of the Art." Soil Erosion: Causes and Mechanisms, Prevention and Control. Special Report No. 135, Highway Research Board, Washington, D.C., pgs. 52 to 74.
- Paaswell, R.E., and E. Partheniades (1968) "Erosion of Cohesive Soil and Channel Stabilization, Part II: Behavior of Cohesive Soils - Study of the Mechanisms of Erosion". Civil Engineering Report No. 19. State University of New York at Buffalo, October, 1968, 51 pgs.
- Pamadi, B.N., I.A. Belov (1980) "A Note on the Heat Transfer Characteristics of Circular Impinging Jet." International Journal of Heat and Mass Transfer. **23**: 783-787.
- Parchure, T.M., and A.J. Mehta (1985) "Erosion of Soft Cohesive Sediment Deposits." Journal of Hydraulic Engineering. **111** (10): 1308-1326.
- Partheniades, E. (1962) A Study of Erosion and Deposition of Cohesive Soils in Saltwater. Ph.D. Thesis, University of California at Berkeley, Berkeley, California.
- Partheniades, E. (1965) "Erosion and Deposition of Cohesive Soils." Journal of the Hydraulics Division. **91** (HY1): 105-139.
- Partheniades, E. (1966) Closure of "Erosion and Deposition of Cohesive Soils." by E. Partheniades. Journal of the Hydraulics Division. **92** (HY3): 79-81.
- Partheniades, E. (1971) "Results of Recent Investigations on Erosion and Deposition of Cohesive Sediments." Chapter 20. Sedimentation. H.W. Shen, ed. pgs. 20-1 to 20-39.
- Partheniades, E. (1984) Discussion of "Cohesive Material Erosion by Unidirectional Current." Journal of the Hydraulics Division. **110** (3): 368-370.
- Partheniades, E., and R.E. Paaswell (1968) "Erosion of Cohesive Soil and Channel Stabilization - Part I: State of Knowledge." Civil Engineering Report No. 19. State University of New York at Buffalo, October, 1968, 68 pgs.
- Perigaud, C. (1984) "Erosion of Cohesive Sediments by a Turbulent Flow: Part II - High Mud Concentration." Journal de Mecanique Theorique et Appliquee. **3** (4): 505-519.
- Poreh, M., Y.G. Tsuei, and J.E. Cermak (1967) "Investigation of a Turbulent Radial Wall Jet." Transactions of the ASME: Journal of Applied Mechanics. **34** (June): 457-463.
- Rajaratnam, N. (1965) "The Hydraulic Jump as a Wall Jet." Journal of the Hydraulics Division. ASCE. **91** (HY5): 107-130.

- Rajaratnam, N. (1967) "Plane Turbulent Wall Jets on Rough Boundaries." Water Power. England, May: 196-201.
- Rajaratnam, N. (1968) "Effect of Side Walls on Plane Turbulent Wall Jets." Journal of Hydraulic Research. 6 (4): 327-334.
- Rajaratnam, N. (1976) Turbulent Jets. Developments in Water Science 5, Elsevier Scientific Publishing Company: New York.
- Rajaratnam, N. (1981) "Erosion by Plane Turbulent Jets." Journal of Hydraulic Research. 19 (4): 339-358.
- Rajaratnam, N. (1982) "Erosion by Submerged Circular Jets." Journal of the Hydraulics Division. 108 (HY2): 262-267.
- Rajaratnam, N., and S. Beltaos (1977) "Erosion by Impinging Circular Turbulent Jets." Journal of the Hydraulics Division. 103 (HY10): 1191-1205.
- Rajaratnam, N and Flint-Petersen, L. (1989). "Low Reynolds Number Circular Turbulent Jets." Proc. Instn. of Civil Engrs. 87: 299-305.
- Raudkivi, A.J., and D.L. Hutchison (1974) "Erosion of Kalonite by Flowing Water." Proceedings of the Royal Society of London (Series A). 337: 537-554.
- Raudkivi, A.J., and S.K. Tan (1984) "Erosion of Cohesive Soils." Journal of Hydraulic Research. 22 (4): 217-233.
- Reddi, L. and M.V.S. Bonala (1996) "Critical Shear Stress and its Relationship with Cohesion for Sand-Kaolinite Mixtures." Canadian Geotechnical Journal. 34: 26-33.
- Rohan, K., G. Lefebvre, and S. Douville (1980) "Erosion Mechanisms of Intact Clay" (in French). Proceedings of the Candian Coastal Conference, Burlington, Ontario, April 22-24, 1980, pgs. 200-219.
- Rohan, K., G., Lefebvre, S. Douville, and J.P. Milette (1986) "A New Technique to Evaluate Erosivity of Cohesive Material." Geotechnical Testing Journal. 9 (2): 87-92.
- Rouse, H. (1939) "A Criteria for Similarity in the Transportation of Sediment." Proceedings of the 1st Hydraulic Conference, Bulletin 20, State Unviersity of Iowa, Iowa City, Iowa, 1939, pgs. 33-49.
- Sargunam, A. (1973) Influence of Mineralogy, Pore Fluid Composition and Structure on the Erosion of Cohesive Soils. Ph.D. Thesis. University of California at Davis Davis, California.
- Sargunam, A., P. Riley, K. Arulanandan, and R.B. Krone (1973) "Physico-Chemical Factors in Erosion of Cohesive Soils." Journal of the Hydraulics Division. 99 (HY3): 555-558.
- Schwarz, W.H., and W.P. Cosart (1961) "The Two-Dimensional Turbulent Wall Jet." Journal of Fluid Mechanics. 10 (4): 481-495.

- Shaikh, A. (1986) Surface Erosion of Compacted Clays. Ph.D. Thesis. Department of Civil Engineering. Colorado State University. Fort Collins, Colorado.
- Shaikh, A., J.F. Ruff, and S.R. Abt (1988) "Erosion Rate of Compacted Na-Montmorillonite Soils." Journal of Geotechnical Engineering. 114 (3): 296-305.
- Shaikh, A., J.F. Ruff, W.A. Charlie, and S.R. Abt (1988) "Erosion Rate of Dispersive and Nondispersive Clays." Journal of Geotechnical Engineering. 114 (5): 589-600.
- Shainberg, I., J.M. Laflen, J.M. Bradford, and L.D. Norton (1994) "Hydraulic Flow and Water Quality Characteristics in Rill Erosion." Soil Science Society of America Journal. 58: 1007-1012.
- Sherard, J.L., R.S. Decker, and N.L. Ryker (1972) "Piping in Earth Dams of Dispersive Clay." Proceedings, ASCE Specialty Conference on the Performance of Earth and Earth Supported Structures. Vol. 1, pgs. 589-626.
- Smerdon, E.T., and R.P. Beasley (1961) "Critical Tractive Forces in Cohesive Soils." Agricultural Engineering. 42: 26-29.
- Stein, O. (1990) Mechanics of Headcut Migration in Rills. Ph.D. Thesis. Colorado State University, Fort Collins, Colorado.
- Stein, O.R., and P.Y. Julien (1994) "Sediment Concentration Below Free Overfall." Journal of Hydraulic Engineering. 120 (9): 1043-1059.
- Stein, O.R., P.Y. Julien, and C.V. Alonso (1993) "Mechanics of Jet Scour Downstream of a Headcut." Journal of Hydraulic Research. 31 (6): 723-738.
- Stein, O.R., and D.D. Nett (1997) "Impinging Jet Calibration of Excess Shear Sediment Detachment Parameters." Transactions of the ASAE. 40 (6): 1573-1580.
- Tarapore, Z.S. (1956) Scour below a submerged sluice gate. M.Sc. Thesis, University of Minnesota, Minneapolis, Minnesota.
- Terwindt, J.H.J., H.N.C. Breusers, J.N. Svasek (1968) "Experimental Investigation on the Erosion-Sensitivity of a Sand-Clay Lamination." Sedimentology. 11: 105-114.
- Thomas, C.W., and P.F. Enger (1961) "Use of an Electronic Computer to Analyze Data from Studies of Critical Tractive Forces for Cohesive Soils." Proceedings of the 9th IAHR Congress, Dubrovnik, 1961, pgs. 760-771.
- Thorn, M.F.C., and J.G. Parsons (1980) "Erosion of Cohesive Sediments in Estuaries: An Engineering Guide." 3rd International Symposium on Dredging Technology, Bordeaux, France, March, 1980, pgs. 349-358.
- Topping, J. (1957) Errors of Observation and their Treatment. The Institute of Physics: London, England.
- Torfs, H., M. Huygens, and L. Tito (1994) "The Influence of the Cross-Section on the Erosion Criteria For Partly Cohesive Sediments." Water Science and Technology.

29 (1-2): 103-111.

Van Olphen, H. (1963) An Introduction to Clay Colloid Chemistry. Interscience Publishers: New York, 301 pgs.

Westrich, B., and H. Kobus (1973) "Erosion of a Uniform Sand Bed by Continuous and Pulsating Jets." Proceedings of the IAHR Congress, Istanbul, Turkey, Paper No. A14, Vol. 1, pgs. A13 1-8.

Zeman, A.J. (1982) "Erosion Resistance of Cohesive Sediments." Proceedings of the Workshop on Great Lakes Coastal Erosion and Sedimentation, Burlington, Ontario, November 1 and 2, 1982, pgs. 93-96.

Zeman, A.J. (1983) "Erosion of Cohesive Sediments: Bibliography and Annotated Abstracts." Study No. 354, Shore Processes Section, Hydraulics Division, National Water Research Institute, Canadian Centre for Inland Waters, February, 1983.

Zreik, D.A., B.G. Krishnappan, J.T. Germaine, O.S. Madsen, and C.C. Ladd (1998) "Erosional and Mechanical Strengths of Deposited Cohesive Sediments." Journal of Hydraulic Engineering. 124 (11): 1076-1085.

Appendix A: Data for the growth of the scour holes for the impinging jet tests.

Test No.	8/8.1/5.0/1	S_v (kPa)	w_c (%)	25.38	Temp (°C)	11.8
Clay	M390	New block	w_p (%)	25.38	Ultimate state	
Clay Lot No.	34281348	Metal confining band #2	w_r (%)			
Test Date:	13-Oct-98					
Q (L/s)	0.25					
H (cm)	6.5					
d (mm)	8					

Time (min)	Time (h)	Max. Disturbance (cm)		ξ (cm ³)	$\sqrt[3]{\xi}$ (cm)	ϵ_m (cm)	ϵ_{cl} (cm)
		Width	Length				
0	0.00	0.0	0.0	0.0	0.00	0.00	0.00
4187	69.78	2.8	1.8	0.3	0.67	0.35	0.20

Test No.	8/8.1/6.1/1	S_v (kPa)	20.5	w_c (%)	26.5	Temp (°C)	14.9
Clay	M390	New block	w_p (%)	26.5	Taken as ultimate state		
Clay Lot No.	34281348	Metal confining band #2	w_r (%)	28.09			
Test Date:	1-Oct-98						
Q (L/s)	0.31						
H (cm)	6.5						
d (mm)	8						

Time (min)	Time (h)	Max. Disturbance (cm)		ξ (cm ³)	$\sqrt[3]{\xi}$ (cm)	ϵ_m (cm)	ϵ_{cl} (cm)
		Width	Length				
0	0.00	0.0	0.0	0.0	0.00	0.00	0.00
415	6.92	3.3	3.4	1.5	1.14	0.55	0.45
600	10.00	4.2	3.5	2.5	1.36	0.65	0.60
1496	24.93	5.2	4.6	6.5	1.87	0.85	0.80
1828	30.47	5.4	4.9	8.0	2.00	0.95	0.85
3070	51.17	6.1	5.6	12.0	2.29	1.00	0.95
4577	76.28	6.4	6.0	16.0	2.52	1.25	1.05
5066	84.43	6.4	6.3	16.5	2.55	1.30	1.20

Test No.	8/8.1/6.1/2	S_v (kPa)	w_c (%)	Temp (°C)	15.1
Clay	M390	1 day wet	w_p (%)	Large chunk removal	
Clay Lot No.	34281348	Metal confining band #2	w_r (%)		
Test Date:	29-Sep-98				
Q (L/s)	0.31				
H (cm)	6.5				
d (mm)	8				

Time (min)	Time (h)	Max. Disturbance (cm)		ξ (cm ³)	$\sqrt[3]{\xi}$ (cm)	ϵ_m (cm)	ϵ_{cl} (cm)
		Width	Length				
0	0.00	0.0	0.0	0.0	0.00	0.00	0.00
15	0.25	6.4	5.3	8.0	2.00	0.85	0.45
60	1.00	6.4	5.4	13.5	2.38	1.45	0.95
141	2.35	6.4	5.4	16.0	2.52	1.45	1.05
237	3.95	6.4	5.9	18.5	2.64	1.60	1.25
456	7.60	6.4	6.2	19.5	2.69	1.65	1.40

Test No.	8/8.1/7.0/1	S_v (kPa)	20.8	w_c (%)	26.18	Temp (°C)	18.9
Clay	M390	2 days wet		w_p (%)	29.99		
Clay Lot No.	34281348	Metal confining band #2		w_r (%)	27.41		
Test Date:	4-Sep-98						
Q (L/s)	0.35						
H (cm)	6.5						
d (mm)	8						

Time (min)	Time (h)	Max. Disturbance (cm)		ξ (cm ³)	$\sqrt[3]{\xi}$ (cm)	ϵ_m (cm)	ϵ_{cl} (cm)
		Width	Length				
0	0.00	0.0	0.0	0.0	0.00	0.00	0.00
15	0.25	4.3	4.7	2.5	1.36	0.65	0.20
30	0.50	4.3	4.7	3.5	1.52	0.75	0.35
60	1.00	4.7	4.7	5.5	1.77	0.90	0.50
150	2.50	5.1	4.7	6.0	1.82	0.95	0.65
440	7.33	5.3	5.0	7.0	1.91	0.95	0.75
1350	22.50	5.5	5.5	9.0	2.08	0.95	0.80
1845	30.75	5.5	5.5	10.0	2.15	1.10	1.00
3044	50.73	6.0	5.7	12.5	2.32	1.20	1.05
4660	77.67	6.3	5.7	13.0	2.35	1.25	1.10
5924	98.73	6.3	5.7	14.0	2.41	1.30	1.20
7077	117.95	6.3	5.7	14.5	2.44	1.30	1.20

Test No.	8/8.1/7.4/1	S_v (kPa)	18.9	w_c (%)	26.20	Temp (°C)	18.3
Clay	M390	2 days wet		w_p (%)	28.23	Ultimate state	
Clay Lot No.	34281348	Metal confining band #2		w_r (%)	27.55		
Test Date:	11-Sep-98						
Q (L/s)	0.374						
H (cm)	6.5						
d (mm)	8						

Time (min)	Time (h)	Max. Disturbance (cm)		ξ (cm ³)	$\sqrt[3]{\xi}$ (cm)	ϵ_m (cm)	ϵ_{cl} (cm)
		Width	Length				
0	0.00	0.0	0.0	0.0	0.00	0.00	0.00
10	0.17	4.8	4.1	3.0	1.44	0.55	0.45
30	0.50	5.3	4.8	7.5	1.96	0.95	0.85
60	1.00	6.3	5.3	10.0	2.15	1.10	1.00
120	2.00	6.6	5.8	13.5	2.38	1.20	1.15
265	4.42	6.7	6.3	15.5	2.49	1.30	1.25
615	10.25	6.8	6.5	18.0	2.62	1.45	1.35
1557	25.95	7.3	6.5	21.5	2.78	1.65	1.50
3131	52.18	7.7	7.4	27.0	3.00	1.75	1.70
4208	70.13	7.8	7.5	28.0	3.04	1.95	1.85
5759	95.98	7.8	7.6	29.0	3.07	1.95	1.90
7046	117.43	7.8	7.6	30.0	3.11	2.10	2.00
8800	146.67	7.8	7.6	30.0	3.11	2.10	2.00

Test No. 8/8.1/8.1/1
 Clay M390
 Clay Lot No. 334027107
 Test Date: 12-Apr-98
 Q (L/s) 0.405
 H (cm) 6.5
 d (mm) 8

S_v (kPa)	18.9	w_c (%)	26.20	Temp (°C)	18.3
2 days wet		w_p (%)	28.23	Ultimate state	
Metal confining band #2		w_r (%)	27.55	(block split apart)	

Time (min)	Time (h)	Max. Disturbance (cm)		ξ (cm ³)	$\sqrt[3]{\xi}$ (cm)	ϵ_m (cm)	ϵ_{cl} (cm)
		Width	Length				
0	0.00	0.0	0.0	0.0	0.00	0.00	0.00
5	0.08	7.3	5.7	11.0	2.22	1.0	
15	0.25	8.1	6.0	20.0	2.71	1.3	
30	0.50	7.4	7.0	26.0	2.96	1.3	
60	1.00	8.3	8.0	28.2	3.04	1.4	
120	2.00	8.3	8.0	30.0	3.11	1.4	
240	4.00	8.5	8.0	34.0	3.24	1.4	
480	8.00	8.5	8.0	35.2	3.28	1.5	
1405	23.42	9.2	8.0	44.0	3.53	1.7	
1875	31.25	9.5	8.5	44.0	3.53	1.7	
2570	42.83	9.5	8.5	47.0	3.61	1.7	
3140	52.33	9.5	8.5	50.0	3.68	1.9	
4110	68.50	9.5	8.5	51.5	3.72	2.1	

Test No. 8/8.1/8.4/1
 Clay M390
 Clay Lot No. 34281348
 Test Date: 20-Sep-98
 Q (L/s) 0.42
 H (cm) 6.5
 d (mm) 8

S_v (kPa)	19.6	w_c (%)	26.43	Temp (°C)	15.6
2 days wet		w_p (%)	30.43	Ultimate state	
Metal confining band #2		w_r (%)			

Time (min)	Time (h)	Max. Disturbance (cm)		ξ (cm ³)	$\sqrt[3]{\xi}$ (cm)	ϵ_m (cm)	ϵ_{cl} (cm)
		Width	Length				
0	0.00	0.0	0.0	0.0	0.00	0.00	0.00
2	0.03	7.8	5.3	9.5	2.12	0.95	0.75
5	0.08	8.6	7.1	40.0	3.42	2.50	1.45
15	0.25	9.6	7.4	55.0	3.80	2.75	2.25
30	0.50	9.7	7.4	60.0	3.91	2.80	2.35
60	1.00	9.7	7.4	67.0	4.06	2.80	2.65
120	2.00	9.9	7.8	73.0	4.18	3.15	3.00
240	4.00	9.9	7.9	81.0	4.33	3.35	3.25
360	6.00	9.9	7.9	82.0	4.34	3.35	3.30
1440	24.00	9.9	7.9	94.0	4.55	3.65	3.60
2797	46.62	9.9	8.0	94.5	4.55	3.85	3.85
4347	72.45	9.9	8.1	102.0	4.67	4.05	4.05
5625	93.75	9.9	8.1	104.0	4.70	4.05	4.05
6946	115.77	9.9	8.1	104.0	4.70	4.05	4.05

Test No.	8/8.1/9.0/1	S_v (kPa)	20.4	w_c (%)		Temp (°C)	16
Clay	M390	New Clay Block		w_p (%)		Ultimate state	
Clay Lot No.	334027107	Metal confining band #1		w_r (%)	28.0425		
Test Date:	5-May-98						
Q (L/s)	0.45						
H (cm)	6.5						
d (mm)	8						

Time (min)	Time (h)	Max. Disturbance (cm)		ξ (cm ³)	$\sqrt[3]{\xi}$ (cm)	ϵ_m (cm)	
		Width	Length				
0	0.00	0.0	0.0	0.0	0.00	0.0	
5	0.08	0.1	0.1	0.5	0.79	0.1	
15	0.25	4.5	4.7	4.0	1.59	1.0	
30	0.50	6.2	4.7	6.0	1.82	1.0	
68	1.13	6.7	4.7	8.0	2.00	1.0	
150	2.50	7.3	6.5	16.0	2.52	1.6	
300	5.00	8.5	6.7	20.0	2.71	1.6	
428	7.13	8.7	7.0	24.0	2.88	1.6	
584	9.73	8.7	7.0	27.5	3.02	1.6	
1401	23.35	8.7	8.3	41.0	3.45	2.1	
1821	30.35	9.2	8.3	46.5	3.60	2.3	
2766	46.10	10.4	8.3	58.5	3.88	2.7	
3342	55.70	10.4	9.1	71.0	4.14	2.7	
4173	69.55	10.4	9.1	75.0	4.22	2.8	
4575	76.25	10.4	9.3	76.0	4.24	2.8	
5796	96.60	10.4	9.5	76.5	4.25	2.8	
7455	124.25	10.4	9.5	78.0	4.27	2.8	
8591	143.18	10.4	9.5	78.0	4.27	2.8	

Test No.	8/8.1/9.0/2	S_v (kPa)	20.5	w_c (%)	26.21	Temp (°C)	22.3
Clay	M390	2 days wet		w_p (%)		Taken as ultimate state	
Clay Lot No.	34281348	Metal confining band #2		w_r (%)	27.9		
Test Date:	16-Aug-98						
Q (L/s)	0.45						
H (cm)	6.5						
d (mm)	8						

Time (min)	Time (h)	Max. Disturbance (cm)		ξ (cm ³)	$\sqrt[3]{\xi}$ (cm)	ϵ_m (cm)	ϵ_{cl} (cm)
		Width	Length				
0	0.00	0.0	0.0	0.0	0.00	0.00	0.00
2	0.03	6.5	7.6	29.0	3.07	2.30	0.70
5	0.08	6.5	7.6	31.5	3.16	2.40	0.90
15	0.25	7.5	8.1	41.0	3.45	2.50	1.15
30	0.50	7.8	8.3	43.0	3.50	2.50	1.55
60	1.00	8.0	8.3	51.0	3.71	2.50	1.85
120	2.00	8.2	8.7	54.0	3.78	2.50	2.30
240	4.00	8.2	9.4	63.0	3.98	2.90	2.80
480	8.00	8.2	10.0	70.0	4.12	3.00	2.90
1345	22.42	8.2	10.0	80.0	4.31	3.30	3.20
1852	30.87	8.2	10.0	81.0	4.33	3.70	3.50
2680	44.67	8.2	10.0	85.0	4.40	3.70	3.50

Test No. 8/8.1/9.0/3
 Clay M390
 Clay Lot No. 34281348
 Test Date: 25-Aug-98
 Q (L/s) 0.45
 H (cm) 6.5
 d (mm) 8

S_v (kPa)	20.2	w_c (%)	25.52	Temp (°C)	19.9
1 day wet		w_p (%)	29.625	Ultimate state	
Metal confining band #2		w_r (%)	27.41		

Time (min)	Time (h)	Max. Disturbance (cm)		ξ (cm ³)	$\sqrt[3]{\xi}$ (cm)	ϵ_m (cm)	ϵ_{cl} (cm)
		Width	Length				
0	0.00	0.0	0.0	0.0	0.00	0.00	0.00
2	0.03	5.5	6.0	5.5	1.77	0.75	0.20
5	0.08	7.5	7.0	16.0	2.52	1.10	0.65
15	0.25	9.0	7.2	26.0	2.96	1.40	0.90
30	0.50	9.2	7.5	28.5	3.05	1.50	1.40
60	1.00	9.2	7.5	32.5	3.19	1.70	1.45
120	2.00	9.2	7.5	38.0	3.36	1.85	1.65
275	4.58	9.2	8.0	42.0	3.48	1.90	1.85
529	8.82	9.3	8.5	46.0	3.58	2.35	2.05
1326	22.10	9.3	8.5	55.0	3.80	2.45	2.35
1793	29.88	9.3	9.2	58.0	3.87	2.55	2.55
2756	45.93	9.5	9.5	64.0	4.00	2.80	2.70
3019	50.32	9.5	12.0	81.0	4.33	2.85	2.80
4394	73.23	9.5	12.0	87.0	4.43	3.05	3.00
5520	92.00	9.5	12.0	89.0	4.46	3.15	3.15
7325	122.08	9.5	12.0	90.0	4.48	3.25	3.25

Test No. 8/8.1/9.0/4
 Clay M390
 Clay Lot No. 34281348
 Test Date: 16-Oct-98
 Q (L/s) 0.45
 H (cm) 6.5
 d (mm) 8

S_v (kPa)	16.1	w_c (%)	26.50	Temp (°C)	11.8
4 days wet		w_p (%)	26.5	Taken as ultimate state	
Metal confining band #2		w_r (%)	27.26		

*From Oct 13th test.

Time (min)	Time (h)	Max. Disturbance (cm)		ξ (cm ³)	$\sqrt[3]{\xi}$ (cm)	ϵ_m (cm)	ϵ_{cl} (cm)
		Width	Length				
0	0.00	0.0	0.0	0.0	0.00	0.00	0.00
2	0.03	6.7	5.1	18.0	2.62	1.60	0.45
5	0.08	7.4	7.5	32.0	3.17	2.55	1.45
15	0.25	7.3	7.7	36.0	3.30	2.65	1.45
30	0.50	7.5	7.7	44.0	3.53	2.85	2.25
60	1.00	7.8	7.7	49.0	3.66	2.85	2.65
120	2.00	7.8	7.9	54.0	3.78	2.85	2.65
222	3.70	7.8	7.9	56.0	3.83	2.85	2.75
480	8.00	8.5	8.2	60.0	3.91	3.00	2.95
1297	21.62	8.7	8.2	78.0	4.27	3.35	3.35
1728	28.80	8.3	8.4	82.0	4.34	3.65	3.50
2927	48.78	8.9	10.2	99.0	4.63	3.95	3.85
4151	69.18	9.3	10.2	104.0	4.70	4.15	4.05
5577	92.95	9.3	10.2	107.0	4.75	4.15	4.15
7009	116.82	9.3	10.2	108.0	4.76	4.40	4.20

Test No. 8/8.1/9.0/5
 Clay M390
 Clay Lot No. 34281348
 Test Date: 9-Mar-99
 Q (L/s) 0.45
 H (cm) 6.5
 d (mm) 8

S_v (kPa)	21.7	w_c (%)	25.50	Temp (°C)	4.8
1 Day Wet		w_p (%)	30.14	Ultimate state	
Metal confining band #2		w_l (%)	27.54		

Time (min)	Time (h)	Max. Disturbance (cm)		ξ (cm ³)	$\sqrt[3]{\xi}$ (cm)	ϵ_m (cm)	ϵ_{cl} (cm)
		Width	Length				
0	0.00	0.0	0.0	0.0	0.00	0.00	0.00
294	4.90	8.8	6.8	44.0	3.53	2.10	2.05
1417	23.62	10.4	10.0	90.0	4.48	3.15	3.05
3066	51.10	10.4	10.8	113.0	4.83	3.45	3.35
4301	71.68	10.8	11.2	127.0	5.03	3.80	3.60
5721	95.35	10.8	11.2	132.0	5.09	3.75	3.70
7514	125.23	10.8	11.2	132.0	5.09	3.80	3.80

Test No. 8/8.1/9.0/6
 Clay M390
 Clay Lot No. 34281348
 Test Date: 16-Mar-99
 Q (L/s) 0.45
 H (cm) 6.5
 d (mm) 8

S_v (kPa)	22.6	w_c (%)	25.81	Temp (°C)	4.8
New Block		w_p (%)	25.81	Ultimate state	
Metal confining band #2		w_l (%)	27.56		

Time (min)	Time (h)	Max. Disturbance (cm)		ξ (cm ³)	$\sqrt[3]{\xi}$ (cm)	ϵ_m (cm)	ϵ_{cl} (cm)
		Width	Length				
0	0.00	0.0	0.0	0.0	0.00	0.00	0.00
1679	27.98	6.7	6.8	27.0	3.00	2.05	2.05
3084	51.40	7.7	8.2	55.0	3.80	3.10	2.60
4494	74.90	7.8	8.6	56.0	3.83	3.10	2.75
6041	100.68	7.8	8.6	58.0	3.87	3.25	3.05
7573	126.22	7.8	8.6	64.0	4.00	3.25	3.05
8570	142.83	7.8	8.8	68.0	4.08	3.40	3.20
9961	166.02	7.9	8.9	70.0	4.12	3.80	3.70

Test No. 8/8.1/9.0/7
 Clay M390
 Clay Lot No. 334027107
 Test Date: 1-May-98
 Q (L/s) 0.45
 H (cm) 6.5
 d (mm) 8

S_v (kPa)	18.3	w_c (%)		Temp (°C)	15
1 day wet		w_o (%)		Large chunk removal	
Metal confining band #1		w_t (%)	28.5267		

Time (min)	Time (h)	Max. Disturbance (cm)		ξ (cm ³)	$\sqrt[3]{\xi}$ (cm)	ϵ_m (cm)
		Width	Length			
0	0.00	0.0	0.0	0.0	0.00	0.0
5	0.08	6.0	5.3	5.0	1.71	0.6
15	0.25	8.5	5.3	16.5	2.55	1.0
30	0.50	9.2	5.5	22.5	2.82	1.6
60	1.00	9.4	7.2	41.0	3.45	2.0
120	2.00	9.4	7.5	45.5	3.57	2.5
240	4.00	9.4	7.8	54.0	3.78	2.5
390	6.50	9.4	7.5	57.5	3.86	2.7
570	9.50	11.2	8.7	65.0	4.02	2.8
1220	20.33	11.5	8.7	76.0	4.24	2.8
1710	28.50	11.5	8.7	77.5	4.26	2.8

Test No. 8/8.1/9.0/8
 Clay M390
 Clay Lot No. 334027107
 Test Date: 28-May-98
 Q (L/s) 0.45
 H (cm) 6.5
 d (mm) 8

S_v (kPa)	19.3	w_c (%)	26.01	Temp (°C)	19
1 day wet		w_o (%)	29.1	Block destroyed	
Metal confining band #1		w_t (%)			
LL (%)	39.7	% clay	43		
PL (%)	18.0	Activity	0.5		
PI (%)	21.7				

Time (min)	Time (h)	Max. Disturbance (cm)		ξ (cm ³)	$\sqrt[3]{\xi}$ (cm)	ϵ_m (cm)	ϵ_{cl} (cm)
		Width	Length				
0	0.00	0.0	0.0	0.0	0.00	0.0	
5	0.08	4.5	5.0	6.0	1.82	0.9	
15	0.25	6.5	6.7	11.0	2.22	0.9	
30	0.50	7.1	6.7	16.0	2.52	1.2	0.70
60	1.00	7.1	7.0	18.5	2.64	1.2	0.80
127	2.12	7.1	7.1	19.0	2.67	1.3	1.00
240	4.00	7.1	7.1	20.0	2.71	1.3	1.00
360	6.00	7.1	7.2	20.5	2.74	1.3	1.30
588	9.80	7.1	7.2	25.5	2.94	1.4	1.40
1344	22.40	7.2	7.3	28.5	3.05	1.6	1.50

Test No.	8/8.1/9.9/1	S_v (kPa)	18.4	w_c (%)	26.85	Temp (°C)	16.9
Clay	M390	2 days wet		w_p (%)	29.15	Ultimate state	
Clay Lot No.	334027107	Metal confining band #1		w_r (%)	28.59		
Test Date:	7-Jun-98	LL (%)	38.5	% clay	43		
Q (L/s)	0.499	PL (%)	18.0	Activity	0.48		
H (cm)	6.5	PI (%)	20.5				
d (mm)	8						

Time (min)	Time (h)	Max. Disturbance (cm)		ξ (cm ³)	$\sqrt[3]{\xi}$ (cm)	ϵ_m (cm)	ϵ_{cl} (cm)
		Width	Length				
0	0.00	3.2	3.8	3.5	0.00	1.0	0.0
2	0.03	9.6	8.2	82.0	4.34	3.3	1.9
5	0.08	9.8	8.9	85.0	4.40	3.3	2.2
15	0.25	9.9	8.9	89.0	4.46	3.3	2.4
30	0.50	9.9	8.9	90.0	4.48	3.3	2.4
60	1.00	11.1	9.1	120.0	4.93	3.3	2.4
120	2.00	11.1	9.3	122.0	4.96	3.3	2.6
240	4.00	11.2	9.3	125.0	5.00	3.3	2.7
459	7.65	11.2	9.3	126.0	5.01	3.3	2.8
1296	21.60	11.2	9.3	133.0	5.10	3.3	3.1
1641	27.35	11.2	9.3	134.0	5.12	3.3	3.3
2726	45.43	11.2	9.3	145.0	5.25	3.7	3.5
4139	68.98	11.2	9.3	145.0	5.25	3.8	3.6
5605	93.42	11.2	9.3	149.0	5.30	3.8	3.7
7046	117.43	11.2	9.8	149.0	5.30	3.8	3.7

Test No.	8/8.1/9.9/2	S_v (kPa)	20.5	w_c (%)	26.95	Temp (°C)	15.8
Clay	M390	2 days wet		w_p (%)	29.185	Large chunk removal	
Clay Lot No.	334027107	Metal confining band #1		w_r (%)	28.07		
Test Date:	3-Jun-98	LL (%)	37.6	% clay	40		
Q (L/s)	0.499	PL (%)	18.3	Activity	0.48		
H (cm)	6.5	PI (%)	19.3				
d (mm)	8						

Time (min)	Time (h)	Max. Disturbance (cm)		ξ (cm ³)	$\sqrt[3]{\xi}$ (cm)	ϵ_m (cm)	ϵ_{cl} (cm)
		Width	Length				
0	0.00	0.0	0.0	0.0	0.00	0.0	0.0
5	0.08	9.4	8.7	26.0	2.96	1.4	0.7
15	0.25	10.1	9.1	43.0	3.50	2.0	1.2
30	0.50	10.8	9.1	49.5	3.67	2.3	1.4
60	1.00	10.8	9.1	54.0	3.78	2.5	1.7
120	2.00	10.8	9.1	58.0	3.87	2.7	1.9
240	4.00	10.8	9.1	63.0	3.98	2.7	2.2
367	6.12	10.8	9.1	66.0	4.04	2.7	2.3
1384	23.07	10.8	9.9	90.0	4.48	2.7	2.4

Notes: * From 5 to 15 min - too high of flow rate for 2 min Q=0.49 L/s (actually about 0.543 L/s)

Test No. 8/8.1/9.9/3
 Clay M390
 Clay Lot No. 34281348
 Test Date: 22-Oct-98
 Q (L/s) 0.5
 H (cm) 6.5
 d (mm) 8

S_v (kPa)	w_c (%)	25.19	Temp (°C)	10.7
1 day wet	w_p (%)	29.63	Block destroyed	
Metal confining band #2	w_l (%)			

* May have been bubbles in clay.

Time (min)	Time (h)	Max. Disturbance (cm)		ξ (cm ³)	$\sqrt[3]{\xi}$ (cm)	ϵ_m (cm)	ϵ_{cl} (cm)
		Width	Length				
0	0.00	0.0	0.0	0.0	0.00	0.00	0.00
2	0.03	5.2	4.8	6.5	1.87	1.75	0.30
5	0.08	6.7	5.3	13.0	2.35	1.10	0.95
15	0.25	6.9	6.0	18.5	2.64	1.65	1.05
30	0.50	7.1	6.3	25.0	2.92	2.00	1.85
60	1.00	7.5	7.7	34.0	3.24	2.95	1.95
163	2.72	7.4	10.0	65.0	4.02	3.95	3.15
307	5.12	8.3	10.2	81.0	4.33	4.65	4.55
552	9.20	9.5	10.4	100.0	4.64	5.00	4.95
1404	23.40	9.6	10.2	124.0	4.99	6.00	5.95

Test No. 8/8.1/9.9/4
 Clay M390
 Clay Lot No. 34281348
 Test Date: 28-Oct-98
 Q (L/s) 0.5
 H (cm) 6.5
 d (mm) 8

S_v (kPa)	w_c (%)	26.15	Temp (°C)	11.8
1 day wet	w_p (%)	29.5	Block Destroyed	
Metal confining band #2	w_l (%)			

* May have been bubbles in clay.

Time (min)	Time (h)	Max. Disturbance (cm)		ξ (cm ³)	$\sqrt[3]{\xi}$ (cm)	ϵ_m (cm)	ϵ_{cl} (cm)
		Width	Length				
0	0.00	0.0	0.0	0.0	0.00	0.00	0.00
2	0.03	6.8	8.1	13.0	2.35	0.80	0.60
5	0.08	6.8	8.1	35.0	3.27	2.20	1.40
15	0.25	7.1	8.2	43.0	3.50	2.25	2.25
30	0.50	7.1	8.3	45.0	3.56	2.40	2.40
60	1.00	7.2	8.3	48.0	3.63	2.45	2.45
150	2.50	7.4	8.4	55.0	3.80	2.50	2.50
372	6.20	7.6	9.1	67.0	4.06	2.75	2.75

Test No.	8/8.1/9.9/5	S_v (kPa)	19.9	w_c (%)	27.12	Temp (°C)	9.7
Clay	M390	1 day wet		w_p (%)	29.73	Slaking affected hole dimensions	
Clay Lot No.	34281348	Metal confining band #2		w_f (%)	27.6		
Test Date:	31-Oct-98	* Rapid surface erosion near beginning of test.					
Q (L/s)	0.5						
H (cm)	6.5						
d (mm)	8						

Time (min)	Time (h)	Max. Disturbance (cm)		ξ (cm ³)	$\sqrt[3]{\xi}$ (cm)	ϵ_m (cm)	ϵ_{cl} (cm)
		Width	Length				
0	0.00	0.0	0.0	0.0	0.00	0.00	0.00
2	0.03	3.1	3.1	2.0	1.26	0.50	0.45
5	0.08	7.3	6.7	26.0	2.96	1.65	0.85
15	0.25	8.1	6.3	33.0	3.21	1.75	1.25
30	0.50	8.4	6.7	35.0	3.27	1.80	1.55
60	1.00	9.1	7.1	40.0	3.42	1.85	1.65
134	2.23	9.2	7.1	45.0	3.56	1.95	1.80
393	6.55	8.8	8.7	60.0	3.91	2.35	2.35
1350	22.50	9.5	9.4	79.0	4.29	2.95	2.95
2920	48.67	9.5	9.9	n/a	n/a	3.40	3.40
4378	72.97	n/a	n/a	n/a	n/a	3.15	3.15

Test No.	8/8.1/9.9/6	S_v (kPa)		w_c (%)	26.24	Temp (°C)	7.9
Clay	M390	New block		w_p (%)	26.24	Block destroyed	
Clay Lot No.	34281348	Metal confining band #2		w_f (%)			
Test Date:	4-Nov-98	* Rapid surface erosion near beginning of test.					
Q (L/s)	0.5						
H (cm)	6.5						
d (mm)	8						

Time (min)	Time (h)	Max. Disturbance (cm)		ξ (cm ³)	$\sqrt[3]{\xi}$ (cm)	ϵ_m (cm)	ϵ_{cl} (cm)
		Width	Length				
0	0.00	0.0	0.0	0.0	0.00	0.00	0.00
2	0.03	0.9	0.5	0.5	0.79	0.45	0.25
5	0.08	2.6	3.6	1.2	1.06	0.60	0.55
15	0.25	3.6	4.6	5.5	1.77	0.85	0.80
30	0.50	4.2	5.2	7.0	1.91	1.00	0.95
60	1.00	4.4	5.2	10.0	2.15	1.25	1.25
120	2.00	5.2	5.4	16.0	2.52	1.55	1.55
252	4.20	5.2	6.0	20.0	2.71	1.80	1.80

Test No.	8/8.1/9.9/7	S_v (kPa)	w_c (%)	Temp (°C)	7.9
Clay	M390	1 day wet	w_p (%)	30.08	Block destroyed
Clay Lot No.	34281348	Metal confining band #2	w_r (%)		
Test Date:	7-Nov-98	* Rapid surface erosion near beginning of test.			
Q (L/s)	0.5				
H (cm)	6.5				
d (mm)	8				

Time (min)	Time (h)	Max. Disturbance (cm)		ξ (cm ³)	$\sqrt[3]{\xi}$ (cm)	ϵ_m (cm)	ϵ_{cl} (cm)
		Width	Length				
0	0.00	0.0	0.0	0.0	0.00	0.00	0.00
5	0.08	8.9	11.4	63.0	3.98	1.75	1.25

Test No.	8/14.5/9.0/1	S_v (kPa)	17.5	w_c (%)	26.06	Temp (°C)	20.1
Clay	M390	2 days wet		w_p (%)	30.05	Ultimate state	
Clay Lot No.	34281348	Metal confining band #1		w_r (%)	27.8325		
Test Date:	10-Jul-98	LL (%)	33.7	% clay	40		
Q (L/s)	0.45	PL (%)	18.1	Activity	0.39		
H (cm)	11.6	PI (%)	15.6				
d (mm)	8						

Time (min)	Time (h)	Max. Disturbance (cm)		ξ (cm ³)	$\sqrt[3]{\xi}$ (cm)	ϵ_m (cm)	ϵ_{cl} (cm)
		Width	Length				
0	0.00	0.0	0.0	0.0	0.00	0.00	0.00
5	0.08	0.0	0.0	0.0	0.00	0.00	0.00
15	0.25	0.0	0.0	0.0	0.00	0.00	0.00
60	1.00	4.3	4.5	1.5	1.14	0.40	0.30
120	2.00	6.1	5.2	4.5	1.65	0.60	0.30
333	5.55	7.2	5.6	8.5	2.04	0.70	0.45
803	13.38	7.2	6.5	15.0	2.47	0.80	0.60
1883	31.38	8.1	7.3	20.5	2.74	0.80	0.75
3031	50.52	8.3	7.4	21.0	2.76	0.80	0.75
4288	71.47	8.4	7.6	24.0	2.88	0.80	0.75
5848	97.47	8.7	7.6	24.5	2.90	0.90	0.80

Test No.	8/14.5/9.0/2	S_v (kPa)	14.8	w_c (%)	26.51	Temp (°C)	20.1
Clay	M390	3 days wet		w_p (%)	29.005	Ultimate state	
Clay Lot No.	34281348	Metal confining band #1		w_r (%)	27.8		
Test Date:	17-Jul-98	LL (%)	35.9	% clay	40		
Q (L/s)	0.45	PL (%)	18.1	Activity	0.45		
H (cm)	11.6	PI (%)	17.8				
d (mm)	8						

Time (min)	Time (h)	Max. Disturbance (cm)		ξ (cm ³)	$\sqrt[3]{\xi}$ (cm)	ϵ_m (cm)	ϵ_{cl} (cm)
		Width	Length				
0	0.00	4.4	5.5	9.0	2.08	1.1	0.0
15	0.25	4.8	5.7	11.0	2.22	1.1	0.3
45	0.75	7.4	5.8	16.0	2.52	1.2	0.4
187	3.12	8.7	6.2	19.0	2.67	1.2	0.6
1257	20.95	9.7	7.8	26.0	2.96	1.3	0.9
1838	30.63	9.7	8.5	35.0	3.27	1.3	1.0
3069	51.15	10.2	8.7	42.0	3.48	1.3	1.2
4239	70.65	10.2	8.7	43.0	3.50	1.4	1.2

Test No.	8/14.5/9.0/3	S_v (kPa)	18.1	w_c (%)	26.16	Temp (°C)	22.2
Clay	M390	1 day wet		w_p (%)	29.42	Ultimate state	
Clay Lot No.	34281348	Metal confining band #2		w_r (%)	27.36		
Test Date:	25-Jul-98						
Q (L/s)	0.45						
H (cm)	11.6						
d (mm)	8						

Time (min)	Time (h)	Max. Disturbance (cm)		ξ (cm ³)	$\sqrt[3]{\xi}$ (cm)	ϵ_m (cm)	ϵ_{cl} (cm)
		Width	Length				
0	0.00	0.0	0.0	0.0	0.00	0.00	0.00
15	0.25	6.2	4.4	5.5	1.77	0.50	0.35
25	0.42	8.6	7.3	20.5	2.74	1.30	0.60
66	1.10	10.5	7.3	24.5	2.90	1.30	0.75
120	2.00	10.5	7.3	31.0	3.14	1.40	0.90
317	5.28	10.5	7.3	35.0	3.27	1.70	1.00
1333	22.22	10.5	8.0	44.0	3.53	1.70	1.30
2721	45.35	11.0	1.5	123.0	4.97	3.30	1.30
4037	67.28	11.5	11.5	127.0	5.03	3.30	1.30
4743	79.05	11.5	11.5	127.0	5.03	3.30	1.40
6329	105.48	13.1	11.5	128.0	5.04	3.30	1.40

Test No.	8/14.5/9.0/4	S_v (kPa)	19.6	w_c (%)		Temp (°C)	22.2
Clay	M390	3 days wet		w_o (%)	29.52	Ultimate state	
Clay Lot No.	34281348	Metal confining band #2		w_f (%)	27.17		
Test Date:	3-Aug-98						
Q (L/s)	0.45						
H (cm)	11.6						
d (mm)	8						

Time (min)	Time (h)	Max. Disturbance (cm)		ξ (cm ³)	$\sqrt[3]{\xi}$ (cm)	ϵ_m (cm)	ϵ_{cl} (cm)
		Width	Length				
0	0.00	0.0	0.0	0.0	0.00	0.00	0.00
20	0.33	6.1	5.5	2.0	1.26	0.50	0.25
40	0.67	6.7	5.6	3.5	1.52	0.60	0.45
60	1.00	7.0	5.7	6.5	1.87	0.70	0.50
120	2.00	7.5	6.2	7.0	1.91	0.70	0.50
240	4.00	7.7	6.4	8.5	2.04	0.70	0.50
520	8.67	7.7	6.4	10.0	2.15	0.75	0.65
1270	21.17	9.4	7.5	14.5	2.44	0.80	0.70
1867	31.12	9.4	7.5	17.0	2.57	0.80	0.70
2917	48.62	9.7	8.2	17.5	2.60	0.80	0.75
4114	68.57	9.7	8.2	18.0	2.62	0.80	0.75

Test No.	8/14.5/9.0/5	S_v (kPa)		w_c (%)	26.72	Temp (°C)	4.4
Clay	M390	3 days wet		w_o (%)		Ultimate state	
Clay Lot No.	34281348	Metal confining band #2		w_f (%)	27.95		
Test Date:	13-Nov-98	* Flake erosion at beginning of test					
Q (L/s)	0.45	*There was slaking off of a piece of clay resulting in a sudden increase in volume.					
H (cm)	11.6						
d (mm)	8						

Time (min)	Time (h)	Max. Disturbance (cm)		ξ (cm ³)	$\sqrt[3]{\xi}$ (cm)	ϵ_m (cm)	ϵ_{cl} (cm)
		Width	Length				
0	0.00	0.0	0.0	0.0	0.00	0.00	0.00
1410	23.50	5.1	4.3	3.0	1.44	0.50	0.35
2970	49.50	5.8	5.2	5.0	1.71	0.50	0.40
4208	70.13	6.1	5.2	7.0	1.91	0.55	0.50
5769	96.15	7.8	5.9	13.5	2.38	0.70	0.60

Test No.	8/14.5/9.0/6	S_v (kPa)		w_c (%)	26.04	Temp (°C)	20.5
Clay	M390	2 days wet		w_o (%)	30.215	Block cracked	
Clay Lot No.	34281348	Metal confining band #1		w_f (%)			
Test Date:	8-Jul-98						
Q (L/s)	0.45						
H (cm)	11.6						
d (mm)	8						

Time (min)	Time (h)	Max. Disturbance (cm)		ξ (cm ³)	$\sqrt[3]{\xi}$ (cm)	ϵ_m (cm)	ϵ_{cl} (cm)
		Width	Length				
0	0.00	0.0	0.0	0.0	0.00	0.0	0.0
5	0.00	0.0	0.0	0.0	0.00	0.0	0.0
15	0.25	6.5	4.9	24.0	2.88	2.1	0.3
30	0.50	7.3	5.1	27.0	3.00	2.1	1.1

Test No. 8/14.5/9.0/7
 Clay M390
 Clay Lot No. 34281348
 Test Date: 7-Aug-98
 Q (L/s) 0.45
 H (cm) 11.6
 d (mm) 8

S_v (kPa)	w_c (%)	26.69	Temp (°C)	23.6
1 day wet	w_p (%)	29.53	Sample cracked	
Metal confining band #2	w_r (%)			

Time (min)	Time (h)	Max. Disturbance (cm)		ξ (cm ³)	$\sqrt[3]{\xi}$ (cm)	ϵ_m (cm)	ϵ_{cl} (cm)
		Width	Length				
0	0.00	0.0	0.0	0.0	0.00	0.00	0.00
2	0.03	9.2	7.2	25.0	2.92	1.70	0.50
5	0.08	9.2	7.7	28.0	3.04	2.25	0.80
15	0.25	9.3	7.8	33.0	3.21	2.30	1.25
30	0.50	9.3	7.8	35.0	3.27	2.30	1.50
60	1.00	9.3	7.8	37.5	3.35	2.30	1.85
120	2.00	9.3	8.5	42.0	3.48	2.30	2.30
302	5.03	9.3	8.5	50.0	3.68	2.70	2.45
487	8.12	9.5	8.5	53.0	3.76	2.80	2.80

Test No. 8/14.5/9.9/1
 Clay M390
 Clay Lot No. 34281348
 Test Date: 21-Nov-98
 Q (L/s) 0.5
 H (cm) 11.6
 d (mm) 8

S_v (kPa)	23.2	w_c (%)		Temp (°C)	3.5
1 day wet		w_p (%)	29.93	Ultimate state at 70 h	
Metal confining band #2		w_r (%)	27.27		

*Last time interval - had large chunk removed which was likely due to slaking

Time (min)	Time (h)	Max. Disturbance (cm)		ξ (cm ³)	$\sqrt[3]{\xi}$ (cm)	ϵ_m (cm)	ϵ_{cl} (cm)
		Width	Length				
0	0.00	0.0	0.0	0.0	0.00	0.00	0.00
290	4.83	5.6	5.2	6.0	1.82	0.50	0.40
521	8.68	6.3	5.7	8.5	2.04	0.65	0.60
1528	25.47	7.6	6.2	18.0	2.62	1.05	0.95
3047	50.78	8.1	8.2	25.5	2.94	1.25	1.15
4255	70.92	8.1	8.2	33.0	3.21	1.50	1.35
4557	75.95	9.7	10.2	92.0	4.51	3.10	1.65

Test No. 8/14.5/9.9/2
 Clay M390
 Clay Lot No. 34281348
 Test Date: 18-Nov-98
 Q (L/s) 0.5
 H (cm) 11.6
 d (mm) 8

S_v (kPa)		w_c (%)	25.87	Temp (°C)	3.7
New block		w_p (%)		Block destroyed	
Metal confining band #2		w_r (%)			

* Flake erosion at beginning of test.

Time (min)	Time (h)	Max. Disturbance (cm)		ξ (cm ³)	$\sqrt[3]{\xi}$ (cm)	ϵ_m (cm)	ϵ_{cl} (cm)
		Width	Length				
0	0.00	0.0	0.0	0.0	0.00	0.00	0.00
355	5.92	4.9	3.6	1.5	1.14	0.35	0.30
1444	24.07	8.1	7.1	26.0	2.96	1.30	1.00

Test No.	8/14.5/10.9/1	S_v (kPa)	21.7	w_c (%)	26.43	Temp (°C)	6.4
Clay	M390	1 day wet		w_p (%)	28.59	Ultimate state	
Clay Lot No.	34281348	Metal confining band #2		w_l (%)	27.56		
Test Date:	3-Dec-98						
Q (L/s)	0.55						
H (cm)	11.6						
d (mm)	8						

Time (min)	Time (h)	Max. Disturbance (cm)		ξ (cm ³)	$\sqrt[3]{\xi}$ (cm)	ϵ_m (cm)	ϵ_{cl} (cm)
		Width	Length				
0	0.00	0.0	0.0	0.0	0.00	0.00	0.00
27	0.45	6.4	8.0	19.0	2.67	1.40	0.40
95	1.58	7.5	8.1	25.0	2.92	1.50	0.75
138	2.30	7.8	9.0	30.0	3.11	1.50	1.00
515	8.58	8.5	9.7	43.0	3.50	1.60	1.30
1353	22.55	8.7	9.7	55.0	3.80	1.75	1.55
3108	51.80	10.2	10.1	70.0	4.12	1.85	1.80
4277	71.28	11.2	10.7	98.0	4.61	2.55	2.15
5572	92.87	11.7	10.9	99.0	4.63	2.55	2.25

Test No.	8/14.5/11.9/1	S_v (kPa)		w_c (%)	26.39	Temp (°C)	4.1
Clay	M390	1 day wet		w_p (%)	29.95	Block destroyed	
Clay Lot No.	34281348	Metal confining band #2		w_l (%)			
Test Date:	8-Dec-98						
Q (L/s)	0.55						
H (cm)	11.6						
d (mm)	8						

Time (min)	Time (h)	Max. Disturbance (cm)		ξ (cm ³)	$\sqrt[3]{\xi}$ (cm)	ϵ_m (cm)	ϵ_{cl} (cm)
		Width	Length				
0	0.00	0.0	0.0	0.0	0.00	0.00	0.00
15	0.25	7.2	4.6	3.5	1.52	0.50	0.40
99	1.65	8.2	6.6	17.5	2.60	1.00	0.95
230	3.83	8.2	7.8	29.0	3.07	1.35	1.20
422	7.03	8.6	8.2	43.0	3.50	1.55	1.50
1420	23.67	8.8	9.4	64.0	4.00	2.05	2.00
3213	53.55	10.8	11.9	110.0	4.79	2.95	2.65
4453	74.22	11.1	13.7	136.0	5.14	3.50	3.10

Test No. 4/10.0/9.9/1
 Clay M390
 Clay Lot No. 34281348
 Test Date: 8-Feb-99
 Q (L/s) 0.125
 H (cm) 4.0
 d (mm) 4

S_v (kPa)	w_c (%)	25.51	Temp (°C)	4.8
New Block	w_p (%)	25.51	Ultimate state	
Metal confining band #2	w_r (%)			

Time (min)	Time (h)	Max. Disturbance (cm)		ξ (cm ³)	$\sqrt[3]{\xi}$ (cm)	ϵ_m (cm)	ϵ_{cl} (cm)
		Width	Length				
0	0.00	0.0	0.0	0.0	0.00	0.00	0.00
1362	22.70	2.6	2.9	1.5	1.14	0.40	0.30
3005	50.08	3.4	3.6	2.5	1.36	0.55	0.45
4305	71.75	3.9	4.0	4.0	1.59	0.75	0.65
5693	94.88	4.2	4.4	6.0	1.82	0.90	0.80
7353	122.55	4.4	4.5	7.0	1.91	0.90	0.80
8510	141.83	4.8	4.5	8.0	2.00	0.95	0.85
10265	171.08	4.8	4.5	8.0	2.00	1.00	0.90

Test No. 4/10.0/11.9/1
 Clay M390
 Clay Lot No. 34281348
 Test Date: 15-Jan-99
 Q (L/s) 0.15
 H (cm) 4.0
 d (mm) 4

S_v (kPa)	23.3	w_c (%)	25.52	Temp (°C)	4.3
New Block		w_p (%)	25.52	Ultimate state	
Metal confining band #2		w_r (%)	27.28		

* Flake erosion at beginning of test

Time (min)	Time (h)	Max. Disturbance (cm)		ξ (cm ³)	$\sqrt[3]{\xi}$ (cm)	ϵ_m (cm)	ϵ_{cl} (cm)
		Width	Length				
0	0.00	0.0	0.0	0.0	0.00	0.00	0.00
1642	27.37	3.9	2.9	2.5	1.36	0.55	0.45
2953	49.22	4.2	4.2	4.0	1.59	0.95	0.80
4290	71.50	4.6	4.2	8.0	2.00	1.10	1.00
7083	118.05	4.6	4.3	12.0	2.29	1.35	1.15
8697	144.95	5.6	6.8	22.5	2.82	1.45	1.30

Test No. 4/10.0/11.9/2
 Clay M390
 Clay Lot No. 34281348
 Test Date: 19-Feb-99
 Q (L/s) 0.15
 H (cm) 4.0
 d (mm) 4

S_v (kPa)	n/a	w_c (%)	25.47	Temp (°C)	4.7
New Block		w_p (%)	25.47	Taken as ultimate state	
Metal confining band #2		w_r (%)	n/a		

Time (min)	Time (h)	Max. Disturbance (cm)		ξ (cm ³)	$\sqrt[3]{\xi}$ (cm)	ϵ_m (cm)	ϵ_{cl} (cm)
		Width	Length				
0	0.00	0.0	0.0	0.0	0.00	0.00	0.00
1668	27.80	2.1	2.3	1.0	1.00	0.30	0.25
3081	51.35	2.7	2.9	1.5	1.14	0.55	0.45
4224	70.40	3.4	3.1	2.0	1.26	0.65	0.60
5659	94.32	3.5	3.1	2.5	1.36	0.70	0.65
7361	122.68	3.7	3.2	4.0	1.59	0.90	0.70
8645	144.08	3.7	3.5	5.0	1.71	0.95	0.90

Test No. 4/10.0/13.9/1
 Clay M390
 Clay Lot No. 34281348
 Test Date: 5-Jul-99
 Q (L/s) 0.175
 H (cm) 4.0
 d (mm) 4

S_v (kPa)	28.4	w_c (%)	25.49	Temp (°C)	14.9
New Block		w_p (%)	25.49	Ultimate state	
Metal confining band #2		w_r (%)	26.94		

* volume may have been influenced by slaking

Time (min)	Time (h)	Max. Disturbance (cm)		ξ (cm ³)	$\sqrt[3]{\xi}$ (cm)	ϵ_m (cm)	ϵ_{cl} (cm)
		Width	Length				
0	0.00	0.0	0.0	0.0	0.00	0.00	0.00
1320	22.00	8.2	6.7	21.5	2.78	2.30	2.10
2542	42.37	9.6	6.9	54.0	3.78	2.90	2.75
4169	69.48	10.7	7.1	61.0	3.94	3.55	3.40
5455	90.92	11.4	7.6	69.0	4.10	3.85	3.40

Test No. 4/10.0/15.9/1
 Clay M390
 Clay Lot No. 34281348
 Test Date: 22-Jan-99
 Q (L/s) 0.2
 H (cm) 4.0
 d (mm) 4

S_v (kPa)	25.6	w_c (%)	25.05	Temp (°C)	5.4
New Block		w_p (%)	25.05	Ultimate state	
Metal confining band #2		w_r (%)	27.35		

Time (min)	Time (h)	Max. Disturbance (cm)		ξ (cm ³)	$\sqrt[3]{\xi}$ (cm)	ϵ_m (cm)	ϵ_{cl} (cm)
		Width	Length				
0	0.00	0.0	0.0	0.0	0.00	0.00	0.00
30	0.50	2.6	2.7	3.5	1.52	1.05	1.05
118	1.97	3.2	3.7	6.5	1.87	1.45	1.45
251	4.18	3.6	4.0	8.0	2.00	1.70	1.70
1562	26.03	3.6	4.0	14.5	2.44	2.10	2.10
2936	48.93	3.6	4.0	17.5	2.60	2.45	2.45
4225	70.42	3.6	4.1	19.0	2.67	2.65	2.65
5587	93.12	3.7	4.1	19.5	2.69	2.65	2.65

Test No. 4/10.0/15.9/2
 Clay M390
 Clay Lot No. 34281348
 Test Date: 9-Jul-99
 Q (L/s) 0.2
 H (cm) 4.0
 d (mm) 4

S_v (kPa)		w_c (%)	25.46	Temp (°C)	16.8
New Block		w_p (%)	25.46	Ultimate state	
Metal confining band #2		w_r (%)			

Time (min)	Time (h)	Max. Disturbance (cm)		ξ (cm ³)	$\sqrt[3]{\xi}$ (cm)	ϵ_m (cm)	ϵ_{cl} (cm)
		Width	Length				
0	0.00	0.0	0.0	0.0	0.00	0.00	0.00
1632	27.20	4.0	4.3	18.0	2.62	2.20	2.20
2994	49.90	4.1	4.6	19.5	2.69	2.55	2.75
4223	70.38	8.8	11.1	81.0	4.33	2.75	2.45
5759	95.98	8.9	11.3	84.0	4.38	3.00	2.80
6964	116.07	9.2	11.4	85.0	4.40	3.05	2.90

Test No.	4/10.0/17.9/1	S_v (kPa)	w_c (%)	Temp (°C)	15.7
Clay	M390	New Block	w_p (%)	Ultimate state	
Clay Lot No.	34281348	Metal confining band #2	w_l (%)		
Test Date:	14-Jul-99				
Q (L/s)	0.225				
H (cm)	4.0				
d (mm)	4				

Time (min)	Time (h)	Max. Disturbance (cm)		ξ (cm ³)	$\sqrt[3]{\xi}$ (cm)	ϵ_m (cm)	ϵ_{cl} (cm)
		Width	Length				
0	0.00	0.0	0.0	0.0	0.00	0.00	0.00
1507	25.12	3.1	4.0	18.0	2.62	3.00	3.00
3000	50.00	3.4	3.9	19.0	2.67	3.20	3.20
4438	73.97	3.4	3.9	19.5	2.69	3.35	3.35
5933	98.88	3.4	4.1	19.5	2.69	3.35	3.35
7433	123.88	3.4	4.1	20.0	2.71	3.50	3.50

Test No.	4/10.0/19.9/1	S_v (kPa)	w_c (%)	25.26	Temp (°C)	4.9
Clay	M390	New Block	w_p (%)	25.26	Assumed end state -	
Clay Lot No.	34281348	Metal confining band #2	w_l (%)		block destroyed	
Test Date:	28-Jan-99					
Q (L/s)	0.25					
H (cm)	4.0					
d (mm)	4					

Time (min)	Time (h)	Max. Disturbance (cm)		ξ (cm ³)	$\sqrt[3]{\xi}$ (cm)	ϵ_m (cm)	ϵ_{cl} (cm)
		Width	Length				
0	0.00	0.0	0.0	0.0	0.00	0.00	0.00
44	0.73	3.4	3.6	5.5	1.77	1.30	1.30
149	2.48	3.7	3.8	8.0	2.00	1.65	1.65
1393	23.22	4.4	4.8	27.0	3.00	2.95	2.95
2852	47.53	5.8	6.0	44.0	3.53	3.70	3.70
4576	76.27	7.4	6.2	55.0	3.80	4.15	4.15
5778	96.30	7.5	6.1	57.0	3.85	4.35	4.35

Test No.	4/16.3/15.9/1	S_v (kPa)	24.1	w_c (%)	25.79	Temp (°C)	11
Clay	M390	New Block		w_p (%)	25.79	Ultimate state	
Clay Lot No.	34281348	Metal confining band #2		w_l (%)	28.08		
Test Date:	12-May-99						
Q (L/s)	0.2						
H (cm)	6.5						
d (mm)	4						

Time (min)	Time (h)	Max. Disturbance (cm)		ξ (cm ³)	$\sqrt[3]{\xi}$ (cm)	ϵ_m (cm)	ϵ_{cl} (cm)
		Width	Length				
0	0.00	0.0	0.0	0.0	0.00	0.00	0.00
1618	26.97	5.5	6.0	11.5	2.26	1.05	1.05
2861	47.68	6.4	7.0	20.0	2.71	1.35	1.35
4477	74.62	7.5	8.3	24.5	2.90	1.45	1.45
6079	101.32	7.5	8.5	30.0	3.11	1.45	1.45
7123	118.72	7.5	8.7	34.0	3.24	1.50	1.45

Test No. 4/16.3/19.9/1
 Clay M390
 Clay Lot No. 34281348
 Test Date: 25-May-99
 Q (L/s) 0.25
 H (cm) 6.5
 d (mm) 4

S_v (kPa)	22.9	w_c (%)	25.57	Temp (°C)	15.9
New Block		w_p (%)	25.57	Ultimate state	
Metal confining band #2		w_t (%)	27.53		

Time (min)	Time (h)	Max. Disturbance (cm)		ξ (cm ³)	$\sqrt[3]{\xi}$ (cm)	ϵ_m (cm)	ϵ_{cl} (cm)
		Width	Length				
0	0.00	0.0	0.0	0.0	0.00	0.00	0.00
345	5.75	5.7	5.5	15.5	2.49	1.55	1.55
1480	24.67	7.6	7.8	43.0	3.50	2.80	2.80
3070	51.17	8.3	7.6	68.0	4.08	3.25	3.25
4435	73.92	9.3	7.7	84.0	4.38	3.50	3.50
6233	103.88	9.3	8.2	90.0	4.48	3.60	3.60

Test No. 4/29.0/19.9/1
 Clay M390
 Clay Lot No. 34281348
 Test Date: 8-Jun-99
 Q (L/s) 0.25
 H (cm) 11.6
 d (mm) 4

S_v (kPa)		w_c (%)	25.56	Temp (°C)	15.9
New Block		w_p (%)	25.56	Large chunk removal	
Metal confining band #2		w_t (%)		due to slaking	

* Flake erosion at beginning of test.

Time (min)	Time (h)	Max. Disturbance (cm)		ξ (cm ³)	$\sqrt[3]{\xi}$ (cm)	ϵ_m (cm)	ϵ_{cl} (cm)
		Width	Length				
0	0.00	0.0	0.0	0.0	0.00	0.00	0.00
2630	43.83	4.9	8.4	34.0	3.24	2.15	0.05
5476	91.27	5.7	8.4	34.0	3.24	2.15	0.20
7347	122.45	8.5	8.0	35.0	3.27	2.15	0.25

Test No. 4/29.0/21.9/1
 Clay M390
 Clay Lot No. 34281348
 Test Date: 30-Jun-99
 Q (L/s) 0.275
 H (cm) 11.6
 d (mm) 4

S_v (kPa)	25.2	w_c (%)	26.01	Temp (°C)	14.9
New Block		w_p (%)	26.01	Ultimate state	
Metal confining band #2		w_t (%)	27.39		

Time (min)	Time (h)	Max. Disturbance (cm)		ξ (cm ³)	$\sqrt[3]{\xi}$ (cm)	ϵ_m (cm)	ϵ_{cl} (cm)
		Width	Length				
0	0.00	0.0	0.0	0.0	0.00	0.00	0.00
1440	24.00	5.8	5.9	5.0	1.71	0.45	0.35
2638	43.97	6.8	7.4	10.5	2.19	0.65	0.55
4457	74.28	7.7	8.4	17.0	2.57	0.80	0.75
5439	90.65	7.6	8.4	20.0	2.71	0.80	0.75

Test No.	4/29.0/25.9/1	S_v (kPa)	22.9	w_c (%)	25.39	Temp (°C)	18.4
Clay	M390	New Block		w_p (%)	25.39	Ultimate state	
Clay Lot No.	34281348	Metal confining band #2		w_l (%)	27.29		
Test Date:	14-Jun-99						
Q (L/s)	0.325						
H (cm)	11.6						
d (mm)	4						

Time (min)	Time (h)	Max. Disturbance (cm)		ξ (cm ³)	$\sqrt[3]{\xi}$ (cm)	ϵ_m (cm)	ϵ_{cl} (cm)
		Width	Length				
0	0.00	0.0	0.0	0.0	0.00	0.00	0.00
1445	24.08	7.4	9.0	29.0	3.07	1.45	0.85
2875	47.92	10.4	9.8	50.0	3.68	2.25	1.85
4195	69.92	11.9	9.9	69.0	4.10	2.50	1.85
5540	92.33	12.9	10.1	92.0	4.51	2.80	2.45
7327	122.12	12.9	11.1	110.0	4.79	2.95	2.45
8482	141.37	13.4	10.9	112.0	4.82	2.95	2.40

Test No.	4/29.0/25.9/2	S_v (kPa)		w_c (%)	25.37	Temp (°C)	15.4
Clay	M390	New Block		w_p (%)	25.37	Ultimate state	
Clay Lot No.	34281348	Metal confining band #2		w_l (%)			
Test Date:	25-Jun-99						
Q (L/s)	0.325						
H (cm)	11.6						
d (mm)	4						

Time (min)	Time (h)	Max. Disturbance (cm)		ξ (cm ³)	$\sqrt[3]{\xi}$ (cm)	ϵ_m (cm)	ϵ_{cl} (cm)
		Width	Length				
0	0.00	0.0	0.0	0.0	0.00	0.00	0.00
1420	23.67	8.5	8.7	34.0	3.24	1.35	1.25
3199	53.32	10.2	10.1	64.0	4.00	1.70	1.65
4251	70.85	10.6	11.1	73.0	4.18	1.95	1.75
5923	98.72	10.6	11.1	86.0	4.41	2.15	2.05
6863	114.38	10.6	10.9	88.0	4.45	2.25	2.05

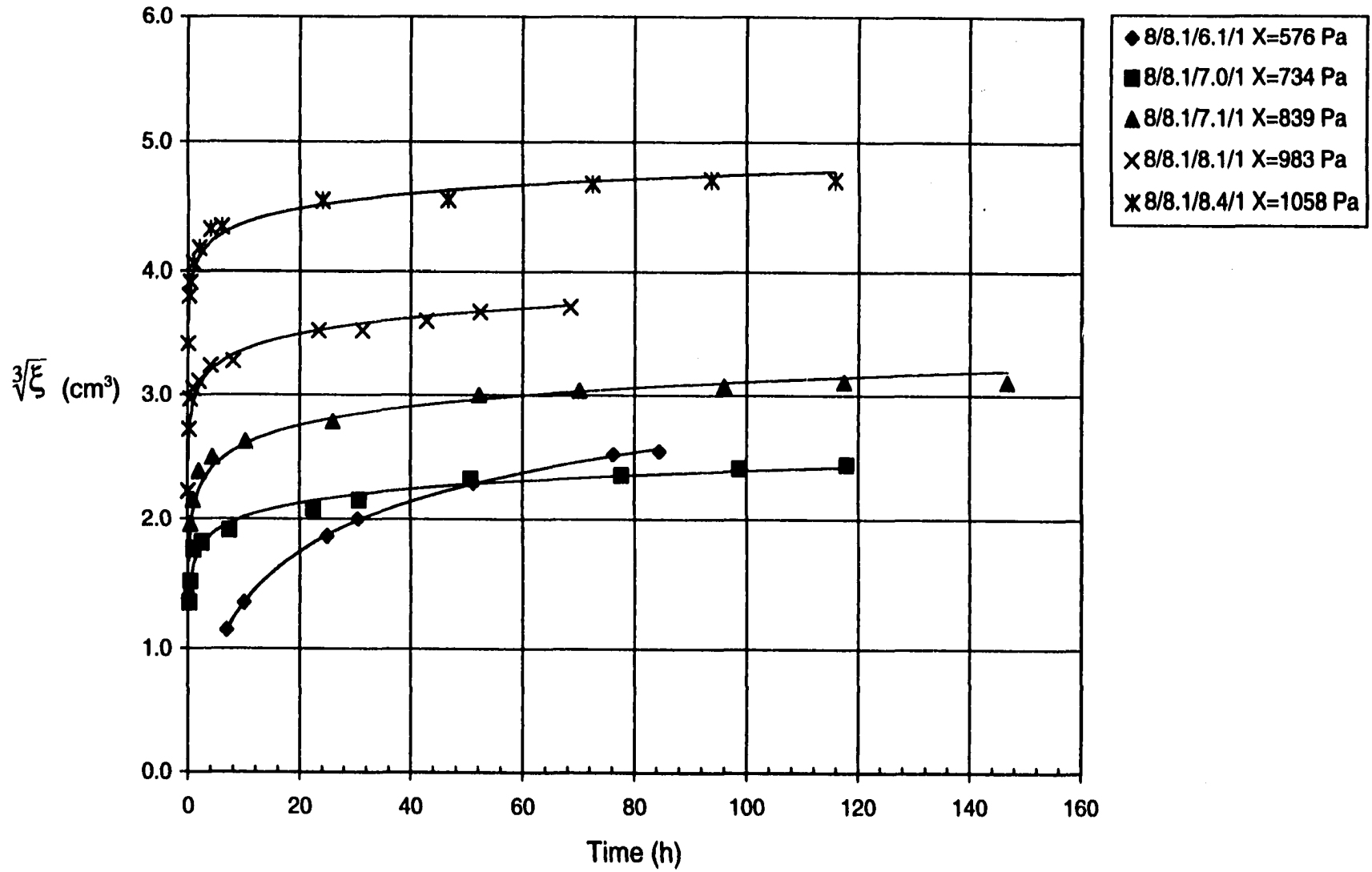


Fig. B-1: Growth of the Scour Hole Volume for tests 8/8.1/6.1/1, 8/8.1/7.0/1, 8/8.1/8.1/1, and 8/8.1/8.4/1.

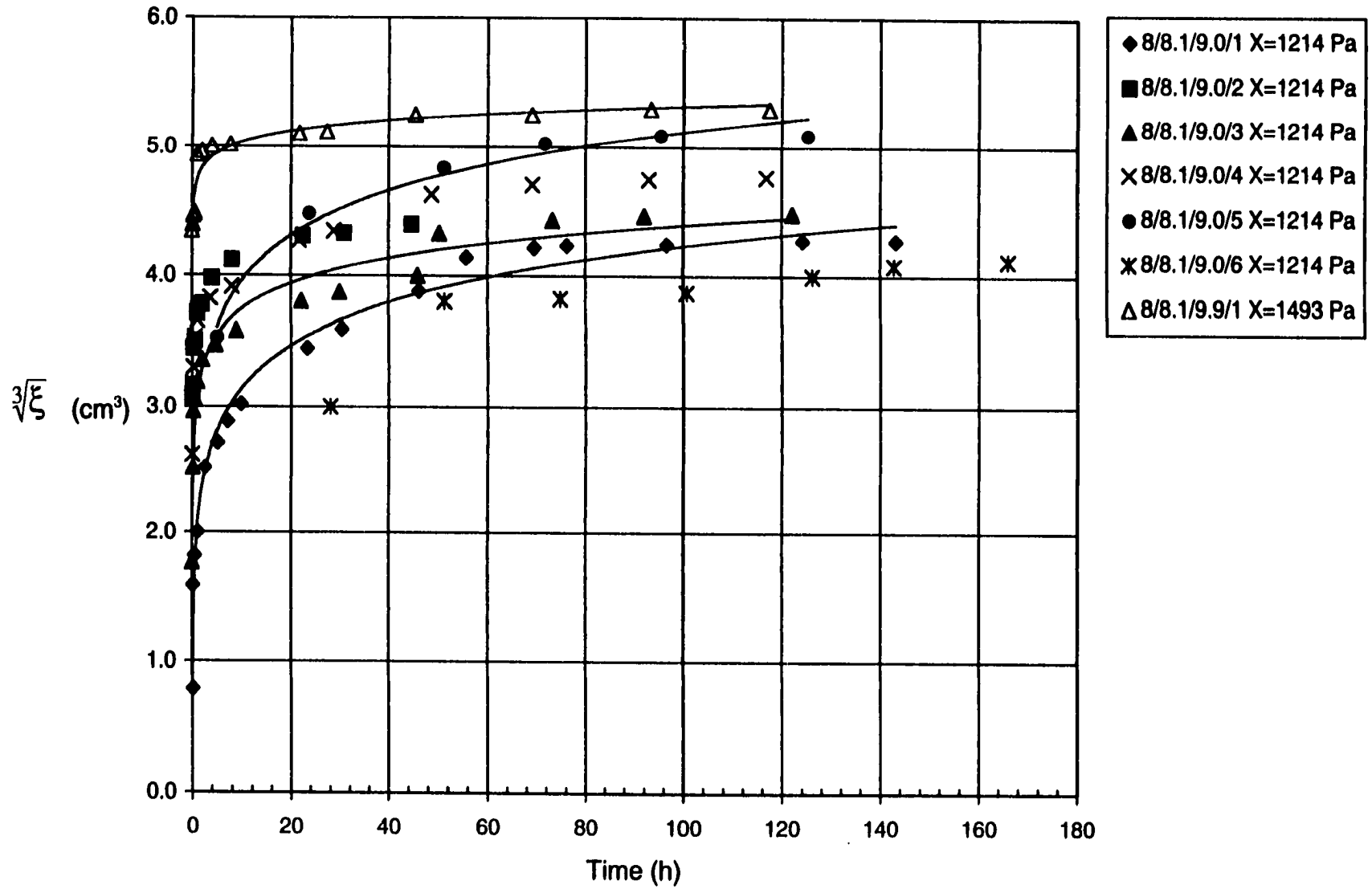


Fig. B-2: Growth of the scour hole volume for tests 8/8.1/9.0/1-6 and 8/8.1/9.9/1.

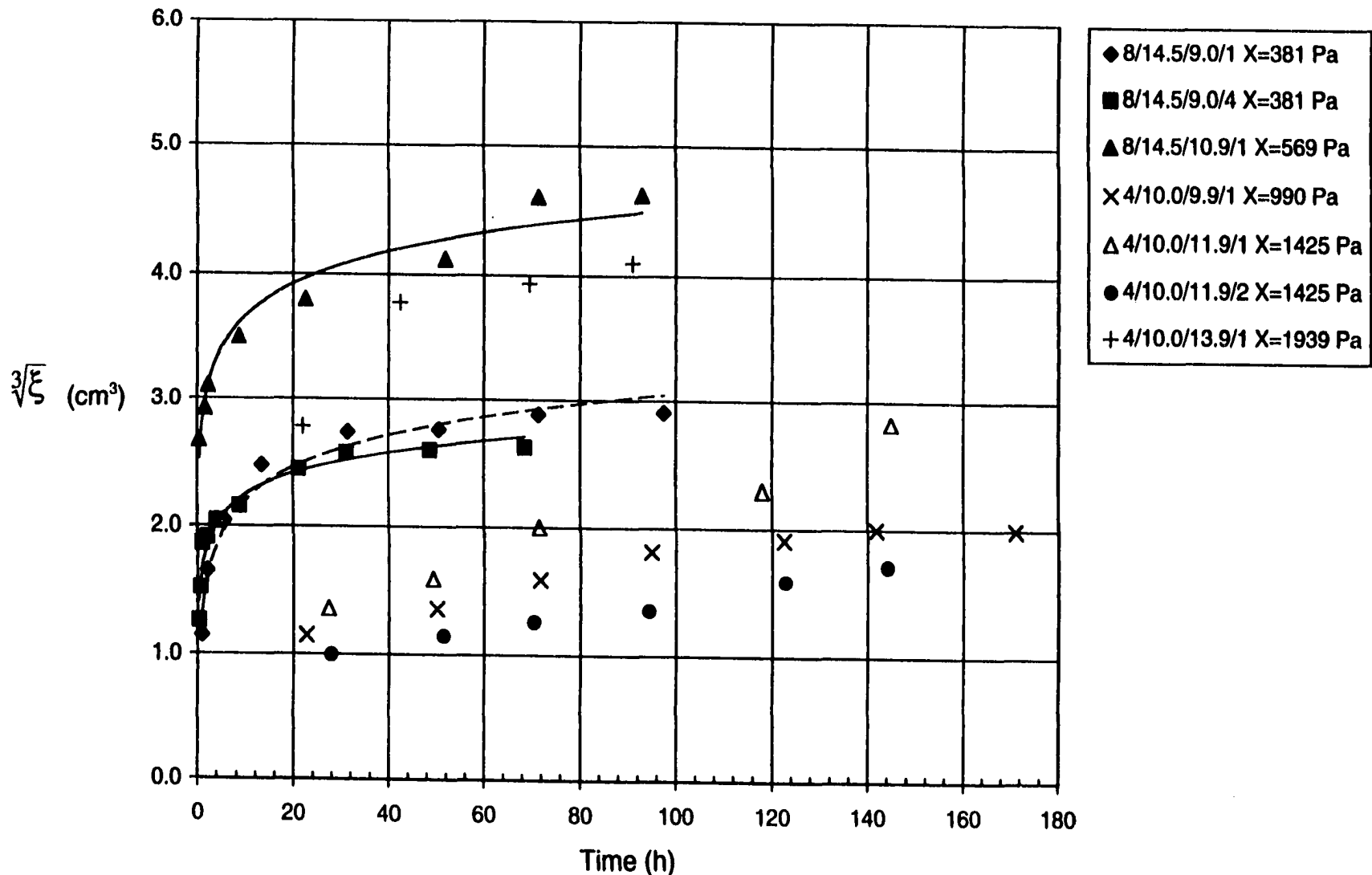


Fig. B-3: Growth of the scour hole volume for Test No. 8/14.5/9.0/1, 8.0/14.5/9.0/4, 8.0/14.5/10.9/1, 4/10.0/9.9/1, 4/10.0/11.9/1-2, and 4/10.0/13.9/1.

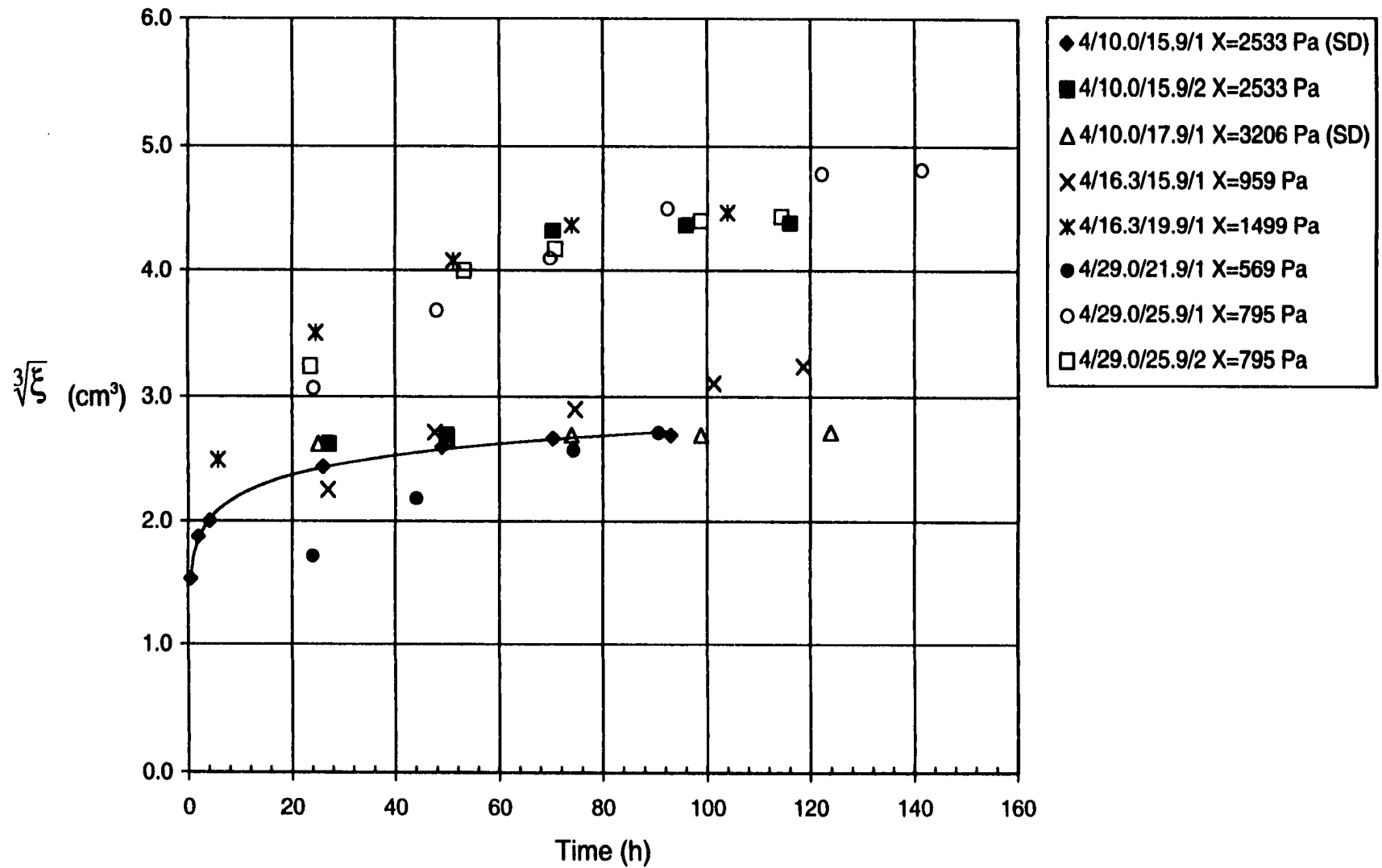


Fig. B-4: Growth of the scour hole volume for Test No. 4/10.0/15.9/1-2, 4/10.0/17.9/1, 4/16.3/15.9/1, 4/16.3/19.9/1, 4/29.0/21.9/1, 4/29.0/25.9/1, and 4/29.0/25.9/2.

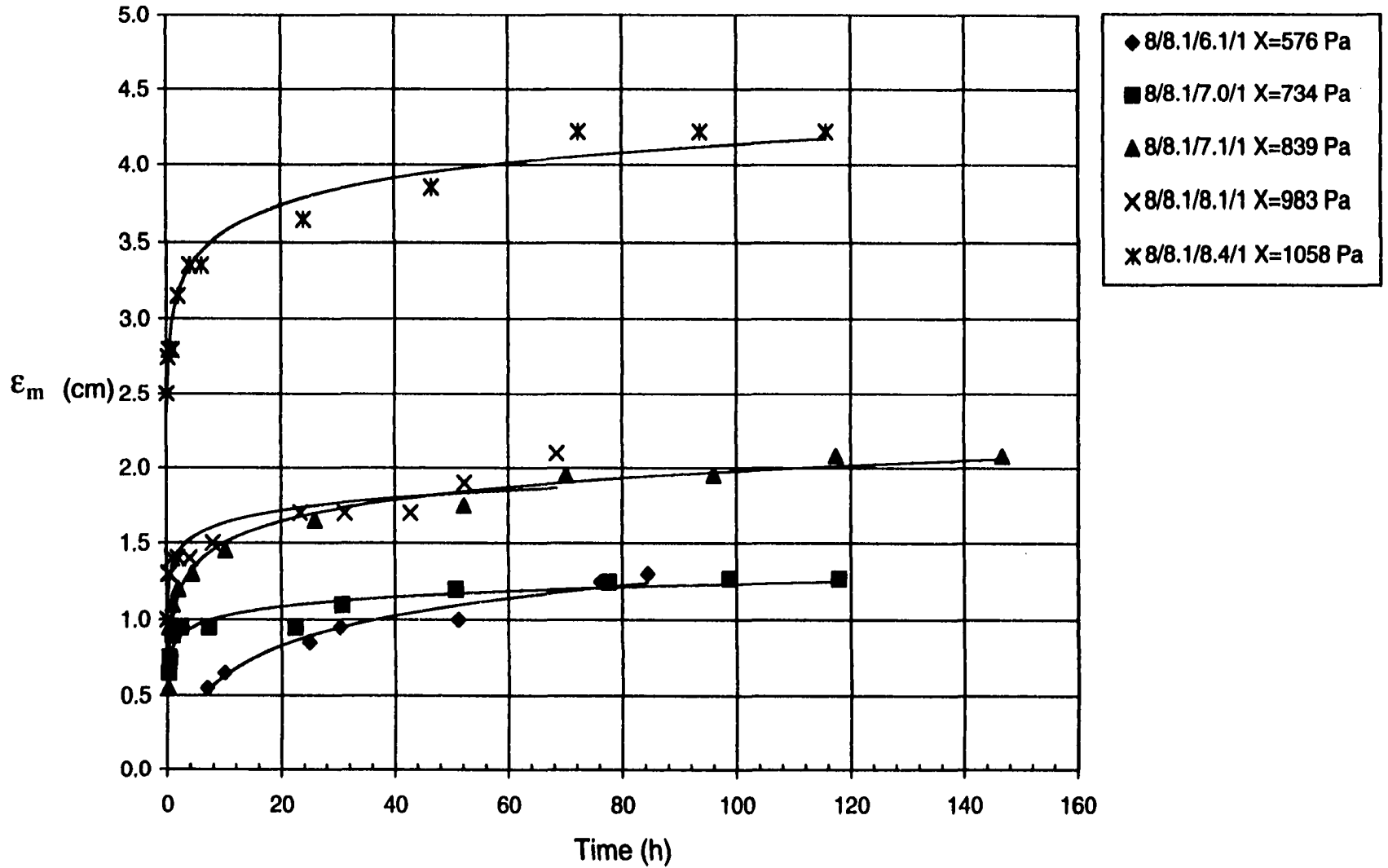


Fig. B-5: Growth of the maximum scour depth for tests 8/8.1/6.1/1, 8/8.1/7.0/1, 8/8.1/7.1/1, 8/8.1/8.1/1, and 8/8.1/8.4/1.

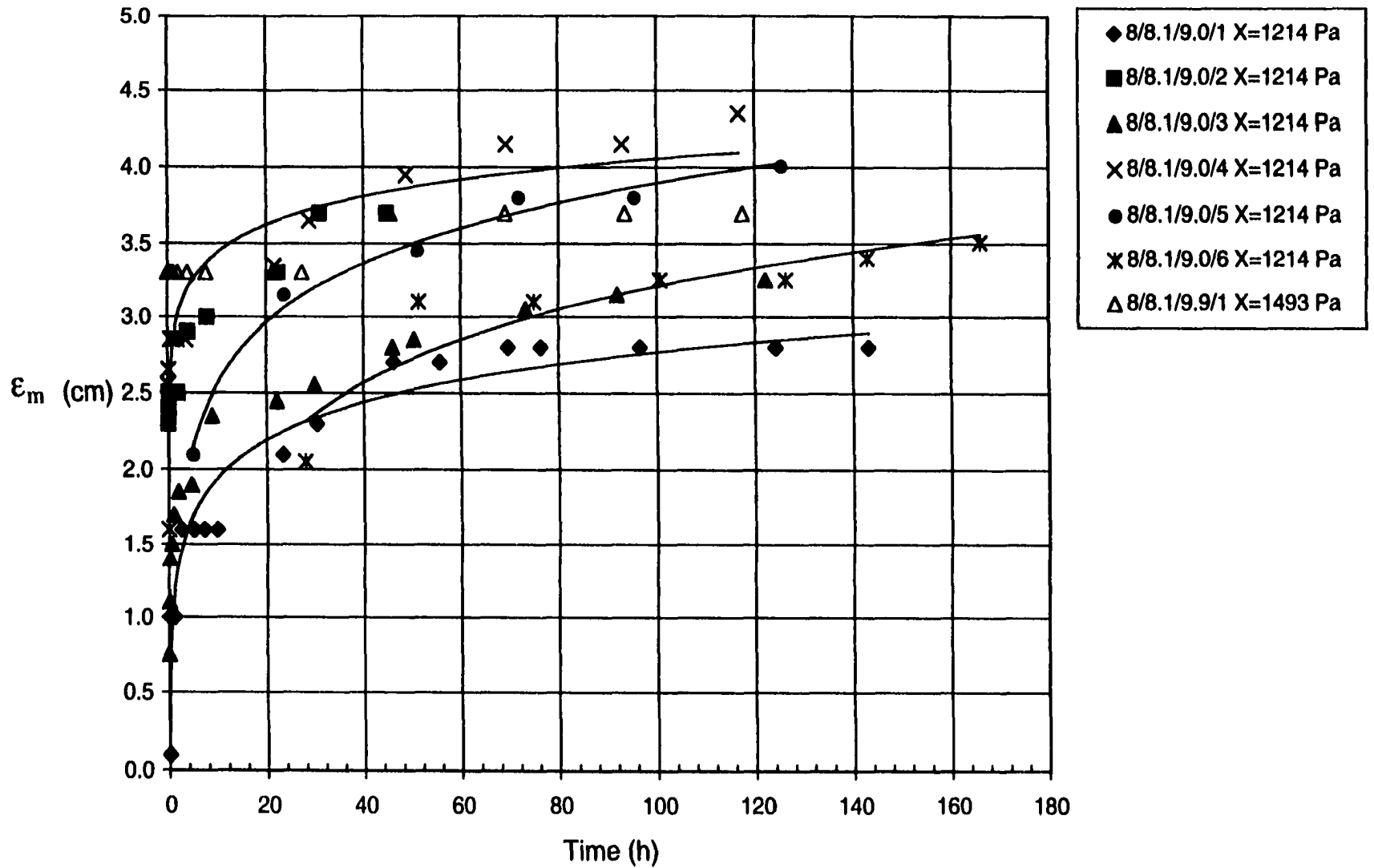


Fig. B-6: Growth of the maximum scour depth for tests 8/8.1/9.0/1-6 and 8/8.1/9.9/1.

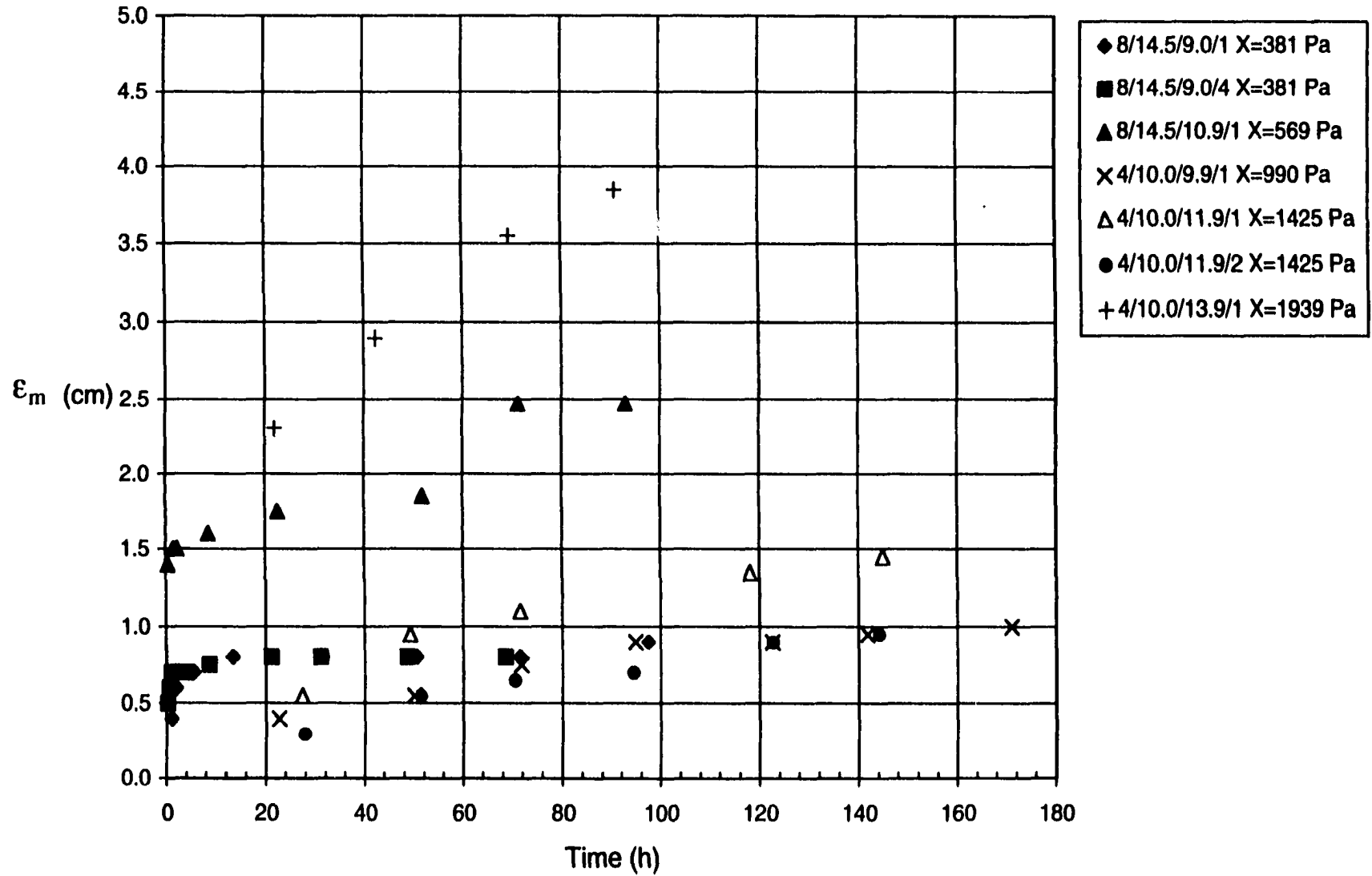


Fig. B-7: Growth of the maximum scour depth for Test No. 8/14.5/9.0/1, 8/14.5/9.0/4, 8/14.5/10.9/1, 4/10.0/9.9/1, 4/10.0/11.9/1-2, and 4/10.0/13.9/1.

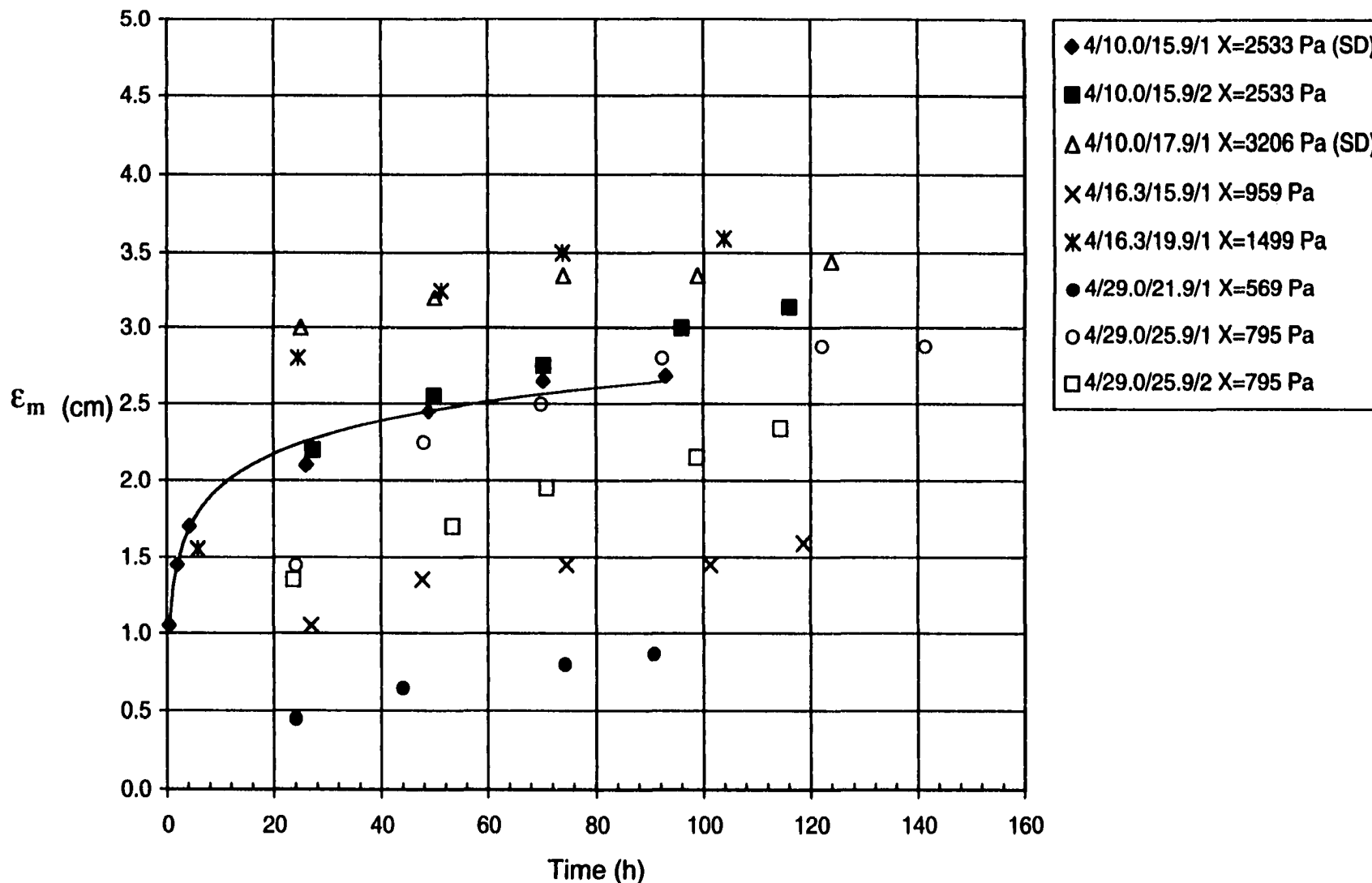


Fig. B-8: Growth of the maximum scour depth for Test No. 4/10.0/15.9/1-2, 4/10.0/17.9/1, 4/16.3/15.9/1, 4/16.3/19.9/1, 4/29.0/21.9/1, 4/29.0/25.9/1, and 4/29.0/25.9/2.

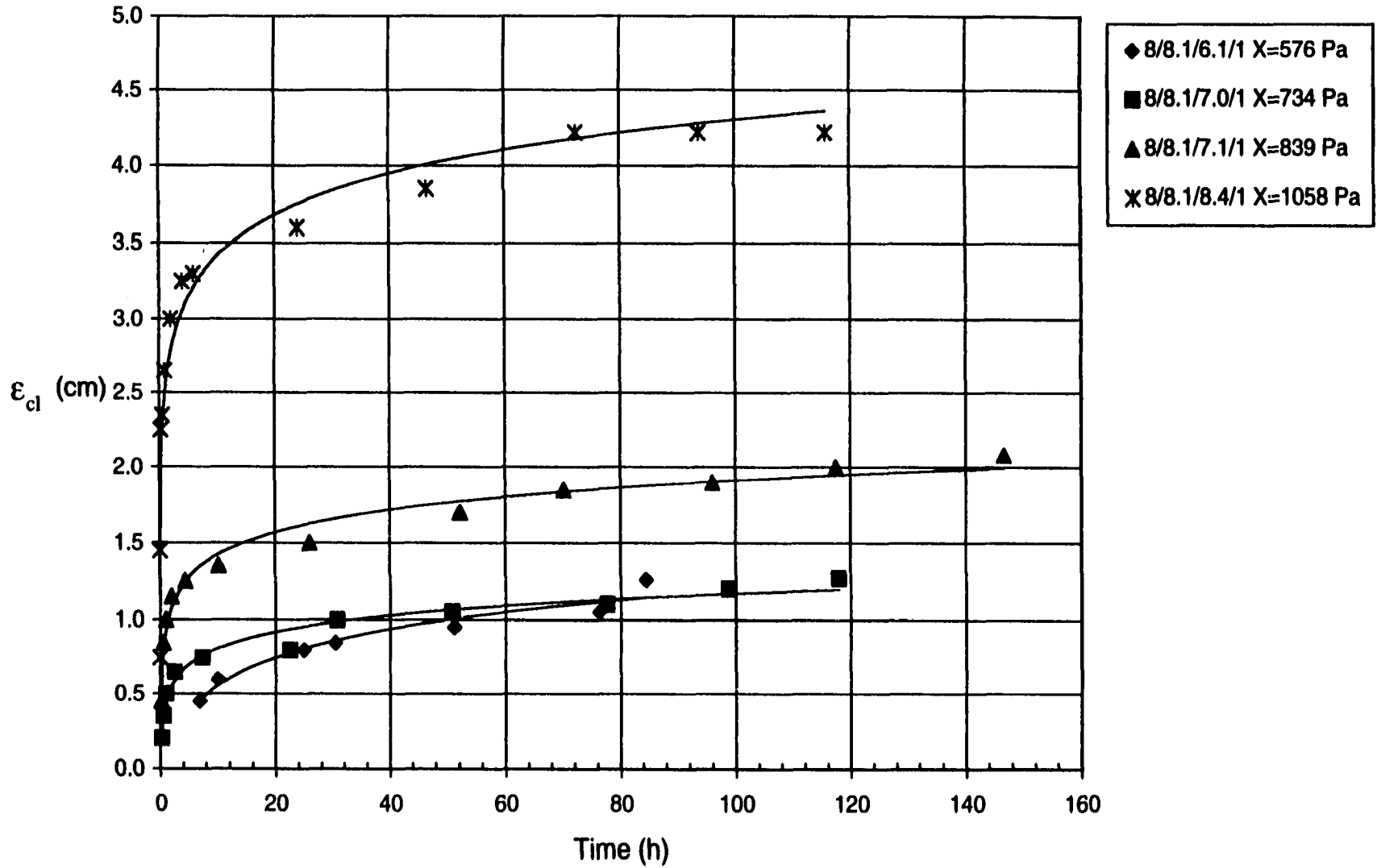


Fig. B-9: Growth of the centreline scour depth for tests 8/8.1/6.1/1, 8/8.1/7.0/1, 8/8.1/7.1/1, and 8/8.1/8.4/1.

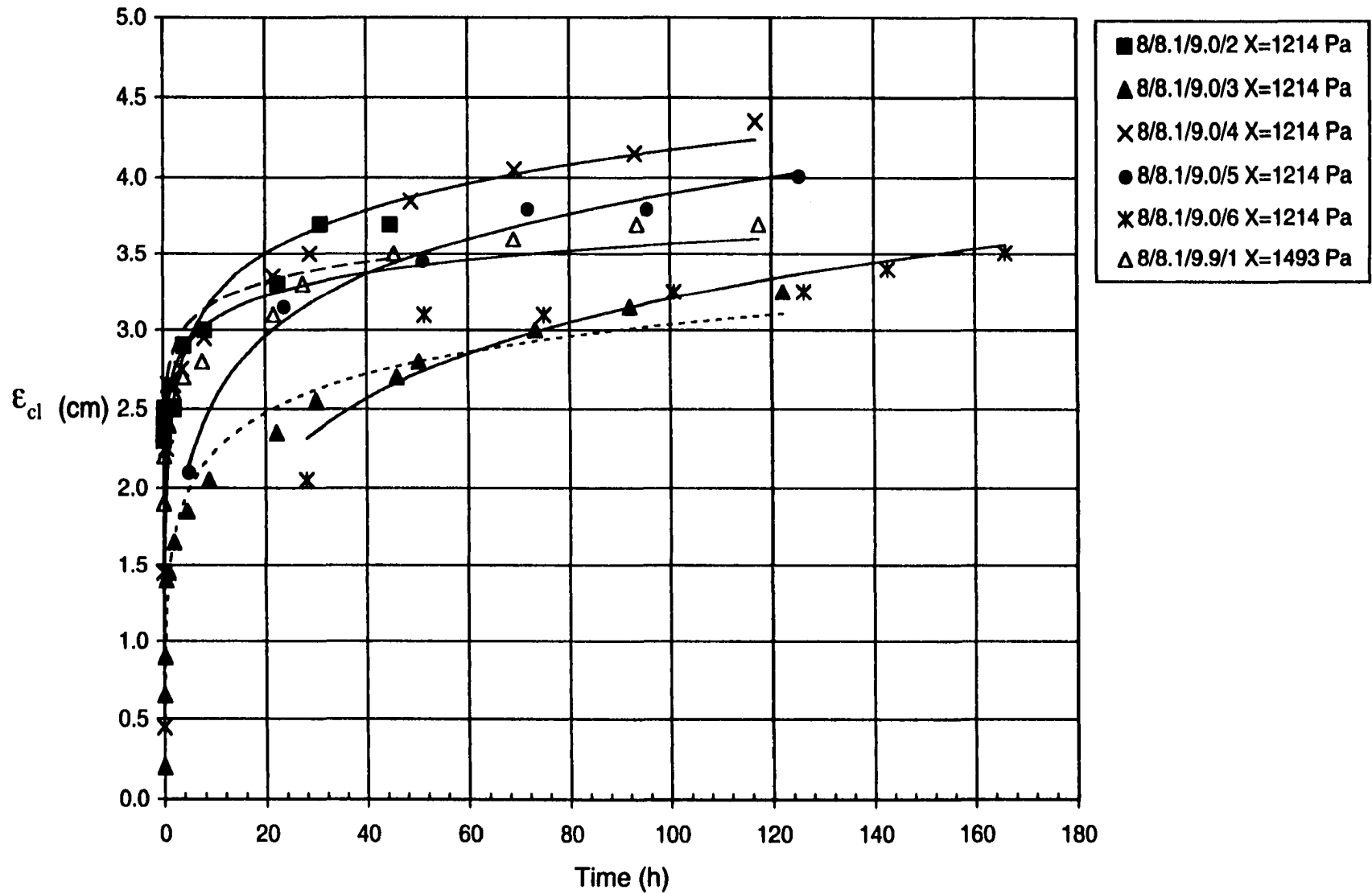


Fig. B-10: Growth of the centreline scour depth for tests 8/8.1/9.0/1-6 and 8/8.1/9.9/1.

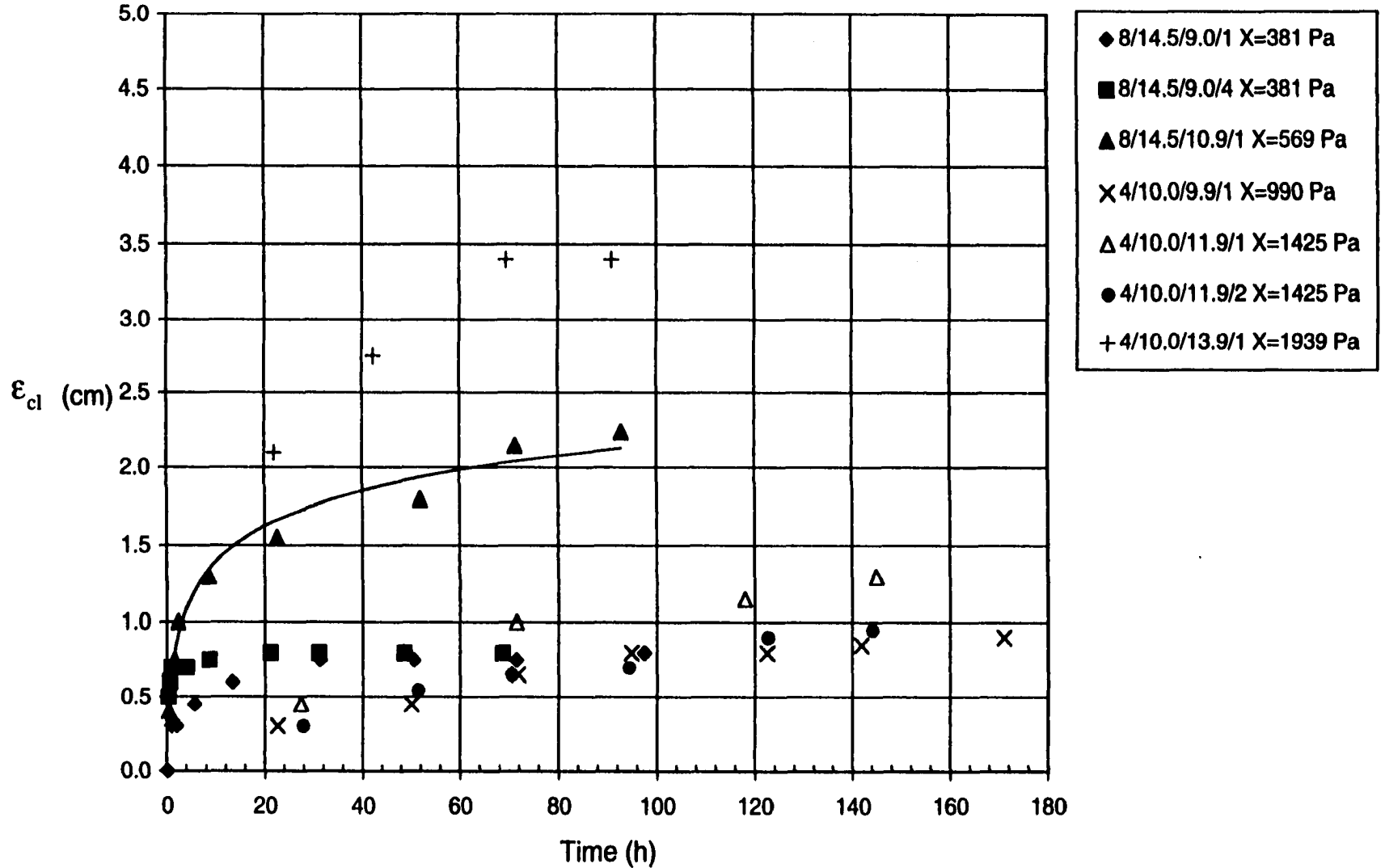


Fig. B-11: Growth of the centreline scour depth for Test No. 8/14.5/9.0/1, 8.0/14.5/9.0/4, 8.0/14.5/10.9/1, 4/10.0/9.9/1, 4/10.0/11.9/1-2, and 4/10.0/13.9/1.

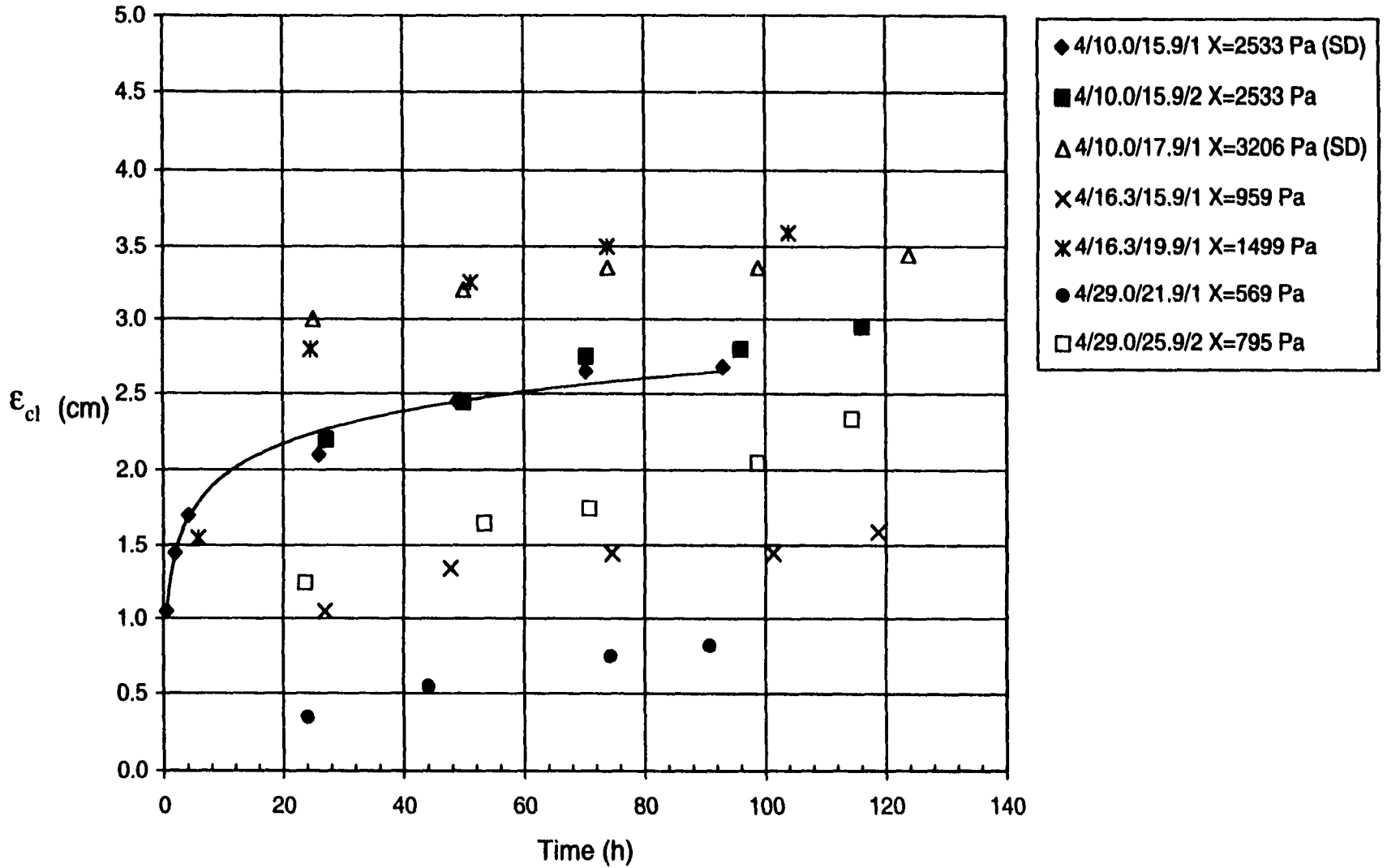


Fig. B-12: Growth of the centreline scour depth for Test No. 4/10.0/15.9/1-2, 4/10.0/17.9/1, 4/16.3/15.9/1, 4/16.3/19.9/1, 4/29.0/21.9/1, 4/29.0/25.9/1, and 4/29.0/25.9/2.

Appendix C: Scour Hole Profile Data for Impinging Jet Tests

Test No.	8/8.1/7.0/1		Test Variables		
Clay	M390		Q (L/s)	H (cm)	d (mm)
Clay Lot No.	34281348		0.35	6.5	8
Test Date:	4-Sep-98				
Lengthwise:	centreline	maximum	Widthwise:	$\epsilon_{max} = \epsilon_{ct}$	
$r_{0\rightarrow}$ (cm)	3.0	3	$r_{0\rightarrow}$ (cm)	4.0	
$r_{0\leftarrow}$ (cm)	3.5	3.5	$r_{0\leftarrow}$ (cm)	3.0	
$\bar{r}_{0\rightarrow}$ (cm)	3.25	3.25	$\bar{r}_{0\leftarrow}$ (cm)	3.5	
ϵ_{\rightarrow} (cm)	1.13	1.27	ϵ_{\leftarrow} (cm)	1.27	
$\epsilon_{\rightarrow}/2$ (cm)	0.565	0.635	$\epsilon_{\leftarrow}/2$ (cm)	0.635	
b_{\rightarrow} (cm)	1.728	1.625	b_{\rightarrow} (cm)	2.020	
b_{\leftarrow} (cm)	2.136	2.036	b_{\leftarrow} (cm)	2.130	
\bar{b}_{\rightarrow} (cm)	1.932	1.831	\bar{b}_{\leftarrow} (cm)	2.075	

Lengthwise section (4 Sep 98)			Widthwise section (4 Sep 98)		
r (cm)	Depth Reading (cm)	ϵ_{\rightarrow} (cm)	r (cm)	Depth Reading (cm)	ϵ_{\leftarrow} (cm)
3.5	79.48	-0.02	4.0	79.52	0.00
3.0	79.48	-0.02	3.5	79.43	-0.09
2.5	79.45	-0.05	3.0	79.31	-0.21
2.0	79.12	-0.38	2.5	79.18	-0.34
1.5	76.78	-0.72	2.0	78.87	-0.65
1.0	78.46	-1.04	1.5	78.60	-0.92
0.5	78.32	-1.18	1.0	78.36	-1.16
0.0	78.37	-1.13	0.5	78.25	-1.27
-0.5	78.23	-1.27	0.0	78.25	-1.27
-1.0	78.34	-1.16	-0.5	78.37	-1.15
-1.5	78.53	-0.97	-1.0	78.47	-1.05
-2.0	78.84	-0.66	-1.5	78.65	-0.87
-2.5	79.19	-0.31	-2.0	78.74	-0.78
-3.0	79.42	-0.08	-2.5	79.31	-0.21
-3.5	79.49	-0.01	-3.0	79.49	-0.03
-4.0	79.50	0.00	-3.5	79.52	0.00

Test No.	8/8.1/7.1/1		Test Variables		
Clay	M390		Q (L/s)	H (cm)	d (mm)
Clay Lot No.	34281348		0.374	6.5	8
Test Date:	11-Sep-98				
Lengthwise:	$\epsilon_{max} = \epsilon_{ct}$		Widthwise:	$\epsilon_{max} = \epsilon_{ct}$	
$r_{0\rightarrow}$ (cm)	3.5		$r_{0\rightarrow}$ (cm)	3.5	
$r_{0\leftarrow}$ (cm)	4.0		$r_{0\leftarrow}$ (cm)	4.0	
$\bar{r}_{0\rightarrow}$ (cm)	3.75		$\bar{r}_{0\leftarrow}$ (cm)	3.75	
ϵ_{\rightarrow} (cm)	-2.08		ϵ_{\leftarrow} (cm)	2.02	
$\epsilon_{\rightarrow}/2$ (cm)	-1.04		$\epsilon_{\leftarrow}/2$ (cm)	1.01	
b_{\rightarrow} (cm)	2.011		b_{\rightarrow} (cm)	1.740	
b_{\leftarrow} (cm)	2.138		b_{\leftarrow} (cm)	2.180	
\bar{b}_{\rightarrow} (cm)	2.075		\bar{b}_{\leftarrow} (cm)	1.960	

Lengthwise section (11 Sep 98)				Widthwise section (11 Sep 98)			
r (cm)	Depth Reading (cm)	Int. Surface(cm)	ϵ_{-} (cm)	r (cm)	Depth Reading (cm)	Int. Surface(cm)	ϵ_{-} (cm)
4.5	85.80	85.83	-0.03	4.5	85.79	85.79	0.00
4.0	85.83	85.83	0.00	4.0	85.79	85.79	0.00
3.5	85.80	85.83	-0.03	3.5	85.78	85.79	-0.01
3.0	85.73	85.84	-0.11	3.0	85.65	85.80	-0.15
2.5	85.46	85.84	-0.38	2.5	85.41	85.80	-0.39
2.0	84.80	85.85	-1.05	2.0	85.05	85.80	-0.75
1.5	84.36	85.85	-1.49	1.5	84.56	85.81	-1.25
1.0	84.06	85.85	-1.79	1.0	84.05	85.81	-1.76
0.5	83.81	85.86	-2.05	0.5	83.85	85.81	-1.96
0.0	83.78	85.86	-2.08	0.0	83.79	85.82	-2.02
-0.5	83.89	85.87	-1.98	-0.5	83.93	85.82	-1.89
-1.0	84.09	85.87	-1.78	-1.0	84.03	85.82	-1.79
-1.5	84.33	85.88	-1.55	-1.5	84.30	85.82	-1.52
-2.0	84.73	85.88	-1.15	-2.0	84.64	85.83	-1.19
-2.5	85.05	85.88	-0.83	-2.5	85.14	85.83	-0.69
-3.0	85.31	85.89	-0.58	-3.0	85.44	85.83	-0.39
-3.5	85.60	85.89	-0.29	-3.5	85.63	85.84	-0.21
-4.0	85.87	85.90	-0.03	-4.0	85.84	85.84	0.00
-4.5	85.90	85.90	0.00	-4.5	85.87	85.84	0.03
-5.0	85.90	85.90	0.00				

Test No.	8/8.1/8.1/1	Test Variables		
Clay	M390	Q (L/s)	H (cm)	d (mm)
Clay Lot No.	34281348	0.42	6.5	8
Test Date:	20-Sep-98			
Lengthwise:	$\epsilon_{m-} = \epsilon_{cl-}$	Widthwise:	$\epsilon_{m-} = \epsilon_{cl-}$	
r_{m-} (cm)	4.6	r_{m-} (cm)	6.1	
r_{c-} (cm)	3.3	r_{c-} (cm)	3.0	
\bar{r}_{m-} (cm)	3.95	\bar{r}_{c-} (cm)	4.6	
ϵ_{-} (cm)	-4.22	ϵ_{-} (cm)	-4.22	
$\epsilon_{-}/2$ (cm)	-2.11	$\epsilon_{-}/2$ (cm)	-2.11	
b_{m-} (cm)	2.766	b_{m-} (cm)	3.629	
b_{c-} (cm)	2.305	b_{c-} (cm)	2.186	
\bar{b}_{m-} (cm)	2.536	\bar{b}_{c-} (cm)	2.908	

Lengthwise section (20 Sep 98)				Widthwise section (20 Sep 98)			
r (cm)	Depth Reading (cm)	Int. Surface(cm)	ϵ_{-} (cm)	r (cm)	Depth Reading (cm)	Int. Surface(cm)	ϵ_{-} (cm)
4.6	85.84	85.84	0.00	6.1	85.78	85.78	0.00
4.5	85.75	85.84	-0.09	6.0	85.77	85.78	-0.01
4.0	85.43	85.85	-0.42	5.5	85.45	85.79	-0.34
3.5	85.18	85.85	-0.67	5.0	85.13	85.79	-0.66
3.0	84.47	85.85	-1.38	4.5	84.64	85.80	-1.16
2.5	82.92	85.86	-2.94	4.0	84.12	85.80	-1.68
2.0	82.39	85.86	-3.47	3.5	83.55	85.81	-2.26
1.5	82.03	85.87	-3.84	3.0	83.08	85.81	-2.73
1.0	81.82	85.87	-4.05	2.5	82.73	85.82	-3.09
0.5	81.66	85.88	-4.22	2.0	82.35	85.83	-3.48
0.0	81.66	85.88	-4.22	1.5	82.01	85.83	-3.82
-0.5	81.68	85.89	-4.21	1.0	81.76	85.84	-4.08
-1.0	81.93	85.89	-3.96	0.5	81.64	85.84	-4.20
-1.5	82.25	85.89	-3.64	0.0	81.63	85.85	-4.22
-2.0	83.04	85.90	-2.86	-0.5	81.67	85.85	-4.18
-2.5	84.27	85.90	-1.63	-1.0	81.87	85.86	-3.99
-3.0	85.27	85.91	-0.64	-1.5	82.18	85.86	-3.68
-3.3	85.91	85.91	0.00	-2.0	82.88	85.87	-2.99
				-2.5	85.24	85.87	-0.63
				-3.0	85.88	85.88	0.00

Test No. 8/8.1/6.1/1
Clay M390
Clay Lot No. 34281348
Test Date: 1-Oct-98

Test Variables		
Q (L/s)	H (cm)	d (mm)
0.31	6.5	8

Lengthwise:			Widthwise:		
	centreline	maximum		centreline	maximum
$r_{0\rightarrow}$ (cm)	3.1	3.1	$r_{0\rightarrow}$ (cm)		
$r_{0\leftarrow}$ (cm)	3.0	3.0	$r_{0\leftarrow}$ (cm)	4.0	4.0
$\bar{r}_{0\rightarrow}$ (cm)	3.05	3.05	$\bar{r}_{0\leftarrow}$ (cm)	4.0	4.0
ϵ_{\rightarrow} (cm)	-1.26	-1.30	ϵ_{\leftarrow} (cm)	-1.25	-1.36
$\epsilon_{\rightarrow}/2$ (cm)	-0.630	-0.650	$\epsilon_{\leftarrow}/2$ (cm)	-0.625	-0.680
b_{\rightarrow} (cm)	1.911	1.875	b_{\leftarrow} (cm)		
b_{\leftarrow} (cm)	2.145	1.875	b_{\rightarrow} (cm)	2.85	2.759
\bar{b}_{\rightarrow} (cm)	2.028	1.875	\bar{b}_{\leftarrow} (cm)	2.85	2.759

Lengthwise section (1 Oct 98)			Widthwise section (1 Oct 98)		
r (cm)	Depth Reading (cm)	ϵ_{\rightarrow} (cm)	r (cm)	Depth Reading (cm)	ϵ_{\leftarrow} (cm)
3.1	46.19	0.00	0.0	44.95	-1.25
3.0	46.15	-0.04	-0.5	44.84	-1.36
2.5	45.98	-0.21	-1.0	44.85	-1.35
2.0	45.61	-0.58	-1.5	44.95	-1.25
1.5	45.33	-0.86	-2.0	45.15	-1.05
1.0	45.18	-1.01	-2.5	45.37	-0.83
0.5	44.96	-1.23	-3.0	45.66	-0.54
0.0	44.93	-1.26	-3.5	46.00	-0.20
-0.5	44.89	-1.30	-4.0	46.20	0.00
-1.0	45.00	-1.19			
-1.5	45.24	-0.95			
-2.0	45.64	-0.55			
-2.5	45.95	-0.24			
-3.0	46.19	0.00			

Test No. 8/8.1/9.0/4
Clay M390
Clay Lot No. 34281348
Test Date: 16-Oct-98

Test Variables		
Q (L/s)	H (cm)	d (mm)
0.45	6.5	8

Lengthwise:		Widthwise:	
	$\epsilon_{\rightarrow} = \epsilon_{c\rightarrow}$		$\epsilon_{\leftarrow} = \epsilon_{c\leftarrow}$
$r_{0\rightarrow}$ (cm)	3.5	$r_{0\rightarrow}$ (cm)	4.7
$r_{0\leftarrow}$ (cm)	4.4	$r_{0\leftarrow}$ (cm)	3.65
$\bar{r}_{0\rightarrow}$ (cm)	3.95	$\bar{r}_{0\leftarrow}$ (cm)	4.2
ϵ_{\rightarrow} (cm)	-4.35	ϵ_{\leftarrow} (cm)	-4.26
$\epsilon_{\rightarrow}/2$ (cm)	-2.175	$\epsilon_{\leftarrow}/2$ (cm)	-2.13
b_{\rightarrow} (cm)	2.463	b_{\leftarrow} (cm)	2.616
b_{\leftarrow} (cm)	2.669	b_{\rightarrow} (cm)	2.482
\bar{b}_{\rightarrow} (cm)	2.566	\bar{b}_{\leftarrow} (cm)	2.549

Lengthwise section (16 Oct 98)			Widthwise section (16 Oct 98)			
r (cm)	Depth Reading (cm)	ϵ_{-} (cm)	r (cm)	Depth Reading (cm)	Int. Surface(cm)	ϵ_{-} (cm)
4.5	44.13	-0.03	5.0	44.16	44.14	0.02
4.0	44.13	-0.03	4.7	44.14	44.14	0.00
3.5	44.07	-0.09	4.5	43.99	44.14	-0.15
3.0	43.19	-0.97	4.0	43.73	44.13	-0.40
2.5	42.06	-2.10	3.5	43.62	44.12	-0.50
2.0	41.05	-3.11	3.0	42.55	44.12	-1.57
1.5	40.56	-3.60	2.5	41.81	44.11	-2.30
1.0	40.20	-3.96	2.0	41.14	44.10	-2.96
0.5	39.99	-4.17	1.5	40.57	44.09	-3.52
0.0	39.81	-4.35	1.0	40.21	44.09	-3.88
-0.5	39.93	-4.23	0.5	39.94	44.08	-4.14
-1.0	40.04	-4.12	0.0	39.81	44.07	-4.26
-1.5	40.32	-3.84	-0.5	39.81	44.07	-4.26
-2.0	40.76	-3.40	-1.0	39.89	44.06	-4.17
-2.5	41.63	-2.53	-1.5	40.14	44.05	-3.91
-3.0	42.68	-1.48	-2.0	40.60	44.04	-3.44
-3.5	43.02	-1.14	-2.5	41.96	44.04	-2.08
-4.0	43.60	-0.56	-3.0	43.29	44.03	-0.74
-4.4	44.15	-0.01	-3.5	43.85	44.02	-0.17
-4.5	44.16	0.00	-3.65	44.02	44.02	0.00
			-4.0	44.04	44.01	0.03

Test No. 8/8.1/9.9/5
Clay M390
Clay Lot No. 34281348
Test Date: 31-Oct-98

Test Variables		
Q (L/s)	H (cm)	d (mm)
0.5	6.5	8

Lengthwise:		centreline	maximum	Widthwise:		centreline	maximum
$r_{0\rightarrow}$ (cm)	4.2	4.2	$r_{0\rightarrow}$ (cm)	3.9	3.9		
$r_{0\leftarrow}$ (cm) *	4.0	4.0	$r_{0\leftarrow}$ (cm)	n/a	n/a		
$\bar{r}_{0\rightarrow}$ (cm)	4.10	4.10	$\bar{r}_{0\rightarrow}$ (cm)	3.90	3.90		
ϵ_{-} (cm)	-3.91	-3.93	ϵ_{-} (cm)	-3.93	-3.95		
$\epsilon_{-}/2$ (cm)	-1.955	-1.965	$\epsilon_{-}/2$ (cm)	-1.965	-1.975		
b_{\rightarrow} (cm)	2.407	2.399	b_{\rightarrow} (cm)	2.262	2.257		
b_{\leftarrow} (cm)	2.800	2.797	b_{\leftarrow} (cm)	n/a	n/a		
\bar{b}_{\rightarrow} (cm)	2.604	2.598	\bar{b}_{\rightarrow} (cm)	2.262	2.257		

Lengthwise section (31 Oct 98)			Widthwise section (31 Oct 98)		
r (cm)	Depth Reading (cm)	ϵ_{-} (cm)	r (cm)	Depth Reading (cm)	ϵ_{-} (cm)
4.5	45.43	-0.74	4.0	46.19	0.00
4.0	45.20	-0.97	3.9	46.18	-0.01
3.5	44.96	-1.21	3.5	45.96	-0.23
3.0	44.65	-1.52	3.0	45.41	-0.78
2.5	44.34	-1.83	2.5	44.73	-1.46
2.0	43.67	-2.50	2.0	43.67	-2.52
1.5	42.97	-3.20	1.5	42.84	-3.35
1.0	42.53	-3.64	1.0	42.50	-3.69
0.5	42.32	-3.85	0.5	42.33	-3.86
0.0	42.26	-3.91	0.0	42.26	-3.93
-0.5	42.24	-3.93	-0.5	42.24	-3.95
-1.0	42.28	-3.89	-1.0	42.31	-3.88
-1.5	42.40	-3.77	-1.5	42.42	-3.77
-2.0	42.75	-3.42	-2.0	42.68	-3.51
-2.5	43.41	-2.76	-2.5	43.09	-3.10
-3.0	44.75	-1.42	-3.0	43.41	-2.78
-3.5	45.38	-0.79	-3.5	43.78	-2.41
-4.0	46.11	-0.06			

Test No. 8/14.5/9.0/5
 Clay M390
 Clay Lot No. 34281348
 Test Date: 13-Nov-98

Test Variables		
Q (L/s)	H (cm)	d (mm)
0.45	11.6	8

Lengthwise:			Widthwise:		
	centreline	maximum		centreline	maximum
$r_{0\rightarrow}$ (cm)	3.25		$r_{0\rightarrow}$ (cm)	2.75	2.75
$r_{0\leftarrow}$ (cm)	2.7		$r_{0\leftarrow}$ (cm)	n/a	n/a
$\bar{r}_{0\rightarrow}$ (cm)	2.98		$\bar{r}_{0\rightarrow}$ (cm)	n/a	n/a
ϵ_{\rightarrow} (cm)	-0.566	-0.574	ϵ_{\rightarrow} (cm)	0.62	-0.66
$\epsilon_{\rightarrow}/2$ (cm)	-0.283	-0.287	$\epsilon_{\rightarrow}/2$ (cm)	0.310	-0.330
b_{\rightarrow} (cm)	2.141	2.129	b_{\rightarrow} (cm)	1.750	1.688
b_{\leftarrow} (cm)	1.684	1.671	b_{\leftarrow} (cm)	n/a	n/a
\bar{b}_{\rightarrow} (cm)	1.913	1.900	\bar{b}_{\rightarrow} (cm)	1.750	1.688

Lengthwise section (13 Nov 98)				Widthwise section (13 Nov 98)		
r (cm)	Depth Reading (cm)	Int. Surface(cm)	ϵ_{\rightarrow} (cm)	r (cm)	Depth Reading (cm)	ϵ_{\rightarrow} (cm)
3.5	45.94	45.92	0.02	3.0	45.96	0.02
3.25	45.92	45.92	0.00	2.75	45.94	0.00
3.0	45.86	45.92	-0.06	2.5	45.89	-0.05
2.5	45.75	45.92	-0.17	2.0	45.71	-0.23
2.0	45.60	45.93	-0.33	1.5	45.55	-0.39
1.5	45.48	45.93	-0.45	1.0	45.36	-0.58
1.0	45.39	45.93	-0.54	0.5	45.28	-0.66
0.5	45.36	45.93	-0.57	0.0	45.32	-0.62
0.0	45.37	45.94	-0.57	-0.5	45.28	-0.66
-0.5	45.46	45.94	-0.48	-1.0	45.22	-0.72
-1.0	45.52	45.94	-0.42	-1.5	45.19	-0.75
-1.5	45.61	45.94	-0.33	-2.0	45.21	-0.73
-2.0	45.75	45.95	-0.20	-2.5	45.27	-0.67
-2.5	45.91	45.95	-0.04			
-2.7	45.95	45.95	0.00			
-3.0	45.98	45.95	0.03			

Test No. 8/14.5/9.9/1
 Clay M390
 Clay Lot No. 34281348
 Test Date: 21-Nov-98

Test Variables		
Q (L/s)	H (cm)	d (mm)
0.5	11.6	8

Lengthwise:			Widthwise:		
	$\epsilon_{\rightarrow} = \epsilon_{\leftarrow}$		centreline	maximum	
$r_{0\rightarrow}$ (cm)	3.5		$r_{0\rightarrow}$ (cm)	n/a	n/a
$r_{0\leftarrow}$ (cm)	n/a		$r_{0\leftarrow}$ (cm)	4.8	4.8
ϵ_{\rightarrow} (cm)	-1.51		ϵ_{\rightarrow} (cm)	-1.54	-1.56
$\epsilon_{\rightarrow}/2$ (cm)	-0.755		$\epsilon_{\rightarrow}/2$ (cm)	-0.770	-0.780
b_{\rightarrow} (cm)	1.820		b_{\rightarrow} (cm)	n/a	n/a
b_{\leftarrow} (cm)	n/a		b_{\leftarrow} (cm)	-3.317	-3.305

Lengthwise section (21 Nov 98)			Widthwise section (21 Nov 98)		
r (cm)	Depth Reading (cm)	ϵ_{\rightarrow} (cm)	r (cm)	Depth Reading (cm)	ϵ_{\rightarrow} (cm)
4.0	46.04	0.04	0.0	44.44	-1.54
3.5	46.00	0.00	-0.5	44.44	-1.54
3.0	45.74	-0.26	-1.0	44.42	-1.56
2.5	45.66	-0.34	-1.5	44.45	-1.53
2.0	45.36	-0.64	-2.0	44.54	-1.44
1.5	45.04	-0.96	-2.5	44.69	-1.29
1.0	44.82	-1.18	-3.0	44.95	-1.03
0.5	44.66	-1.34	-3.5	45.36	-0.62
0.0	44.49	-1.51	-4.0	45.72	-0.26
			-4.5	45.85	-0.13
			-4.8	45.96	-0.02
			-5.0	45.98	0.00

Test No. 8/14.5/10.9/1
 Clay M390
 Clay Lot No. 34281348
 Test Date: 3-Dec-98

Test Variables		
Q (L/s)	H (cm)	d (mm)
0.55	11.6	8

Lengthwise:		centreline	maximum	Widthwise:		centreline	maximum
$r_{o\rightarrow}$ (cm)	5.0	5.0	5.0	$r_{o\rightarrow}$ (cm)	5.4	5.4	5.4
$r_{o\leftarrow}$ (cm)	5.4	5.4	5.4	$r_{o\leftarrow}$ (cm)	5.8	5.8	5.8
$\bar{r}_{o\rightarrow}$ (cm)	5.20	5.20	5.20	$\bar{r}_{o\leftarrow}$ (cm)	5.60	5.60	5.60
ϵ_{\rightarrow} (cm)	2.23	2.28	2.28	ϵ_{\leftarrow} (cm)	-2.24	-2.47	-2.47
$\epsilon_{\rightarrow}/2$ (cm)	1.115	1.140	1.140	$\epsilon_{\leftarrow}/2$ (cm)	-1.120	-1.235	-1.235
b_{\rightarrow} (cm)	2.809	2.735	2.735	b_{\leftarrow} (cm)	3.708	3.549	3.549
b_{\leftarrow} (cm)	3.699	3.673	3.673	b_{\rightarrow} (cm)	4.36	4.13	4.13

Lengthwise section (3 Dec 98)				Widthwise section (3 Dec 98)			
r (cm)	Depth Reading (cm)	Int. Surface (cm)	ϵ_{\rightarrow} (cm)	r (cm)	Depth Reading (cm)	Int. Surface (cm)	ϵ_{\leftarrow} (cm)
5.0	45.86	45.86	0.00	5.5	45.97	45.96	0.01
4.5	45.66	45.86	-0.20	5.4	45.96	45.96	0.00
4.0	45.27	45.87	-0.60	5.0	45.78	45.96	-0.18
3.5	45.06	45.87	-0.81	4.5	45.44	45.96	-0.52
3.0	44.83	45.88	-1.05	4.0	45.04	45.95	-0.91
2.5	44.66	45.88	-1.22	3.5	44.68	45.95	-1.27
2.0	44.29	45.88	-1.59	3.0	44.04	45.95	-1.91
1.5	44.05	45.89	-1.84	2.5	43.72	45.94	-2.22
1.0	43.82	45.89	-2.07	2.0	43.61	45.94	-2.33
0.5	43.75	45.89	-2.14	1.5	43.47	45.94	-2.47
0.0	43.67	45.90	-2.23	1.0	43.50	45.94	-2.44
-0.5	43.62	45.90	-2.28	0.5	43.54	45.93	-2.39
-1.0	43.67	45.91	-2.24	0.0	43.69	45.93	-2.24
-1.5	43.69	45.91	-2.22	-0.5	43.77	45.93	-2.16
-2.0	43.78	45.91	-2.13	-1.0	43.79	45.93	-2.14
-2.5	44.00	45.92	-1.92	-1.5	43.83	45.92	-2.09
-3.0	44.29	45.92	-1.63	-2.0	43.92	45.92	-2.00
-3.5	44.62	45.93	-1.31	-2.5	44.03	45.92	-1.89
-4.0	45.11	45.93	-0.82	-3.0	44.20	45.92	-1.72
-4.5	45.44	45.93	-0.49	-3.5	44.44	45.91	-1.47
-5.0	45.81	45.94	-0.13	-4.0	44.61	45.91	-1.30
-5.4	45.94	45.94	0.00	-4.5	44.86	45.91	-1.05
				-5.0	45.15	45.90	-0.75
				-5.5	45.72	45.90	-0.18
				-5.8	45.86	45.90	-0.04
				-6.0	45.90	45.90	0.00

Test No. 4/10.0/11.9/1
 Clay M390
 Clay Lot No. 34281348
 Test Date: 15-Jan-99

Test Variables		
Q (L/s)	H (cm)	d (mm)
0.15	4	4

Lengthwise:		$\epsilon_{\rightarrow} = \epsilon_{\leftarrow}$	Widthwise:		$\epsilon_{\rightarrow} = \epsilon_{\leftarrow}$
$r_{o\rightarrow}$ (cm)	2.1		$r_{o\rightarrow}$ (cm)	2.0	
$r_{o\leftarrow}$ (cm)	n/a		$r_{o\leftarrow}$ (cm)	n/a	
$\bar{r}_{o\rightarrow}$ (cm)	n/a		$\bar{r}_{o\leftarrow}$ (cm)	n/a	
ϵ_{\rightarrow} (cm)	-1.45		ϵ_{\leftarrow} (cm)	-1.45	
$\epsilon_{\rightarrow}/2$ (cm)	-0.725		$\epsilon_{\leftarrow}/2$ (cm)	-0.725	
b_{\rightarrow} (cm)	1.277		b_{\leftarrow} (cm)	1.232	
b_{\leftarrow} (cm)	n/a		b_{\rightarrow} (cm)	n/a	

Lengthwise section (15 Jan 99)			Widthwise section (15 Jan 99)		
r (cm)	Depth Reading (cm)	ϵ_{-} (cm)	r (cm)	Depth Reading (cm)	ϵ_{-} (cm)
2.5	46.22	0.00	2.0	46.21	-0.01
2.1	46.22	0.00	1.5	45.74	-0.48
2.0	46.16	-0.06	1.0	45.17	-1.05
1.5	45.78	-0.44	0.5	44.86	-1.36
1.0	45.14	-1.08	0.0	44.77	-1.45
0.5	44.82	-1.40			
0.0	44.77	-1.45			
-0.5	44.79	-1.43			
-1.0	44.92	-1.30			
-1.5	45.23	-0.99			
-2.0	45.64	-0.58			
-2.5	45.69	-0.53			

Test No. 4/10.0/15.9/1
 Clay M390
 Clay Lot No. 34281348
 Test Date: 22-Jan-99

Test Variables		
Q (L/s)	H (cm)	d (mm)
0.2	4	4

* observed jet turned almost 90° in hole (came almost straight up out of hole).

Lengthwise: $\epsilon_{m+} = \epsilon_{cl+}$		Widthwise: $\epsilon_{m+} = \epsilon_{cl+}$	
r_{m+} (cm)	2.1	r_{m+} (cm)	2.1
r_{m-} (cm)	1.9	r_{m-} (cm)	1.7
\bar{r}_{m+} (cm)	2.00	\bar{r}_{m+} (cm)	1.90
ϵ_{m+} (cm)	-2.63	ϵ_{m+} (cm)	-2.68
$\epsilon_{m+}/2$ (cm)	-1.315	$\epsilon_{m+}/2$ (cm)	-1.340
b_{m+} (cm)	1.553	b_{m+} (cm)	1.565
b_{m-} (cm)	1.650	b_{m-} (cm)	1.232
\bar{b}_{m+} (cm)	1.602	\bar{b}_{m+} (cm)	1.399

Lengthwise section (22 Jan 99)				Widthwise section (22 Jan 99)			
r (cm)	Depth Reading (cm)	Int. Surface (cm)	ϵ_{-} (cm)	r (cm)	Depth Reading (cm)	Int. Surface (cm)	ϵ_{-} (cm)
2.1	46.12	46.12	0.00	2.5	46.12	46.08	0.04
2.0	46.03	46.12	-0.09	2.1	46.09	46.09	0.00
1.8	45.91	46.12	-0.21	2.0	46.05	46.09	-0.04
1.5	44.56	46.11	-1.55	1.9	46.03	46.09	-0.06
1.0	43.98	46.11	-2.13	1.5	44.51	46.10	-1.59
0.5	43.59	46.10	-2.51	1.0	43.74	46.10	-2.36
0.0	43.47	46.10	-2.63	0.5	43.51	46.11	-2.60
-0.5	43.46	46.09	-2.63	0.0	43.44	46.12	-2.68
-1.0	43.57	46.09	-2.52	-0.5	43.49	46.12	-2.63
-1.5	43.98	46.08	-2.10	-1.0	43.77	46.13	-2.36
-1.9	46.07	46.08	-0.01	-1.5	45.98	46.14	-0.16
-2.0	46.08	46.08	0.00	-1.7	46.14	46.14	0.00
				-2.0	46.15	46.14	0.01

Test No. 4/10.0/9.9/1
 Clay M390
 Clay Lot No. 34281348
 Test Date: 8-Feb-99

Test Variables		
Q (L/s)	H (cm)	d (mm)
0.125	4	4

Lengthwise:			Widthwise:		
	centreline	maximum		centreline	maximum
$r_{o\rightarrow}$ (cm)	2.2	2.2	$r_{o\rightarrow}$ (cm)	2.75	2.75
$r_{o\leftarrow}$ (cm)	2.3	2.3	$r_{o\leftarrow}$ (cm)	2.3	2.3
$\bar{r}_{o\rightarrow}$ (cm)	2.25	2.25	$\bar{r}_{o\leftarrow}$ (cm)	2.53	2.53
ϵ_{\rightarrow} (cm)	-1.03	-1.04	ϵ_{\rightarrow} (cm)	-1.00	-1.09
$\epsilon_{\rightarrow}/2$ (cm)	-0.515	-0.520	$\epsilon_{\rightarrow}/2$ (cm)	-0.500	-0.545
b_{\rightarrow} (cm)	1.343	1.337	b_{\rightarrow} (cm)	1.761	1.663
b_{\leftarrow} (cm)	1.412	1.405	b_{\leftarrow} (cm)	1.487	1.428
\bar{b}_{\rightarrow} (cm)	1.378	1.371	\bar{b}_{\leftarrow} (cm)	1.624	1.546

Lengthwise section (8 Feb 99)			Widthwise section (8 Feb 99)			
r (cm)	Depth Reading (cm)	ϵ_{\rightarrow} (cm)	r (cm)	Depth Reading (cm)	Int. Surface (cm)	ϵ_{\leftarrow} (cm)
2.5	46.28	0.01	3.0	46.27	46.27	0.00
2.2	46.26	-0.01	2.75	46.27	46.27	0.00
2.0	46.22	-0.05	2.5	46.11	46.27	-0.16
1.5	45.89	-0.38	2.0	45.88	46.27	-0.39
1.0	45.46	-0.81	1.5	45.64	46.26	-0.62
0.5	45.29	-0.98	1.0	45.36	46.26	-0.90
0.0	45.24	-1.03	0.5	45.17	46.26	-1.09
-0.5	45.23	-1.04	0.0	45.26	46.26	-1.00
-1.0	45.45	-0.82	-0.5	45.28	46.26	-0.98
-1.5	45.82	-0.45	-1.0	45.39	46.26	-0.87
-2.0	46.14	-0.13	-1.5	45.76	46.25	-0.49
-2.3	46.27	0.00	-2.0	46.12	46.25	-0.13
-2.5	46.28	0.01	-2.3	46.24	46.25	-0.01
			-2.5	46.25	46.25	0.00

Test No. 8/8.1/9.0/5
 Clay M390
 Clay Lot No. 34281348
 Test Date: 9-Mar-99

Test Variables		
Q (L/s)	H (cm)	d (mm)
0.45	6.5	8

Lengthwise:			Widthwise:	
	centreline	maximum	$\epsilon_{\rightarrow} = \epsilon_{\leftarrow}$	
$r_{o\rightarrow}$ (cm)	5.2	5.2	$r_{o\rightarrow}$ (cm)	4.80
$r_{o\leftarrow}$ (cm)	5.3	5.3	$r_{o\leftarrow}$ (cm)	5.3
$\bar{r}_{o\rightarrow}$ (cm)	5.25	5.25	$\bar{r}_{o\leftarrow}$ (cm)	5.05
ϵ_{\rightarrow} (cm)	-4.00	4.01	ϵ_{\rightarrow} (cm)	-3.98
$\epsilon_{\rightarrow}/2$ (cm)	-2.000	2.005	$\epsilon_{\rightarrow}/2$ (cm)	-1.990
b_{\rightarrow} (cm)	3.083	3.080	b_{\rightarrow} (cm)	3.019
b_{\leftarrow} (cm)	3.442	3.438	b_{\leftarrow} (cm)	3.442

Lengthwise section (9 Mar 99)			Widthwise section (9 Mar 99)			
r (cm)	Depth Reading (cm)	ϵ_w (cm)	r (cm)	Depth Reading (cm)	Int. Surface(cm)	ϵ_w (cm)
5.2	46.14	0.00	5.0	46.06	46.04	0.02
5.0	46.08	-0.06	4.8	46.04	46.04	0.00
4.5	45.73	-0.41	4.5	45.34	46.05	-0.71
4.0	45.42	-0.72	4.0	44.95	46.05	-1.10
3.5	44.84	-1.30	3.5	44.81	46.06	-1.25
3.0	44.00	-2.14	3.0	44.05	46.07	-2.02
2.5	43.26	-2.88	2.5	43.30	46.08	-2.78
2.0	42.72	-3.42	2.0	42.79	46.09	-3.30
1.5	42.38	-3.76	1.5	42.41	46.10	-3.69
1.0	42.22	-3.92	1.0	42.21	46.10	-3.89
0.5	42.16	-3.98	0.5	42.14	46.11	-3.97
0.0	42.14	-4.00	0.0	42.14	46.12	-3.98
-0.5	42.13	-4.01	-0.5	42.19	46.13	-3.94
-1.0	42.20	-3.94	-1.0	42.24	46.14	-3.90
-1.5	42.32	-3.82	-1.5	42.36	46.15	-3.79
-2.0	42.60	-3.54	-2.0	42.63	46.15	-3.52
-2.5	43.01	-3.13	-2.5	42.93	46.16	-3.23
-3.0	43.46	-2.68	-3.0	43.50	46.17	-2.67
-3.5	44.23	-1.91	-3.5	44.28	46.18	-1.90
-4.0	45.28	-0.86	-4.0	44.98	46.19	-1.21
-4.5	45.51	-0.63	-4.5	45.58	46.20	-0.62
-5.0	45.99	-0.15	-5.0	46.12	46.20	-0.08
-5.3	46.14	0.00	-5.3	46.21	46.21	0.00
			-5.5	46.22	46.21	0.01

Test No. 8/8.1/9.0/6
Clay M390
Clay Lot No. 34281348
Test Date: 16-Mar-99

Test Variables		
Q (L/s)	H (cm)	d (mm)
0.45	6.5	8

Lengthwise:		maximum	Widthwise:		centreline	maximum
$r_{w\rightarrow}$ (cm)	3.2	3.2	$r_{w\rightarrow}$ (cm)	4.2	4.2	
$r_{w\leftarrow}$ (cm)	3.6	3.6	$r_{w\leftarrow}$ (cm)	3.75	3.8	
\bar{r}_w (cm)	3.40	3.40	\bar{r}_w (cm)	3.98	3.98	
ϵ_w (cm)	-3.45	-3.49	ϵ_w (cm)	-3.45	-3.51	
$\epsilon_w/2$ (cm)	-1.725	-1.745	$\epsilon_w/2$ (cm)	-1.725	-1.755	
$b_{w\rightarrow}$ (cm)	1.703	1.695	$b_{w\rightarrow}$ (cm)	2.782	2.758	
$b_{w\leftarrow}$ (cm)	2.622	2.596	$b_{w\leftarrow}$ (cm)	2.271	2.257	
\bar{b}_w (cm)	2.163	2.146	\bar{b}_w (cm)	2.527	2.508	

Lengthwise section (16 Mar 99)				Widthwise section (16 Mar 99)			
r (cm)	Depth Reading (cm)	Int. Surface(cm)	ϵ_w (cm)	r (cm)	Depth Reading (cm)	Int. Surface(cm)	ϵ_w (cm)
3.5	45.96	45.94	0.02	4.5	46.00	45.98	0.02
3.2	45.94	45.94	0.00	4.2	45.98	45.98	0.00
3.0	45.86	45.94	-0.08	4.0	45.91	45.98	-0.07
2.5	45.60	45.95	-0.35	3.5	45.05	45.99	-0.94
2.0	45.01	45.95	-0.94	3.0	44.54	45.99	-1.45
1.5	43.70	45.96	-2.26	2.5	43.92	46.00	-2.08
1.0	42.96	45.96	-3.00	2.0	43.19	46.00	-2.81
0.5	42.68	45.97	-3.29	1.5	42.78	46.01	-3.23
0.0	42.52	45.97	-3.45	1.0	42.61	46.02	-3.41
-0.5	42.49	45.98	-3.49	0.5	42.55	46.02	-3.47
-1.0	42.57	45.98	-3.41	0.0	42.58	46.03	-3.45
-1.5	42.72	45.99	-3.27	-0.5	42.52	46.03	-3.51
-2.0	43.39	45.99	-2.60	-1.0	42.71	46.04	-3.33
-2.5	44.18	46.00	-1.82	-1.5	43.16	46.04	-2.88
-3.0	44.57	46.00	-1.43	-2.0	43.74	46.05	-2.31
-3.5	45.98	46.01	-0.03	-2.5	44.83	46.06	-1.23
-3.6	46.01	46.01	0.00	-3.0	45.57	46.06	-0.49
-4.0	46.05	46.01	0.04	-3.5	45.96	46.07	-0.11
				-3.75	46.07	46.07	0.00

Test No. 4/16.3/15.9/1
 Clay M390
 Clay Lot No. 34281348
 Test Date: 12-May-99

Test Variables		
Q (L/s)	H (cm)	d (mm)
0.2	6.5	4

Lengthwise:		centreline	maximum	Widthwise:		centreline	maximum
r_{om+} (cm)	4.6	4.6	r_{om+} (cm)	3.7	3.7		
r_{om-} (cm)	3.8	3.8	r_{om-} (cm)	3.75	3.75		
\bar{r}_{om} (cm)	4.20	4.20	\bar{r}_{om} (cm)	3.73	3.73		
ϵ_{-} (cm)	-1.55	-1.59	ϵ_{-} (cm)	-1.52	-1.59		
$\epsilon_{-}/2$ (cm)	-0.777	-0.795	$\epsilon_{-}/2$ (cm)	-0.760	-0.796		
b_{-+} (cm)	2.277	2.240	b_{-+} (cm)	1.971	1.918		
b_{--} (cm)	2.522	2.491	b_{--} (cm)	2.436	2.398		
\bar{b}_{-} (cm)	2.400	2.366	\bar{b}_{-} (cm)	2.204	2.158		

Lengthwise section (12 May 99)				Widthwise-section (12 May 99)			
r (cm)	Depth Reading (cm)	Int. Surface(cm)	ϵ_{-} (cm)	r (cm)	Depth Reading (cm)	Int. Surface(cm)	ϵ_{-} (cm)
5.0	46.11	46.09	0.02	4.0	46.21	46.19	0.02
4.6	46.09	46.09	0.00	3.7	46.19	46.19	0.00
4.5	46.08	46.09	-0.01	3.5	46.10	46.19	-0.09
4.0	45.93	46.10	-0.17	3.0	45.98	46.18	-0.20
3.5	45.73	46.10	-0.37	2.5	45.73	46.17	-0.44
3.0	45.62	46.11	-0.49	2.0	45.42	46.16	-0.74
2.5	45.44	46.11	-0.67	1.5	45.07	46.15	-1.08
2.0	45.20	46.11	-0.91	1.0	44.83	46.15	-1.32
1.5	44.91	46.12	-1.21	0.5	44.69	46.14	-1.45
1.0	44.66	46.12	-1.46	0.0	44.61	46.13	-1.52
0.5	44.54	46.13	-1.59	-0.5	44.53	46.12	-1.59
0.0	44.58	46.13	-1.55	-1.0	44.55	46.11	-1.56
-0.5	44.56	46.14	-1.58	-1.5	44.69	46.11	-1.42
-1.0	44.62	46.14	-1.52	-2.0	44.93	46.10	-1.17
-1.5	44.76	46.15	-1.39	-2.5	45.39	46.09	-0.70
-2.0	45.09	46.15	-1.06	-3.0	45.75	46.08	-0.33
-2.5	45.37	46.16	-0.79	-3.5	46.08	46.07	0.01
-3.0	45.67	46.16	-0.49	-3.75	46.08	46.07	0.01
-3.5	46.03	46.17	-0.14	-4.0	46.10	46.07	0.03
-3.8	46.17	46.17	0.00				

Test No. 4/16.3/19.9/1
 Clay M390
 Clay Lot No. 34281348
 Test Date: 25-May-99

Test Variables		
Q (L/s)	H (cm)	d (mm)
0.25	6.5	4

Lengthwise:		centreline	maximum	Widthwise:		centreline	maximum
r_{om+} (cm)	4.4	4.4	r_{om+} (cm)	4.8	4.8		
r_{om-} (cm)	3.8	3.8	r_{om-} (cm)	3.75	3.75		
\bar{r}_{om} (cm)	4.10	4.10	\bar{r}_{om} (cm)	4.28	4.28		
ϵ_{-} (cm)	-3.52	-3.59	ϵ_{-} (cm)	-3.48	-3.49		
$\epsilon_{-}/2$ (cm)	-1.760	-1.795	$\epsilon_{-}/2$ (cm)	-1.739	-1.747		
b_{-+} (cm)	3.229	3.210	b_{-+} (cm)	2.775	2.765		
b_{--} (cm)	2.600	2.577	b_{--} (cm)	2.871	2.868		
\bar{b}_{-} (cm)	2.915	2.894	\bar{b}_{-} (cm)	2.823	2.817		

Lengthwise section (25 May 99)			Widthwise-section (25 May 99)			
r (cm)	Depth Reading (cm)	ϵ_{-} (cm)	r (cm)	Depth Reading (cm)	Int. Surface(cm)	ϵ_{-} (cm)
4.5	46.16	0.02	5.0	46.01	46.01	0.00
4.4	46.14	0.00	4.8	46.00	46.01	-0.01
4.0	45.59	-0.55	4.5	45.56	46.01	-0.45
3.5	44.89	-1.25	4.0	45.34	46.02	-0.68
3.0	43.95	-2.19	3.5	44.94	46.02	-1.08
2.5	43.35	-2.79	3.0	44.47	46.02	-1.55
2.0	42.91	-3.23	2.5	44.05	46.02	-1.97
1.5	42.66	-3.48	2.0	43.46	46.03	-2.57
1.0	42.56	-3.58	1.5	42.98	46.03	-3.05
0.5	42.55	-3.59	1.0	42.70	46.03	-3.33
0.0	42.62	-3.52	0.5	42.62	46.04	-3.42
-0.5	42.70	-3.44	0.0	42.56	46.04	-3.48
-1.0	42.84	-3.30	-0.5	42.55	46.04	-3.49
-1.5	43.10	-3.04	-1.0	42.55	46.04	-3.49
-2.0	43.62	-2.52	-1.5	42.59	46.05	-3.46
-2.5	44.23	-1.91	-2.0	42.84	46.05	-3.21
-3.0	44.98	-1.16	-2.5	43.28	46.05	-2.77
-3.5	45.55	-0.59	-3.0	44.68	46.06	-1.38
-3.8	46.12	-0.02	-3.5	45.97	46.06	-0.09
-4.0	46.14	0.00	-3.75	46.06	46.06	0.00
			-4.0	46.08	46.06	0.02

Test No. 4/29.0/25.9/1
Clay M390
Clay Lot No. 34281348
Test Date: 14-Jun-98

Test Variables		
Q (L/s)	H (cm)	d (mm)
0.325	11.6	4

Lengthwise:			Widthwise:		
	centreline	maximum		centreline	maximum
$r_{0\rightarrow}$ (cm)	5.9	5.9	$r_{0\rightarrow}$ (cm)	5.7	5.7
$r_{0\leftarrow}$ (cm)	6.2	6.2	$r_{0\leftarrow}$ (cm)	5.10	5.10
$\bar{r}_{0\rightarrow}$ (cm)	6.05	6.05	$\bar{r}_{0\leftarrow}$ (cm)	5.40	5.40
ϵ_{-} (cm)	-2.68	-2.79	ϵ_{-} (cm)	-2.64	-2.68
$\epsilon_{-}/2$ (cm)	-1.340	-1.396	$\epsilon_{-}/2$ (cm)	-1.318	-1.342
b_{\rightarrow} (cm)	4.352	4.289	b_{\rightarrow} (cm)	2.878	2.848
b_{\leftarrow} (cm)	3.750	3.623	b_{\leftarrow} (cm)	2.968	2.941

Abs. Min at 43.18
Absolute Minimum = 2.88 cm

Lengthwise section (14 Jun 99)				Widthwise-section (14 Jun 99)			
r (cm)	Depth Reading (cm)	Int. Surface(cm)	ϵ_{-} (cm)	r (cm)	Depth Reading (cm)	Int. Surface(cm)	ϵ_{-} (cm)
5.9	46.07	46.07	0.00	6.0	46.10	46.08	0.02
5.5	45.66	46.07	-0.41	5.7	46.08	46.08	0.00
5.0	45.17	46.07	-0.90	5.5	46.05	46.08	-0.03
4.5	44.86	46.07	-1.21	5.0	45.89	46.08	-0.19
4.0	44.42	46.07	-1.65	4.5	45.67	46.09	-0.42
3.5	44.19	46.07	-1.88	4.0	45.44	46.09	-0.65
3.0	43.78	46.07	-2.29	3.5	45.18	46.09	-0.91
2.5	43.50	46.06	-2.56	3.0	44.88	46.10	-1.22
2.0	43.35	46.06	-2.71	2.5	44.48	46.10	-1.62
1.5	43.27	46.06	-2.79	2.0	44.04	46.10	-2.06
1.0	43.28	46.06	-2.78	1.5	43.84	46.11	-2.27
0.5	43.30	46.06	-2.76	1.0	43.50	46.11	-2.51
0.0	43.38	46.06	-2.68	0.5	43.43	46.11	-2.68
-0.5	43.38	46.06	-2.68	0.0	43.48	46.12	-2.64
-1.0	43.39	46.06	-2.67	-0.5	43.49	46.12	-2.63
-1.5	43.46	46.06	-2.60	-1.0	43.65	46.12	-2.47
-2.0	43.76	46.06	-2.30	-1.5	43.81	46.13	-2.32
-2.5	43.96	46.06	-2.10	-2.0	44.06	46.13	-2.07
-3.0	44.22	46.06	-1.84	-2.5	44.40	46.13	-1.73
-3.5	44.60	46.05	-1.45	-3.0	44.85	46.14	-1.29
-4.0	44.82	46.05	-1.23	-3.5	45.30	46.14	-0.84
-4.5	45.14	46.05	-0.91	-4.0	45.65	46.14	-0.49
-5.0	45.36	46.05	-0.69	-4.5	45.89	46.15	-0.26
-5.5	45.71	46.05	-0.34	-5.0	46.09	46.15	-0.06
-6.0	46.02	46.05	-0.03	-5.1	46.15	46.15	0.00
-6.2	46.05	46.05	0.00	-5.5	46.16	46.15	0.01

Test No. 4/29.0/25.9/2
 Clay M390
 Clay Lot No. 34281348
 Test Date: 25-Jun-99

Test Variables		
Q (L/s)	H (cm)	d (mm)
0.325	11.6	4

Lengthwise: $\epsilon_{cm} = \epsilon_{cl}$		Widthwise: centreline		maximum
r_{cm+} (cm)	5.5	r_{cm+} (cm)	5.1	5.1
r_{cm-} (cm)	5.5	r_{cm-} (cm)	5.90	5.90
\bar{r}_{cm} (cm)	5.50	\bar{r}_{cm} (cm)	5.50	5.50
ϵ_{cm} (cm)	-2.34	ϵ_{cm} (cm)	-2.25	-2.26
$\epsilon_{cm}/2$ (cm)	-1.171	$\epsilon_{cm}/2$ (cm)	-1.124	-1.132
b_{cm+} (cm)	3.077	b_{cm+} (cm)	3.533	3.525
b_{cm-} (cm)	3.480	b_{cm-} (cm)	4.032	4.022

Lengthwise section (25 Jun 99)				Widthwise section (25 Jun 99)			
r (cm)	Depth Reading (cm)	Int. Surface (cm)	ϵ_{cm} (cm)	r (cm)	Depth Reading (cm)	Int. Surface (cm)	ϵ_{cm} (cm)
5.5	46.07	46.07	0.00	5.1	46.16	46.16	0.00
5.0	45.90	46.07	-0.17	5.0	46.15	46.16	-0.01
4.5	45.72	46.08	-0.36	4.5	45.91	46.16	-0.25
4.0	45.49	46.08	-0.59	4.0	45.53	46.15	-0.62
3.5	45.23	46.08	-0.85	3.5	44.99	46.15	-1.16
3.0	44.85	46.08	-1.23	3.0	44.65	46.14	-1.49
2.5	44.65	46.08	-1.43	2.5	44.46	46.14	-1.68
2.0	44.16	46.08	-1.92	2.0	44.32	46.13	-1.81
1.5	43.86	46.09	-2.23	1.5	44.17	46.13	-1.96
1.0	43.85	46.09	-2.24	1.0	44.10	46.13	-2.03
0.5	43.78	46.09	-2.31	0.5	43.98	46.12	-2.14
0.0	43.75	46.09	-2.34	0.0	43.87	46.12	-2.25
-0.5	43.83	46.09	-2.26	-0.5	43.85	46.11	-2.26
-1.0	44.06	46.10	-2.04	-1.0	43.85	46.11	-2.26
-1.5	44.15	46.10	-1.95	-1.5	43.96	46.11	-2.15
-2.0	44.24	46.10	-1.86	-2.0	44.13	46.10	-1.97
-2.5	44.43	46.10	-1.67	-2.5	44.33	46.10	-1.77
-3.0	44.66	46.10	-1.44	-3.0	44.52	46.09	-1.57
-3.5	44.94	46.10	-1.16	-3.5	44.77	46.09	-1.32
-4.0	45.35	46.11	-0.76	-4.0	44.94	46.09	-1.15
-4.5	45.71	46.11	-0.40	-4.5	45.34	46.08	-0.74
-5.0	45.96	46.11	-0.15	-5.0	45.64	46.08	-0.44
-5.5	46.11	46.11	0.00	-5.5	45.90	46.07	-0.17
				-5.9	46.07	46.07	0.00

Test No. 4/29.0/21.9/1
 Clay M390
 Clay Lot No. 34281348
 Test Date: 30-Jun-99

Test Variables		
Q (L/s)	H (cm)	d (mm)
0.275	11.6	4

Lengthwise: $\epsilon_{cm} = \epsilon_{cl}$		Widthwise: centreline		maximum
r_{cm+} (cm)	3.8	r_{cm+} (cm)	5.1	5.1
r_{cm-} (cm)	4.4	r_{cm-} (cm)	5.90	5.90
\bar{r}_{cm} (cm)	4.10	\bar{r}_{cm} (cm)	5.50	5.50
ϵ_{cm} (cm)	-0.82	ϵ_{cm} (cm)	-0.80	-0.87
$\epsilon_{cm}/2$ (cm)	-0.412	$\epsilon_{cm}/2$ (cm)	-0.400	-0.435
b_{cm+} (cm)	2.395	b_{cm+} (cm)	2.875	2.813
b_{cm-} (cm)	2.762	b_{cm-} (cm)	3.222	3.157
\bar{b}_{cm} (cm)	2.579	\bar{b}_{cm} (cm)	3.049	2.985

Lengthwise section (30 Jun 99)				Widthwise section (30 Jun 99)		
r (cm)	Depth Reading (cm)	ht. Surface(cm)	ϵ_{-} (cm)	r (cm)	Depth Reading (cm)	ϵ_{-} (cm)
3.8	45.97	45.97	0.00	3.8	45.96	0.00
3.5	45.92	45.97	-0.05	3.5	45.89	-0.07
3.0	45.79	45.97	-0.18	3.0	45.63	-0.33
2.5	45.61	45.98	-0.37	2.5	45.35	-0.61
2.0	45.41	45.98	-0.57	2.0	45.20	-0.76
1.5	45.34	45.98	-0.64	1.5	45.15	-0.81
1.0	45.22	45.99	-0.77	1.0	45.09	-0.87
0.5	45.21	45.99	-0.78	0.5	45.14	-0.82
0.0	45.17	45.99	-0.82	0.0	45.16	-0.80
-0.5	45.18	46.00	-0.82	-0.5	45.18	-0.78
-1.0	45.19	46.00	-0.81	-1.0	45.16	-0.80
-1.5	45.31	46.00	-0.69	-1.5	45.13	-0.83
-2.0	45.38	46.01	-0.63	-2.0	45.23	-0.73
-2.5	45.53	46.01	-0.48	-2.5	45.31	-0.65
-3.0	45.66	46.01	-0.35	-3.0	45.44	-0.52
-3.5	45.83	46.01	-0.18	-3.5	45.71	-0.25
-4.0	45.98	46.02	-0.04	-4.0	45.90	-0.06
-4.4	46.02	46.02	0.00	-4.25	45.94	-0.02
				-4.5	45.96	0.00

Test No. 4/10.0/13.9/1
Clay M390
Clay Lot No. 34281348
Test Date: 5-Jul-99

Test Variables		
Q (L/s)	H (cm)	d (mm)
0.175	4	4

* slaking may have influenced scour hole radii and profile.

	Lengthwise:			Widthwise:	
	centreline	maximum		centreline	maximum
$r_{0\rightarrow}$ (cm)	2.8	2.8	$r_{0\rightarrow}$ (cm)	2.80	2.8
$r_{0\leftarrow}$ (cm)	4.60	4.60	$r_{0\leftarrow}$ (cm)	3.75	3.75
$\bar{r}_{0\rightarrow}$ (cm)	3.70	3.70	$\bar{r}_{0\leftarrow}$ (cm)	3.28	3.28
ϵ_{-} (cm)	-3.34	-3.78	ϵ_{-} (cm)	-3.36	-3.71
$\epsilon_{-}/2$ (cm)	-1.672	-1.888	$\epsilon_{-}/2$ (cm)	-1.679	-1.853
b_{\rightarrow} (cm)	1.499	1.413	b_{\rightarrow} (cm)	2.283	2.205
b_{\leftarrow} (cm)	3.246	3.112	b_{\leftarrow} (cm)	1.327	1.281
\bar{b}_{\rightarrow} (cm)	2.373	2.263	\bar{b}_{\leftarrow} (cm)	1.805	1.743

Lengthwise section (5 Jul 99)				Widthwise section (5 Jul 99)			
r (cm)	Depth Reading (cm)	Int. Surface(cm)	ϵ_{-} (cm)	r (cm)	Depth Reading (cm)	Int. Surface(cm)	ϵ_{-} (cm)
2.8	46.06	46.08	-0.02	-3.75	45.99	46.05	-0.06
2.5	46.00	46.07	-0.07	-3.5	45.87	46.05	-0.18
2.0	45.34	46.07	-0.73	-3.0	45.29	46.04	-0.75
1.5	44.39	46.06	-1.67	-2.5	44.78	46.04	-1.26
1.0	43.13	46.06	-2.93	-2.0	43.72	46.03	-2.31
0.5	42.77	46.05	-3.28	-1.5	42.79	46.03	-3.24
0.0	42.70	46.04	-3.34	-1.0	42.32	46.03	-3.71
-0.5	42.50	46.04	-3.54	-0.5	42.38	46.02	-3.64
-1.0	42.32	46.03	-3.71	0.0	42.66	46.02	-3.36
-1.5	42.25	46.03	-3.78	0.5	42.96	46.01	-3.05
-2.0	42.44	46.02	-3.58	1.0	43.18	46.01	-2.83
-2.5	42.64	46.01	-3.37	1.5	44.97	46.01	-1.04
-3.0	43.94	46.01	-2.07	2.0	45.48	46.00	-0.52
-3.5	44.74	46.00	-1.26	2.5	45.71	46.00	-0.29
-4.0	45.29	46.00	-0.71	2.8	46.04	46.00	0.04
-4.5	45.90	45.99	-0.09				
-4.6	45.99	45.99	0.00				

Test No. 4/10.0/15.9/2
 Clay M390
 Clay Lot No. 34281348
 Test Date: 9-Jul-99

Test Variables		
Q (L/s)	H (cm)	d (mm)
0.2	4	4

*slaking likely

Lengthwise:	centreline		maximum		Widthwise:	centreline		maximum	
	$r_{0\rightarrow}$ (cm)					$r_{0\rightarrow}$ (cm)			
$r_{0\rightarrow}$ (cm)	6.3		6.3		$r_{0\rightarrow}$ (cm)	2.7		2.7	
$r_{0\leftarrow}$ (cm)	4.70		4.70		$r_{0\leftarrow}$ (cm)	6.10		6.10	
$\bar{r}_{0\rightarrow}$ (cm)	5.50		5.50		$\bar{r}_{0\rightarrow}$ (cm)	4.40		4.40	
ϵ_{\rightarrow} (cm)	-2.95		-3.00		ϵ_{\rightarrow} (cm)	-2.91		-3.14	
$\epsilon_{\rightarrow}/2$ (cm)	-1.475		-1.502		$\epsilon_{\rightarrow}/2$ (cm)	-1.453		-1.568	
b_{\rightarrow} (cm)	2.283		2.247		b_{\rightarrow} (cm)	1.297		1.265	
b_{\leftarrow} (cm)	1.989		1.970		b_{\leftarrow} (cm)	4.585		4.523	

Lengthwise section (9 Jul 99)				Widthwise section (9 Jul 99)			
r (cm)	Depth Reading (cm)	Int. Surface (cm)	ϵ_{\rightarrow} (cm)	r (cm)	Depth Reading (cm)	Int. Surface (cm)	ϵ_{\rightarrow} (cm)
6.3	46.01	46.01	0.00	2.7	46.08	46.08	0.00
6.0	45.68	46.01	-0.33	2.5	45.94	46.08	-0.14
5.5	45.50	46.02	-0.52	2.0	45.71	46.07	-0.36
5.0	45.24	46.03	-0.79	1.5	45.33	46.07	-0.74
4.5	45.14	46.03	-0.89	1.0	43.56	46.06	-2.50
4.0	45.05	46.04	-0.99	0.5	43.13	46.06	-2.93
3.5	44.96	46.05	-1.09	0.0	43.15	46.06	-2.91
3.0	44.89	46.05	-1.16	-0.5	43.04	46.05	-3.01
2.5	44.75	46.06	-1.31	-1.0	42.91	46.05	-3.14
2.0	44.37	46.06	-1.69	-1.5	43.03	46.04	-3.01
1.5	43.79	46.07	-2.28	-2.0	43.09	46.04	-2.95
1.0	43.31	46.08	-2.77	-2.5	43.31	46.03	-2.72
0.5	43.08	46.08	-3.00	-3.0	43.62	46.03	-2.41
0.0	43.14	46.09	-2.95	-3.5	43.90	46.02	-2.12
-0.5	43.18	46.10	-2.92	-4.0	44.24	46.02	-1.78
-1.0	43.22	46.10	-2.88	-4.5	44.40	46.01	-1.61
-1.5	43.94	46.11	-2.17	-5.0	45.32	46.01	-0.69
-2.0	44.66	46.12	-1.46	-5.5	45.71	46.01	-0.30
-2.5	44.91	46.12	-1.21	-6.0	45.99	46.00	-0.01
-3.0	45.19	46.13	-0.94	-6.1	46.00	46.00	0.00
-3.5	45.50	46.13	-0.63				
-4.0	45.76	46.14	-0.38				
-4.5	46.05	46.15	-0.10				
-4.7	46.15	46.15	0.00				

Test No. 4/10.0/17.9/1
 Clay M390
 Clay Lot No. 34281348
 Test Date: 14-Jul-99

Test Variables		
Q (L/s)	H (cm)	d (mm)
0.225	4	4

Lengthwise:	$\epsilon_{\rightarrow} = \epsilon_{\leftarrow}$		Widthwise:	$\epsilon_{\rightarrow} = \epsilon_{\leftarrow}$	
	$r_{0\rightarrow}$ (cm)			$r_{0\rightarrow}$ (cm)	
$r_{0\rightarrow}$ (cm)	2.20		$r_{0\rightarrow}$ (cm)	1.90	
$r_{0\leftarrow}$ (cm)	1.90		$r_{0\leftarrow}$ (cm)	1.90	
$\bar{r}_{0\rightarrow}$ (cm)	2.05		$\bar{r}_{0\rightarrow}$ (cm)	1.90	
ϵ_{\rightarrow} (cm)	-3.44		ϵ_{\rightarrow} (cm)	-3.44	
$\epsilon_{\rightarrow}/2$ (cm)	-1.719		$\epsilon_{\rightarrow}/2$ (cm)	-1.719	
b_{\rightarrow} (cm)	1.606		b_{\rightarrow} (cm)	1.197	
b_{\leftarrow} (cm)	1.638		b_{\leftarrow} (cm)	1.291	

Lengthwise section (14 Jul 99)				Widthwise section (14 Jul 99)			
r (cm)	Depth Reading (cm)	Int. Surface(cm)	ϵ_{-} (cm)	r (cm)	Depth Reading (cm)	Int. Surface(cm)	ϵ_{-} (cm)
2.5	46.07	46.07	0.00	2.0	46.07	46.07	0.00
2.2	46.06	46.07	-0.01	1.9	46.04	46.07	-0.03
2.0	45.92	46.07	-0.15	1.5	45.63	46.06	-0.43
1.5	43.92	46.06	-2.14	1.0	43.49	46.05	-2.56
1.0	43.16	46.06	-2.90	0.5	42.90	46.04	-3.14
0.5	42.73	46.05	-3.32	0.0	42.59	46.03	-3.44
0.0	42.61	46.05	-3.44	-0.5	42.70	46.02	-3.32
-0.5	42.69	46.04	-3.35	-1.0	43.01	46.01	-3.00
-1.0	42.99	46.04	-3.05	-1.5	45.20	46.00	-0.80
-1.5	43.41	46.03	-2.62	-1.9	45.99	45.99	0.00
-1.9	46.03	46.03	0.00				

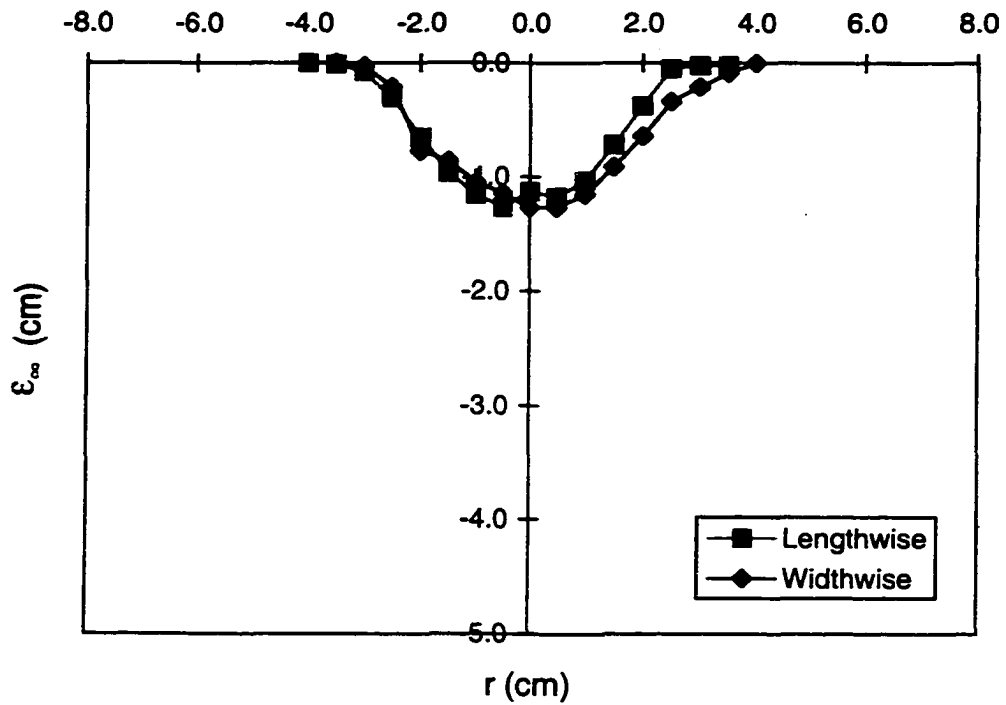


Fig. D-1: Impinging Jet Test (8/8.1/7.0/1): September 4, 1998 $Q=0.35$ L/s $H=6.5$ cm $d=8$ mm $X=734$ Pa

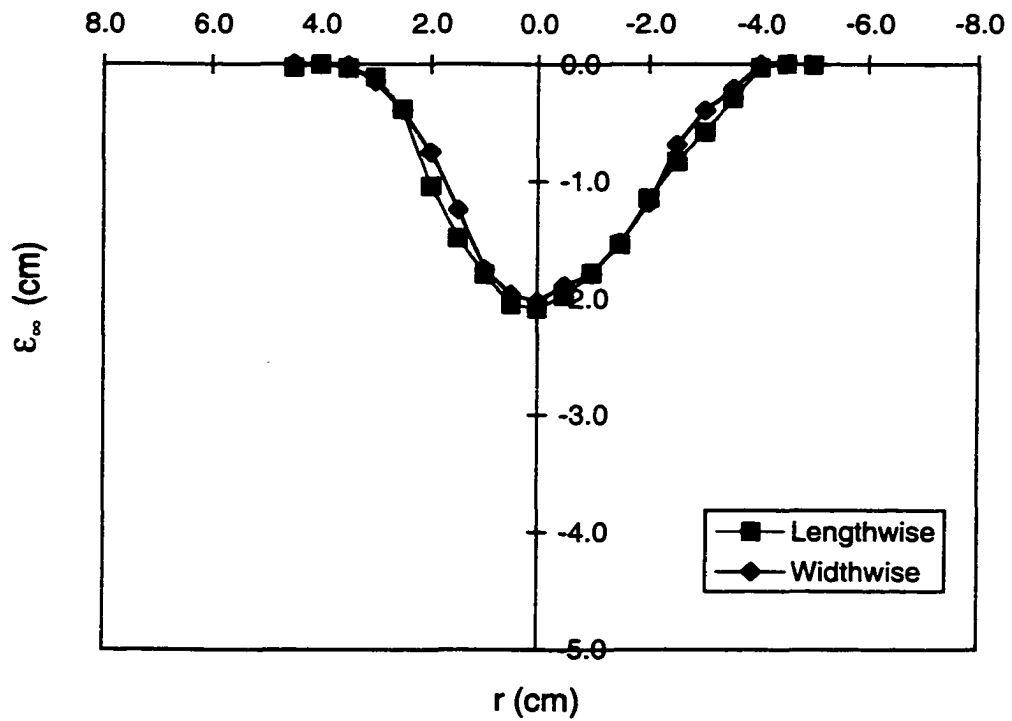


Fig. D-2: Impinging Jet Test (8/8.1/7.4/1): September 11, 1998 $Q=0.374$ L/s $H=6.5$ cm $d=8$ mm $X=839$ Pa

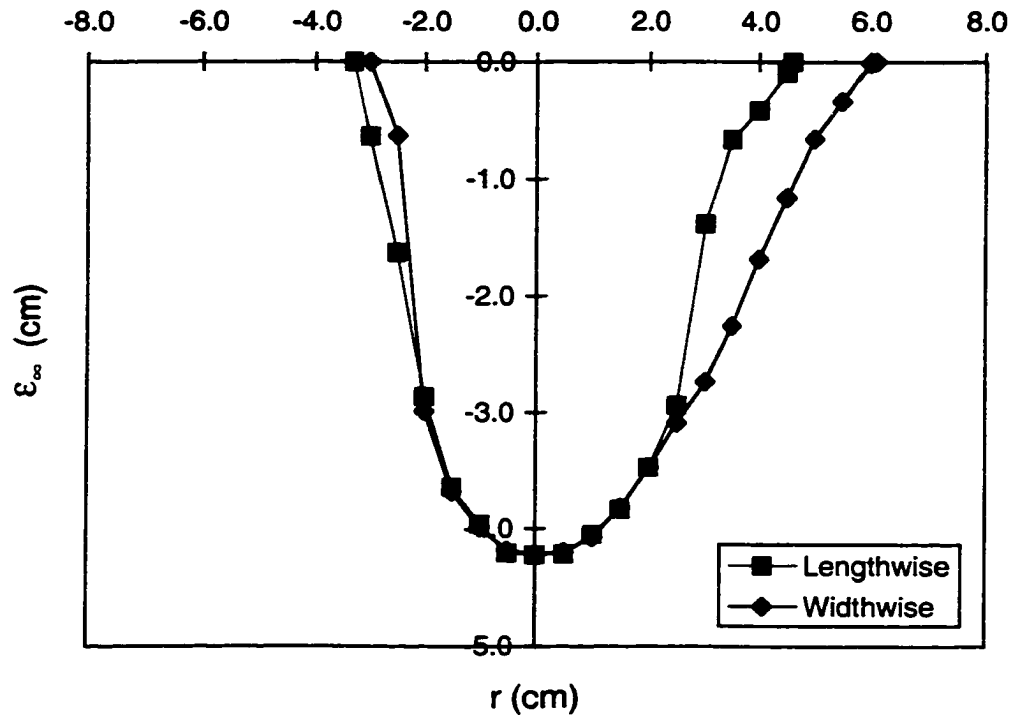


Fig. D-3: Impinging Jet Test (8/8.1/8.4/1): September 20, 1998 Q=0.40 L/s H=6.5 cm d=8 mm X=1058 Pa

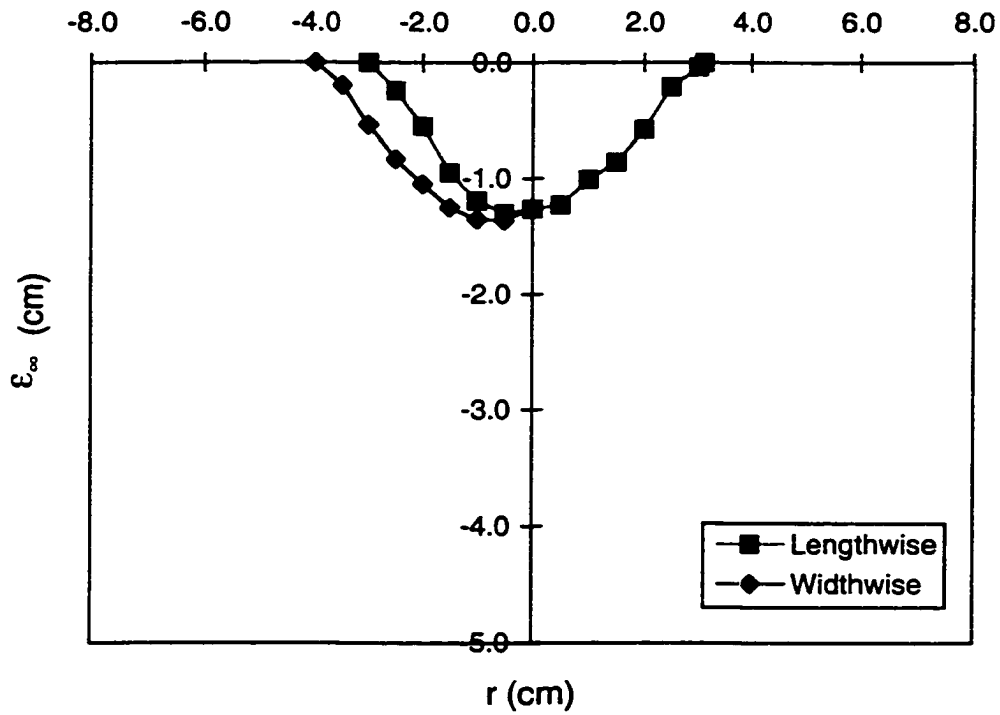


Fig. D-4: Impinging Jet Test (8/8.1/6.1/1): October 1, 1998 Q=0.31 L/s H=6.5 cm d=8 mm X=576 Pa

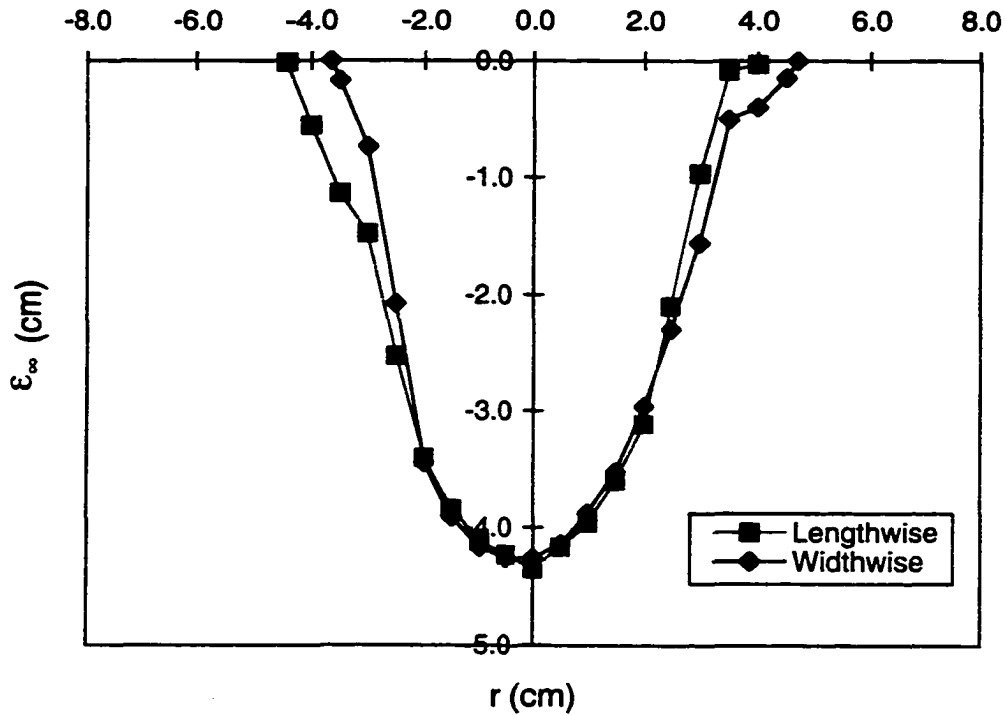


Fig. D-5: Impinging Jet Test (8/8.1/9.0/4): October 16, 1998 $Q=0.45$ L/s $H=6.5$ cm $d=8$ mm $X=1214$ Pa

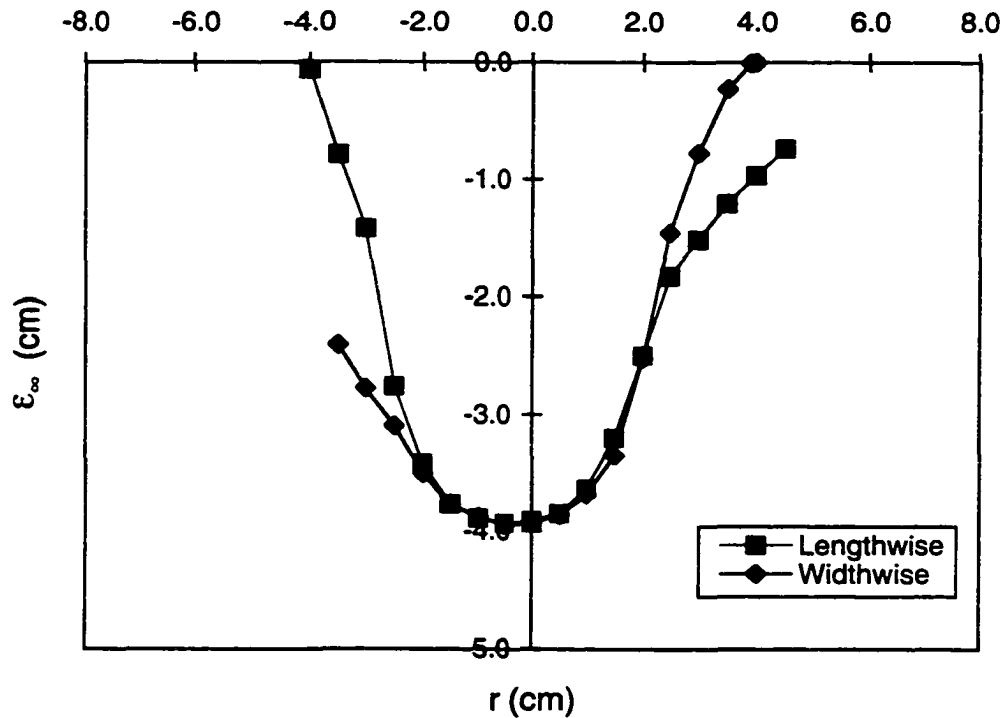


Fig. D-6: Impinging Jet Test (8/8.1/9.9/5): October 31, 1998 $Q=0.50$ L/s $H=6.5$ cm $d=8$ mm $X=1499$ Pa

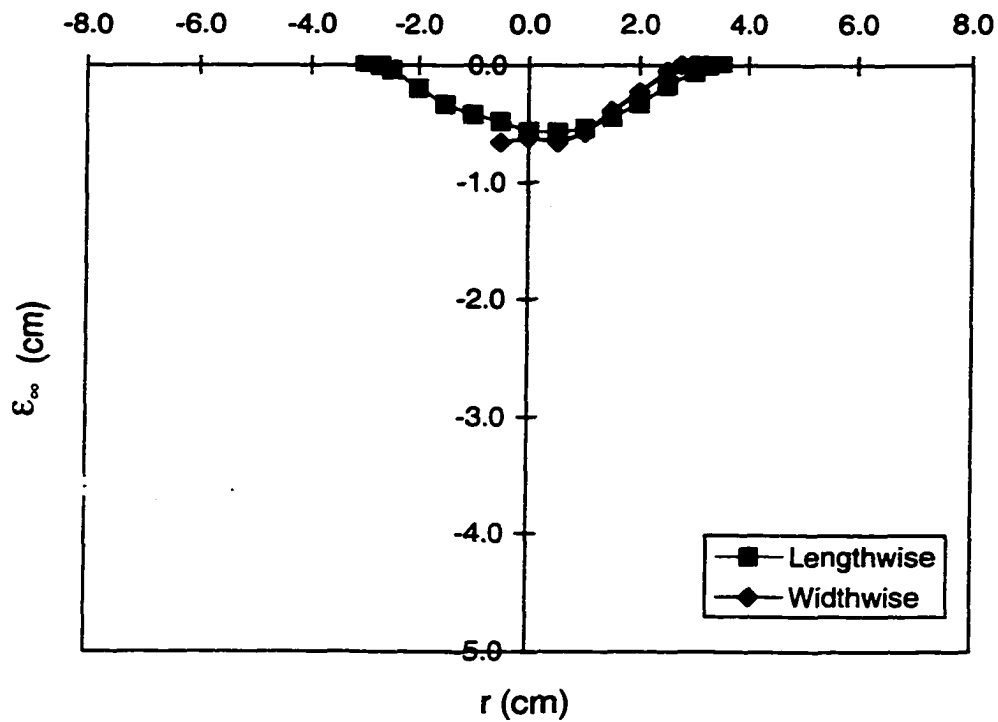


Fig. D-7: Impinging Jet Test (8/14.5/9.0/5): November 13, 1998 Q=0.45 L/s H=11.6 cm d=8 mm X=381 Pa

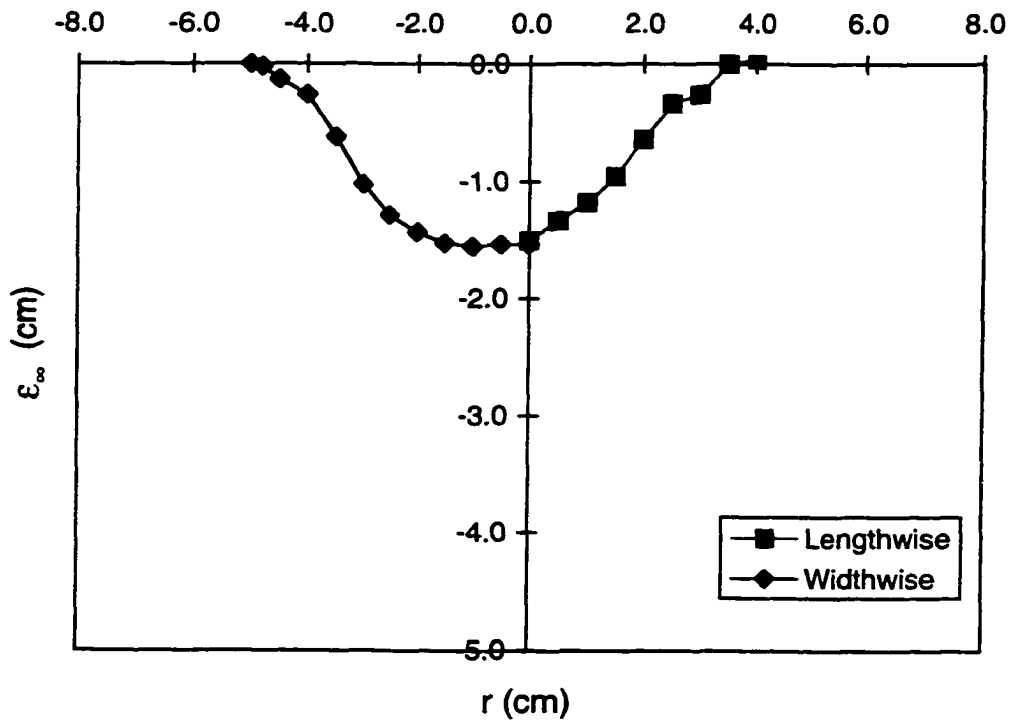


Fig. D-8: Impinging Jet Test (8/14.5/9.9/1): November 21, 1998 Q=0.5 L/s H=11.6 cm d=8 mm X=471 Pa

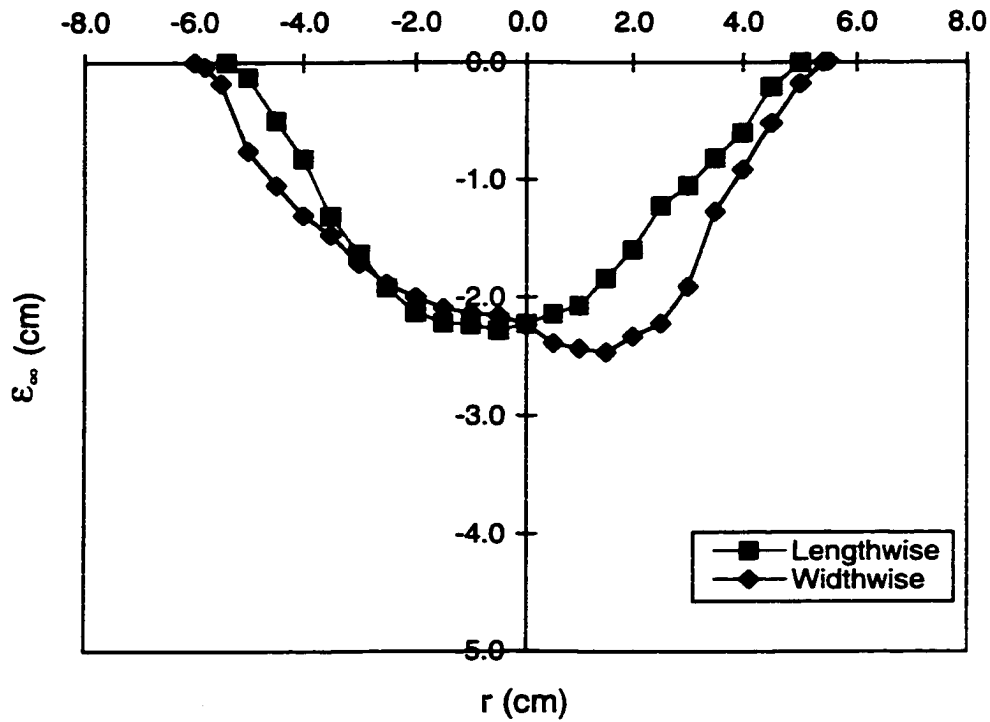


Fig. D-9: Impinging Jet Test (8/14.5/10.9/1): December 3, 1998 Q=0.55 L/s H=11.6 cm d=8 mm X=569 Pa

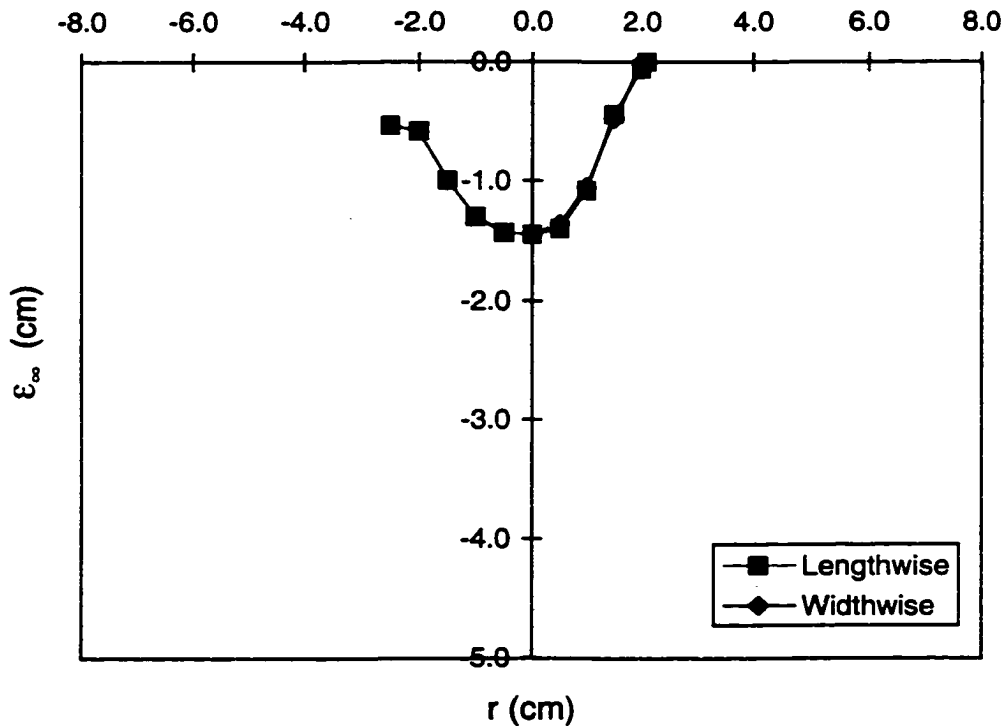


Fig. D-10: Impinging Jet Test (4/10.0/11.9/1): January 15, 1999 Q=0.15 L/s H=4.0 cm d=4 mm X=1424 Pa

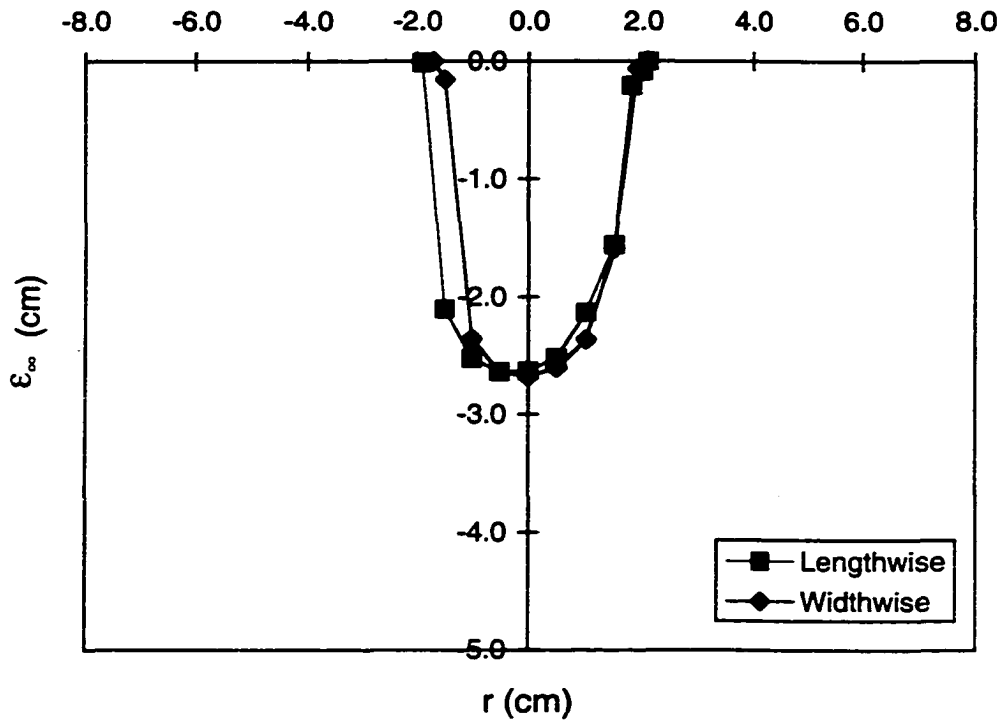


Fig. D-11: Impinging Jet Test (4/10.0/15.9/1): January 22, 1999 $Q=0.20$ L/s $H=4.0$ cm $d=4$ mm $X=2533$ Pa

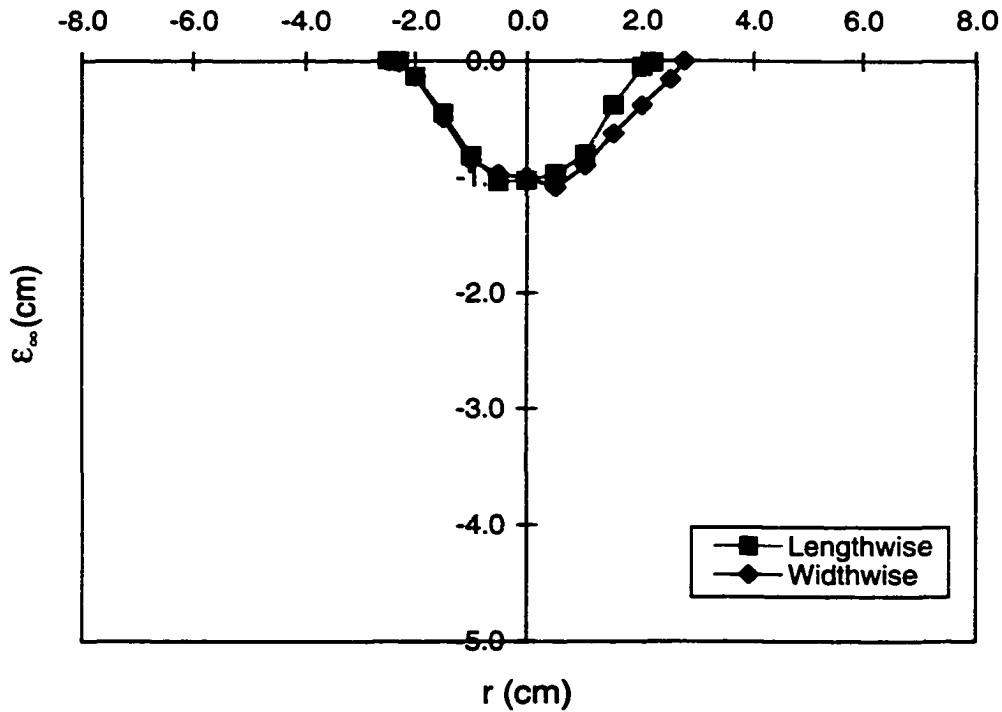


Fig. D-12: Impinging Jet Test (4/10.0/9.9/1): February 8, 1999 $Q=0.125$ L/s $H=4.0$ cm $d=4$ mm $X=989$ Pa

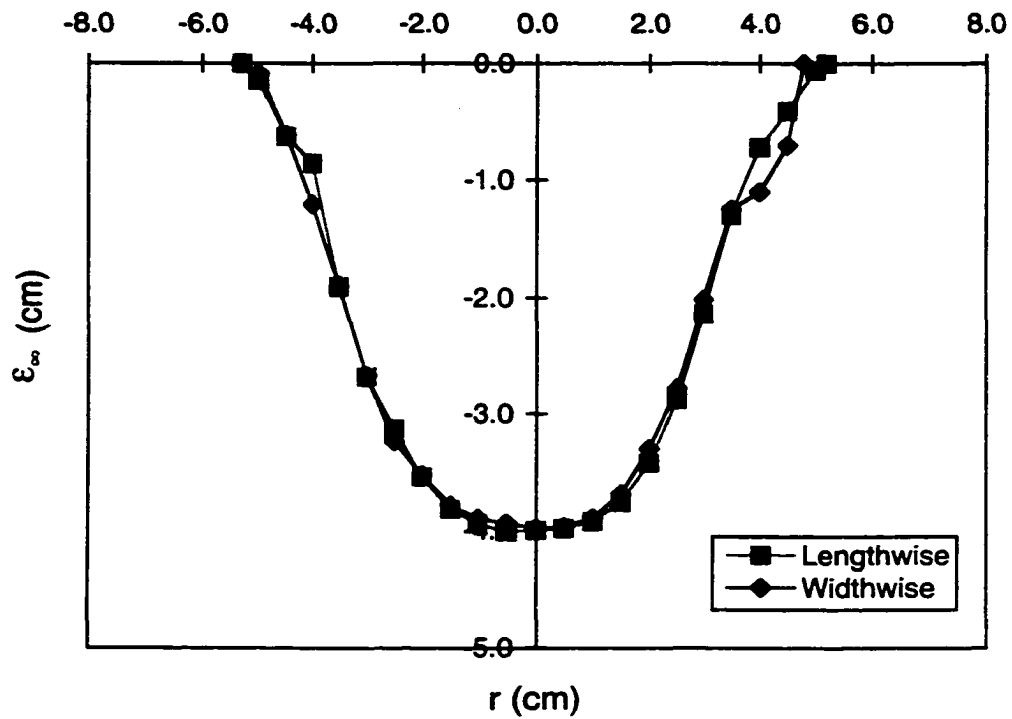


Fig. D-13: Impinging Jet Test (8/8.1/9.0/5): March 9, 1999 $Q=0.45$ L/s $H=6.5$ cm $d=8$ mm $X=1214$ Pa

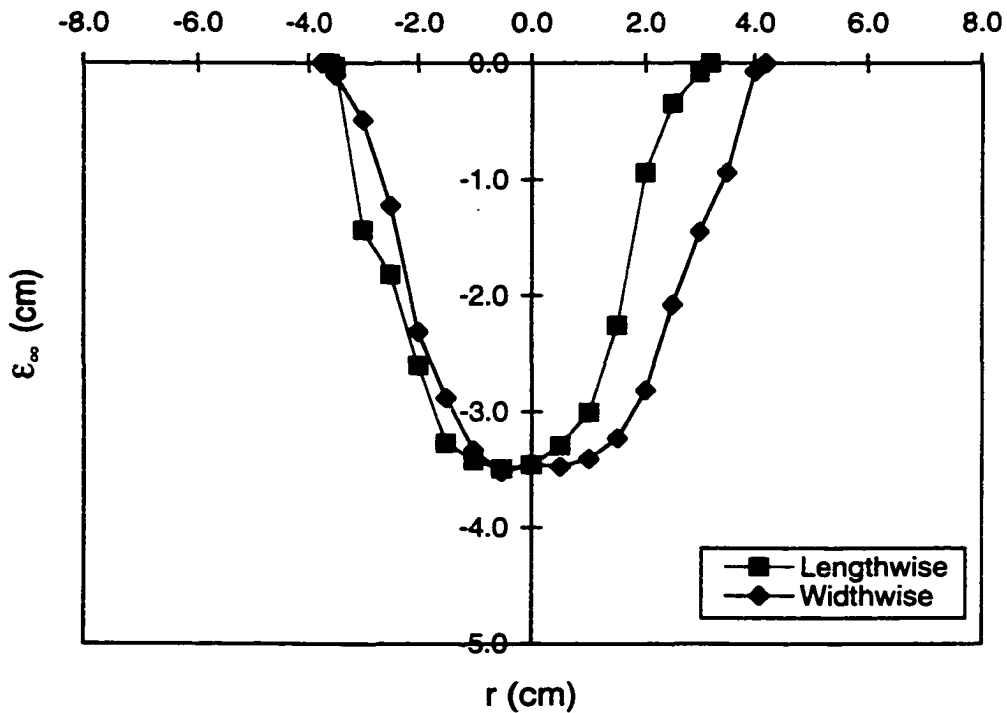


Fig. D-14: Impinging Jet Test (8/8.1/9.0/6): March 16, 1999 $Q=0.45$ L/s $H=6.6$ cm $d=8$ mm $X=1214$ Pa

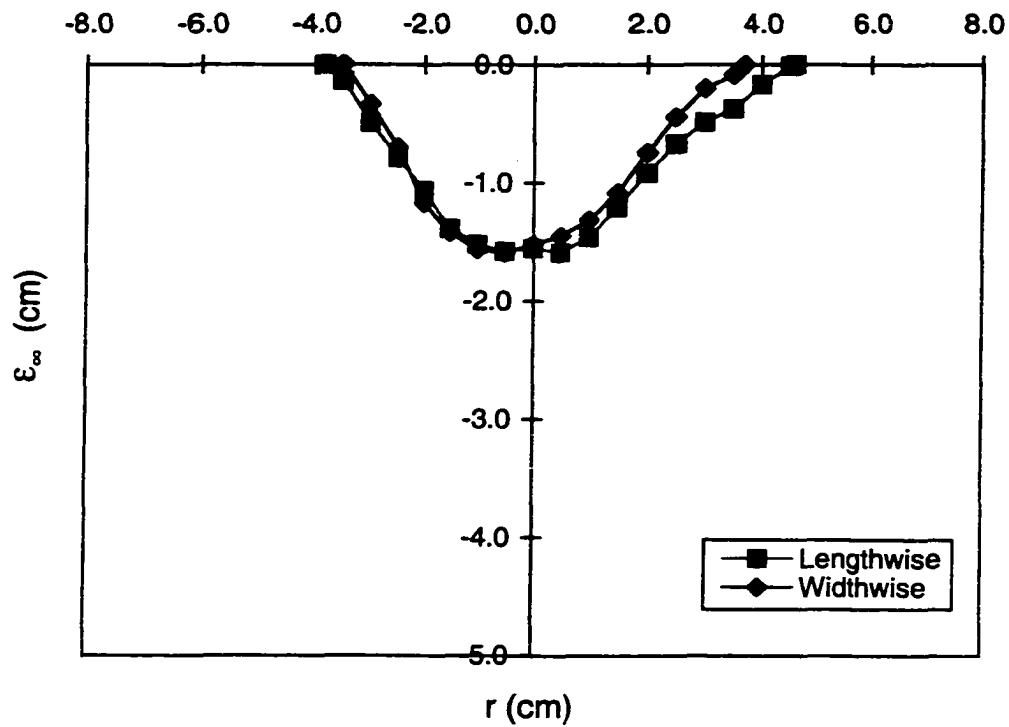


Fig. D-15: Impinging Jet Test (4/16.3/15.9/1): May 12, 1999 Q=0.2 L/s H=6.5 cm d=4 mm X=959 Pa

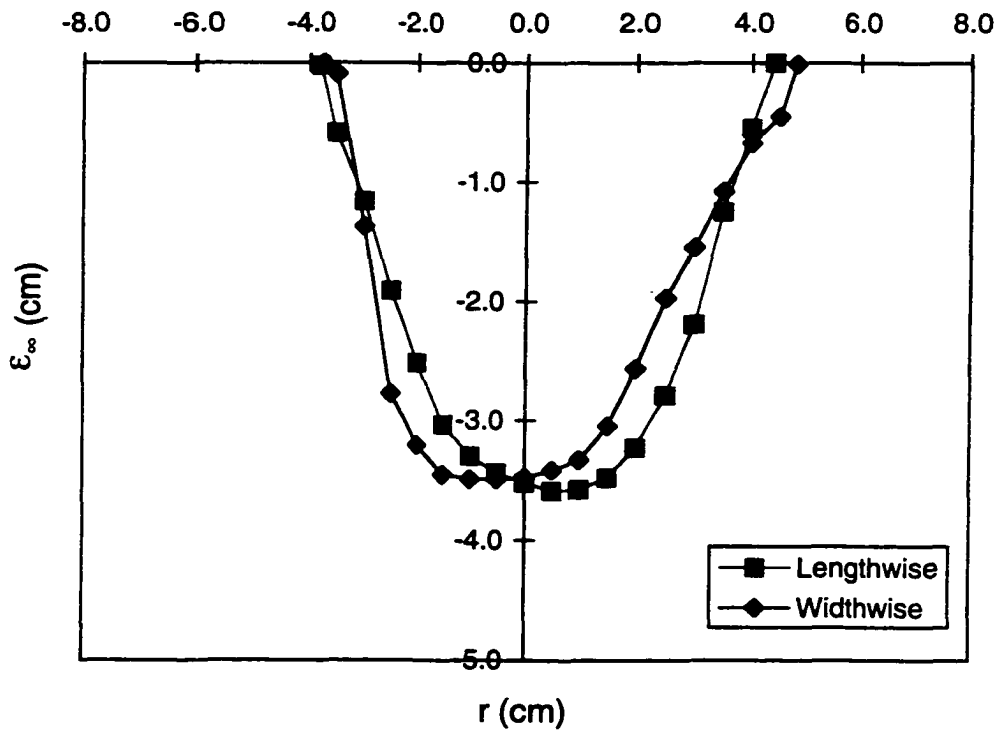


Fig. D-16: Impinging Jet Test (4/16.3/19.9/1): May 25, 1999 Q=0.25 L/s H=6.5 cm d=4 mm X=1499 Pa

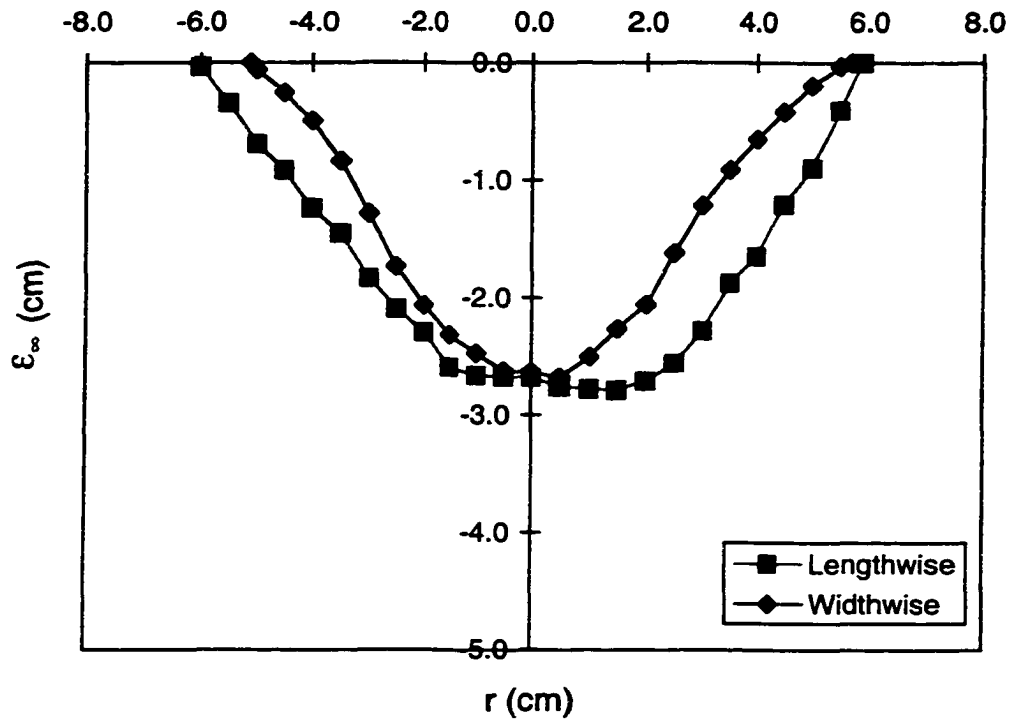


Fig. D-17: Impinging Jet Test (4/29.0/25.9/1): June 14, 1999 $Q=0.325$ L/s $H=11.6$ cm $d=4$ mm $X=795$ Pa

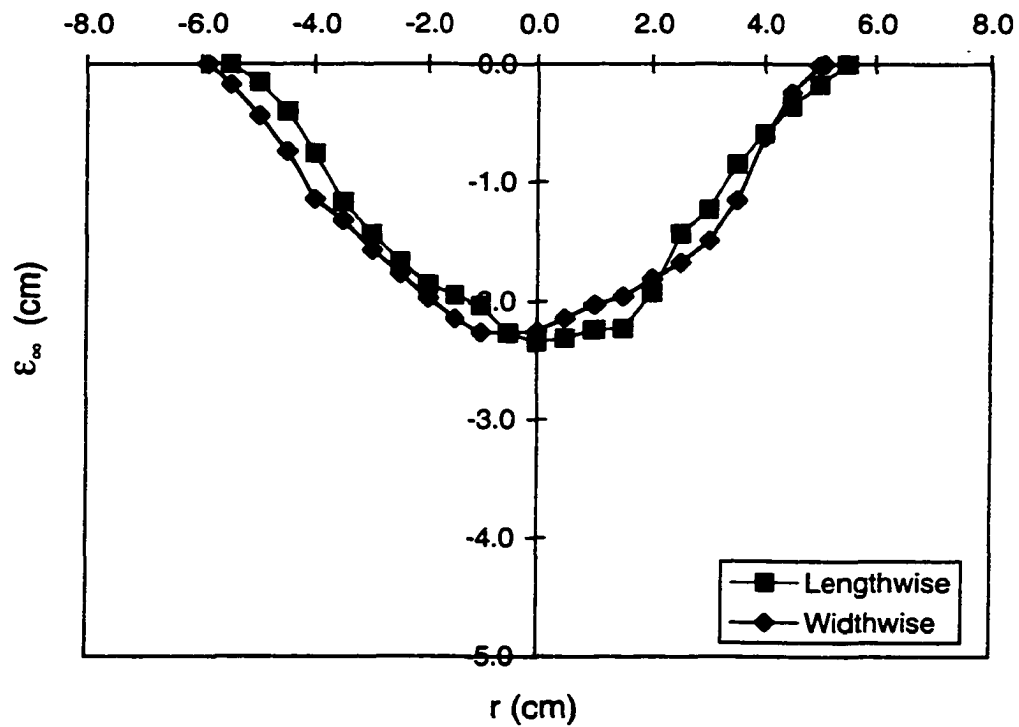


Fig. D-18: Impinging Jet Test (4/29.0/25.9/2): June 25, 1999 $Q=0.325$ L/s $H=11.6$ cm $d=4$ mm $X=795$ Pa

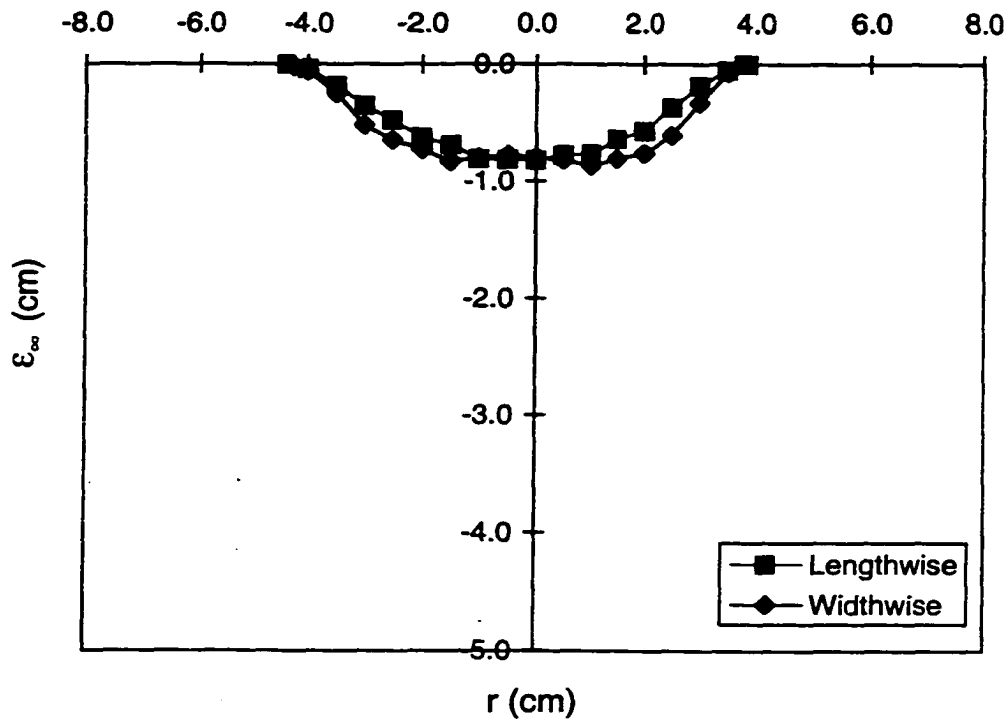


Fig. D-19: Impinging Jet Test (4/29.0/21.9/1): June 30, 1999 Q=0.275 L/s H=11.6 cm d=4 mm X=569 Pa

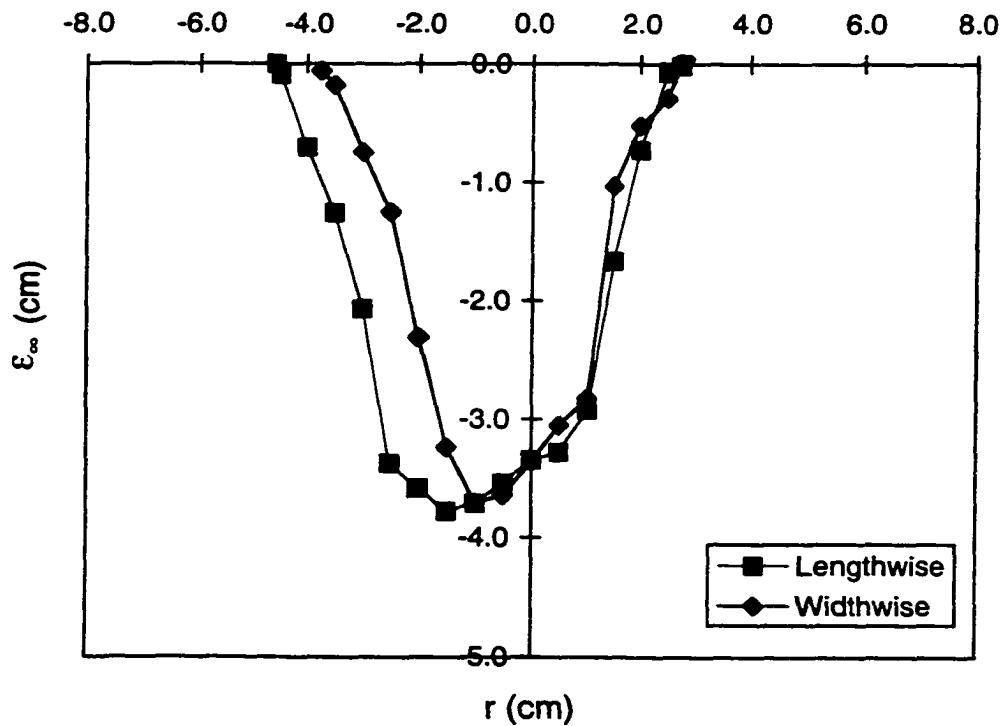


Fig. D-20: Impinging Jet Test (4/10.0/13.9/1): July 5, 1999 Q=0.175 L/s H=4.0 cm d=4 mm X=1939 Pa

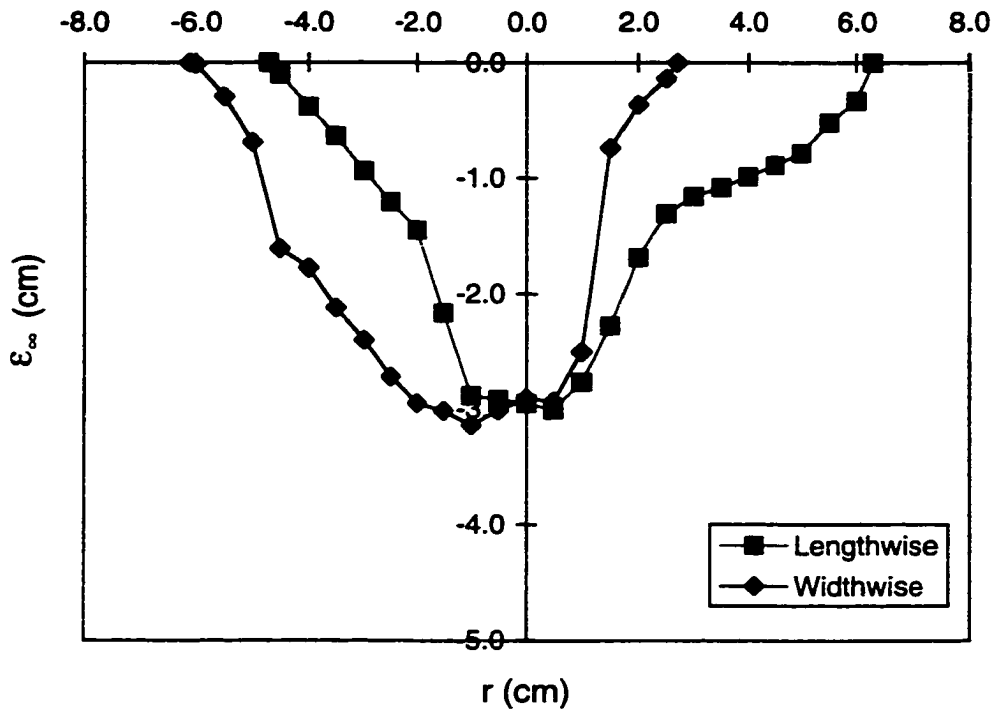


Fig. D-21: Impinging Jet Test (4/10.0/15.9/2): July 9, 1999 $Q=0.20$ L/s $H=4.0$ cm $d=4$ mm $X=2533$ Pa

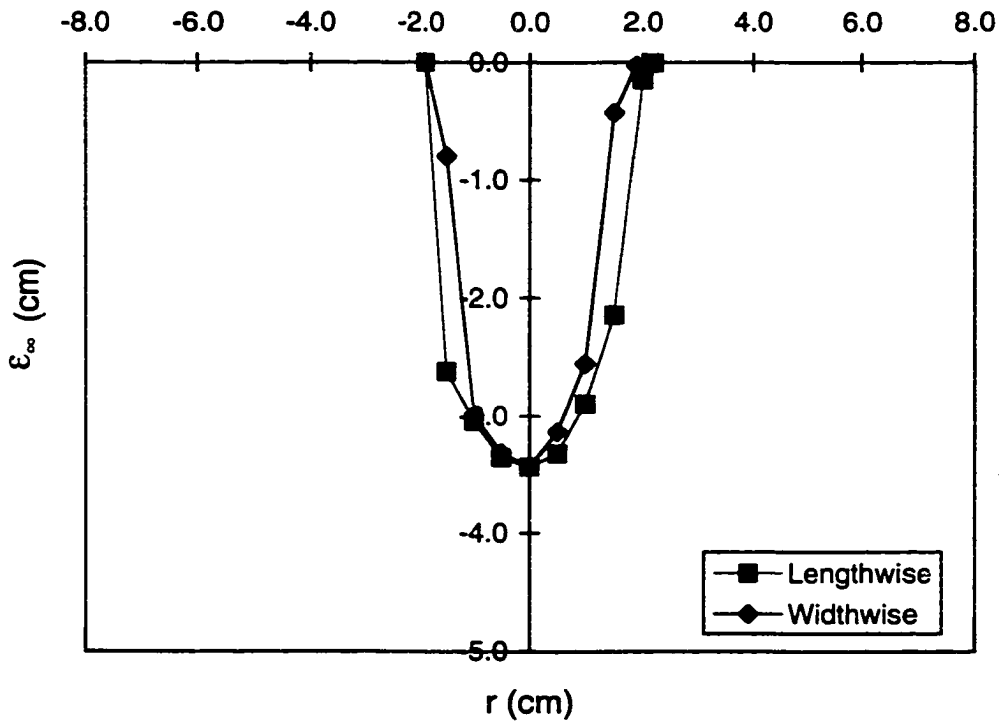


Fig. D-22: Impinging Jet Test (4/10.0/17.9/1): July 14, 1999 $Q=0.225$ L/s $H=4.0$ cm $d=4$ mm $X=3206$ Pa

Appendix E: Equilibrium dimensions of the scour holes for the wall jet tests.

Test No.	2.33/9.3/1	Test Variables		
Clay	M390	Q (L/s)	U _o (m/s)	a (mm)
Clay Lot No.	34281348	3.12	9.31	2.33
Test Date:	12-Nov-98			

Δh_m (mm)	326	
Section	1	2
Located at y (mm)	38.5	76.5
ϵ_{m-} (mm)	-20.6	-16.2
x_{m-} (mm)	20	27
x_{o-} (mm)	140	130
b (mm)	80.3	77.5

Section 1 (12 Nov 98)			Section 2 (12 Nov 98)		
x (mm)	Reading (cm)	ϵ_{-} (mm)	x (mm)	Reading (cm)	ϵ_{-} (mm)
0	44.66	-14.3	0	45.13	-9.8
10	44.17	-19.2	10	44.98	-11.3
15	44.04	-20.5	20	44.66	-14.5
20	44.03	-20.6	27	44.49	-16.2
30	44.21	-18.8	30	44.67	-14.4
40	44.52	-15.7	40	44.86	-12.5
50	44.55	-15.4	50	44.93	-11.8
60	44.69	-14.0	60	45.05	-10.6
70	44.79	-13.0	70	45.18	-9.3
80	45.05	-10.4	80	45.34	-7.7
90	45.35	-7.4	90	45.72	-3.9
100	45.53	-5.6	100	45.82	-2.9
110	45.71	-3.8	110	45.97	-1.4
120	45.74	-3.5	120	46.03	-0.8
130	45.94	-1.5	124	46.07	-0.4
137	46.05	-0.4	130	46.11	0.0
140	46.09	0.0			

Test No.	2.33/9.7/1	Test Variables		
Clay	M390	Q (L/s)	U _o (m/s)	a (mm)
Clay Lot No.	34281348	3.27	9.74	2.33
Test Date:	18-Nov-98			

Δh_m (mm)	357	
Section	1	2
Located at y (mm)	38.5	76.5
ϵ_{m-} (mm)	-31.3	-36.8
x_{m-} (mm)	38	43
x_{o-} (mm)	190	193
b (mm)	112.0	88.3

Section 1 (18 Nov 98)			Section 2 (18 Nov 98)		
x (mm)	Reading (cm)	ϵ_{-} (mm)	x (mm)	Reading (cm)	ϵ_{-} (mm)
0	44.15	-20.1	0	43.23	-29.5
13	43.63	-25.3	13	43.06	-31.2
23	43.19	-29.7	23	42.72	-34.6
33	43.09	-30.7	33	42.60	-35.8
38	43.03	-31.3	43	42.50	-36.8
43	43.07	-30.9	53	42.61	-35.7
53	43.28	-28.8	63	43.27	-29.1
63	43.66	-25.0	73	44.07	-21.1
73	43.89	-22.7	83	44.25	-19.3
83	44.03	-21.3	93	44.42	-17.6
93	44.19	-19.7	103	44.59	-15.9
103	44.38	-17.8	113	44.71	-14.7
113	44.62	-15.4	123	44.84	-13.4
123	44.74	-14.2	133	44.93	-12.5
133	44.79	-13.7	143	45.07	-11.1
143	45.06	-11.0	153	45.31	-8.7
153	45.21	-9.5	163	45.48	-7.0
163	45.42	-7.4	173	45.69	-4.9
173	45.73	-4.3	183	45.93	-2.5
183	45.96	-2.0	193	46.18	0.0
190	46.16	0.0			

Test No.	2.33/8.8/1	Test Variables	
Clay	M390	Q (L/s)	U _c (m/s)
Clay Lot No.	34281348	2.97	8.84
Test Date:	7-Dec-98	a (mm)	2.33

Test No.	2.33/8.1/1	Test Variables	
Clay	M390	Q (L/s)	U _c (m/s)
Clay Lot No.	34281348	2.73	8.13
Test Date:	14-Dec-98	a (mm)	2.33

Δh_w (mm)	294
Section	1
Located at y (mm)	38.5
ϵ_{max} (mm)	-16.0
x_{max} (mm)	30
x_{min} (mm)	97.5
b (mm)	61.1

Δh_w (mm)	249
Section	2
Located at y (mm)	76.5
ϵ_{max} (mm)	-14.1
x_{max} (mm)	7.5
x_{min} (mm)	108.0
b (mm)	56.5

Section 1 (7 Dec 98)			Section 2 (7 Dec 98)		
x (mm)	Reading (cm)	ϵ_w (mm)	x (mm)	Reading (cm)	ϵ_w (mm)
0	44.95	-9.4	0	45.86	-0.3
10	44.73	-11.8	10	45.05	-8.6
20	44.36	-15.7	20	44.19	-17.4
30	44.35	-16.0	30	44.07	-18.7
40	44.55	-14.1	40	44.32	-16.4
50	44.90	-10.8	50	44.74	-12.4
60	45.18	-8.2	60	45.09	-9.1
70	45.41	-6.1	70	45.29	-7.3
80	45.66	-3.8	80	45.46	-5.8
90	45.90	-1.6	90	45.70	-3.5
97.5	46.07	0.0	100	46.02	-0.5
			104	46.08	0.0

Section 2 (14 Dec 98)		
x (mm)	Reading (cm)	ϵ_w (mm)
0	45.03	-10.5
7.5	44.68	-14.1
10	44.71	-13.8
20	44.93	-11.7
30	45.32	-7.9
40	45.33	-7.9
50	45.41	-7.3
60	45.46	-6.9
70	45.52	-6.4
80	45.74	-4.3
90	45.76	-4.2
100	46.05	-1.4
108	46.20	0.0

Test No.	2.33/8.5/1	Test Variables	
Clay	M390	Q (L/s)	a (mm)
Clay Lot No.	34281348	U _s (m/s)	2.33
Test Date:	4-Jan-99		

Test No.	2.33/8.7/1	Test Variables	
Clay	M390	Q (L/s)	a (mm)
Clay Lot No.	34281348	U _s (m/s)	2.33
Test Date:	12-Jan-99		

Δh _m (mm)	273		
Section	1	2	
Located at y (mm)	38.5	76.5	
ε _m (mm)	-15.4	-22.9	
X _m (mm)	29	22.5	
X ₀ (mm)	122	122	
b (mm)	89.7	70.6	

Δh _m (mm)	283		
Section	2		
Located at y (mm)	76.5		
ε _m (mm)	-22.0		
X _m (mm)	23		
X ₀ (mm)	120		
b (mm)	59.2		

Section 1 (4 Jan 99)			Section 2 (4 Jan 99)		
x (mm)	Reading (cm)	ε _m (mm)	x (mm)	Reading (cm)	ε _m (mm)
0	45.59	-5.6	0	44.36	-18.7
10	45.72	-4.3	10	44.28	-19.5
20	44.89	-12.6	20	43.95	-22.8
29	44.61	-15.4	23	43.94	-22.9
30	44.63	-15.2	30	44.14	-20.9
40	44.86	-12.9	40	44.73	-15.0
50	44.88	-12.7	50	44.96	-12.7
60	44.87	-12.8	60	44.99	-12.4
70	44.93	-12.2	70	45.08	-11.5
80	45.09	-10.6	80	45.16	-10.7
90	45.39	-7.6	90	45.34	-8.9
100	45.72	-4.3	100	45.61	-6.2
110	45.77	-3.8	110	45.94	-2.9
120	46.13	-0.2	120	46.19	-0.4
122	46.15	0.0	122	46.23	0.0

Section 2 (12 Jan 99)		
x (mm)	Reading (cm)	ε _m (mm)
0	44.30	-18.9
10	44.29	-19.0
20	44.14	-20.5
23	43.99	-22.0
30	44.07	-21.2
40	44.43	-17.6
43	44.68	-15.1
50	44.74	-14.5
60	45.12	-10.7
70	45.14	-10.5
80	45.37	-8.2
90	45.61	-5.8
100	45.82	-3.7
110	46.00	-1.9
120	46.19	0.0

Test No.	2.337.4/1	Test Variables	
Clay	M390	Q (L/s)	U_e (m/s)
Clay Lot No.	34281348	2.47	7.36
Test Date:	22-Jan-99	ρU_e^2 (Pa)	

Test No.	2.33/8.1/2	Test Variables	
Clay	M390	Q (L/s)	U_e (m/s)
Clay Lot No.	34281348	2.70	8.05
Test Date:	28-Jan-99	a (mm)	2.33

Δh_a (mm)	204
Section	1 2
Located at y (mm)	38.5 76.5
ϵ_{max} (mm)	-12.5 -16.2
X_{max} (mm)	10 15
X_{min} (mm)	86 84
b (mm)	55.8 30.9

Δh_a (mm)	244
Section	1 2 3
Located at y (mm)	38.5 76.5 115
ϵ_{max} (mm)	-21.1 -18.6 -15.5
X_{max} (mm)	25 23 4
X_{min} (mm)	106 100 98
b (mm)	52.25 52.5 24.3

Section 1 (22 Jan 99)		Section 2 (22 Jan 99)	
x (mm)	Reading (cm)	ϵ_- (mm)	Reading (cm)
0	45.19	-9.7	44.75
10	44.91	-12.5	44.69
20	44.97	-11.9	44.48
28	45.36	-8.0	44.61
30	45.38	-7.8	45.21
40	45.44	-7.2	45.38
50	45.46	-7.0	45.50
60	45.59	-5.7	45.54
70	45.75	-4.1	45.77
80	45.99	-1.7	45.96
86	46.16	0.0	46.04
			84
			46.10
			0.0
			0.0

Section 1 (28 Jan 99)		Section 2 (28 Jan 99)		Section 3 (28 Jan 99)	
x (mm)	Reading (cm)	ϵ_- (mm)	Reading (cm)	x (mm)	Reading (cm)
0	44.83	-13.6	44.33	0	44.90
10	44.46	-17.3	44.46	10	44.68
20	44.11	-20.8	44.39	20	44.92
25	44.08	-21.1	44.37	28	45.29
30	44.34	-18.5	44.55	30	45.52
40	44.95	-12.4	45.01	40	45.47
44	45.08	-11.1	45.26	50	45.40
50	45.12	-10.7	45.42	60	45.39
60	45.19	-10.0	45.65	70	45.43
70	45.39	-8.0	45.88	80	45.64
80	45.59	-6.0	46.05	90	45.92
90	45.82	-3.7	46.23	100	46.14
100	46.06	-1.3		98	46.23
106	46.19	0.0			

Test No.	2.337,0/1	Test Variables	
Clay	M390	Q (L/s)	a (mm)
Clay Lot No.	34281348	U _s (m/s)	2.33
Test Date:	11-Feb-99		

Δh_{10} (mm)	198
Section	1 2
Located at y (mm)	45 72
ϵ_{100} (mm)	-14.4 -16.0
X_{100} (mm)	32.5 36.0
X_{50} (mm)	68 70
b (mm)	47.7 49.4

Section 1 (11 Feb 99)			Section 2 (11 Feb 99)		
x (mm)	Reading (cm)	ϵ_{-} (mm)	x (mm)	Reading (cm)	ϵ_{-} (mm)
0	45.92	-1.8	0	45.46	-6.5
10	45.61	-4.9	10	45.32	-7.9
20	45.11	-9.9	20	44.84	-12.7
30	44.80	-13.0	30	44.58	-15.3
32.5	44.66	-14.4	36	44.51	-16.0
40	44.97	-11.3	40	44.67	-14.4
50	45.50	-6.0	50	45.35	-7.6
60	45.88	-2.2	60	45.74	-3.7
68	46.10	0.0	70	46.11	0.0

Test No.	2.337,2/1	Test Variables	
Clay	M390	Q (L/s)	a (mm)
Clay Lot No.	34281348	U _s (m/s)	2.33
Test Date:	17-Feb-99		

Δh_{10} (mm)	108
Section	1 2
Located at y (mm)	59 83
ϵ_{100} (mm)	-12.3 -12.7
X_{100} (mm)	26.0 25.0
X_{50} (mm)	70 72
b (mm)	39.7 44.8

Section 1 (11 Feb 99)			Section 2 (11 Feb 99)		
x (mm)	Reading (cm)	ϵ_{-} (mm)	x (mm)	Reading (cm)	ϵ_{-} (mm)
0	45.33	-8.7	0	45.66	-5.4
10	45.37	-8.3	10	45.43	-7.7
20	45.01	-11.9	15	45.19	-10.1
26	44.97	-12.3	20	45.01	-11.9
30	45.01	-11.9	25	44.93	-12.7
35	45.22	-9.8	30	45.00	-12.0
40	45.61	-5.9	35	45.25	-9.5
45	45.86	-3.4	40	45.45	-7.5
50	45.96	-2.4	45	45.57	-6.3
55	46.07	-1.3	50	45.66	-5.4
60	46.17	-0.3	60	45.94	-2.6
65	46.17	-0.3	65	46.12	-0.8
70	46.20	0.0	70	46.18	-0.2
			72	46.20	0.0

Test No.	2.33/8.0/1	Test Variables	
Clay	M390	Q (L/s)	U _c (m/s)
Clay Lot No.	34281348	2.67	7.97
Test Date:	15-Mar-99	a (mm)	
Δh _m (mm)	258	2.33	

Test No.	2.33/8.5/2	Test Variables	
Clay	M390	Q (L/s)	U _c (m/s)
Clay Lot No.	34281348	2.84	8.46
Test Date:	30-Mar-99	a (mm)	
Δh _m (mm)	291	2.33	

Section	1	2
Located at y (mm)	61	76.5
ε _{max} (mm)	-55.4	-57.0
X _{max} (mm)	45	48.0
X _{min} (mm)	116	132.5
b (mm)	73.4	74.7

Section	1	2
Located at y (mm)	67	85
ε _{max} (mm)	-31.3	0.0
X _{max} (mm)	55	55.0
X _{min} (mm)	141	136.0
b (mm)	77.1	74.6

Section 1 (15 Mar 99)			Section 2 (15 Mar 99)		
x (mm)	Reading (cm)	ε ₋ (mm)	x (mm)	Reading (cm)	ε ₋ (mm)
0	44.42	-17.8	0	44.74	-15.5
5	44.32	-18.8	5	44.75	-15.4
10	44.28	-19.2	10	44.68	-16.1
15	43.54	-26.6	15	43.90	-23.9
20	42.99	-32.1	20	43.21	-30.8
25	42.46	-37.4	25	42.68	-36.1
30	41.90	-43.0	30	42.15	-41.4
35	41.58	-46.2	35	41.62	-46.7
40	41.19	-50.1	40	41.20	-50.9
45	40.66	-55.4	45	40.77	-55.2
50	41.01	-51.9	48	40.59	-57.0
55	41.57	-46.3	50	40.71	-55.8
60	41.92	-42.8	55	41.27	-50.2
65	42.32	-38.8	60	41.76	-45.3
70	42.88	-33.2	65	42.22	-40.7
75	43.68	-25.2	70	42.74	-35.5
80	44.59	-16.1	75	43.48	-28.1
85	45.00	-12.0	80	44.51	-17.8
90	45.23	-9.7	85	44.80	-14.9
95	45.59	-6.1	90	45.11	-11.8
100	45.70	-5.0	95	45.30	-9.9
105	45.76	-4.4	100	45.42	-8.7
110	46.00	-2.0	110	45.73	-5.6
115	46.22	0.2	120	46.10	-1.9
116	46.26	0.6	130	46.27	-0.2
			132.5	46.29	0.0

Section 1 (30 Mar 99)			Section 2 (30 Mar 99)		
x (mm)	Reading (cm)	ε ₋ (mm)	x (mm)	Reading (cm)	ε ₋ (mm)
0	42.17	-40.6	0	42.35	-39.3
10	42.06	-41.7	10	42.32	-39.6
15	42.02	-42.1	15	42.02	-42.6
20	41.70	-45.3	20	41.37	-49.1
25	41.17	-50.6	30	40.50	-57.8
35	40.53	-57.0	40	40.28	-60.0
45	40.22	-60.1	50	40.17	-61.1
50	40.11	-61.2	55	40.09	-61.9
55	40.09	-61.4	60	40.74	-55.4
60	40.74	-54.9	70	42.45	-38.3
70	41.95	-42.8	80	44.05	-22.3
80	43.66	-25.7	90	44.55	-17.3
85	44.52	-17.1	100	45.06	-12.2
90	44.73	-15.0	110	45.49	-7.9
100	45.19	-10.4	120	45.90	-3.8
110	45.57	-6.6	130	46.16	-1.2
120	45.85	-3.8	136	46.28	0.0
130	45.96	-2.7			
141	46.23	0.0			

Test No.	2.33/8.2/1	Test Variables		
Clay	M390	Q (L/s)	U _o (m/s)	a (mm)
Clay Lot No.	34281348	2.75	8.18	2.33
Test Date:	6-Apr-99			

Δh_m (mm)	272	
Section	1	2
Located at y (mm)	59	81
ϵ_{mm} (mm)	-31.3	0.0
x_{mm} (mm)	32	25
x_{om} (mm)	89	88
b (mm)	51.5	49.3

Section 1 (6 Apr 99)			Section 2 (6 Apr 99)		
x (mm)	Reading (cm)	ϵ_{--} (mm)	x (mm)	Reading (cm)	ϵ_{--} (mm)
0	44.67	-15.0	0	43.56	-26.2
10	44.72	-14.5	10	43.57	-26.1
20	44.31	-18.6	20	43.58	-26.0
30	43.85	-23.2	25	43.51	-26.7
32	43.84	-23.3	30	43.68	-25.0
35	43.91	-22.6	35	43.94	-22.4
40	44.06	-21.1	40	44.29	-18.9
50	44.91	-12.6	50	44.89	-12.9
55	45.23	-9.4	60	45.32	-8.6
60	45.26	-9.1	70	45.59	-5.9
70	45.74	-4.3	80	45.96	-2.2
80	46.02	-1.5	88	46.18	0.0
85	46.11	-0.6			
89	46.17	0.0			

Test No.	2.33/9.5/1	Test Variables		
Clay	M390	Q (L/s)	U _o (m/s)	a (mm)
Clay Lot No.	34281348	3.19	9.50	2.33
Test Date:	13-Apr-99			

Δh_m (mm)	367	
Section	1	2
Located at y (mm)	62	83
ϵ_{mm} (mm)	-31.3	0.0
x_{mm} (mm)	25	30
x_{om} (mm)	147	120
b (mm)	67.4	68.5

Section 1 (13 Apr 99)			Section 2 (13 Apr 99)		
x (mm)	Reading (cm)	ϵ_{--} (mm)	x (mm)	Reading (cm)	ϵ_{--} (mm)
0	41.69	-43.1	0	41.36	-46.4
10	41.60	-44.1	10	41.21	-48.0
15	41.60	-44.2	15	41.17	-48.5
20	41.32	-47.0	20	41.01	-50.2
25	41.23	-48.0	25	40.86	-51.7
30	41.35	-46.9	30	40.82	-52.2
35	41.27	-47.7	35	40.87	-51.8
40	41.27	-47.8	40	40.85	-52.0
45	41.51	-45.5	45	41.15	-49.1
50	41.73	-43.3	50	41.48	-45.9
60	42.67	-34.0	60	42.38	-37.0
70	44.05	-20.4	70	43.67	-24.2
80	44.73	-13.7	80	44.51	-16.0
90	45.32	-7.9	90	45.16	-9.6
110	45.73	-4.0	110	45.90	-2.5
120	45.78	-3.7	120	46.16	0.0
130	45.89	-2.7			
140	46.06	-1.1			
147	46.18	0.0			

Test No.	2.33/9.8/1	Test Variables		
Clay	M390	Q (L/s)	U _o (m/s)	a (mm)
Clay Lot No.	34281348	3.31	9.85	2.33

Test Date: 3-May-99

Δh _m (mm)	394	
Section	1	2
Located at y (mm)	82	107
ε _m (mm)	-31.3	0.0
x _m (mm)	40	42
x _o (mm)	107	116
b (mm)	63.0	64.1

Section 1 (3 May 99)			Section 2 (3 May 99)		
x (mm)	Reading (cm)	ε _m (mm)	x (mm)	Reading (cm)	ε _m (mm)
0	44.81	-13.7	0	44.36	-18.2
5	44.74	-14.4	5	44.29	-18.9
10	44.63	-15.5	10	44.16	-20.2
15	44.53	-16.5	15	43.96	-22.2
20	43.80	-23.8	20	43.54	-26.4
25	43.35	-28.3	25	43.22	-29.6
30	43.19	-29.9	30	42.95	-32.3
35	43.09	-30.9	35	42.81	-33.7
40	43.05	-31.3	40	42.65	-35.3
45	43.29	-28.9	42	42.64	-35.4
50	43.67	-25.1	45	42.74	-34.4
60	44.47	-17.1	50	43.06	-31.2
70	44.96	-12.2	60	43.99	-21.9
80	45.33	-8.5	65	44.50	-16.8
90	45.76	-4.2	70	44.75	-14.3
100	46.05	-1.3	80	45.09	-10.9
107	46.18	0.0	90	45.30	-8.8
			100	45.82	-3.6
			110	46.15	-0.3
			116	46.18	0.0

Test No.	2.33/11.3/1	Test Variables		
Clay	M390	Q (L/s)	U _o (m/s)	a (mm)
Clay Lot No.	34281348	3.80	11.31	2.33

Test Date: 13-May-99

Δh _m (mm)	520	
Section	1	2
Located at y (mm)	56.5	78
ε _m (mm)	-59.4	-60.4
x _m (mm)	60	60
x _o (mm)	155	180
b (mm)	92.8	94.9

Section 1 (13 May 99)			Section 2 (13 May 99)		
x (mm)	Reading (cm)	ε _m (mm)	x (mm)	Reading (cm)	ε _m (mm)
0	42.58	-35.5	0	42.44	-37.4
10	42.19	-39.4	10	42.02	-41.6
20	41.81	-43.2	20	41.74	-44.4
30	41.31	-48.2	30	41.30	-48.8
40	40.76	-53.7	40	40.87	-53.1
50	40.46	-56.7	50	40.49	-56.9
60	40.19	-59.4	60	40.14	-60.4
65	40.22	-59.1	61	40.15	-60.3
70	40.53	-56.0	65	40.25	-59.3
75	40.91	-52.2	70	40.45	-57.3
80	41.51	-46.2	75	40.91	-52.7
90	42.85	-32.8	80	41.23	-49.5
100	43.96	-21.7	85	41.81	-43.7
105	44.29	-18.4	90	42.49	-36.9
110	44.56	-15.7	100	43.87	-23.1
115	44.85	-12.8	105	44.51	-16.7
120	45.08	-10.5	110	44.77	-14.1
130	45.48	-6.5	120	45.19	-9.9
140	45.71	-4.2	130	45.37	-8.1
150	45.96	-1.7	140	45.41	-7.7
155	46.13	0.0	150	45.59	-5.9
			160	45.72	-4.6
			170	46.09	-0.9
			180	46.18	0.0

Test No. 2.33/8.9/1
 Clay M390
 Clay Lot No. 34281348
 Test Date: 19-May-99

Test Variables		
Q (L/s)	U _o (m/s)	a (mm)
3.03	9.03	2.33

Section	1	2
Located at y (mm)	50	85
E _{m=} (mm)	-19.7	-23.7
x _{m=} (mm)	32	32
x _{o=} (mm)	122.5	132
b (mm)	79.5	68.2

Section 1 (19 May 99)			Section 2 (19 May 99)		
x (mm)	Reading (cm)	E ₋ (mm)	x (mm)	Reading (cm)	E ₋ (mm)
0	44.98	-11.9	0	44.44	-17.5
10	45.11	-10.6	10	44.32	-18.7
15	44.95	-12.2	15	44.13	-20.6
20	44.59	-15.8	20	43.95	-22.4
25	44.30	-18.7	25	43.85	-23.4
30	44.22	-19.5	30	43.83	-23.6
32	44.20	-19.7	32	43.82	-23.7
35	44.25	-19.2	40	43.90	-22.9
40	44.56	-16.1	45	44.77	-14.2
45	44.91	-12.6	50	44.85	-13.4
50	45.06	-11.1	60	44.85	-13.4
60	45.10	-10.7	70	45.04	-11.5
70	45.06	-10.9	80	45.12	-10.7
80	45.19	-9.8	90	45.21	-9.8
90	45.39	-7.8	100	45.38	-8.1
100	45.56	-6.1	110	45.69	-5.0
110	45.83	-3.4	120	45.99	-2.0
120	46.15	-0.2	130	46.17	-0.2
122.5	46.17	0.0	132	46.19	0.0

Test No. 2.33/10.2/1
 Clay M390
 Clay Lot No. 34281348
 Test Date: 25-May-99

Test Variables		
Q (L/s)	U _o (m/s)	a (mm)
3.43	10.23	2.33

Section	1	2
Located at y (mm)	53	94.5
E _{m=} (mm)	-40.5	-40.7
x _{m=} (mm)	41	38
x _{o=} (mm)	175	152
b (mm)	87.2	89.3

Section 1 (25 May 99)			Section 2 (25 May 99)		
x (mm)	Reading (cm)	E ₋ (mm)	x (mm)	Reading (cm)	E ₋ (mm)
0	42.97	-32.5	0	42.91	-33.7
10	42.87	-33.5	10	42.93	-33.5
20	42.78	-34.4	15	42.82	-34.6
25	42.63	-35.9	20	42.61	-36.7
30	42.48	-37.4	25	42.47	-38.1
35	42.25	-39.7	30	42.31	-39.7
40	42.20	-40.2	35	42.22	-40.6
41	42.17	-40.5	37.5	42.21	-40.7
45	42.25	-39.7	40	42.23	-40.5
50	42.32	-39.0	45	42.30	-39.8
60	42.46	-37.6	50	42.44	-38.4
65	42.69	-35.3	55	42.70	-35.8
70	43.00	-32.2	60	42.96	-33.2
75	43.49	-27.3	70	43.42	-28.6
80	43.87	-23.5	80	43.92	-23.6
90	44.32	-19.0	90	44.27	-20.1
100	44.46	-17.6	100	44.74	-15.4
110	44.64	-15.8	110	45.20	-10.8
120	44.93	-12.9	120	45.52	-7.6
130	45.12	-11.0	130	45.93	-3.5
140	45.56	-6.6	140	46.08	-2.0
150	45.81	-6.1	150	46.27	-0.1
160	45.85	-3.7	152	46.28	0.0
170	46.17	-0.5			
175	46.22	0.0			

Test No.	2.33/6.2/1	Test Variables		
Clay	M390	Q (L/s)	U _s (m/s)	a (mm)
Clay Lot No.	34281348	2.07	6.16	2.33

Test Date: 8-Jun-99

Δh_m (mm) 154

Section	1
Located at y (mm)	71.5
$\epsilon_{m=}$ (mm)	-14.6
$x_{m=}$ (mm)	7
$x_{o=}$ (mm)	67
b (mm)	21.8

Section 1 (8 Jun 99)		
x (mm)	Reading (cm)	$\epsilon_{=}$ (mm)
0	44.67	-15.0
5	44.68	-14.9
7	44.71	-14.6
10	44.74	-14.3
15	44.86	-13.1
20	45.28	-8.9
23	45.54	-6.3
25	45.60	-5.7
30	45.64	-5.3
35	45.70	-4.7
45	45.90	-2.7
55	46.02	-1.5
65	46.15	-0.2
67	46.17	0.0

Test No.	2.33/8.0/2	Test Variables		
Clay	M390	Q (L/s)	U _s (m/s)	a (mm)
Clay Lot No.	34281348	2.69	8.00	2.33

Test Date: 15-Jun-99

Δh_m (mm) 260

Section	1	2
Located at y (mm)	59.5	96.5
$\epsilon_{m=}$ (mm)	-17.4	-17.1
$x_{m=}$ (mm)	24	21
$x_{o=}$ (mm)	67.0	70
b (mm)	38.7	38.1

Section 1 (15 Jun 99)			Section 2 (15 Jun 99)		
x (mm)	Reading (cm)	$\epsilon_{=}$ (mm)	x (mm)	Reading (cm)	$\epsilon_{=}$ (mm)
0	45.85	-2.6	0	45.68	-4.6
5	45.61	-5.0	5	45.62	-5.2
10	45.26	-8.5	10	44.94	-12.0
15	44.85	-12.6	15	44.59	-15.5
20	44.46	-16.5	20	44.45	-16.9
24	44.37	-17.4	21	44.43	-17.1
25	44.41	-17.0	25	44.56	-15.8
30	44.64	-14.7	30	44.99	-11.5
35	44.96	-11.5	35	45.23	-9.1
40	45.34	-7.7	40	45.32	-8.2
45	45.60	-5.1	45	45.46	-6.8
50	45.76	-3.5	50	45.57	-5.7
55	45.91	-2.0	55	45.75	-3.9
60	46.00	-1.1	60	45.95	-1.9
65	46.09	-0.2	65	46.05	-0.9
67	46.11	0.0	70	46.11	-0.3
			75	46.14	0.0

Test No. 2.33/12.0/1
 Clay M390
 Clay Lot No. 34281348
 Test Date: 25-Jun-99

Test Variables		
Q (L/s)	U _o (m/s)	a (mm)
4.04	12.03	2.33

Δh_m (mm) 588

Section	1	2
Located at y (mm)	52	76.5
ε _m (mm)	-40.7	-42.9
x _m (mm)	42.5	32
x _o (mm)	138.0	144
b (mm)	80.5	86.7

* section 1 is most representative section (42.5 mm as minimum)

Section 1 (25 Jun 99)			Section 2 (25 Jun 99)		
x (mm)	Reading (cm)	ε _m (mm)	x (mm)	Reading (cm)	ε _m (mm)
0	43.91	-22.7	0	44.81	-16.1
5	43.76	-24.2	5	44.46	-17.6
10	43.53	-26.5	10	43.77	-24.5
15	43.19	-29.9	15	43.02	-32.0
20	42.84	-33.4	20	42.65	-35.7
25	42.51	-36.7	25	42.22	-40.0
30	42.38	-38.0	30	41.95	-42.7
35	42.17	-40.1	32	41.93	-42.9
40	42.12	-40.6	35	41.95	-42.7
42.5	42.11	-40.7	40	41.96	-42.6
45	42.20	-39.8	45	42.09	-41.3
50	42.25	-39.3	50	42.20	-40.2
55	42.50	-36.8	55	42.36	-38.6
60	42.69	-34.9	60	42.58	-36.4
70	43.28	-29.2	70	43.08	-31.4
80	44.12	-20.6	80	43.72	-25.0
90	44.65	-15.3	90	44.25	-19.7
100	45.05	-11.3	100	44.93	-12.9
110	45.40	-7.8	110	45.24	-9.8
120	45.70	-4.8	120	45.66	-5.6
130	45.97	-2.1	130	45.76	-4.6
138	46.18	0.0	140	46.12	-1.0
			144	46.22	0.0

Test No. 2.33/12.7/1
 Clay M390
 Clay Lot No. 34281348
 Test Date: 9-Jul-99

Test Variables		
Q (L/s)	U _o (m/s)	a (mm)
4.27	12.72	2.33

Δh_m (mm) 657

Section	1	2
Located at y (mm)	51	96.0
ε _m (mm)	-80.8	-68.7
x _m (mm)	81	63
x _o (mm)	past end	past end
b (mm)	166.6	147.4

Section 1 (9 Jul 99)			Section 2 (9 Jul 99)		
x (mm)	Reading (cm)	ε _m (mm)	x (mm)	Reading (cm)	ε _m (mm)
0	41.30	-47.5	0	41.27	-47.5
10	41.17	-48.8	10	41.10	-49.3
20	40.82	-52.4	15	41.05	-49.8
25	40.57	-54.9	25	40.50	-55.3
30	40.16	-59.0	35	40.10	-59.4
35	39.49	-65.8	45	39.59	-64.6
45	38.76	-73.1	55	39.31	-67.4
55	38.56	-75.2	63	39.19	-68.7
65	38.28	-78.0	65	39.24	-68.2
75	38.02	-80.7	75	39.28	-67.8
81	38.01	-80.8	85	39.51	-65.6
85	38.03	-80.6	95	40.17	-59.0
95	38.04	-80.6	105	41.10	-49.8
105	38.11	-79.9	115	41.57	-45.2
115	38.22	-78.9	125	41.91	-41.8
125	38.47	-76.4	135	42.19	-39.1
135	39.49	-66.3	145	42.54	-35.6
145	40.06	-60.6	155	43.09	-30.2
155	41.13	-50.0	165	43.62	-25.0
165	41.97	-41.6	175	44.31	-18.1
175	42.72	-34.2	185	44.87	-12.6
185	43.42	-27.2	195	45.23	-9.0
195	43.95	-22.0	205	45.47	-6.7
205	44.31	-18.4	215	45.63	-5.1
215	44.65	-15.1	225	45.71	-4.4
225	45.02	-11.4	234	45.77	-3.9
235	45.34	-8.3	240	45.82	-3.4
240	45.42	-7.5			

Test No. 2.33/12.3/1
 Clay M390
 Clay Lot No. 34281348
 Test Date: 15-Jul-99

Test Variables		
Q (L/s)	U ₀ (m/s)	a (mm)
4.11	12.25	2.33

Δh _m (mm)	610	
Section	1	2
Located at y (mm)	54	96
ε _{m=} (mm)	-60.0	-44.3
x _{m=} (mm)	45	35
x ₀₌ (mm)	past end	past end
b (mm)	81.8	129.4

Section 1 (15 Jul 99)			Section 2 (15 Jul 99)		
x (mm)	Reading (cm)	ε _m (mm)	x (mm)	Reading	ε _m (mm)
0	41.83	-42.4	0	42.14	-40.1
10	41.72	-43.5	5	42.13	-40.2
15	41.36	-47.1	10	41.92	-42.2
20	41.17	-49.0	15	41.76	-43.8
25	40.75	-53.2	20	41.73	-44.0
30	40.61	-54.6	25	41.75	-43.8
35	40.35	-57.2	30	41.70	-44.3
40	40.22	-58.5	35	41.69	-44.3
45	40.07	-60.0	40	41.77	-43.5
50	40.09	-59.8	45	41.79	-43.2
55	40.16	-59.1	50	41.84	-42.7
60	40.44	-56.3	55	42.15	-39.6
70	41.54	-45.3	60	42.55	-35.5
80	42.80	-31.7	65	42.91	-31.9
85	43.37	-27.0	70	43.05	-30.5
90	43.59	-24.8	75	43.11	-29.8
100	43.94	-21.3	80	43.06	-30.3
110	44.16	-19.1	90	43.15	-29.3
120	44.34	-17.3	100	43.21	-28.6
130	44.53	-15.3	110	43.53	-25.3
140	44.77	-12.9	120	43.56	-25.0
150	44.92	-11.4	130	43.85	-22.0
160	45.05	-10.1	140	43.98	-20.6
170	45.23	-8.3	150	44.26	-17.7
180	45.46	-6.0	160	44.55	-14.7
190	45.50	-5.6	170	44.70	-13.2
200	45.20	-8.6	180	45.07	-9.4
210	45.27	-7.9	190	45.13	-8.7
220	45.55	-5.1	200	45.19	-8.0
230	45.93	-1.3	210	45.33	-6.6
240	45.89	-1.7	220	45.43	-5.5
			230	45.60	-3.7
			240	45.46	-5.0

Test No. 2.33/7.2/2
 Clay M390
 Clay Lot No. 34281348
 Test Date: 9-Sep-99

Test Variables		
Q (L/s)	U ₀ (m/s)	a (mm)
2.40	7.16	2.33

Δh _m (mm)	208		
Section	1	2	3
Located at y (mm)	50	75.5	110
ε _{m=} (mm)	-9.8	-12.2	-17.9
x _{m=} (mm)	14	14.5	21
x ₀₌ (mm)	60	63	61
b (mm)	24.1	23.9	32.5

Section 1 (9 Sep 99)			Section 2 (9 Sep 99)			Section 3 (9 Sep 99)		
x (mm)	Reading (cm)	ε _m (mm)	x (mm)	Reading (cm)	ε _m (mm)	x (mm)	Reading (cm)	ε _m (mm)
0	45.73	-2.3	0	45.71	-2.6	0	45.47	-5.4
5	45.44	-5.3	5	45.32	-6.6	5	44.99	-10.2
10	45.14	-8.4	10	44.99	-10.0	10	44.69	-13.3
14	45.00	-9.8	14.5	44.78	-12.2	15	44.44	-15.8
15	45.02	-9.6	15	44.79	-12.1	20	44.25	-17.8
20	45.23	-7.6	20	45.05	-9.5	21	44.24	-17.9
25	45.57	-4.3	25	45.50	-5.1	25	44.50	-15.3
30	45.62	-3.8	27.5	45.57	-4.5	30	44.91	-11.3
35	45.73	-2.8	30	45.64	-3.8	35	45.39	-6.5
40	45.73	-2.9	35	45.69	-3.4	40	45.59	-4.6
45	45.84	-1.9	40	45.75	-2.9	45	45.73	-3.2
50	45.91	-1.3	45	45.79	-2.6	50	45.92	-1.4
55	46.02	-0.2	55	45.95	-1.2	60	46.06	-0.1
60	46.05	0.0	60	46.05	-0.2	61	46.07	0.0
			63	46.08	0.0			

Test No.	2.33/5.2/1		
Clay	M390		
Clay Lot No.	34281348		
Test Date:	24-Sep-99 * Section 1 only surface erosion.		
Δh_m (mm)	108 * Section 3 is most representative section.		
Section	1	2	3
Located at y (mm)	50	75.5	99
ϵ_{m-} (mm)	0	-1.8	-2.1
x_{m-} (mm)	0	12.5	12.5
x_{o-} (mm)	0	29	33
b (mm)	0	20.3	23.3

Section 2 (24 Sep 99) (centreline)			Section 3 (24 Sep 99)		
x (mm)	Reading (cm)	ϵ_{-} (mm)	x (mm)	Reading (cm)	ϵ_{-} (mm)
0	45.86	-1.3	0	45.98	-0.2
3	45.79	-2.1	5	45.88	-1.4
5	45.91	-1.0	10	45.85	-1.9
10	45.87	-1.6	12.5	45.84	-2.1
12.5	45.86	-1.8	15	45.86	-2.0
15	45.92	-1.3	20	45.94	-1.4
20	45.97	-0.96	25	46.02	-0.9
25	46.08	0.0	30	46.12	-0.1
29	46.10	0.0	33	46.14	0.0

Test No.	2.33/11.7/1		
Clay	M390		
Clay Lot No.	34281348		
Test Date:	30-Sep-99		
Δh_m (mm)	552		
Section	1	2	3
Located at y (mm)	50	75.5	100
ϵ_{m-} (mm)	-38.8	-43.7	-45.1
x_{m-} (mm)	44	42.5	39
x_{o-} (mm)	141	120	143
b (mm)	75.6	72.1	72.4

Section 1 (30 Sep 99)			Section 2 (30 Sep 99)			Section 3 (30 Sep 99)		
x (mm)	Reading (cm)	ϵ_{-} (mm)	x (mm)	Reading (cm)	ϵ_{-} (mm)	x (mm)	Reading (cm)	ϵ_{-} (mm)
0	44.78	-11.8	0	45.31	-6.7	0	45.46	-5.0
5	44.56	-14.1	5	45.16	-8.3	5	45.20	-7.7
10	44.33	-16.5	10	45.01	-9.9	10	44.90	-10.8
15	43.80	-21.9	15	44.51	-15.0	15	44.53	-14.6
20	43.51	-24.9	20	43.80	-22.2	20	43.51	-24.9
30	42.82	-32.0	30	42.52	-35.2	25	42.85	-31.6
35	42.51	-35.2	35	42.09	-39.6	30	42.28	-37.4
40	42.27	-37.7	40	41.75	-43.1	35	41.93	-41.0
44	42.16	-38.8	42.5	41.70	-43.7	39	41.53	-45.1
45	42.18	-38.7	45	41.82	-42.5	40	41.54	-45.0
50	42.34	-37.2	50	42.08	-40.0	45	41.86	-41.9
55	42.67	-34.0	55	42.39	-37.0	50	42.26	-38.0
60	43.08	-29.9	60	42.83	-32.8	55	42.49	-35.8
70	43.81	-22.8	70	43.76	-23.7	60	42.84	-32.4
80	44.44	-16.7	80	44.64	-15.1	65	43.18	-29.1
90	44.88	-12.5	90	45.19	-9.8	70	43.63	-24.7
100	45.25	-9.0	100	45.64	-5.5	80	44.57	-15.5
110	45.57	-6.0	110	46.02	-1.9	85	44.91	-12.2
120	45.84	-3.5	115	46.18	-0.4	90	45.18	-9.6
130	46.08	-1.3	120	46.23	0.0	100	45.48	-6.8
135	46.17	-0.5				110	45.83	-3.5
140	46.22	-0.1				115	45.94	-2.5
141	46.23	0.0				120	45.88	-3.2
						130	45.94	-2.8
						140	46.17	-0.7
						143	46.25	0.0

Test Variables		
Q (L/s)	U _c (m/s)	a (mm)
5.02	6.54	5.10

Test No. 5.10/6.5/1
 Clay M390
 Clay Lot No. 34281348
 Test Date: 10-Jan-00
 Δh_m (mm) 174

Section	1	2	3
Located at y (mm)	50	75.5	100
ϵ_{me} (mm)	-20.7	-16.1	-10.2
x_{me} (mm)	42.5	30.0	35
x_{ms} (mm)	153	149	130
b (mm)	86.0	74.8	95.5

Section 1 (10 Jan 00)				Section 2 (10 Jan 00)				
x (mm)	Reading (cm)	ϵ_m (mm)	x (mm)	Reading (cm)	ϵ_m (mm)	x (mm)	Reading (cm)	ϵ_m (mm)
0	44.99	-10.0	0	45.09	-9.0	0	45.09	-9.0
5	44.71	-12.9	5	44.86	-11.4	5	44.86	-11.4
10	44.52	-14.8	10	44.74	-12.6	10	44.74	-12.6
15	44.35	-16.6	15	44.50	-15.1	15	44.50	-15.1
20	44.28	-17.3	20	44.32	-16.9	20	44.32	-16.9
25	44.23	-17.9	25	44.44	-15.8	25	44.44	-15.8
30	44.10	-19.3	30	44.41	-16.1	30	44.41	-16.1
35	44.02	-20.1	35	44.45	-15.8	35	44.45	-15.8
40	44.00	-20.4	40	44.54	-15.0	40	44.54	-15.0
42.5	43.97	-20.7	45	44.72	-13.2	45	44.72	-13.2
45	43.99	-20.5	50	44.85	-12.0	50	44.85	-12.0
50	44.11	-19.4	55	44.94	-11.1	55	44.94	-11.1
55	44.29	-17.6	60	44.99	-10.7	60	44.99	-10.7
60	44.55	-15.1	65	45.11	-9.5	65	45.11	-9.5
65	44.66	-14.1	70	45.22	-8.5	70	45.22	-8.5
75	44.76	-13.2	80	45.32	-7.6	80	45.32	-7.6
80	44.87	-12.1	90	45.39	-7.0	90	45.39	-7.0
85	45.05	-10.4	100	45.52	-5.8	100	45.52	-5.8
90	45.08	-10.2	110	45.64	-4.8	110	45.64	-4.8
95	45.21	-8.9	120	45.73	-4.0	120	45.73	-4.0
100	45.25	-8.6	130	45.89	-2.5	130	45.89	-2.5
110	45.31	-8.1	140	46.08	-0.7	140	46.08	-0.7
120	45.46	-6.7	149	46.16	0.0	149	46.16	0.0
130	45.68	-4.6						
140	45.92	-2.3						
150	46.15	-0.2						
153	46.17	0.0						

Section 3 (10 Jan 00)			
x (mm)	Reading (cm)	ϵ_m (mm)	x (mm)
0	45.49	-5.0	0
5	45.36	-6.4	5
10	45.28	-7.2	10
15	45.25	-7.6	15
20	45.10	-9.1	20
25	45.05	-9.7	25
30	45.03	-10.0	30
35	45.01	-10.2	35
40	45.07	-9.7	40
45	45.15	-9.0	45
50	45.17	-8.8	50
55	45.19	-8.7	55
60	45.21	-8.5	60
65	45.24	-8.3	65
70	45.24	-8.4	70
75	45.27	-8.1	75
80	45.33	-7.6	80
90	45.47	-6.3	90
100	45.70	-4.1	100
110	45.87	-2.6	110
120	46.11	-0.3	120
125	46.14	0.0	125
130	46.15	0.0	130

Test No.	5.10/7.0/1	Test Variables		
Clay	M390	Q (L/s)	U _s (m/s)	a (mm)
Clay Lot No.	34281348	5.40	7.03	5.10
Test Date:	20-Jan-00			
Δh _m (mm)	201			

* Italics indicate areas that may have been affected by siaking.

Section 1 (20 Jan 00)			Section 2 (20 Jan 00)		
x (mm)	Reading (cm)	ε _z (mm)	x (mm)	Reading (cm)	ε _z (mm)
0	37.23	-88.2	0	39.98	-60.5
25	37.23	-88.4	5	40.10	-59.4
30	39.21	-68.6	10	40.27	-57.7
35	39.29	-67.9	15	40.30	-57.5
40	39.39	-66.9	20	40.34	-57.2
45	39.40	-66.8	25	40.47	-56.0
50	39.89	-62.0	30	40.59	-54.8
55	40.12	-59.7	35	40.64	-54.4
60	40.48	-56.1	40	40.68	-54.1
65	41.08	-50.2	45	40.80	-52.9
70	41.52	-45.8	50	40.73	-53.7
75	42.04	-40.6	55	40.69	-54.2
80	42.53	-35.8	60	40.78	-53.3
85	43.09	-30.2	65	40.96	-51.6
90	43.39	-27.2	70	41.22	-49.1
95	43.62	-25.0	75	41.59	-45.5
100	43.80	-23.2	76	42.14	-40.0
105	44.04	-20.9	80	42.35	-37.9
110	44.19	-19.4	90	43.02	-31.4
120	44.54	-16.0	100	43.82	-23.5
130	44.73	-14.1	105	44.07	-21.1
140	45.03	-11.2	110	44.23	-19.6
150	45.46	-7.0	120	44.50	-17.0
160	45.74	-4.3	130	44.78	-14.3
170	45.92	-2.5	140	45.05	-11.8
180	46.18	0.0	150	45.19	-10.5
			160	45.09	-11.7
			170	45.09	-11.8
			180	45.15	-11.3
			190	45.58	-7.2
			200	45.75	-5.6
			210	45.99	-3.4
			220	46.34	0.0

Section	1	2	3
Located at y (mm)	35	76.0	100
ε _m (mm)	-66.8	-54.2	-51.6
x _m (mm)	45	55.0	50
x _{cm} (mm)	182	220	216
b (mm)	82.1	95.4	94.7
Section 3 (20 Jan 00)			
x (mm)	Reading (cm)	ε _z (mm)	
0	40.19	-58.5	
5	39.74	-63.1	
10	39.95	-61.0	
15	40.14	-59.2	
25	40.62	-54.6	
35	40.91	-51.8	
40	40.99	-51.1	
45	40.96	-51.4	
50	40.95	-51.6	
55	41.04	-50.8	
60	41.17	-49.6	
65	41.32	-48.1	
70	41.64	-45.0	
75	41.90	-42.5	
80	42.21	-39.4	
85	42.55	-36.1	
90	43.13	-30.4	
100	44.12	-20.6	
110	44.51	-16.9	
120	44.83	-13.8	
130	44.94	-12.9	
140	45.04	-12.0	
150	45.05	-12.1	
160	45.00	-12.7	
170	45.14	-11.4	
180	45.39	-9.1	
190	45.51	-8.0	
200	45.82	-5.1	
210	46.17	-1.7	
216	46.35	0.0	

Test No. 5.10/6.0/1
 Clay M390
 Clay Lot No. 34281348
 Test Date: 26-Jan-00
 Δh_s (mm) 148

Test Variables		
Q (L/s)	U _c (m/s)	a (mm)
4.63	6.04	5.10

*estimate of b for section 1 and 2

Section 1 (26 Jan 00)			Section 2 (26 Jan 00)		
x (mm)	Reading (cm)	ϵ_{ms} (mm)	x (mm)	Reading (cm)	ϵ_{ms} (mm)
0	45.05	-10.0	0	45.70	-3.4
5	44.21	-18.5	5	45.06	-9.9
10	43.64	-24.2	10	44.52	-15.3
15	43.14	-29.3	15	44.04	-20.2
20	42.55	-35.2	20	43.55	-25.1
25	42.01	-40.7	25	43.05	-30.2
30	41.66	-44.2	30	42.50	-35.8
32.5	41.50	-45.9	35	41.78	-43.0
35	41.59	-45.0	36	41.66	-44.2
40	41.59	-45.1	40	41.81	-42.8
45	41.75	-43.5	45	42.18	-39.1
50	41.89	-42.2	50	42.30	-38.0
55	42.06	-40.5	55	42.38	-37.3
60	42.21	-39.1	60	42.60	-35.1
65	42.46	-36.7	65	42.89	-32.3
70	42.71	-34.2	70	43.04	-30.8
75	42.98	-31.6	75	43.21	-29.2
80	43.22	-29.2	80	43.45	-26.9
85	43.29	-28.6	85	43.49	-26.5
90	43.25	-29.0	90	43.41	-27.4
95	43.31	-28.5	100	43.22	-29.4
100	43.34	-28.3	110	42.99	-31.8
105	43.29	-28.8	120	42.86	-33.2
110	43.23	-29.5	130	43.12	-30.8
115	43.10	-30.8	140	43.65	-25.6
120	42.87	-33.2	150	44.63	-15.9
125	42.98	-32.2	160	45.10	-11.3
130	43.37	-28.3	170	45.11	-11.3
140	44.03	-21.8	180	45.46	-8.0
145	43.96	-22.6	190	45.98	-2.9
150	44.29	-19.3	200	46.28	0.0
160	44.82	-14.2			
170	45.15	-11.0			
180	45.73	-5.3			
190	46.14	-1.3			
197.5	46.28	0.0			

Section	1	2	3
Located at y (mm)	52	75.5	107
ϵ_{ms} (mm)	-45.9	-44.2	-44.3
x_{ms} (mm)	32.5	36.0	39
x_{os} (mm)	197.5	200	199
b (mm)	145	144	137.8

Section 3 (26 Jan 00)		
x (mm)	Reading (cm)	ϵ_{ms} (mm)
0	45.25	-8.0
5	45.16	-9.0
10	44.90	-11.6
15	44.53	-15.4
20	43.91	-21.6
25	43.33	-27.5
30	42.67	-34.1
35	42.12	-39.7
39	41.67	-44.3
40	41.76	-43.4
45	42.05	-40.5
50	42.37	-37.4
55	42.54	-35.7
65	43.09	-30.4
75	43.71	-24.3
80	43.85	-22.9
90	43.64	-25.1
100	43.77	-24.0
110	43.41	-27.7
120	43.37	-28.2
130	43.57	-26.3
140	44.12	-20.9
150	44.35	-18.7
160	44.72	-15.1
170	45.29	-9.6
180	45.83	-4.3
190	45.92	-3.5
199	46.28	0.0

Test Variables		
Q (L/s)	U _s (m/s)	a (mm)
3.73	4.86	5.10

Test No. 5.10/4.9/1
 Clay M390
 Clay Lot No. 34281348
 Test Date: 8-Feb-00
 Δh_m (mm) 96

Section	1	2	3
Located at y (mm)	55	75.5	105
ε _{max} (mm)	-31.3	-30.8	-21.4
X _{max} (mm)	25	32	30
X _{0%} (mm)	96	92	83
b (mm)	53.1	54.0	50.2

Section 1 (8 Feb 00)		Section 2 (8 Feb 00)	
x (mm)	ε _m (mm)	x (mm)	ε _m (mm)
0	-29.6	0	-22.8
5	-29.2	5	-23.3
10	-30.7	10	-24.8
15	-30.5	15	-26.8
20	-30.7	20	-28.5
25	-31.3	25	-29.4
28	-31.1	30	-30.7
30	-30.4	32	-30.8
35	-28.3	35	-29.1
40	-25.9	40	-26.3
45	-22.7	50	-18.9
55	-14.0	60	-10.1
59	-11.1	65	-7.0
60	-10.9	70	-5.2
65	-10.9	75	-4.2
70	-10.2	80	-2.7
75	-9.0	85	-1.0
85	-3.6	90	-0.4
90	-1.5	92	0.0
95	-0.2		
96	0.0		

Section 3 (8 Feb 00)		
x (mm)	Reading (cm)	ε _m (mm)
0	44.60	-14.4
5	44.55	-15.0
10	44.36	-16.9
15	44.18	-18.8
20	44.02	-20.4
25	43.97	-21.0
30	43.94	-21.4
35	44.12	-19.6
40	44.30	-17.9
45	44.64	-14.5
50	45.02	-10.8
55	45.32	-7.9
60	45.57	-5.4
65	45.70	-4.2
70	45.79	-3.3
75	45.90	-2.3
80	46.07	-0.7
83	46.14	0.0

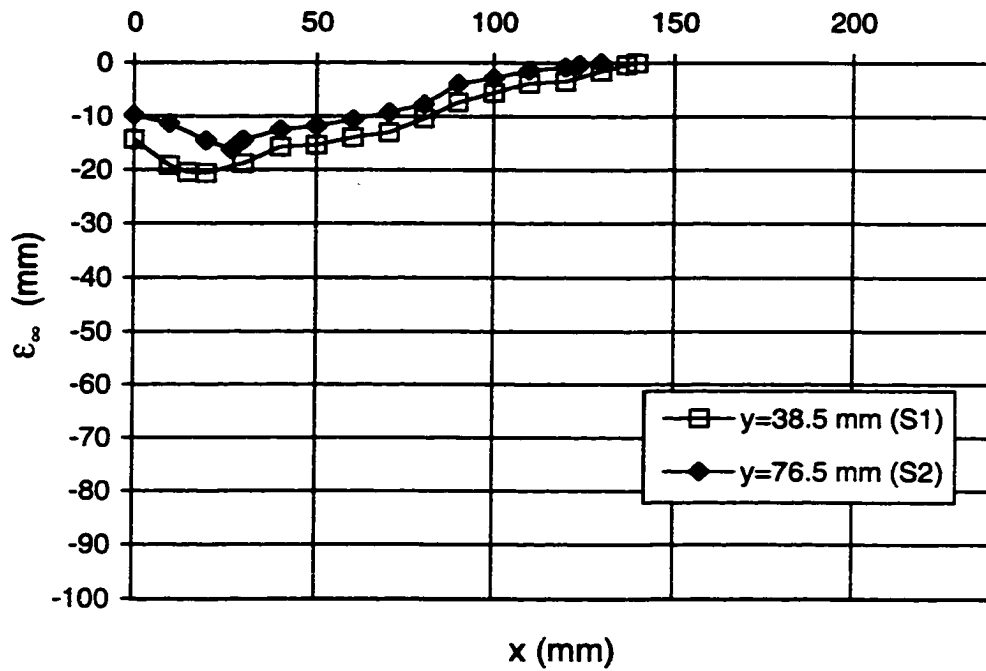


Fig. F-1: Scour hole profile at ultimate state for Wall Jet
 Test No. 2.33/9.3/1 - 12 Nov 98
 $U_o=9.31$ m/s $a=2.33$ mm $(\lambda-\lambda_c)/\lambda_c=3.33$

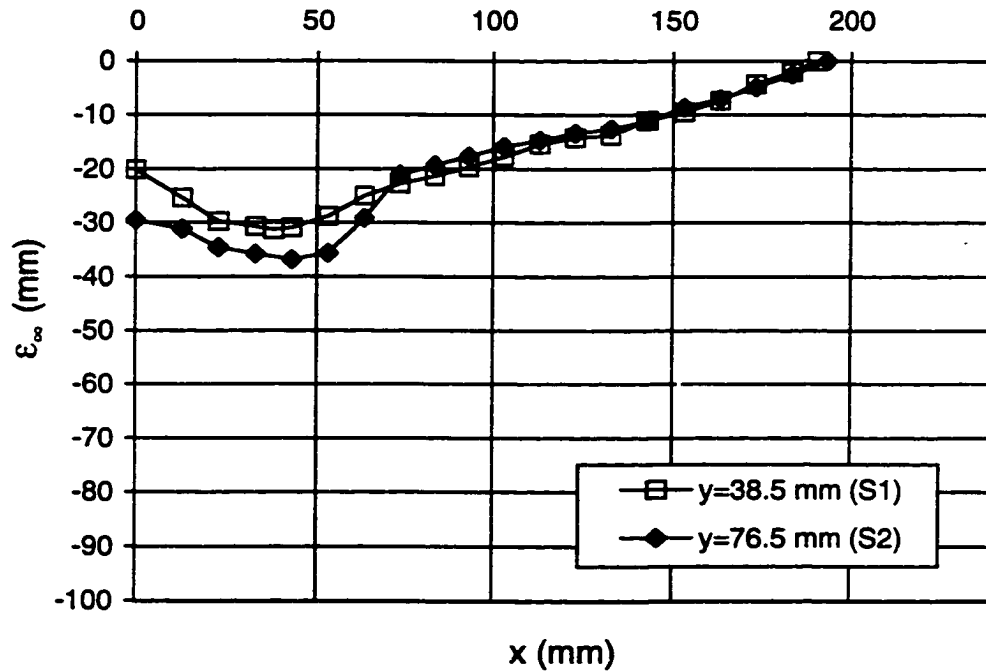


Fig. F-2: Scour hole profile at ultimate state for Wall Jet
 Test No. 2.33/9.7/1 - 18 Nov 98
 $U_o=9.74$ m/s $a=2.33$ mm $(\lambda-\lambda_c)/\lambda_c=3.74$

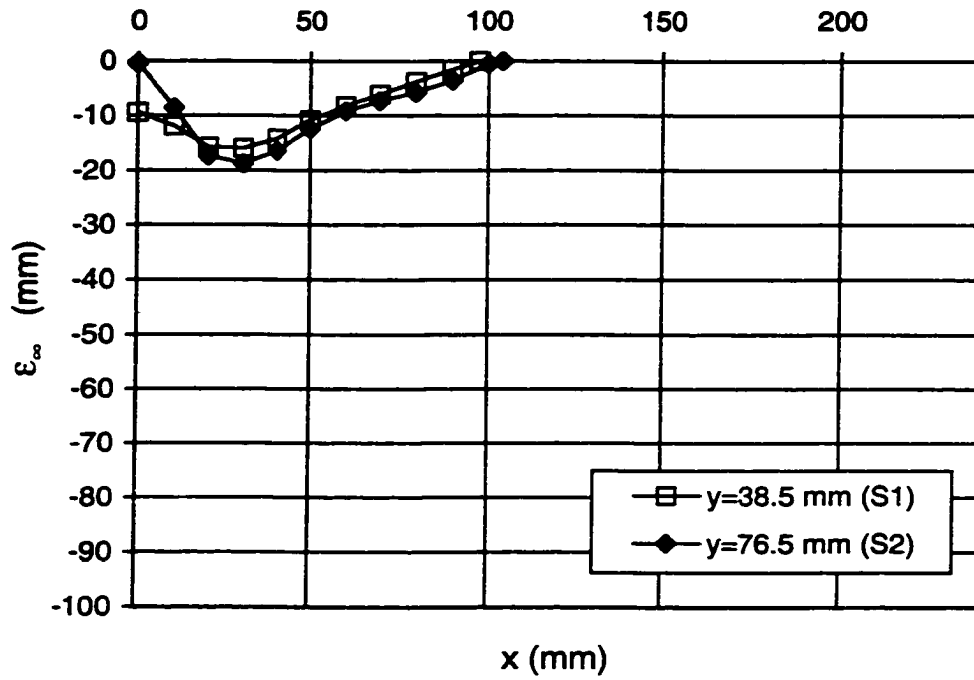


Fig. F-3: Scour hole profile at ultimate state for Wall Jet
 Test No. 2.33/8.8/1 - 7 Dec 98
 $U_o=8.84$ m/s $a=2.33$ mm $(\lambda-\lambda_c)/\lambda_c=2.91$

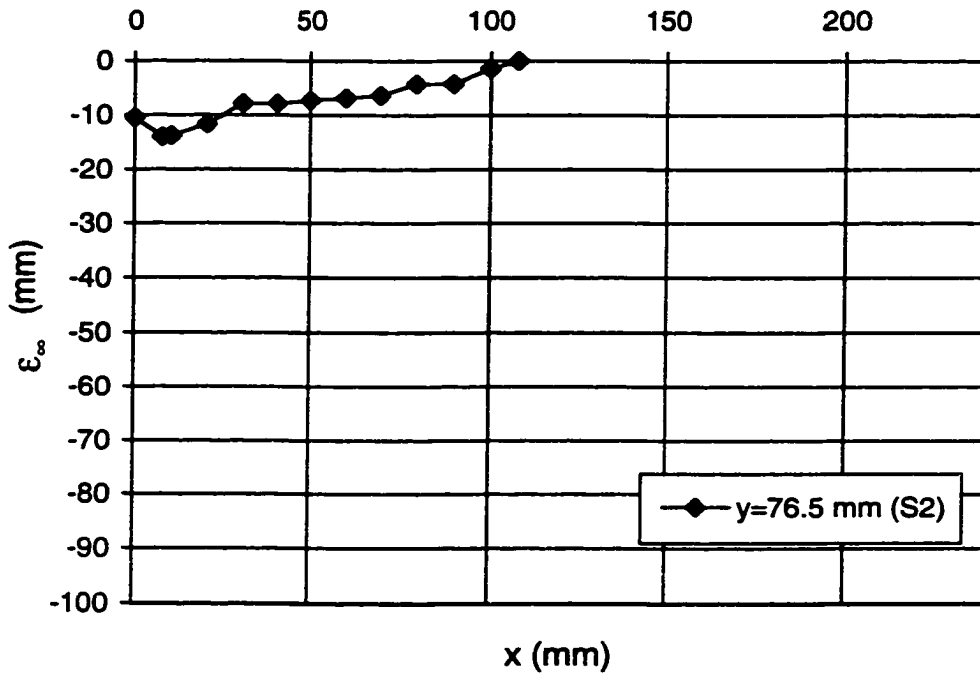


Fig. F-4: Scour hole profile at ultimate state for Wall Jet
 Test No. 2.33/8.1/1 - 14 Dec 98
 $U_o=8.13$ m/s $a=2.33$ mm $(\lambda-\lambda_c)/\lambda_c=2.31$

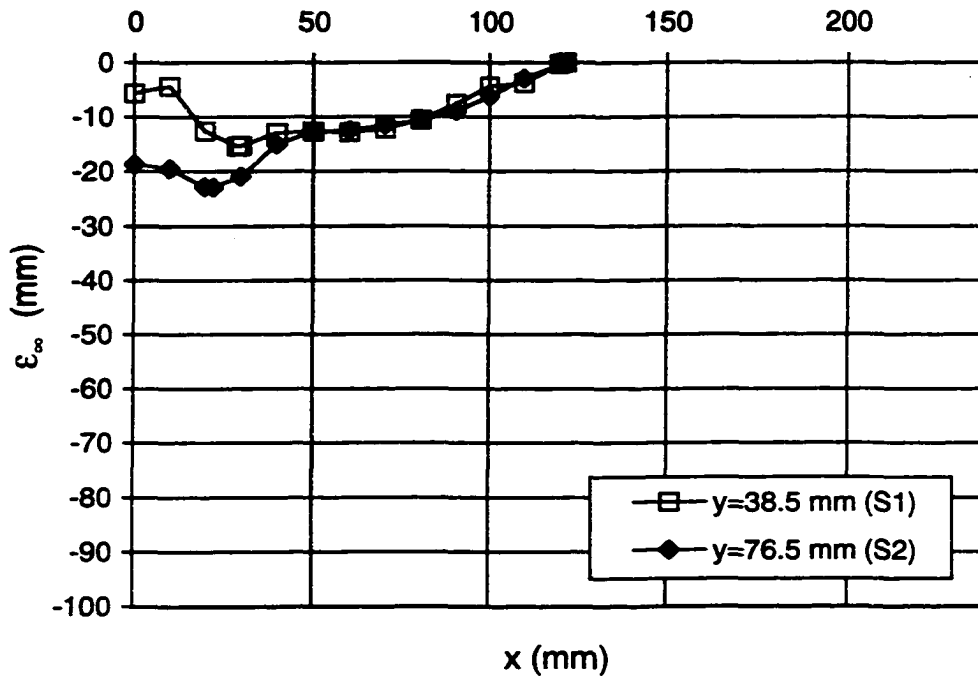


Fig. F-5: Scour hole profile at ultimate state for Wall Jet
Test No. 2.33/8.5/1 - 4 Jan 99

$U_o=8.52$ m/s $a=2.33$ mm $(\lambda-\lambda_c)/\lambda_c=2.63$

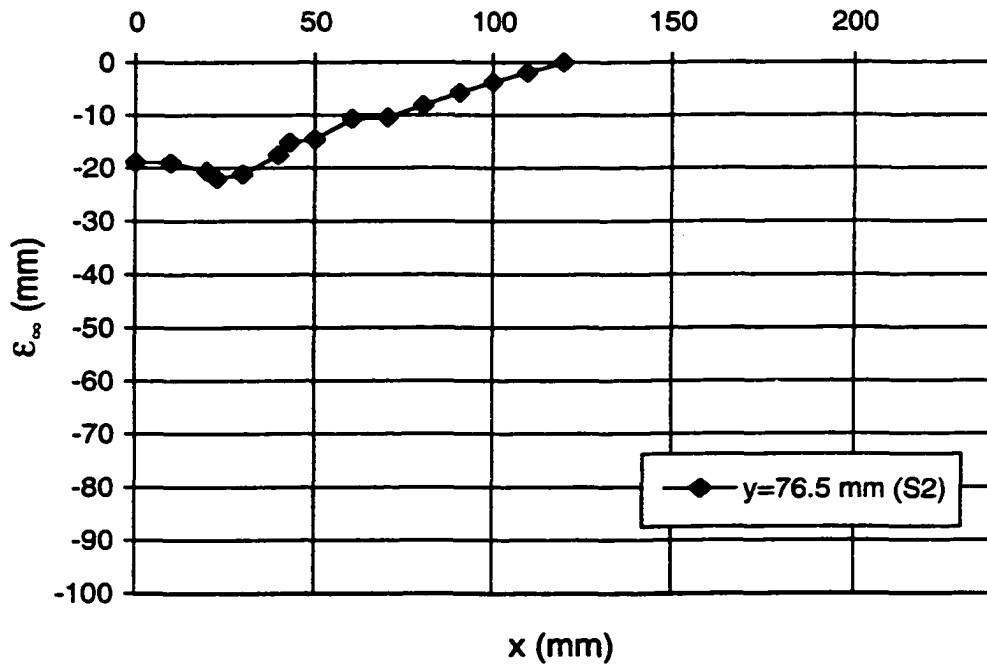


Fig. F-6: Scour hole profile at ultimate state for Wall Jet
Test No. 2.33/8.7/1 - 12 Jan 99

$U_o=8.67$ m/s $a=2.33$ mm $(\lambda-\lambda_c)/\lambda_c=2.76$

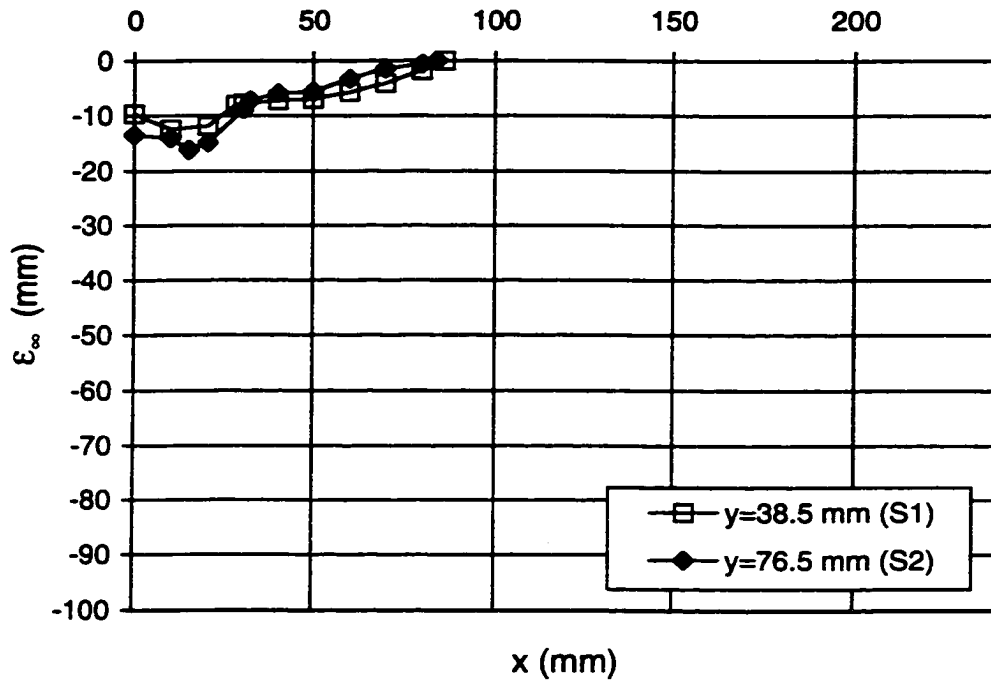


Fig. F-7: Scour hole profile at ultimate state: Wall Jet
 Test No. 2.33/7.4/1 - 22 Jan 99
 $U_o=7.36$ m/s $a=2.33$ mm $(\lambda-\lambda_c)/\lambda_c=1.71$

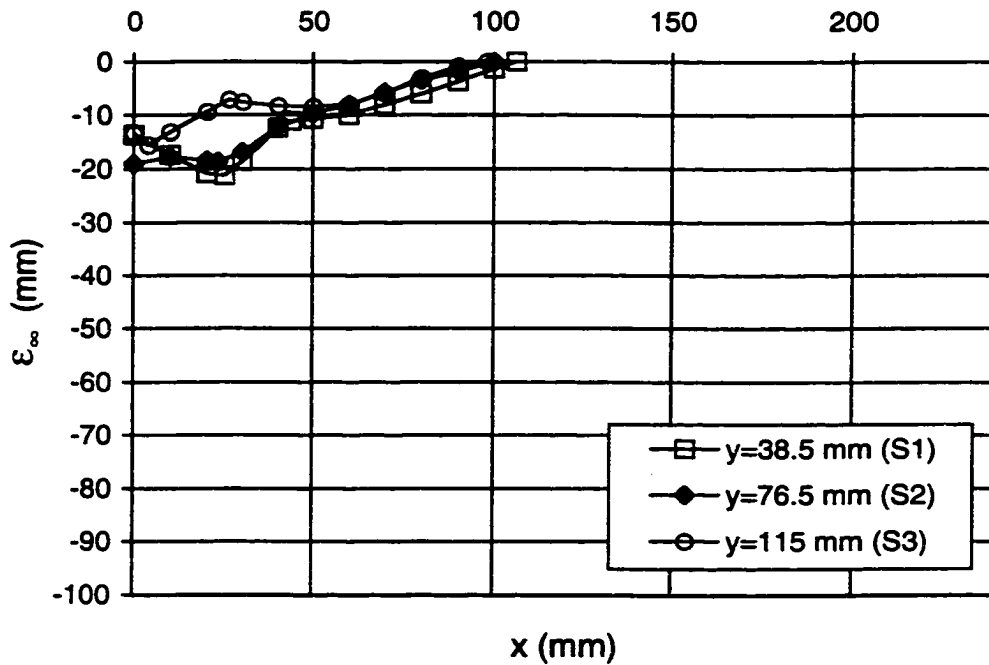


Fig. F-8: Scour hole profile at ultimate state for Wall Jet
 Test No. 2.33/8.1/2 - 28 Jan 99
 $U_o=8.05$ m/s $a=2.33$ mm $(\lambda-\lambda_c)/\lambda_c=2.24$

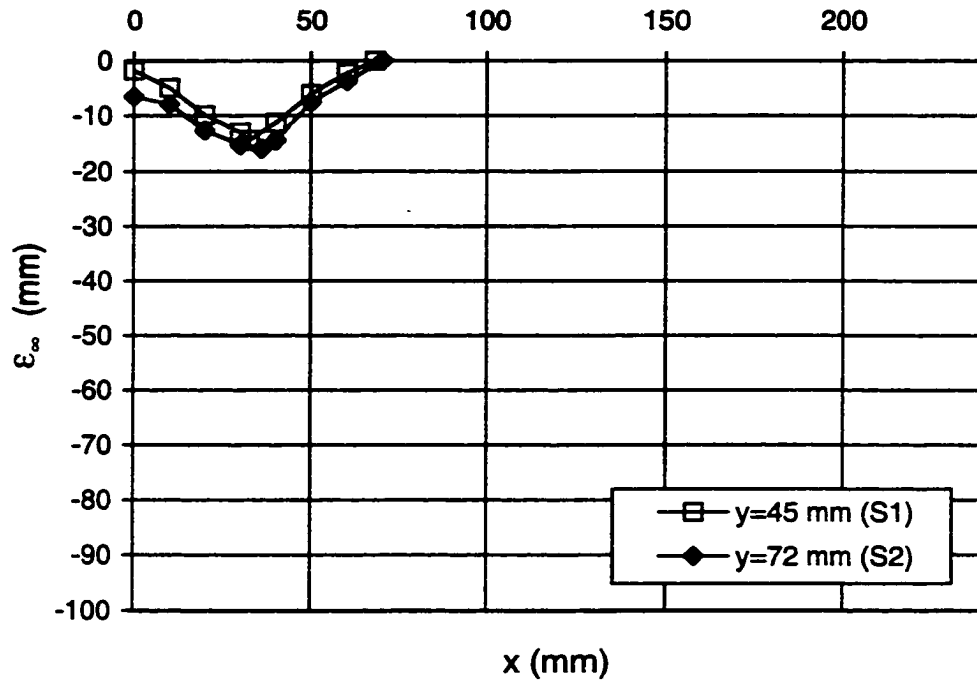


Fig. F-9: Scour hole profile at ultimate state for Wall Jet Test No. 2.33/7.0/1 - 11 Feb 99

$$U_o=6.98 \text{ m/s } a=2.33 \text{ mm } (\lambda-\lambda_c)/\lambda_c=1.44$$

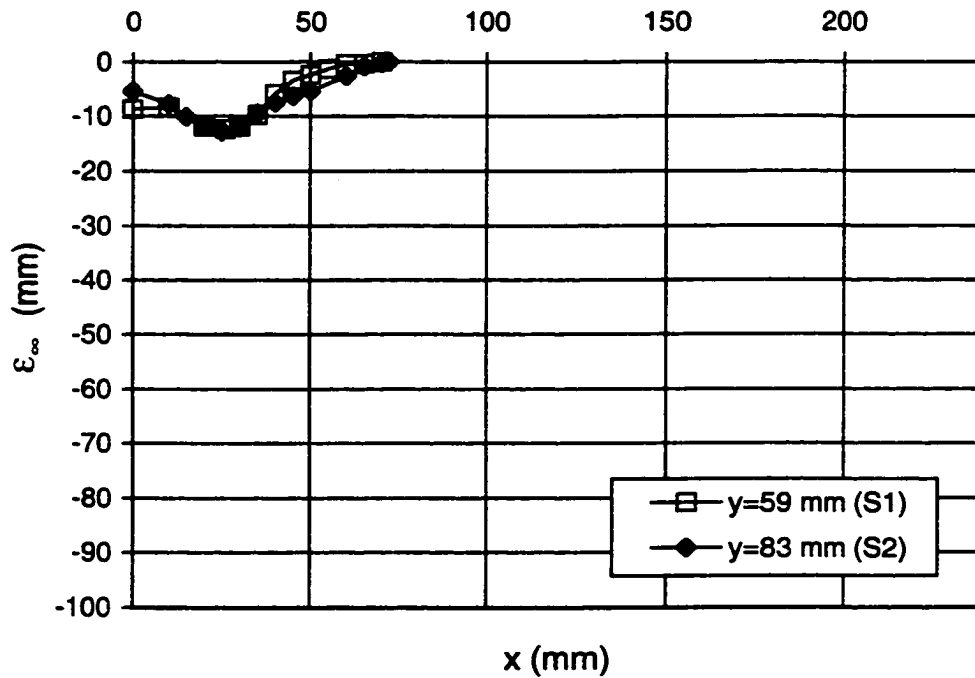


Fig. F-10: Scour hole profile at ultimate state for Wall Jet Test No. 2.33/7.2/1 - 17 Feb 99

$$U_o=7.17 \text{ m/s } a=2.33 \text{ mm } (\lambda-\lambda_c)/\lambda_c=1.57$$

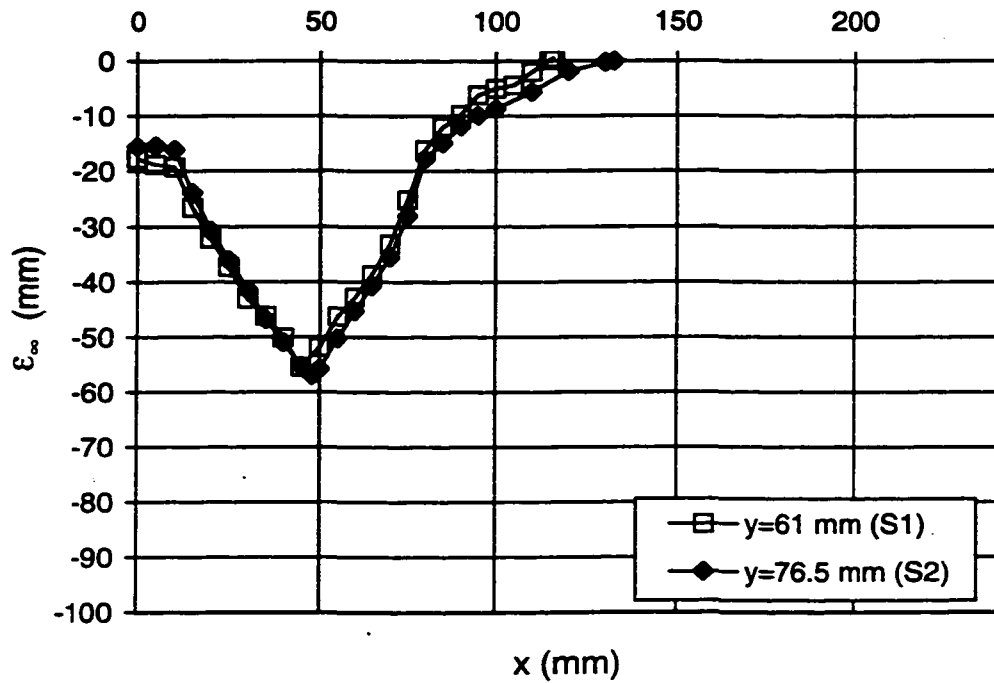


Fig. F-11: Scour hole profile at ultimate state for Wall Jet
 Test No. 2.33/8.0/1 - 15 Mar 99
 $U_o=7.97$ m/s $a=2.33$ mm $(\lambda-\lambda_c)/\lambda_c=2.18$

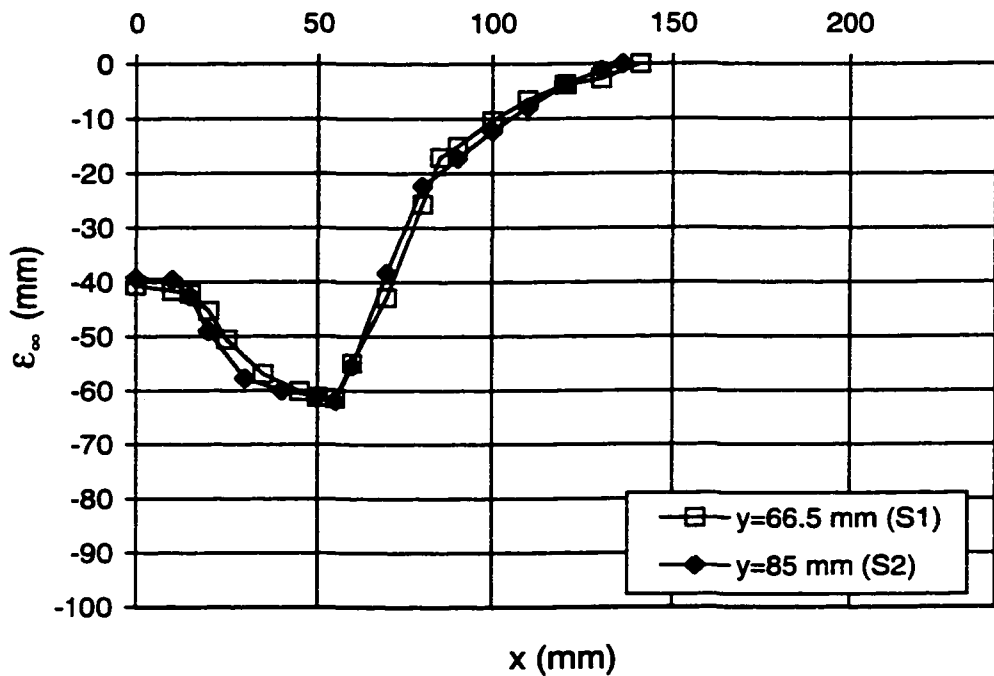


Fig. F-12: Scour hole profile at ultimate state for Wall Jet
 Test No. 2.33/8.5/2 - 30 Mar 99
 $U_o=8.46$ m/s $a=2.33$ mm $(\lambda-\lambda_c)/\lambda_c=2.58$

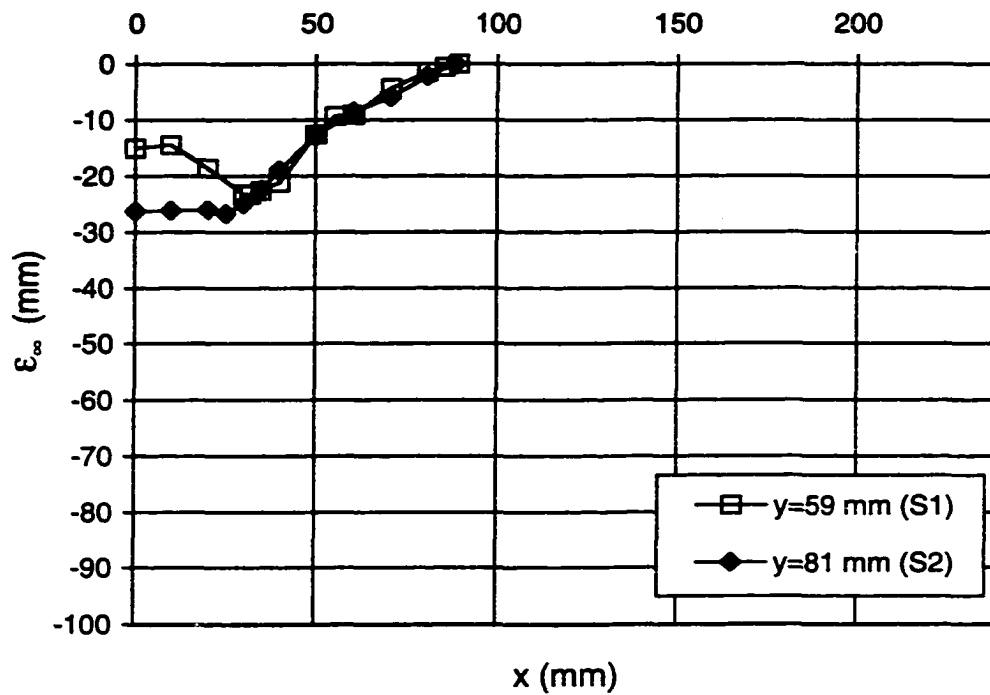


Fig. F-13: Scour hole profile at ultimate state: Wall Jet
 Test No. 2.33/8.2/1 - 6 Apr 99
 $U_o=8.18$ m/s $a=2.33$ mm $(\lambda-\lambda_c)/\lambda_c=2.35$

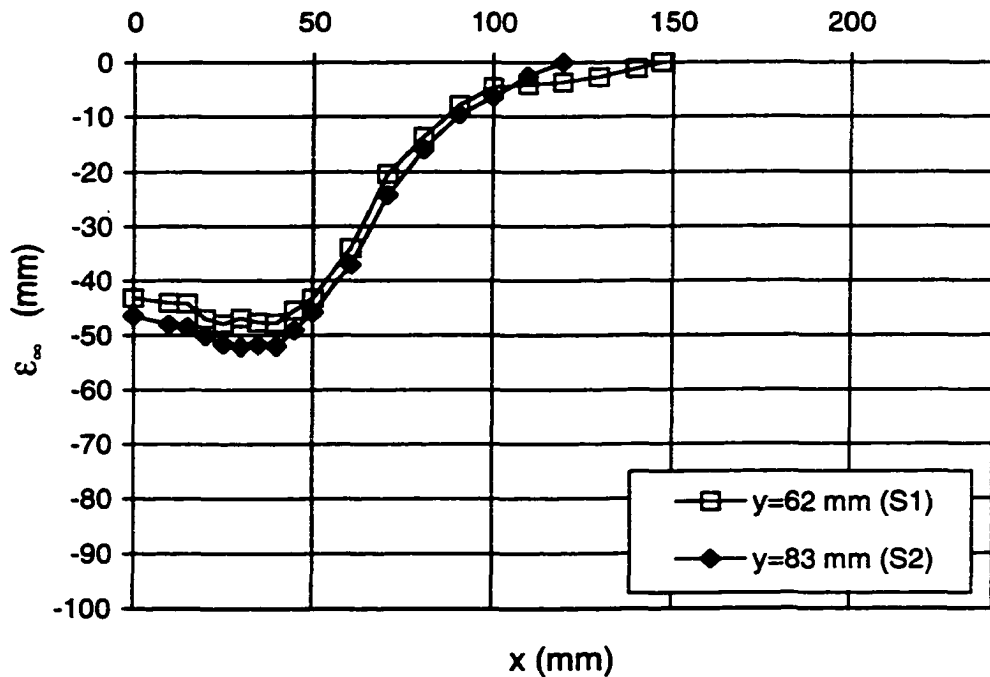


Fig. F-14: Scour hole profile at ultimate state for Wall Jet
 Test No. 2.33/9.5/1 - 13 Apr 99
 $U_o=9.50$ m/s $a=2.33$ mm $(\lambda-\lambda_c)/\lambda_c=3.52$

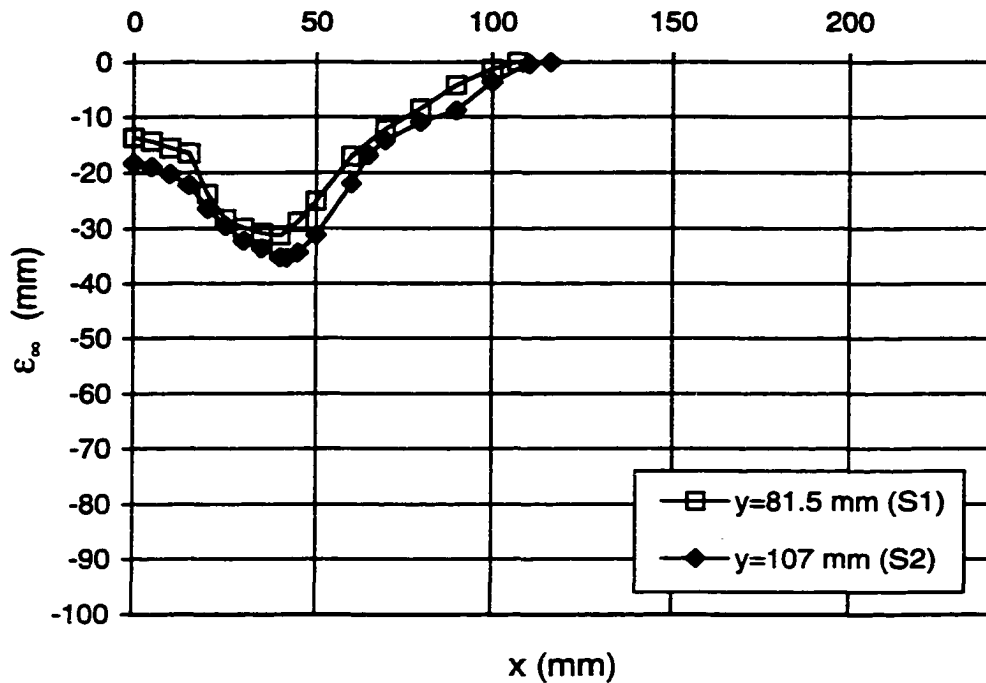


Fig. F-15: Scour hole profile at ultimate state: Wall Jet
 Test No. 2.33/9.8/1 - 3 May 99
 $U_o=9.85$ m/s $a=2.33$ mm $(\lambda-\lambda_c)/\lambda_c=3.85$

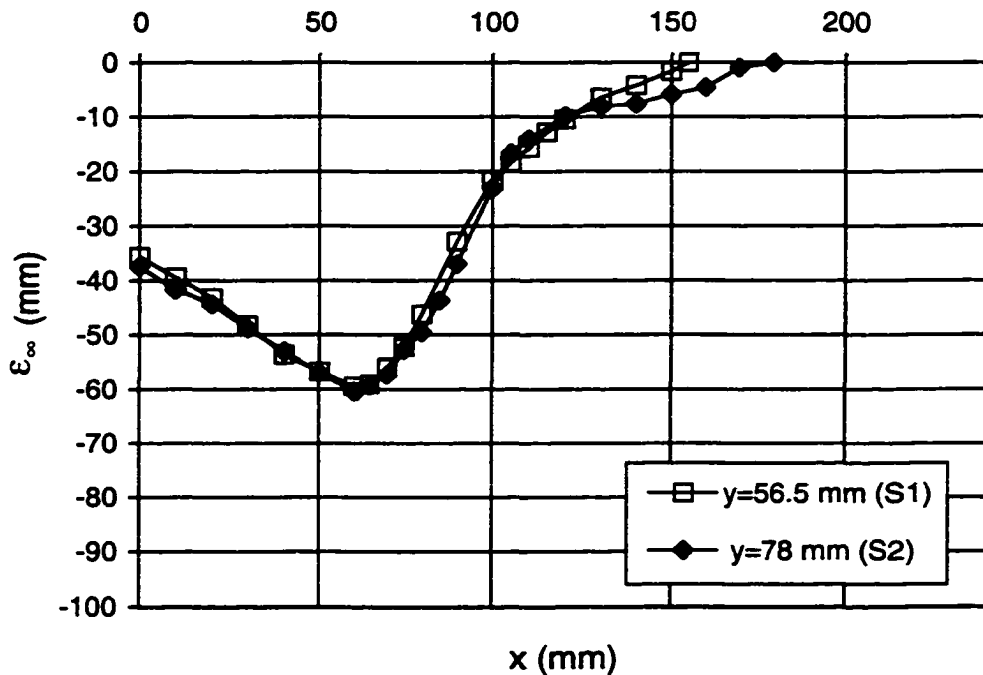


Fig. F-16: Scour hole profile at ultimate state for Wall Jet
 Test No. 2.33/11.3/1 - 13 May 99
 $U_o=11.31$ m/s $a=2.33$ mm $(\lambda-\lambda_c)/\lambda_c=5.40$

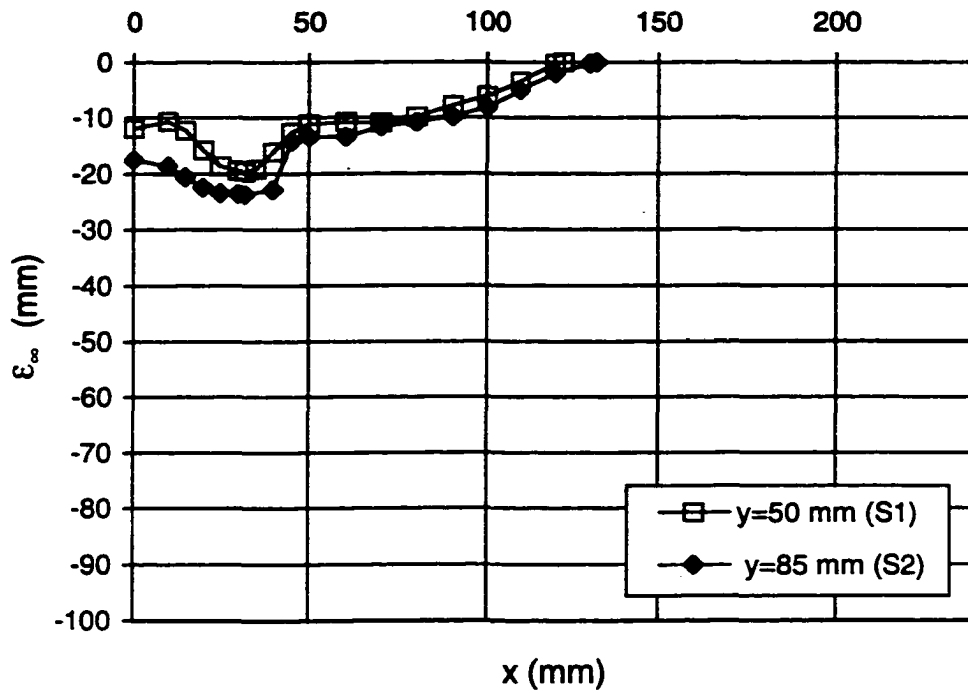


Fig. F-17: Scour hole profile at ultimate state for Wall Jet
 Test No. 2.33/9.0/1 - 19 May 99
 $U_o=9.03$ m/s $a=2.33$ mm $(\lambda-\lambda_c)/\lambda_c=3.07$

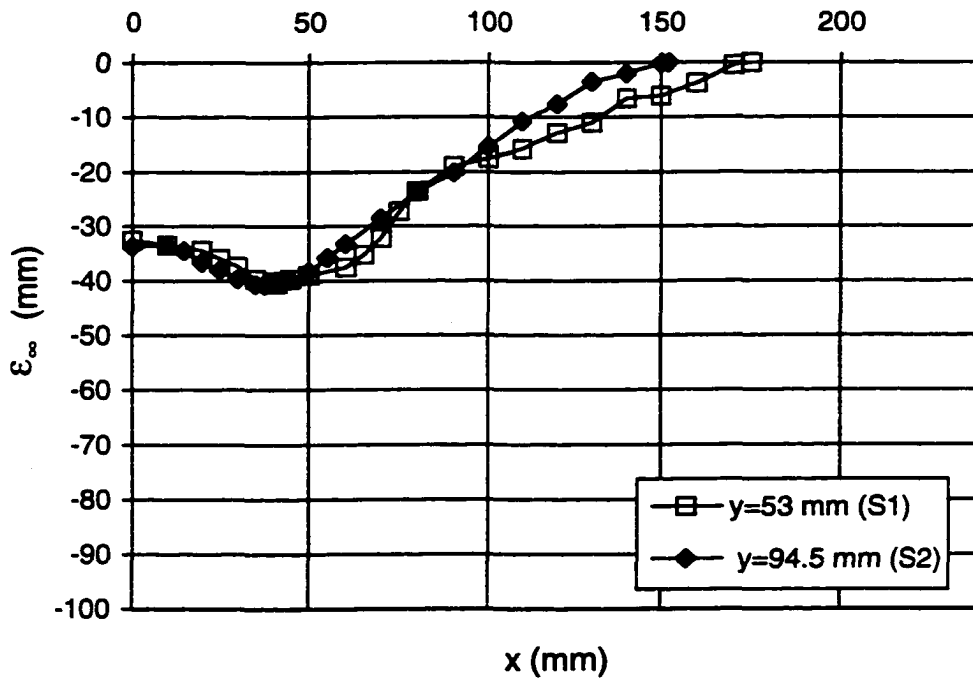


Fig. F-18: Scour hole profile at ultimate state for Wall Jet
 Test No. 2.33/10.2/1 - 25 May 99
 $U_o=10.23$ m/s $a=2.33$ mm $(\lambda-\lambda_c)/\lambda_c=4.23$

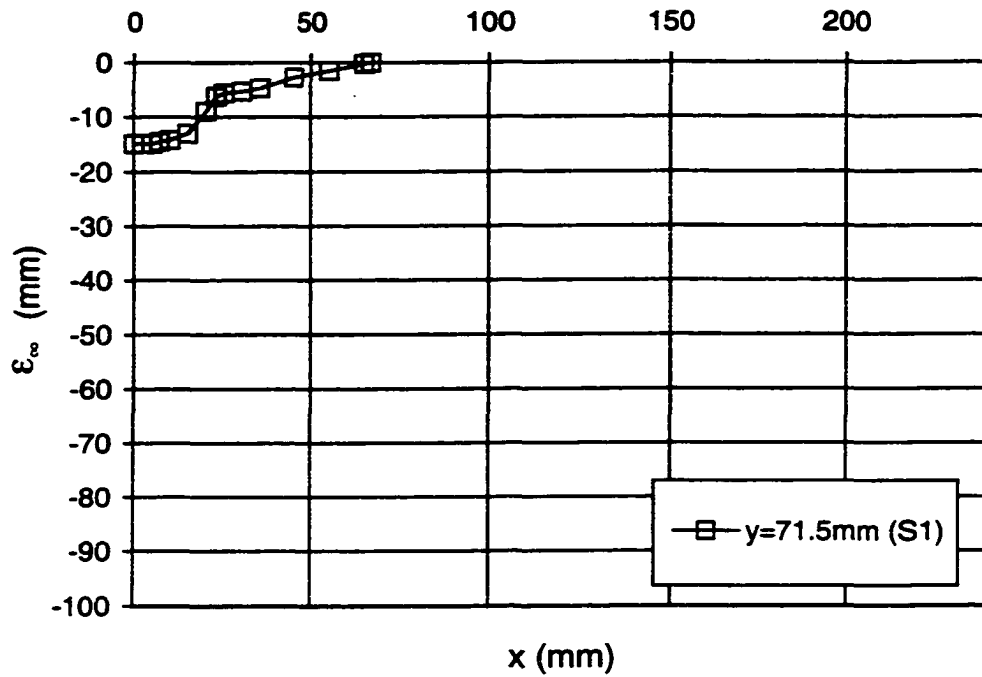


Fig. F-19: Scour hole profile at ultimate state for Wall Jet
 Test No. 2.33/6.2/1 - 8 Jun 99
 $U_o=6.16$ m/s $a=2.33$ mm $(\lambda-\lambda_c)/\lambda_c=0.89$

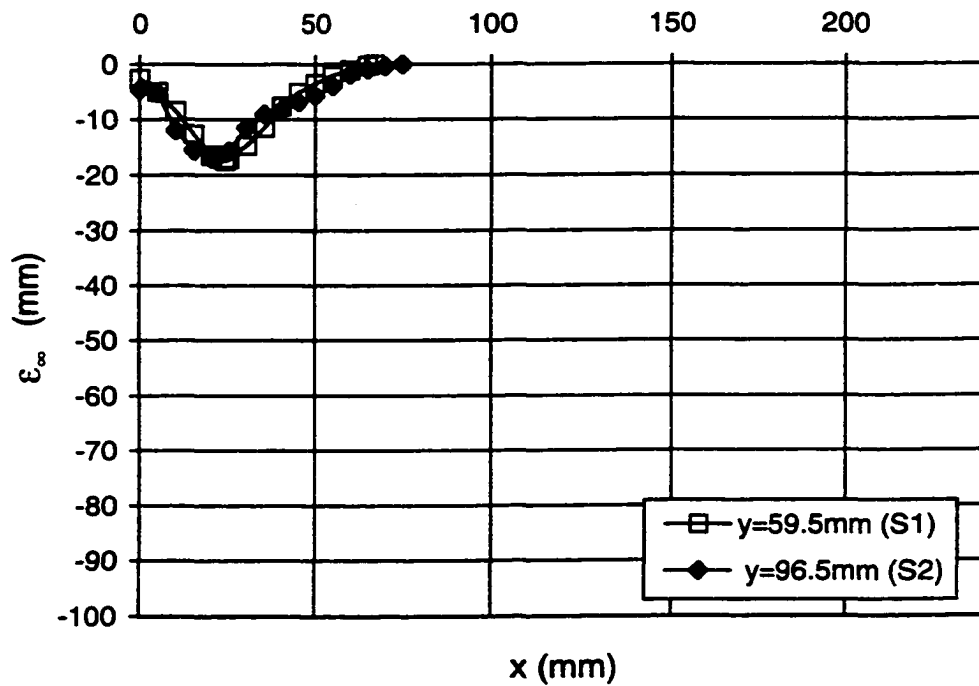


Fig. F-20: Scour hole profile at ultimate state for Wall Jet
 Test No. 2.33/8.0/2- 15 Jun 99
 $U_o=8.00$ m/s $a=2.33$ mm $(\lambda-\lambda_c)/\lambda_c=2.19$

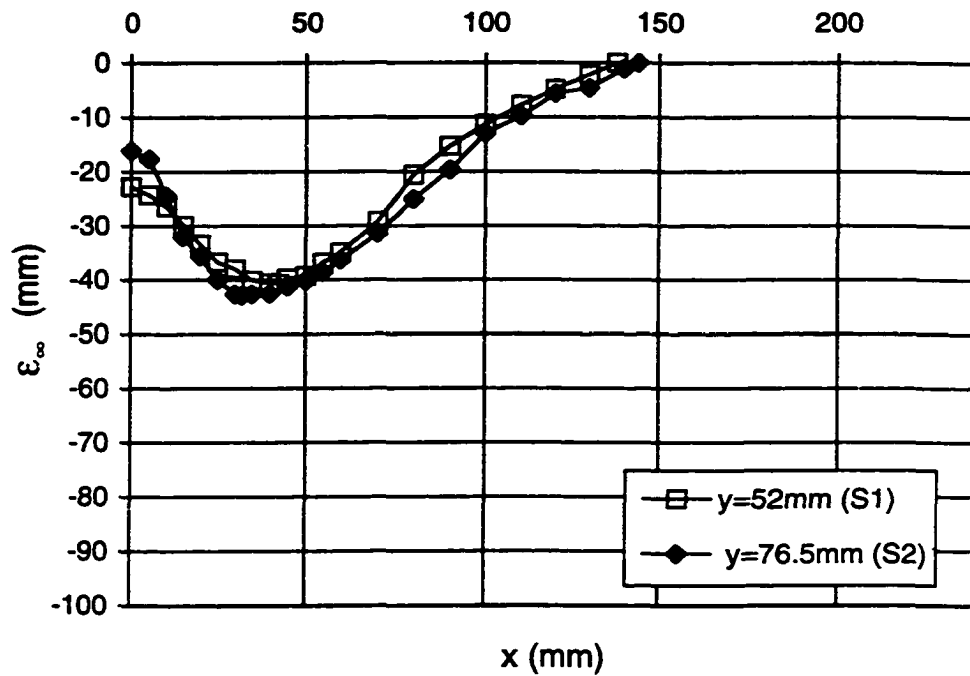


Fig. F-21: Scour hole profile at ultimate state for Wall Jet
 Test No. 2.33/12.0/1 - 25 Jun 99
 $U_o=12.03$ m/s $a=2.33$ mm $(\lambda-\lambda_c)/\lambda_c=6.23$

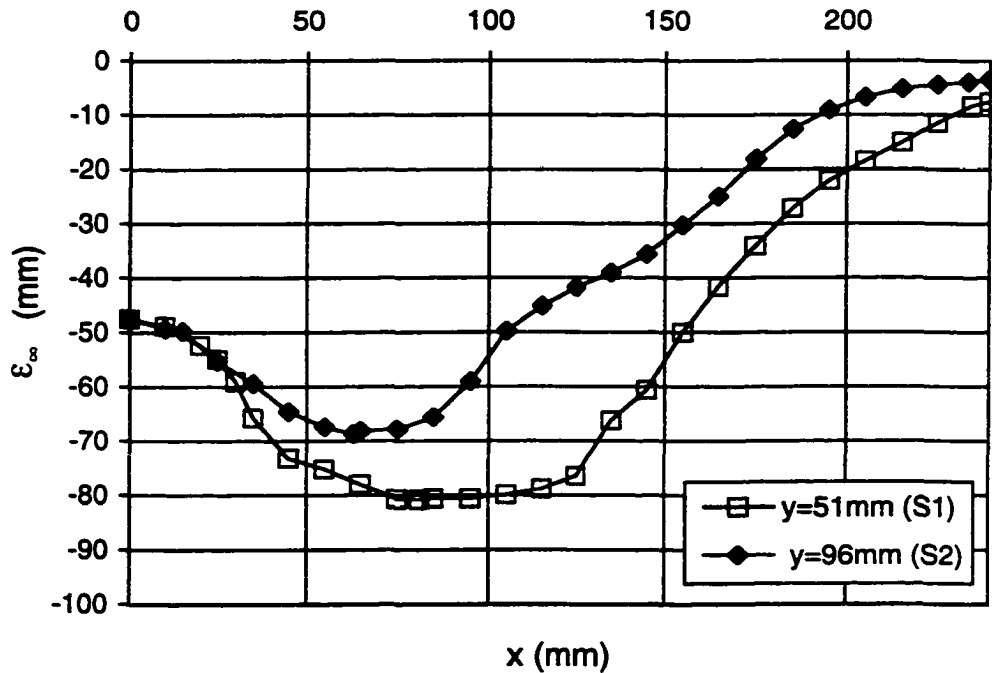


Fig. F-22: Scour hole profile at ultimate state for Wall Jet
 Test No. 2.33/12.7/1 - 9 Jul 99
 $U_o=12.72$ m/s $a=2.33$ mm $(\lambda-\lambda_c)/\lambda_c=7.10$

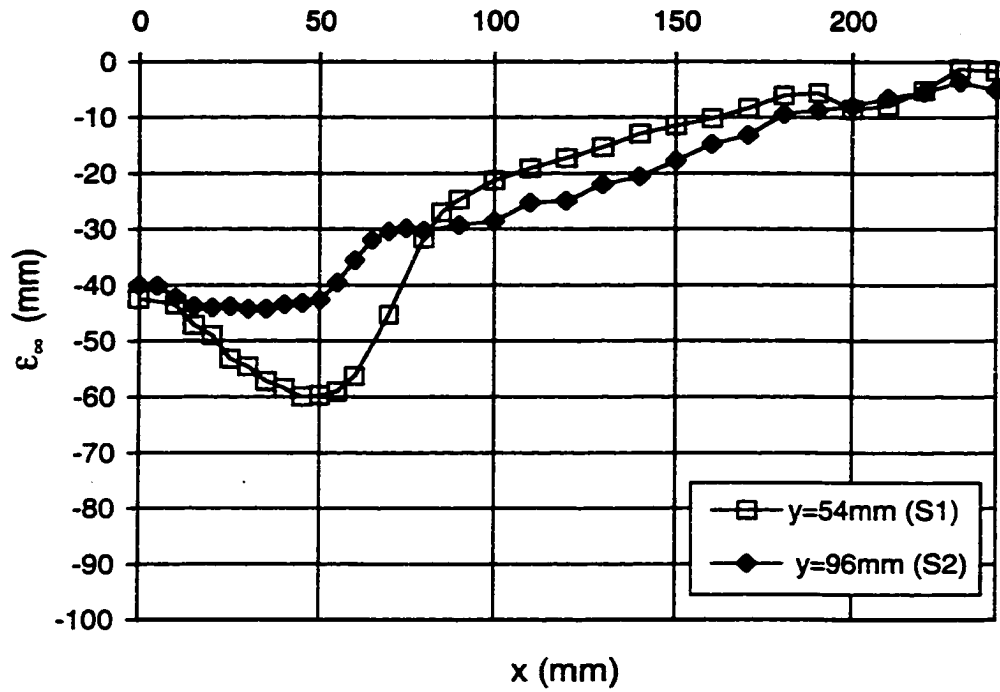


Fig. F-23: Scour hole profile at ultimate state for Wall Jet
 Test No. 2.33/12.3/1 - 15 Jul 99
 $U_o=12.25\text{ m/s}$ $a=2.33\text{ mm}$ $(\lambda-\lambda_c)/\lambda_c=6.50$

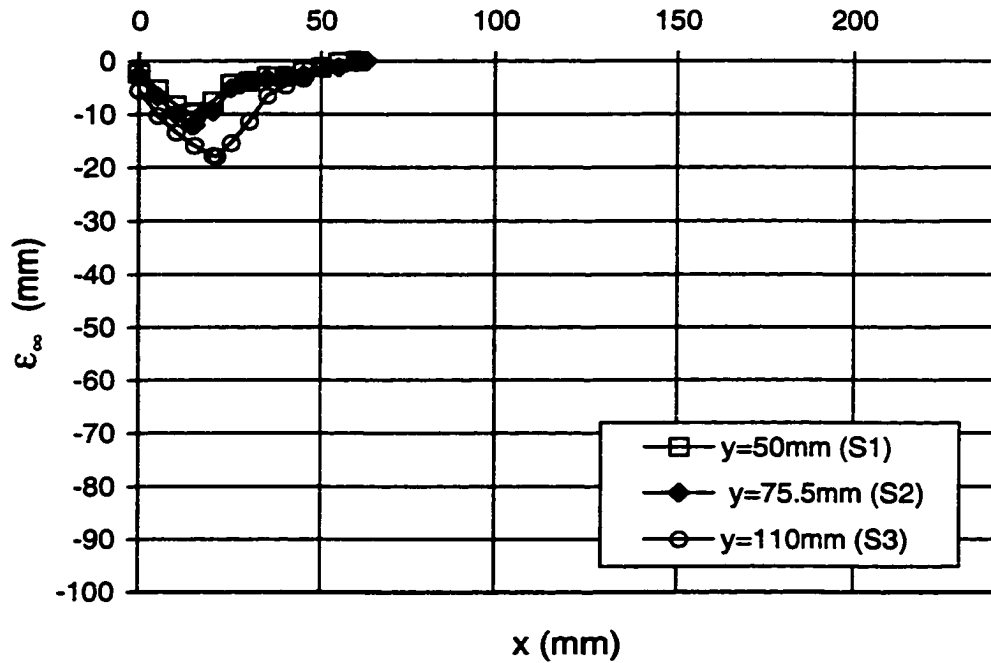


Fig. F-24: Scour hole profile at ultimate state for Wall Jet
 Test No. 2.33/7.2/2 - 9 Sep 99
 $U_o=7.16\text{ m/s}$ $a=2.33\text{ mm}$ $(\lambda-\lambda_c)/\lambda_c=1.56$

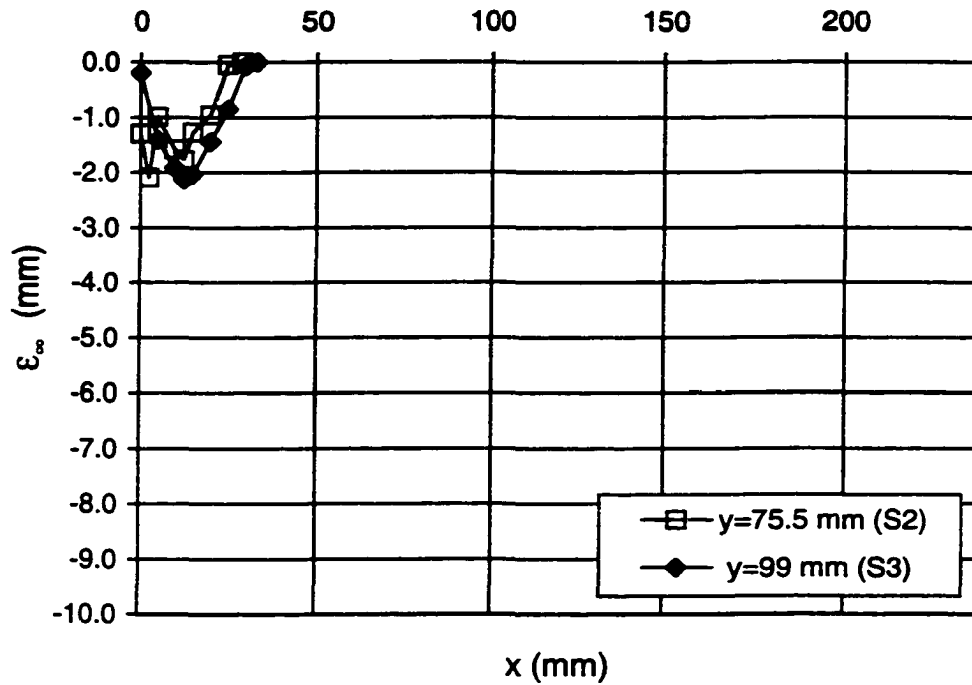


Fig. F-25: Scour hole profile at ultimate state for Wall Jet
 Test No. 2.33/5.2/1 - 24 Sep 99
 $U_o=5.16$ m/s $a=2.33$ mm $(\lambda-\lambda_c)/\lambda_c=0.33$

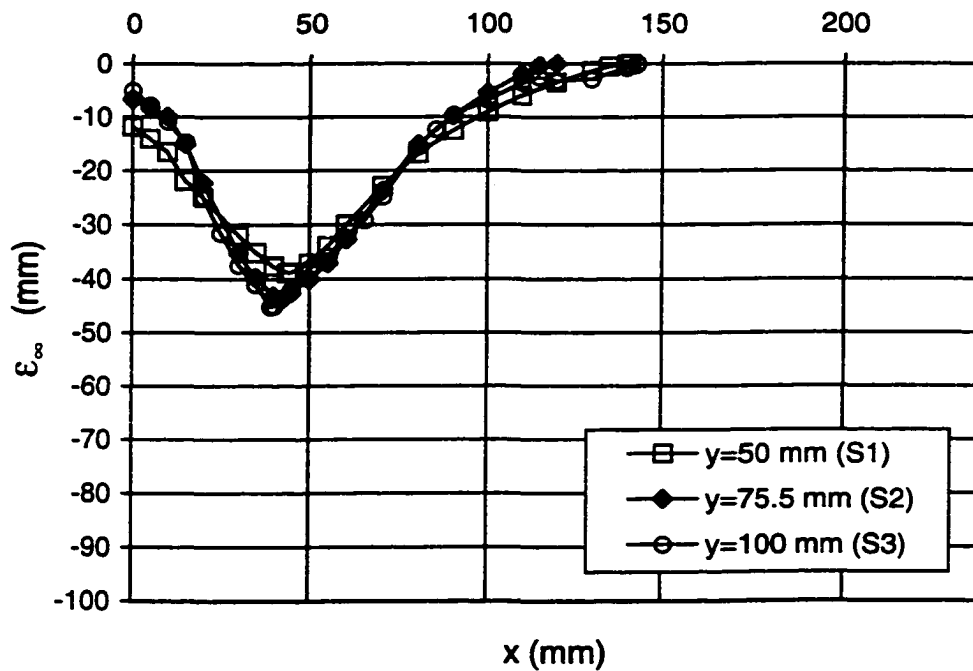


Fig. F-26: Scour hole profile at ultimate state for Wall Jet
 Test No. 2.33/11.7/1 - 30 Sep 99
 $U_o=11.66$ m/s $a=2.33$ mm $(\lambda-\lambda_c)/\lambda_c=5.79$

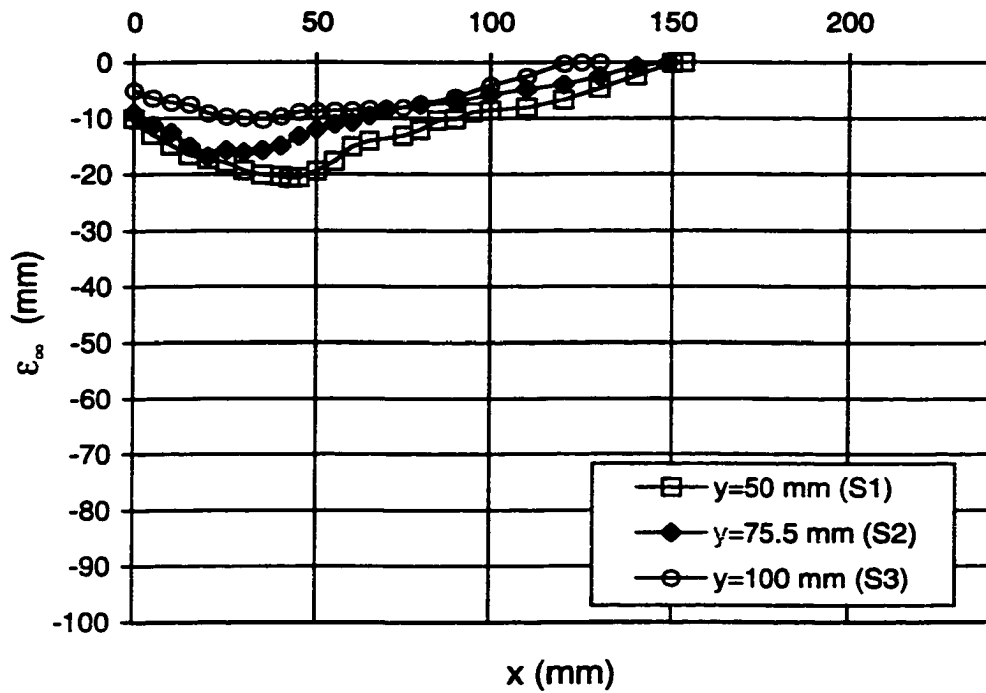


Fig. F-27: Scour hole profile at ultimate state for Wall Jet
 Test No. 5.10/6.5/1 - 10 Jan 00
 $U_o=6.54$ m/s $a=5.10$ mm $(\lambda-\lambda_c)/\lambda_c=1.14$

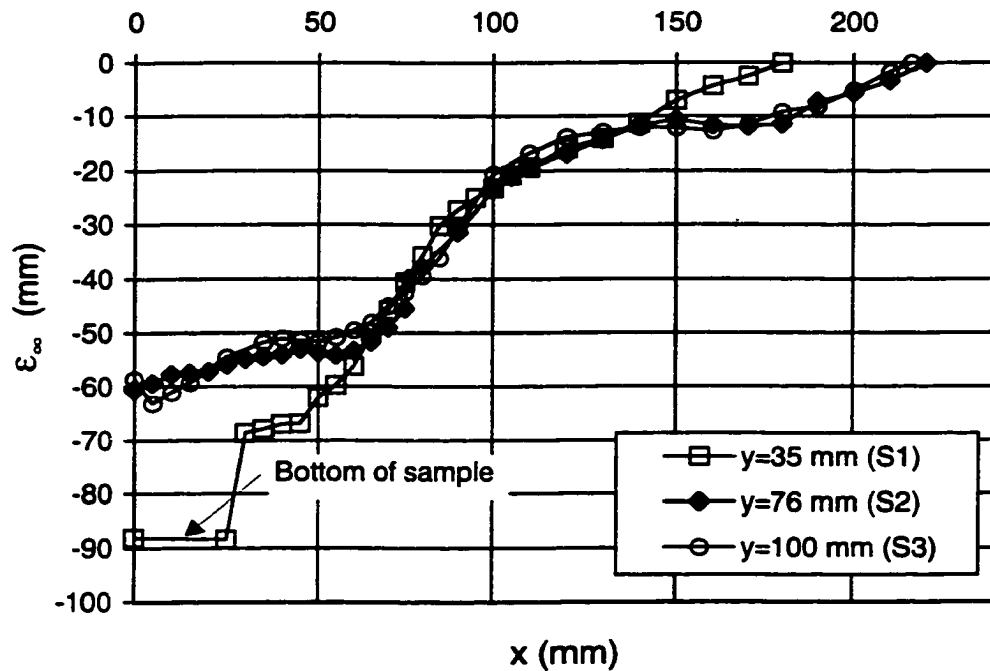


Fig. F-28: Scour hole profile at ultimate state for Wall Jet
 Test No. 5.10/7.0/1 - 20 Jan 00
 $U_o=7.03$ m/s $a=5.10$ mm $(\lambda-\lambda_c)/\lambda_c=1.47$

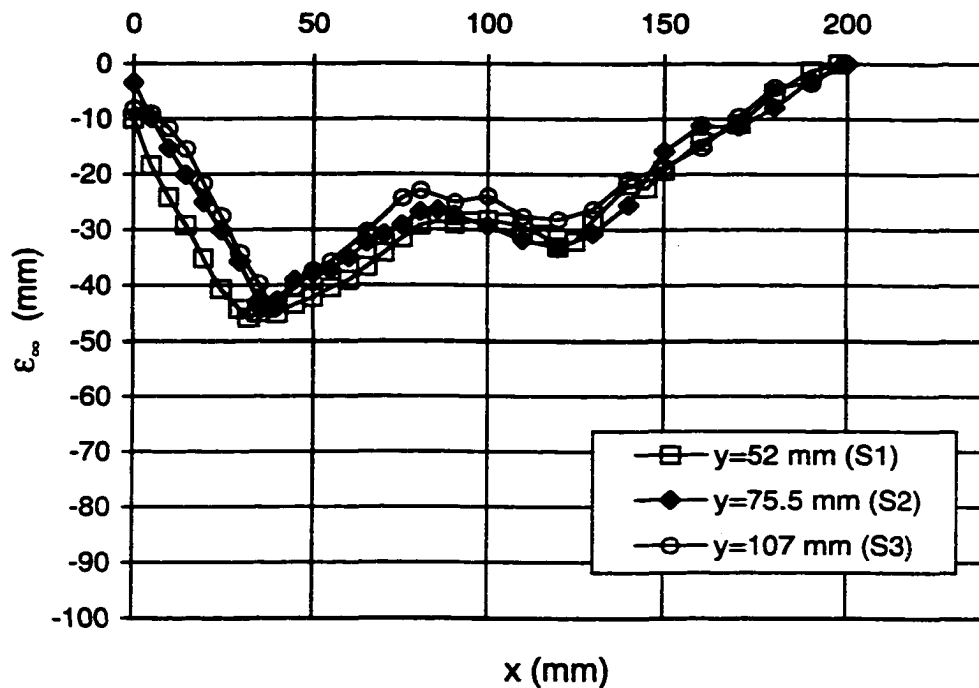


Fig. F-29: Scour hole profile at ultimate state for Wall Jet
 Test No. 5.10/6.0/1 - 26 Jan 00
 $U_o=6.04$ m/s $a=5.10$ mm $(\lambda-\lambda_c)/\lambda_c=0.82$

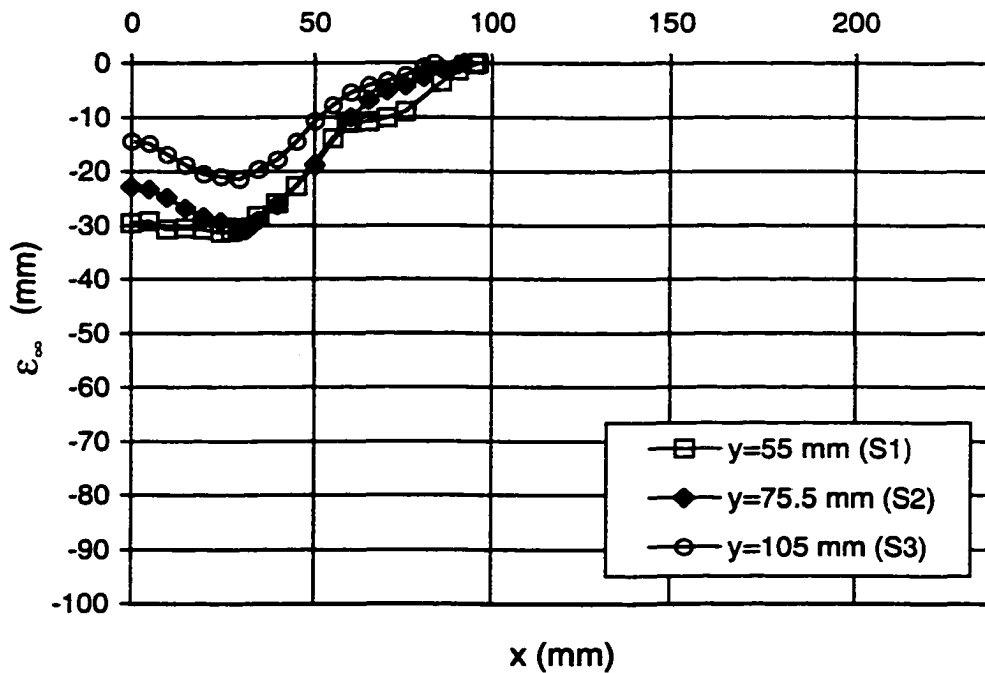


Fig. F-30: Scour hole profile at ultimate state for Wall Jet
 Test No. 5.10/4.9/1 - 8 Feb 00
 $U_o=4.86$ m/s $a=5.10$ mm $(\lambda-\lambda_c)/\lambda_c=0.18$

Appendix G: Data for Wall Jet Evolution Tests

Test No.	2.33/10.5/1/E	Test Variables		
Clay	M390	Q (L/s)	U _a (m/s)	a (mm)
Clay Lot No.	34281348	3.54	10.54	2.33

Test Date: 2-Nov-99

Δh_m (mm) 451

*all measurements along centreline at y=75.5mm

Time (h)	ε _m (mm)	x _m (mm)	x _o (mm)	b (mm)	U _a /a	x/a
0.5	5.83	14	34	22.7	8139580	14.59
1	7.80	19	45	28.0	16279160	19.31
2	9.84	24	64	37.362794	32558320	27.47
4	13.31	25	67	43.726868	65116639	28.76

After 30 min - 2 Nov 99				After 1 h - 2 Nov 99				After 2 h - 2 Nov 99			
x (mm)	Reading (cm)	Int. Surface	ε _w (mm)	x (mm)	Reading (cm)	Int. Surface	ε _w (mm)	x (mm)	Reading (cm)	Int. Surface	ε _w (mm)
Top of Band	45.94			Top of Band	45.94			Top of Band	45.94		
0	45.92	45.94	-0.20	0	45.72	45.94	-2.20	0	45.89	45.94	-0.50
5	45.61	45.93	-3.17	5	45.51	45.93	-4.22	5	45.40	45.94	-5.41
7.5	45.47	45.92	-4.50	10	45.28	45.92	-6.44	10	45.27	45.94	-6.72
10	45.38	45.91	-5.34	15	45.19	45.92	-7.27	15	45.16	45.94	-7.82
14	45.32	45.90	-5.83	17	45.14	45.91	-7.74	20	45.01	45.94	-9.33
15	45.33	45.90	-5.70	18	45.14	45.91	-7.72	24	44.96	45.94	-9.84
17.5	45.37	45.89	-5.24	19	45.13	45.91	-7.80	25	44.98	45.94	-9.64
20	45.45	45.89	-4.37	20	45.14	45.91	-7.69	30	45.08	45.94	-8.65
25	45.71	45.87	-1.64	25	45.29	45.90	-6.11	35	45.35	45.95	-5.95
27.5	45.77	45.87	-0.97	30	45.65	45.89	-2.43	40	45.57	45.95	-3.76
30	45.81	45.86	-0.51	35	45.73	45.89	-1.56	45	45.73	45.95	-2.17
32.5	45.83	45.85	-0.24	40	45.83	45.88	-0.48	50	45.83	45.95	-1.18
34	45.85	45.85	0.00	45	45.87	45.87	0.00	55	45.89	45.95	-0.59
								60	45.92	45.95	-0.29
								64	45.95	45.95	0.00

After 4 h - 2 Nov 99			
x (mm)	Reading (cm)	Int. Surface	ϵ_{-} (mm)
Top of Band	45.93		
0	45.60	45.93	-3.30
5	45.37	45.93	-5.62
10	45.19	45.93	-7.44
15	44.95	45.94	-9.87
20	44.70	45.94	-12.39
25	44.61	45.94	-13.31
30	44.68	45.94	-12.63
35	44.87	45.95	-10.76
40	45.12	45.95	-8.28
45	45.34	45.95	-6.10
50	45.51	45.95	-4.42
55	45.72	45.95	-2.35
60	45.82	45.96	-1.37
65	45.92	45.96	-0.39
67	45.96	45.96	0.00

Test No. 2.33/8.9/1/E
 Clay M390
 Clay Lot No. 34281348
 Test Date: 22-Nov-99
 Δh_m (mm) 321

Test Variables		
Q (L/s)	U_o (m/s)	a (mm)
2.98	8.89	2.33

*all measurements along centreline at $y=75.5\text{mm}$

Time (h)	ϵ_{m-} (mm)	x_{m-} (mm)	x_{o-} (mm)	b (mm)	U_o/a	x_o/a
0.5	7.38	17	38	26.23	6866987	16.31
1	10.23	21	47	32.30	13733974	20.17
2	14.31	27	58	39.30	27467949	24.89
4.5	20.29	32.5	70	49.59	61802885	30.04
25	41.23	48	90	65.08	343349359	38.63
50	47.88	50	115	71.80	686698717	49.36
72	55.76	49	123	71.80	988846153	52.79

*Int. Surface - interpolated surface of clay (from top of clay and measurement of clay surface at x_o).

After 30 min - 22 Nov 99				After 1 h - 22 Nov 99				After 2 h - 22 Nov 99			
x (mm)	Reading (cm)	Int. Surface	ϵ_{-} (mm)	x (mm)	Reading (cm)	Int. Surface	ϵ_{-} (mm)	x (mm)	Reading (cm)	Int. Surface	ϵ_{-} (mm)
Top of Band	45.90			Top of Band	45.93			Top of Band	45.94		
0	45.87	45.90	-0.30	0	45.84	45.93	-0.90	0	45.74	45.94	-2.00
5	45.61	45.89	-2.83	5	45.50	45.92	-4.24	5	45.37	45.94	-5.68
10	45.36	45.89	-5.27	10	45.27	45.92	-6.47	10	45.10	45.94	-8.37
15	45.15	45.88	-7.30	15	45.05	45.91	-8.61	15	44.89	45.93	-10.45
17	45.14	45.88	-7.38	20	44.91	45.90	-9.94	20	44.65	45.93	-12.83
20	45.19	45.87	-6.84	21	44.88	45.90	-10.23	25	44.52	45.93	-14.11
25	45.44	45.87	-4.27	25	44.96	45.90	-9.38	27	44.50	45.93	-14.31
30	45.67	45.86	-1.91	30	45.23	45.89	-6.62	30	44.57	45.93	-13.60
35	45.83	45.85	-0.24	35	45.55	45.89	-3.35	35	44.85	45.93	-10.78
38	45.85	45.85	0.00	40	45.77	45.88	-1.09	40	45.27	45.93	-6.56
				45	45.83	45.87	-0.43	45	45.58	45.92	-3.44
				47	45.87	45.87	0.00	50	45.77	45.92	-1.53
								55	45.88	45.92	-0.41
								58	45.92	45.92	0.00

After 4.5 h - 22 Nov 99				After 25 h - 22 Nov 99				After 50 h - 22 Nov 99			
x (mm)	Reading (cm)	Int. Surface	ϵ_{-} (mm)	x (mm)	Reading (cm)	Int. Surface	ϵ_{-} (mm)	x (mm)	Reading (cm)	Int. Surface	ϵ_{-} (mm)
Top of Band	45.93			Top of Band	45.94			Top of Band	45.93		
0	45.56	45.93	-3.70	0	45.65	45.94	-2.90	0	42.72	45.93	-32.10
5	45.37	45.93	-5.61	5	45.29	45.95	-6.56	5	42.74	45.94	-31.98
10	45.06	45.93	-8.73	10	44.96	45.95	-9.91	10	42.94	45.95	-30.06
15	44.84	45.93	-10.94	15	44.36	45.96	-15.97	15	43.06	45.95	-28.93
20	44.57	45.94	-13.66	20	43.62	45.96	-23.42	20	42.72	45.96	-32.41
25	44.32	45.94	-16.17	25	43.00	45.97	-29.68	25	42.30	45.97	-36.69
30	44.04	45.94	-18.99	30	42.67	45.97	-33.03	30	42.07	45.98	-39.07
32.5	43.91	45.94	-20.29	35	42.40	45.98	-35.79	35	41.90	45.98	-40.85
35	44.02	45.94	-19.20	40	42.21	45.98	-37.74	40	41.67	45.99	-43.23
40	44.29	45.94	-16.51	45	41.97	45.99	-40.20	45	41.50	46.00	-45.00
45	44.59	45.94	-13.53	48	41.87	45.99	-41.23	50	41.22	46.01	-47.88
50	44.96	45.94	-9.84	50	42.04	46.00	-39.56	55	41.74	46.02	-42.76
55	45.37	45.95	-5.76	55	42.76	46.00	-32.41	60	42.19	46.02	-38.34
60	45.78	45.95	-1.67	60	43.96	46.01	-26.47	65	42.75	46.03	-32.82
65	45.91	45.95	-0.39	65	43.94	46.01	-20.72	70	43.35	46.04	-26.90
70	45.95	45.95	0.00	70	44.64	46.02	-13.78	75	44.18	46.05	-18.67
				75	45.32	46.02	-7.03	80	44.89	46.06	-11.65
				80	45.66	46.03	-3.69	85	45.37	46.06	-6.93
				85	45.86	46.03	-1.74	90	45.53	46.07	-5.41
				90	46.04	46.04	0.00	95	45.84	46.08	-2.39
								100	45.87	46.09	-2.17
								105	45.89	46.09	-2.04
								110	46.06	46.10	-0.42
								115	46.11	46.11	0.00

After 72 h - 22 Nov 99			
x (mm)	Reading (cm)	Int. Surface	ϵ_{-} (mm)
Top of Band	45.94		
0	42.76	45.94	-31.80
5	42.80	45.95	-31.50
10	42.91	45.96	-30.50
15	42.79	45.97	-31.79
20	42.10	45.98	-38.79
25	41.54	45.99	-44.49
30	40.92	46.00	-50.79
35	40.66	46.01	-53.48
40	40.53	46.02	-54.88
45	40.54	46.03	-54.88
49	40.46	46.04	-55.76
50	40.76	46.04	-52.78
55	41.54	46.05	-45.07
60	42.03	46.06	-40.27
65	42.66	46.07	-34.07
70	43.08	46.08	-29.97
75	43.67	46.09	-24.16
80	44.31	46.10	-17.86
85	44.93	46.11	-11.76
90	45.19	46.12	-9.26
95	45.28	46.13	-8.45
100	45.49	46.14	-6.45
105	45.55	46.14	-5.95
110	45.78	46.15	-3.75
115	45.96	46.16	-2.04
120	46.14	46.17	-0.34
123	46.18	46.18	0.00